

https://dspace.org/

Linking solution and solid state studies of bismuth and cadmium complexes

Vieira, Vanessa Lourenco

2014-08-01
http://hdl.handle.net/10539/15106

Downloaded from a DSpace repository. https://dspace.org/

Linking Solution and Solid State Studies of Bismuth and Cadmium Complexes

by Vanessa Lourenço Vieira

A thesis submitted to the Faculty of Science, University of the Witwatersrand, Johannesburg, in fulfillment of the requirements for the degree of Doctor of Philosophy.

May 2014

Declaration

I declare that this thesis is my own, unaided work. It is being submitted for the Degree of Doctor of Philosophy in the University of the Witwatersrand, Johannesburg. It has not been submitted before for any degree or examination in any other University.

_____ (Signature of Candidate)

_____ day of _____ 2014

Abstract

In this project the link between species in solution and the solid state was considered. This is relevant due to the many applications in life where there is this interchange between solid and solution state, for example drug design, environmental metal speciation and the manufacture of materials that are in contact with solution (such as outdoor surface coatings, containers and so on). Complexation of two metal ions, namely cadmium(II) and bismuth(III), was studied. With bismuth showing so much promise in medicinal applications it was pertinent to investigate this interchange since the intake of medication is generally in the solid form which then converts to solution species as it dissolves in the body where it becomes active. For cadmium it is mainly the environmental concerns which we are faced with that call for the examination of speciation of complexes in solution, as well as their disposition upon precipitation or crystallization.

A correlation was found between solution species and the complex that was isolated in the crystalline form with regards to pH for a number of metal-ligand species. We show how the results from solution experiments (achieved using direct current polarography) and those of crystalline complexes can complement each other when using species distribution diagrams as the intermediary. The distribution of species can be varied by changing the concentration and ligand-to-metal ratio at which the species distribution diagram is plotted. It is this characteristic which allows the solution and crystalline complexes – which are achieved using differing experimental conditions – to be correlated.

The speciation diagram for a metal-ligand system, calculated using formation constants derived from solutions studies, was used in most instances to target specific species for their growth in the solid state. In some cases the solid state structure was used to confirm a suspected solution species, and in others the result was used to identify minor solution species which cannot be detected by the techniques used in

determining formation constants. Further, we show that doing solution experiments at a range of temperatures can also aid in elucidating these minor species.

The growth of crystalline species at low pH was important for this work because the pH titrations used for solution experiments were conducted from below pH 2 where the diffusion junction potential is large and changing. An in-situ witness ion was incorporated into the experiment to monitor the shifts due to the diffusion junction potential so that they could be compensated for. Additionally, for bismuth-ligand systems, hydrolysis and complexation with nitrates occurs in this same pH region. The formation constants and the species identified below pH 2 therefore do carry some uncertainty, so obtaining crystalline complexes of these species provides further confidence in their prediction in solution.

Acknowledgements

Caren, my supervisor and my mentor, I admire your work ethic and your determination to produce work of the best quality! Thank you for all the time you spent with me in the laboratory as well as analyzing data - through your dedication I learnt so much! I must also express my gratitude for the support, advice, assistance and encouragement that you offered consistently throughout my research!

Thank you Demi, my co-supervisor, for all the effort you put into proof-reading my thesis and for assisting me with the crystallography. Your guidance and expertise are greatly valued!

Manny, your assistance and unwavering offer of support throughout my degree are truly appreciated! Your knowledge in crystallography is admirable and I appreciate the time you spent imparting it.

Thank you to friends and colleagues whose encouragement and friendship was much needed throughout my studies. Thank you to the School of Chemistry and the University of the Witwatersrand for the wonderful experience you have given me as a student, a tutor and a part-time lecturer.

Thank you to Caren, Helder, the NRF (National Research Foundation) and The Financial Aid and Scholarships Office for the magnificent opportunity of presenting my work at an international conference.

The financial assistance towards this research from the NRF is hereby acknowledged. Opinions expressed, and conclusions arrived at, are those of the author and are not necessarily to be attributed to the NRF.

Dedication

My family is my reason for being! Without them I would not be who I am! I love them very dearly and I dedicate this work to them. Let my effort and determination towards my PhD be a small representation of how greatly I love and appreciate each one of them! They all have attributes which I adore and respect: my extremely hard-working father, Kevin, who is my moral compass; my happy, loving and dedicated mother, Luisa, who has blessed me with creativity which has helped me tremendously through this degree; my extremely knowledgeable and versatile *big* brother, Marco, who has just submitted his MSc, my determined *little* sister, Bianca, who has obtained her degree and is already out in the working world; my *little* brother, Filipe, who against all odds is on the road to achieving his goal of a degree in Food Technology, and last but not least my loving fiancé, George, who has created his own business through determination, courage, hard work and persistence! I admire you all, and I thank you all for your support and encouragement along the way.

The secret of success is to be like a duck – smooth and unruffled on top, but paddling furiously underneath. ~ Anonymous

Publications and Presentations

- Published a short communication in the South African Journal of Chemistry entitled "The Crystal Structures of Two Novel Cadmium-Picolinic Acid Complexes in Relation to the Solution Species". Journal reference: C. Billing, D.C. Levendis and V.L. Vieira (2011). *S. Afr. J. Chem.,* 64, 38–41.
- SACI Young Chemists Symposium in Johannesburg (2013) – Oral presentation entitled "Can Solid Complexes be Linked with their Respective Species in Solution?" Obtained the 1st place award in the PhD category.
- 40th International Conference on Coordination Chemistry (ICCC 40) in Valencia, Spain (2012) - Poster entitled "Elucidating complexes using solution and solid state as complimentary techniques".
- Indaba 7 Conference "Insights from Structure" in The Kruger National Park (2012) - Poster entitled "Adopting solid state chemistry as a tool to assist in elucidating species that potentially exist in solution".
- 40th SACI Convention incorporating the 15th Inorganic Conference (INORG2011) and the 3rd FASC Congress in Johannesburg (2011) - Presented a poster that described the research conducted on cadmium-dipicolinic acid and cadmium-picolinic acid systems.
- University of the Witwatersrand's Chemistry Society's Postgraduate Colloquium in Johannesburg (2010) – Oral presentation which covered various cadmium-ligand systems in solution and their link to solid state structures. Obtained the 2nd place award.
- University of the Witwatersrand's Cross Faculty Symposium in Johannesburg (2010) - Poster presentation on how solution species are linked to solid state crystal structures.
- Indaba 6 Conference "Structure and Properties" in The Kruger National Park (2009) - Poster presentation on coordination compounds (2009).

Contents

Chapter One

1.1 LITERATURE REVIEW 1

1.1.1 Meet the Metal Ions of Interest 2

1.1.2 Solution Studies 3

1.1.2.1 The Polarography Technique and its Associated Pitfalls 4

1.1.3 Crystallographic studies 8

1.1.3.1 Single-crystal X-ray Diffraction (SCXRD) 8

1.1.3.2 Powder X-ray Diffraction (PXRD) 10

1.1.4 The Link between Solution Species and Crystalline Complexes 10

1.2 AIMS 14

1.3 REFERENCES 16

Chapter Two

2.1 INTRODUCTION 20

2.2 SOLUTION STUDIES 20

2.2.1 Experiments and Data Analyses 28

2.2.1.1 Standardization of Solutions 28

2.2.1.2 Calibration of the Glass Electrode 29

2.2.1.3 Polarographic Experiments 32

2.2.1.4 Curve Fitting 37

2.2.1.5 Solving Formation Constants 40

2.2.1.6 Relating Solution Species to Crystalline Complexes 42

2.3 CRYSTALLOGRAPHIC STUDIES 42

2.3.1 Crystal Structure Determination 46

2.3.2 Crystalline Complexes 48

2.4 REFERENCES 50

Chapter Three

3.1 INTRODUCTION 51

3.2 EXPERIMENTS MONITORING THE DIFFUSION JUNCTION POTENTIAL 57

3.3 THE COMPENSATION MODEL 66

3.3.1 Testing the Various Models 70

3.3.1.1 Testing Accuracy 70

3.3.1.1 Testing Precision 72

3.4 COMPARING E_j CALCULATED USING THE HENDERSON EQUATION TO THAT DETERMINED EXPERIMENTALLY IN THE ABSENCE OF LIGAND 76

3.5 COMPARING E_j CALCULATED USING THE HENDERSON EQUATION TO THAT USING THE COMPENSATION MODEL 81

3.6 CONCLUSION 82

3.7 REFERENCES 84

Chapter Four

4.1 INTRODUCTION 86

4.1.1 Formation Constants 91

4.1.2 The Distribution of Species in Solution 94

4.2 AIMS 98

4.3 EXPERIMENTAL 99

4.3.1 Diaquadinitrato(pyridine-2-carboxylato-O,O)cadmium(II) (Cd(PIC-H)) 99

4.3.2 Tri(pyridine-2-carboxylato-N,O)cadmium(II)dinitrate ($Cd(PIC\text{-}H)_3$) 100

4.3.3 Crystallographic Data collection, Structure Solution and Refinement 100

4.4 RESULTS AND DISCUSSION 102

4.4.1 Diaquadinitrato(pyridine-2-carboxylato-O,O)cadmium(II) Complex (Cd(PIC-H)) 102

4.4.1.1 Analysis of the Crystal Structure 102

4.4.1.2 A Comparative Study with Literature Structures 106

4.4.2 Tri(pyridine-2-carboxylato-N,O)cadmium(II)dinitrate Complex ($Cd(PIC\text{-}H)_3$) 109

4.4.2.1 Analysis of the Crystal Structure 109

4.4.2.2 A Comparative Study with Literature Structures 112

4.5 RELATING SOLUTION SPECIES TO CRYSTALLINE COMPLEXES 114

4.6 CONCLUSIONS 122

4.7 REFERENCES 124

Chapter Five

5.1 INTRODUCTION 127

5.1.1 Solution Complexes for the Cadmium(II)-Dipicolinic Acid System 129

5.2 AIMS 131

5.3 EXPERIMENTAL, DATA ASSESSMENT AND PROBLEM IDENTIFICATION 132

5.3.1 Unresolved Waves at Low pH 134

5.3.2 Complex Formation with the In-situ Witness Ion, Thallium(I) 138

5.4 RESULTS AND DISCUSSION 142

5.4.1 Cadmium(II)-Dipicolinic Acid Formation Constants at 25 °C 142

5.4.2 The van't Hoff equation and Adjustment of Protonation Constants 157
5.4.3 Cadmium(II)-Dipicolinic Acid Formation Constants at 32 °C 159
5.4.4 Cadmium(II)-Dipicolinic Acid Formation Constants at 40 °C 164
5.5 COMPARISON OF RESULTS 176
5.6 CONCLUSIONS 184
5.7 REFERENCES 186
Chapter Six
6.1 INTRODUCTION 190
6.2 AIMS 193
6.3 EXPERIMENTAL 194
6.3.1 Crystal Growth of hexa-aqua-bis(μ_2-pyridine-2,6-dicarboxylato-N,O,O,O')-di-cadmium(II) bis(pyridine-2,6-dicarboxylic acid) 194
6.3.2 Other Attempts at Crystallization of Cadmium(II)-Dipicolinic acid Complexes 196
6.3.3 Crystallographic Data Collection, Structure Solution and Refinement 200
6.4 RESULTS AND DISCUSSION 202
6.4.1 Hexa-aqua-bis(μ_2-pyridine-2,6-dicarboxylato-N,O,O,O')-di-cadmium(II) bis(pyridine-2,6-dicarboxylic acid) 202
6.3.3.1 Analysis of the Crystal Structure 202
6.3.3.2 A Comparative Study with Literature Structures 205
6.3.4 Analysis of Doubly Protonated Dipicolinic acid (DIPIC-H_2) 211
6.3.5 Analysis of the Salt Crystal 211
6.5 RELATING SOLUTION SPECIES TO CRYSTALLINE COMPLEXES 213
6.6 CONCLUSION 216
6.7 REFERENCES 218
Chapter Seven
7.1 INTRODUCTION 221
7.1.1 Crystalline Complexes for the Cadmium(II)-Quinolinic Acid System 224
7.1.2 Solution Complexes for the Cadmium(II)-Quinolinic Acid System 224
7.2 AIMS 225
7.3 RESULTS AND DISCUSSION 225
Part A: Solution Complex Formation 226
7.3.1 Interference From Ligand Reduction at Low pH 226
7.3.2 Complex Formation with the In-situ Witness Ion, Thallium(I) 227
7.3.3 Cadmium(II)-Quinolinic Acid Formation Constants 229
Part B: Crystalline Complex Formation 242

7.3.4 Experimental Overview 242
7.3.5 Crystallographic Data Collection, Structure Solution and Refinement 247
7.3.6 Analysis of the Crystal Structure of catena-[(μ_2-Pyridine-2,3-dicarboxylato-κ^3n,O,O')-triaqua-cadmium(II)] or catena-Poly[[triaquacadmium(II)]-μ-pyridine-2,3-carboxylato-$\kappa^3 n,O^2$:O^3] 250
7.3.6.1 A Comparative Study with Literature Structures 254
7.3.7 Analysis of the Crystal Structure of Tri(quinolinato-N,O)-cadmium(II)) hexa-aqua-cadmium 259
7.3.7.1 A Comparative Study with Literature Structures 263
7.3.8 Analysis of the Crystal Structure of Pyridine-2,3-dicarboxylic Acid 266
7.4 RELATING SOLUTION SPECIES TO CRYSTALLINE COMPLEXES 266
7.5 CONCLUSIONS 272
7.6 REFERENCES 275

Chapter Eight

8.1 INTRODUCTION 278
8.2 AIMS 287
8.3 EXPERIMENTAL 287
8.3.1 Crystallographic Data Collection, Structure Solution and Refinement 291
8.4 RESULTS AND DISCUSSION 292
8.4.1 Structure Analysis of the Bismuth(III)-Quinolinate Crystal Complex 292
8.4.2 A Comparative Study with Literature Structures 298
8.5 CONCLUSIONS 301
8.6 REFERENCES 303

Chapter Nine

9.1 INTRODUCTION 305
9.1.1 Solution Complexes for the Bismuth(III)-EDTA System 307
9.1.2 Crystalline Complexes for the Bismuth(III)-EDTA System 309
9.2 AIMS 312
9.3 EXPERIMENTAL 312
9.3.1 Solution Complex Formation 312
9.3.2 Crystalline Complex Formation 313
9.3.2.1 Crystal Growth of catena((m3-hydrogen-ethylenediaminetetra-acetato)-bismuth(III)) dihydrate 313
9.3.2.2 Crystallographic Data Collection, Structure Solution and Refinement of catena((m3-Hydrogen-ethylenediaminetetra-acetato)bismuth(III))dihydrate 314
9.4 RESULTS AND DISCUSSION 316

9.4.1 Solution Studies 316

9.4.1.1 Analysis of Composite Waves where the Reduction of Bismuth(III) is Irreversible 316

9.4.1.2 Determination of the Diffusion Junction Potential 325

9.4.1.3 Modelling the Free Bismuth(III) Ion Potential 326

9.4.1.4 Model to Determine the Free Bi(III) Potential in Complexation Experiments 330

9.4.1.5 Solving for $E(Bi_{free})$ in a Complexation Experiment using the "Difference" Models 333

9.4.2 Crystallographic Studies 344

9.4.2.1 Analysis of the Crystal Structure of catena((μ_3-Hydrogen-ethylenediaminetetra-acetato)-bismuth(III)) dihydrate 344

9.4.2.2 A Comparative Study with Literature Structures 347

9.5 RELATING SOLUTION SPECIES TO CRYSTALLINE COMPLEXES 349

9.6 CONCLUSIONS 351

9.7 REFERENCES 352

Chapter Ten

10.1 INTRODUCTION 355

10.2 AIMS 360

10.3 EXPERIMENTAL 361

10.4 RESULTS AND DISCUSSION 362

10.4.1 Approach 1 364

10.4.2 Approach 2 380

10.4.3 Comparison of Approach 1 and 2 384

10.5 CONCLUSIONS 387

10.6 REFERENCES 389

Chapter Eleven

Concluding Summary 391

Chapter Twelve

Appendix A 395

Chapter Thirteen

Appendix B 410

List of Figures

Figure 1.1 Crystal structure of the self-assembled adduct ((pydc)(pyda.H_2)) from Moghimi *et al.* (2002).

Figure 1.2 The electronic spectra of pydc·H_2, pyda and (pydc)(pyda·H_2) obtained spectrophotometrically, from Moghimi *et al.* (2002).

Figure 1.3 ORTEP diagram obtained from Moghimi *et al.* (2004) showing the structure of the complex formed by reacting the self-assembled adduct with $HgCl_2$.

Figure 2.1 Typical polarographic cell.

Figure 2.2 Schematic representation of the automated polarographic and potentiometric setup. Abbreviations have the following meanings: PC - personal computer, CE -counter electrode, WE - working electrode, EU - exchange unit, W – water for humidification of gas, RE - reference electrode, GE - glass electrode, TP - temperature probe, MS - magnetic stirrer and UHP N_2 – ultra high purity nitrogen. The black stars represent valves that are found on the cell stand

Figure 2.3 Comparison of calibration titration curves taken before and after a polarographic experiment, using 25 mL of ~0.5 M HNO_3 and 50 mL of ~0.5 M KOH (added in 0.5 mL increments).

Figure 2.4 Calibration curve showing the slope for evaluation of the long-term performance of the glass electrode.

Figure 2.5 Calibration curve in the highly acidic region showing the deviation from linearity below pH 0.5.

Figure 2.6 Polarogram showing a typical background scan in ~0.5 M HNO_3, pre- and post- N_2 purge.

Figure 2.7 Three consecutive polarograms showing the half-wave potentials of a) cadmium(II) and thallium(I) and b) bismuth(III) and thallium(I) in 0.5 M HNO_3.

Figure 2.8 The fitting procedure of each portion of a cadmium(II) and thallium(I) polarogram.

Figure 2.9 Apparatus used in temperature controlled crystallizations.

Figure 2.10 a) The APEX II diffractometer, and b) a close up of the crystal mount, area detector and CRYOSTREAM.

Figure 3.1 Schematic representation of a portion of the electrolytic cell and the diffusion junction between the sample solution and the salt bridge solutions.

Figure 3.2 Polarograms showing Cd(II) and Tl(I) reduction in nitrate solution at varying pH.

Figure 3.3 The half-wave potentials plotted as a function of pH for both Cd(II) and Tl(I) reduction. Coloured points correspond to polarograms plotted in Figure 3.2.

Figure 3.4 Quadratic and straight line functions fitted through the data points for cadmium(II) and thallium(I) reduction processes.

Figure 3.5 The magnitude of the diffusion junction potential at low pH values for thallium(I) calculated using the difference between $E(Tl_{free})$ and $E_{½}$.

Figure 3.6 The diffusion junction potential for thallium(I) and cadmium(II) in nitrate solutions at low pH.

Figure 3.7 The volume of KOH used to adjust the pH of the sample solution by 0.1 units together with its effect on the ionic strength and ΔE_j.

Figure 3.8 Simulation showing that the effect of changing ionic strength on the diffusion junction potential for thallium(I) is greater than what it would be if ionic strength was maintained at 0.5 M.

Figure 3.9 P-model at low pH calculated from five datasets.

Figure 3.10 C-model at low pH calculated from five datasets.

Figure 3.11 Comparison of all the C- and P-models.

Figure 3.12 Comparison of actual and predicted cadmium(II) half-wave potential data for experiment 2 using various compensation models.

Figure 3.13 Comparison of the change in measured diffusion junction potential for cadmium(II) with that calculated using the Henderson equation (using limiting ionic mobilities).

Figure 3.14 Comparison of the diffusion junction potential measured for thallium(I) and cadmium(II) with that calculated using the Henderson equation, with mobilities at infinite dilution or mobilities calculated at varying ionic strength

Figure 3.15 Comparison of the E_j calculated by the Henderson equation and that calculated for cadmium(II) using the compensation model, C(I).

Figure 4.1 Deprotonation equilibria of picolinic acid with stepwise protonation constants given in brackets (quoted as log *K* values at 25 °C and μ = 0.5 M (Martell, Smith and Motekaitis, 2004)).

Figure 4.2 Species distribution diagram (SDD) showing the percentage distribution of the ligand species that predominate in specific pH regions in solution.

Figure 4.3 Coordination modes for a) REHLIA and b) NISJEE which are rare for picolinic acid. The locations of the protons in each of these were not certain.

Figure 4.4 SDD showing the difference in species distributions when including (solid lines) or excluding (dashed lines) the MLH species. [Cd] = $1x10^{-4}$ M and [L] = $1x10^{-2}$ M. Cadmium(II) hydroxide species have been omitted for clarity.

Figure 4.5 SDD showing the effect of increasing both the concentration and [L]:[M] ratio by a hundred. Solid lines represent [L]:[M] = 1 where [Cd] = 0.001 M, dotted lines represent [L]:[M] = 100 where [Cd] = 0.001 M and dashed lines represent [L]:[M] = 1 where [Cd] = 0.1 M. M_{free} and hydroxide species have been omitted for clarity.

Figure 4.6 The molecular structure of Cd(PIC-H) with displacement ellipsoids drawn at the 50% probability level.

Figure 4.7 Packing of Cd(PIC-H) as viewed down the *a* axis. Hydrogen atoms have been omitted for clarity.

Figure 4.8 The layered structure of Cd(PIC-H). Hydrogen atoms have been omitted for clarity.

Figure 4.9 Hydrogen bond pair of Cd(PIC-H) molecules showing the bifurcated H-bond.

Figure 4.10 Coordination geometry around Cd1 for DEQDIN. The coordination number is seven which reduces to 5 if the nitrate ions are considered to be effectively monodentate (Wu, Zhang and Lin, 2006). Only a portion of the molecule is shown.

Figure 4.11 The structures of a) YILBIF and b) QUFKUY showing their coordination modes.

Figure 4.12 The molecular structure of $Cd(PIC\text{-}H)_3$ with displacement ellipsoids drawn at the 50% probability level.

Figure 4.13 Hydrogen bonding between two $Cd(PIC\text{-}H)_3$ molecules related by a centre of inversion showing the disordered H1 positions.

Figure 4.14 Hydrogen bonded chains of $Cd(PIC\text{-}H)_3$ as seen down the b-axis.

Figure 4.15 A view down the c-axis showing a) the channel occupied by the nitrate ions, and H-bonds between the $Cd(PIC\text{-}H)_3$ complexes, and b) the short contacts between the nitrate anion and the $Cd(PIC\text{-}H)_3$ complexes.

Figure 4.16 SDDs predicting the pH region where the MLH species exists when using liquor conditions of the crystal experiment. [Cd] = 0.5 M (solid lines) and [Cd] = 5 M (dotted lines) where [L]:[M] = 1:1.

Figure 4.17 Powder patterns showing the calculated pattern for the Cd(PIC-H) complex (black) compared to that measured on the remaining crystals (red). Other powder patterns also shown are cadmium(II) nitrate (blue), and picolinic acid (PICOLA02) (pink) and cadmium(II) nitrate dihydrate (green).

Figure 4.18 SDD showing the distribution effects of changing the [L]:[M] ratios, where the cadmium(II) concentration remains 0.125 M. Dashed lines represent [L]:[M] = 2:1 and solid lines represent [L]:[M] = 3:1.

Figure 4.19 SDD of the acidic region showing the distribution of $M(LH)_3$ which (from below pH 0 to 4). [L]:[M] = 12:1 (dotted lines) and 3:1 (solid lines) where [Cd] = 0.125 M, log β(MLH) = 6.27, log β(ML) = 4.23, log $\beta(ML_2)$ =7.81 and log $\beta(ML_3)$ =10.53, and log $\beta(ML_3H_3)$ = 20.

Figure 5.1 Chemical structure of dipicolinic acid.

Figure 5.2 Deprotonation equilibria of dipicolinic acid with stepwise protonation constants given in brackets (quoted as log *K* values for 25 °C and 0.5 M ionic strength (Martell, Smith and Motekaitis, 2004).

Figure 5.3 Polarograms showing potential shifts due to complex formation and E_j recorded during a pH titration, where [DIPIC]:[Cd] = 21 at 25 °C.

Figure 5.4 Polarograms measured at pH 0.3 before and after the addition of dipicolinic acid, where [DIPIC]:[Cd] = 52 and [Cd] = 1.00 x 10^{-4} M.

Figure 5.5 Polarograms showing the interference from the reduction of dipicolinic acid at different [L]:[M] ratios, all measured at pH 0.3.

Figure 5.6 Simulation showing the effect of concentration, at the same pH, on reduction potentials.

Figure 5.7 Polarograms showing the dependence of the reduction potential on pH.

Figure 5.8 At increased temperatures the reduction occurs at less negative potentials. [L]:[M] = 20 where [Cd] = 1.00 x 10^{-4} M and the pH was 0.3 in all cases.

Figure 5.9 Experimental half-wave potential values for thallium(I) and expected values above pH 2 for uncomplexed thallium(I), where [L]:[Tl] = 11 and [Tl] = 2 x 10^{-4} M.

Figure 5.10 The potential shift due to complex formation between thallium(I) and dipicolinic acid collected at 32 °C, where [L]:[Tl]= 10, 20 and 25 (which corresponds to [L]:[Cd] = 20, 40 and 50 respectively).

Figure 5.11 Species distribution diagram plotted using log β values for thallium(I)-dipicolinic acid complexes estimated by Billing (2012). [Tl] = 2 x 10^{-4} M and [L] = 2 x 10^{-3} M.

Figure 5.12 Thallium(I) and cadmium(II) half-wave potential values as pH is increased for [L]:[M] = 21 at 25 °C.

Figure 5.13 The determined free metal ion potential for thallium(I) where [L]:[M] = 21, at 25 °C.

Figure 5.14 Graph showing the experimental half-wave potential for cadmium(II) and the predicted uncomplexed cadmium(II) data. The magnitude of E_j is the difference between $E(Cd_{free})$ and the predicted uncomplexed-cadmium(II) data.

Figure 5.15 The experimental half-wave potentials that have been compensated for the diffusion junction potential, where [L]:[M] = 21, at 25 °C.

Figure 5.16 ECFC and CCFC showing the poor fit when the ML and ML_2 species are used for refinement of formation constants. ([L]:[M] = 21.)

Figure 5.17 Slope analysis performed on the ECFC for [DIPIC]:[Cd] = 21.

Figure 5.18 Comparative plot showing two models used in calculating the CCFC for [L]:[M] = 21 at 25 °C.

Figure 5.19 The structure of the ML_3 Cd-dipicolinic acid crystal found by Li, Wang, Fu and Chen (2005) and Fu, Wang and Liu (2004).

Figure 5.20 ECFC and CCFC fitted with the MLH, ML and ML_2 model for each [DIPIC]:[Cd] ratio at 25 °C.

Figure 5.21 Species distribution diagram including ML_3 and MLH for [DIPIC]:[Cd] = 21 using log β values from Table 5.5. The hydroxide complexes have been omitted from the plot for clarity.

Figure 5.22 Species distribution diagram excluding the ML_3 complex for [L]:[M] = 21 using log β values from Table 5.6. The hydroxide complexes have been omitted from the plot for clarity.

Figure 5.23 Compensation model (C(I)) formed using the difference in half-wave potentials of thallium(I) and cadmium(II), using all three datasets obtained at 32 °C.

Figure 5.24 ECFC and CCFC calculated using the MLH, ML and ML_2 species model at each [L]:[M] ratio.

Figure 5.25 ECFC and CCFC calculated using MLH, ML, ML_2 and ML_3 species model at each [L]:[M] ratio.

Figure 5.26 Compensation model (C(I)) determined using the difference in half-wave potentials of thallium(I) and cadmium(II), using all three datasets obtained at 40 °C.

Figure 5.27 Comparison of the C(I) Compensation models for each temperature.

Figure 5.28 Overlap of the polarograms at pH 0.3 collected at each temperature. [Cd] = 1.00×10^{-4} M and [Tl] = 2.00×10^{-4} M.

Figure 5.29 The change in shape of a DC polarogram when the temperature is increased from 2.8 to 79.0 °C, by Janik and Sommer (1973).

Figure 5.30 ECFC and CCFC fitted using an MLH, ML and ML_2 model for each [DIPIC]:[Cd] ratio at 40 °C.

Figure 5.31 ECFC and CCFC fitted using the MLH, ML, ML_2 and ML_3 model for each [L]:[M] ratio at 40 °C.

Figure 5.32 ECFC and CCFC for each [L]:[M] ratio (at 40 °C) fitted with the ML, ML_2 and ML_3 model.

Figure 5.33 Comparison of the predicted current (due to dilution) and that measured during experimentation at 40 °C, where no ligand is present.

Figure 5.34 van't Hoff plot for the calculation of ΔH values for the formation of the MLH, ML, ML_2 and ML_3 complexes.

Figure 5.35 Comparison of two SDDs at 25 °C plotted using formation constants where the ML_3 complex was excluded (solid lines) and included (dashed lines) in the model. [Cd] = 1×10^{-4} M and [DIPIC] = 2×10^{-3} at 0.5 – 0.25 M ionic strength.

Figure 5.36 Comparison of the SDDs plotted using a MLH, ML, ML_2 and ML_3 species model for the 32 °C (dashed lines) and 40 °C (solid lines) data. [Cd] = 1 x 10^{-4} M and [DIPIC] = 2 x 10^{-3} M at 0.5 - 0.25 M ionic strength.

Figure 5.37 Comparison of SDDS at different temperatures plotted using an MLH, ML and ML_2 complex model. 25 °C is represented with solid lines, 32 °C with dotted lines and 40 °C with dashed lines. [Cd] = 1 x 10^{-4} M and [DIPIC] = 2 x 10^{-3} at an ionic strength of 0.25M to 0.5 M.

Figure 5.38 Comparison of SDDS at different temperatures plotted using an MLH, ML, ML_2 and ML_3 complex model. 25 °C is represented with solid lines, 32 °C with dotted lines and 40 °C with dashed lines. [Cd] = 1 x 10^{-4} M and [DIPIC] = 2 x 10^{-3} at an ionic strength of 0.25M to 0.5 M.

Figure 6.1 Coordination mode *x* with dinuclear bridging.

Figure 6.2 SDD plotted using MLH, ML, ML_2 and ML_3 formation constants calculated at 25 (solid lines) and 40 °C (dotted lines), where [L]:[M] = 1 and [Cd] = 0.01 M.

Figure 6.3 ORTEP diagram showing the structure of $Cd_2DIPIC_2 \cdot DIPIC\text{-}H_2$ at the 50% probability level. The inset highlights the planarity of the dinuclear portion of the structure.

Figure 6.4 ORTEP diagram of $Cd_2DIPIC_2 \cdot DIPIC\text{-}H_2$, showing the distorted pentagonal bipyramidal geometry around the cadmium(II) centre.

Figure 6.5 Intra- and inter-molecular hydrogen bonding within the crystal structure of $Cd_2DIPIC_2 \cdot DIPIC\text{-}H_2$.

Figure 6.6 ORTEP diagram showing the packing of a unit cell as seen down the b-axis.

Figure 6.7 a) The distorted trigonal bipyramidal geometry, and b) the intraligand distances of the nitrate anions, in the structure of XESHUY.

Figure 6.8 A portion of the structure of XESHOS with seven coordinate geometry around the cadmium ion, showing the intraligand distances of the nitrate anions.

Figure 6.9 The structure of XESJAG with seven coordinate geometry around the cadmium ion, showing the intraligand distances of the nitrate anions.

Figure 6.10 Portions of the structure of DEQDIN with seven coordinate geometry around the cadmium ions, showing intraligand distances of the nitrate anions around a) Cd1 and b) Cd2.

Figure 6.11 Structure of AFEBUI showing the disordered hydrogen atom.

Figure 6.12 KNO_3 salt structure by Holden and Dickinson (1975).

Figure 6.13 SDD plotted using MLH, ML, ML_2 and ML_3 formation constants calculated at 32 °C (solid lines) and 40 °C (dotted lines), where [L]:[M] = 1 and [Cd] = 0.01 M. LH_2 is represented by the dashed line. Cadmium(II) hydroxide species were omitted for clarity.

Figure 6.14 SDD plotted using MLH, ML, ML_2 and ML_3 formation constants calculated at 40 °C, where [L]:[M] = 2:1 and [Cd] = 0.005 M. Cadmium(II)hydroxide species have been omitted for clarity.

Figure 6.15 SDD plotted in terms of the remaining uncomplexed dipicolinic acid at 40 °C where [L]:[M] = 1 and [Cd] = 0.01 M.

Figure 7.1 Chemical structure of quinolinic acid (pyridine-2,3-dicarboxylic acid).

Figure 7.2 Deprotonation equilibria of quinolinic acid with stepwise protonation constants given in brackets and quoted as log *K* values.

Figure 7.3 Selected polarograms from pH 0.3 to 1.3 showing the overlap of quinolinic acid and cadmium(II) reduction waves and highlighting the shift of the quinolinic acid wave as the pH is increased ([L]:[M] = 196 data).

Figure 7.4 Comparison of the half-wave potential data for thallium(I) at different [L]:[M] ratios.

Figure 7.5 Difference between $E(Tl_{free})$ (averaged between approximately pH 2 and 3.5) and the half-wave potentials for thallium(I) at each pH.

Figure 7.6 Thallium(I) half-wave potential vs. pH plots showing $E(Tl_{free})$ for each data set.

Figure 7.7 Comparison of the diffusion junction potential calculated using the Henderson equation with that determined from thallium(I) for each data set.

Figure 7.8 ECFC and CCFC calculated using the ML and ML_2 complex for each [L]:[M] ratio for the cadmium(II)-quinolinate system.

Figure 7.9 Slope analysis performed on the ECFC for [QUIN]:[Cd] of a) 101 and b) 21.

Figure 7.10 ECFC and CCFC calculated using the MLH, ML and ML_2 complex for each [L]:[M] ratio for the cadmium(II)-quinolinate system.

Figure 7.11 SDD for the protonation of quinolinic acid: LH^-, LH_2 and LH_3^+ where log K_3 is -0.8 (solid green line) and where log K_3 is +0.8 (dashed green line).

Figure 7.12 ECFC and CCFC calculated using the MLH_2, MLH, ML and ML_2 complex for each [L]:[M] ratio for the cadmium(II)-quinolinate system.

Figure 7.13 Comparative SDD showing the variation in species distribution when the value of log K_3 is -0.8 (solid lines) or +0.8 (dashed lines), [L]:[M] = 100 where [Cd] = 1×10^{-4} M.

Figure 7.14 a) The start of crystal formation, and b) the formation of many more crystals within the following 26 hours. ([Cd] = 0.1 M, [QUIN]:[Cd] = 1)

Figure 7.15 The fine Cd(QUIN) (ML) crystals, that resembled dandelion seeds, as viewed under a microscope using polarized light.

Figure 7.16 The molecular structure of Cd(QUIN) with displacement ellipsoids drawn at the 50% probability level.

Figure 7.17 Distorted octahedral geometry of the cadmium(II) metal centre in Cd(QUIN).

Figure 7.18 Polymeric head-to-tail chains a) as viewed down the c-axis and b) down the b-axis. Hydrogen atoms omitted for clarity.

Figure 7.19 View down the a-axis showing a zigzag pattern. Hydrogen atoms omitted for simplicity.

Figure 7.20 Hydrogen bonded monomers forming the polymeric chain.

Figure 7.21 Intermolecular hydrogen bonding in Cd(QUIN).

Figure 7.22 Ball and stick representation of catena-((m3-Pyridine-2,3-dicarboxylato)-diaqua-cadmium) (REFCODE: PEPXOY) (Li et al., 2006b).

Figure 7.23 ORTEP diagram of the molecular structure of $Cd(QUIN\text{-}H)_3$. Displacement ellipsoids are drawn at the 50% probability level.

Figure 7.24 The unit cell of $Cd(QUIN\text{-}H)_3$ as viewed down the c-axis.

Figure 7.25 Packing diagram of $Cd(QUIN\text{-}H)_3$, as seen down the c-axis showing the hydrate down the channels of the hydrogen bonded cadmium complexes.

Figure 7.26 Diagram highlighting the hydrogen bonding shown in Figure 7.25. Hydrogen bonding between a) the hydrate and the tris complex ($Cd(QUIN\text{-}H)_3$) and b) two adjacent $Cd(QUIN\text{-}H)_3$ complexes.

Figure 7.27 Packing diagram as seen down the *c*-axis showing the hydrate down the channels of the hydrogen bonded manganese complexes (REFCODE: HAZSIK).

Figure 7.28 Packing diagram of $Cd(Pic\text{-}H)_3$ as seen down the c-axis showing the disordered nitrate ions down the channels of the hydrogen bonded cadmium complexes (Billing, Levendis and Vieira, 2011).

Figure 7.29 Tautomeric diagram illustrating the structure of the doubly protonated quinolinic acid crystals.

Figure 7.30 SDDs plotted under solution conditions from which crystals of the ML complex was formed: a) a [L]:[M] of 1, where [Cd] = 0.005 M and b) a [L]:[M] of 2:1, where [Cd] = 0.005 M. The pH of the solution is also indicated. (Log $\beta(ML_2H_2)$ = 8.6, log $\beta(MLH)$ = 6.6, log $\beta(ML)$ = 3.9 and log $\beta(ML_2)$ = 6.6 when log K_3 = -0.8.)

Figure 7.31 Partial SDD showing the different protonated forms of ligand available in solution using under the following conditions: a) [L]:[M] = 1 where [Cd] = 0.1 M and b) where [L]:[M] = 2 and [Cd] = 0.05 M.

Figure 7.32 ECFC and CCFC calculated using the $M(LH)_3$, ML and ML_2 complex for each [L]:[M] ratio for the cadmium(II)-quinolinate system.

Figure 7.33 Comparison of SDDs plotted at an [L]:[M] of 1 where [Cd] = 0.05 M (solid lines) and at an [L]:[M] of 20 where [Cd] = 1 x 10^{-4} M (dashed lines), using average formation constants of log $\beta(M(LH)_3)$ = 21.2, log $\beta(ML)$ = 3.7 and log $\beta(ML_2)$ = 6.7.

Figure 7.34 Suggested coordination mode for a MLH_2 crystal complex.

Figure 8.1 Schematic representation by Kragten, Decnop-Weever and Gründler (1993) which shows how the solution species and precipitates are formed from various equilibrium reactions taking place in solution. A symbolizes NO_3^- (or ClO_4^- or Cl^-).

Figure 8.2 SDD showing the possible bismuth(III) nitrate and hydroxide species found in solution when [NO_3^-] = 0.5 M and [Bi] = 5 x 10^{-5} M, using log β values given in Table 8.2 and 8.3.

Figure 8.3 SDDs plotted using the MLH, ML, ML_2, ML_3 and ML_3OH species model where [Bi] = 0.05 M. Solid lines represent [L]:[M] = 1:1,dashed lines represent [L]:[M] = 2:1 and dotted lines represent [L]:[M] = 3:1. All hydroxides have been omitted for clarity.

Figure 8.4 The coordination modes for Bi1 and Bi2 have been shown in a) and b), respectively, where the shaded region indicates the ligand which is common to both illustrations. The overall view of the structure is given in c).

Figure 8.5 Extended structure of the bismuth(III)-quinolinic acid complex generated using the program Schakal. The pink balls represent Bi1 and the large grey balls Bi2. Solvent molecules were omitted for clarity.

Figure 8.6 Packing diagram seen down the b-axis, created by an extensive hydrogen bond network, which forms clusters of molecules in the a-direction.

Figure 8.7 A view down the c-axis which shows the solvent molecules of water present in the structure.

Figure 8.8 Structural diagram showing the coordination of the bismuth(III) ion when complexed by picolinic acid, and the ring formation it forms (REFCODE: GERGOA).

Figure 8.9 Structural diagrams showing the complexity of lanthanum(III)-quinolinic acid complexes: a) CEXWEI, b) ILEJUF and c) NOCPUR.

Figure 9.1 Chemical structure of EDTA (ethylenediaminetetraacetic acid).

Figure 9.2 SDD showing the percentage distribution of the EDTA species that predominate in specific pH regions in aqueous solution at 25°C.

Figure 9.3 Structural diagram of HAYPEC (Summers, Abboud, Farrah and Palenik, 1994).

Figure 9.4 Polarograms showing negative shifts in Bi(III) reduction potential due to complex formation as pH is increased. (The small positive shift in the reduction potentials for Tl(I) is due to E_j.) [EDTA]:[Bi] = 100 at 25 °C.

Figure 9.5 An illustration of the log analysis plot from Ružić and Branica (1969). It should be noted that the log analyses described in the article by Ružić and Branica (1969) were done on theoretical polarograms and the procedure was not applied to experimental data as done in this work.

Figure 9.6 Comparison of the polarograms collected at pH 1.85 and 1.95, with the log plot drawn for that obtained at pH 1.95.

Figure 9.7 Log plot for the polarogram measured at pH 1.95 showing the tangents drawn using different data points, which were extrapolated to the x-axis to obtain E_k values.

Figure 9.8 Half-wave potential vs. pH plot for thallium(I) obtained for resolved waves. The red data point indicates the next point in the series according to calculation based on the log analysis.

Figure 9.9 The average magnitude of the diffusion junction potential.

Figure 9.10 SDD showing the possible bismuth(III) nitrate and hydroxide species found in solution when $[NO_3^-]$ = 0.5 M and [Bi] = 1 x 10^{-5} M, using log β values given in Table 8.2 and 8.3. (The protonation constant for nitric acid was set as -5.00).

Figure 9.11 Experimental bismuth data and where E_j has been compensated for. The free metal ion potential of bismuth was calculated in two ways: by considering complexation with hydroxides only and by considering complexation with hydroxides and nitrates.

Figure 9.12 Overlap of the three polarograms that were collected manually at the start of EXP 1. The inset shows the average $E_{½}$ value for these three polarograms that were obtained at pH 0.297.

Figure 9.13 Calculation of ΔE_{OH} and ΔE_{OH+NO3} as the differences between $E_{½}$ and $E(Bi_{free})_T$ and $E(Bi_{free})_{OH}$, respectively.

Figure 9.14 The quadratic function obtained when fitting the half-wave potential vs. pH data up until pH 1.3 for EXP 1.

Figure 9.15 The δ value as a function of pH for Bi(III) during a ligand experiment where [L]:[M] = 100.

Figure 9.16 Comparison of the experimental polarogram (where δ = 0.988) and the polarograms fitted by forcing δ to 0.4. The blue crosses represent the points that were removed when fixing δ to 0.4.

Figure 9.17 Half-wave potential for Bi(III) where δ is fixed at 0.4 throughout the pH range, together with the compensation of E_j.

Figure 9.18 Graph showing the calculation of the free bismuth potentials using the difference models determined in Table 9.4.

Figure 9.19 Comparison of CCFCs obtained using $E(Bi_{free})_T$ and the MLH and ML species set (purple) and the MLH, ML and ML_2 species set (red). The log β values for the MLH and ML species set (Table 9.6) did not refine.

Figure 9.20 Slope analysis performed on the ECFC.

Figure 9.21 Polarograms showing the effect of varying a) the standard heterogonous rate constant and b) the timescale of a measurement on the degree of reversibility of the process. This figure has been reproduced from Gileadi (2011).

Figure 9.22 ORTEP diagram showing the structure of Bi(EDTA-H) at the 50% probability level. Labels of hydrogen atoms have been omitted for clarity.

Figure 9.23 Polymerization occurring in two directions (b and c), as seen down the a-axis.

Figure 9.24 Water molecules responsible for linking polymerized chains together by hydrogen bonding in the a-direction, as seen down the b-axis. Hydrogen atoms have been omitted for clarity.

Figure 9.25 SDD was plotted using the MLH and ML species set with log β values of 26.58 and 25.68, respectively. Solid lines represent [L]:[M] = 100 and [Bi] = 5 x 10^{-3} M (polarographic solution conditions) and dotted lines represent [L]:[M] = 1 and [Bi] = 0.1 M (crystal growth conditions). Bismuth(III) hydroxide species have been omitted for clarity.

Figure 10.1 Doubly protonated pyrazinecarboxylic acid complex (REFCODE: NIBLUG).

Figure 10.2 Coordination modes of the pyrazinecarboxylic acid ligands around the bismuth(III) centre. (The water molecule was omitted for simplicity.)

Figure 10.3 The magnitude of the diffusion junction potential as a function of pH.

Figure 10.4 Illustration showing the experimental data (green) for bismuth(III) which is compensated for the shifts by E_j (orange) and complex formation with hydroxides (blue) and nitrates + hydroxides (purple).

Figure 10.5 Calculation of the difference values ΔE_{OH} and ΔE_{OH+NO3} for EXP 3.

Figure 10.6 Polarograms collected at increasing pH showing the movement in the reduction potential of the ligand, where [L]:[M] = 49. (Note that the current of the polarogram at pH 0.330 is saturated at 25 µA.)

Figure 10.7 ECFC for each [L]:[M] ratio with its corresponding CCFC obtained using the ML species and $E(Bi_{free})_{OH}$.

Figure 10.8 The current of bismuth for each complexation experiment which shows the point where precipitation occurs.

Figure 10.9 Overlapping polarograms recorded before (pink lines) and after (blue lines) the ligand was added to the complexation experiment, where a) [L]:[M] = 100, b) [L]:[M] = 49 and c) [L]:[M] = 77.

Figure 10.10 Comparison of the ligand-free and corresponding complexation experiment for a) [L]:[M] = 100, b) [L]:[M] = 49 and c) [L]:[M] = 77. (The actual value of the half-wave potential is meaningless because some of the data was manipulated to obtain an overlay of the initial points.)

Figure 10.11 ECFC and CCFC calculated using MLH, ML and ML_2 species model at each [L]:[M] ratio.

Figure 10.12 ECFC and CCFC calculated using MLH, ML and MLOH species model at each [L]:[M] ratio.

Figure 10.13 Plot showing how the free metal ion potentials ($E(Bi_{free})_{OH}$ and $E(Bi_{free})_T$) (a) are affected by the changing distribution of nitrate and hydroxide species that vary with pH (b) in solution.

Figure 10.14 ECFC and CCFC for each [L]:[M] ratio showing the pH region where the MLH species affects the CCFC.

Figure 10.15 Comparative SDDs showing the pH region where MLOH and ML_2 would exist if they were present in solution. Average log β values of 6.6, 5.3 and 16.86 were used for MLH, ML and MLOH, respectively, (solid lines), and 6.6, 5.0 and 9.6 were used for MLH, ML and ML_2, respectively, (dashed lines), both plotted at [L]:[M] = 100. Hydroxide species have been omitted for clarity.

Figure 10.16 Slope analysis performed on the ECFC for [L]:[M] = 100.

Figure 10.17 Thallium(I) half-wave potential vs. pH data fitted with a polynomial using the same data points that were used in measuring the diffusion junction potential (EXP 1).

Figure 10.18 Compensation of E_j and calculation of the $E(Bi_{free})$ values obtained using the model for the [L]:[M] = 100 dataset.

Appendix

Figure A5.1 Monomeric unit making up the polymers of GIZKEG, WARYEU and WARYEU01.

Figure A5.2 Comparison of a normal polarogram with one that is noisy and cannot be used.

Figure A5.3 ECFC and CCFC for [L]:[M] = 21 and 52 (at 25 °C), fitted with the MLH, ML, ML_2 and ML_3 model.

Figure A5.4 Comparison showing the closeness of the raw and fitted half-wave potentials for thallium(I) and cadmium(II) of EXP 3.

Figure A5.5 ECFC and CCFC fitted using the MLH, ML, ML_2 and ML_3 species model, for each [L]:[M] dataset at 32 °C.

Figure A5.6 ECFC and CCFC fitted using the MLH, ML, and ML_2 species model, for each [L]:[M] dataset at 32 °C.

Figure A5.7 Comparison of the CCFC fitted using the MLH, ML, and ML_2 and MLH, ML, ML_2 and ML_3 species models, for the [L]:[M] = 20 dataset at 32 °C.

Figure A5.8 Comparison of glass electrode calibration curves at 25, 32 and 40 °C.

Figure A8.1 Comparison of SDDs plotted using species set 1 (MLH, ML, ML2 and ML2OH) (solid lines) and species set 2 (MLH, ML, ML2, ML3 and ML3OH) (dashed lines), where [L]:[M] = 1:1 and [Bi] = 0.05 M. All hydroxides have been omitted for clarity. Refer to Table 8.4, E(Bifree)T, for log β values.

Figure A9.1 Structural diagram of FAFSAH from the CSD (Allen, 2002).

List of Tables

Table 1.1 Ratio of the substituents of the most abundant mercury(II) species in solution, together with their formation constants and maximum percentage distribution with its corresponding pH (25 °C and 0.1 M ionic strength). (Moghimi *et al.*, 2004).

Table 2.1 Metrohm glass electrode (Ecotrode) specifications.

Table 2.2 Parameters used for the automated collection of polarograms as a function of pH.

Table 2.3 Metrohm LL Biotrode specifications

Table 2.4 Summary of the experimental details for obtaining crystalline Cd(II) and Bi(III) complexes.

Table 3.1 Limiting ionic mobility for some important ions (Harris, 1995).

Table 3.2 Functions corresponding to each of the Compensation models.

Table 3.3 The standard deviation of the fit calculated for models P(I), C(I), P(II) and C(II).

Table 3.4 Results for the student's t-test comparing points and curves models used on two separate experiments.

Table 3.5 Comparison of ionic mobilities at infinite dilution and those calculated at the given ionic strengths using the Onsager limiting law. The actual E_j was calculated using the Henderson equation.

Table 4.1 Coordination modes of picolinic acid with various metals, M, as found in literature.

Table 4.2 Summary of the formation constants for the cadmium(II)-picolinate system that are published in literature.

Table 4.3 Effects on the SDD when changing the solution conditions as given in Figure 4.5.

Table 4.4 Crystal data and structure refinement for CdPIC-H and $Cd(PIC\text{-}H)_3$.

Table 4.5 Selected bond lengths (Å) and angles (°) for Cd(PIC-H).

Table 4.6 Selected bond lengths (Å) and angles (°) for $Cd(PIC\text{-}H)_3$.

Table 4.7 The change in percentage distribution at pH 0.4 of the MLH species as the concentration of the solution increases and [L]:[M] = 1:1.

Table 5.1 Formation constants for cadmium-dipicolinic acid as quoted by literature.

Table 5.2 Information required for solving formation constants for the Cd(II)-Dipicolinic acid system, using 3D-CFC (Cukrowski, 2000).

Table 5.3 Possible reduction reactions in the given pH regions with their respective calculated slopes.

Table 5.4 Formation constants obtained for the [L]:[M] = 21 system using two different models for the calculation of the CCFC.

Table 5.5 Formation constants determined for each [DIPIC]:[Cd] ratio at 25 °C using the MLH, ML and ML_2 model.

Table 5.6 Formation constants used in calculating the CCFC for [L]:[M] = 21 and 52 using the MLH, ML, ML_2 and ML_3 model.

Table 5.7 Enthalpy and protonation constants for dipicolinic acid at 25 °C (Martell, Smith and Motekaitis, 2004) and protonation constants calculated at 32 and 40 °C using the van't Hoff equation.

Table 5.8 Some adjusted cadmium(II)hydroxide stability complexes at 32 and 40 °C using the van't Hoff equation.

Table 5.9 Formation constants obtained for each [L]:[M] ratio at 32 °C incorporating MLH, ML and ML2 in the species model.

Table 5.10 Formation constants obtained for each [L]:[M] ratio at 32 °C incorporating MLH, ML, ML_2 and ML_3 in the species model.

Table 5.11 The average difference in half-wave potentials for thallium(I) and cadmium(II) above pH 2 ($\Delta E_{C>pH}$) for each temperature.

Table 5.12 Free metal ion potentials for thallium(I) and cadmium(II) for each ligand-free experiment. The average $\pm$ the standard deviation is shown in italics due to the large uncertainty associated with these values.

Table 5.13 Formation constants obtained for each [L]:[M] ratio at 40 °C using the species model containing an MLH, ML and ML_2 species.

Table 5.14 Formation constants for each [DIPIC]:[Cd] ratio using the species model containing MLH, ML, ML_2 and ML_3.

Table 5.15 Average formation constants calculated by excluding and including the ML_3 complex at each temperature.

Table 5.16 Approximate values for the enthalpy associated with each complexation reaction.

Table 5.17 Maximum percentage distribution of species at respective pH or pH ranges, corresponding to the SDDs plotted in Figure 5.38.

Table 6.1 Coordination modes of dipicolinic acid (Park *et al.*, 2007) which depend on the protonated form of the ligand.

Table 6.2 Unit cell data for the salt, obtained by SCXRD.

Table 6.3 Crystal data and structure refinement for hexa-aqua-bis(μ_2-pyridine-2,6-dicarboxylato-N,O,O,O')-di-cadmium(II) bis(pyridine-2,6-dicarboxylic acid).

Table 6.4 Comparison of the crystallographic data for the Cd(II)-dipicolinic acid crystal, $Cd_2DIPIC_2 \cdot DIPIC\text{-}H_2$, from this work and that of Odoko, Kusano and Okabe (2002).

Table 6.5 Comparison of the crystal data found in this work and that for KNO_3 found in the ICSD.

Table 7.1 Coordination modes of quinolinic acid with various metal ions, M, as found in literature.

Table 7.2 Reduction reactions with their respective calculated slopes given for possible species in solution.

Table 7.3 Formation constants for each [QUIN]:[Cd] ratio using MLH, ML and ML_2 complexes in the model.

Table 7.4 Log K_3 values for quinolinic acid and its isomers as found in literature (at 25 °C).

Table 7.5 Formation constants for each [QUIN]:[Cd] ratio using the MLH_2, MLH, ML and ML_2 complex model and log $K_3 = -0.8$

Table 7.6 Average formation constants for the [QUIN]:[Cd] = 21, 101 and 196 data using the MLH_2, MLH, ML and ML_2 complex model.

Table 7.7 Crystals produced using Cd(II) and quinolinic acid and their associated experimental conditions.

Table 7.8 Crystal data and structure refinement for Cd(QUIN) and Cd(QUIN-H)$_3$.

Table 7.9 Selected bond lengths [Å] and angles [°] for Cd(QUIN).

Table 7.10 Comparison of our ML crystal characteristics with that by Aghabozorg *et al*. (2008).

Table 7.11 Selected bond lengths [Å] and angles [°] for Cd(QUIN-H)$_3$.

Table 7.12 Comparison of Cd(QUIN-H)$_3$ with two isormorphous structures and a similar picolinate complex (Cd(Pic-H)$_3$).

Table 7.13 Comparison of the formation constants of picolinic acid, dipicolinic acid and quinolinic acid at 25 °C and ionic strength 0.5 – 0.25 M.

Table 8.1 Comparison of number of crystal structures for various metal ions.

Table 8.2 The overall stability constants for bismuth hydroxide species at 25 °C.

Table 8.3 The overall stability constants for bismuth nitrate species at 25 °C as given by the NIST database (Martell, Smith and Motekaitis, 2004).

Table 8.4 Average log β values calculated by Billing (2012) using $E(Bi_{free})_T$ and $E(Bi_{free})_{OH}$.

Table 8.5 Experimental conditions used when trying to grow specific bismuth(III)-quinolinic acid species in an initial solution volume of 20 mL.

Table 8.6 Crystallographic data for the bismuth(III)-quinolinate structure.

Table 9.1 Formation constants for Bi-EDTA complexes from literature.

Table 9.2 Crystal data and structure refinement for Bi(EDTA-H).

Table 9.3 The differences between the free metal ion potentials and the average half-wave potential of Bi(III) from the initial polarograms.

Table 9.4 The calculated $E_{½}$ values at pH 0.345, together with the differences calculated between $E_{½}$ and the free metal ion potentials for each ligand-free experiment. The E_j = 32.5 mV at pH 0.345, according to the quadratic function in Figure 9.9.

Table 9.5 Protonation constants of EDTA at 25 °C.

Table 9.6 Formation constants for the bismuth(III)-EDTA system when using species set 1 (MLH and ML) and species set 2 (MLH, ML and ML_2) and $E(Bi_{free})_T$. Refinement on species set 1 was not possible thus standard deviations cannot be quoted.

Table 9.7 Possible reduction reactions in the given pH regions with their respective calculated slopes.

Table 9.8 Comparison of the Bi(EDTA-H) crystal $(C_{10}H_{13}N_2O_8Bi)_n,2(H_2O)_n$ from this work and that grown by Summers, Abboud, Farrah and Palenik (1994). An antimony analogue (SBEDTA10) has been included for comparison.

Table 10.1 Coordination modes of pyrazinecarboxylic acid with various metals (M), which depend on the extent of protonation of the ligand.

Table 10.2 Protonation constants for pyrazinecarboxylic acid as quoted by the NIST database (Martell, Smith and Motekaitis, 2004).

Table 10.3 Differences calculated using Approach 1

Table 10.4 Values for $E(Bi_{free})$ calculated using Approach 1.

Table 10.5 Formation constants calculated using Approach 1 and $E(Bi_{free})_{OH}$.

Table 10.6 Formation constants calculated using Approach 1 and $E(Bi_{free})_T$ for the MLH, ML and ML_2 species model.

Table 10.7 Formation constants calculated using Approach 1 and $E(Bi_{free})_T$ for the MLH, ML and MLOH species model.

Table 10.8 Possible reduction reactions in the given pH regions with their respective calculated slopes.

Table 10.9 The equation fitted to thallium(I) data in the ligand-free experiments which was used to obtain the $E_{½}$ value for thallium(I) at the initial pH for the corresponding complexation experiment.

Table 10.10 Differences calculated between the $E_{½}$ and $E(Bi_{free})$ values for thallium(I), for each ligand-free experiment.

Table 10.11 Calculated values for the $E(Bi_{free})$ values using background thallium data as the reference point.

Table 10.12 Formation constants calculated using Approach 2 and $E(Bi_{free})_T$.

Table 10.13 Summary of the difference models obtained from ligand-free experiments for Approach 1 and 2.

Table 10.14 Summary of the data $E(Bi_{free})$ values determined for complexation experiments.

Table 10.15 Formation constants calculated using Approach 3 and $E(Bi_{free})_T$.

Appendix

Table A2.1 Reagents used for experimentation

Table A2.2 Parameters for standardizing KOH and HNO_3 using the autotitrator

Table A2.3 Parameters used for the calibration of the glass electrode.

Table A2.4 Parameters and their settings used when manually collecting a polarogram.

Table A3.1 Data table for students t-test.

Table A5.1 Standard redox potentials of the silver/silver chloride reference electrode ([KCl] = 3 mol/L) as a function of the temperature and concentration (Metrosensor electrodes, 2012).

Table A5.2 Table highlighting the variation in pH (x-intercept) and potential (y-intercept) of the glass electrode calibration curves at 25, 32 and 40 °C.

Table A5.3 Formation constants and their respective standard deviations for the cadmium(II) dipicolinate system at 32 °C.

Table A5.4 Formation constants and their respective standard deviations for the cadmium(II) dipicolinate system at 32 °C.

TableA5.5 Formation constants and their respective standard deviations for the [L]:[M] = 20 ratio at 32 °C.

Table A7.1 Summary of the data obtained when incorporating the third protonation constant (0.8) and then calculating the CCFC with the following four species: MLH_2, MLH, ML and ML_2.

Table A9.1 Experimental conditions used for solving formation constants of the Bi(III)-EDTA system using the 3DCFC program.

Table B13.1 Alphabetized REFCODES of the CSD (Allen, 2002) with corresponding references.

List of Abbreviations

AC	Alternating current
Adj	adjustment
CE	counter electrode
CSD	Cambridge Structural Database
DC	Direct current
DCP	direct current polarography
DIPIC	dipicolinic acid
ECFC	experimental complex formation curve
EDTA	ethylenediaminetetraacetic acid
GE	glass electrode
GEP	glass electrode potentiometry
IR	Infra-red
ISE	ion selective electrode
IUPAC	International Union of Pure and Applied Chemistry
MOF	molecular organic framework
NIST	National Institute of Standards and Technology
PIC	picolinic acid
Polarog	polarography
PXRD	powder x-ray diffraction
QUIN	quinolinic acid
RE	reference electrode
Recryst.	recrystallization
REFCODE	reference code (CSD)
SCXRD	single crystal x-ray diffraction
SDD	species distribution diagram
Std Dev	standard deviation
T	temperature
Vol	volume
Voltam	voltammetry
VP	virtual potentiometry
XRD	x-ray diffraction

List of Symbols

a	activity
c	concentration
D	diffusion coefficient
E	potential
$E\ 1/2$	half-wave potential
$E(M_{free})$	free metal ion potential
E°	standard potential
E_j	diffusion junction potential
F	Faradays constant
γ	activity coefficient
$\imath$	current
i_d	diffusion limited current
k	wave 1 or wave 2
K	stepwise stability constants
Kw	autoprotolysis constant for water
λ°	conductivity
m	inflection point
n	number of electrons transferred
pH	-log[H+]
R	Gas constant
T	temperature
u	ionic mobility
u°	limiting ionic mobility
z	charge
β	overall stability constant
δ	slope of the DC wave
ΔE	potential difference
$\Delta E_{C > pH\ 2}$	potential difference above pH 2
λ	ionic conductivity
μ	ionic strength

Chapter One

Introduction

1.1 LITERATURE REVIEW

"Crystal structures are in a sense misleading … thus, without the stability constants, our understanding of the chemistry of a metal ion with any particular ligand must be regarded as incomplete"

(Martell and Hancock, 1996)

This quote encapsulates the essence of why this research is relevant – both solution and structural studies have been utilized to create a strong understanding of metal-ligand complexation. The crux of this project was to study a possible link between solution species and crystalline complexes at specific and controlled experimental conditions. In doing so it was noted that in some cases the results from solution experiments allowed for the elucidation of crystal complexes that had not before been found, and at other times it was the crystalline complexes that supported species found in solution or assisted in identifying minor solution species. As we delve into the various chapters which look at different metal-ligand systems we explore the possibility of a relationship between the two phases and discuss the viability of creating such a comparison.

1.1.1 Meet the Metal Ions of Interest

Metal ions form complexes with naturally and anthropogenically occurring complexing agents. The metal complexes are thus mobilized and transported in both environmental and biological systems. The impact of such metal complexes depends on the kinetic and/or thermodynamic stability in these systems (Fernando, 1995). It is therefore clearly of great importance to be able to distinguish between the individual species present in a particular sample. The metal ions used for investigation are cadmium(II) and bismuth(III) due to the impact they have on society.

Cadmium(II) is a toxic heavy metal that has dire environmental consequences and is carcinogenic in humans and animals at relatively low levels. Humans and animals are poisoned by cadmium through inhalation of contaminated dusts, aerosols and cigarette smoke, as well as through ingestion of contaminated food and water (Misra *et al.*, 1998). For many years now it has been known that cadmium leaching from particular items (pigmented plastic bags for example) in landfills can lead to contamination of soil and water in surrounding areas thus having adverse health effects on inhabitants (Wilson, Young, Hudson and Baldwin, 1982). Environmental concentrations of cadmium are of grave concern because cadmium accumulates in the human body, throughout life, where a large portion of it remains stored in the kidneys and the liver (Blood and Grant, 1975).

In contrast bismuth is extremely beneficial and has many applications in the medicinal field; since the 1970s bismuth salts have been used in combating *Helicobacter pyloris* (Ford *et al.*, 2008), a gut colonizing bacteria (Chaturvedi *et al.*, 2001). Bismuth compounds are most commonly used to treat gastrointestinal disorders, for example gastric ulcers (Sun *et al.*, 1999) which are caused by *Helicobacter pyloris*. Bismuth subsalicylate, an antidiarrheal agent, is useful as it shortens the duration and severity of diarrhea and is also safe for use in children

older than 3 years (Stauffer, Christenson and Fischer, 2008). Bismuth in medication has, since the 17th century (Tobon-Zapata, Etcheverry and Baran, 1997), and up until today, function to alleviate many different disorders. To date it has been found useful in the treatment of tumors, eye infections, syphilis, heartburn, radio-isotope therapies, and in the reduction of the renal toxicity of cisplatin (in cancer patients) (Briand and Burford, 1999). Bismuth subnitrate ($Bi_5O(OH)_9(N0_3)_4$) was probably one of the first compounds to be utilized as an x-ray contrast agent for human patients, where bismuth is the element having the contrast-enhancing ability (Yu and Watson, 1999). It was found that large doses of bismuth subnitrate were proving to be poisonous and so it is now only used in dental filling composites and intravascular catheters, for the same application (Yu and Watson, 1999). Also, bismuth trioxide has been incorporated into Teflon in order to produce radio-opaque catheters (Sherken and Friedman, 1973). Bismuth subcarbonate ($Bi_2O_2(CO_3)$) is excellent as a protector of the ulcer cavity as it is oily in nature and does not absorb hydrochloric acid or pepsin (Ehrmann, 1945). This fascinating element has many more applications but, surprisingly, its chemistry is not well documented. We therefore have undertaken the task to create more of a knowledge-base for bismuth and to improve our understanding of its complex forming abilities.

1.1.2 Solution Studies

Identification and stability of species in solution was accomplished using an electrochemical technique namely sampled direct current polarography (DCP). pH titrations were implemented in order to obtain reliable results starting at very low pH values (well below pH 2). The experimental procedure employed collects data via a combination of successive pH measurements as well as current vs. potential recordings. This method is preferred to the more familiar glass electrode potentiometry (GEP) because GEP acquires results solely on the basis of pH measurements in the cell. This technique fails to produce reliable data when used in

the very low pH range (Cukrowski and Loader, 1998), the region we are interested in exploring. Bismuth is particularly difficult to study and can only be studied if one starts at an extremely low pH (< 2). The reason for this is that weakly acidic (to basic) conditions cause bismuth salts to become hydrolyzed (Briand and Burford, 1999), thus impacting on the solubility of the species in solution.

1.1.2.1 The Polarography Technique and its Associated Pitfalls

Polarography uses a dropping mercury electrode for the measurement of polarization curves which occur due to the response obtained by diffusive mass transport. Polarographic curves are potential-current plots that depict the dependence of the current passing through the system on the voltage applied to the electrodes. The potential at which the current reaches half of the total wave height is referred to as the half-wave potential ($E_{½}$). The half-wave potential for a particular reversible redox process is constant and independent of concentration. The total height that the wave reaches is representative of the diffusion limited current which signifies the concentration of the analyte solution.

Quantitative analytical measurements obtained via polarography are limited by a number of factors. One of these arises due to the fact that mercury is oxidized at potentials more positive than about +0.2 V versus the standard calomel electrode (SCE), which makes analysis impossible in the positive potential region (Kounaves, 1997). Another limitation arises due to the fact that the current is being measured continuously. Current due to capacitance (charging current) decreases rapidly in the life time of the mercury drop, but as the drop grows gradually in size, the surface area increases and so there is an increase in the faradaic current during the drop life. A change in capacitance and faradaic current, as the size of the drop varies, causes the measure of current to be unreliable. These changing current effects combined with experiments where the potential is continuously changed can result in extremely noisy traces.

Charging current, due to the formation of the double layer at the working electrode interface, cannot be easily predicted as it is not directly related to any change that is easily measured or accounted for. Due to this difficulty Sampled DCP (also called DC_{TAST}) is the chosen method for experimentation. The current measurement is sampled for a short time near the end of the drop's lifetime because charging current is at a minimum and faradaic current at a maximum, at the end of the potential step (Harris, 1995). The rate of change of current is also the smallest when the drop is the largest, just before it falls from the capillary tip.

Over and above this, another major difficulty faced by most electrochemical measurements is the formation of a diffusion junction potential (E_j) at the interface between the sample solution and the salt bridge solution in which the reference electrode is placed (if no salt bridge was present the difference would between the sample solution and the filling solution of the reference electrode). A diffusion junction potential is set up when two dissimilar solutions are placed in contact with each other. The ions contained in the solutions move across the interface at differing velocities which leads to the unequal distribution of charge on either side of the interface. If one solution is highly acidic, this phenomenon is more pronounced because of the large concentration of fast moving H^+ ions that are present. The problem is that the magnitude of the overall measured potential is a combination of the applied potential and the diffusion junction potential, and they cannot be isolated from each other. Since this issue cannot be rectified or avoided, a witness ion was introduced into the solution and functions by providing information indirectly about the magnitude of the diffusion junction potential. It is most accurate if this measurement is done in-situ for each experiment because the diffusion junction potential has been known to vary slightly with each new experiment (Billing, Cukrowski and Jordan, 2013). The magnitude of the diffusion junction potential in the extreme pH regions (at very low and very high pH) is

greatest and changes significantly with variations in pH, while at more intermediate pH values it is largely pH independent.

Taking all of these aspects into account has allowed for the system to be tweaked in order for the process to yield optimal results. Introduction of the in-situ witness ion, together with the timing of current measurements, reduces experimental error as far as possible. Technique specific issues, as well as the use of varying scientific methods of experimentation produce experimental results which could differ from each other, and are dependent on the scientist and the technique implemented. Cukrowski and Loader (1998) highlight the fact that the literature offers quite a spread of values when it comes to stability constants of cadmium-picolinic acid complexes, for example. A literature survey on the cadmium-dipicolinic acid system also proved that the formation constant values were in a fairly broad range. This has led to the questioning of the reliability of polarographic techniques of speciation that have been used in the past.

Polarographic experiments have been conducted over a number of years using the ligand titration method where the ligand is required in large concentrations so that it's concentration at the electrode surface is essentially equal to that in the bulk solution (Cukrowski, 1996). All measurements need to be taken at constant ionic strength and so the background electrolyte is in excess (approximately 100 times that of the ligand concentration), so that as the species in solution vary the ionic strength remains essentially constant. More than half a century ago Lingane (1941) presented an equation that described the shift of a half-wave potential as a function of excess ligand, but only a single predominant complex in solution could be considered at a time. DeFord and Hume (1951) then improved on this equation which allowed for the calculation of formation constants for metal-ligand systems where several complexes formed in a stepwise manner. However, it became evident that this only applied to simple ligands. Also, the degree of uncertainty of

the formation constant values increased as each successive one was being solved for. These theories were improved upon, where potentially the ligand concentration could be minimized, both ligand and pH titrations could be performed, and more than one competing species in solution could be identified (Cukrowski, 1996). Minimizing the ligand concentration aids solubility of the ligand as well as its complexes, and it also serves to reduce the amount of chemical usage and therefore benefit the environment. Also, in the case where the ligand is synthesized, obtaining large amounts is often extremely difficult. In glass electrode potentiometry (GEP) large concentrations of ligand are used generally so that pH changes can be determined as accurately as possible. New theories for the analysis of polarographic data were developed in speciation studies of both labile and non-labile systems, where the ligand was not needed in such high concentrations. Reducing the amount of ligand was possible because the entire process was not only dependent on pH measurement; thus mass-balance calculations not only involving the H^+ ion concentrations (as in GEP) were performed, but also included the mass balances for both total metal ion and ligand concentrations. Both labile and non-labile systems were successfully studied by Cukrowski (1996) using differential pulse polarography (DPP) provided that each species was a major species in solution (Cukrowski, 1996).

Further steps were then taken to devise an analysis technique specific to non-labile systems. Non-labile species require larger amounts of energy (in comparison to labile species) to reduce the metal centre and so the reduction signal is formed at significantly more negative potentials than that of the free metal ion. A method proposed by Cukrowski, Hancock and Luckay (1996) relies on the computation of mass-balance equations that describe the formation constant for the non-labile complex that is formed in solution. For both labile and non-labile systems a method was then deciphered where the ligand to metal ratio was kept constant, and the pH was varied. This is commonly referred to as a pH titration, which differs significantly

from a ligand titration. (Ligand titration involves the maintenance of a constant pH while the ligand concentration is increased.) This approach will be used in the following study where we ultimately sought to determine formation constants of complexes formed with Cd(II) or Bi(III) and specified ligands. These formation constants can be used to plot species distribution diagrams (SDDs), which indicate the percentage of each species present in solution at different pH values

1.1.3 Crystallographic studies

From searches of the literature and the Cambridge Structural Database (CSD) (Allen, 2002) it is apparent that not much research has been conducted on crystal-forming systems where the authors specifically tried to grow crystals of targeted species, especially in only aqueous media. Very often organic solvents were incorporated into the crystallization technique. Also, in depth studies on the effect of complex formation due to the control of pH during crystal formation have not been conducted.

Crystal structures of different metal complexes could indicate how the conditions used to grow the crystal influenced the structure and stoichiometry of the complex formed, and therefore allow for comparison of data obtained in solution.

1.1.3.1 Single-crystal X-ray Diffraction (SCXRD)

X-ray diffraction is a modern, almost routine , non-destructive technique used in the analysis of a wide variety of crystallographic samples for the determination of the location of all the atoms within the molecule. It is a standard technique for determining crystal structures by the integration of intensities of diffraction peaks for constructing the electron density map within the unit cell in the crystal. The reconstruction is achieved by Fourier transformations of the diffraction intensities with the appropriate phase assignment. Redundancy in diffraction data (all possible reflections are measured multiple times) is necessary to ensure reduced systematic

and statistical error. High intensity molybdenum radiation is used as it allows the data collection time to be somewhat minimized compared to when other x-ray sources are applied. Molybdenum radiation is generally used for structures containing metal ions because of its great penetrating ability as well as it having a low absorption coefficient. (Rogers, 1996).

X-rays are electromagnetic radiation with wavelengths of the order of 10^{-10} m (Atkins and de Paula, 2006). X-ray photons collide with electrons in atoms and some of these photons from the incident beam are deflected away from the original direction of travel. The scattered x-rays are measured and depending on their wavelength we learn of the process that has taken place. X-rays with unchanged wavelengths indicate an elastic scattering process and x-rays with wavelengths different to that of the incident beam are characteristic of inelastic scattering processes. Inelastic scattering occurs when x-rays collide with electrons and transfer some of their energy to the electrons. Diffracted waves from different atoms can interfere with each other constructively to create the resultant intensity distribution which provides information about the electron distribution in the material being studied (Clark and Dutrow, 2009a). In the case of a crystal where the atoms are arranged periodically the waves will consist of sharp interference maxima with the same symmetry as in the distribution of atoms.

The determination of the arrangement of atoms in the unit cell is accomplished by analysis of the relative intensities of all unique reflections in the diffraction pattern. Once the entire molecular structure has been solved, the approximate positions of the atoms are refined to give the best fit between the calculated and observed intensity data for the specimen. The refinement process produces accurate values for atomic positions which then allows for good calculation of bond lengths and angles. (Hammond, 2001)

1.1.3.2 Powder X-ray Diffraction (PXRD)

Powder x-ray diffraction is an analytical technique used for phase identification of a crystalline material that has been finely ground. The crystalline substance acts as a three-dimensional diffraction grating for x-ray wavelengths similar to the spacing of planes in a crystal lattice. The diffracted x-rays are continually recorded as the sample and detector rotate through their respective angles. Intensity maximizes when the mineral contains lattice planes with d-spacings that are appropriate in diffracting x-rays at that particular value of theta (θ). The d-spacing of each peak is then obtained by calculation of the wavelength (λ) in the Bragg equation ($\lambda = 2d \sin \theta$). Complete determination of the unknown materials d-spacings will then allow for a comparison of d-spacings of known materials because each mineral or molecular solid has a specific set of d-spacings unique to it only, just like a fingerprint. (Clark and Dutrow, 2009b). The Inorganic Crystal Structure Database (ICSD) (Belsky, Hellenbrandt, Karen and Luksch, 2002) is a powder diffraction pattern database which houses each determined material's "fingerprint", which makes for easy and automated comparisons with your determined "fingerprint". This method is used as a tool in deciding whether the material is a novel complex or a mixture containing various complexes. The experimental PXRD pattern can also be compared with the PXRD pattern calculated from the single-crystal data, if the crystal structure is known.

1.1.4 The Link between Solution Species and Crystalline Complexes

Some work has been conducted on the comparisons between solution and solid state species on proteins (Deisenhofer (1981) Williams, Clayden, Moore and Williams (1985) Heidorn and Trewhella (1988), Berndt, Güntert, Orbons and Wüthrich (1992), and Gouda *et al.* (1992)), but not much was found pertaining to metal-ligand complexes in this respect. Comparative solution-solid state studies

have been found in literature involving charge transfer complexes. This work is possibly most similar to that which was done in this thesis. Aghabozhorg and his co-authors (Moghimi *et al.*, 2002, Moghimi *et al.*, 2004, Aghabozorg *et al.*, 2009) made comparisons between single crystal complexes and solution species that were identified using potentiometry and in some cases absorbance spectrometry and spectroscopic techniques (IR, FT-IR, MS, and solid phase NMR ^{13}C). In each case the main conclusion between the two states was a simple similarity between the stoichiometry of the species in both states, and in some instances the crystal structure correlated to one of the species that was relatively dominant in solution. An example of their work is discussed here.

Moghimi *et al.* (2002) synthesized a proton transfer compound (pyda·H_2)(pydc) (where pyda is 2,6-pyridinediamine and pydc·H_2 is dipicolinic acid) as a yellow powder from a solution of pyridinediamine and dipicolinic acid in the presence of triethylamine in tetrahydrofuran. The structure, in Figure 1.1, of the resulting compound shows that the there was a proton transfer from the diacid to the diamine. The self-assembled unit was then studied spectrophotometrically in aqueous solution, and the electronic spectra of pydc·H_2 and pyda as well as the adduct (pydc)(pyda·H_2) are given in Figure 1.2. The shift that is seen for pyda, from 304.8 nm to 328.2 nm, is a consequence of the same proton transfer that was witnessed in forming the product of the yellow powder. When titrating pydc with pyda, it was found that when the mole ratio of pydc:pyda was 1:1 the absorbance didn't change, evidence that the product being formed had a 1:1 ratio. The formation of this 1:1 product was then further confirmed when a well-defined isosbestic point was obtained from a pH-dependent study of the diamine spectra. This study also showed that the (pydc)(pyda·H_2) adduct is stable in acidic media (pH 4.74 – 4.96) (with log K = 5.65 ± 0.13) and completely dissociates to pydc·H_2 and pyda from pH 9. Unfortunately the authors did not mention the pH at which the crystals were formed.

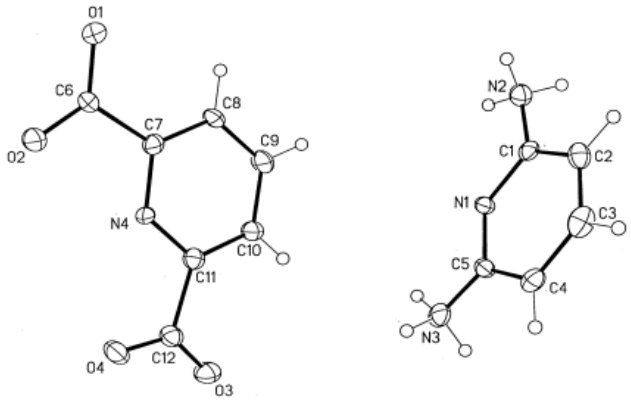


Figure 1.1 Crystal structure of the self-assembled adduct ((pydc)(pyda.H_2)) from Moghimi *et al.* (2002).

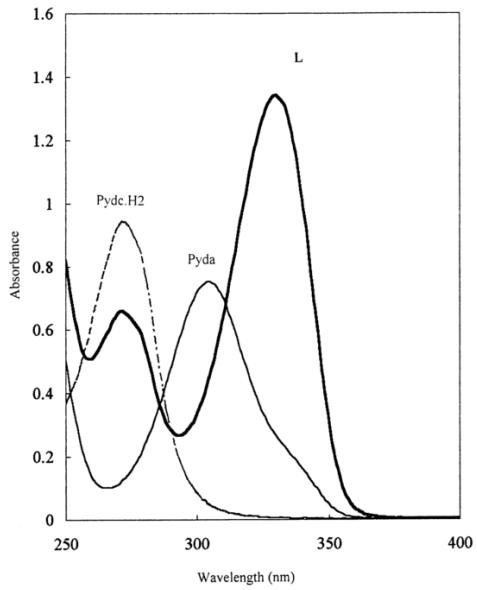


Figure 1.2 The electronic spectra of pydc·H_2, pyda and (pydc)(pyda·H_2) obtained spectrophotometrically, from Moghimi *et al.* (2002).

In a separate paper Moghimi *et al.* (2004) proceeded with potentiometric pH titrations (under the same conditions – 25 °C and 0.1 M ionic strength) where reaction of pydc·H_2 and pyda were studied to obtain formation constants for various self-assembling units. They found that the H_2(pyda)(pydc) species was the most abundant in solution (63.5% distribution) and existed at around pH 3.8, having a log

K value of 6.15. This was evidence that the *stoichiometry* of the solution species that was most abundant in solution was similar to that of the crystalline complex.

Further potentiometric pH titrations were done to study the complexation of mercury(II) with the proton transfer compound (pydc)(pyda.H_2) in aqueous solution. The three species that were most abundant in solution, at their respective pH values, are given in Table 1.1, together with their log *β* values. The self-assembled adduct, (pydc)(pyda·H_2), was dissolved in water and added to a solution of $HgCl_2$. After two weeks golden needle-shaped crystals were produced. Single crystal XRD was used to determine that the structure was a $(pydaH)_2(Hg\ pydcCl)_2$ complex, as shown in Figure 1.3. This complex was then compared to the solution complex and found to have the same stoichiometry, which existed in solution at pH 3.9.

Table 1.1 Ratio of the substituents of the most abundant mercury(II) species in solution, together with their formation constants and maximum percentage distribution with its corresponding pH (25 °C and 0.1 M ionic strength). (Moghimi *et al.*, 2004).

Hg(II)	**pyda**	**pydc**	**H^+**	**log *β***	**Max %**	**pH**
2	2	2	2	34.55	35.8	3.9
1	2	1	1	19.66	53.0	5.9
1	2	2	0	15.94	86.5	>9.0

The obvious question to ask is why did the species which predominated in solution, $Hg(pydc)_2(pyda)_2$, not form in the crystalline state preferentially, as was observed when the adduct alone, H_2(pyda)(pydc), was crystallized? It is clear that one needs to be cautious when trying to compare the solution chemistry to the occurrence of selected crystalline complexes. However it is evident from their report that they have not considered the conditions under which the complexes were actually

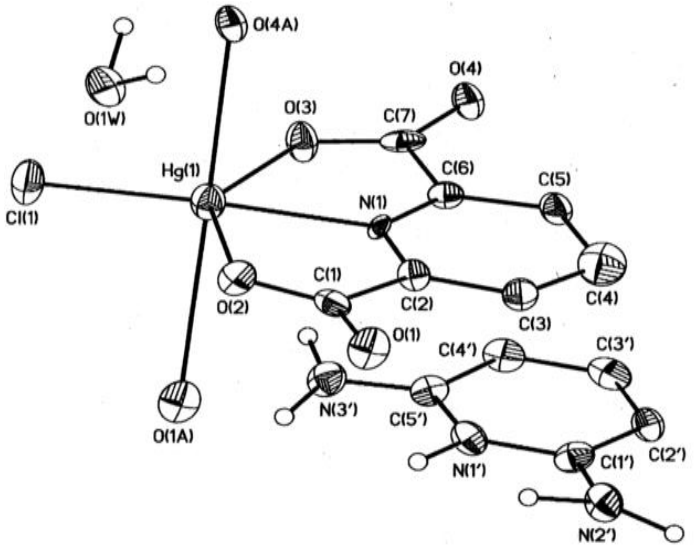


Figure 1.3 ORTEP diagram obtained from Moghimi *et al.* (2004) showing the structure of the complex formed by reacting the self-assembled adduct with $HgCl_2$.

formed when comparing the solution and solid-state complexes. It must be noted that the solution studies were done using the nitrate salt of mercury, whereas the chloride salt of mercury was used in forming the crystalline complex. The anion clearly plays a role in determining the species that will be formed. If the crystalline complex and corresponding solution species were obtained under similar conditions (such as pH) then a more acceptable comparison could be made, and potentially a good correlation between solution and crystalline species could be drawn. This is one of the questions that this research seeks to address.

1.2 AIMS

The central aim of this project was to obtain an understanding of metal-ligand complexation in solution and the solid state, and to investigate whether conditional (pH, concentration, metal-to-ligand ratio and temperature) correlations were

present between the two phases for a specific complex. In order to achieve this for each metal-ligand system, four main objectives had to be met. (i) The metal-ligand species in solution had to be identified at different pH values, starting in strongly acidic solutions, and the formation constants of each of these species determined. Due to the solution studies starting below pH 2 the in-situ witness was used to monitor the diffusion junction potential and the data obtained were modeled in various ways to determine the most accurate method of compensation. The effect of temperature on the magnitude of formation constants was investigated using the cadmium(II)-dipicolinic acid system. (ii) Species distribution diagrams plotted using the calculated formation constants were used to illustrate the species composition of the solution at different pH, concentrations and temperature. (iii) Attempts were made to crystallize the various metal-ligand complexes from solution liquors that were set up at, and performed under, controlled conditions. The effect of pH and ligand-to-metal concentration ratios was investigated. (iv) The crystal structure of any solids formed were studied using SCXRD in order to determine whether there was any correlation between species found in the crystalline form and those found in solution, particularly with respect to composition. Any other solids or powders formed were studied using PXRD.

The finer details of these aims will be discussed in each chapter where the specific metal-ligand systems will be introduced.

1.3 REFERENCES

Aghabozorg, H., Daneshvar, S., Motyeian, E., Manteghi, F., Khadivi, R., Ghadermazi, M., Shokrollahi, A., Ghaedi, M., Derki, S. and Shamsipur, M., 2009. Synthesis and crystal structure of Mn(II) and Hg(II) compounds and solution studies of Mn(II), Zn(II), Cd(II) and Hg(II) compounds based on piperazinediium pyridine-2,3-dicarboxylate. *Journal of the Iranian Chemical Society,* 6 (3)**,** pp 620-637.

Allen, F. H., 2002. Acta Crystallographica, B58, pp 380-388. Cambridge Structural Database. Version 5.34, November 2012 update.

Atkins, P. and de Paula, J., 2006. *Atkins' Physical Chemistry*, Oxford University Press.

Belsky, A., Hellenbrandt, M., Karen, V. L. and Luksch, P., 2002. Acta Crystallographica, B58, pp 364-369. Inorganic Crystal Structure Database.

Berndt, K. D., Güntert, P., Orbons, L. P. and Wüthrich, K., 1992. Determination of a high-quality nuclear magnetic resonance solution structure of the bovine pancreatic trypsin inhibitor and comparison with three crystal structures. *Journal of Molecular Biology,* 227 (3)**,** pp 757-775.

Billing, C., Cukrowski, I. and Jordan, B., 2013. A Novel Approach to Monitoring of the Diffusion Junction Potential in Speciation Studies by Polarography Under very Acidic Conditions. Part I: The Reversible Cd(II)-Picolinic Acid System. *Electroanalysis,* 25 (9)**,** pp 2221-2230.

Blood, E. R. and Grant, G. C., 1975. Determination of cadmium in fish tissue by flameless atomic absorption with a tantalum ribbon. *Analytical Chemistry,* 47 (8)**,** pp 1438-1441.

Briand, G. G. and Burford, N., 1999. Bismuth Compounds and Preparations with Biological or Medicinal Relevance. *Chemical Reviews,* 99 (9)**,** pp 2601-2658.

Chaturvedi, G., Tewari, R., Mrigank, A., N, Vishwakarma, R. A. and Ganguly, N. K., 2001. Inhibition of Helicobacter pylori adherence by a peptide derived from neuraminyl lactose binding adhesion. *Molecular and Cellular Biochemistry,* 228**,** pp 83–89.

Clark, C. M. and Dutrow, B. L. 2009a. *Single-Crystal X-Ray Diffraction* [Online]. Available: http://serc.carleton.edu/research_education/geochemsheets/techniques/SXD.html [Accessed 14 September 2009].

Clark, C. M. and Dutrow, B. L. 2009b. *X-ray Powder Diffraction (XRD)* [Online]. Available: http://serc.carleton.edu/research_education/geochemsheets/techniques/XRD.html [Accessed 14 September 2009].

Cukrowski, I., 1996. A polarographic method of speciation for labile metal-ligand systems based on mass-balance equations. A differential pulse polarographic study at fixed ligand to metal ratio and varied pH. *Analytica Chimica Acta,* 336 (1)**,** pp 23-36.

Cukrowski, I., Hancock, R. D. and Luckay, R. C., 1996. Formation constant calculation for non-labile complexes based on a labile part of the metal-ligand system. A DPP study at a fixed ligand to metal ratio and varied pH. Application to polarographically inactive complexes. *Analytica Chimica Acta,* 319**,** pp 39 - 48.

Cukrowski, I. and Loader, S. A., 1998. Evaluation of a Peak Potential of an Uncomplexed Metal Ion in Speciation Study of Labile Metal–Ligand Systems by Polarography. Stability Constant Determination of Cd^{II} and Pb^{II} with Picolinic Acid at a Fixed L_T:M_T Ratio and Varied pH. *Electroanalysis,* 10 (13)**,** pp 877-885.

DeFord, D. D. and Hume, D. N., 1951. The Determination of Consecutive Formation Constants of Complex Ions from Polarographic Data. *Journal of the American Chemical Society,* 73 (11)**,** pp 5321-5322.

Deisenhofer, J., 1981. Crystallographic refinement and atomic models of a human Fc fragment and its complex with fragment B of protein A from Staphylococcus aureus at 2.9- and 2.8-Å resolution. *Biochemistry,* 20 (9)**,** pp 2361-2370.

Ehrmann, R., 1945. Drugs in the treatment of Peptic ulcer and hypersecretion. *American Journal of Digestive Diseases,* 12**,** pp 154-156.

Fernando, Q., 1995. Metal Speciation in Environmental and Biological Systems. *Environmental Health Perspectives,* 103 (Supplement 1)**,** pp 13-16.

Ford, A. C., Malfertheiner, P., Khan, M., Santana, J. O., Giguere, M. and Moayyedi, P., 2008. Adverse events with bismuth salts for Helicobacter pylori eradication: Systematic review and meta-analysis. *World Journal of Gastroenterology,* 14 (48)**,** pp 7361-7370.

Gouda, H., Torigoe, H., Saito, A., Sato, M., Arata, Y. and Shimada, I., 1992. Three-dimensional solution structure of the B domain of staphylococcal protein A:

comparisons of the solution and crystal structures. *Biochemistry,* 31 (40)**,** pp 9665-9672.

Hammond, C., 2001. *Basics of crystallography and diffraction,* Oxford, Oxford University Press.

Harris, D. C., 1995. *Quantitative Chemical Analysis,* New York, W.H. Freeman and Company.

Heidorn, D. B. and Trewhella, J., 1988. Comparison of the crystal and solution structures of calmodulin and troponin C. *Biochemistry,* 27 (3)**,** pp 909-915.

Kounaves, S. P., 1997. Voltammetric Techniques *In:* Settle, F. A. (ed.) *Handbook of Instrumental Techniques for Analytical Chemistry.* Upper Saddle River, New Jersey: Prentice Hall pp 711-729.

Lingane, J. J., 1941. Interpretation of the Polarographic Waves of Complex Metal Ions. *Chemical Reviews,* 29**,** pp 1.

Martell, A. E. and Hancock, R. D., 1996. *Metal Complexes in Aqueous Solutions*, New York, Plenum Press.

Misra, R. R., Page, J. E., Smith, G. T., Waalkes, M. P. and Dipple, A., 1998. Effect of cadmium exposure on background and anti-5-methylchrysene-1,2-dihydrodiol 3,4-epoxide-Induced mutagenesis in the supF gene of pS189 in Human Ad293 Cells. *Chemical Research in Toxicology,* 11 (3)**,** pp 211-216.

Moghimi, A., Ranjbar, M., Aghabozorg, H., Jalali, F., Shamsipur, M., Yap, G. and Rahbarnoohi, H., 2002. A novel pyridine containing self-assembling system: synthesis, characterization, X-ray crystal structure, ^{13}C solid phase NMR and solution studies. *Journal of Molecular Structure,* 605 (2)**,** pp 133-149.

Moghimi, A., Shokrollahi, A., Shamsipur, M., Aghabozorg, H. and Ranjbar, M., 2004. X-ray crystal structure and solution studies of hexacoordinated mercury(II) complex of a pyridine containing proton transfer compound. *Journal of Molecular Structure,* 701 (1)**,** pp 49-56.

Rogers, R. D., 1996. Chemical Crystallography. *In:* Seddon, K. R. and Zaworotko, M. (eds.) *Crystal Engineering: The Design and Application of Functional Solids.* Netherlands: Kluwer Academic Publishers pp 155-189.

Sherken, S. and Friedman, E. J., 1973. Quantitative determination of bismuth trioxide in teflon catheters using decomposition by molten salt fusion followed by standard

addition and conventional direct current polarography. *Analytical Chemistry,* 45 (14)**,** pp 2399-2400.

Stauffer, W., Christenson, J. C. and Fischer, P. R., 2008. Preparing children for International Travel. *Travel Medicine and Infectious Disease,* 6 (3)**,** pp 101-113.

Sun, H., Li, H., Mason, A. B., Woodworth, R. C. and Sadler, P. J., 1999. N-lobe versus C-lobe complexation of bismuth by human transferrin. *Journal of Biochemistry,* 337**,** pp 105-111.

Tobon-Zapata, G. E., Etcheverry, S. B. and Baran, E. J., 1997. Vibrational Spectrum of bismuth subcarbonate. *Journal of Material Science Letters,* 16**,** pp 656-657.

Williams, G., Clayden, N. J., Moore, G. R. and Williams, R. J., 1985. Comparison of the solution and crystal structures of mitochondrial cytochrome *c.* Analysis of paramagnetic shifts in the nuclear magnetic resonance spectrum of ferricytochrome *c*. *Journal of Molecular Biology,* 183 (3)**,** pp 447-460.

Wilson, D. C., Young, P. J., Hudson, B. C. and Baldwin, G., 1982. Leaching of Cadmium from Pigmented Plastics in a Landfill Site. *Environmental Science and Technology,* 16 (9)**,** pp 560.

Yu, S.-B. and Watson, A., 1999. Metal-Based X-ray Contrast Media. *Chemical Reviews,* 99**,** pp 2353-2377.

Chapter Two

Experimental

2.1 INTRODUCTION

Glassware was acid (HNO_3) washed, rinsed with deionized water and air-dried. The acid serves to solubilize and oxidize any bacteria or particulates that may be present, as well as protonate the outermost layer of the glass to avoid adsorption of cations from solution. Throughout experimentation deionized water was used, which came from a Milli-Q water purification unit, resistivity = 18 MΩ cm, and all solutions were made using analytical grade chemicals. All reagents that were used are listed in Table A2.1, Appendix A, together with their supplier and manufacturer assay. The equipment will be discussed in detail in the relevant sections of this chapter. pH is a central theme in this research and therefore it should be stated upfront that when pH is referred to it is the concentration of the H^+ ions in solution (not the activity) measured by a glass electrode.

2.2 SOLUTION STUDIES

Complex formation of various metal-ligand systems were studied as a function of pH. Sampled direct current polarography (DC_{TAST}) was used for measuring polarograms at specific pH intervals in an acid-base titration, starting at pH 0.3 where not much research has been conducted. At low pH values a small degree of complexation is generally expected, and as the pH slowly increases so the degree of complex formation should increase (Harris, 1995). Formation constants were

determined for the metal-ligand systems of interest, at an initial ionic strength of 0.5 M and at specified temperatures.

The electrolytic cell used is a combination of two cells – a potentiometric cell and a polarographic cell. The potentiometric cell is responsible for measuring the potential difference between a Metrohm glass electrode and a combined external reference system (particulars of this electrode are given in Table 2.1) which is used for determining pH via a calibration curve. The glass electrode is an ion-sensitive electrode, specific to H^+ ions. It is made up of a silicate framework containing lithium ions, amongst others. When the electrode is submerged in a sample solution, a solvated layer around the glass is formed where ion exchange occurs. As the concentration of the ions in the sample changes, a new equilibrium needs to be achieved within the solvated layer which results in a change of the potential at the glass membrane (Metrohm, 2012).

Table 2.1 Metrohm glass electrode (Ecotrode) specifications.

Electrode Features	**Description**
Shaft material	glass
Membrane glass type	T*
Membrane resistance	200-500 MΩ
Diaphragm	Ceramic frit
Diaphragm resistance	0.4-0.9 kΩ
Electrolyte flow rate	5-15 µL/hr.
pH range	0 - 14
Temperature range	0 - 80 °C

* T glass is blue glass, having specific properties (response time, thermal resistance, chemical stability, shape, size and electrical properties) which are particular for the application of the electrode (Metrohm, 2012).

The outer reference's filling solution is 3 M KCl, as it results in only a small diffusion junction potential at the ceramic frit, because of the high concentration used and

since the K^+ and Cl^- ions move at similar rates. When the glass electrode is not in use it is kept in Metrohm storage solution (6.2323.000, which is made up of 3 M KCl and other additives which the company does not divulge) which is said to prolong the lifetime of the glass membrane in terms of response times and alkali error (Metrohm, 2012). Also the electrode is ready for immediate use if stored in this solution.

The polarographic cell incorporates the following Metrohm electrodes: a dropping mercury electrode (DME- filled with triple distilled mercury from Saarchem), a silver-silver chloride reference electrode (with a 3 M KCl internal solution) in a salt bridge containing 0.5 M KNO_3 and a platinum counter electrode. The actual electrolytic cell set up can be seen in Figure 2.1.

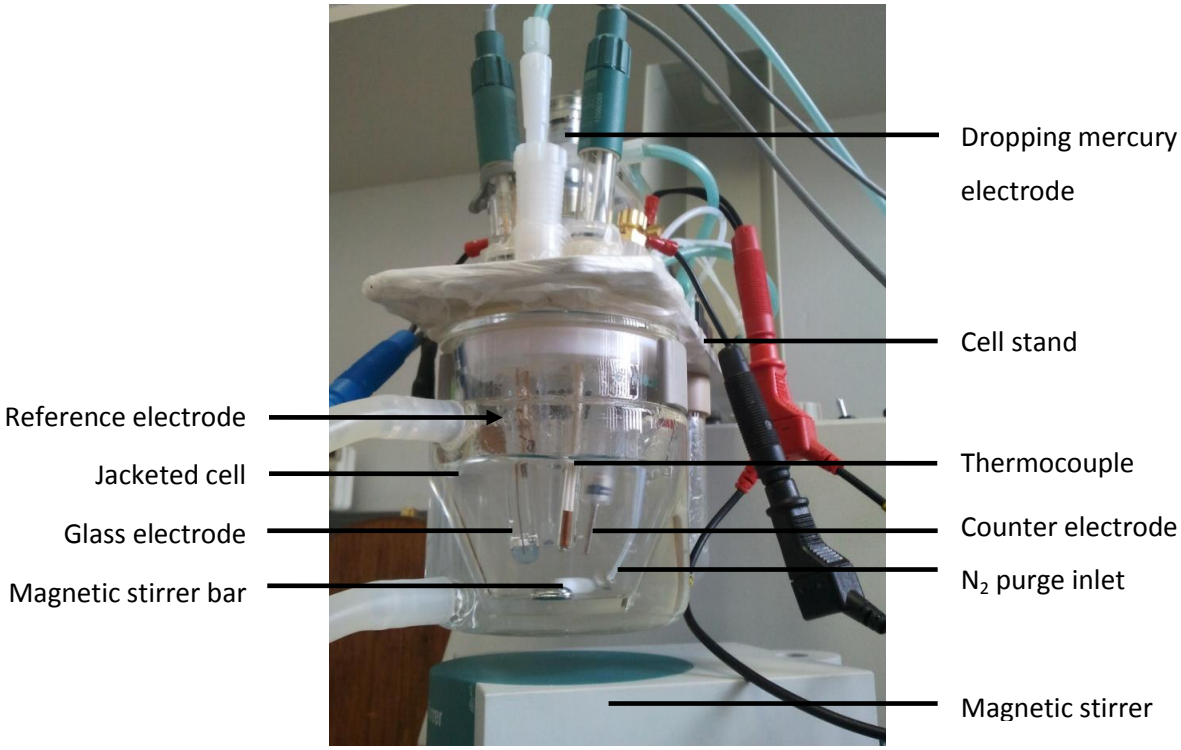


Figure 2.1 Typical polarographic cell.

Polarograms, a current vs. potential plot, were recorded at each pH interval. The counter electrode is used in conjunction with the DME for current flow and measurement. The potential is measured between the working electrode (DME) and the reference electrode. All potentials quoted are with respect to the Ag/AgCl/3 M KCl reference electrode. The electrodes all sit within the jacketed cell which is maintained at a constant temperature using a homemade water bath (containing a Labcon CPE 100 thermostat). Solution temperature was measured with a Metrohm Pt 1000 thermocouple (measurement range: -50 to 180 °C). The cell is held in place by the 663 VA stand (which houses all the gas connections and valves), with the Metrohm 728 magnetic stirrer carefully positioned just below it. The Metrohm 765 Dosimat is responsible for accurate automated additions of solutions to the cell. The entire system comprising a potentiostat (BAS Voltammograph CV-27), a Metrohm 713 pH-meter, the Dosimat, the VA stand and the magnetic stirrer is linked to the computer via a homemade interface. The LabVIEW software package (version 7) and the NI-6036-E data acquisition card (National Instruments, Austin, Texas, USA) link these components together via the interface to produce an automated system that can be controlled from the computer. A schematic representation showing how the components link together, with the general setup of the apparatus for an experiment, can be seen in Figure 2.2.

The N_2 has a feed to the DME allowing for a continuous flow of mercury, to the drop knocker for the DME (in the cell stand) and to the sample solution (humidified first by passing through deionized water). Valves on the cell stand control the flow of the nitrogen from the gas bottle to the three outlet points.

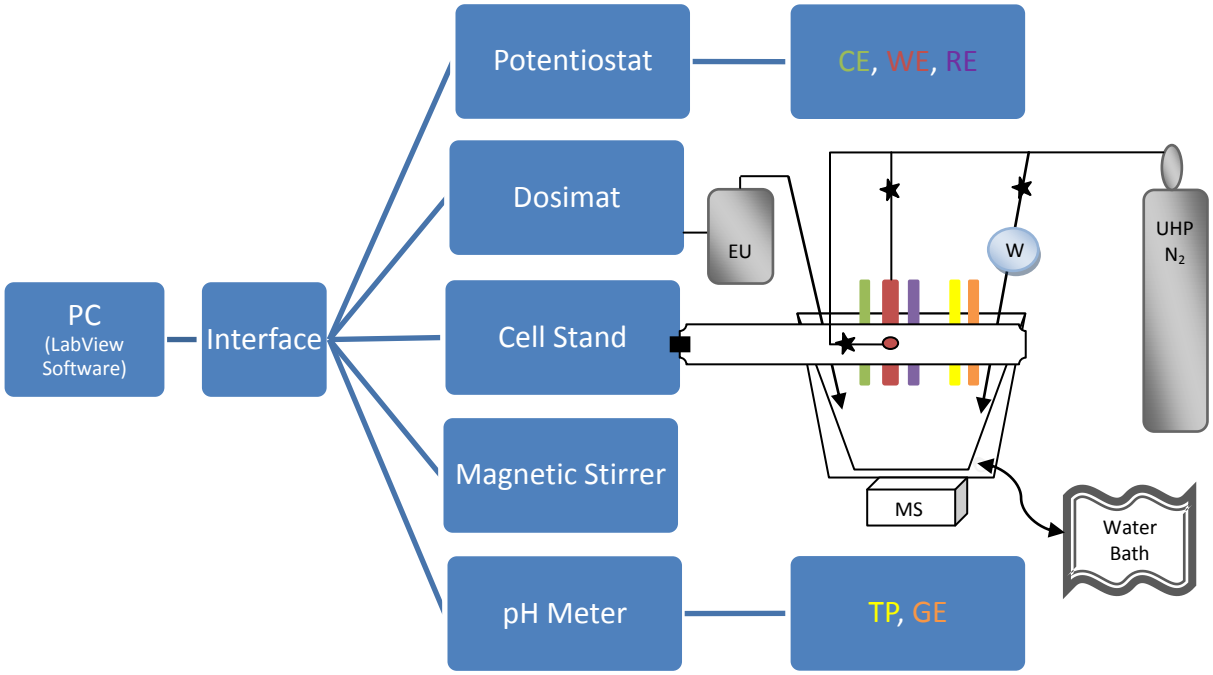


Figure 2.2 Schematic representation of the automated polarographic and potentiometric setup. Abbreviations have the following meanings: PC - personal computer, CE -counter electrode, WE - working electrode, EU - exchange unit, W – water for humidification of gas, RE - reference electrode, GE - glass electrode, TP - temperature probe, MS - magnetic stirrer and UHP N_2 – ultra high purity nitrogen. The black stars represent valves that are found on the cell stand.

In a polarographic pH titration, shifts in potential for reduction processes are studied as a function of pH. The ligand and metal ions are present in a particular concentration ratio, which remains the same throughout the experiment. As the pH changes, different complexes are present in solution and are therefore reduced at different potentials. Shifting of polarographic signals is thereby presented as a function of pH. The pH titrations done in this study were of a strong acid and a strong base with equivalence point at pH 7, described by the following reaction:

$$HNO_3 + KOH \rightarrow KNO_3 + H_2O$$

25.000 mL of the 0.5 M HNO_3 was delivered to the cell accurately by means of a Dosimat. The metal ions of interest (and ligand for complexation experiments) were added to this titrand before the experiment began. The 0.5 M KOH was the titrant, stored in an exchange unit that was controlled by the Dosimat for dispensing accurate volumes of solution to the cell. The exchange unit containing the potassium hydroxide solution was equipped with a CO_2 adsorbing unit that was prepared in a layered fashion using cotton wool, sodium hydroxide pellets and Ascarite© or Soda Lime. This adsorbs carbon dioxide from the air by reacting with it to form sodium bicarbonate, as follows:

$$NaOH + CO_2\,(g) \rightarrow NaHCO_3$$

KOH additions are made to the cell until the pH changes by 0.1 which is monitored by the potentiometric cell. The solution is stirred and purged throughout the titration, except during polarographic measurements. Initially, 0.5 mL of base is added and allowed to equilibrate (for 5 - 15 seconds) and the approximate pH is then recorded. If the pH has not changed by 0.1 then another base addition is made. This continues until $\Delta pH = 0.1$. Thereafter, the solution is allowed a 60 s period for equilibration to occur. Then a maximum of 15 minutes is allowed to obtain ten consecutive potential difference readings which have a maximum standard deviation of 0.04 mV, sampled at 2 s intervals. Initial readings that do not satisfy this criterion are discarded. The average of the selected ten values is recorded as the potential difference (which is converted to pH) at which a polarogram will be recorded. The temperature of the solution is then recorded, followed by a 10 s rest time and the polarographic cell is initiated, where stirring and purging is stopped for the measurement. The potential is applied, and the current measured between the working and counter electrode. Once a polarogram is obtained, the Dosimat once again makes small base additions to the solution being

stirred and purged. As the titration approaches the end point, smaller volumes of base are added because less KOH is required to change the pH by 0.1. This procedure continues until a stop condition is met. Parameters used to control the automated polarographic and potentiometric data collections for cadmium(II) and bismuth(III) experiments, via the LabView software, are given in Table 2.2. The above paragraph explains the procedure using particulars for data collection of cadmium(II) experiments; however, it can all be applied to the bismuth(III) system by using the respective values given in Table 2.2.

Table 2.2 Parameters used for the automated collection of polarograms as a function of pH.

Parameter	Setting	
	Cadmium	**Bismuth**
Potentiometric Data:		
Initial pause	10 s	15 s
Equilibration time	60 s	300 s
Sample rate	2 s	2 s
Criterion for stability	0.04	0.04
Maximum waiting time	15 min	15 min
Number of readings saved	100	100
Polarographic Data:		
Initial potential	-0.20 V	0.18 V
Final potential	-0.85 V	-0.70 V
Step potential	-0.004 V	-0.004 V
Step time (drop life)	1s	1s
Current integration time	100 ms	120 ms
pH step	0.1	0.1
CV-gain	0.005 mA/V	0.005 mA/V
Potential input range	± 1.0 V	± 1.0 V
Current input range	± 1.0 V	± 1.0 V
Rest time	5 s	5 s
Stop conditions:		
Stop potential	-400 mV	0 mV
Stop pH*	7	7
Stop volume	30 mL	30 mL
Dosimat configuration:		
Mode	DisC	DisC
Rate of addition	5 mL/min	5 mL/min
Rate of filling	30 mL/min (for a 10 mL burette)	30 mL/min (for a 10 mL burette)
Volume increment	0.2 mL until about 16 mL, then 0.05 mL until about 20 mL, and then 0.01 mL thereafter	0.1 mL until 20 mL, and then 0.01 mL thereafter.

* Stop pH was attained before the other stop conditions.

2.2.1 Experiments and Data Analyses

Solutions used for electrochemical titrations were made up in order to achieve initial ionic strength (μ) of 0.5 M. Stock solutions of the metal ions used consisted of 0.100 M thallium(I) nitrate in 0.5 M HNO_3, 0.100 M cadmium(II) nitrate tetrahydrate in 0.5 M HNO_3, and 0.0100 M bismuth(III) nitrate in 1 M HNO_3. 0.5 M HNO_3 and KOH solutions were standardized and used to calibrate the pH electrode before any pH measurements were taken.

2.2.1.1 Standardization of Solutions

The 0.5 M potassium hydroxide was standardized using potassium hydrogen phthalate (KHP) that was dried at 120 °C in an oven for about three hours. Around 0.5 g of KHP was accurately weighed out to five decimal places and dissolved in 5 mL of deionized water. A titration was then carried out with the KOH solution using the Metrohm 848 Titrino Plus autotitrator and Metrohm glass electrode (Ecotrode) sensor until the equivalence point of the titration was obtained. Standardization of the 0.5 M HNO_3 solution was achieved by titration of 5 mL of the acid with the previously standardized KOH solution, again using the autotitrator. Titration instrument parameters for the standardization of the acid and base can be found in Table A2.2, Appendix A. Replicate measurements of both standardizations were done until the relative standard deviation of the calculated concentrations of HNO_3 and KOH were below 1%, allowing for concentrations to be quoted to four significant figures. Solutions were standardized each time they were replenished or if they had been standing for about a month or longer.

The reason solutions were standardized was so that the exact pH at each titration step in the glass electrode calibration procedure could be calculated. This pH was related to the potential difference measured by the glass electrode and a calibration

curve was plotted. The calibration was then used throughout the experiment for accurate pH readings.

2.2.1.2 Calibration of the Glass Electrode

Calibration of the glass electrode was not done using buffer solutions because the results will not be accurate due to the buffer and test solution not having the same ionic strength and composition. Instead a potentiometric pH titration of 0.5 M KOH and 0.5 M HNO_3 was conducted according to the procedure described by Billing and Cukrowski (2009). The calibrations were done by the addition of 35, 45 or 50 mL of 0.5 M KOH in small increments (0.1 or 0.5 mL) to 25 mL of 0.5 M HNO_3. The titration is done from approximately pH 0.3 to 12.8, and at these extreme pHs there is the possibility of an acid and/or alkaline error occurring, as well as an error due to the diffusion junction potential.

The acid solution was purged for half an hour before the titration started, and stirring and purging occurred throughout the calibration. It is extremely important that the results of the calibration of the glass electrode are obtained under the same conditions used for polarographic experiments. Between base additions and the glass electrode readings a minimum time of 15 s was allowed for equilibration to be attained. Potential data at the glass electrode were read in 2 s intervals but was only recorded once the standard deviation of the last ten measurements was calculated to be lower than 0.040 mV. Temperature was measured after every ten potential difference readings in order to ensure that the desired temperature was maintained. Instrument parameters used for the calibration of the glass electrode can be seen in Table A2.3, Appendix A. In Figure 2.3 the pH, calculated from the potential readings, was plotted vs. volume of KOH added at each point in the titration.

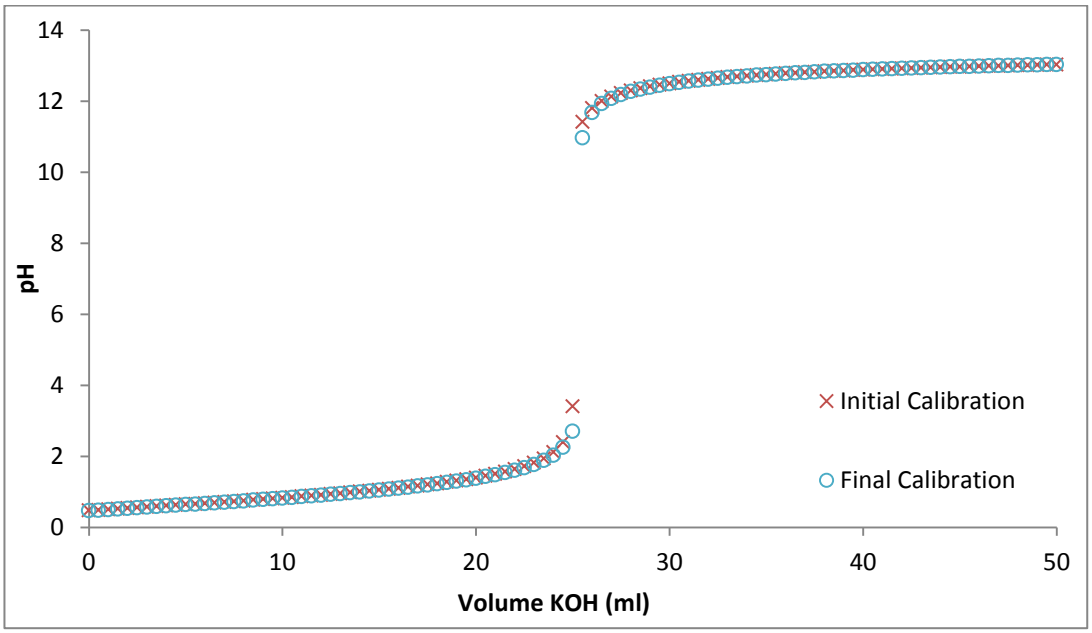


Figure 2.3 Comparison of calibration titration curves taken before and after a polarographic experiment, using 25 mL of ~0.5 M HNO_3 and 50 mL of ~0.5 M KOH (added in 0.5 mL increments).

Calibration was carried out before and after each polarographic experiment which is crucial since it gives an indication of whether the glass electrode is performing consistently throughout. The semi-permeable frit permits the movement of ions between the outer reference solution and the surrounding contents of the cell. This movement of ions could cause changes in the reference solution over time. The calibration done after an experiment therefore serves to demonstrate the extent of these changes. If these changes are too extreme then we would have very little confidence in our pH measurements that were recorded (as potential values) during the actual experiment. The data in the basic region can additionally be used to evaluate the quality of the glass membrane. The reason for this is at pH values larger than about 9, the glass of the electrode becomes highly susceptible to corrosion. A straight line fitted to the calibration curve (potential vs. pH data)

between pH 12.2 and 12.8 should render a gradient of between -56 and -60 for an acceptable glass electrode, according to Billing and Cukrowski (2009) (Figure 2.4).

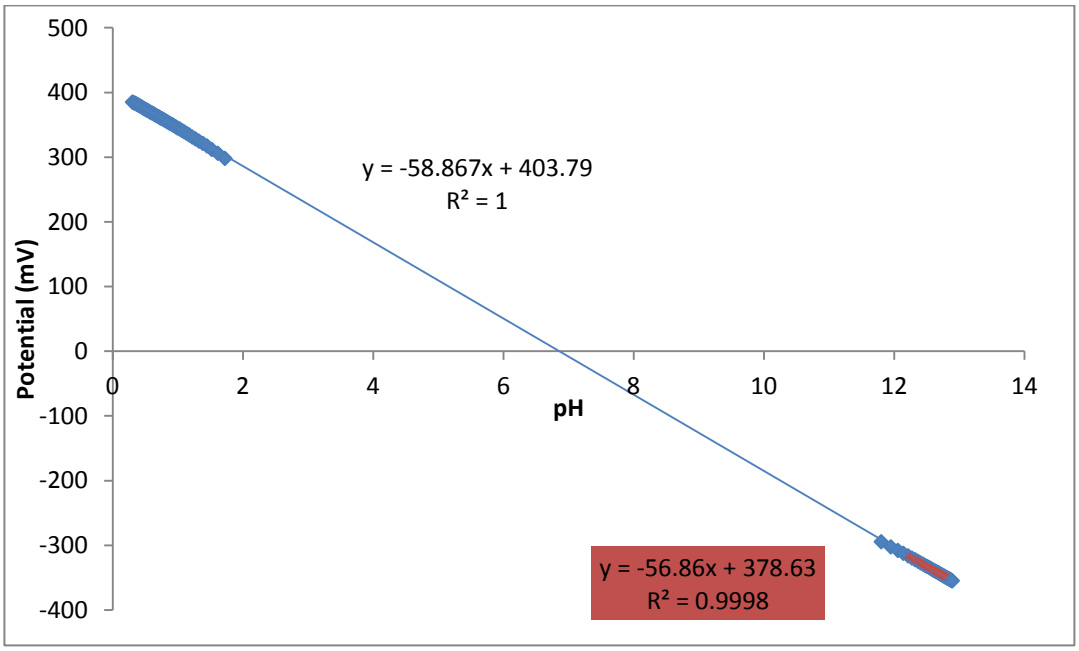


Figure 2.4 Calibration curve showing the slope for evaluation of the long-term performance of the glass electrode.

Billing and Cukrowski (2009) describe a novel approach to evaluating titration data in the low pH region (between 0 and 2) obtained for the calibration of a glass electrode. At very low and very high pH the calibration curve is seen to deviate from linearity due to the diffusion junction potential and alkaline errors respectively. This needs to be accounted for, and fitting a straight line through the data does not give an accurate calibration curve in these regions. Their method was therefore used to obtain the best possible calibration curve for accurate calculation of pH for the subsequent polarographic experiment. Calibration curves were plotted using the potential data obtained from these calibration titrations with pH as the independent variable. (The actual concentrations and volumes of the acid and base at each point in the titration were used to calculate pH.) Points in the low buffer region were then removed from the data. Due to the deviation from linearity at very low pH, two

curves were fitted to the data in different pH ranges. A straight line was fitted to the data between pH 0.6 and 12.8, and a quadratic function was fitted to the data in the acidic region. These two graphs were overlaid to establish the intersection, which has been emphasized in Figure 2.5 by only showing the data below pH 0.5.

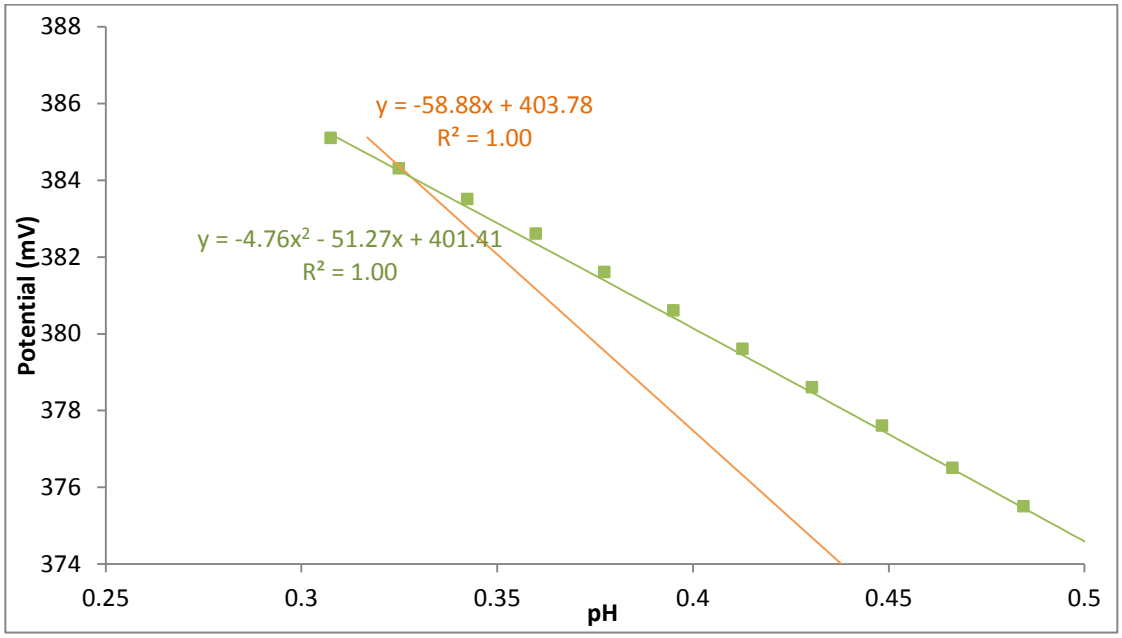


Figure 2.5 Calibration curve in the highly acidic region showing the deviation from linearity below pH 0.5.

For potentials above the first intersection, the quadratic calibration curve is used for calculating pH, and below the first intersection the straight line is used. This approach allows the calibration curve to predict pH measurements having uncertainty better than ± 0.01 pH unit in the acid region (Billing and Cukrowski, 2009), the pH region of interest in our research.

2.2.1.3 Polarographic Experiments

Initially a pH titration was performed where only the metal ion of interest and Tl(I) were present in the test solution (i.e. no ligand was introduced into the system). This set of data is vital because it provides information about the diffusion junction

potential when no complexes are being formed. This can almost be viewed as a reference set of data. Experiments to study complex formation were then conducted with the metal ions as well as the ligand of interest. Complex formation of each system was studied at different ligand-to-metal concentration ratios and in one case even at varied temperature.

For each experiment 25.000 mL of standardized 0.5 M HNO_3 was placed in the jacketed cell equipped with a stirrer bar and a few grains of gelatine. The gelatine's main function was to prevent current maxima. For the polarographic measurements we ideally wanted movement of ions to be purely diffusive, so this, together with the fact that a high concentration of background electrolyte is required to maintain ionic strength, was the reason for doing the experiment in a concentrated background solution of 0.5 M HNO_3. The acid solution was stirred and purged with Ultra High Purity (UHP - 99.999%) nitrogen to rid the cell environment of any oxygen. A background scan (manually set) was recorded to ensure an inert nitrogen atmosphere and that no other impurities were present (Figure 2.6, post-purge). (Parameters used for the manual collection of background polarograms can be seen in Table A2.4, Appendix A.) Removal of O_2 is essential because it is an electro-active species that can undergo reduction, as the pre-purge dataset in Figure 2.6 shows. The very low concentrations (of the order of 10^{-5} M) of metal ions in solution produce currents which are far lower than that due to the reduction of oxygen. The reduction half-wave potential for the first step of a two-step process occurs at 0.695 V with respect to the standard hydrogen electrode (Harris, 1998) (seen in Figure 2.6) according to the following reaction:

$$O_2 + 2H^+ + 2e^- \rightleftharpoons H_2O_2$$

The second step of the reaction is:

$$H_2O_2 + 2H^+ + 2e^- \rightleftharpoons 2H_2O$$

Additionally, the presence of oxygen can oxidize electrode surfaces because of its electro-active characteristic. In the post purge polarograms in Figure 2.6, the sharp increase in the current from a potential of about -600 mV is due to the reduction of hydrogen ions in solution, as follows:

$$2H^{+}(aq) + 2e^{-} \rightleftharpoons H_2(g)$$

This phenomenon will always occur in solutions containing high concentrations of acid. This cannot be avoided in such experiments, and so it must just be affirmed that the signal does not interfere with the reduction of any of the metal ions of interest (or their complexes).

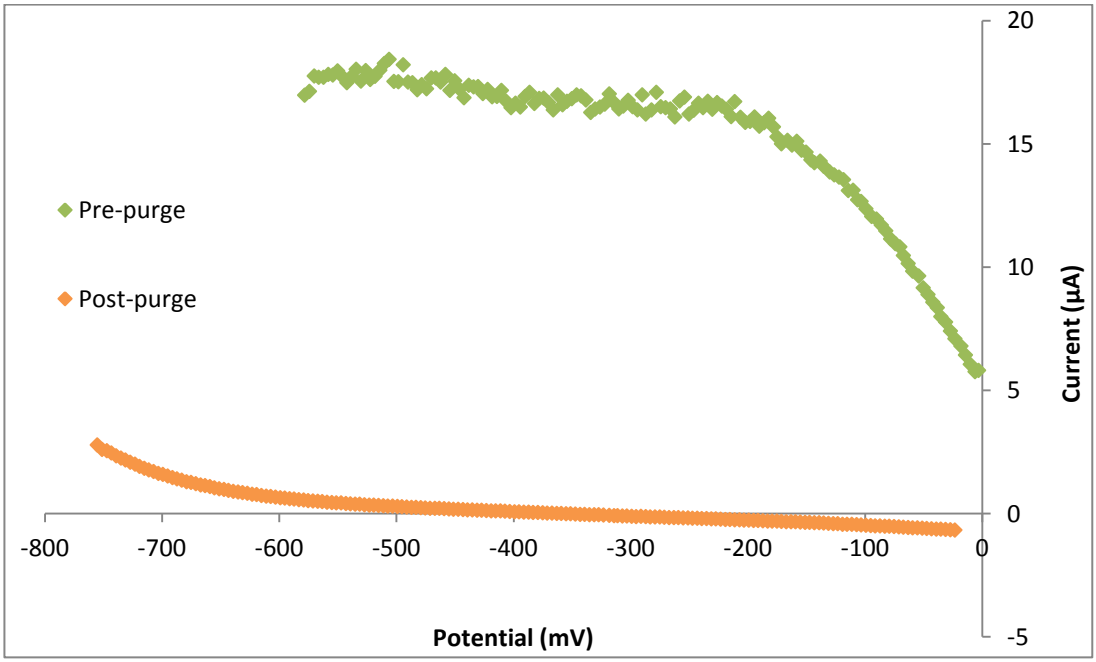


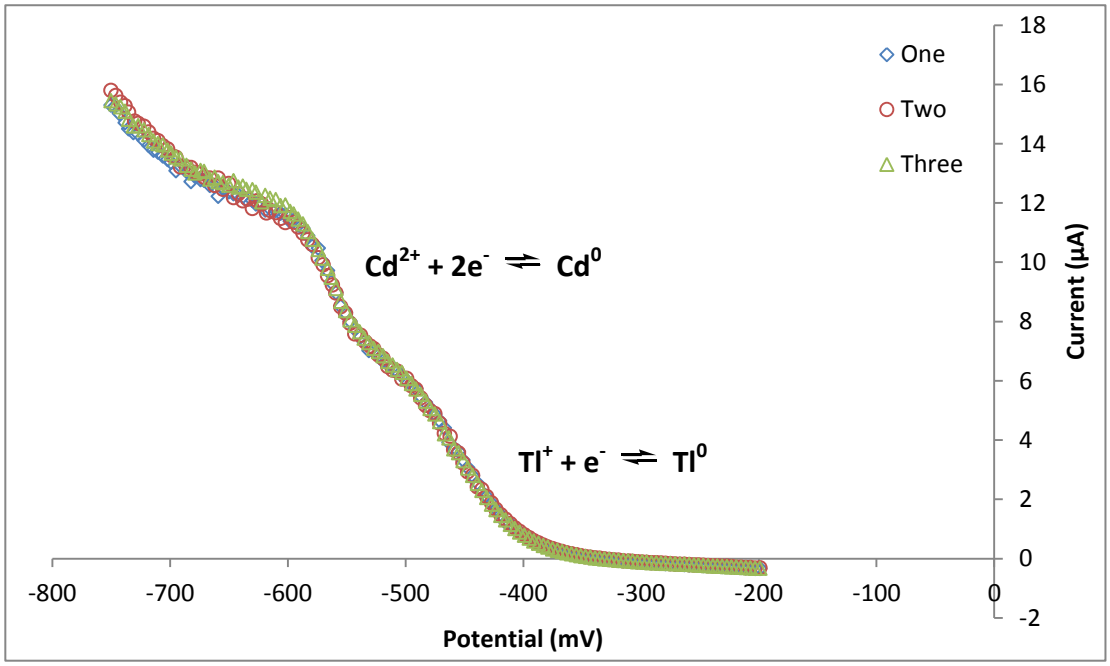
Figure 2.6 Polarogram showing a typical background scan in ~0.5 M HNO_3, pre- and post- N_2 purge.

The two metal ion species (Cd(II) and Tl(I), or Bi(III) and Tl(I)) in the form of stock solutions were added to the titrand using a Hamilton syringe to get an accurate volume in the microlitre scale. After stirring and purging again for thirty minutes

another polarogram was measured. The system was purged for a further five minutes and then another polarogram was recorded. Three consecutive polarograms that overlapped proved that the atmosphere was completely inert and that the dropping mercury electrode was in good working order. Figure 2.7 a) is a typical example for the cadmium experiments, and Figure 2.7 b) for bismuth).

Figure 2.7 a) shows two waves, one at an approximate half-wave potential of -450 mV representing the reduction of thallium(I), and the other at about -570 mV for cadmium(II). Figure 2.7 b) also shows two waves, at approximately 25 mV the reduction of Bi(III) occurs, and at -450 mV again thallium(I). These initial polarograms were used as an indication of the error associated with measuring data and curve fitting (see section 2.2.1.4). Once these polarograms are collected the system is set to automatically run a pH titration, as described in the introductory section of this chapter.

a)



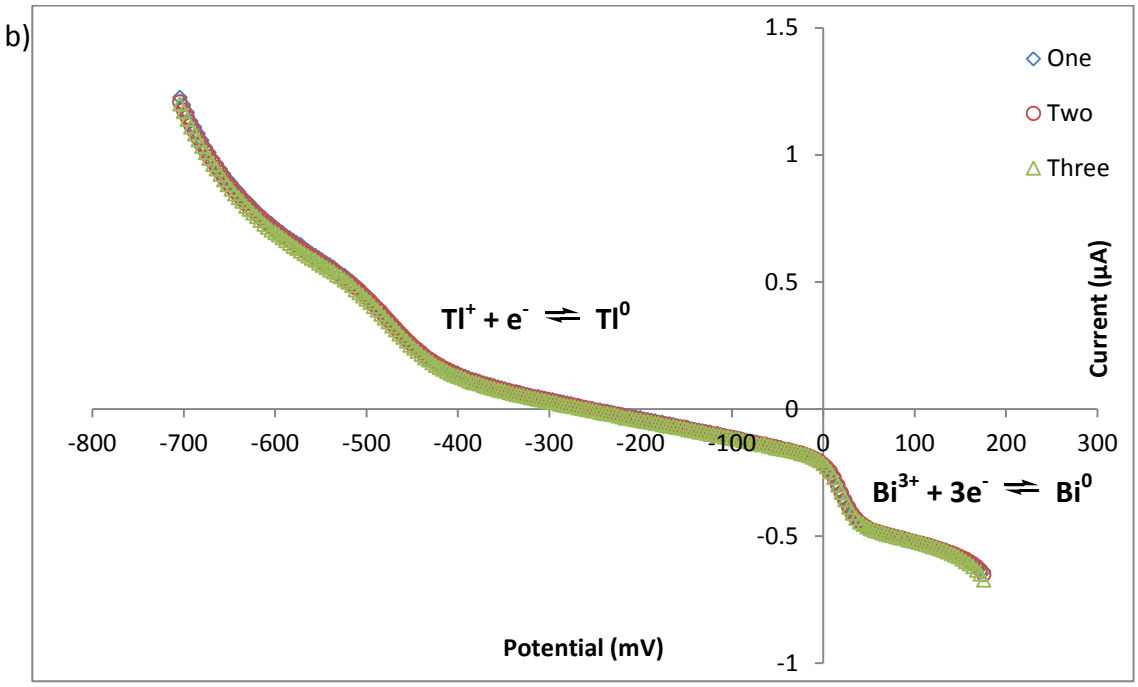


Figure 2.7 Three consecutive polarograms showing the half-wave potentials of a) cadmium(II) and thallium(I) and b) bismuth(III) and thallium(I) in 0.5 M HNO_3.

The pH at which each polarogram was recorded at was calculated using the potential data recorded by the glass electrode. The pH was calculated by substituting these potentials into the calibration curve equations (either the quadratic or the straight line) obtained from both the initial and final calibrations of the glass electrode. The values were then averaged to obtain pH. A maximum standard deviation of 0.02 mV between the two calibrations was allowed.

In experiments where complex formation of a metal-ligand system was studied, addition of the ligand was required. The same experiment was performed, but now the accurately weighed (five decimal places in grams) ligand was introduced to the solution containing the metal ions, and the solution was stirred and purged again for thirty minutes. In this case manual polarograms were collected of the background, then after the addition of the metal ions and then after the addition of ligand as

well. The automated system commenced in the same manner as described above for the experiment where no ligand was present. The only difference was that the polarograms were recorded to more negative potentials to ensure shifting of the reduction potential didn't cause essential data to be out of the measured frame.

Polarographic experiments carried out with the metal ion/s where no ligand was present for chelation produced a set of polarograms that represented data where any shift in half-wave potential with changing pH is essentially due to the diffusion junction potential. These data were therefore used to create a model representing the magnitude of the diffusion junction potential. Experiments performed where ligand was present produces polarograms which were more complicated as they contain shifts in half-wave potentials due to the diffusion junction potential as well as complex formation. We therefore used the model to compensate the diffusion junction potential in the complex formation experiments, thereby producing data which purely represented the shift in potential due to complexes being formed in solution.

Polarographic data were analyzed by plotting graphs of half-wave potential, current and delta versus calculated pH, for each metal ion. These values were obtained by the fitting of the polarographic waves.

2.2.1.4 Curve Fitting

The polarograms were fitted manually using locally developed software called FitBrink, or automatically using software developed under LabView which uses the previous polarograms parameters to fit the next polarogram until the whole series has been fitted. Both programs fit the polarograms using the following equation:

$$f(x) = \frac{I_d}{10^{\left(\frac{n\delta\left(x-E_{1/2}\right)}{s}\right)}+1} + I_b \qquad (2.1)$$

I_d represents the diffusion limited current, I_b represents the background current, n represents the number of electrons transferred, δ represents the steepness of the curve, $E_{1/2}$ represents the half-wave potential and s is the Nernstian slope for a single electron transfer process. The reduction waves of Tl(I) and Cd(II) were fitted together as they were close in potential, whereas Bi(III) and Tl(I) were fitted separately.

Curve fitting of polarograms was done to obtain accurate values for the half-wave potential and the diffusion limited current for each reduction process. The half-wave potential is the potential where the current is equal to half of the diffusion limited current. When the thallium(I) and cadmium(II)/bismuth(III) waves were fitted together the following equation (Equation 2.2) was used, which takes into consideration both electron transfer processes:

$$f(x) = \left[\frac{I_d}{\left(\frac{n\delta\left(x-E_{\frac{1}{2}}\right)}{0.05916}\right)+1}\right]_{Tl} + \left[\frac{I_d}{\left(\frac{n\delta\left(x-E_{\frac{1}{2}}\right)}{0.05916}\right)+1}\right]_{Cd/Bi} + I_b \qquad (2.2)$$

The background current was described using equation 2.3 which contained a linear term representing the charging current and an exponential term for the H_2 evolution in very acidic solutions. The same equation was also used for the bismuth data, where the exponential function now represented any mercury oxidation of the electrode, which unfortunately could not be totally avoided.

$$I_b = a + bx + c \times \exp(dx) \qquad (2.3)$$

Figure 2.8 was plotted to show an example of the fit of each reduction wave separately for thallium(I) and cadmium(II), as well as the background current for the linear and exponential terms.

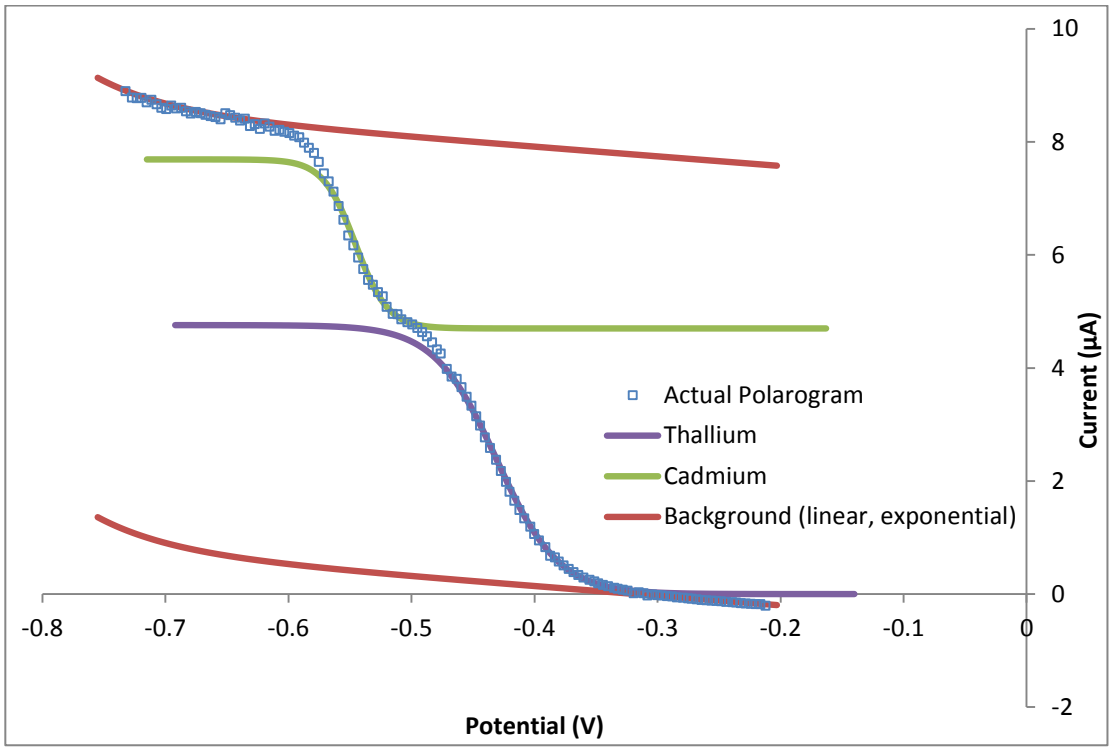


Figure 2.8 The fitting procedure of each portion of a cadmium(II) and thallium(I) polarogram.

A delta value of one is indicative of a completely reversible reduction process. (When curve fitting produced values of delta close to one, delta was set equal to one as the process was then known to be reversible). In order to apply the theory used in this research for solving formation constants, the processes had to be reversible. It was found that all Cd(II) and Tl(I) reduction processes were reversible. For the bismuth experiments, the delta value was allowed to vary when the reduction waves were fitted and the reversibility of the reduction processes will be discussed separately in the respective chapters to follow.

The rate of electron transfer for a reversible process is greater than the rate of mass transport and can be described by Nernstian behaviour (Harris, 1995). The Nernstian slope at 25 °C has a constant value of 0.05916 units per electron

transferred. This value was recalculated for experiments conducted at elevated temperatures, according to the following equation:

$$\text{Nernstian slope} = \frac{R \times T}{F} \times \ln 10 \qquad (2.4)$$

where *R* represents the gas constant, *T* the temperature measured in kelvin and *F* Faraday's constant.

The three initial polarograms for both metal-ions and ligand are also fitted. The variation in these values again indicates the error in measuring and fitting data. It is expected that the fitted data for each of the three curves to be similar because all three polarograms were obtained in close succession without any conditional changes to the experiment (except for additional purging).

2.2.1.5 Solving Formation Constants

A method proposed by Cukrowski (1996) to calculate formation constants using polarographic data relies on the computation of mass-balance equations that contain the formation constants for each complex that is formed. Equation 2.5 was used to calculate formation constants by relating the shift in half-wave potential and a decrease in polarographic half-wave height to the concentration of free metal ion as determined by the mass balance equations which contain formation constants (Cukrowski, 1996).

$$\left\{E\left(M_{free}\right) - E\left(M_{comp}\right)_i\right\} - \frac{RT}{nF} ln \frac{I\left(M_{comp}\right)_i}{I\left(M_{free}\right)_i} = \frac{RT}{nF} ln \frac{[M_T]_i}{\left[M_{free}\right]_i} \qquad (2.5)$$

$E(M_{free})$ is the free (uncomplexed) metal ion potential, $E(M_{comp})$ is the complexed metal ion potential, $I(M_{free})$ is the current for the free metal ion, $I(M_{comp})$ is the current for the complexed metal ion, $[M_T]$ is the total metal ion concentration, $[M_{free}]$ is the free metal ion concentration and *i* refers to the value obtained at each pH step in a pH titration experiment.

The left side of the equation (called the corrected potential shift) plotted vs. pH represents the experimental complex formation curve (ECFC) which was calculated based upon the data that were obtained experimentally. The right side of the equation was computed using mass-balance equations and stability constants to yield the calculated complex formation curve (CCFC) when plotted versus pH. The a mass-balance equations which consider the total metal ion concentration [M_T] (Equation 2.6) and the total ligand concentration [L_T] (Equation 2.7), at each pH (at which a polarogram is recorded), are as follows, respectively:

$$[M_T]_{(i)} = \left[M_{free}\right]_{(i)} + \sum_p \sum_q \sum_r p\,\beta_{M_pL_qH_r}\left[M_{free}\right]^p_{(i)}\left[L_{free}\right]^q_{(i)}[H]^r_{(i)} + \sum_x \sum_y x\,\beta_{M_x(OH)_y}\left[M_{free}\right]^x_{(i)}[OH]^y_{(i)} \tag{2.6}$$

$$[L_T]_i = \sum_k \beta_{H_kL}[H]^k_{(i)}\,[L_{free}]_{(i)} + \sum_p \sum_q \sum_r q\beta_{M_pL_qH_r}\,[M_{free}]^p_{(i)}[L_{free}]^q_{(i)}[H]^r_{(i)} \tag{2.7}$$

The total metal ion and ligand concentrations are known for each experiment and the hydrogen ion and hydroxide concentrations are obtained through calculation of the measured pH. (The value of *r* is negative when representing a hydroxide concentration.) The mass-balance equations were refined concurrently so that the difference between the ECFC and CCFC was minimized. Metal-hydroxide formation constants, ligand protonation constants and the dissociation constant for water remain constant for the refinement process. The refinement process was accomplished with the 3D-CFC software (Cukrowski, 2000) which uses a non-linear least-squares method. The standard deviation of the fit (s_{yx}) (Equation 2.8) is then used to calculate a value for the overall fit.

$$s_{yx} = \frac{\sum(Y_{obs}-Y_{calc})^2}{N-P} \tag{2.8}$$

where Y_{obs} represents the value of the experimental corrected potential shift, Y_{calc} is the predicted value (based on solving the mass-balance equations), *N* is the number of data points and *P* is the number of parameters fitted. Species are speculated and their formation constants are estimated, then following the refinement process the fit indicates whether that species is likely to exist in solution or not. The important aspect when predicting species is the ratio between the ligand and the metal ion, (including hydrogen or hydroxides) – the exact structure or number of atoms in the species cannot be determined with this technique. The CCFC will be most similar to the ECFC when the complexes in solution are identified correctly and used in the calculation and refinement of formation constants. For an accurately described composition of the system, the CCFC will overlap well with the ECFC and the value of the overall fit will be small.

2.2.1.6 Relating Solution Species to Crystalline Complexes

Formation constants were used to plot species distribution diagrams for specific metal – ligand systems. This provides information about the species that are present in solution at particular pH values. The protonation constants for the ligand as well as the log β values for complexation of the metal ion with hydroxides and the ligand are taken into consideration. The SDDs are plotted for specific metal and ligand concentrations. The output is useful in making reasonable projections of pH values at which investigation for the formation of a particular crystal, containing the complexed metal ion, would be attempted.

2.3 CRYSTALLOGRAPHIC STUDIES

Solid state experiments involved the crystallization of complexes from solution under controlled conditions. Controlling the solution conditions from which crystallizations were to occur was of utmost importance for this research. Solutions

were made using analytical grade chemicals diluted with deionized water. Crystallizations were done strictly in aqueous media as we wanted to keep conditions as close to the solution studies as possible for the formation of a solid complex. The metal salt together with the ligand of interest was dissolved in deioinized water and acidified with HNO_3 where necessary, to allow complexes to form. At times solutions of the ligands were prepared and added to the metal ion solution, and other times the ligand was added as a solid to the metal ion solution. Two crystallization techniques (carried out in small glass vials) were employed: temperature-controlled slow-cooling in closed vials and room temperature crystallizations that were performed in closed or open vials where evaporation occurred at different rates.

The slow-cooling method was used predominantly when the ligand showed low solubility. The closed vial containing solid reagent and the metal ion solution was immersed into an oil bath heated to a specific temperature. That temperature was then maintained until the solid vial-contents completely dissolved. The oil bath was then set to cool to 25 °C at a specified rate. Temperature regulation was achieved using a locally modified oil bath, equipped with a programmable proportional-integral-derivative controller, in conjunction with a heating-stirring plate and a thermocouple. The set up can be seen below in Figure 2.9.

The other method that was used was achieved simply by placing the vial, either open or closed, with its solution (which sometimes did require heating, stirring or shaking to ensure complete dissolution of the solid ligand) on a bench top at room temperature. The solutions in the open vials undergo evaporation that eventually leads to the formation of single crystals or sometimes just powders. The closed vials, too, underwent evaporation but at a far lower rate than the open vials.

Experiments were conducted at various initial concentrations, temperatures, ligand-to-metal concentration ratios ([L]:[M]) and pHs. All pH adjustments were



Figure 2.9 Apparatus used in temperature controlled crystallizations.

accomplished by adding differing concentrations of HNO_3 or KOH to the solution before crystal growth. Solutions were allowed to reach point of crystallization regardless of the time required. Once crystals were formed, a small pH glass electrode (a Metrohm LL Biotrode and Metrohm 780 pH Meter) was used to measure the pH of the solution, and then crystals were immediately harvested, air-dried and stored in clean vials for single-crystal X-ray diffraction (SCXRD) and/or X-ray powder diffraction (PXRD).

The pH electrode was calibrated using three Metrohm buffer solutions (pH 3, 7 and 9). It was not necessary to calibrate using the titration method because as the SDDs indicate – that species are found in pH ranges, not at a specific pH value. Since pH is temperature dependent the electrode was calibrated at the temperature of the solution (which had to be within the temperature range where the electrode is fully

functional) and a Metrohm Pt 1000 thermocouple was used to measure the temperature. The Metrohm Biotrode was specifically used because of its low immersion depth (7 mm) and its reduced electrode tip (diameter 3 mm) allowing for pH measurements in very small volumes of solution. (Other particulars for this electrode are given in Table 2.3.) The functioning and storage of this electrode is the same as that discussed for the Ecotrode.

Table 2.3 Metrohm LL Biotrode specifications

Electrode characteristic	**Specification**
Shaft material	Glass
Membrane glass type	M*
Membrane resistance	300 - 600 MΩ
Diaphragm	Plied platinum wire
Diaphragm resistance	30 kΩ
pH range	0 - 14
Temperature range	0 - 60 °C
Catalogue number	6.0224.100

* M glass is colourless glass, having specific properties (response time, thermal resistance, chemical stability, shape, size and electrical properties) which are particular for the application of the electrode (Metrohm, 2012).

The potential measured by a glass electrode is dependent on the temperature of the solution (Haider, 2004), described by the Nernst equation:

$$E = E_0 + \frac{2.303RT}{z_i F} \times \log a_i \qquad (2.9)$$

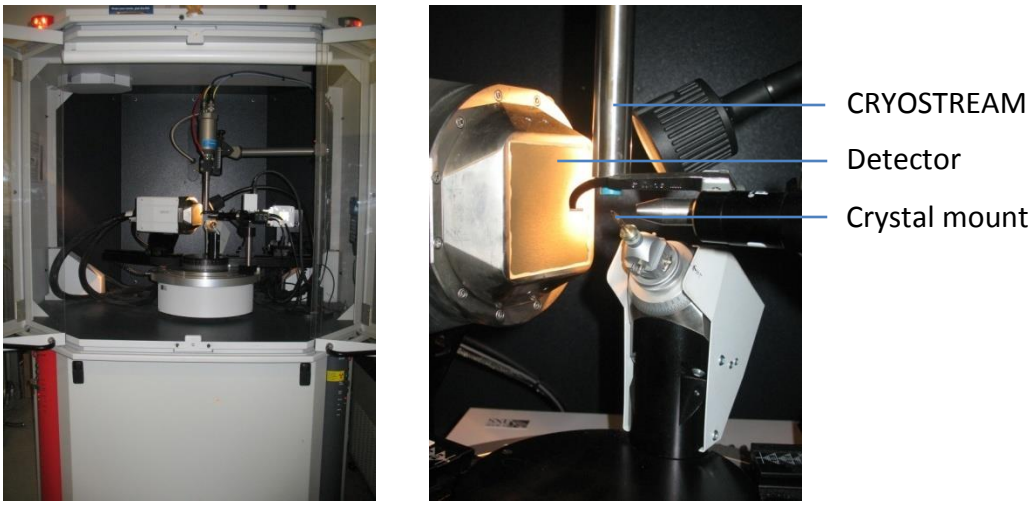
where E_0 is the standard potential of the GE, z_i the charge of the ion *i* measured (including sign) and a_i the activity of ion *i*. The Nernst slope differs at different temperatures. The Metro sensor pH electrodes with optimized inner buffer and long-life reference system allow for pH measurements throughout the whole temperature range – even if only calibrated at 25 °C. Although for increased

accuracy Metrohm suggests calibrating at the temperature at which the measurements are to be made (Metrohm, 2012).

The pH electrode was therefore calibrated at the temperature of solutions when the pH was adjusted and again when crystals were formed. The calibration was done using buffer solutions of pH 4, 7 and 9, which have slightly different pH values at different temperatures which the pH meter accounts for. The Metrohm pH Meter calculates the slope of the line when potential is plotted vs. pH. As discussed previously the ideal slope at 25, 32 and 40 °C are 59.16, 60.55 and 62.14 mV respectively (Haider, 2004).

2.3.1 Crystal Structure Determination

Analysis of crystals was done using two different x-ray diffractometers: a BRUKER SMART 1K Single Crystal diffractometer and a Bruker APEX II (see Figure 2.10). Each crystal was studied at -100 °C using a CRYOSTREAM which is designed for operation over a wide temperature range.



a) b)

Figure 2.10 a) The APEX II diffractometer, and b) a close up of the crystal mount, area detector and CRYOSTREAM.

Intensity data were collected on the Bruker SMART 1K CCD area detector diffractometer with graphite monochromated Mo K_α radiation (40kV, 40mA). The collection method involved ω-scans of width 0.3°. Data reduction was carried out using the program *SAINT+* (Bruker, 1999a) and face indexed absorption corrections were made (on certain structure data, to be discussed in the relevant chapters) using the program XPREP (Bruker, 1999a). Intensity data were collected on the Bruker APEX II CCD area detector diffractometer with graphite monochromated Mo K_α radiation (50kV, 30mA), and data collection was accomplished using the APEX II (Bruker, 2005a) software. The collection method involved ω-scans of a width of either 0.3° or 0.5° and 512 x 512 bit data frames. Data reduction was carried out using the program *SAINT+* (Bruker, 2005b) and face indexed absorption corrections were made using the program *XPREP* (Bruker, 2005b) where necessary. The crystal structures were solved by direct methods using *SHELX-97* (Sheldrick, 1997). Non-hydrogen atoms were first refined isotropically followed by anisotropic refinement by full matrix least-squares calculations based on F^2 using *SHELX-97* (exceptions will be discussed in the relevant chapters). In general, hydrogen atoms were positioned geometrically and allowed to ride on their respective parent atoms. Diagrams and publication material were generated using *Win*GX (Farrugia, 1999), *SHELX-97* (Sheldrick, 1997), *PLATON* (Spek, 2003), *ORTEP-3 (Farrugia, 1997)* and Mercury (Macrae *et al.*, 2006).

In the case of extremely small crystals the PROTEUM x-ray diffractometer was used for data collection. It is equipped with a PLATINUM 135 CCD detector and Montel 200 optics, using Cu K_α radiation (45 kV, 20 mA) from a Microstar rotating-anode generator. The collection method involved ω-scans of width 0.5° and 1024 × 1024 bit data frames.

PXRD was used in certain instances to ascertain whether the single crystal chosen for evaluation was representative of the entire sample. A bench top Bruker D2

diffractometer was used for this purpose. It was operated at 30 kV and 10 mA using a sealed copper tube. The detector was a LynxEye PSD with a 5 ° angular range and 2.5 ° radial soller slits for the primary and secondary beams. The measuring circle of the instrument was set at 141.4 mm.

2.3.2 Crystalline Complexes

A summary of the crystals of Cd(II) and Bi(III) complexes successfully prepared for this research is given in Table 2.4, where PIC represents picolinic acid, DIPIC represents dipicolinic acid, QUIN represents quinolinic acid and EDTA is ethylenediaminetetraacetic acid. The table includes each crystalline metal-ligand complex that was studied using SCXRD. The species name given represents the actual composition of the crystalline complex, except in the case of the bismuth(III)-quinolinate where the exact molecular formula could not be established due to the difficulty experienced in resolving the disordered crystal structure. The last column in Table 2.4 includes extra information specific to each crystal complex formed. An experimental section will be incorporated into each chapter where a number of attempts at growing crystals of metal-ligand complexes will be discussed, together with any other crystalline compounds that were identified.

Table 2.4 Summary of the experimental details for obtaining crystalline Cd(II) and Bi(III) complexes.

Species	[L]:[M] Ratio	[Metal] (Molar)	Initial Temp	pH Adjustment	Vial	Other Information
Cd(PIC-H)	1:1	0.5	Room	Slightly acidified	Open	Crystals at pH 0.4
$Cd(PIC\text{-}H)_3$	2:1	0.125	Room	None	Open	Crystals at pH 1.003
	3:1	0.125	Room	None	Open	Crystals at pH 1.293
Cd_2DIPIC_2·DIPIC-H_2	1:1	0.01	55 °C	HNO_3, pH 1.020	Closed	Slow cooled: 1°C/hr.
	2:1	0.005	55 °C	HNO_3, pH 1.088	Closed	Slow cooled: 1°C/hr.
$Cd(QUIN\text{-}H)_3$	1:1	0.05	65 °C	HNO_3, pH 1.480	Open	Crystals at pH 1.240
	2:1	0.05	65 °C	HNO_3, pH 1.366	Open	Crystals at pH 1.322
	3:1	0.05	65 °C	HNO_3, pH 1.268	Closed	Crystals at pH 1.268
Cd(QUIN)	1:1	0.005	Room	KOH, pH 4.078.	Open	pH not remeasured
	1:1	0.01	Room	KOH, pH 3.239.	Open	pH not remeasured
Bi-QUIN complex	3:1	0.05	40 °C	None	Open	Crystals at pH -0.198
Bi(EDTA-H)	1:1	0.01	40 °C	None	Open	Crystals at pH 0.380

2.4 REFERENCES

Billing, C. and Cukrowski, I., 2009. Glass Electrode Calibration for Use in the Voltammetric Determination of Stability Constants under Extreme Acidic Conditions. *South African Journal of Chemistry,* 62**,** pp 168-178.

Cukrowski, I., 1996. A polarographic method of speciation for labile metal-ligand systems based on mass-balance equations. A differential pulse polarographic study at fixed ligand to metal ratio and varied pH. *Analytica Chimica Acta,* 336 (1)**,** pp 23-36.

Cukrowski, I., 2000. 3D Complex Formation Curves. 5.00 ed.

Farrugia, L. F., 1997. ORTEP-3 for Windows - a version of ORTEP-III with a Graphical User Interface (GUI). *Journal of Applied Crystallography,* 30**,** pp 565.

Farrugia, L. F., 1999. WinGX suite for small molecule single-crystal crystallography. *Journal of Applied Crystallography,* 32**,** pp 837–838.

Haider, C. 2004. *Monograph: Electrodes in Potentiometry* [Online]. Herisau. Available: file:///C:/Documents%20and%20Settings/Administrator/My%20Documents/Downloads/955207_80155013.pdf.

Harris, D. C., 1995. *Quantitative Chemical Analysis,* New York, W.H. Freeman and Company.

Harris, D. C., 1998. *Quantitative Chemical Analysis,* New York, W.H. Freeman and Company.

Macrae, C. F., Edgington, P. R., McCabe, P., Pidcock, E., Shields, G. P., Taylor, R., Towler, M. and van de Streek, J., 2006. *Mercury*: visualization and analysis of crystal structures. *Journal of Applied Crystallography,* 39**,** pp 453-457.

Metrohm, 2012. Metrosensor electrodes 2012. Metrohm Ltd.

Spek, A. L., 2003. Single-crystal structure validation with the program *PLATON*. *Journal of Applied Crystallography,* 36**,** pp 7–13.

Chapter Three

The Diffusion Junction Potential

3.1 INTRODUCTION

One of the major problems faced when solving formation constants starting at low pH is the presence of the diffusion junction potential. The diffusion junction potential (E_j) exists at the interface of any two dissimilar solutions, i.e. the composition and/or concentration is different. In the cell used here, it occurs between the reference electrode solution and the salt bridge solution, as well as the salt bridge solution and the sample solution. Figure 3.1 shows a cell containing the three electrodes in the sample solution with the enlarged portion representing the diffusion junction potential which is created at the interface between the salt bridge and the sample solution. This is the largest contribution to E_j because of the type of ions present in both solutions, as well as the concentration of the sample solution that is changing throughout the titration. The two solutions in contact at this interface are 0.5 M KNO_3 in the salt bridge and initially 0.5 M HNO_3 (which gradually decreases in concentration and changes in composition as KOH additions are made) in the sample solution. The presence of the junction potential is caused by the movement of the ions (K^+, H^+ and NO_3^-) at differing ionic mobilities across the permeable ceramic frit. Ionic mobility is a quantitative measure of an ion's ability to move under the influence of a 1 V potential difference. The hydrogen ions pose the main problem because of their ability to move significantly faster than that of any other ion. The H^+ ion moves approximately 1.8 times faster than the OH^- ion, the ion that has the second highest mobility. (See Table 3.1 for the mobility of some ions of

interest.) When the sample solution is at its lowest pH, the E_j is greatest because of the high concentration of the H^+ ions which move through the permeable frit at a faster rate than the K^+ ions moving in the opposite direction. This creates a surplus of positively charged ions at the boundary in the salt bridge solution and leaves an excess of negatively charged ions in the sample solution, hence setting up a potential difference across the interface. This potential has to be accounted for as it is large and changing throughout the titration.

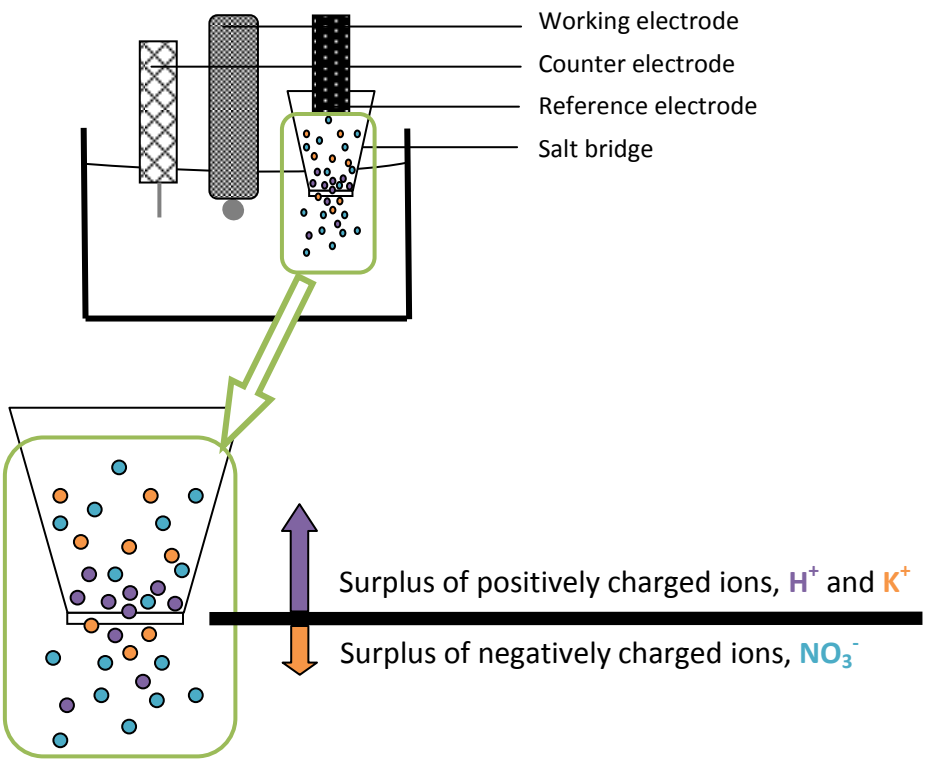


Figure 3.1 Schematic representation of a portion of the electrolytic cell and the diffusion junction between the sample solution and the salt bridge solutions.

The junction between the reference electrode solution (3 M KCl) and the salt bridge solution (0.5 M KNO_3) is relatively small because the mobility of the ions (K^+, Cl^- and NO_3^-) are similar and relatively low. The junction remains almost constant due to

the concentrations of the solutions essentially not changing throughout the experiment.

Table 3.1 Limiting ionic mobility for some important ions (Harris, 1995).

Ion	Mobility ($\times 10^{-8}$ m^2/sV)
H^+	36.3
OH^-	20.5
Cl^-	7.91
K^+	7.62
NO_3^-	7.4

The E_j at this interface was calculated to be approximately 2.8 mV (using the Henderson equation) and doesn't have to be compensated for, thus can be ignored.

In the polarographic experiments the current passing through the system is measured as a function of the applied potential. The overall potential is the sum of the reduction potential of the metal ion (or complex) of interest, measured relative to the potential of the reference electrode, and the diffusion junction potential. In order to calculate the reduction potential of the metal ion we need to obtain a measure of the E_j so that it can be subtracted from the overall recorded potential. This value can unfortunately not be measured directly during the experiment and so other approaches need to be undertaken to obtain its magnitude.

The junction potential between two solutions is described by the following equation:

$$E_j = -\left(\frac{RT}{F}\right)\int_1^2 \sum\left(\frac{t_i}{z_i}\right) d\ln a_i \qquad (3.1)$$

where t_i is the transference number, z_i the charge and a_i the activity of the *i*th ion in solutions *1* and *2* (Bagg, 1990). The transference number of an ion is the fraction of the total current that is carried by that ion during electrolysis. Different types of ions carry different fractions of the current because each ion has its own characteristic electrical mobility under the same potential gradient (Generalic,

2011). Transference numbers can be determined in a number of ways, the most common being the Hittorf method (Surampudi and Meeting, 2000). Others include electrophoretic nuclear magnetic resonance (Surampudi and Meeting, 2000), the direct moving-boundary method (Esteso, Esparza, Grandoso and Gonzalez-Diaz, 1987), electrochemical polarization, or they can be calculated on the basis of diffusion coefficients (obtained by NMR measurement) (Zhao *et al.*, 2008).

Activity of an ion, as featured in equation 3.1, is related to the concentration of that ion by the following equation:

$$a_i = \gamma_i c_i \tag{3.2}$$

The activity coefficient (γ) of a single ion cannot be measured directly because every electrolyte solution must be electrically neutral and therefore must contain both positively and negatively charged ions. For an ideal solution the activity coefficients for all the ions are unity and therefore activity is equal to concentration. At high ionic strength there are many more ionic interactions between ions and so the activity deviates considerably from the concentration (Zoski, 2007) and ionic mobility is also affected.

Henderson and Planck both derived equations from this fundamental model (Equation 3.1) in order to make the calculation accessible and quick. Henderson (1907) made a number of assumptions in order to arrive at the following equation:

$$E_j = \frac{RT}{F}\frac{(U_1-V_1)-(U_2-V_2)}{(U_1'+V_1')-(U_2'+V_2')} ln \frac{(U_1'+V_1')}{(U_2'-V_2')} \tag{3.3}$$

where $U = \Sigma c_+\lambda_+^\circ$, $V = \Sigma c_-\lambda_-^\circ$, $U' = \Sigma z_+c_+\lambda_+^\circ$ and $V' = \Sigma z_-c_-\lambda_-^\circ$. λ° denotes the conductivity, *c* the molar concentration and *z* the charge on each ion, and *1* and *2* denote two solutions having different compositions. The assumptions made by this equation include: (i) the presence of a linear concentration gradient in the transition zone (i.e. a constant activity gradient across the junction (Banica, 2012)), (ii)

diffusion takes place in one dimension, (iii) the mobility of ions is independent of the concentration (Rieger, 1994, Angst, Vennesland and Myrdal, 2009) and (iv) solutions are assumed to be ideal (activity coefficients are equal to unity (Winkelman *et al.*, 1984)). The Henderson equation has been used countless times because it "*generally leads to fairly accurate results"* (Angst, Vennesland and Myrdal, 2009).

The Henderson approximation is used more frequently than Planck's original equation as the latter is somewhat tedious and requires numerical evaluation by graph work or by trial and error (Morf, 1977). Morf (1977) simplified the original Planck equation in order to allow for effortless calculation of the response behaviour of any type of ion-selective liquid-membrane electrode. The extended Planck model is given by:

$$E_j = \frac{RT}{F} ln \frac{\sum(c_+u_+)_1 + \sum(c_-u_-)_2}{\sum(c_+u_+)_2 + \sum(c_-u_-)_1} \qquad (3.4)$$

where $u = \lambda \backslash IzIF$ and is valid if the concentrations of solutions *1* and *2* are the same and all ions are singly charged. The diffusion potential of biological membranes, described by Goldman (1943), equates to this extended Planck model. In the extended Planck model the following assumptions concerning the diffusion layer are made: (i) a steady-state potential is present, (ii) electroneutrality exists and (iii) only one class of mobile cations and anions are in solution (i.e. cations and anions must have the same magnitude of charge) (Morf, 1977).

Since these equations are based on a number of assumptions, they often do not necessarily fit the conditions of the specific experiment.

Cukrowski and Loader (1998) noticed a positive shift in reduction potential from pH 1 to pH 2.5 when comparing half-wave potential data for cadmium(II) when a pH titration experiment was conducted both without the ligand present, as well as when the ligand was included. At that stage they did not realize that this positive shift was in fact due to the diffusion junction potential but rather put it down to the

varying composition of the background electrolyte only (which theoretically is true). Later Cukrowski, Zhang and van Aswegen (2004) - more aware now of the presence of the diffusion junction potential - tried to experimentally obtain the change in diffusion junction potential with varying pH. However, they errantly ascribed complex formation of bismuth with nitrates from the background as part of the potential shift due to the diffusion junction. The general idea to determine the magnitude of the junction potential experimentally was useful and further work was done to improve its accuracy.

An important factor here is that the diffusion junction potential varies slightly for each titration and therefore doing two successive experiments (with and without the ligand as described by Cukrowski, Zhang and Van Aswegen (2004)) would still introduce some discrepancy. In order to overcome this concern the idea of incorporating a witness metal ion into the sample solution in a titration experiment was considered. The role of the witness ion is to indirectly monitor the diffusion junction potential in-situ, without it interfering with the metal ion or ligand of interest (Billing, Cukrowski and Jordan, 2013). Billing, Cukrowski and Jordan (2013) showed that using thallium(I) as the witness metal ion when studying the cadmium-picolinic acid system allowed for the experimental determination of the diffusion junction potential because thallium(I) did not form complexes with the ligand, nor did it overlap with the reduction signal of the metal ion. Experiments carried out with the aim to solely measure the diffusion junction potential have also been compared to calculated values and found to give a good correlation: “Diffusion potential values predicted by the Henderson formula are in fair accord with the experimental ones” (Banica, 2012) and “the calculated E_j values (using the Henderson or Planck equations) gave similar trends to those obtained experimentally” (Billing, Cukrowski and Jordan, 2013).

Calculated diffusion potentials, even though quite similar to measured values, are not sufficient for compensation within an experiment because the diffusion junction potential is specific for each titration. Also, during a titration in this work, the ionic strength varied and this was accounted for within the compensation of the diffusion junction potential. Without the in-situ witness these variations could not be determined.

3.2 EXPERIMENTS MONITORING THE DIFFUSION JUNCTION POTENTIAL

As an example we will look at a cadmium-ligand system and explain how the diffusion junction potential is monitored. The experimental determination of E_j using the in-situ witness ion for compensation of the polarographic data has been applied to complexation studies of dipicolinic acid and quinolinic acid with cadmium(II). Thallium(I) was used as the witness ion.

Polarographic studies from low pH, where the diffusion junction potential needs to be compensated for, require two types of experiments to be performed – one where the sample solution contains the metal ions as well as the ligand and one where the ligand is absent. The experiment without the ligand is important because it allows for an accurate determination of the diffusion junction potential (i.e. it acts as a reference data set). This experiment was repeated a number of times in order to obtain an average representation of the behaviour of the metal ions.

In the polarographic pH titration method, pH data and a polarogram are collected at intervals of ~0.1 pH unit. Figure 3.2 shows selected polarograms that were collected from a sample solution containing cadmium(II) and thallium(I) (without ligand) at increasing pH.

The waves at approximately -440 mV and -560 mV represent the reduction of the thallium(I) and cadmium(II) ions, respectively. The half reactions representing these processes are:

$$Tl^{+} + e^{-} \rightarrow Tl^{0}$$

$$Cd^{2+} + 2e^{-} \rightarrow Cd^{0}$$

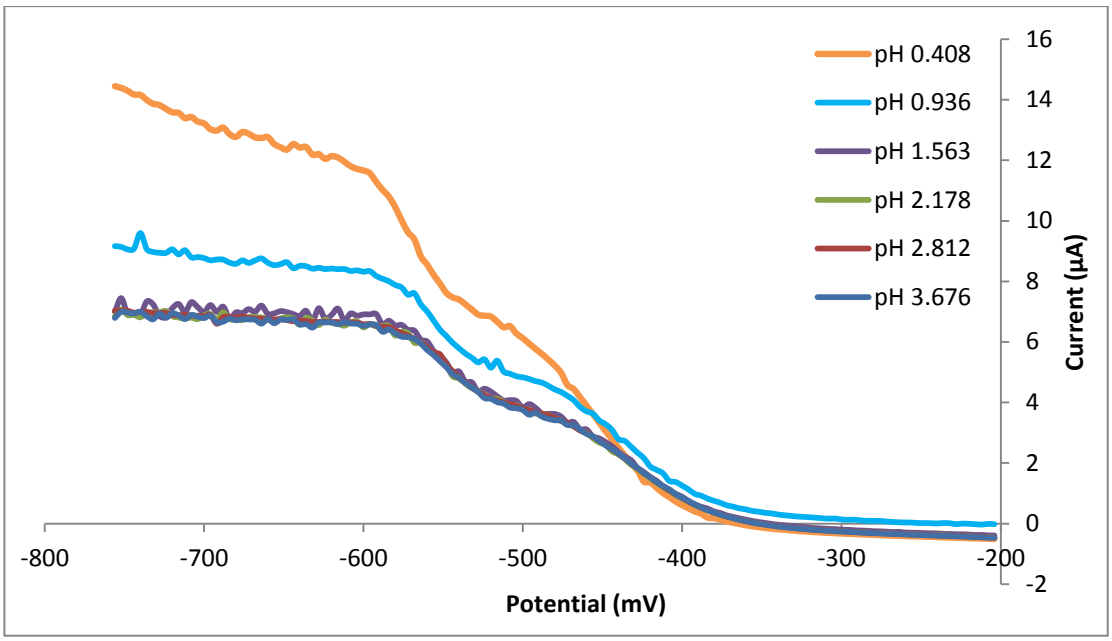


Figure 3.2 Polarograms showing Cd(II) and Tl(I) reduction in nitrate solution at varying pH.

The decrease in current is due to dilution of the metal ions in solution on addition of the KOH solution. In solutions of low pH, the onset of H_2 evolution is evident at the most negative potentials recorded as indicated by the increasing currents. As the pH increases the concentration of H^+ ions in solution decreases and therefore, so does H_2 evolution. The positive shift of the half-wave potential as pH is increased due to the changing E_j is clearly observed, especially below 2. Between pH values of 2 and 12 the junction potential remains relatively constant and so it can be ignored.

A graph of half-wave potential vs. pH (Figure 3.3) clearly shows the effect of the E_j. The half-wave potentials reach a plateau (above pH ~2) which corresponds to the free metal ion potentials ($E(M_{free})$) for cadmium(II) and thallium(I) where the E_j remains constant.

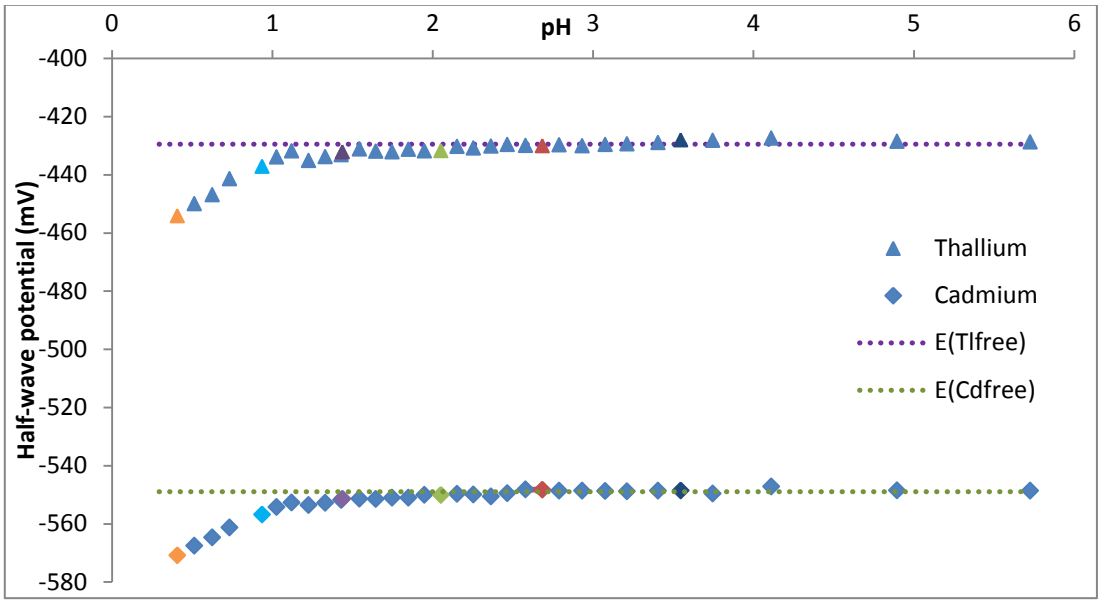


Figure 3.3 The half-wave potentials plotted as a function of pH for both Cd(II) and Tl(I) reduction. Coloured points correspond to polarograms plotted in Figure 3.2.

The free metal ion potential - the reduction potential of the metal ion when it is not complexed by a ligand - was determined for both cadmium(II) ($E(Cd_{free})$) and thallium(I) ($E(Tl_{free})$) by finding the average half-wave potential in the pH region where the junction potential was constant (above approximately pH 2), as indicated in Figure 3.3. At low pH, where the data points lie below the horizontal line, the magnitude of the diffusion junction potential is evident. The half-wave potential vs. pH curves (Figure 3.4) can be represented by two functions: a quadratic where the diffusion junction potential is changing, and a straight line (zero slope) where the

diffusion junction potential is constant and negligible. The functions serve to smooth the data.

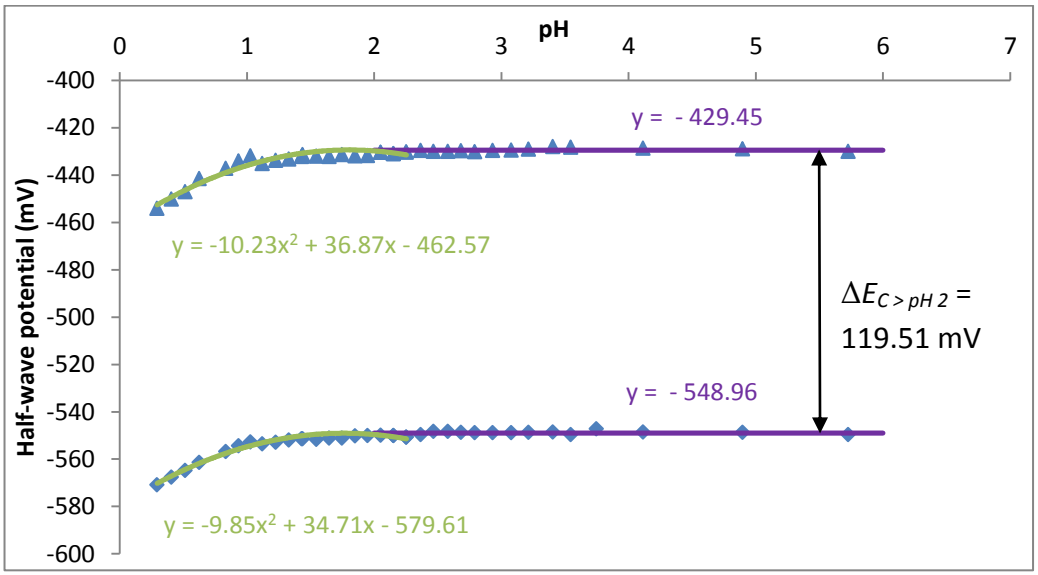


Figure 3.4 Quadratic and straight line functions fitted through the data points for cadmium(II) and thallium(I) reduction processes.

The potential difference between the thallium(I) and cadmium(II) straight line functions (above pH 2) (represented as $\Delta E_{C\ >\ pH\ 2}$, where *C* represents the compensation model) produces an average value of 120.0 ± 0.5 mV for five experiments. The values of $E(Tl_{free})$, the average $\Delta E_{C>pH\,2}$ and a compensation model (to be discussed shortly) will be used throughout the cadmium-ligand experiments to compensate for the positive shift of the cadmium(II) wave with increasing pH due to the diffusion junction potential. This positive shift has to be accounted for because complex formation is measured by the negative shift in half-wave potentials relative to that of the free metal ion potential as pH is increased. These two phenomena counteract each other and hence the E_j could possibly mask the presence of a complex, especially at very low pH where the E_j shift is largest. Figure 3.5 shows that the half-wave potentials determined from the initial polarograms, i.e.

the polarograms at the lowest pH, are most affected by the E_j. As the pH increases so the effect of E_j decreases and eventually becomes negligible and unchanging.

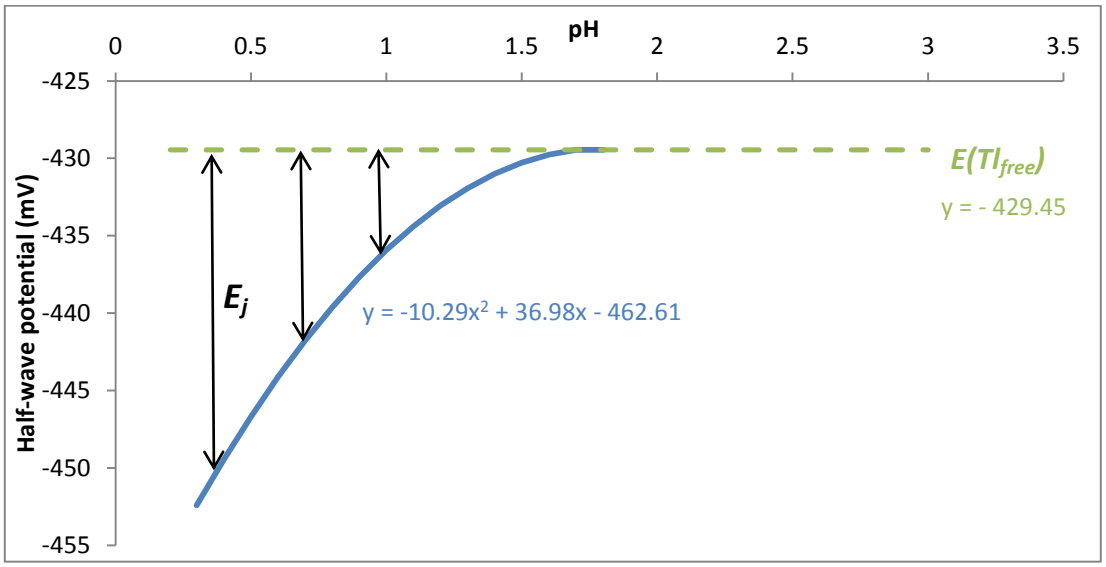


Figure 3.5 The magnitude of the diffusion junction potential at low pH values for thallium(I) calculated using the difference between $E(Tl_{free})$ and $E_{½}$.

The E_j was calculated at particular pH values by subtracting the fitted quadratic potential values from $E(M_{free})$. Magnitudes of the diffusion junction potential for both cadmium(II) and thallium(I) can be seen in Figure 3.6.

In Figure 3.6 there appears to be a difference in the E_j calculated for the two metal ions. The diffusion junction potential was calculated to be 2.97 mV greater for thallium(I) than for cadmium(II) at pH 0.3. This cannot be so because any ion present in a sample solution is equally affected by the diffusion junction potential. This small difference also cannot be due to experimental error because it was seen for every experiment, and was also seen by Billing, Cukrowski and Jordan (2013) who ascribe it to the changing ionic strength which affects the half-wave potential of the ions being reduced. Lingane (1939) first showed that the half-wave potentials experience a negative shift when the ionic strength is increased, and this can be

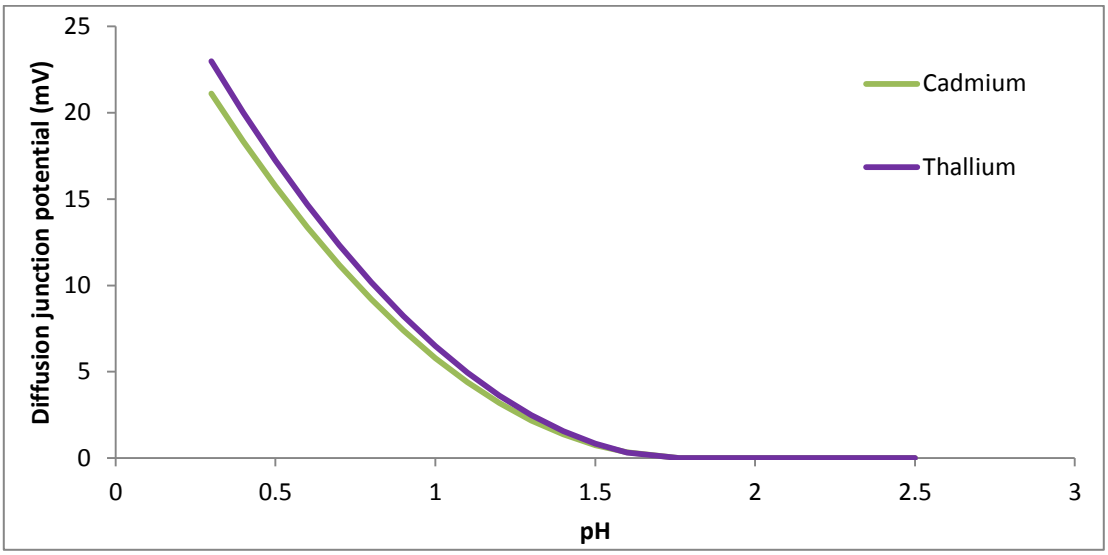


Figure 3.6 The diffusion junction potential for thallium(I) and cadmium(II) in nitrate solutions at low pH.

described mathematically. The magnitude of the half-wave potential ($E_{½}$) is dependent on diffusion rates and activity coefficients, and can be described by the following equation if the oxidized and reduced species remain in solution (at 25 °C) (Harris, 1998):

$$E_{1/2} = E^{\circ} - \frac{0.05916}{n} \log\left(\frac{\gamma_{red}\sqrt{D_{ox}}}{\gamma_{ox}\sqrt{D_{red}}}\right) \qquad (3.5)$$

where E° is the standard reduction potential (with respect to the standard calomel electrode), γ and D are the activity coefficient and diffusion coefficient, respectively, for the reduced (*red*) and oxidized (*ox*) species in solution. The log term is usually close to unity but an increase in the ionic strength of the solution causes a deviation from ideal behaviour. The activity coefficient of the ions in the supporting electrolyte then becomes less than one, hence causing the value for $E_{½}$ to shift in the negative direction (in relation to the value for E°).

Ideally we should keep the ionic strength the same throughout the experiment. Unfortunately this is not possible because experiments are conducted at relatively

low ionic strength and start at a very highly acidic pH. Addition of a supporting electrolyte would assist in maintaining the ionic strength, but it would mean that experiments would be run at a higher ionic strength. Also, the ionic strength of the solution affects the magnitude of the log β values.

The ionic strength is related to the sum of the squares of the electrical charges in solution per unit volume (McQuarrie and Simon, 1997), and can be calculated using the following equation:

$$\mu = \frac{1}{2}\sum_{i=1}^{n} c_i z_i^2 \qquad (3.6)$$

where c_i is the concentration and z_i the charge of the ith ion.

Initially thallium(I) and cadmium(II) were added to a 0.5 M HNO_3 solution which was then titrated with 0.5 M KOH. The metal ions had essentially no effect on the ionic strength of the solution due to their low concentrations. Small increments of the hydroxide solution were added to the acid to alter the pH, which led to the decrease in ionic strength because the HNO_3 reacts with the KOH to produce KNO_3 and H_2O. The KNO_3 contributes to the ionic strength of the solution because it is a salt and ionizes completely in solution, but water has an insignificant tendency to dissociate (as indicated by a low K_w value). The ions in solution are therefore diluted and consequently decrease the ionic strength, as shown in Figure 3.7.

In the low pH region the ionic strength changes rapidly with an increase in pH because larger amounts of hydroxide are required to change the pH by 0.1 units at low pH. As the pH is increased, less hydroxide is required to change the pH and therefore the dilution effect gradually becomes negligible. The ionic strength therefore remains relatively constant at about 0.25 M, and thus the $\Delta E_{C\ pH>2}$ value - a constant value - can be used to describe data in this region.

Billing, Cukrowski and Jordan (2013) measured $E_{½}$ values of cadmium(II) and thallium(I) in KNO_3 solutions of 0.5 M and 0.25 M ionic strengths. They found that the potential for thallium(I) decreased by 2 mV when going from a 0.5 M to a 0.25 M

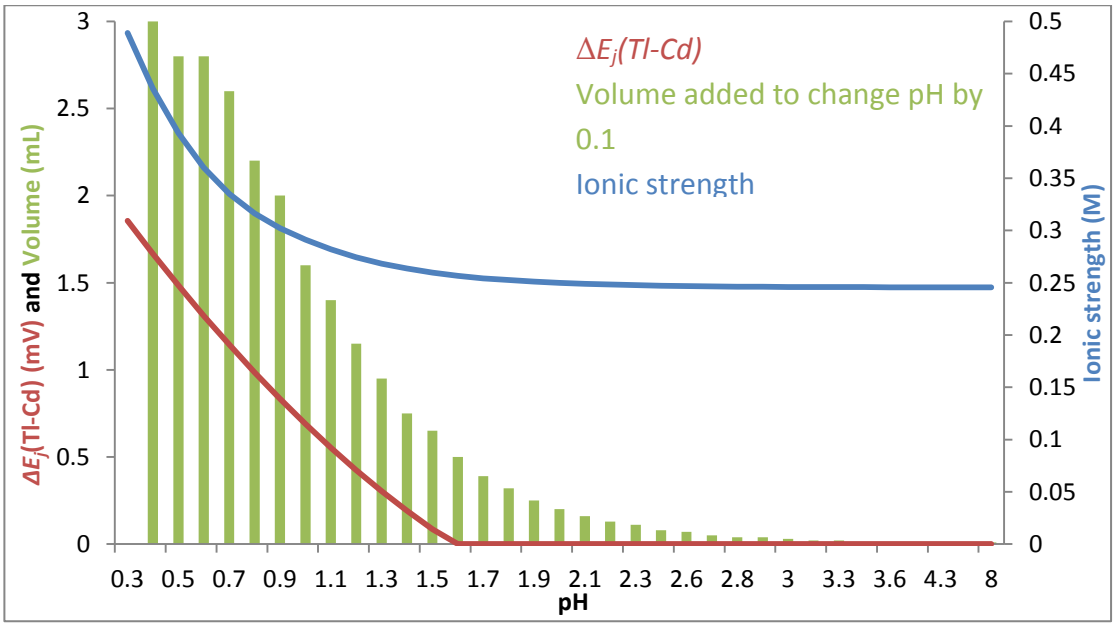


Figure 3.7 The volume of KOH used to adjust the pH of the sample solution by 0.1 units together with its effect on the ionic strength and ΔE_j.

solution, while that of cadmium(II) remained unchanged. The discrepancy in E_j magnitudes in Figure 3.6 depicts this finding. If the ionic strength was maintained at 0.5 M throughout the pH range, we would expect that the cadmium(II) and thallium(I) graphs of E_j vs. pH be the same. Figure 3.8 demonstrates this point by showing that the difference between the thallium and cadmium E_j data is caused by the changing ionic strength which affects the magnitude of the free metal ion potential for thallium(I).

The free metal ion potential used to calculate E_j for thallium(I) is not representative of its value at 0.5 M ionic strength. For cadmium(II) this problem does not exist because its $E_{½}$ value is the same at 0.5 M and 0.25 M ionic strength. The $E(Tl_{free})$

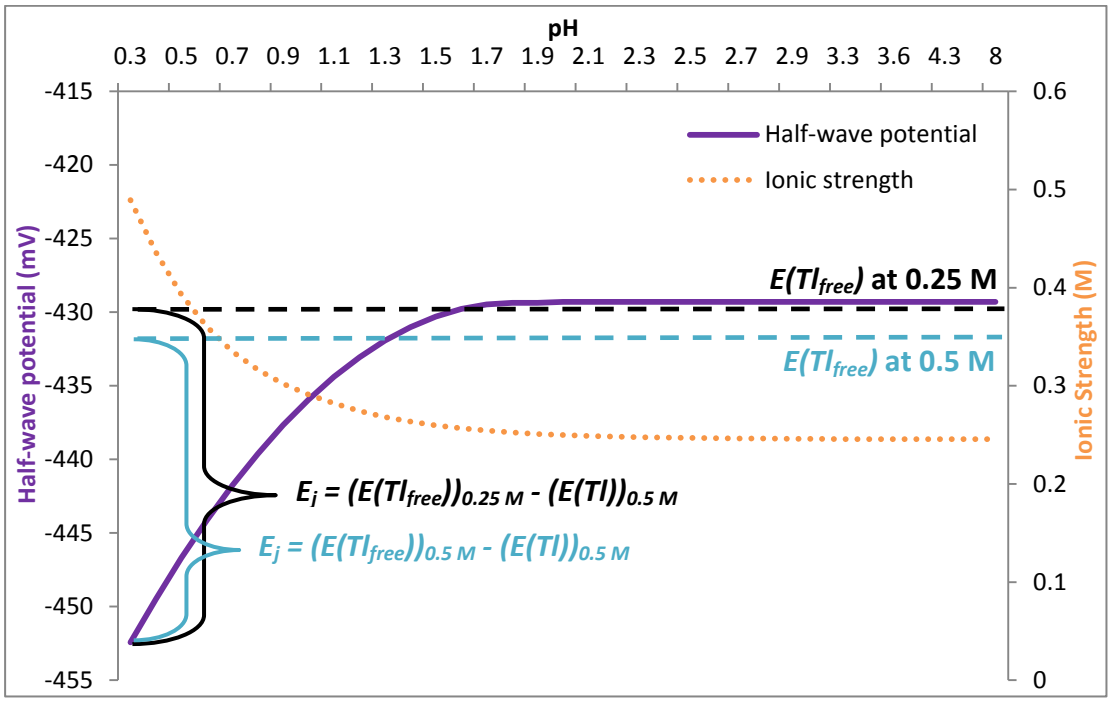


Figure 3.8 Simulation showing that the effect of changing ionic strength on the diffusion junction potential for thallium(I) is greater than what it would be if ionic strength was maintained at 0.5 M.

value calculated from experimental data (the average of the $E_{½}$ values above pH 2) is where the ionic strength of the solution is approximately 0.25 M (Figure 3.8). It is evident that the deviation in ΔE between the thallium(I) and cadmium(II) data is largest at the lowest pH, and gradually decreases as the pH is increased, or more importantly, as the ionic strength decreases. The same ΔE value could be used throughout the pH range, and not only above pH 2, if and only if, both metal ions were affected equally by the change in ionic strength. Unfortunately this is not the case and therefore this difference is accounted for in the calculated E_j for the two metal ions by modelling the behaviour of the metal ions in solution below pH 2.

When ligand is present in the experiment we do not have this plot of E_j vs. pH for cadmium(II); we only have it for thallium. We therefore have to use thallium(I) data

to predict this plot for cadmium(II) as closely as would be obtained experimentally, which is why the model is so important. Increasing the number of replicate experiments performed without ligand provides greater confidence in this model.

For bismuth experiments this same approach cannot be used because hydrolysis and complex formation with the background electrolyte occurs, thus the free metal ion potential cannot be determined from bismuth(III) half-wave potential values. We therefore do not have a reference point from which a model can be built. In this case it is assumed that the calculated diffusion junction potential for thallium(I) is the same for bismuth(III) - a fair assumption since the change in the half-wave potential for thallium(I) was only about 2 mV due to ionic strength changes. Compensation and calculation of the diffusion junction potential for this system will be discussed in Chapters Nine and Ten.

3.3 THE COMPENSATION MODEL

The compensation model presented in this section of work was applied to the cadmium(II)-ligand systems of quinolinic acid and dipicolinic acid (at 25 °C only).

The potential shift of the cadmium(II) wave was studied relative to that of the witness ion (thallium(I)) for a number of experiments and the average relationship was modeled. When the titration experiment is then conducted with ligand (a complex formation experiment), the shift of the witness ion wave is again only due to the diffusion junction, while that of cadmium(II) occurs because of the diffusion junction as well as complex formation (in opposite directions with increasing pH). The model is used together with the witness ion data to compensate for the diffusion junction potential for cadmium(II) so that its resulting potential shift represents complex formation only.

Five experiments were conducted without ligand (interspersed between complex formation experiments). The difference between the half-wave potentials of thallium(I) and cadmium(II) were calculated at each pH for every dataset. The data were modeled and is called the "compensation model" in this work. Two types of compensation models were considered. Firstly, the actual raw data points were used to calculate the difference and this is referred to as a POINTS (P) model (Figure 3.9). Secondly, the quadratic and horizontal lines fitted to the raw data points of each dataset (below and above approximately pH 2, respectively) as discussed previously (see Figure 3.4) were used to calculate the difference and this is referred to as a CURVES (C) model (Figure 3.10). A third order polynomial was fitted through the combined data for each model. These models represent the average behavior of the difference in the half-wave potentials of the metal ions when no complexes are being formed.

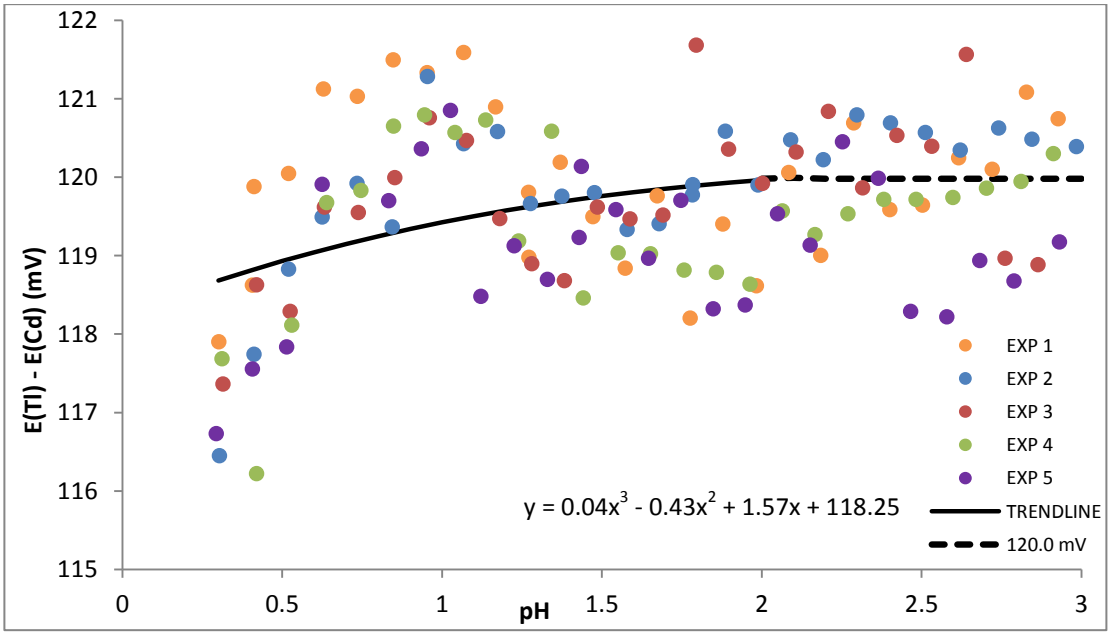


Figure 3.9 P-model at low pH calculated from five datasets.

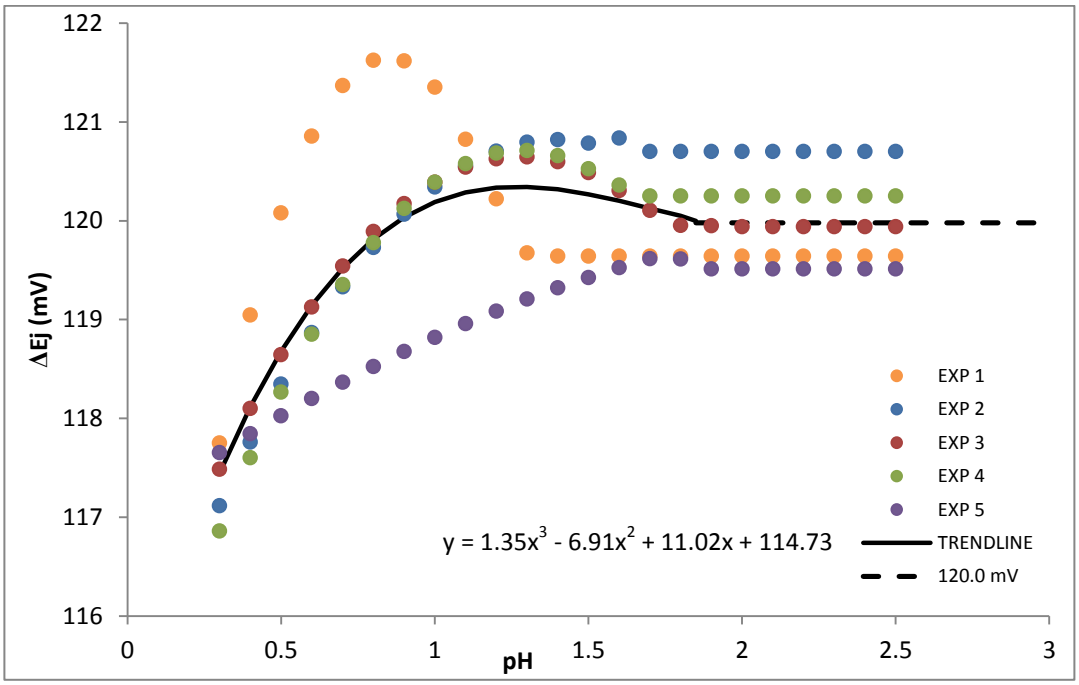


Figure 3.10 C-model at low pH calculated from five datasets.

Three of the five datasets were very similar, but experiment 1 and 5 differed from them and from each other and is particularly pronounced in the C-model. The question was if data from these two experiments should be included in the model or not? How should the model be created? Which model best represents the data more accurately – P or C? To answer these questions, either all or only a select few of the five datasets were combined to build different models. Five different C-models and three different P-models were created to test whether there was a significant difference between them, and if so, which model was the most representative.

Models C(I) and P(I) include all five datasets, C(II) and P(II) exclude experiment 1 (which was obtained using a different glass electrode which essentially should not make a difference), C(III) excludes experiment 5, C(IV) also excludes experiment 5 but only data up to pH 1.8 for each experiment is used, C(V) excludes experiment 2 and 3 (which were collected successively with experiment 4, and should therefore

not weight the average too heavily), and P(III) includes all five datasets but the extreme outliers were removed. Figures 3.9 and 3.10 show models P(I) and C(I), respectively.

The average model in each case is given in Table 3.2. The trinomial describes data below pH 2, and the averaged ΔE describes data above pH 2 (named to $\Delta E_{C>pH\ 2}$). The averaged $\Delta E_{C>pH\ 2}$ value was calculated the same way for the C- and P-models using the difference of the average value of the experimental thallium(I) and cadmium(II) points. Figure 3.11 is a comparison of all the different points and curves models.

Table 3.2 Functions corresponding to each of the Compensation models.

Model	**Average $\Delta E_{C>pH\ 2}$ (mV)**	**Compensation Equation**
C(I).	120.0 ± 0.5	y= 1.35 x^3- 6.91 x^2+11.02 x+ 114.73
C(II).	120.1 ± 0.5	y=0.99 x^3- 5.48 x^2+9.70 x + 114.76
C(III).	120.1 ± 0.4	y=1.70 x^3- 8.53 x^2+ 13.18 x+ 114.17
C(IV).	120.1 ± 0.4	y=2.63 x^3- 11.65 x^2+ 16.23 x + 113.36
C(V).	119.8 ± 0.3	y=1.43 x^3- 7.04 x^2+ 10.71 x + 114.99
P(I).	120.0 ± 0.5	y= 0.04 x^3- 0.43 x^2+ 1.57 x + 118.25
P(II).	120.1 ± 0.5	y=0.05 x^3- 0.59 x^2+ 2.08 x + 117.75
P(III).	120.0 ± 0.5	y=0.04 x^3-0.42 x^2+ 1.53 x + 118.28

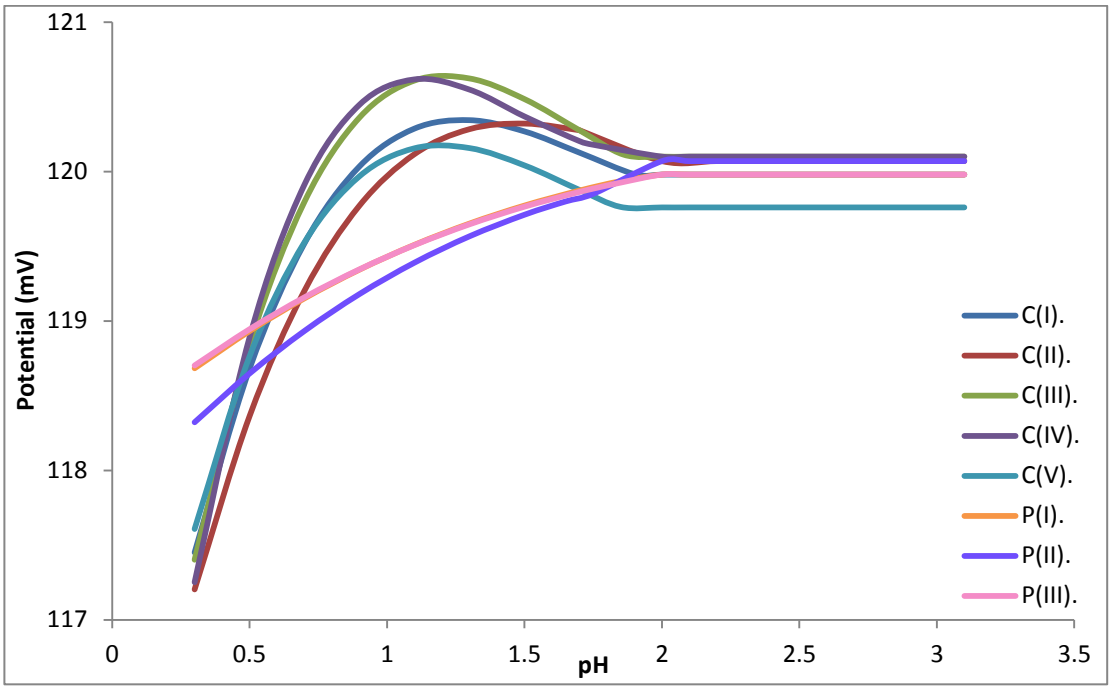


Figure 3.11 Comparison of all the C- and P-models.

3.3.1 Testing the Various Models

The compensation models can be tested in two ways, for:

1) Accuracy: using an experiment where no complexation occurs, the cadmium data are predicted using the models and compared to the actual experimental data.
2) Precision: using a complexation experiment, different models are applied and resulting formation constants are compared.

3.3.1.1 Testing Accuracy

Two ligand-free experiments (experiments 2 and 4) that were used in creating some of the compensation models were tested by comparing the predicted cadmium(II) potential data with the experimentally obtained data. Comparison of only models P(I) and C(I), and then P(II) and C(II) were done because using the other models

would create a bias depending on whether experiment 2 or 4 was purposefully included or excluded from the model.

The thallium(I) data for experiments 2 and 4 reach a maximum half-wave potential at about pH 2.4 and so the compensation model was used up to this pH in each case. From above pH 2.4 the $\Delta E_{C>pH\ 2}$ value is used to calculate the cadmium potential. Throughout the pH range the raw thallium (I) half-wave potential data are used. Figure 3.12 shows the actual experimental cadmium(II) data obtained for experiment 2, and that predicted using the P(I), C(I), P(II) and C(II) compensation models.

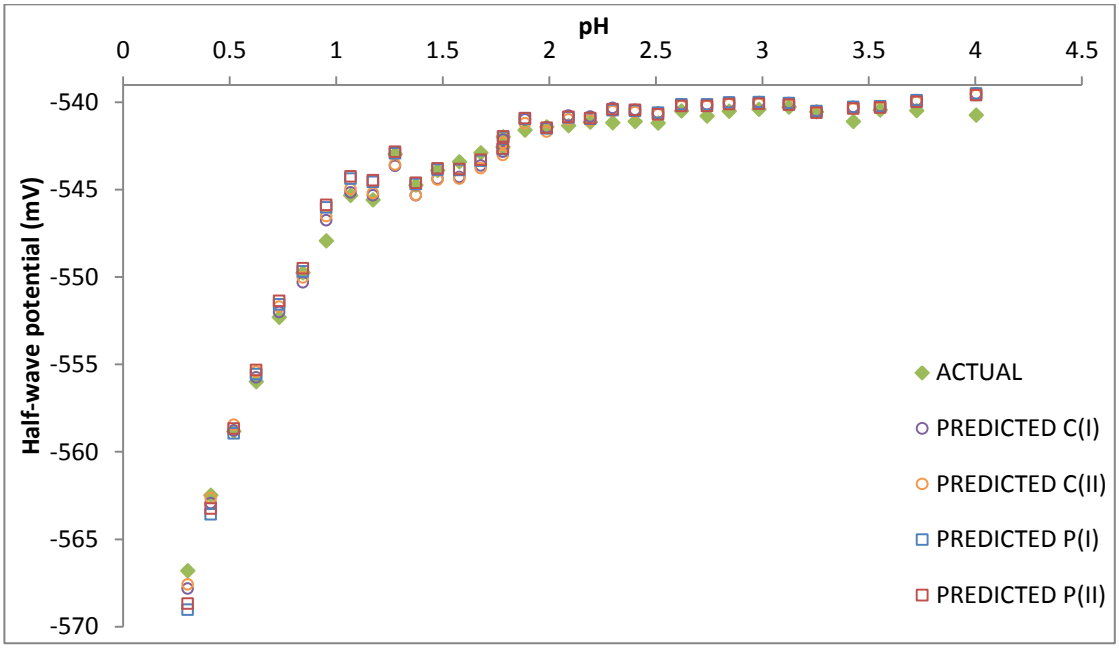


Figure 3.12 Comparison of actual and predicted cadmium(II) half-wave potential data for experiment 2 using various compensation models.

To compare the actual and predicted data across the pH range the standard deviation of the fit (s_{yx}) (see Equation 2.8) was calculated for each model. Although this relationship is usually used to compare raw data to a function fitted to the data,

it was applied here and, since a trinomial is usually fitted to the data below pH 2, the number of parameters (*P*) was set equal to 3. The results are given for each experiment in Table 3.3. The closer a s_{yx} value is to zero the better because you summing the errors.

Table 3.3 The standard deviation of the fit calculated for models P(I), C(I), P(II) and C(II).

	s_{yx}	
Model	**EXP 2**	**EXP 4**
P (I).	0.6304	0.9286
C (I).	0.3852	0.7200
P (II).	0.5944	0.8918
C (II).	0.3628	0.8372

The compensation for experiment 2 was more accurate than that for experiment 4 for all these models which would be an indication of how closely the data follow the average model and also the noise associated with the actual raw experimental data. According to these results the C-models best predict the cadmium(II) data for both experiments.

3.3.1.1 Testing Precision

Hypothesis: The model used for E_j compensation affects the magnitude of the formation constants.

Null hypothesis: There is a significant difference between the formation constants calculated when using different compensation models.

Alternative hypothesis: There is no significant difference between the formation constants calculated when using different compensation models.

Two complex formation experiments were used to test the null hypothesis, one using dipicolinic acid and the other quinolinic acid, both present in 50 times the concentration of cadmium(II). Each of the eight models was used to calculate the E_j for cadmium(II) and the resulting data, which represented potential shifts only due to complex formation of cadmium(II), was used to calculate formation constants. Three appropriate metal-ligand complexes were fitted to the dipicolinic acid data and two to the quinolinic acid data. At this stage it is not important to explain what these complexes were or what the value of their formation constants were. Each metal-ligand complex was considered separately and an average value obtained for both the C- and P-models. It is the size of the standard deviation of this average for each complex that is necessary when testing the precision of the models. The results can be seen in Table 3.4.

The standard deviation of the average of the C-models was small for each complex. Complex 1 for both dipicolinic and quinolinic acid have the largest deviations due to their existence in the low pH region where the E_j and changing ionic strength have their greatest effect. (It should be noted that complex 1 forms at a lower pH for dipicolinic than for quinolinic acid and so it is not surprising that there is a larger discrepancy in the formation constants of the former.) Their values are still small enough though to conclude that the prediction with the various models is not significantly different from each other. The standard deviation of the average of the P-models was very low for each complex, thus we can conclude that there is no significant difference between the P-models. The standard deviations are lower for the P-models which was expected because they are obtained from only three values, as opposed to the curves models which average five different values.

Comparing the average of the C-models with that of the P-models for each complex was achieved by using the student's *t*-test for the comparison of replicate

measurements for two sets of data where their sample sizes and means differ. The following equation is used to calculate the value of t_{calc}:

$$t_{calc} = \frac{|\bar{x}_1 - \bar{x}_2|}{s_{pooled}} \sqrt{\frac{n_1 n_2}{n_1 + n_2}} \quad (3.7)$$

where $\bar{x}_1$ and $\bar{x}_2$ are the mean values for replicates 1 and 2 respectively, n_1 and n_2 are the number of measurements for replicate 1 and 2 respectively, and s_{pooled} is the pooled standard deviation, which is calculated as follows:

$$s_{pooled} = \sqrt{\frac{{s_1}^2(n_1 - 1) + {s_2}^2(n_2 - 1)}{n_1 + n_2 - 2}} \quad (3.8)$$

where ${s_1}^2$ and ${s_2}^2$ represent the variance of replicate measurements for 1 and 2 respectively, and (n_1 + n_2 - 2) represents the degrees of freedom. For 6 degrees of freedom (n_1 = 5, n_2 = 3) the t_{table} value at the 99.9% confidence interval is 5.959 (see Table A3.1, Appendix A). The calculated *t* values for each complex for both ligand experiments are shown in Table 3.4.

Table 3.4 Results for the student's t-test comparing points and curves models used on two separate experiments.

	CURVES		POINTS		CURVES vs. POINTS	
50x DIPIC	**Average ($\bar{x}_1$)**	**Std Dev**	**Average ($\bar{x}_2$)**	**Std Dev**	**t_{calc}**	**t_{table} @ 99.9%**
Complex 1	8.263	0.013	8.310	0.006	5.860	
Complex 2	6.631	0.008	6.618	0.003	2.891	5.959
Complex 3	11.132	0.004	11.134	0.002	0.968	
50x QUIN	**Average ($\bar{x}_1$)**	**Std Dev**	**Average ($\bar{x}_2$)**	**Std Dev**	**t_{calc}**	**t_{table} @ 99.9%**
Complex 1	3.97	0.01	3.976	0.003	0.183	5.959
Complex 2	6.42	0.02	6.4123	0.0006	0.900	

$t_{calc} < t_{table}$ at the 99.9% confidence level and therefore we reject the null hypothesis, i.e. there is no significant difference between the two types of compensation models. To keep the process standard a single compensation model must be

selected and used throughout. The curves models consistently gave the lowest standard deviation of fit for the accuracy test (as seen in Table 3.3). This outcome makes sense as the curves models are produced from smoothed data where any outliers are taken into consideration by a best fit curve. Because there is no significant difference in the precision between the C-models all data were compensated for using the C(I) model because it contains all five datasets and is therefore most representative (Figure 3.9). This model is used to predict the uncomplexed (free) cadmium(II) data in experiments where complexes are formed so that the diffusion junction potential for cadmium(II) can be calculated and compensated for. This model is specific to cadmium(II)-ligand systems for particular background conditions where complexation occurs at 25 °C. For experiments conducted at different temperatures a new model must be created where the diffusion junction potential and ionic strength changes are monitored at the required temperature.

Compensation for E_j is done by substituting the pH values (pH < 2) at which each polarogram was recorded into the equation of the C(I) model to obtain potential values which represent the difference between the thallium(I) and cadmium(II) data if no complexation was taking place. Above pH 2, where the ionic strength is essentially constant, the difference in potential between thallium(I) and cadmium(II) is constant, and so the average $\Delta E_{C>pH\ 2}$ value is used (120.0 mV - Table 3.2). These values are then subtracted from thallium(I) data points at corresponding pH values to obtain "predicted uncomplexed cadmium potential shifts". The free metal ion potential for cadmium ($E(Cd_{free})$) is calculated by subtracting the average $\Delta E_{C>pH\ 2}$ value from the free metal ion potential of thallium ($E(Tl_{free}) - \Delta E_{C>pH\ 2}$ (120.0)). Now the magnitude of the E_j can be calculated by subtracting the "predicted uncomplexed cadmium potential shifts" from the free metal ion potential ($E(Cd_{free})$). The complexed-cadmium potential data are then compensated for by adding the

value of E_j at the corresponding pH values. These new data represents shifts in potential due to complexation only (i.e. E_j has been compensated for).

3.4 COMPARING E_j CALCULATED USING THE HENDERSON EQUATION TO THAT DETERMINED EXPERIMENTALLY IN THE ABSENCE OF LIGAND

The E_j values were calculated by the Henderson equation (Equation 3.3) using limiting ionic mobilities and a constant ionic strength of 0.5 M for the background solution. These values were then manipulated to reflect the difference in magnitude of the E_j, i.e. E_j at pH < 2 (when it is changing with pH) is subtracted from E_j at pH > 2 (where it is basically constant). Figure 3.13 shows that the measured diffusion junction potential was zero from pH 1.8; importantly the zero reading on the y-axis indicates that the E_j is not changing. Since the measured half-wave potentials only allow for the calculation of the change in the magnitude of E_j, the change in E_j as calculated by the Henderson equation is also considered here. Above pH 2 E_j is zero (up to about pH 10) and any deviation from this was calculated. The relationship between the experimentally determined E_j and that calculated by the Henderson equation was found to be similar for all experiments (see Figure 3.13).

It is evident that the calculation of the E_j using the Henderson equation does not fully agree with the diffusion junction potential calculated using the free metal ion potential together with the potentials measured by the in-situ witness ion. A similar deviation was seen for all experiments. The mobilities of the ions in solution are used in the Henderson equation and these mobilities depend on a number of variables such as temperature, the type of solvent, ion-specific properties (such as particle size, shape and charge) as well as on the ionic strength of the solution (Jouyban and Kenndler, 2006). Since the ionic strength varied throughout the titration (see Figure 3.8) it was decided to take this into account when calculating E_j.

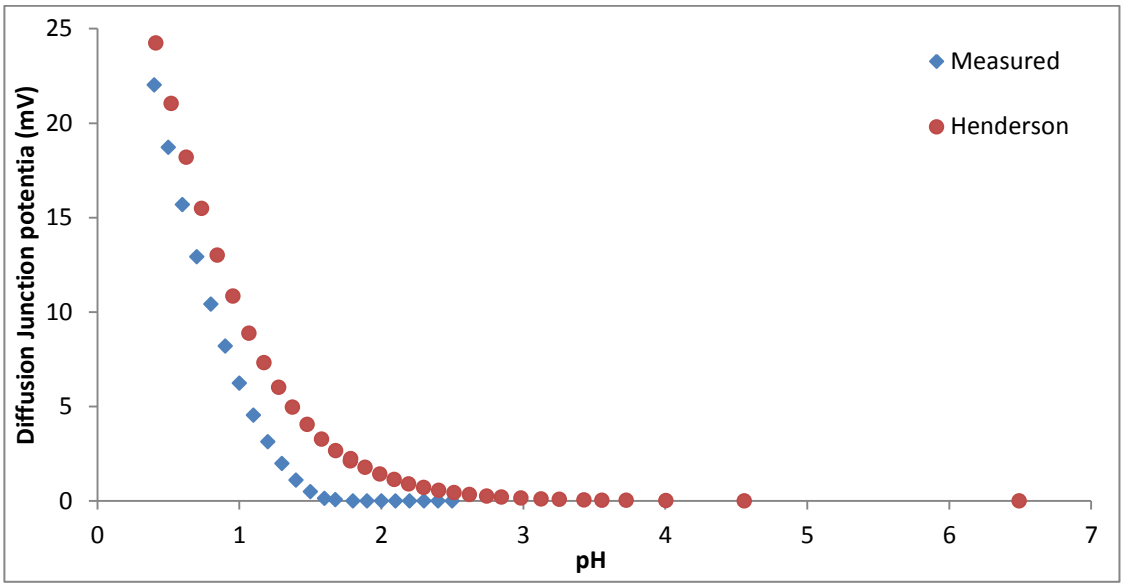


Figure 3.13 Comparison of the change in measured diffusion junction potential for cadmium(II) with that calculated using the Henderson equation (using limiting ionic mobilities).

At the lowest pH where ionic strength is 0.5 M, the E_j calculated by Henderson is similar to that predicted using thallium(I). As the pH is increased (and hence the ionic strength decreased) the deviation is increasing in accordance with the decrease in ionic strength. Simply considering ionic strength and mobility it was assumed that the deviation could possibly be minimized.

The ionic strength of the sample solution decreases and so the mobility of the ions should increase. The Onsager limiting law can be used to calculate mobility of ions with respect to the ionic strength. Its validity has been verified for ionic strengths up to 0.1 M in the article by Zusková, Novotná, Včeláková and Gaš (2006). Here experiments are conducted at much higher ionic strengths (0.25 to 0.5 M) where more interactions between ions occur and therefore values predicted by the Onsager equation would only be an estimate. The following equation (manipulated from the original Onsager equation) is written for a cation but it can be equally applied to an anion (Zusková, Novotná, Včeláková and Gaš, 2006):

$$u_+ = u_+^o - \left(u_+^o z_+ |z_-| B_1 \left(\frac{q}{1+\sqrt{q}}\right) + B_2 z_+\right)\left(\frac{\sqrt{\mu}}{1+Ba\sqrt{\mu}}\right) \quad (3.9)$$

where u_+ is the mobility of the cation, u_+^o is the limiting cationic mobility (i.e. the mobility at infinite dilution), z_+ and z_- are the charges on the cation and anion, respectively, and μ is the ionic strength. B_1, B_2 and B are constants which are dependent on the solvent and the temperature used. a is a parameter which describes the effective diameter of the cation, which ranges between 0.3 and 0.5 nm, and therefore Ba can be approximated to 1.5 $(\text{mol.dm}^{-3})^{-½}$. For an aqueous solution at 25 °C the parameters are: B_1 = 0.7817 $\text{mol}^{-½}$ and B_2 = 3.14 × 10^{-8} $\text{m}^2\text{V}^{-1}\text{s}^{-1}\text{mol}^{-½}$. q is a parameter which is calculated for the background electrolyte using the following equation:

$$q = \left(\frac{z_+|z_-|}{z_+ + |z_-|}\right)\left(\frac{u_+^o + u_-^o}{|z_-|u_+^o + z_+ u_-^o}\right) \quad (3.10)$$

If the electrolyte is symmetrical (i.e. $z_+ = z_-$) then q = 0.5 (Zusková, Novotná, Včeláková and Gaš, 2006).

Ibrahim, Ohshima, Allison and Cottet (2012) describe the mobility of a cation (also applicable to the anion) with a more simple equation – the extended Onsager model or Debye−Hückel−Onsager equation:

$$u_+ = u_+^o - (A_1 + A_2 u_+^o)\left(\frac{\sqrt{\mu}}{1+Ba\sqrt{\mu}}\right) \quad (3.11)$$

This equation is applied to studying the electrophoretic mobility of an ion as a function of ionic strength particularly for small ions that are singly charged (Ibrahim, Ohshima, Allison and Cottet, 2012). A_1, A_2 and B are Pitts parameters which are defined for fully dissociated 1:1 electrolytes, having a specific temperature, electrolyte viscosity and relative dielectric constant. For an aqueous solution at 25 °C the parameters are: A_1 = 3.14 × 10^{-8} $\text{m}^2\text{V}^{-1}\text{s}^{-1}\text{mol}^{-½}$, A_2 = 0.229 $\text{mol}^{-½}$ and B = 0.3288 $\text{Åmol}^{-½}$. Ibrahim, Ohshima, Allison and Cottet (2012) suggest determining

the radius and limiting mobility of the ion by nonlinear curve fitting of experimental effective mobilities. No electrophoretic experiments were done here so the assumption by Zusková, Novotná, Včeláková and Gaš (2006) that $Ba \approx 1.5$ units (i.e. $(mol.dm^{-3})^{-½}$) was used, together with the limiting mobilities given by Harris (1995) in Table 3.1.

Ionic strength and corresponding mobilities of ions were calculated at each pH at which a polarogram was recorded. The H^+ mobility was calculated at each solution composition using both the Debye−Hückel−Onsager equation and the Onsager limiting law, but the difference between the values was not significant (the largest difference giving a relative standard deviation of 0.0027%). Thereafter the mobilities of all ions were calculated at each pH as a function of ionic strength using only the Onsager limiting law (Equation 3.9). Table 3.5 shows these values at selected pHs. These mobilities had to be related to conductivities in order to be used in the Henderson equation. The relationship between conductivity and mobility is given by the following equation:

$$\lambda = u|z|F \tag{3.12}$$

where λ denotes the conductivity, *F* is Faraday's constant and *z* is the charge on the ion. The Henderson equation was then employed to calculate the diffusion junction potential (Table 3.5 shows selected values).

As the ionic strength increases so the mobility decreases, as expected. The actual mobility at 0.1 M was calculated because this is the highest ionic strength at which the Onsager limiting law should be used. The values calculated at higher ionic strengths are just an estimate. The diffusion junction potential calculated using the Henderson equation using these values increases at higher ionic strengths. Figure 3.14 shows the measured diffusion junction potential for thallium(I) and

cadmium(II), as well as that calculated using the Henderson equation with mobilities at infinite dilution and mobilities at the ionic strength of the solution for each pH.

Table 3.5 Comparison of ionic mobilities at infinite dilution and those calculated at the given ionic strengths using the Onsager limiting law. The actual E_j was calculated using the Henderson equation.

pH	Ionic strength (M)	Mobility (x10^{-8} m^2/sV)			E_j (mV)
		H^+	NO_3^-	K^+	
0.312	Infinite dilution	36.26	7.41	7.62	27.046
	0.489	32.35	5.76	5.95	29.935
	0.1	33.8	6.37	6.57	28.72815
0.945	Infinite dilution	36.26	7.41	7.62	10.715
	0.303	32.81	5.95	6.15	12.221
	0.1	33.8	6.37	6.57	12.221
8.062	Infinite dilution	36.26	7.41	7.62	-0.459
	0.246	33	6.03	6.23	-0.5064
	0.1	33.8	6.37	6.57	-0.5064

Surprisingly the E_j calculated using adjusted mobilities based on the ionic strength of the solution causes a larger deviation from the measured diffusion junction potential than when using limiting mobilities. The equation for calculating mobility was only reliable for solutions having ionic strength values of up to 0.1 M. Our solutions have ionic strengths up to five times larger and so it is obvious that the predicted mobilities are smaller than what they should be, which was also found by Robinson and Stokes (1959). Regardless, the decrease in mobility of the ions causes an increase in the magnitude of the diffusion junction potential and hence an even larger deviation between the experimental values and those from the Henderson prediction. It therefore appears that using the Henderson equation in its simplest form, where the mobilities of ions are at infinite dilution at each pH in the experiment, gives better results.

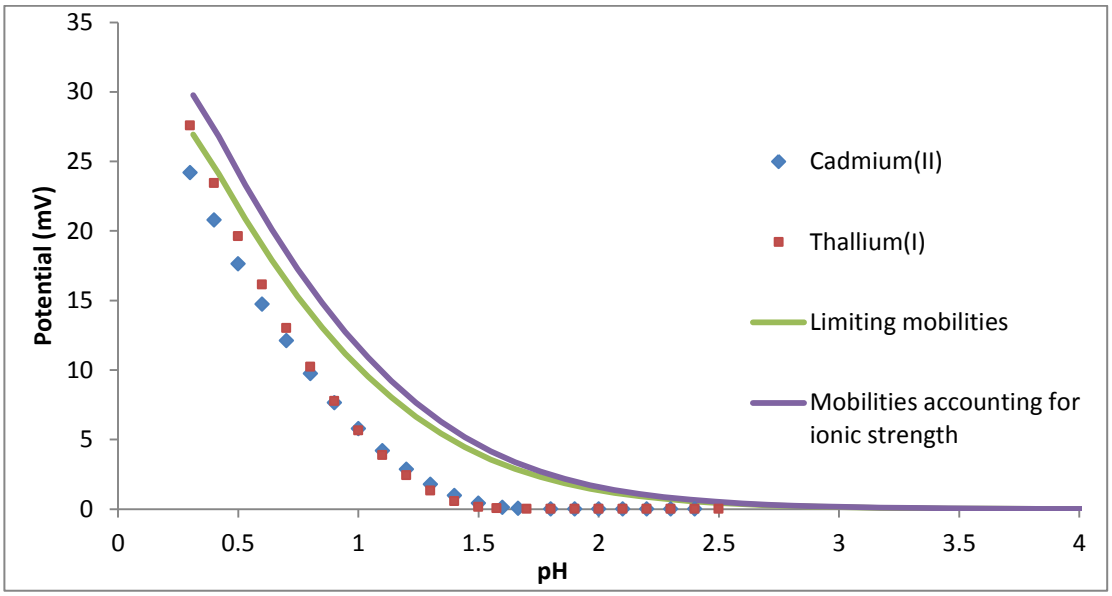


Figure 3.14 Comparison of the diffusion junction potential measured for thallium(I) and cadmium(II) with that calculated using the Henderson equation, with mobilities at infinite dilution or mobilities calculated at varying ionic strength.

3.5 COMPARING E_j CALCULATED USING THE HENDERSON EQUATION TO THAT USING THE COMPENSATION MODEL

The diffusion junction potential for an experiment containing dipicolinic acid in 50 times the concentration with cadmium(II) was also considered. The magnitude of the E_j was calculated using the compensation model C(I) at each pH value below 2 and was compared to that calculated E_j using the Henderson equation utilising limiting mobilities (Figure 3.15). The E_j predicted by Henderson should be most comparable to that of cadmium(II) (rather than thallium(I)) because cadmium's half-wave potential is not affected by the changing ionic strength, unlike that of thallium.

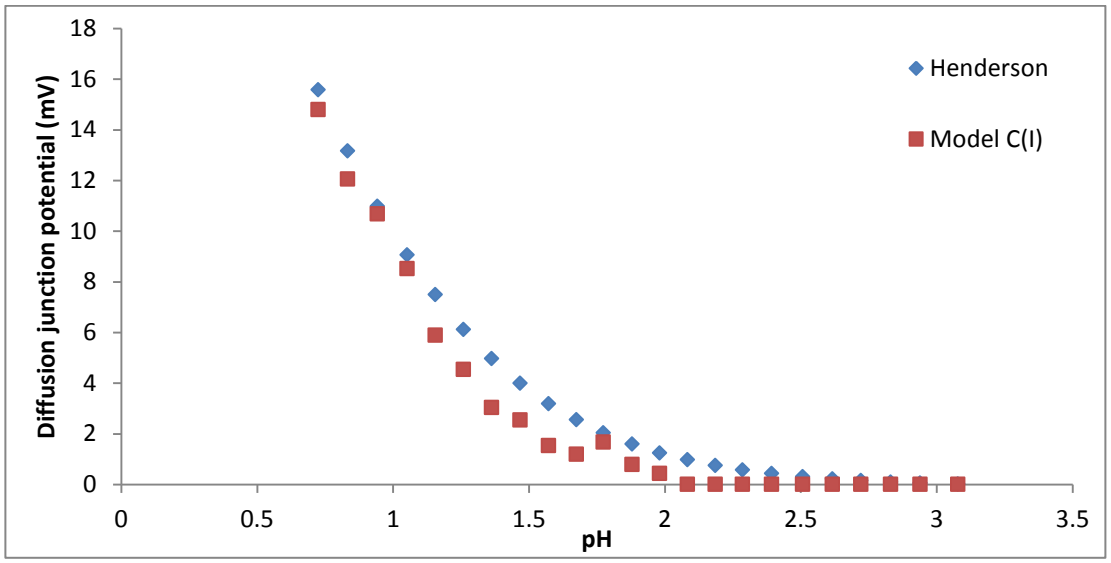


Figure 3.15 Comparison of the E_j calculated by the Henderson equation and that calculated for cadmium(II) using the compensation model, C(I).

As expected, the prediction by Henderson was somewhat larger than it was calculated to be using experimental data. This trend gives confidence that the C(I) compensation model is functioning adequately.

3.6 CONCLUSION

In conclusion the following points can be drawn: (1) Below pH 2 "E_j" changes with pH differently for thallium(I) and cadmium(II) because of the changing ionic strength. Half-wave potentials for thallium(I) and cadmium(II) are not equally affected by the change in ionic strength. The difference between their behaviour was therefore modelled. (2) The C(I) compensation model takes into account the changing E_j with increasing pH as well as the differences in half-wave potential values experienced by cadmium(II) and thallium(I) due to ionic strength changes. (3) Above pH 2 ΔE is constant because the ionic strength is essentially 0.25 M throughout this pH range and the E_j is constant, thus an average $\Delta E_{C>pH\,2}$ value was

calculated for all experiments. (4) Ligand-free experiments were used to create the compensation model that was used to calculate the diffusion junction potential in experiments where complex formation between the ligand and cadmium(II) occurs (to be discussed in Chapters 5 and 7). (5) An E_j calculated using the Henderson equation could not be used to accurately compensate for the diffusion junction potential. The E_j had to be measured experimentally and preferably was monitored in the same experiment in which complex formation was taking place. This was achieved using an in-situ witness ion.

3.7 REFERENCES

Angst, U., Vennesland, Ø. and Myrdal, R., 2009. Diffusion potentials as source of error in electrochemical measurements in concrete. *Materials and Structures,* 42 (3), pp 365-375.

Bagg, J., 1990. Computer calculation of liquid-junction potentials—I. Concentration profiles at junctions with concentrated KCl. *Electrochimica Acta,* 35 (2), pp 361-365.

Banica, F. G., 2012. *Chemical Sensors and Biosensors: Fundamentals and Applications,* West Sussex, Wiley.

Billing, C., Cukrowski, I. and Jordan, B., 2013. A Novel Approach to Monitoring of the Diffusion Junction Potential in Speciation Studies by Polarography Under very Acidic Conditions. Part I: The Reversible Cd(II)-Picolinic Acid System. *Electroanalysis,* 25 (9), pp 2221-2230.

Cukrowski, I. and Loader, S. A., 1998. Evaluation of a Peak Potential of an Uncomplexed Metal Ion in Speciation Study of Labile Metal-Ligand Systems by Polarography. Stability Constant Determination of Cd(II) and Pb(II) with Picolinic Acid at a Fixed LT:MT Ratio and Varied pH. *Electroanalysis,* 10, pp 877-885.

Cukrowski, I., Zhang, J. M. and van Aswegen, A., 2004. Voltammetry as a Virtual Potentiometric Sensor in Modelling of a Metal/Ligand System and Refinement of Stability Constants. Part 2. *Helvetica Chimica Acta,* 87 (8), pp 2135-2158.

Esteso, M. A., Esparza, M., Grandoso, D. M. and Gonzalez-Diaz, O. M., 1987. Transference number measurements in aqueous solutions at 25 °C. 3. Lithium bromide. *Journal of Chemical & Engineering Data,* 32 (4), pp 474-476.

Generalic, E. 2011. *Croatian-English Chemistry Dictionary & Glossary* [Online]. Available: http://glossary.periodni.com [Accessed 16 November 2012].

Goldman, D. E., 1943. Potential, impedance, and rectification in membranes. *The Journal of General Physiology,* 27 (1), pp 37-60.

Harris, D. C., 1995. *Quantitative Chemical Analysis,* New York, W.H. Freeman and Company.

Harris, D. C., 1998. *Quantitative Chemical Analysis,* New York, W.H. Freeman and Company.

Henderson, P., 1907. Zur Thermodynamik der Flüssig Keitsketten. *Zeitschrift für Physikalische Chemie,* 59, pp 118.

Ibrahim, A., Ohshima, H., Allison, S. A. and Cottet, H., 2012. Determination of effective charge of small ions, polyelectrolytes and nanoparticles by capillary electrophoresis. *Journal of Chromatography A*, pp 154-164.

Jouyban, A. F. and Kenndler, E., 2006. Theoretical and empirical approaches to express the mobility of small ions in capillary electrophoresis. *Electrophoresis*, 25 (5-6) pp 992 - 1005.

Lingane, J. J., 1939. Thermodynamic Significance of Polarographic Half-Wave Potentials of Simple Metal Ions at the Dropping Mercury Electrode. *Journal of the American Chemical Society,* 61 (8), pp 2099-2103.

McQuarrie, D. A. and Simon, J. D., 1997. *Physical Chemistry: A Molecular Approach,* California, University Science Books.

Morf, W. E., 1977. Calculation of liquid-junction potentials and membrane potentials on the basis of the Planck theory. *Analytical Chemistry,* 49 (6), pp 810-813.

Rieger, P. H., 1994. *Electrochemistry,* New York, Chapman and Hall.

Robinson, R. A. and Stokes, R. H., 1959. *Electrolyte Solutions – The Measurement and Interpretation of Conductance, Chemical Potential and Diffusion in Solutions of Simple Electrolytes,* London, Butterworth and Co.

Surampudi, S. and Meeting, E. S., 2000. *Lithium Batteries: Proceedings of the International Symposium*, Electrochemical Society.

Winkelman, J., Merritt, C., Scott, W., Kumar, A. and Baum, G., 1984. Effects of residual liquid junction potential in direct potentiometry of potassium. *Clinical Chemistry,* 30 (3), pp 482-484.

Zhao, J., Wang, L., He, X., Wan, C. and Jiang, C., 2008. Determination of Lithium-Ion Transference Numbers in $LiPF_6$–PC Solutions Based on Electrochemical Polarization and NMR Measurements. *Journal of The Electrochemical Society,* 155 (4), pp A292-A296.

Zoski, C. G., 2007. *Handbook of Electrochemistry,* Amsterdam, Elsevier Science.

Zusková, I., Novotná, A., Včeláková, K. and Gaš, B., 2006. Determination of limiting mobilities and dissociation constants of 21 amino acids by capillary zone electrophoresis at very low pH. *Journal of Chromatography B,* 841 (1–2), pp 129-134.

Chapter Four

Complex Formation of Cadmium(II)-Picolinic Acid

4.1 INTRODUCTION

Picolinic acid is of biological importance and has been found to possess a wide range of neuro-protective, immunological and anti-proliferative effects within the human body (Grant, Coggan and Smythe, 2009). Picolinic acid is endogenously produced in the liver by an enzymatic decarboxylation of quinolinic acid – an intermediate of tryptophan metabolism. The picolinic acid functions as a chelating agent of elements such as chromium, zinc, manganese, copper, iron and molybdenum. Many years ago young children were being diagnosed with acrodermatitis enteropathica – a disease having symptoms of diarrhoea, skin rash, hair loss and infections, all which occurred after being weaned off of breast milk (Evans, 1982). The disease was caused by the malabsorption of zinc, which sparked interest in a possible zinc-binding ligand present in human milk. After rigorous separation of breast milk samples and various ligand identifications it was established to be picolinic acid. It has since been known for its great importance to humans, as well as animals, in the transport and absorption of zinc and other essential metal ions.

Picolinic acid can occur either as a cation, a zwitterion, a neutral ligand, or as a picolinate anion depending on the pH of the solution, as indicated by its protonation constants (see Figure 4.1). Figure 4.2 is a species distribution diagram (SDD) which shows the entire pH range where each form of the ligand can be found to exist and it also indicates where each form predominates. Protonation constants indicate the

point where 50% of the one form of the ligand is present and 50% of the other form is present.

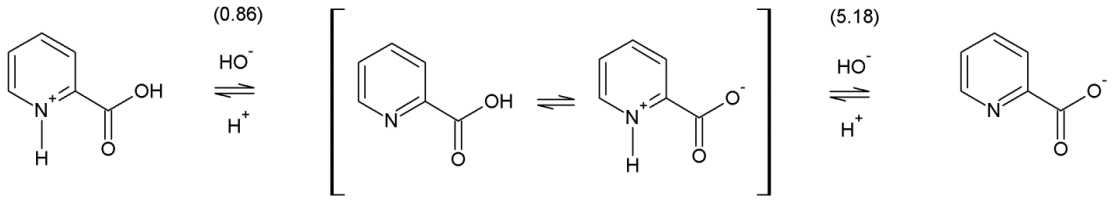


Figure 4.1 Deprotonation equilibria of picolinic acid with stepwise protonation constants given in brackets (quoted as log *K* values at 25 °C and μ = 0.5 M (Martell, Smith and Motekaitis, 2004)).

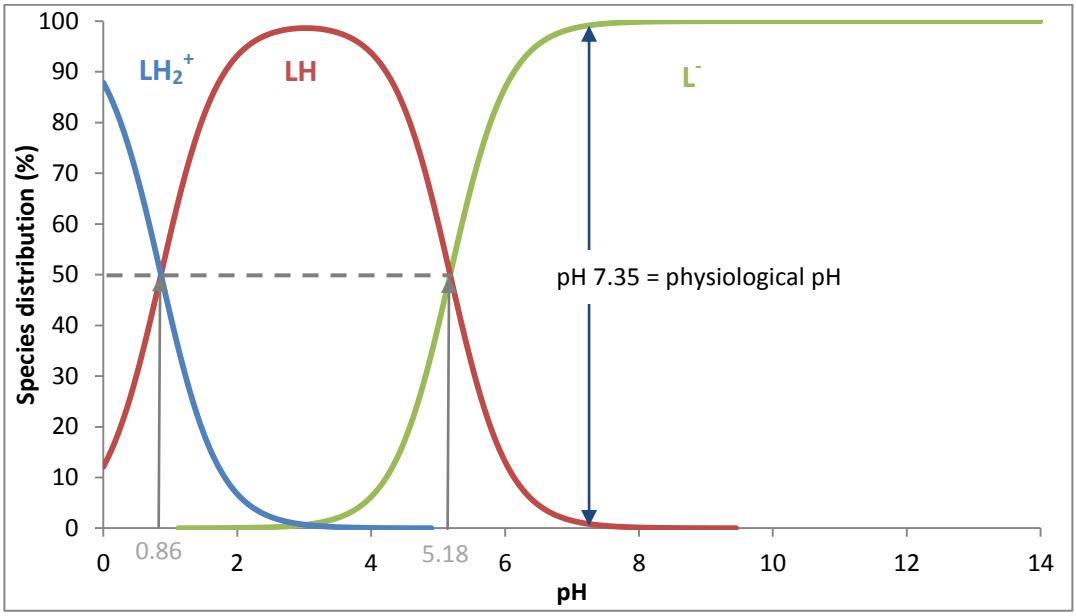


Figure 4.2 Species distribution diagram (SDD) showing the percentage distribution of the ligand species that predominate in specific pH regions in solution.

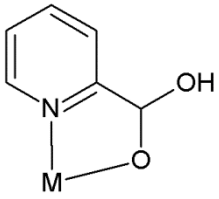
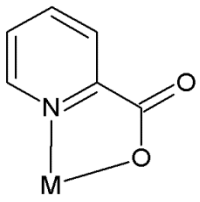
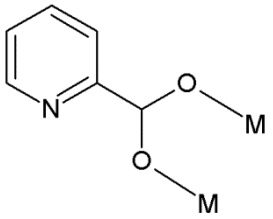
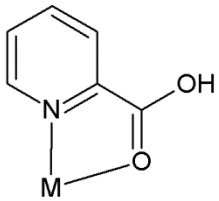
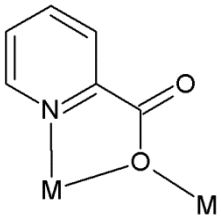
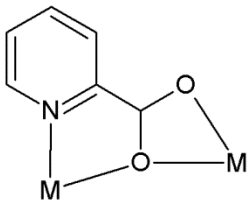
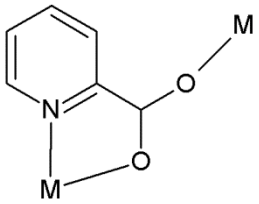
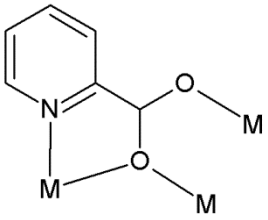
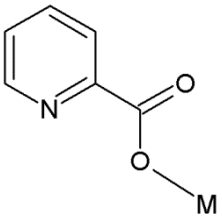
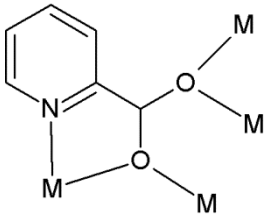
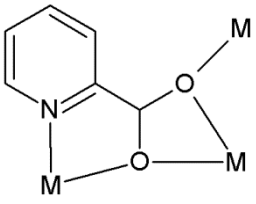
In literature various structures have been found where the picolinate anion acts as a bidentate chelating ligand or even as a tridentate chelating bridging ligand, coordinating via the pyridine nitrogen as well as the two carboxylate oxygen atoms

(Mautner, Abu-Youssefb and Goher, 1997). At physiological pH (approximately 7.35) the ligand is fully deprotonated and forms very strong complexes with a number of metal ions (Evans, 1982). Table 4.1 shows the various coordination modes that picolinic acid has been found to adopt in the crystalline form, as obtained from a search of the Cambridge Structural Database (CSD) (Allen, 2002). (Throughout this thesis, all structures from the CSD will be referred to using the reference code (REFCODE) as quoted per the CSD. For all corresponding journal references please see Table B13.1, Appendix B.)

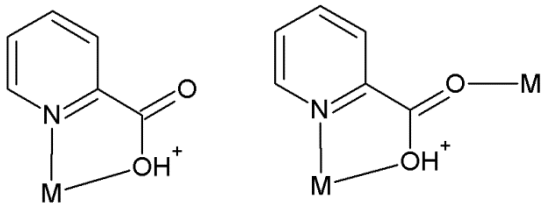
The singly protonated form of picolinic acid has fewer coordination modes than the completely deprotonated ligand, as would be expected. There are two coordination modes which involve the singly protonated picolinate ligand and the carboxylate oxygen which is protonated in each case. No such complexes were found for cadmium(II) in particular. Only three examples of coordination mode *i* (shown in Table 4.1) were found in literature where the protonated ligand was bonded to thallium (REFCODE: SAHCOU), manganese (REFCODE: PYCXMN01) or copper (REFCODE: KANQOG). Two other protonated coordination modes were found, but having only one example of each, REFCODES: NISJEE and REHLIA (Figure 4.3). They were not included in the coordination mode table because of the uncertainty associated with the published data (positions of hydrogen atoms are rather unreliable), as well as the lack of similar examples. Coordination mode *ii* (Table 4.1) is far more common and complexes of cobalt, zinc, manganese, copper, potassium, mercury, sodium and many other cations were found.

All the other coordination modes for picolinic acid involve the completely deprotonated ligand. Looking specifically at the cadmium-picolinate system we find that the most common coordination mode for crystalline complexes includes chelation of all three electron rich sites, as shown by coordination mode *viii* in Table 4.1. The pyridyl nitrogen is often involved in chelation because it is electron rich

Table 4.1 Coordination modes of picolinic acid with various metals, M, as found in literature.

LH_2^+	LH	L^-	
	 *i*	 *iii*	 *vii*
	 *ii*	 *iv*	 *viii*
		 *v*	 *ix*
		 *vi*	 *x*
			 *xi*

and from a relatively low pH is not protonated if the ligand exists in the neutral form. The pyridine nitrogen is a soft donor that favours stabilization of transition metals of lower oxidation states, whereas the carboxylate oxygen is a hard donor that stabilizes higher oxidation state transition metals (Basu, Peng, Lee and Bhattacharya, 2005). Ma *et al.* (2009) show an O,O-bidentate bond, where N is uncoordinated, to be a possible coordination mode for the picolinate anion when bonding to any transition metal. They do not give an example of this though and so it hasn't been included as a possible coordination mode in the above table.



a) b)

Figure 4.3 Coordination modes for a) REHLIA and b) NISJEE which are rare for picolinic acid. The locations of the protons in each of these were not certain.

Solution studies of metal-ligand equilibria provide information about different complexes that exist and predominate at specific pH values, while crystal structures can be used to study the precise geometry of the complexes formed and provide insight into the mode of coordination of the ligand. Our interest lies in the relationship between species that are found in solution and those crystallized at specific pH values.

Literature shows that in the past a number of different experimental techniques have been used for growing crystals of cadmium-picolinate complexes. There is no single or common method for doing so, although it was evident that organic solvents

feature quite extensively in the solution mixture. Kang *et al.* (2005) (REFCODE: RAZXUF) and Wang, Fan, Wang and Chen (2005) (REFCODE: DARYEB) both used high temperatures and organic solvents (ethanol and 2-(2-pyridyl)-5-(4-pyridyl)-1,3,4-oxadiazole, respectively) to obtain picolinate crystals. Odoko, Isomoto and Okabe (2001) (REFCODE: NELNIB) grew crystals by slow evaporation of an ethanol-water solution at room temperature. Deloume and Loiseleur (1974) (REFCODE: CDPICO) produced crystals by slow evaporation of an aqueous solution (no comment was made on the exact temperature used, presumably room temperature). Papatriantafyllopoulou *et al.* (2007) (REFCODE: YILBIF) used an aqueous solution of picolinic acid and cadmium(II) sulfate which was layered with dimethylcarbon(II)monoxide, where again the temperature of the experiment was not reported. In this work only aqueous solutions are considered for the growth of picolinate crystals and so the literature results do not offer very many techniques or methods that are of use in this context.

4.1.1 Formation Constants

Cukrowski and Loader (1998) did a comprehensive literature review on the formation constants available for the cadmium-picolinate system that were obtained using various techniques. Table 4.2 summarizes the information for this metal-ligand system. Cukrowski and Loader (1998) found that the values reported in literature were inconsistent and that there was a substantial difference between those obtained by polarography and glass electrode potentiometry (GEP).

Cukrowski and Loader (1998) then went on to obtain their own formation constants for the cadmium-picolinate system using differential pulse polarography, at ionic strengths of 0.1 and 0.5 M at a temperature of 25 °C. They detected the ML, ML_2 and ML_3 species having the following respective log β values at 0.5 M ionic strength: 4.29 ± 0.03, 7.89 ± 0.03 and 10.49 ± 0.02. These values compared very closely to those obtained by GEP and are available on the NIST Database (Martell, Smith and

Motekaitis, 2004) meaning that they have been "critically assessed". By critically assessed the authors mean that the

Table 4.2 Summary of the formation constants for the cadmium(II)-picolinate system that are published in literature.

Author	Log β(ML)	Log $\beta(ML_2)$	Log $\beta(ML_3)$	Other Log β	Technique	Temp (°C)	Ionic Strength (M)
Anderegg (1960)	4.55	8.16	10.76	-	GEP	20	0.1
Buffle, Mota and Gonçalves (1985)	4.5-4.8	8.3-9.0	-	-	Voltam		
Jain, Prakash and Bhasin (1976)	4.70	8	9.48	**(ML_4)** 10.82	Polarog		
Martell, Smith and Motekaitis (2004)**	4.36	7.99	-	-	GEP		
Matsui and Ohtaki (1982)	4.47	8.17			GEP	25	3
Evtimova, Scharff and Paris (1969)*	4.18	7.61	10.76		GEP	25	0.5
Cukrowski and Loader (1998)	4.34	8.01	10.79		Voltam	25	0.1
	4.29	7.89	10.49		Voltam	25	0.5-0.25
Billing, Cukrowski and Jordan (2013)*	4.23	7.81	10.53	**(MLH)** 6.27	Voltam	25	0.5-0.25

*Does not appear on the NIST Database (Martell, Smith and Motekaitis, 2004).
**Quoted in Cukrowski and Loader (1998)

stability constants were acquired under specific and controlled reaction conditions where all apparatus, measurements and calibrations were made and described clearly (Martell and Hancock, 1996).

Formation constants for this same system were later calculated by (Billing, Cukrowski and Jordan, 2013) using polarography, by both pH and ligand titrations. In their study, the background solution was made up of nitric acid and sodium hydroxide (NaOH) solutions at a fixed ionic strength of 0.5 M for the ligand titrations

and an ionic strength range of 0.25 to 0.5 M for the pH titrations. Three pH titrations were conducted of which two started from pH 0.3 while the third was started at pH 2 in order to avoid the region where the diffusion junction potential is changing. Thallium(I) was used as the witness ion for monitoring the diffusion junction potential. Fortunately no complex formation took place between the picolinic acid and the thallium(I), thus all shifts in potential were due to the diffusion junction potential. Once the diffusion junction potential was compensated for, complex formation between cadmium(II) and picolinic acid was studied. Slope analysis (to be discussed in Chapter Five) and the refinement process identified MLH, ML, ML_2 and ML_3 species for the two experiments that were started at low pH. For the data starting at pH 2 the MLH species could not be incorporated into the system.

Three ligand titrations were performed at constant pH values of 3.0, 3.8 and 5.1 where the [L]:[M] ratio varied from 10 to 200. The diffusion junction potential remains constant throughout the titration because the pH is fixed and also because each experiment was done at a pH above 2. The formation constants for the ML and ML_2 species were calculated with the data from ligand titrations done at pH 3.0 and 3.8, while that at pH 5.1 was used to calculate the formation constants of ML_2 and ML_3. A pH titration done at pH 2 produced noisy data which would either only refine a formation constant for MLH or ML, but not a combination of the two, so these data were not included.

Billing, Cukrowski and Jordan (2013) obtained an average of the formation constants calculated from the pH and ligand titrations (see Table 4.2). The MLH formation constant was however determined from an average of only two values. The authors expressed concern in their level of confidence in the MLH species, as it has never before been reported and its existence is also in the pH region where compensation of the diffusion junction potential was done. Excluding it from the model did not

change the magnitude of the remaining log β values significantly (4.26 ± 0.03, 7.86 ± 0.11 and 10.47 ± 0.12 for ML, ML_2 and ML_3, respectively.)

4.1.2 The Distribution of Species in Solution

Plotting SDDs using the formation constants for both models proposed by Billing, Cukrowski and Jordan (2013) indicates the differences in the distribution of the species when the MLH complex is included or not (Figure 4.4).

The ML and ML_2 formation constants increase slightly to compensate for the exclusion of the MLH species and more of the metal ion remains free in solution. MLH is a minor species in solution under these conditions and so the general species distribution does not change too drastically when it is excluded. The difficulty in deciding whether MLH is definitely present in solution or not, is due to its low concentration under these conditions.

One of the aims of this study was to grow crystals of the cadmium(II) complexes under conditions similar to those used in the polarographic studies. The SDDs were used as a guide to decide on a suitable pH range that could be used to target specific crystalline complexes. It should be noted at the outset that concentrations at which crystal growth takes place is actually be quite different to the concentrations used in electrochemical studies.

Obtaining crystal structures for these metal-ligand species could potentially provide evidence for their existence in solution. A SDD is used as a guide to what pH and solution conditions to use in order to try obtain a specific complex. Using the same formation constants but altering solution concentration and [L]:[M] ratios affects the distribution of species. For example, Figure 4.5 shows the effect of changing the concentration and the [L]:[M] ratio by a hundred times.

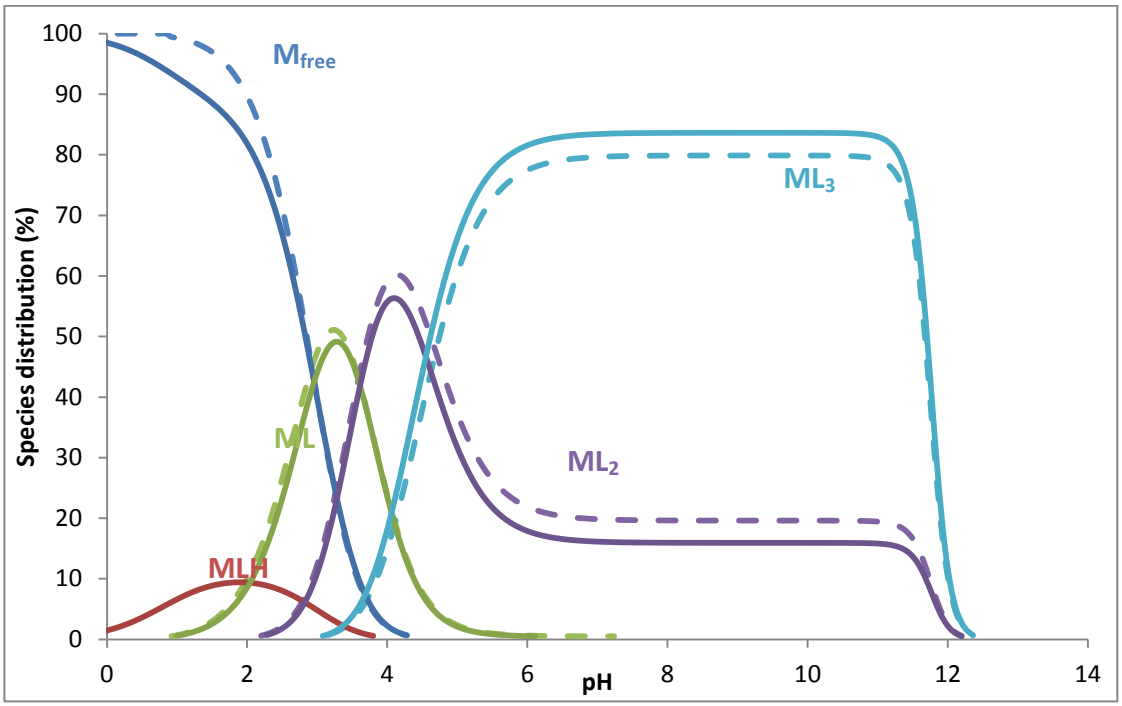


Figure 4.4 SDD showing the difference in species distributions when including (solid lines) or excluding (dashed lines) the MLH species. [Cd] = $1x10^{-4}$ M and [L] = $1x10^{-2}$ M. Cadmium(II) hydroxide species have been omitted for clarity.

Table 4.3 gives a summary of the changes experienced by each species in accordance with Figure 4.5. Conditions were manipulated in this way to find the optimum combination of conditions for targeting a specific complex for crystal growth.

Increasing the [L]:[M] ratio or the concentration promotes the formation of the MLH species in solution, but solutions at high ratios for crystal growth may result in crystallization of just the ligand because of its large excess. Also dissolution of the ligand in such excess may be problematic at the concentration levels needed for crystal growth. The production of the ML_2 and ML_3 species is also promoted at increased concentrations and ratios and so the same issues may apply. For these

two species though the increase in the ratio (i.e. introducing an excess of ligand) assists in creating such species due to the stoichiometry of the reaction requiring more ligand than metal.

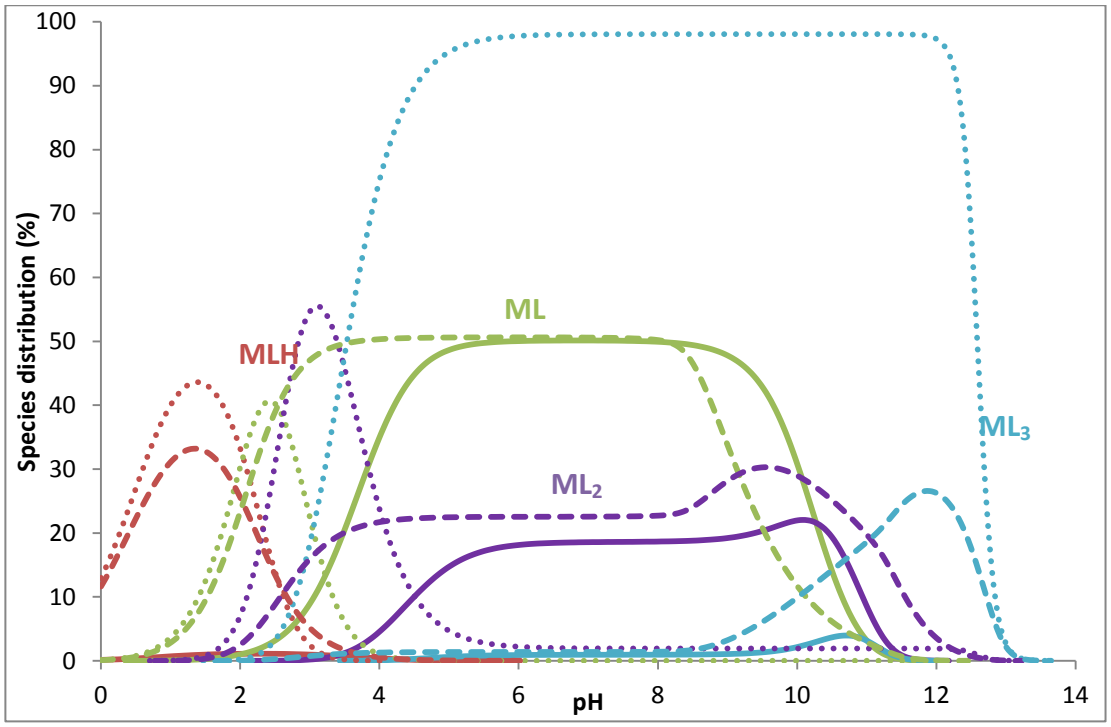


Figure 4.5 SDD showing the effect of increasing both the concentration and [L]:[M] ratio by a hundred. Solid lines represent [L]:[M] = 1 where [Cd] = 0.001 M, dotted lines represent [L]:[M] = 100 where [Cd] = 0.001 M and dashed lines represent [L]:[M] = 1 where [Cd] = 0.1 M. M_{free} and hydroxide species have been omitted for clarity.

In this research all crystallization experiments were performed in purely aqueous solutions so that they could be as similar as possible to the solutions used in determining formation constants. Formation constants were used to plot SDDs at experimental conditions suitable for crystal growth, and so they needed to be measured in a solution as comparable as possible to that of the crystal growth

solution. The magnitude of formation constants vary when measured in different solvents due to the different

Table 4.3 Effects on the SDD when changing the solution conditions as given in Figure 4.5.

Species	Increasing concentration	Increasing [L]:[M] ratio
M_{free}	Decreased	Decreased
MLH	Increased by 30%	Increased by 40%
ML	Forms from a lower pH	Decreased, found over a narrower pH range and at lower pH.
ML_2	Increased and found over a larger pH range.	Increased considerably at lower pH, but decreased from above pH 4.5.
ML_3	Increased by 30% at high pH	Increased drastically (90%)

interactions (primarily hydrogen bonding and dipole-dipole interactions) between the solvent and the solute (Reichardt and Welton, 2011). The solvent may preferentially stabilize either the product or the reactant, thereby shifting the equilibrium in the direction of the stabilized compound, hence affecting the magnitude of the formation constants. Also, different solvents would affect the ionic strength of the solution. If the ionic strength of the solution changes, the magnitude of the log β values would change due to their magnitude being a function of the activity of the ions in solution (Bond, 1970). Therefore the closer the conditions are between the solutions and crystalline experiments the more closely they can be compared. Unfortunately, in order to form crystals the concentrations of metal and ligand need to be significantly higher than those used in the polarographic experiments. Also the concentration ratios of ligand to metal should be closer to unity, like those used for GEP. GEP is done using low [L]:[M] ratios, but this technique cannot be used to confirm the presence of species that form below pH 2 and above pH 11 because it is not accurate when there is a large concentration

of either H^+ or OH^- ions in solution. Nuclear magnetic resonance (NMR) spectroscopy can also be used to determine formation constants and it utilizes concentrations of approximately 0.5 x 10^{-3} M and also requires low [L]:[M] ratios, however the sample has to be diamagnetic (http://qudev.ethz.ch/content/courses/phys4/studentspresentations/nmr/James_Fundamentals_of_NMR.pdf). Spectrophotometric methods based on absorbance and luminescence measurements are generally done at low [L]:[M] ratios too, but they require that the complex being formed has colour. Although the log β values obtained are not affected by the [L]:[M] ratios and the values should be comparable irrespective of the technique used to determine these values, the actual species present in solution could change, for example more polynuclear species could form at lower ratios. Comparing the solution species models determined by the various techniques, it is generally found that they are in good agreement. A direct comparison of the species in the solid state and solution state (especially under polarographic conditions) therefore does have its limitations. That being said, there must be some formation of complexes and preorganization in solution before crystallization occurs. Thus species distribution diagrams plotted employing the calculated formation constants for the cadmium(II)-picolinate system were used to try and target particular species to crystallize by controlling the pH and/or the [L]:[M] ratios in the liquors for crystal growth.

4.2 AIMS

For the cadmium(II)-picolinate system we aimed to grow crystalline complexes of the species that were proposed in solution studies carried out by Billing, Cukrowski and Jordan (2013). SDDs were used as a guide to see if the crystal complexes grown under similar conditions would correlate to the species in solution. Any crystal

grown was analysed using single crystal x-ray diffraction (SCXRD). Powder x-ray diffraction (PXRD) was used to confirm that the crystal chosen for SCXRD represented the bulk of the solid material, as well as to identify any other products that may be present (for example salts or uncomplexed ligand) in the crystal mixture. The final objective was to decide if there was any correlation between the crystalline complexes and the species identified in solution at similar pH values, according to a SDD which is plotted using formation constants from solution experiments, and concentrations and ratios that correspond to the conditions used for crystal growth. The complexing ability of picolinic acid in terms of cadmium(II) was investigated under various conditions in this research.

4.3 EXPERIMENTAL

Growth of picolinate complexes were achieved because picolinic acid readily dissolves in water (887 g/L at 20 °C, according to http://www.chemicalbook.com/ChemicalProductProperty_EN_CB8196640.htm) and has a high affinity for forming metal complexes. Two crystalline metal-ligand complexes were grown using the following experimental methods:

4.3.1 Diaquadinitrato-(pyridine-2-carboxylato-O,O)-cadmium(II) (Cd(PIC-H))

Cadmium(II) nitrate tetrahydrate and picolinic acid were dissolved in deionized water in a 1:1 [L]:[M] ratio to produce concentrations of 0.5 M and the solution was slightly acidified using HNO_3. No specific pH adjustment was done as the pH was sufficiently low. Evaporation of the solvent at room temperature led to the formation of hard, colourless, block-shaped crystals which took almost two months to grow.

Initially no crystals had formed but there were crystalline threads on the walls of the vial. At this point the measured pH was 0.35. The next day a cluster of crystals started growing on the base of the vial and the solution pH was measured to be -0.55. The vial was then closed. The following day more crystals appeared that formed large, colourless crystal aggregates. A pH of 0.51 was measured in the small amount of liquid remaining in the vial.

4.3.2 Tri(pyridine-2-carboxylato-N,O)-cadmium(II) dinitrate ($Cd(PIC\text{-}H)_3$)

Picolinic acid and cadmium(II) nitrate tetrahydrate were dissolved in deionized water in a [L]:[M] ratio of 2:1 and a 3:1, where the concentration of cadmium(II) was 0.125 M in both cases. Evaporation of the solvent at room temperature led to the formation of colourless, needle-shaped crystals at a pH of 1.0 and 1.3, respectively. In both cases crystal formation took 11 weeks. Crystals from each [L]:[M] ratio were analysed using SCXRD and produced the same structure.

4.3.3 Crystallographic Data collection, Structure Solution and Refinement

Intensity data were collected on a Bruker SMART CCD area detector diffractometer with graphite monochromated Mo K_α radiation (50 kV, 30 mA). The collection method involved ω-scans of width 0.3 °. Data reduction was carried out using the program *SAINT+,* version 6.02 (Bruker, 1999). Empirical absorption corrections were made for Cd(PIC-H) using the program SADABS, while this was not necessary for $Cd(PIC\text{-}H)_3$ as no changes in the refinement were observed when applied. All crystals were studied at -100 °C (173.15 K) and structures were solved by direct methods using *SHELX-97* (Sheldrick, 2008). Non-hydrogen atoms were first refined isotropically followed by anisotropic refinement by full matrix least-squares calculations based on F^2 using *SHELX-97*. All hydrogen atoms were positioned geometrically and allowed to ride on their respective parent atoms, except those of O9 and O10 in Cd(PIC-H) which were placed according to electron density and

refined freely. A summary of the crystallographic data for both structures can be seen in Table 4.4.

Table 4.4 Crystal data and structure refinement for Cd(PIC-H) and Cd(PIC-H)$_3$.

Complex	Cd(PIC-H)	Cd(PIC-H)$_3$
Empirical formula	$C_6H_9Cd\ N_3O_{10}$	$C_{18}H_{13.5}Cd\ N_4O_9$
Formula weight (g/mol)	395.56	1022.45
Temperature	173(2) K	173(2) K
Wavelength	0.71073 Å	0.71073 Å
Crystal system	Triclinic	Trigonal
Space group	P -1	P-3
a	8.4374(8) Å	14.0290(5) Å
b	9.2353(7) Å	14.0290(5) Å
c	9.5588(8) Å	5.6564(2) Å
α	111.409(5)°	90°
β	116.156(5)°	90°
γ	94.582(6)°	120°
Volume	596.03(9) Å^3	964.10(6) Å^3
Z	2	2
Density (calculated)	2.204 Mg/m^3	1.761 Mg/m^3
Absorption coefficient	1.892 mm^{-1}	1.184 mm^{-1}
F(000)	388	508
Crystal size	0.46 x 0.36 x 0.28 mm^3	0.499 x 0.152 x 0.121 mm^3
Theta range for data collection	2.47 to 27.99°	1.68 to 27.97°
Index ranges	$-11 \le h \le 10, -12 \le k \le 12, -12 \le l \le 12$	$-9 \le h \le 18, -18 \le k \le 15, -7 \le l \le 7$
Reflections collected	11730	7838
Independent reflections	2863 [R(int) = 0.0223]	1556 [R(int) = 0.0453]
Completeness to theta	99.80%	99.90%
Absorption correction	Semi-empirical from equivalents	None
Max. and min. transmission	0.6194 and 0.3273	
Refinement method	Full-matrix least-squares on F^2	Full-matrix least-squares on F^2
Data / restraints / parameters	2863 / 0 / 197	1556 / 1 / 91
Goodness-of-fit on F^2	1.184	1.104
Final R indices [I>2sigma(I)]	R_1 = 0.0166, wR_2 = 0.0440	R_1 = 0.0293, wR_2 = 0.0762
R indices (all data)	R_1 = 0.0171, wR_2 = 0.0442	R_1 = 0.0333, wR_2 = 0.0782
Largest diff. peak and hole	0.294 and -0.857 e.Å^{-3}	0.772 and -0.984 e.Å^{-3}

4.4 RESULTS AND DISCUSSION

4.4.1 Diaquadinitrato-(pyridine-2-carboxylato-O,O)-cadmium(II) Complex (Cd(PIC-H))

4.4.1.1 Analysis of the Crystal Structure

Cd(PIC-H), $[Cd(NO_3)_2(C_5H_4NHCO_2)(H_2O)_2]$, crystallized in the P-1 space group, having two molecules in the asymmetric unit (Z = 2). The defining feature of this structure is the novel coordination mode (for this particular metal-ligand system) that picolinic acid adopts in forming the cadmium complex. The molecular structure and numbering scheme are shown in Figure 4.6. Selected bond lengths and angles are listed in Table 4.5. The pyridyl nitrogen is protonated while the two carboxylate oxygen atoms are responsible for chelating bidentately to the cadmium(II) metal centre. This crystal also contains two water molecules and two nitrate anions, one of which bonds bidentately to the metal centre creating a three-membered chelate ring. Both nitrate groups and two water molecules are arranged in *trans* dispositions from each other. The two water molecules are axial ligands and the remaining groups all lie within the equatorial plane (torsion angle -1.11 ° (O1-Cd1-O4-N2), -174.16 ° (N3-O6-Cd1-O1) and 1.63 ° (O6-Cd1-O1-C1).

The cadmium(II) ion is seven coordinate as a result of binding bidentately to the picolinate ion and a nitrate group, as well as monodentately to the other nitrate ion and two water molecules. However, the intra-ligand O3…O4 distance of the bidentate nitrate is somewhat smaller than 2.2 Å (2.162(2) Å), and therefore “the mean position of the two chemically equivalent atoms can be considered to lie roughly at the vertex of one of the usual coordination polyhedrons” (Pons, 2007). Bergman and Cotton (1966) suggest that an intra-ligand distance of less than 2.2 Å reduces the effective coordination number of a metal centre. As a consequence of

this phenomenon the coordination number is reduced from seven to six and the resulting geometry can be described as a distorted octahedron.

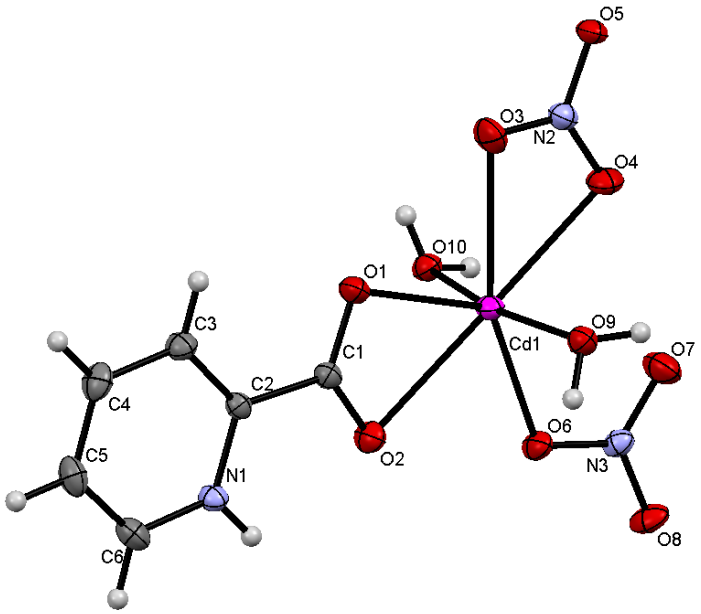


Figure 4.6 The molecular structure of Cd(PIC-H) with displacement ellipsoids drawn at the 50% probability level.

There are two symmetry equivalent positions within the unit cell due to the presence of the inversion centre (see Figure 4.7). The two molecules that are related by an inversion centre are linked together via two sets of hydrogen bonds, of the form O10—H2WA…O1 and O10-H2WB…O8. Axial water molecules act as hydrogen bond donors, linking neighbouring molecules via the carboxylate oxygen and the nitrogen of the bidentate nitrate. It is this hydrogen bond that is responsible for the stacking of the molecules. A layered structure is created by these hydrogen bonds as well as other short contacts, as shown in Figure 4.8.

Table 4.5 Selected bond lengths (Å) and angles (°) for Cd(PIC-H).

Cd(PIC-H)			
O(1)-Cd(1)	2.3540(12)	O(10)-Cd(1)-O(4)	82.15(5)
O(2)-Cd(1)	2.5509(13)	O(6)-Cd(1)-O(4)	107.82(4)
O(3)-Cd(1)	2.5217(14)	O(1)-Cd(1)-O(4)	126.12(4)
O(4)-Cd(1)	2.4802(14)	O(9)-Cd(1)-O(3)	88.74(5)
O(6)-Cd(1)	2.3157(12)	O(10)-Cd(1)-O(3)	90.51(5)
O(9)-Cd(1)	2.2438(13)	O(6)-Cd(1)-O(3)	159.02(4)
		O(1)-Cd(1)-O(3)	74.90(4)
O(9)-Cd(1)-O(10)	167.51(5)	O(4)-Cd(1)-O(3)	51.22(4)
O(9)-Cd(1)-O(6)	91.38(5)	O(9)-Cd(1)-O(2)	93.34(5)
O(10)-Cd(1)-O(6)	84.88(5)	O(10)-Cd(1)-O(2)	96.85(4)
O(9)-Cd(1)-O(1)	92.27(5)	O(6)-Cd(1)-O(2)	72.32(4)
O(10)-Cd(1)-O(1)	99.57(4)	O(1)-Cd(1)-O(2)	53.72(4)
O(6)-Cd(1)-O(1)	126.04(4)	O(4)-Cd(1)-O(2)	178.96(4)
O(9)-Cd(1)-O(4)	87.68(5)	O(3)-Cd(1)-O(2)	128.62(4)

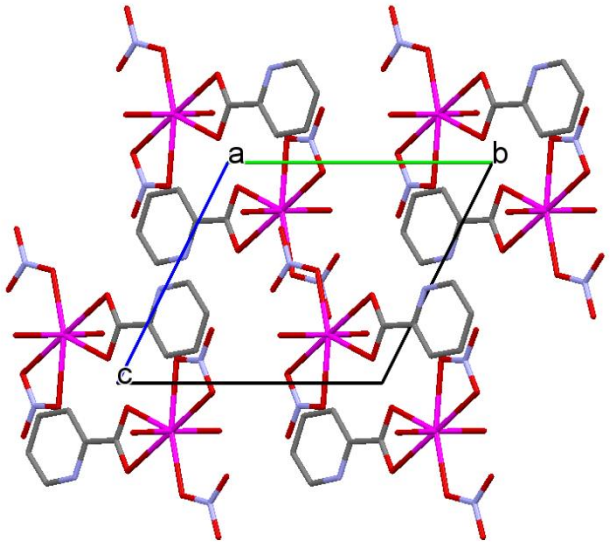


Figure 4.7 Packing of Cd(PIC-H) as viewed down the *a* axis. Hydrogen atoms have been omitted for clarity.

A bifurcated intermolecular hydrogen bond exists between O10 of the axial water and O1 and O3 of a neighbouring molecule, where one of the hydrogen atoms

(H2WA) on O10 is shared between the two oxygen acceptors (see Figure 4.9). The crystals are hard probably due to the extensive hydrogen bonding network within this structure. The only oxygen atoms which do not take part in hydrogen bonding are O2 and O7.

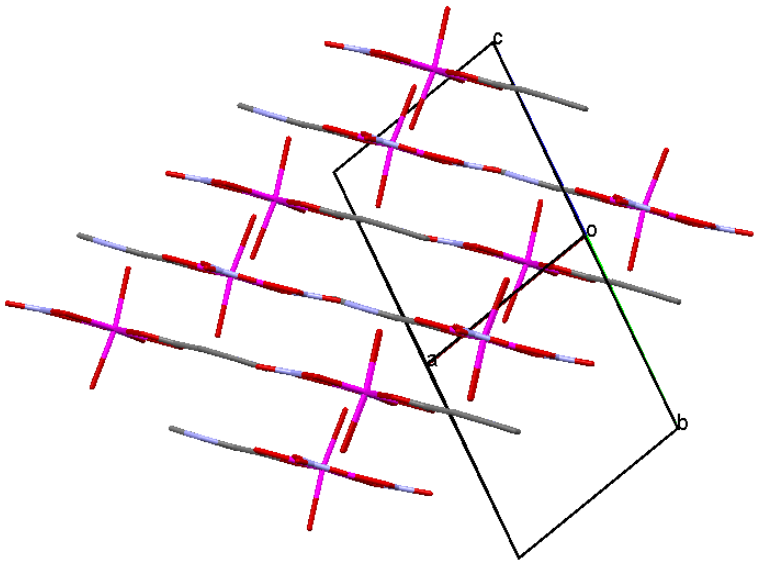


Figure 4.8 The layered structure of Cd(PIC-H). Hydrogen atoms have been omitted for clarity.

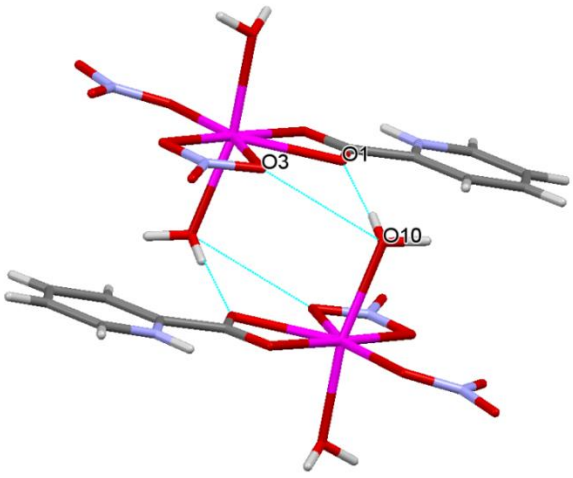


Figure 4.9 Hydrogen bond pair of Cd(PIC-H) molecules showing the bifurcated H-bond.

4.4.1.2 A Comparative Study with Literature Structures

Pons (2007) (REFCODE: HISSAE) produced crystals of cadmium(II) nitrate tetrahydrate bonded to ethyl picolinate from an aqueous solution. In this structure the cadmium ion appears to be eight coordinate having an antiprismatic geometry. The chelating ring shows short intra-ligand O···O distances (of the nitrate) and therefore the mean position of the two chemically equivalent atoms can be considered to lie roughly at the vertex of one of the usual co-ordination polyhedrons, as before. The cadmium coordination number therefore reduces to 6, as was found for Cd(PIC-H), and a very irregular co-ordination polyhedron becomes a distorted octahedral geometry. The cadmium metal centre bonds to the picolinate ligand via the nitrogen and one carboxylate oxygen. The Cd-$O_{picolinate}$ distance of 2.511(4) Å lies in the range of 2.361(2) Å (DARYEB) and 2.629(7) Å (TEQTAK, bridging ligation) which was found for 4 similar complexes (DARYEB, TEQTAK, YILBIF and RASXUF). The metal-ligand bonding in our complex occurs via the two carboxylate oxygen atoms. Both bonds undergo terminal ligation and no bridging takes place. The Cd-$O_{picolinate}$ bonding distances are 2.354(1) Å (Cd1-O1) and 2.551(1) Å (Cd1-O2), which are within the range of Cd-O distances stated above. The C-O distances in the carboxylate of the picolinic acid are not equal (C1-O1, 1.264(2) Å; C1-O2, 1.248(2) Å).

Another similar example is the structure by Wu, Zhang and Lin (2006) (REFCODE:DEQDIN) where the coordination number of Cd1 is seven, having two nitrates bonded bidentately, a substituted pyridine ring bonded monodentately through the nitrogen and two other ligands bonded monodentately to the cadmium ion. In this structure (Figure 4.10) the average O···O intra-ligand distances for the nitrate groups are 2.111(1) and 2.164(5) Å, and so the coordination reduces from seven to five.

A search of the CSD (Allen, 2002) reveals that cadmium metal ions bind to picolinate-type ligands mostly via both oxygen atoms and the nitrogen of the pyridine ring. The structure reported in this work is interesting because the nitrogen is protonated and is not involved in the coordination. A new coordination mode can therefore be added to the table in the introductory section of this chapter (Table 4.1). This mode would fit in column two which

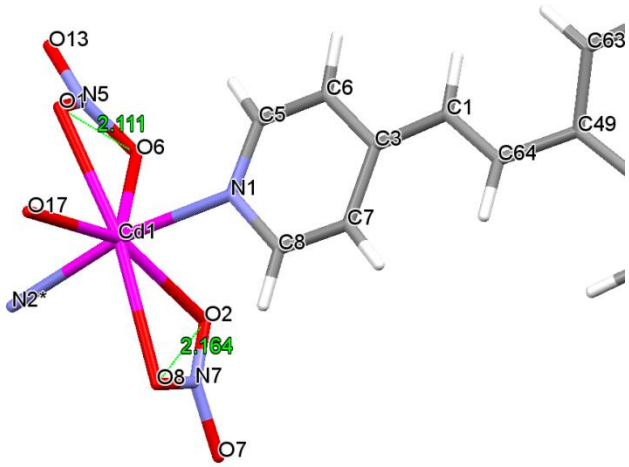
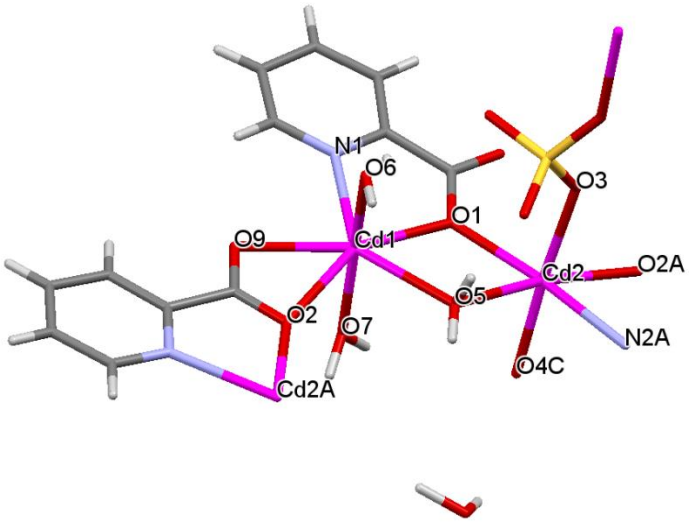


Figure 4.10 Coordination geometry around Cd1 for DEQDIN. The coordination number is seven which reduces to 5 if the nitrate ions are considered to be effectively monodentate (Wu, Zhang and Lin, 2006). Only a portion of the molecule is shown.

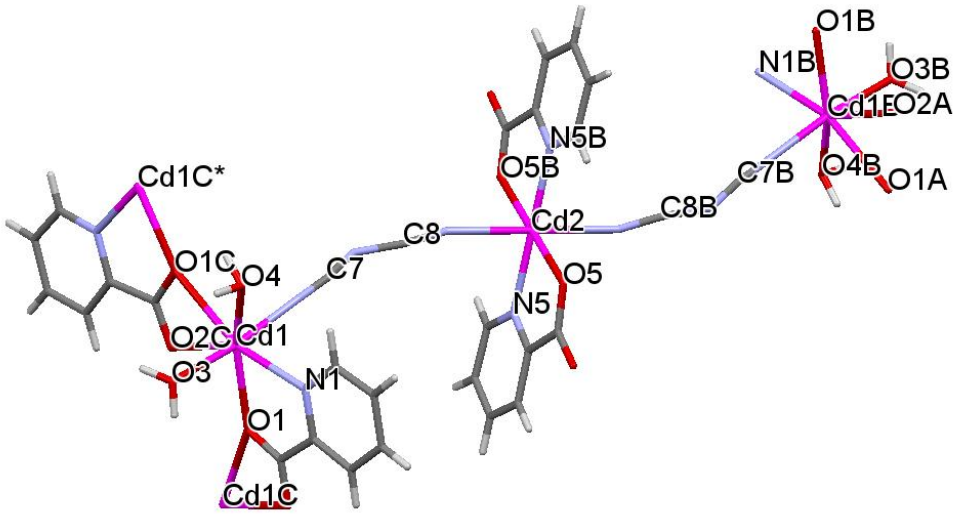
contains all of the LH forms of the ligand. This would be the first coordination complex of cadmium and picolinic acid in which the nitrogen is protonated.

The two cadmium complexes that show the most similarity to our Cd(PIC-H) complex, are those of YILBIF (Papatriantafyllopoulou *et al.*, 2007) and QUFKUY (Ma *et al.*, 2009) where the two oxygens of the carboxyl group of the picolinate ligand form a bidentate bond to the metal. However in both cases the pyridyl nitrogen

bridges cadmium ions to form polymeric structures. Their structures are shown in Figure 4.11, and are best described by coordination mode (*viii)* in Table 4.1.



a)



b)

Figure 4.11 The structures of a) YILBIF and b) QUFKUY showing their coordination modes.

In our case the resulting octahedron is distorted. The angle closest to 180° is that between O9 and O10 (O9-Cd-O10) which has a value of 167.51(5)°. If the geometry is reduced to 6 the one angle would be measured using the midpoint of the vertex between the bidentately bonded groups and O2, passing through Cd. This angle, measured as the N2-Cd-O2 angle, has a value of 154.25(5) °. The O1-Cd-O6 angle having a measure of 126.04(5) ° is furthest from linearity and is mostly responsible for the distortion of the octahedron.

4.4.2 Tri(pyridine-2-carboxylato-N,O)-cadmium(II) dinitrate Complex ($Cd(PIC\text{-}H)_3$)

4.4.2.1 Analysis of the Crystal Structure

Crystals of $Cd(PIC\text{-}H)_3$, $[Cd(C_5H_4NCO_2H)_3 \cdot NO_3]$, belong to the trigonal crystal system and crystallized in the P-3 space group. The cadmium(II) atom is coordinated octahedrally by an oxygen atom of the carboxylic acid group and the nitrogen atom of the pyridine ring of three separate picolinic acid ligands. The geometry is distorted octahedral, having an average bite angle (O-Cd-N) of 72.14° (0.02). Figure 4.12 shows the coordination and numbering scheme of this crystal structure. Selected bond lengths and angles are given in Table 4.6. Picolinic acid being an unsymmetrical, bidentate ligand is able to exist in two different isomeric forms, namely facial and meridional (Basu, Peng, Lee and Bhattacharya, 2005). The structure of $Cd(PIC\text{-}H)_3$ reported here shows the presence of the facial isomer in this complex since the three pyridine nitrogens are adjacent and occupy the corners of one triangular face of the octahedron, as the facial geometry is described in Shriver and Atkins (1999).

Within the asymmetric unit there is one coordination complex and a nitrate ion disordered over two positions. The unit cell contains two $Cd(PIC\text{-}H)_3$ molecules that are related by a centre of inversion. The nitrogen of the nitrate ion occupies a special position (0.0, 0.0, z), and therefore the oxygen atoms of the nitrate group are

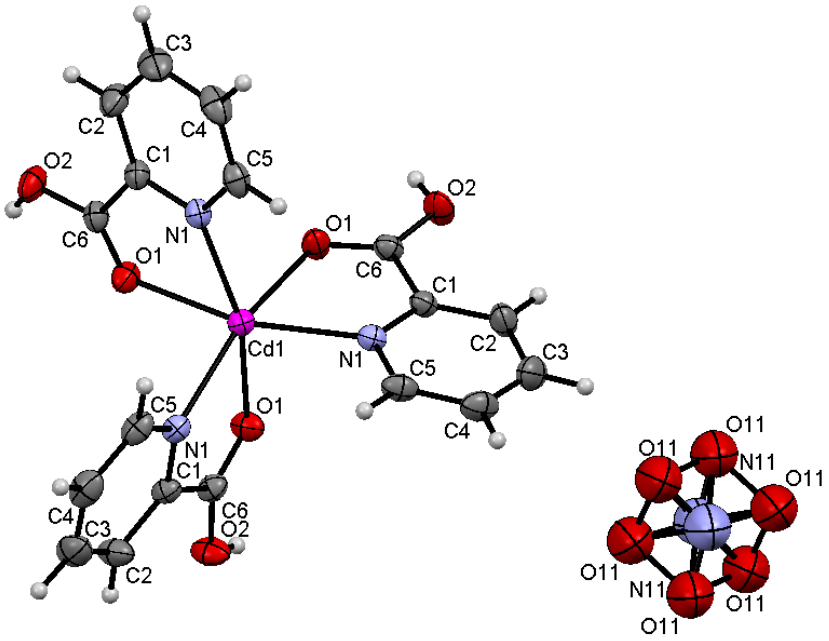


Figure 4.12 The molecular structure of Cd(PIC-H)$_3$ with displacement ellipsoids drawn at the 50% probability level.

disordered over three positions. In the crystal packing the centrosymmetric pair of molecules within the unit cell is linked by a hydrogen bond (1.644(2) Å) between O2-H1...H1-O2 (Figure 4.13). H1 is disordered over two positions; hence the distance between the oxygens is unusually short (O2…O2, 2.457(3) Å), compared to a typical hydrogen bond O…O distance of about 2.65 Å (Allen *et al.*, 2004).

A view down the b-axis (Figure 4.14) shows chains of Cd(PIC-H)$_3$ molecules connected by hydrogen bonds. Hydrogen bonding between the metal complexes as well as Van der Waals forces between the oxygens of the nitrate ion and C-H of the pyridine rings results in a channel centred around the nitrate ion (looking down the c-axis) (Figure 4.15).

This structure may have an application in molecular organic framework (MOF) chemistry due to the channels it possesses. Basu, Peng, Lee and Bhattacharya

(2005) also state the importance of tris-picolinate complexes with transition metals in the biological field.

Table 4.6 Selected bond lengths (Å) and angles (°) for $Cd(PIC\text{-}H)_3$.

$Cd(PIC\text{-}H)_3$			
O(1)-Cd(1)	2.3209(16)	N(1)#1-Cd(1)-O(1)#1	72.15(6)
N(1)-Cd(1)	2.2949(19)	N(1)-Cd(1)-O(1)#1	162.19(7)
		N(1)#2-Cd(1)-O(1)#1	91.75(7)
N(1)#1-Cd(1)-N(1)	105.68(5)	O(1)-Cd(1)-O(1)#1	90.15(6)
N(1)#1-Cd(1)-N(1)#2	105.68(5)	N(1)#1-Cd(1)-O(1)#2	162.19(7)
N(1)-Cd(1)-N(1)#2	105.68(5)	N(1)-Cd(1)-O(1)#2	91.75(7)
N(1)#1-Cd(1)-O(1)	91.75(7)	N(1)#2-Cd(1)-O(1)#2	72.15(6)
N(1)-Cd(1)-O(1)	72.15(6)	O(1)-Cd(1)-O(1)#2	90.15(6)
N(1)#2-Cd(1)-O(1)	162.19(7)	O(1)#1-Cd(1)-O(1)#2	90.15(6)

#1 and #2 refer to two symmetry related molecules

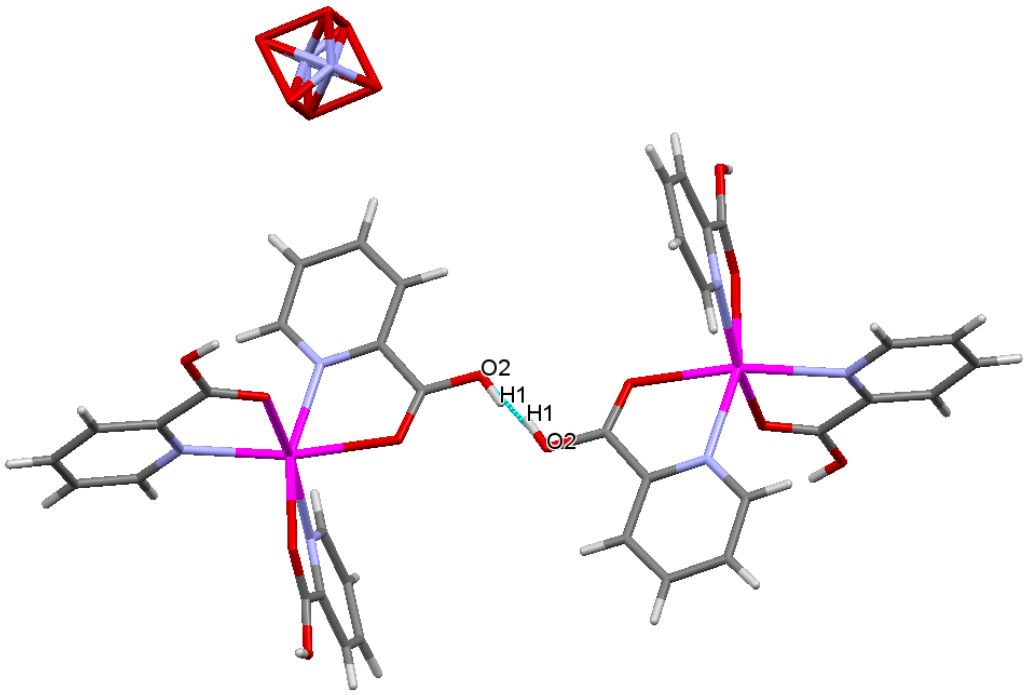


Figure 4.13 Hydrogen bonding between two $Cd(PIC\text{-}H)_3$ molecules related by a centre of inversion showing the disordered H1 positions.

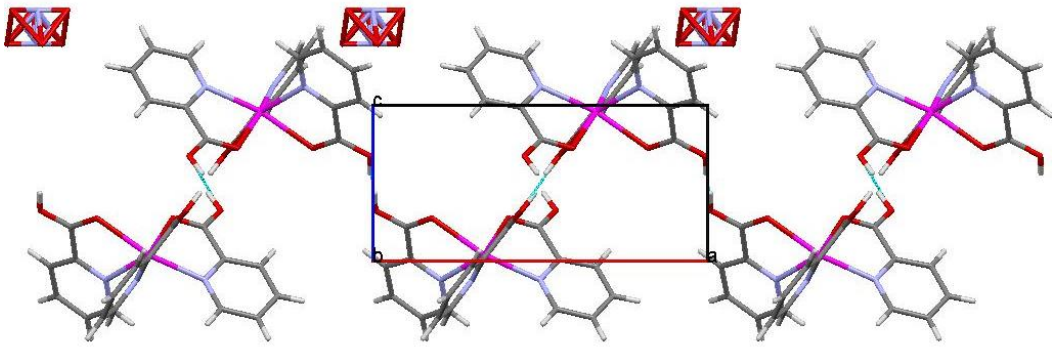
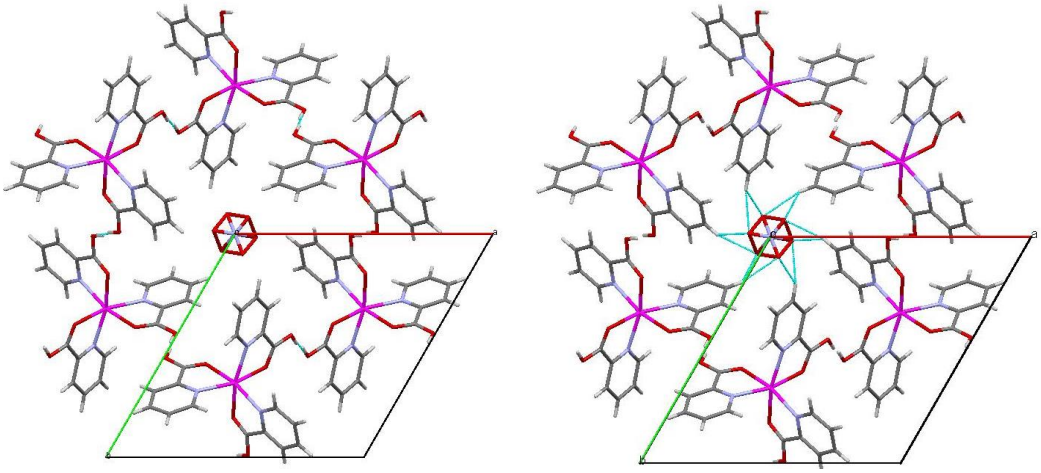


Figure 4.14 Hydrogen bonded chains of Cd(PIC-H)$_3$ as seen down the b-axis.



a) b)

Figure 4.15 A view down the c-axis showing a) the channel occupied by the nitrate ions, and H-bonds between the Cd(PIC-H)$_3$ complexes, and b) the short contacts between the nitrate anion and the Cd(PIC-H)$_3$ complexes.

4.4.2.2 A Comparative Study with Literature Structures

A CSD search for cadmium(II)-picolinate type structures having an octahedral arrangement, as in Cd(PIC-H)$_3$, produced zero hits. The same octahedral arrangement produced by three picolinate ligands has been observed with other

transition metals though. Basu, Peng, Lee and Bhattacharya (2005) produced two tris-picolinate complexes, one with iridium(III) (REFCODE: FISTUX) and the other with rhodium(III) (REFCODE: FISTOR). Both complexes contain three picolinate ligands each bonded to the metal centre via bidentate N, O-donors and each forming a five membered chelate ring. The Ir(III) and Rh(III) structures both exhibit the meridional stereochemistry which is the more common form found for these specific metal centres (Basu, Peng, Lee and Bhattacharya, 2005). A tris-ruthenium(III) complex (REFCODE: KIVROW) of the same ligand, by Barral *et al.* (1991), and a tris-manganese(III) complex (REFCODE: PYCXMN) by Figgis, Raston, Sharma and White (1978) also shows the meridional arrangement. However, this was not observed in our tris-cadmium(II) complex ($Cd(PIC\text{-}H)_3$) which has facial stereochemistry. The picolinate ligand in the *tris* complexes with Ru(III) and Mn(III) chelated to the metal centre in the same way as described above for both Basu, Peng, Lee and Bhattacharya's (2005) complexes. Each complex can be described with the generic formula $[M(C_5H_4NCO_2)_3]\cdot H_2O$ (where M = metal ion) because the ligands are not protonated. The structure reported here is different though, in that all three ligands are singly protonated, and therefore its formula would rather be expressed as $[Cd(C_5H_4NCO_2H)_3]\cdot NO_3$, taking into account that each hydrogen is disordered over two positions. There are very few structures in the CSD (there is PYCXMN01 which contains picolinic acid, and BOKRID and OPOVUL which have ligands that are similar to picolinic acid) that have a *cis* coordination of picolinic acid similar to the structure that we report here, and it has been found that the ligand rather exists in the trans arrangement: BENVEV, FISTOR, FISTUX, KIVROW, KIVROW01 and LOBGUF to mention a few. None of the picolinic acid structures reported in the literature contain the ligand in its protonated form when coordinating in the *tris* or *cis* manner as the structure presented in this work does. It therefore appears that a novel coordination mode for a tris-picolinate structure has been identified.

Odoko, Isomoto and Okabe (2001) reported a cadmium(II) complex (REFCODE: NELNIB) that is octahedrally coordinated to two bidentately bonded picolinate ligands, and two chlorine atoms which bridge to a second identical cadmium(II) metal ion. Two of the four picolinate ligands are protonated, while the others are anionic (the structure also contains an ethanol solvent molecule). The N,O-bidentate bond lengths (2.326(4) and 2.313(3) Å, respectively) between the cadmium(II) and picolinate ligands compare very closely to those found in Cd(PIC-H)$_3$: Cd1-N1 and Cd1-O1 bond distances are 2.295(2) and 2.321(2) Å respectively.

The three bite angles of the pyridine rings in Cd(PIC-H)$_3$ differ slightly, but average to 72.14(2)°. The bite angles reflect the octahedral distortion and compare well with the angles observed in a similar complex produced by Odoko, Isomoto and Okabe (2001) (O1-Cd1-N1: 72.0(1)°), as well as to many other similar structures. In the structure reported by Odoko, Isomoto and Okabe's (2001) the carboxyl group and the pyridine ring are almost in the same plane, with torsion angles O1-C7-C2-N1 and O3-C14-C9-N8 of 3.7(10)° and 3.4(9)° respectively. However, in Cd(Pic-H)$_3$, the carboxyl group is not coplanar with the pyridine ring creating a much larger torsion angle (O1-C6-C1-N1) of 9.34 °.

4.5 RELATING SOLUTION SPECIES TO CRYSTALLINE COMPLEXES

Both of the cadmium(II) complexes reported here have significantly different structures which are each interesting in their own right. In both complexes the ligand is protonated, which is not very common for picolinic acid crystal structures, as discussed in the introduction. Cd(PIC-H) is the first picolinic acid crystal reported to adopt this coordination mode. Cd(PIC-H)$_3$ has a coordination mode not previously observed in Cd(II)-picolinate structures, although it has been observed

(albeit rarely) in complexes of other metal ions. Cd(PIC-H) corresponds to an MLH species found in solution and $Cd(PIC\text{-}H)_3$ to an $M(LH)_3$ species.

We aimed to grow a MLH species by adjusting the pH of the solution from which crystals were to be grown, and using low [L]:[M] ratios. Fortunately we obtained the structure that was meant to be formed, but the question was: does it correlate to what the SDD predicted? The SDD (Figure 4.16) plotted with conditions used to grow the crystals, indicates that at around pH 0.4 there are about equal quantities of free metal ion and the MLH species. Only from above pH 2 do the ML and other species start to predominate. MLH is therefore the dominant complexed species between pH 0 and 2 in solution, which includes the pH at which the crystal was formed.

Evaporation of the solution during crystal growth leads to an increase in the concentration of the solution. Since the concentration was not monitored, the effect of evaporation is shown by plotting SDDs at increasing concentrations, where the [L]:[M] ratio remains constant, and in this case at a ratio of 1:1. The dotted lines of Figure 4.16 were calculated at a concentration of 5 M (in the event of 90% of the solution evaporating) which indicates the changes in the distribution of species. Table 4.7 shows the percentage distribution of the MLH species at pH 0.4 for different solution concentrations. It is clear that as the concentration increases, so does the percentage of MLH in solution. From a concentration of 2 M it becomes dominant and the free metal ion (cadmium(II)) decreases substantially.

Figure 4.16 clearly shows why the experimental solution produced the MLH crystalline complex at a fluctuating pH of between -0.5 and 0.5 as it shows that the MLH complex is formed even before pH 0. Due to the large fluctuation of the solution's pH over such a short time, the pH for crystal growth was averaged to

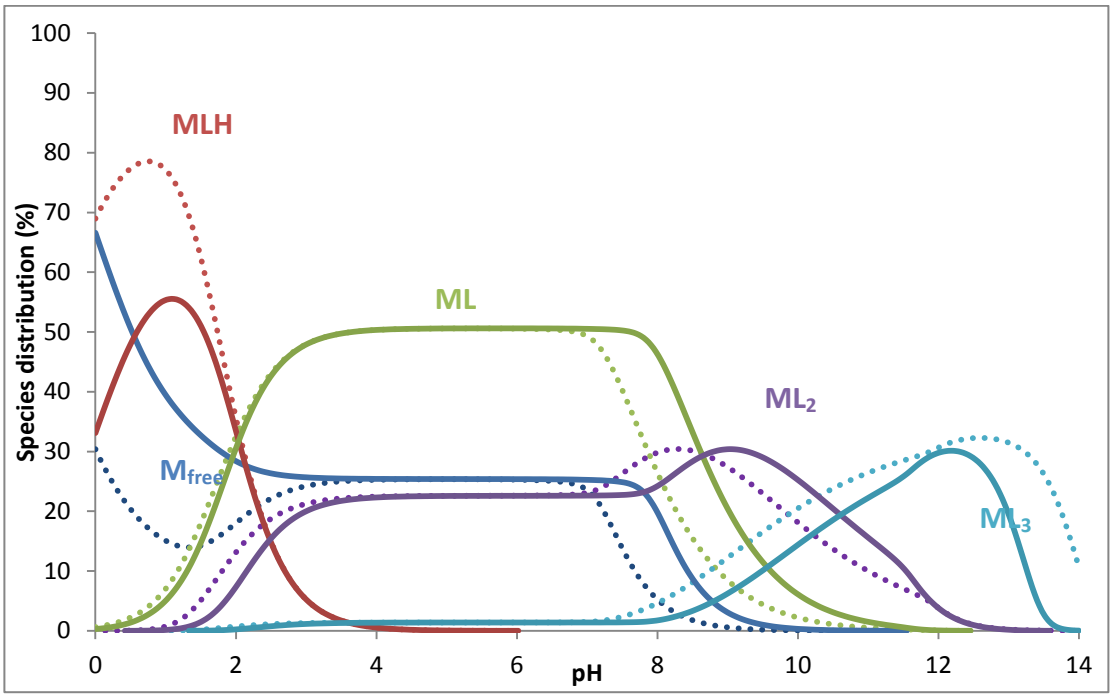


Figure 4.16 SDDs predicting the pH region where the MLH species exists when using liquor conditions of the crystal experiment. [Cd] = 0.5 M (solid lines) and [Cd] = 5 M (dotted lines) where [L]:[M] = 1:1.

about 0.4. The concentration of H^+ ions in solution was 0.45 M (calculated using pH = –log[H]) just before crystal growth. Just after the appearance of a few crystals it increased drastically to 3.6 M, and then upon formation of many more crystals it decreased to 0.31 M. This fluctuation in pH appears to indicate a more complicated process occurring in solution with the ligand deprotonating and then reprotonating to an extent again as crystallization occurs. Seen as this experiment was only conducted once, far more investigation is required to see whether these fluctuations are reproducible.

Table 4.7 The change in percentage distribution at pH 0.4 of the MLH species as the concentration of the solution increases and [L]:[M] = 1:1.

Solution Concentration (M)	MLH Distribution (%)
0.5	45.9
1	56.9
2	66.5
2.5	69.2
5	76.5

Another aspect to consider is that as evaporation occurs and the concentrations increases significantly, the ionic strength also increases considerably. In turn, the ionic strength affects the magnitude of the log β values due to their reliance on the activity coefficients (Bond, 1970) and hence the SDDs would be influenced. The Davies equation (Equation 4.1) can be used to calculate the activity coefficients ($f_{\pm}$) of electrolyte solutions at specific ionic strengths (μ), when the electrolyte dissociates into ions having charges z_1 and z_2. At very low concentration, when μ = 0, the second term (0.15μ) falls away and the Davies equation reduces to the Debye-Hückel equation. As the ionic strength increases so the formation of a complex is more difficult to achieve and hence the magnitude of the log β value decreases.

$$-logf_{\pm} = 0.5z_1z_2\left(\frac{\sqrt{\mu}}{1+\sqrt{\mu}} - 0.15\mu\right) \quad (4.1)$$

PXRD – a qualitative technique – was used in order to test whether the crystal chosen for single crystal XRD was representative of the sample. A small sample of crystals was crushed to a fine powder and carefully placed in the sample holder. The results obtained from PXRD can be seen in Figure 4.17. The Cd(PIC-H) complex is a novel complex and was therefore not in the database. Mercury was used to obtain a powder pattern that was calculated from coordinates using the SCXRD data. This pattern was expected to overlap with that obtained by PXRD but there were extra

peaks present in the sample analysed by PXRD. The pattern from PXRD shows other species existing together with the MLH complex. According to the SDD we infer that these species may possibly include the cadmium nitrate salt (as free metal ion (Cd_{free}) was present) as well as the ML species which also formed in solution at the same pH as the MLH complex. Comparison of the powder patterns of PICOLA02 (Hamazaki *et al.*, 1998), cadmium(II) nitrate (ICSD collection code 6185) and cadmium(II) nitrate dehydrate (ICSD collection code 297) with the powder pattern of our sample shows that none of these are represented in our powder pattern at this detection limit and therefore are not expected to be in our sample. Further analyses would need to be done before any conclusive deductions about the powdered sample can be made.

The experiments conducted where the $M(LH)_3$ structure was obtained were aimed at studying the effect of different [L]:[M] ratios. The SDDs plotted at varying [L]:[M] ratios produced rather different distributions at high pH, mostly due to the increase in the ML_2 and ML_3 species as expected (Figure 4.18). The pH of our solutions was not adjusted and the vials were left open until crystallisation occurred. Crystals were produced at pH 1.0 for the [L]:[M] ratio of 2:1 and at pH 1.3 for the [L]:[M] ratio of 3:1. In both cases the same complex structure was formed, but the crystallite size differed with the higher ratio producing larger crystals. The fact that the same complex was produced agrees with what the SDD predicts at the pH that the crystals were formed. Possibly a different result would have come about if the solutions were adjusted to higher pH, where the SDDs at different [L]:[M] ratios differ considerably. The formation of the $M(LH)_3$ complex was completely unexpected and has also never been reported by literature in solution studies before. This is probably because it is not a major species in solution under the more dilute conditions that are used for determining formation constants.

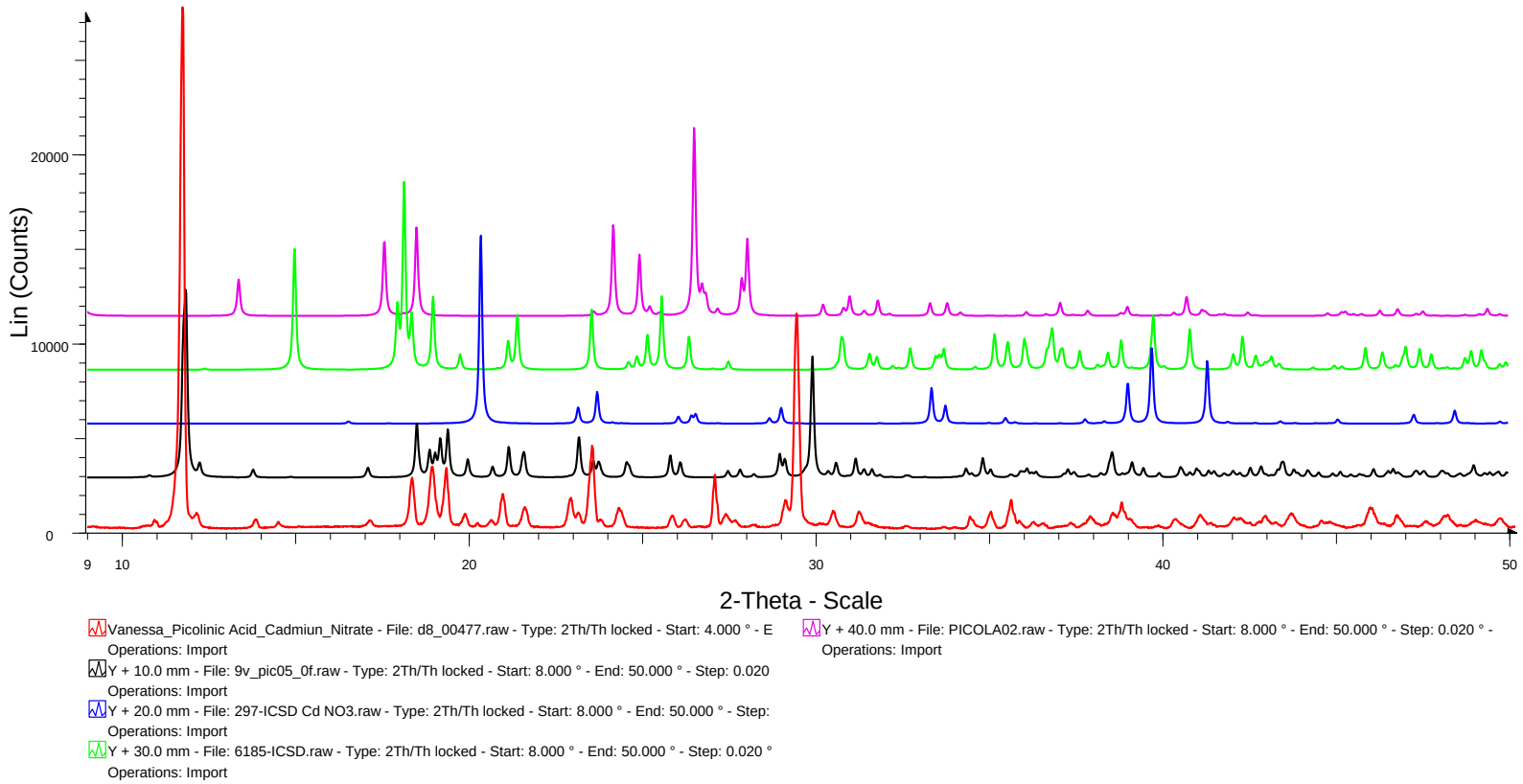


Figure 4.17 Powder patterns showing the calculated pattern for the Cd(PIC-H) complex (black) compared to that measured on the remaining crystals (red). Other powder patterns also shown are cadmium(II) nitrate (blue), and picolinic acid (PICOLA02) (pink) and cadmium(II) nitrate dihydrate (green).

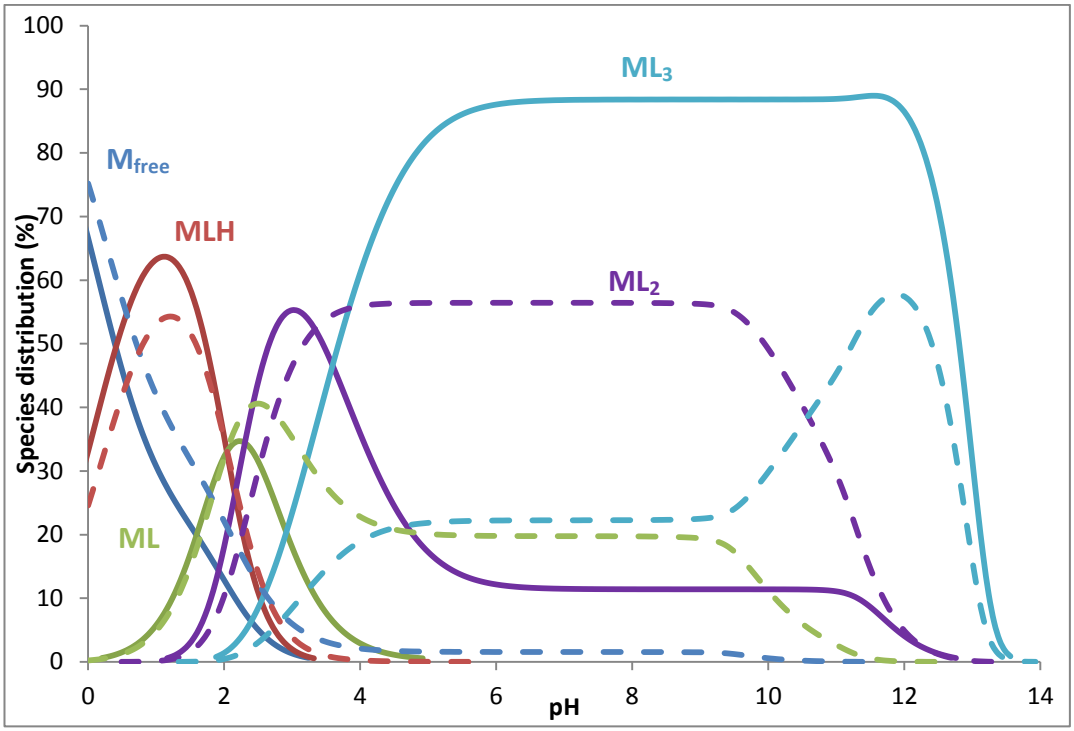


Figure 4.18 SDD showing the distribution effects of changing the [L]:[M] ratios, where the cadmium(II) concentration remains 0.125 M. Dashed lines represent [L]:[M] = 2:1 and solid lines represent [L]:[M] = 3:1.

When revisiting the polarographic data used to calculate the formation constants, it was possible to include the $M(LH)_3$ species in the model, but the standard deviation of the formation constant was large ($\log \beta = 20 \pm 3$) and the overall fit of the CCFC did not change. This is typical for minor species in solution. SDDs were plotted including the $M(LH)_3$ species ($\log \beta(M(LH)_3) = 20$) for [L]:[M] of 2:1 and 3:1 with a cadmium(II) concentration of 0.125 M (Figure 4.19). This clearly shows that $M(LH)_3$ is the dominant species at low pH under these conditions. At a [L]:[M] of 1:1 it was found that MLH and $M(LH)_3$ were present at comparable concentrations, but the MLH species started forming at slightly lower pH than $M(LH)_3$ (pH -1 vs. 0, respectively). For interest, SDDs were also plotted with $\log \beta$ values of 17 and 23 for $M(LH)_3$ (since $\log \beta = 20 \pm 3$) for [L]:[M] of 3:1 and the same cadmium(II) concentration. This gave a maximum percentage distribution for this species of 6% and 97%, respectively, so there is a

huge uncertainty as to its actual concentration in solution if it is formed. What was of importance here was that this species was predicted to exist in solution below pH 4 which correlates to the pH values at which the crystals were grown.

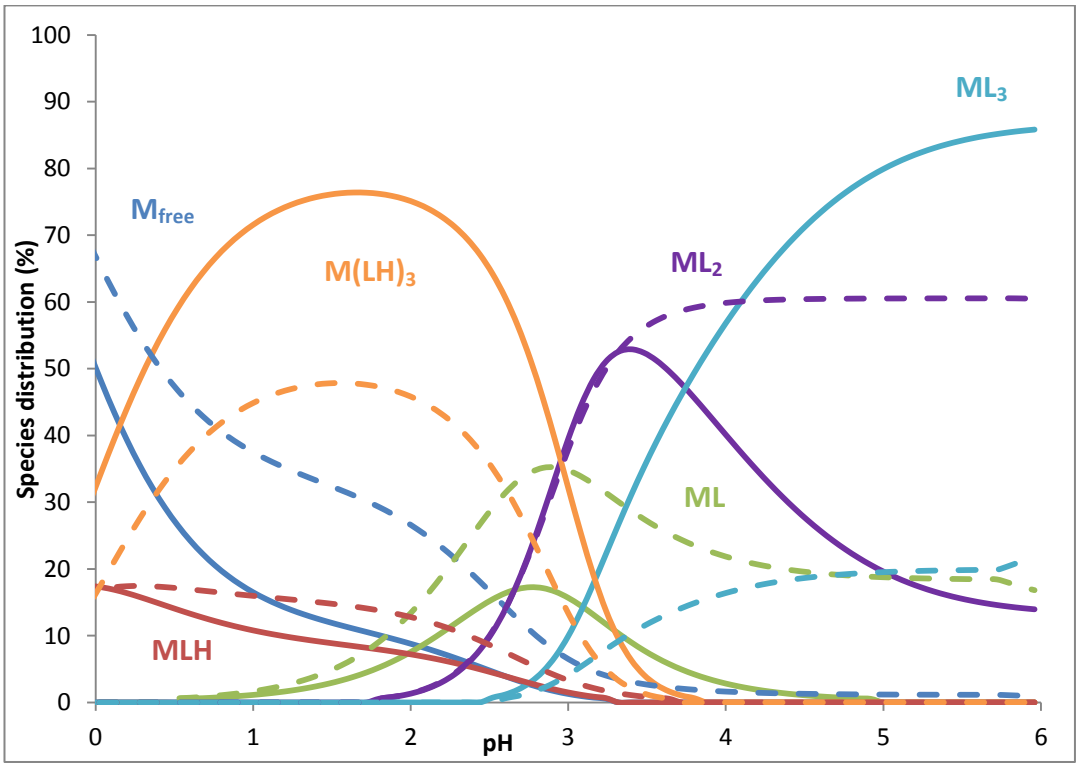


Figure 4.19 SDD of the acidic region showing the distribution of $M(LH)_3$ which (from below pH 0 to 4). [L]:[M] = 12:1 (dotted lines) and 3:1 (solid lines) where [Cd] = 0.125 M, log β(MLH) = 6.27, log β(ML) = 4.23, log $\beta(ML_2)$ =7.81 and log $\beta(ML_3)$ =10.53, and log $\beta(ML_3H_3)$ = 20.

Even though both the crystalline complexes contain protonated ligands, they are protonated at different sites resulting in different bonding arrangements. In the Cd(PIC-H) complex the nitrogen is protonated and in the $Cd(PIC\text{-}H)_3$ complex the carboxylate oxygen is protonated. It is interesting that both these complexes were produced at low pH but with such differing bonding between the metal and the ligand. To try and understand this, the protonation constants for pyridine and benzoic acid were considered, where each of these contain one of the functional groups found in picolinic acid. Their respective log *K* protonation constants are 5.22 and 3.95 (at 25 °C and ionic strength of 0.5 M). This can be

related to picolinic acid to deduce that the carboxylate oxygen would be deprotonated at lower pH than the nitrogen of the pyridine ring. Obtaining the Cd(PIC-H) complex below pH 0.86 (log *K* = 0.86 for the second protonation constant of picolinic acid) where the ligand is predominantly doubly protonated suggests that the cadmium(II) ion competed with the proton for a site on the ligand, and as a result the weaker protonation bond (O-H) was broken and the metal ion bonded to the ligand at this site. In the case of the $Cd(PIC\text{-}H)_3$ complex, the carboxylate oxygen was protonated and therefore bonding occurred through the nitrogen and remaining carboxylate oxygen. This complex was formed at approximately pH 1 where the picolinic acid is predominantly singly protonated, thus existing either as a zwitterion or as its neutral isomer which are in equilibrium with each other (as seen in Figure 4.1). Bonding through the N,O-arrangement, thus forming five-membered rings, appears to be the more stable conformation, as indicated by the list of coordination modes in Table 4.1.

4.6 CONCLUSIONS

Both crystal structures that were solved in this work are novel and also have novel coordination modes. Both crystalline complexes contained the singly protonated form of the ligand. The Cd(PIC-H) complex was grown from solutions at about pH 0.4 which is in the region where the doubly protonated form of the ligand is dominant and suggests that the metal ion possibly competed with the H^+ ion to form a bond to the carboxylate oxygen atom of the ligand. Obtaining the Cd(PIC-H) crystalline complex was exceptional not only because it was novel, but also because it supported the suggestion of its presence in solution by Billing, Cukrowski and Jordan (2013).

The $Cd(PIC\text{-}H)_3$ species has not been found in solution studies before, but elucidating the crystal form allowed for its inclusion in the solution species

model, albeit with a very high standard deviation. This certainly would be a minor species in solution under the conditions used in the solution experiments which explains why it was not incorporated into the species model. Obtaining a solid complex of this species could indicate its preorganized arrangement in solution and would thus support its existence in solution.

It can be concluded that the calculated complex formation curve is not sensitive enough to detect minor species in solution and so they can easily be overlooked when solving formation constants. It appears that crystalline complexes could be used to aid the speculation of solution species. This research has indicated a possible relationship between crystalline complexes and solution species.

4.7 REFERENCES

Allen, F., Watson, D., Brammer, L., Orpen, A. and Taylor, R., 2004. Typical interatomic distances: organic compounds. *International Tables for Crystallography Volume C: Mathematical, physical and chemical tables.* Springer pp 790-811.

Allen, F. H., 2002. Acta Crystallographica, B58, pp 380-388. Cambridge Structural Database. Version 5.31, November 2008 update.

Anderegg, G., 1960. Pyridinderivate als Komplexbildner I. Pyridincarbonsäuren. *Helvetica Chimica Acta,* 43 (1)**,** pp 414-424.

Barral, M. C., Jimenez-Aparicio, R., Royer, E. C., Saucedo, M. J., Urbanos, F. A., Gutierrez-Puebla, E. and Ruiz-valero, C., 1991. Reaction of tetraacetatochlorodiruthenium(II,III) with pyridine-2-carboxylic acid. X-Ray crystal structures of tris(pyridine-2-carboxylato-κ*N,O*)ruthenium(III) monohydrate and trans-bis(pyridine-2-carboxylato-κ*N,O*)bis(triphenylphosphine)ruthenium(II)-methanol(1/2). *Journal of the Chemical Society, Dalton Transactions,* 0 (6)**,** pp 1609-1613.

Basu, S., Peng, S.-M., Lee, G.-H. and Bhattacharya, S., 2005. Synthesis, structure and electrochemical properties of tris-picolinate complexes of rhodium and iridium. *Polyhedron,* 24**,** pp 157-163.

Bergman, M. M. and Cotton, F. A., 1966. *Inorganic Chemistry,* 5**,** pp 1208-1213.

Billing, C., Cukrowski, I. and Jordan, B., 2013. A Novel Approach to Monitoring of the Diffusion Junction Potential in Speciation Studies by Polarography Under very Acidic Conditions. Part I: The Reversible Cd(II)-Picolinic Acid System. *Electroanalysis,* 25 (9)**,** pp 2221-2230.

Bond, A. M., 1970. Some considerations of the electrolyte used to maintain constant ionic strength in studies on concentration stability constants in aqueous solutions. Application to the polarographic evaluation of thallium(I) complexes. *The Journal of Physical Chemistry,* 74 (2)**,** pp 331-338.

Bruker, S. a. S., 1999. Ver. 6.02 (including XPREP) ed. Madison, WI, USA.: Bruker AXS Inc.

Buffle, J., Mota, A. M. and Gonçalves, M. L., 1985. Determination of stability constants using ASV technique (Surface concentration effect). . *Portugaliae Electrochimica Acta,* 3**,** pp 293-310.

Cukrowski, I. and Loader, S. A., 1998. Evaluation of a Peak Potential of an Uncomplexed Metal Ion in Speciation Study of Labile Metal–Ligand Systems by Polarography.

Stability Constant Determination of Cd^{II} and Pb^{II} with Picolinic Acid at a Fixed L_T:M_T Ratio and Varied pH. *Electroanalysis,* 10 (13)**,** pp 877-885.

Deloume, J.-P. and Loiseleur, H., 1974. Structure Cristalline du Pyridine-2 Carboxylate de Cadmium. *Crystal Chemistry,* B30**,** pp 607.

Evans, G. W., 1982. The role of picolinic acid in metal metabolism. *Life Chemistry Reports,* 1**,** pp 57-67.

Evtimova, B., Scharff, J.-P. and Paris, M. R., 1969. *Bulletin de la Societe Chimique de France* pp 81.

Figgis, B., Raston, C., Sharma, R. and White, A., 1978. Crystal structure of Tris (pyridine-2-carboxylato) manganese(III) monohydrate. *Australian Journal of Chemistry,* 31 (11)**,** pp 2545-2548.

Grant, R. S., Coggan, S. E. and Smythe, G. A., 2009. The Physiological Action of Picolinic Acid in the Human Brain. *International Journal of Tryptophan Research,* 2**,** pp 71.

Hamazaki, H., Hosomi, H., Takeda, S., Kataoka, H. and Ohba, S., 1998. 2-Pyridinecarboxylic acid. *Acta Crystalographica,* 54**,** pp IUC9800049-IUC9800049.

Jain, D. S., Prakash, O. and Bhasin, S. K., 1976. *J. Electrochem. Soc. India* 25**,** pp 139.

Kang, Y., Zhang, J., Li, Z.-J., Qin, Y.-Y. and Yao, Y.-G., 2005. Rare 4.8^2 net in a fluorescent Cd-organic framework. *Inorganic Chemistry Communications,* 8 (8)**,** pp 722-724.

Ma, K., Shi, Q., Hu, M., Cai, X. and Huang, S., 2009. Two Cd(II) and Ni(II) complexes constructed with dicyanamide and picolinate ligands. *Inorganica Chimica Acta,* 362 (14)**,** pp 4926-4930.

Martell, A. E. and Hancock, R. D., 1996. *Metal Complexes in Aqueous Solutions*, New York, Plenum Press.

Martell, A. E., Smith, R. M. and Motekaitis, R. J., 2004. NIST Standard Reference Database 46. 8.0 ed. Gaithersburg, USA: U.S Department of Commerce, National Institute of Standards and Technology.

Matsui, H. and Ohtaki, H., 1982. A potentiometric study on mixed ligand cadmium (II) complexes with 2-pyridinecarboxylic acid and 2-aminoalkanoic acids. *Bulletin of the Chemical Society of Japan,* 55 (7)**,** pp 2131-2133.

Mautner, F. A., Abu-Youssefb, M. A. M. and Goher, M. A. S., 1997. Polymeric complexes of cadmium(II) bridged simultaneously by tetradentate picolinato and μ(1,1)-azido or μ(N,S)-thiocyanato anions. Synthesis and structural characterization of $[Cd(picolinato)(N_3)]_n$ and $[Cd(picolinato)(NCS)]_n$. *Polyhedron.,* 16 (2)**,** pp 235-242.

Odoko, M., Isomoto, N. and Okabe, N., 2001. Di-μ-chloro-bis[(2-pyridinecarboxylato-*N,O*)(2-pyridinecarboxylic acid-*N,O*)cadmium(II)] ethanol solvate. *Acta Crystallographica Section E,* 57 (8)**,** pp m371-m372.

Papatriantafyllopoulou, C., Raptopoulou, C. P., Terzis, A., Janssens, J. F., Manessi-Zoupa, E., Perlepes, S. P. and Plakatouras, J. C., 2007. Assembly of a helical zinc(II) chain and a two-dimensional cadmium(II) coordination polymer using picolinate and sulfate anions as bridging ligands. *Polyhedron,* 26 (15)**,** pp 4053-4064.

Pons, J., Garcia-Anton, J., Jimenez, R., Solans, X., Font-Bardia, M., and Ros, J, 2007. Preparation and structural characterisation of a Cd(II) complex with unusual geometry. *Inorg.Chem.Commun,* 10**,** pp 1554-1556.

Reichardt, C. and Welton, T., 2011. *Solvents and Solvent Effects in Organic Chemistry,* Weinheim, Wiley-VCH Verlag & Co.

Sheldrick, G. M., 2008. A short history of *SHELX*. *Acta Crystallographica,* A64**,** pp 112–122.

Shriver, D. F. and Atkins, P. W., 1999. *Inorganic Chemistry,* New York, Oxford University Press.

Wang, Y.-T., Fan, H.-H., Wang, H.-Z. and Chen, X.-M., 2005. A solvothermally in situ generated mixed-ligand approach for NLO-active metal-organic framework materials. *Inorganic Chemistry,* 44 (12)**,** pp 4148-4150.

Wu, C.-D., Zhang, L. and Lin, W., 2006. 1D and 2D Homochiral Metal-Organic Frameworks Built from a New Chiral Elongated Binaphthalene-Derived Bipyridine. *Inorganic Chemistry,* 45 (18)**,** pp 7278-7285.

Chapter Five

Solution Studies of Cadmium(II)-Dipicolinic Acid Complexes

5.1 INTRODUCTION

Pyridinecarboxylic acids are ligands that have been extensively researched due to their application in a broad range of fields. These fields include catalysis, magnetism as well as electronic and chemical separation (Li *et al.*, 2006). Multidentate nitrogen- or oxygen- donors are popular in the construction of metal-organic frameworks (MOFs) (Li *et al.*, 2006), and metal-organic coordination polymers for the formation of new functional materials (Kang *et al.*, 2006). Some pyridinedicarboxylic acids have shown great application in this field because these ligands can construct "versatile structural motifs, which finally aggregate to generate various supramolecular architectures with interesting properties" (Kang *et al.*, 2006). In biological systems, pyridinecarboxylates function in the transport of metal ions and in cell membrane protection (Mendoza-Díaz, Rigotti, Piro and Sileo, 2005).

Dipicolinic acid (see Figure 5.1) is an example of a pyridinedicarboxylic acid. It is found in nature existing in the spore cortex of certain bacteria, making up about 5 to 10% of the dry weight of the spores (Hachisuka, Tochikubo and Murachi, 1965). The function of dipicolinic acid in bacterial spores has been linked to the ability of the organism to oxidize glucose (Harrell and Mantini, 1957). Dipicolinic acid was initially thought to be responsible for the heat resistance of bacterial spores, but in later research it was shown that the ability of it to resist heat was actually related to the dipicolinic acid forming chelates with metal ions (Kalle and Khandekar, 1983). Calcium(II) is an important divalent metal cation in this process. It has been noted

that the ligand also acts as an activator (by a chelate mechanism) of spore enzymes during germination (Doi and Halvorson, 1961). Dipicolinic acid has a strong affinity to chelate to metal cations, and this can be witnessed in the large number of crystal structures published in literature (Allen, 2002) (detailed in Chapter Six). Dipicolinic acid coordinates to numerous metal ions, to mention a few: Ca(II), Ag(II), Ti(II), Ni(II), Fe(II), Cu(II), Zn(II), Mn(II), Cd(II), Tb(III), Cr(III), V(III). Some of these complexes have been found to be extremely important in the development of anti-HIV and insulin-mimetic agents (Park *et al.*, 2007).

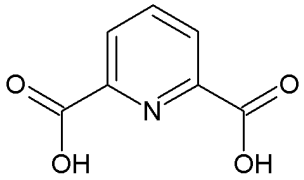


Figure 5.1 Chemical structure of dipicolinic acid.

Dipicolinic acid as a chelating agent has limited steric hindrance and depending on the level of protonation (hence pH of the solution), this ligand can bind to metal ions monodentately, bidentately, tridentately, or can even form bridged complexes with transition metals. Below pH 2.05 the ligand is predominantly doubly protonated and between pH 2.05 and 4.51 it is singly protonated, and in both cases can act as a zwitterion. Above pH 4.51 it is fully deprotonated (Figure 5.2).

The protonation of dipicolinic acid has been described as an interesting process by Calí, Rizzarelli, Sammartano and Pettit (1980) due to the fact that the protonation of the pyridine ring nitrogen differs remarkably from that of pyridine itself. They justify the difference by the loss of resonance of the dianion of dipicolinic acid upon protonation.

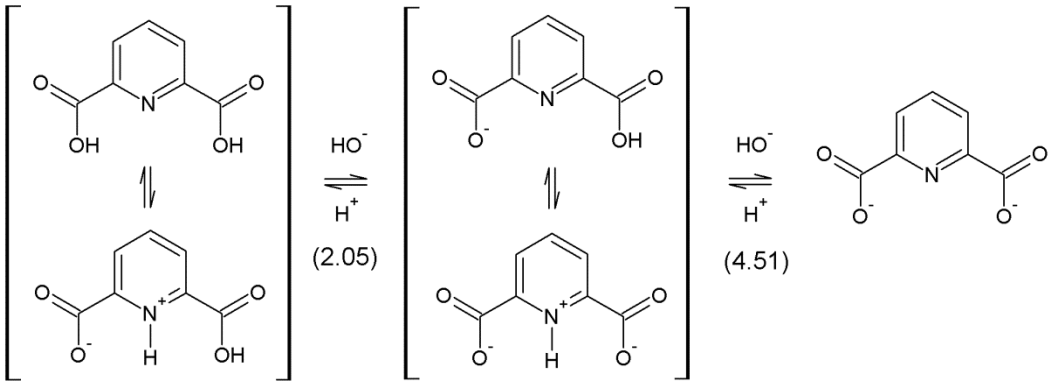


Figure 5.2 Deprotonation equilibria of dipicolinic acid with stepwise protonation constants given in brackets (quoted as log *K* values for 25 °C and 0.5 M ionic strength (Martell, Smith and Motekaitis, 2004).

5.1.1 Solution Complexes for the Cadmium(II)-Dipicolinic Acid System

Norkus, Stalnioniene and Crans (2002) studied complexation of Cd(II) (as well as Pb(II) and Cu(II)) with dipicolinic acid (DIPIC-H_2) in aqueous solutions at 20 °C (ionic strength of 0.4 M) by polarography. They showed that cadmium(II) in the presence of excess dipicolinic acid forms the ML_2 complex with log β_2 = 11.0 ± 0.1 when performing a ligand titration at pH 10 (from 5 to 50 mM of ligand). Interestingly the same complex was seen to predominate in solution just above pH 1.5. Data obtained by pH titration (done between pH 1.8 and 5.1 at a [L]:[M] of 10 where [Cd(II)] = 0.0005 M) allowed calculation of this species' formation constant (log β_2) to be of similar value (11.0 ± 0.3) to that same species obtained at pH 10. In neutral and alkaline solutions dipicolinic acid exists as a doubly deprotonated ion, however, in strongly acidic solutions the carboxylate groups are protonated which therefore act as electron acceptors and reduce the back donation of electrons to the nitrogen atom. Even so, the same complex was formed in both acidic and basic pH regions which indicates, firstly, the ability of the cadmium(II) ion to compete with the protons for chelation to the carboxylate oxygen atoms (at low pH), and secondly the high stability of this ML_2 complex.

Suzuki and Yamasaki (1957) conducted pH titrations at 25 °C (ionic strength of 0.1 M) and found two complexes, ML and ML_2, having respective log β values of 5.7 and 10. According to the authors the large stability constant for the ML complex implies that the ligand bonds tridentately to a single metal centre (Suzuki and Yamasaki, 1957). The chelate effect predicts that ligands with many donor atoms (multidentate ligands) form thermodynamically more stable complexes than analogous complexes containing unidentate ligands, because they are more preorganized (Martell and Hancock, 1996).

Anderegg (1960) used a copper amalgam electrode (CAE) for measuring the reduction potentials of cadmium complexes in solution at 20 °C and 0.1 M ionic strength ($NaNO_3$) using a titration method. Two complexes were identified; ML and ML_2, and their log β values are given in Table 5.1.

Evtimova, Scharff and Paris (1969) also studied the formation of complexes in solution for the cadmium(II)-dipicolinic acid system. An ion selective electrode (ISE) was used for experiments done in NH_4NO_3 at 25 °C and ionic strength of 1.0 M. The formation constants are also quoted in Table 5.1.

Table 5.1 Formation constants for cadmium-dipicolinic acid as quoted by literature.

	Suzuki and Yamasaki (1957)	**Anderegg (1960)**	**Evtimova, Scharff and Paris (1969)**	**Norkus, Stalnioniene and Crans (2002)**
Log β(ML)	5.7	6.75	6.51	Not considered
Log β(ML_2)	10	11.15	10.77	11.0
Log K(ML_2)	4.3	4.40	4.26	-
Temp (°C)	25	20	25	20
μ (M)	0.1 (-)	0.1 ($NaNO_3$)	1.0 (NH_4NO_3)	0.4 (KNO_3)
Method	Polarography	CAE	ISE	Polarography

The spread of the formation constants for the ML complex is wide. Considering the stepwise formation constant (log *K*) for the ML_2 complex, there is far greater agreement for this constant. Although some variation in formation constants is expected due to the different solution conditions, there may also be differences due to poor experimentation and lack of taking the E_j into consideration. The fact that the magnitude of the ML species is so broad may possibly be due to the E_j as this species is dominant below pH 2 where the E_j has its greatest effect.

5.2 AIMS

We aimed to study the cadmium(II)-dipicolinic acid system by collecting polarographic and potentiometric data, which was then analyzed and used to calculate formation constants of all identified solution species. We intended on calculating a more accurate value for the ML formation constant which varies considerably in literature. It is possible that this variation is due to potential shifting caused by the E_j (which was not necessarily accounted for) and so we used an in-situ witness ion to monitor the behaviour of the E_j so that the data could be corrected. The pH region below 2 was carefully studied for any species which may exist in this region. This potentially could have led to a more accurate and comprehensive species model to describe the cadmium(II)-dipicolinic acid system.

Polarographic experiments were also conducted at higher temperatures so that the effect on the formation constants and the species model could be observed and compared. Applying the van't Hoff relationship to determine reaction enthalpies using our results was also considered.

5.3 EXPERIMENTAL, DATA ASSESSMENT AND PROBLEM IDENTIFICATION

Complex formation with dipicolinic acid and cadmium(II) was studied at three different temperatures (namely 25, 32 and 40 °C) at an initial ionic strength of 0.5 M. At each temperature, three different ligand-to-metal concentration ratios ([L]:[M]) of approximately 20, 40 and 50 were studied. The solution pH was varied between 0.3 and 7 and polarograms were collected in the potential range of -200 to -850 mV. Doing replicate experiments at different [L]:[M] ratios should produce the same formation constants. The effect that the increased ligand concentration has is increasing the rate at which complexes are formed and shifting the equilibrium to form more products (complexes). Neither of these should have an effect on the magnitude of formation constants because the reaction times were much faster than the times allowed for complex formation to occur in the experiment. After each adjustment of pH the system was allowed a 60 s equilibration time before the pH was measured and the criterion for stability of the glass electrode (GE) potential readings (sampled every 2 s) was 0.04 mV before the system continued to measure the polarogram. This allowed sufficient time for equilibrium to be attained for this system before data were collected. At higher temperatures complex formation of endothermic processes are promoted and exothermic processes are reduced, thus a change in the magnitude of stability constants was expected. The data obtained at each temperature will be discussed separately in this chapter and then compared.

The automated process of measuring polarograms for the study of complex formation was conducted in the same way as described in Chapter 3, but now with the incorporation of the ligand. The polarograms were studied for changes in potential as this represents the formation of complexes. Visual changes in both the potential and current data as pH is increased can easily be seen when these polarograms are represented on the same set of axes and an example is depicted in Figure 5.3. The polarograms collected at pH 4.097 and 6.164 clearly show a negative

shift (as pH is increased) in the half-wave potential for the cadmium(II) wave at about -560 mV which was due to complex formation; different complexes are reduced at different potentials. Below pH 2 the reduction potential is influenced by two factors (with increasing pH): complex formation (in the negative direction) and E_j (in the positive direction). The effect of the E_j was expected and so the witness ion was incorporated in the solution to monitor its behaviour and hence allow for compensation thereof.

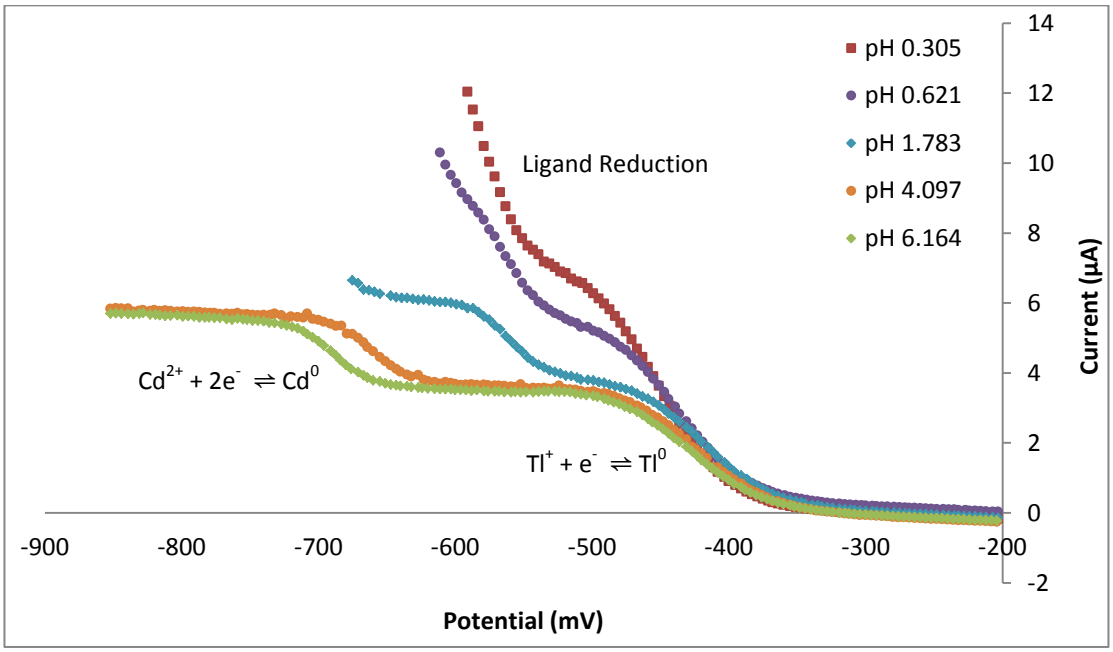


Figure 5.3 Polarograms showing potential shifts due to complex formation and E_j recorded during a pH titration, where [DIPIC]:[Cd] = 21 at 25 °C.

Two unexpected challenges were found when analyzing the data obtained for the cadmium(II)-dipicolinic acid system for all temperature experiments. Firstly, the cadmium(II) wave could not be resolved at low pH due to the reduction of the ligand at a similar potential (see Figure 5.3), and secondly, the witness ion, thallium(I) formed complexes with the dipicolinic acid from about pH 3.

5.3.1 Unresolved Waves at Low pH

A polarogram collected from solutions where dipicolinic acid was added showed that a large reduction wave overlapped with the cadmium(II) reduction wave. This wave was not H^+ reduction which only occurs at more negative potentials. Figure 5.4 shows two polarograms, both collected at pH 0.3, one containing cadmium(II) and thallium(I) only, and one with dipicolinic acid added to it. The polarogram taken after adding dipicolinic acid shows a sharp increase in current at a less negative potential than where the H^+ reduction wave would be. This could only be due to reduction of the ligand itself because its addition was the only change made to the system. (The thallium(I) wave was also slightly affected by this reduction process for the higher [L]:[M] ratio data.)

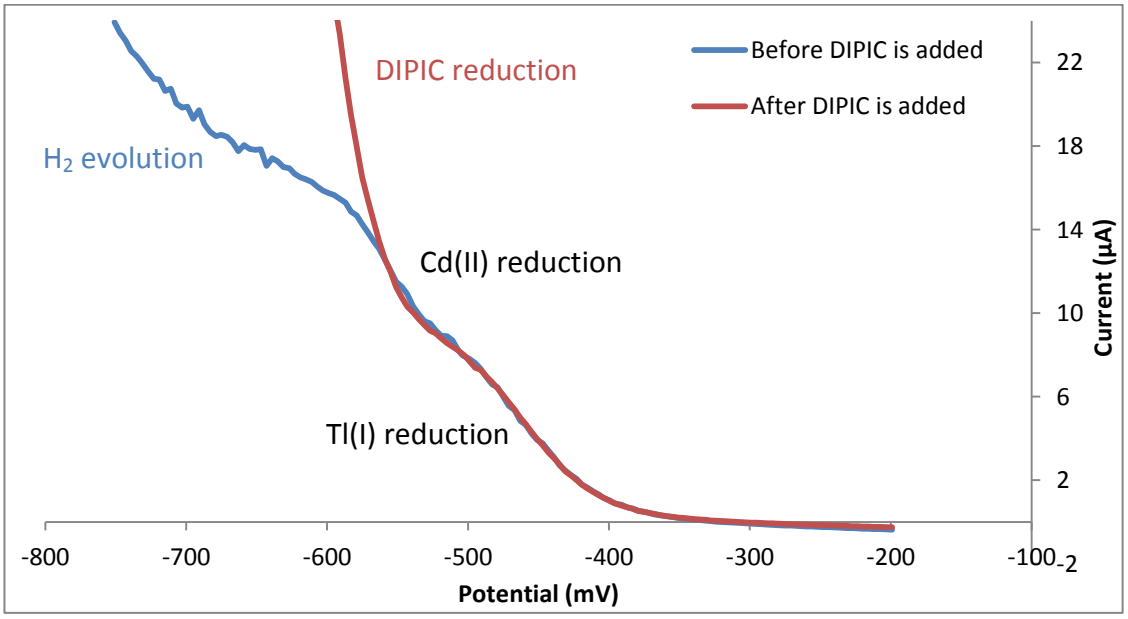


Figure 5.4 Polarograms measured at pH 0.3 before and after the addition of dipicolinic acid, where [DIPIC]:[Cd] = 52 and [Cd] = 1.00×10^{-4} M.

Typical polarographic experiments use small total metal concentrations (of around 10^{-4} M) and large [L]:[M] ratios (around 100 to 200). Cukrowski and Loader (1998)

conducted similar polarographic experiments using picolinic acid at 100 and 150 times the concentration of Cd(II), where [Cd] = 1 x10^{-4} M. For the dipicolinic acid system these ratios were too high, and it was found that decreasing this ratio minimized the effects caused by the ligand reduction wave. To demonstrate this polarograms were recorded at pH 0.3 having ligand in 100 times, 75 times and 50 times the concentration of a metal ion (Figure 5.5). It is evident that as the [L]:[M] ratio is decreased, so the onset of reduction of the ligand occurs at more negative potentials.

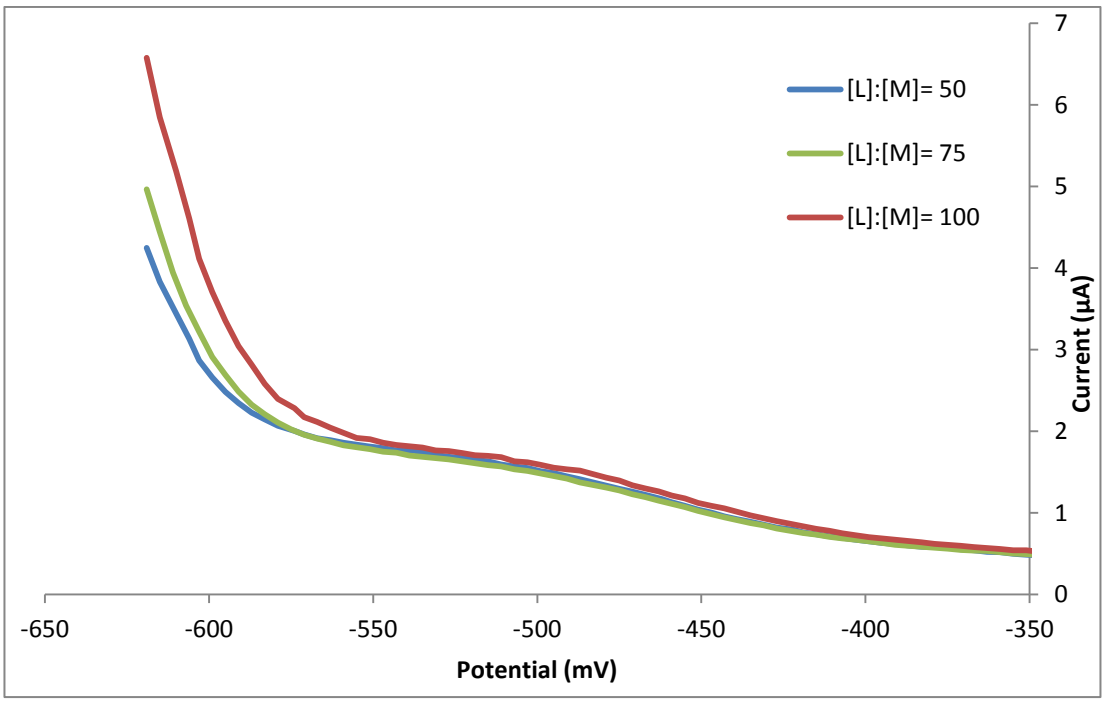


Figure 5.5 Polarograms showing the interference from the reduction of dipicolinic acid at different [L]:[M] ratios, all measured at pH 0.3.

A simulation has been constructed using an arbitrary compound "A" to demonstrate this point further (Figure 5.6). For the reduction of the same compound the reduction half-wave potential is constant, regardless of the concentration, and for this simulation it was arbitrarily chosen as 0 mV. The wave produced by the highest concentration (where the concentration is arbitrarily chosen as a multiple of *x*) of

this compound ([A] = 20*x*) begins to form at approximately 80 mV, whereas if the concentration were only *x* the wave begins at a much lower potential of about 40 mV. An increase in the concentration of the ligand results in an increase in the current. The larger the current, the less negative or more positive the potential at which the wave starts to form. Therefore reducing the ligand concentration postpones the onset of the reduction of the dipicolinic acid to more negative potentials and thus reduces the overlap with cadmium(II) as far as possible. For this study, lower [L]:[M] ratios of 20, 40 and 50 were thus chosen.

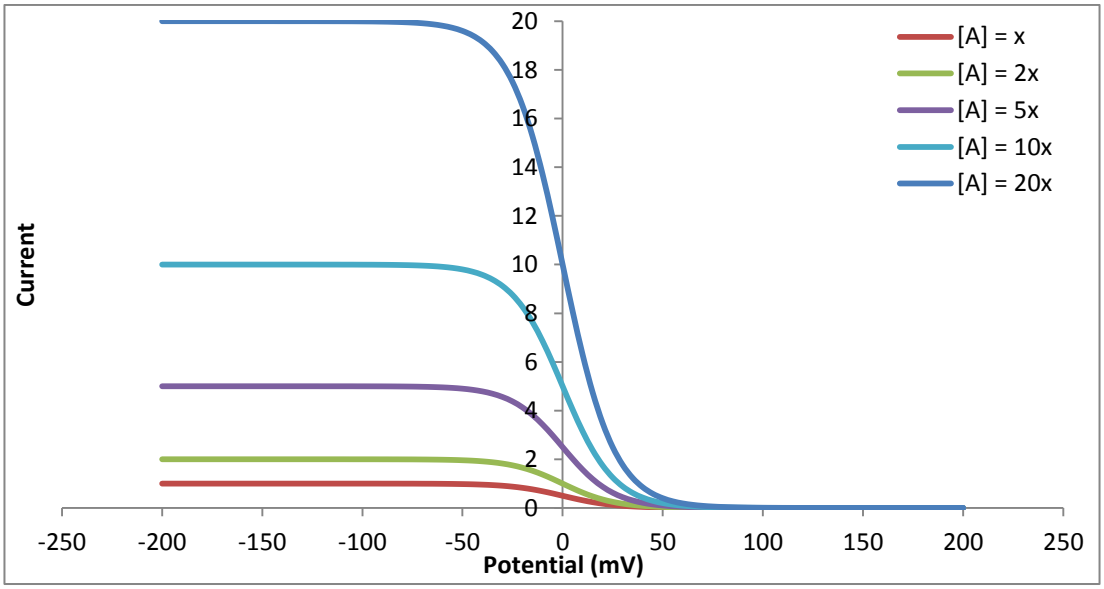


Figure 5.6 Simulation showing the effect of concentration, at the same pH, on reduction potentials.

Fortunately, this phenomenon plays a role only at low pH because as the pH increases the ligand's reduction potential shifts in a negative direction (as was also found by Samota, Garg and Pandey (2010)), allowing the thallium(I) and cadmium(II) data to be easily resolved. This is indicated in Figure 5.7 where polarograms were collected at 25 °C for [L]:[M] = 40 at increasing pH.

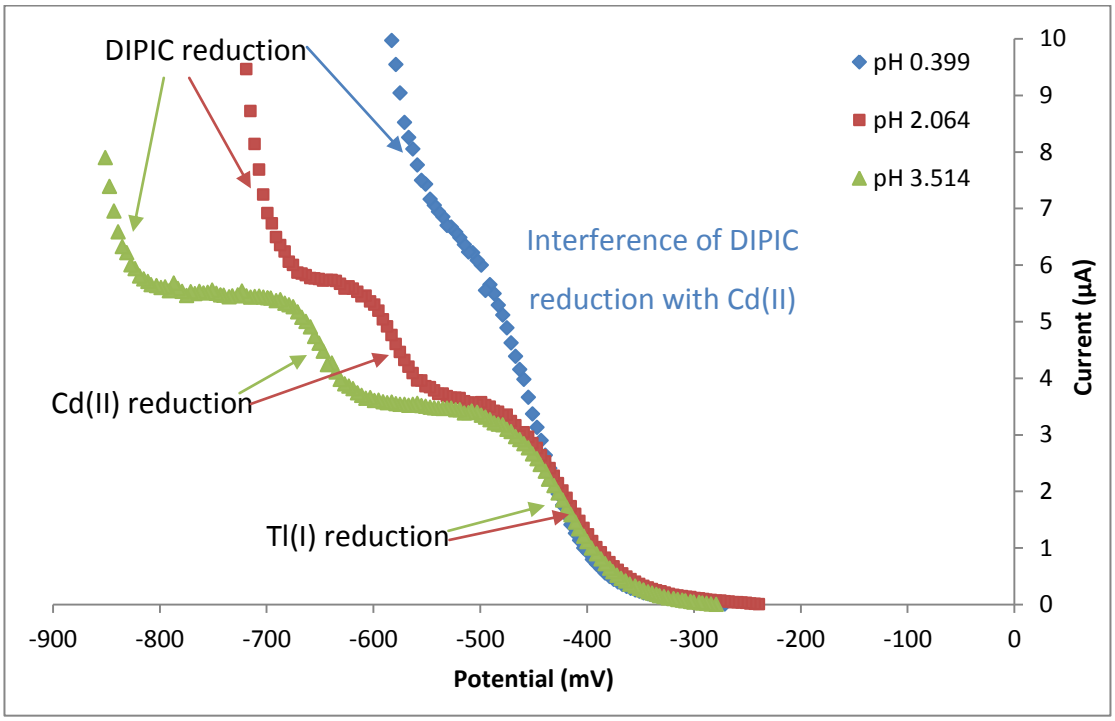


Figure 5.7 Polarograms showing the dependence of the reduction potential on pH.

At low pH reduction of the ligand overlaps reduction of thallium(I) and cadmium(II). Determining the parameters for the cadmium reduction wave accurately is difficult where there is still some overlap between cadmium(II) and the ligand. By about pH 2 both thallium(I) and cadmium(II) reduction waves are fully resolved from the ligand reduction wave. The reduction of dipicolinic acid is still responsible for the sharp increase in current after the reduction wave of cadmium(II). It is not due to the reduction of H^+ ions as this wave would have decreased substantially by pH 3.5 due to the decrease in the concentration of available H^+ ions. Additionally, as the pH increases and complex formation occurs the reduction of the cadmium(II) complex occurs at more negative potentials, compared to the uncomplexed cadmium(II), resulting in improved resolution between the cadmium(II) and thallium(I) reduction waves.

For experiments done at higher temperatures, the onset of the reduction potential of dipicolinic acid starts at less negative potentials (Figure 5.8), but so does that of the thallium(I) and cadmium(II) waves thus the data can be used from almost the same pH at each temperature. (For interest, Table A5.1 in Appendix A, shows the effect that temperature change has on a potential reading of the Ag/AgCl reference electrode.)

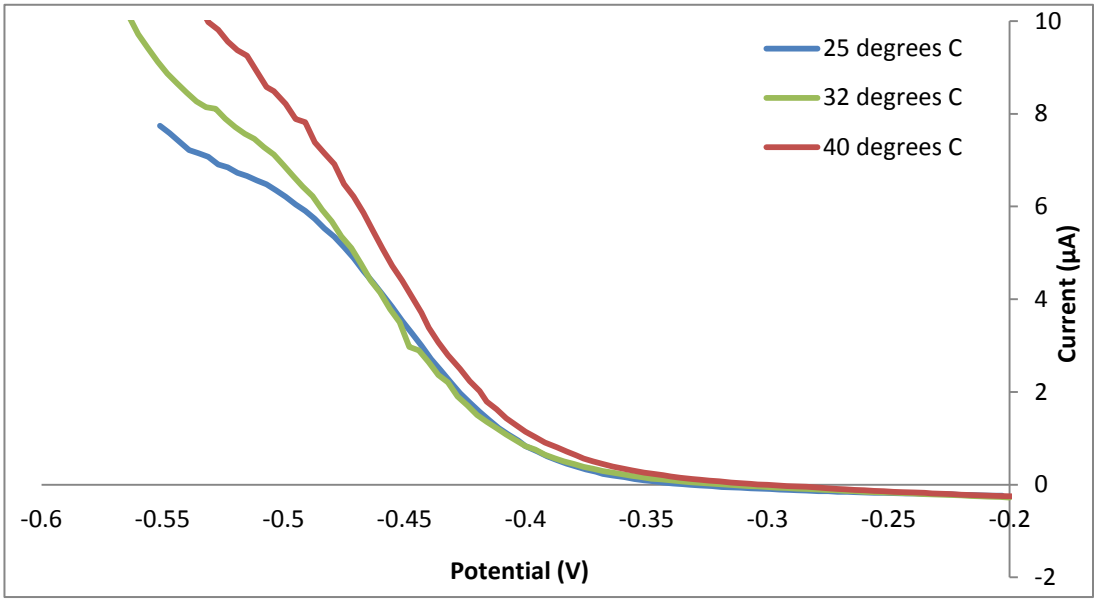


Figure 5.8 At increased temperatures the reduction occurs at less negative potentials. [L]:[M] = 20 where [Cd] = 1.00 x 10^{-4} M and the pH was 0.3 in all cases.

5.3.2 Complex Formation with the In-situ Witness Ion, Thallium(I)

The second challenge was the complexation of the thallium(I) ion by dipicolinic acid. A positive shift in potential occurred below pH 2 due to the changing E_j with pH and a negative shift in potential was observed above about pH 3 due to complex formation. For an ideal witness ion – any shift in the potential should be attributed to the change in the diffusion junction potential, and hence changes in shifts are only expected to occur below about pH 2 – which means that thallium(I) was not an

ideal witness for this system. The problem arose when obtaining the free cadmium(II) potential for experiments starting below pH 2, which relied on the free thallium(I) potential which is calculated by averaging the half-wave potential values of thallium(I) at pH > 2 where the magnitude of the half-wave potential should be constant. Figure 5.9 shows the experimental half-wave potentials of thallium(I) together with the predicted values for uncomplexed thallium(I) above pH 2. The predicted data were obtained by extrapolating the free metal ion potential that was determined by averaging the potential values between pH 2 and 3, to higher pHs. Above pH 2 the diffusion junction potential is small and no longer changing with pH, so a constant half-wave potential is expected if no complexation occurs. The decrease in the experimental half-wave potentials from pH 3.1 indicates that complex formation is taking place with dipicolinic acid.

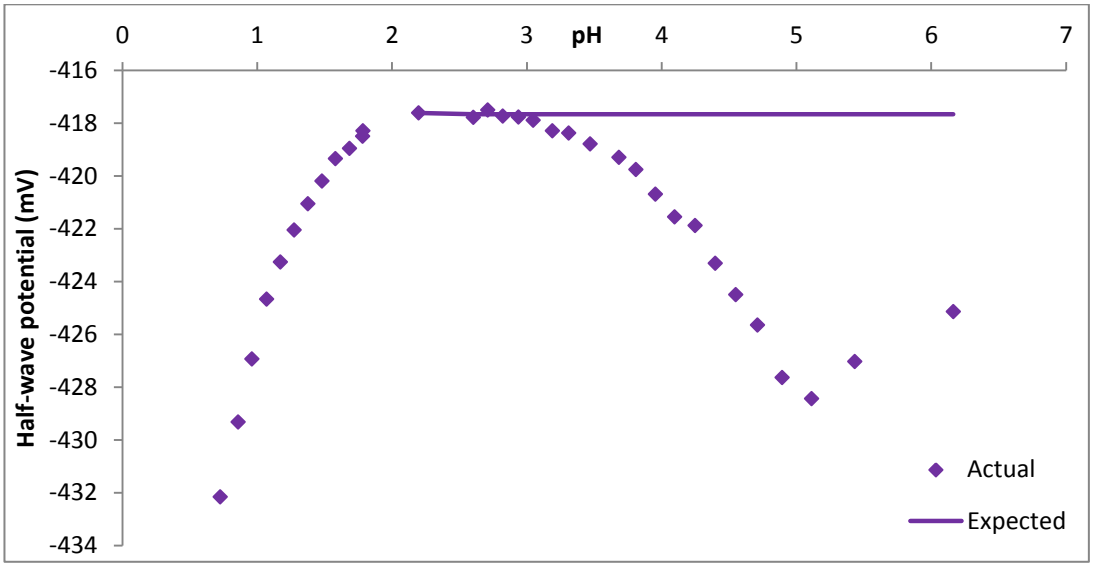


Figure 5.9 Experimental half-wave potential values for thallium(I) and expected values above pH 2 for uncomplexed thallium(I), where [L]:[Tl] = 11 and [Tl] = 2 x 10^{-4} M.

Figure 5.10 highlights this region using a plot where the half-wave potentials were subtracted from the free metal ion potential. If complex formation started at lower

pH then thallium(I) could not be used as an in-situ witness ion because it would be impossible to determine the free metal ion potential. The shifts above pH 3, due to complex formation, vary considerably with ligand concentration as expected. The larger shifts experienced by the thallium(I) ion for experiments performed at higher ligand concentrations represents a greater concentration of the complexes formed. An increase in the ligand concentration promotes formation of complexes which is seen in the magnitude of the potential shifts. For each experiment in Figure 5.10 there is a sudden decrease in the potential at pH 5.5 which measures between 2.5 and 2.7 mV. The reason for this recurring characteristic was not studied as the thallium data were simply used for compensation of the E_j.

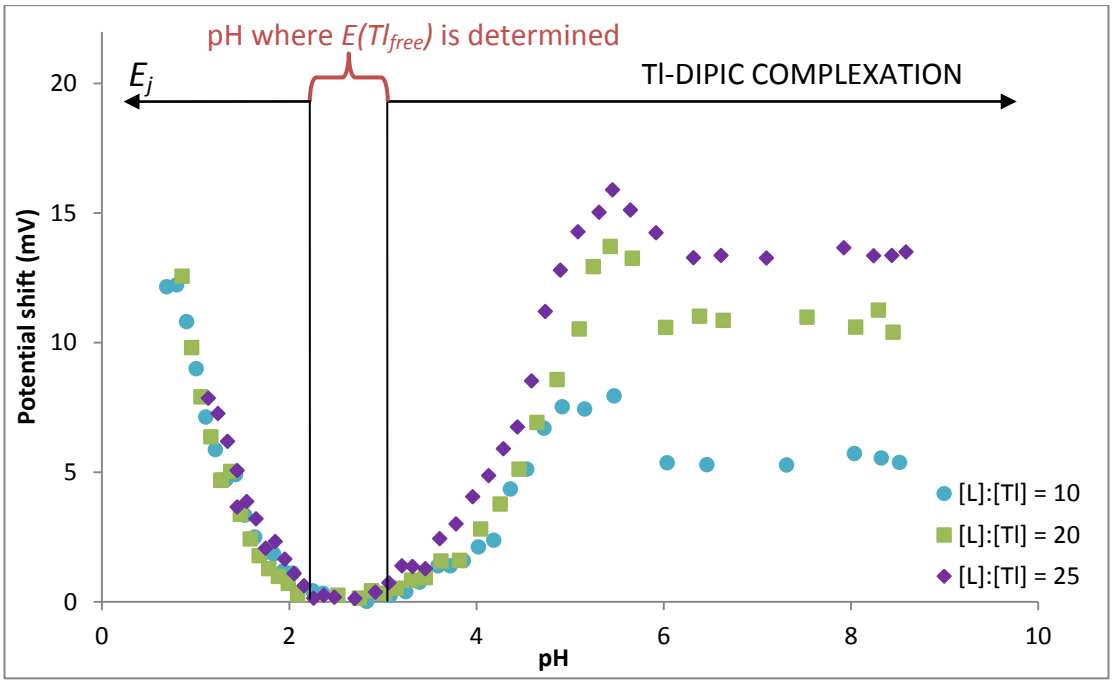


Figure 5.10 The potential shift due to complex formation between thallium(I) and dipicolinic acid collected at 32 °C, where [L]:[Tl]= 10, 20 and 25 (which corresponds to [L]:[Cd] = 20, 40 and 50 respectively).

Dipicolinic acid is a strong complexing agent, so it is not a surprise that it has formed complexes with thallium(I). Lainé, Gourdon, Launay and Tuchagues (1995) affirm

that dipicolinic acid has the ability to stabilize unusual oxidation states and form stable chelates, which was supported by Park *et al.* (2007). No stability constants for the thallium(I)-dipicolinic acid system were found in literature. Rough estimates of log β values found at 25 °C and 0.5 M ionic strength were obtained by Billing (2012). The data were not ideal for obtaining accurate results specifically for thallium(I) as the experiments were actually geared towards studying bismuth(III)-dipicolinic acid complex formation. Nevertheless, it was shown that the possible complexes formed in solution were ML and MLH with respective log β values of 3.56 ± 0.03 and 6.4 ± 0.2. Figure 5.11 is a species distribution diagram plotted using these formation constants at conditions used for the experiments in this work. In this specific case it is especially important to know that a species distribution diagram provides data only as significant as the formation constants that were used in plotting it, as Martell and Hancock (1996) so eloquently put it:

"The construction of a species diagram always starts with the total concentration of each component and its accuracy depends on the quality of all of the equilibrium constants"

The MLH complex is a minor species in solution, reaching a maximum of 10% at pH 3 and the ML complex is a major species predominating between pH 4 and 14. Complex formation with thallium(I) only begins at higher pH where the ligand is singly protonated or fully deprotonated, and therefore very little or no competition is required to form a complex. These observations are in line with our finding of complex formation starting just above pH 3 and becoming more significant at higher pHs.

Further evidence of thallium(I)-dipicolinic acid complexes were found on the CSD. Only three structures showing dipicolinic acid bonded to thallium(I) were reported in the CSD (REFCODES: GIZKEG, WARYEU and WARYEU01) and in each case they were polymers made up of ML units, as shown in Figure A5.1, Appendix A

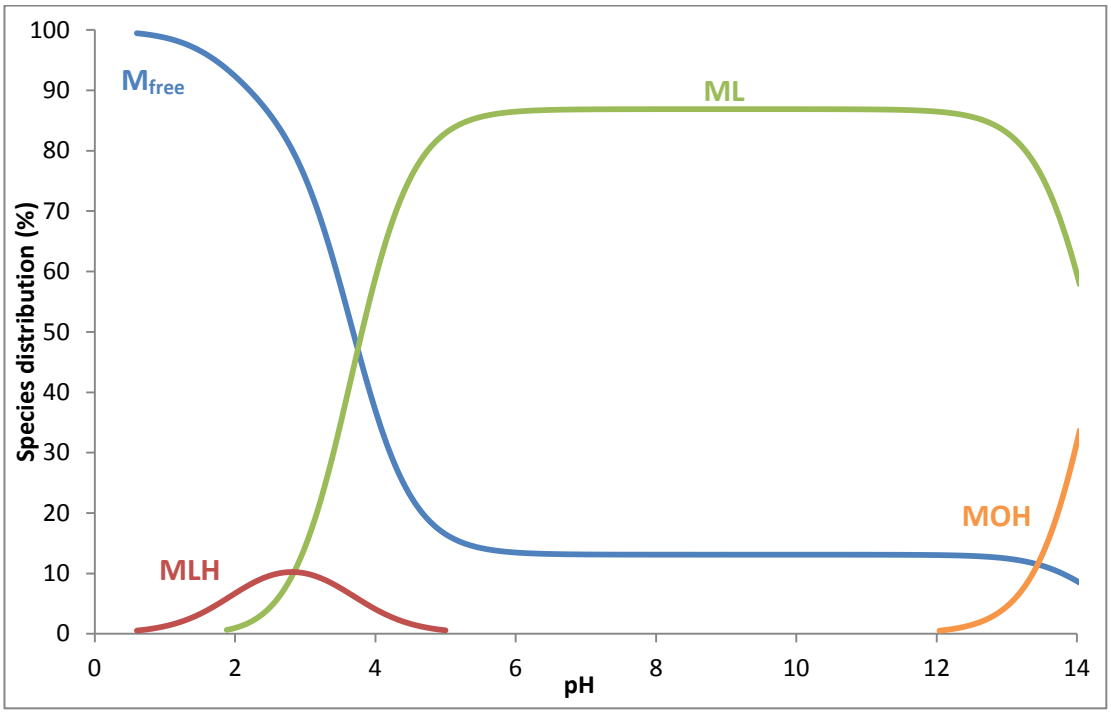


Figure 5.11 Species distribution diagram plotted using log β values for thallium(I)-dipicolinic acid complexes estimated by Billing (2012). [Tl] = 2 x 10^{-4} M and [L] = 2 x 10^{-3} M.

5.4 RESULTS AND DISCUSSION

5.4.1 Cadmium(II)-Dipicolinic Acid Formation Constants at 25 °C

Polarographic experiments were conducted at 25.0 ± 0.1 °C where cadmium(II)-dipicolinic acid complexation was studied at three [L]:[M] ratios, namely 21, 41 and 52. The initial concentrations of cadmium(II) and thallium(I) for each experiment were 1.00 x 10^{-4} M and 2.00 x 10^{-4} M, respectively. Polarograms collected for each experiment were fitted using Equation 2.2 to obtain half-wave potentials of the reduced metal species, diffusion limited currents, the value of δ, which indicates the reversibility of the process, and the parameters describing the background currents.

The [L]:[M] = 21 ratio data will be used as an example to explain the procedure followed to determine formation constants. The plot of half-wave potential vs. pH is shown in Figure 5.12.

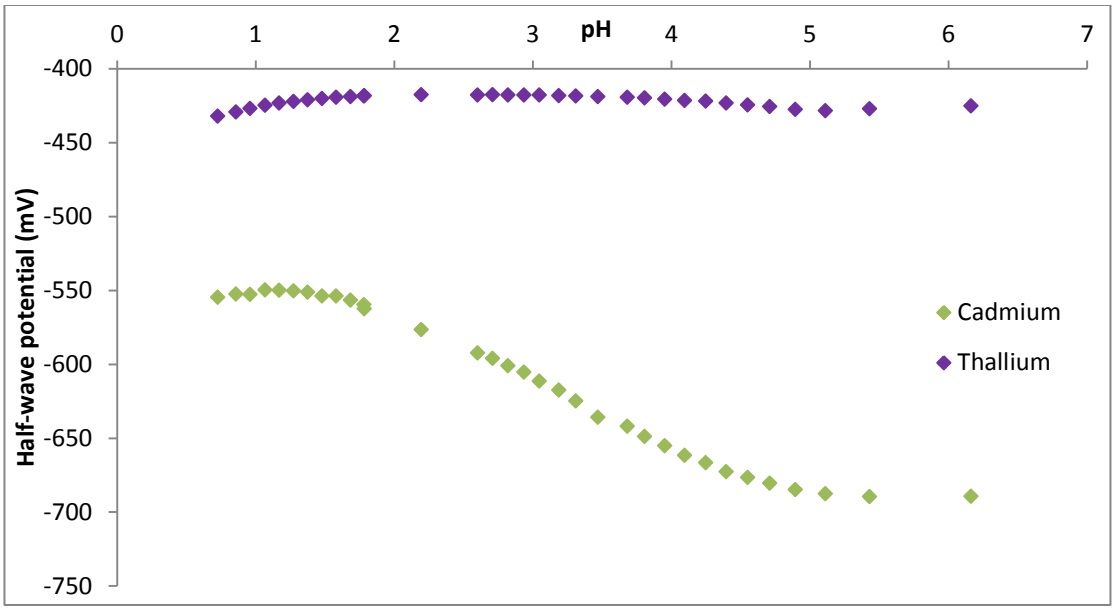


Figure 5.12 Thallium(I) and cadmium(II) half-wave potential values as pH is increased for [L]:[M] = 21 at 25 °C.

The first usable data (where the reduction waves could be resolved) were from pH 0.76 for this dataset. Polarograms from pH 2.07 to 2.27 and 2.48 to 2.68 could not be used because the data collected in these regions had background noise that could not be explained. An example of a noisy polarogram, in comparison with what it should in fact resemble, is shown in Appendix A, Figure A5.2.

Obtaining the correct free metal ion potential for cadmium(II) is essential because all potential shifts are calculated in relation to it (see Equation 2.5). In order to obtain the free metal ion potential for cadmium(II), the thallium(I) data are relied upon. Figure 5.13 shows the half-wave potential data for thallium(I) with complex formation occurring from pH 3.1 onwards. The free metal ion potential ($E(Tl_{free})$) is indicated with a solid line.

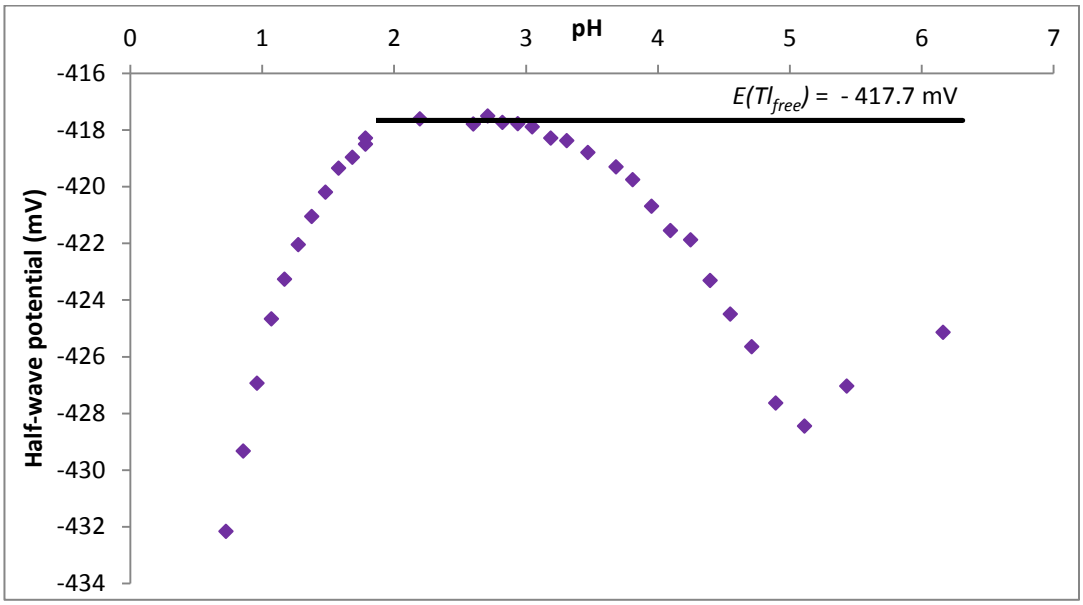


Figure 5.13 The determined free metal ion potential for thallium(I) where [L]:[M] = 21, at 25 °C.

Employing $E(Tl_{free})$ and the $\Delta E_{C>pH\ 2}$ value obtained from the C(I) Compensation model (Table 3.2), the value of $E(Cd_{free})$ can be calculated.

$E(Cd_{free}) = E(Tl_{free}) - \Delta E_{C>pH\ 2} = -417.66 - 119.98 =$ **-537.64 mV**

The C(I) Compensation Model was also used to simulate uncomplexed cadmium data below pH 2 for this experiment. Figure 5.14 shows the experimental cadmium(II) data and the predicted uncomplexed-cadmium potential values. The magnitude of the diffusion junction potential for cadmium(II) was then calculated from the difference between $E(Cd_{free})$ and the uncomplexed-cadmium(II) potential at each pH step below pH 2.

The experimental cadmium(II) half-wave potential data in the presence of ligand was then compensated for the E_j below pH 2.2 in this case. Figure 5.15 shows the effect of this compensation. Any changes in potential from that of the free metal ion are

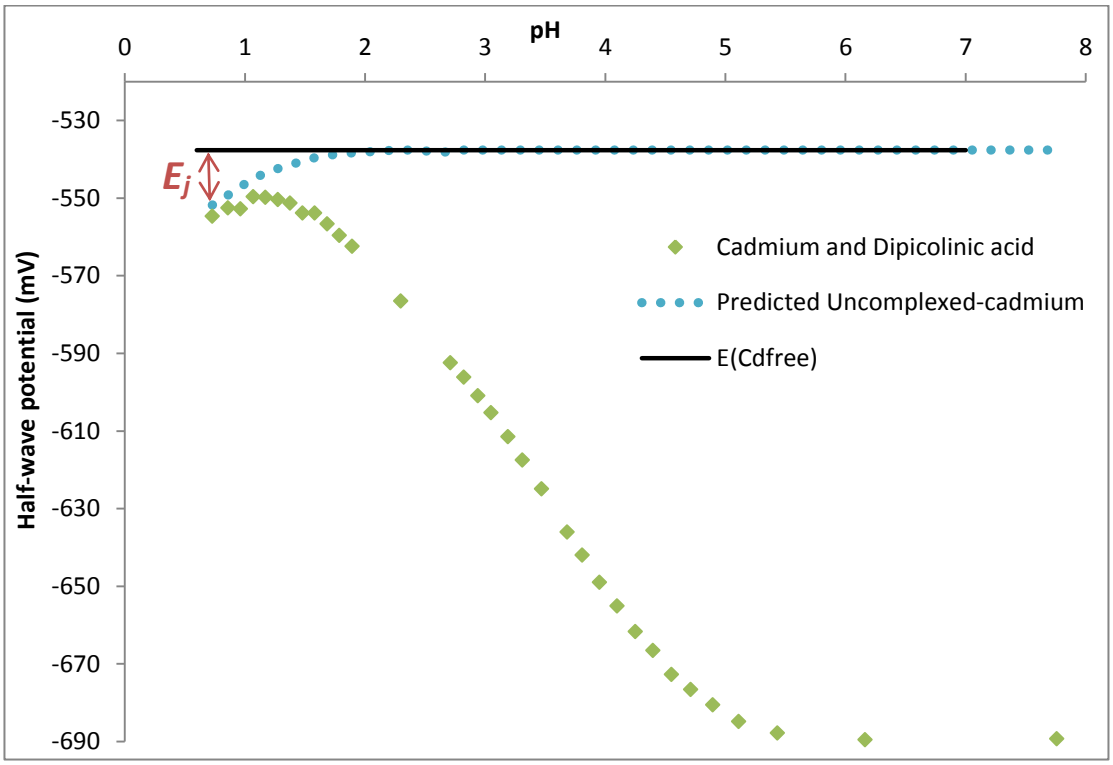


Figure 5.14 Graph showing the experimental half-wave potential for cadmium(II) and the predicted uncomplexed cadmium(II) data. The magnitude of E_j is the difference between $E(Cd_{free})$ and the predicted uncomplexed-cadmium(II) data.

now due to complexation only and hence these data can be used to determine which complexes are formed in solution and their respective formation constants.

In order to calculate formation constants based on Cukrowski's equation (Equation 2.5) using the 3D-CFC program (Cukrowski, 2000) the information in Table 5.2 is required. The following information at each pH step is also required: pH of solution, total volume of KOH added, diffusion limited current ($I(M_{comp})$) and the half-wave potential ($E(M_{comp})$).

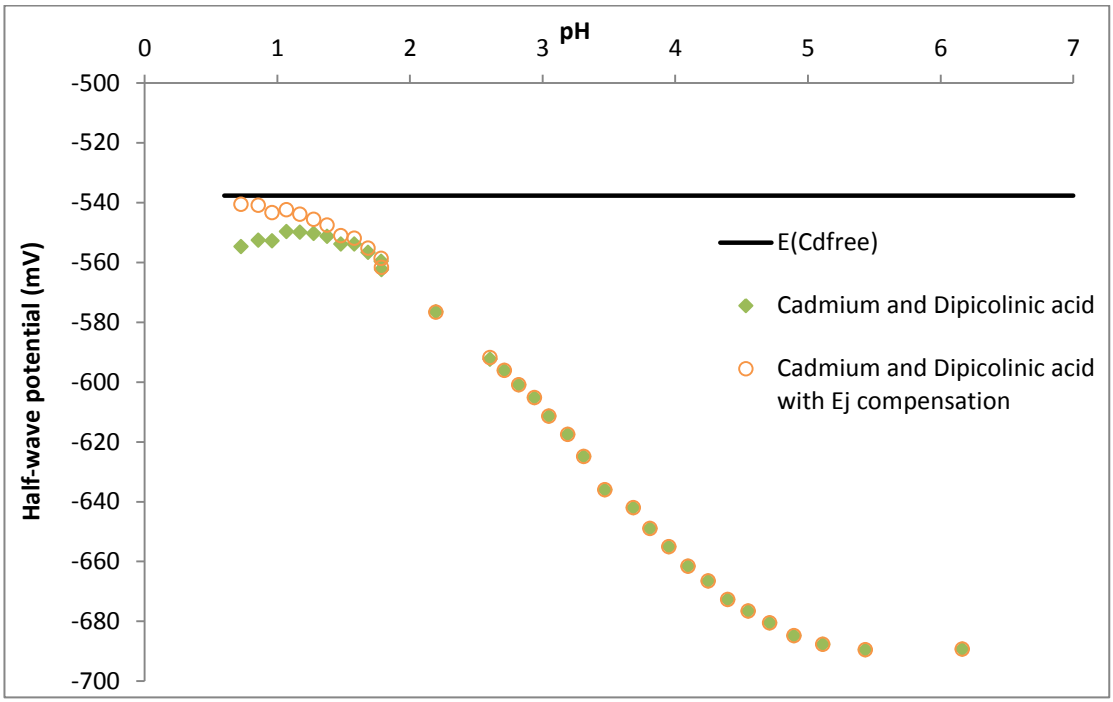


Figure 5.15 The experimental half-wave potentials that have been compensated for the diffusion junction potential, where [L]:[M] = 21, at 25 °C.

The program generates the expected diffusion limited current (which is calculated by applying the dilution factor to the initial diffusion limited current value) and the corrected value (which is the quotient of the experimental current and the expected current), as well as the potential shift which is the difference between the free cadmium potential and the measured half-wave potential. This difference together with the current term is referred to as the corrected potential shift due to complexation, and represents the experimental complex formation curve (ECFC) when plotted vs. pH. The type of cadmium-ligand complexes formed and their respective formation constants are initially speculated (using literature data and slope analysis) and then adjusted through a refinement process using mass-balance equations. The right hand side of Cukrowski's equation (Equation 2.5) gives the CCFC (calculated complex formation curve). This represents the mass-balance equations which incorporate the log β values of each anticipated complex. The 3D-

Table 5.2 Information required for solving formation constants for the Cd(II)-Dipicolinic acid system, using 3D-CFC (Cukrowski, 2000).

Temp (°C) *		25
Ionic strength (M)		0.5
pK_w		13.74
Number of electrons transferred		2
Slope		29.58
Concentration of KOH (M)*		0.4986
Initial total volume (ml)*		25.075
Initial concentration of ligand (M)*		0.002095
Initial concentration of metal (M)*		9.98E-05
Initial potential (mV)*	$E(M_{free})$	-537.64
Initial current (µA)*	$I(M_{free})$	4.019
Ligand protonation constants**		
Log*K*:		4.51
		2.05
Metal hydroxide formation constants***		
Log*β*:		
CdOH		4.0
$Cd(OH)_2$		7.7
$Cd(OH)_3$		10.3
$Cd(OH)_4$		12.0
Cd_2OH		5.06
$Cd_4(OH)_4$		23.7

* Experiment specific details.
** 25 °C and 0.5 M ionic strength (Martell, Smith and Motekaitis, 2004).
*** 25 °C and 3.0 M ionic strength (Martell, Smith and Motekaitis, 2004).

CFC software refines the formation constants by minimizing the difference between the CCFC and ECFC.

Previous work done by other authors identified an ML and ML_2 complex for this system (see Table 5.1 above) and so this combination was tested first on our data as shown in Figure 5.16. The overall standard deviation of the fit (referred to throughout as the "overall fit") calculated using Equation 2.8 was 16.7 in this case,

indicating a poor fit (especially below pH 3.5). The formation constants (log β) for ML and ML_2, respectively, were 6.77 ± 0.01 and 11.14 ± 0.01. The log β values that Anderegg (1960) calculated for ML and ML_2 (6.75 and 11.11, respectively, at 20 °C and an ionic strength of 0.1 M) are almost identical to the values we obtained (bearing in mind that experimental conditions do differ somewhat). Figure 5.16 clearly indicates that these two complexes alone do not fully describe the experimental data, especially in the low pH region. This could be an indication that Anderegg (1960) only considered data above pH 2, as is generally the case.

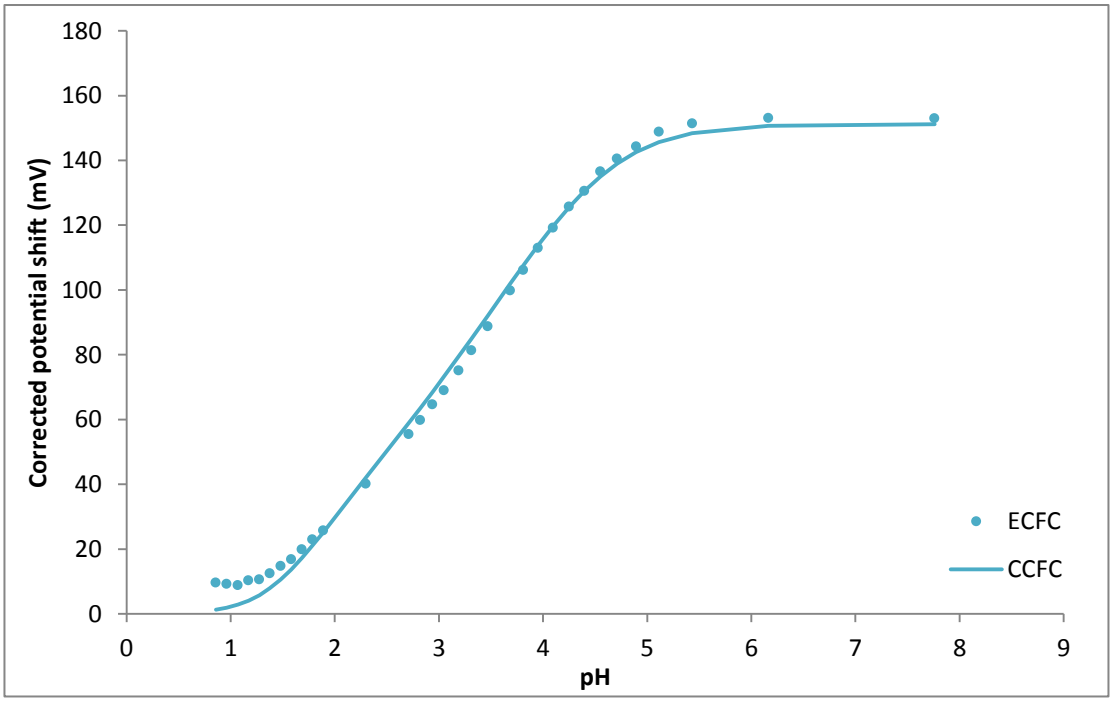


Figure 5.16 ECFC and CCFC showing the poor fit when the ML and ML_2 species are used for refinement of formation constants. ([L]:[M] = 21.)

Slope analysis can be used to predict which complexes possibly exist in solution. The protonation constants of the ligand give an indication of the pH regions in which each form of the ligand predominates. This allows prediction of what reactions could occur in each pH range. Slope analysis therefore relies on the degree of protonation of the ligand, as well as the number of electrons transferred for the

reduction of the complexed metal ion, in comparison to the slope of the ECFC. The magnitude of the slope can be calculated for a predicted reaction occurring, using the following equation:

$$\text{Theoretical Slope} = \frac{\text{number of protons involved}}{\text{number of electrons transferred}} \times \text{Nernstian slope} \qquad (5.1)$$

The Nernstian slope can be rounded off to 60 mV at 25 °C as this equation merely gives an indication of the complexes that could potentially exist in solution. For dipicolinic acid the possible reduction reactions occurring are shown in Table 5.3.

Table 5.3 Possible reduction reactions in the given pH regions with their respective calculated slopes.

pH range	Possible reduction reactions	Calculated slope
pH < 2.05	$CdLH^+ + 2e^- + H^+ \rightleftharpoons Cd^0 + H_2L$	30
	$CdL + 2e^- + 2H^+ \rightleftharpoons Cd^0 + H_2L$	60
2.05 < pH < 4.51	$CdL + 2e^- + H^+ \rightleftharpoons Cd^0 + HL^-$	30
	$CdL_2^{2-} + 2e^- + 2H^+ \rightleftharpoons Cd^0 + 2HL^-$	60
	$CdL_3^{4-} + 2e^- + 3H^+ \rightleftharpoons Cd^0 + 3HL^-$	90
pH > 4.51	$CdL_2^{2-} + 2e^- \rightleftharpoons Cd^0 + 2L^{2-}$	0
	$CdL_3^{4-} + 2e^- \rightleftharpoons Cd^0 + 3L^{2-}$	0

In certain pH regions more than one type of species can exist. If this occurs, the slope will be a value which is approximately a weighted average (where greater weight for a species present indicates a greater concentration of that species) of the calculated slopes for these species. This obviously makes it more difficult to decide which species are present as there is no set rule or equation for determining this accurately. If the slope is zero, either no hydrogen ions are involved in the reaction, or no complexes are being formed.

pH regions indicated on the ECFC in Figure 5.17 describe the form in which the ligand is found to mainly exist. The different slopes found in each region were determined and compared to those calculated by Table 5.3. In the low pH region the slope is almost 30 mV which means there is a possibility of an MLH complex present in solution. Between pH 2.1 and 4.5 the slope is 45 mV which indicates a combination of the ML (calculated slope 30 mV) and the ML_2 (calculated slope 60 mV) complexes in this pH region. Just above pH 4.5 there is still some HL^- present and so the slope of 15 mV could indicate a combination of the ML_2 and ML_3 species or just the ML_2 species and no further complex formation. The final two points of the ECFC have zero slope between them which, as mentioned above, could either indicate no complex formation or the presence of an ML_3 complex.

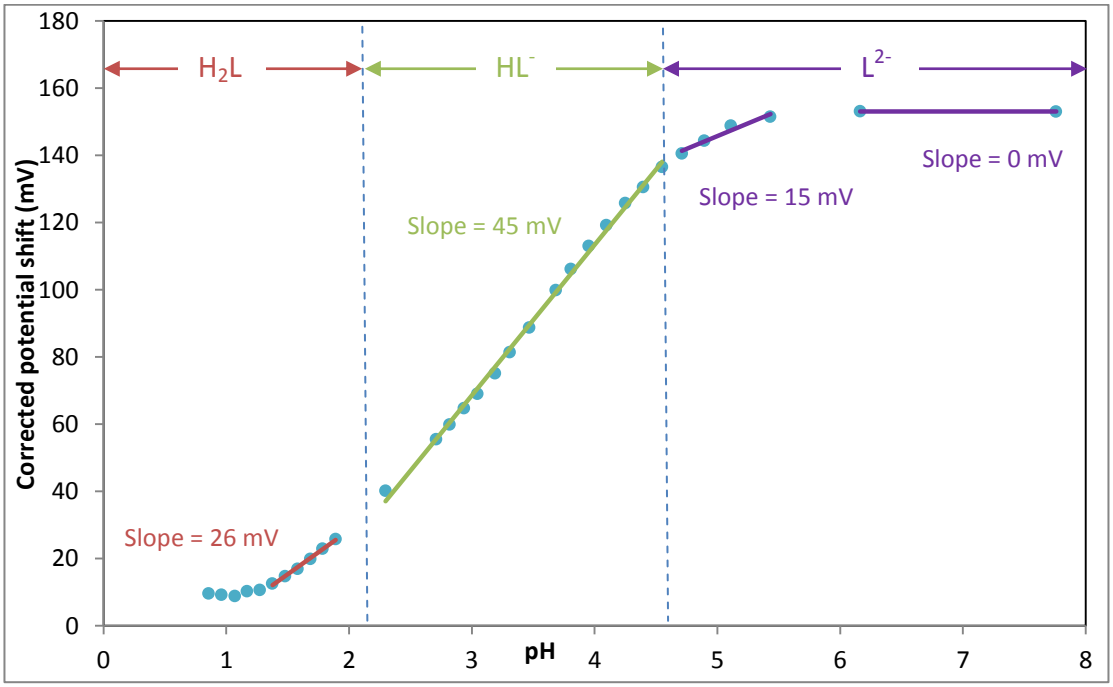


Figure 5.17 Slope analysis performed on the ECFC for [DIPIC]:[Cd] = 21.

Introducing the MLH species improved the fit of the CCFC significantly (values of the overall standard deviation are given in Table 5.4). Even though the fit of the CCFC

was much improved and described the data well, it was interesting to include the ML_3 complex into the model to see what effect it would have (Figure 5.18).

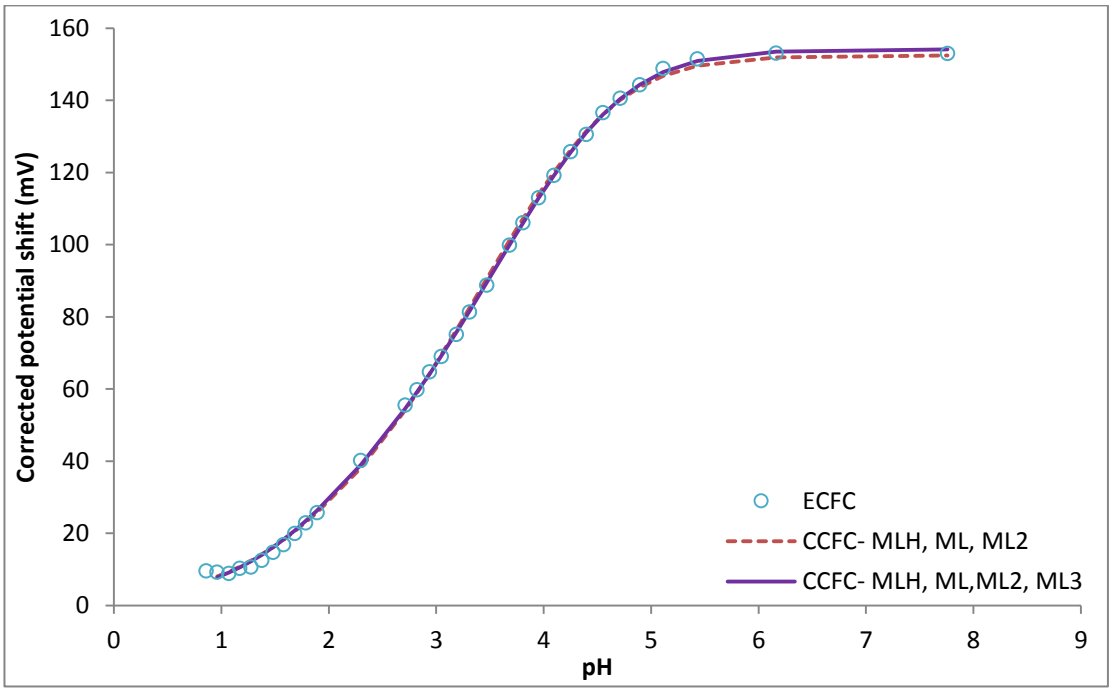


Figure 5.18 Comparative plot showing two models used in calculating the CCFC for [L]:[M] = 21 at 25 °C.

Table 5.4 Formation constants obtained for the [L]:[M] = 21 system using two different models for the calculation of the CCFC.

Complex	[L]:[M] = 21			
	Log *β*	Std Dev	Log *β*	Std Dev
MLH	8.43	0.02	8.40	0.03
ML	6.44	0.03	6.51	0.03
ML_2	11.19	0.01	11.11	0.02
ML_3	-	-	13.8	0.1
OVERALL FIT	**2.39**		**1.82**	

The overall fit only improved slightly by incorporating the ML_3 complex. Also, the standard deviation (which represents the error associated with refinement of that

particular species) of the ML_3 complex is rather high (due to such small shifts associated with this species) and so we cannot be confident in this value or even of the existence of the species in solution. Since formation of the ML_3 complex is pH independent, slope analysis cannot be used to determine conclusively whether this complex is present or not. Another technique could be used to verify whether this species actually exists in solution at this pH, for example electrospray ionization-mass spectrometry (ESI-MS). This was attempted but the results could not be interpreted. GEP could not be used because this technique relies on the change in pH which is observed only if the metal displaces a proton attached to the ligand. The only evidence that the ML_3 species exists thus far is a reported crystal structure (Li, Wang, Fu and Chen, 2005).

Li, Wang, Fu and Chen (2005) (REFCODE: CEBPEF) determined the crystal structure of a cadmium-dipicolinic acid complex of the form ML_3 (Figure 5.19). This crystal was grown by adding a solution of dipicolinic acid and ammonia at 60 °C to an aqueous solution of $Cd(NO_3)_2$. The resulting mixture was stirred, parts of the solvent evaporated, the remaining solution filtered and then left for about two weeks in air until crystals were formed. This same structure was also solved when using ethylenediamine as a solvent at 60 °C (Fu, Wang and Liu, 2004) (REFCODE: OBUZOB). Both these reports indicate that there is a high probability that the ML_3 species exists in solution under certain conditions.

To achieve a good overall fit involved taking the MLH, ML and ML_2 species into account (and in some cases ML_3 as well). Below pH 1 the CCFC did not fit the ECFC very well which could have been due to insufficient compensation of the E_j; but it is more likely that the half-wave potentials for the cadmium(II) reduction waves are inaccurate because of the difficulty in resolving them from the dipicolinic acid reduction wave. The MLH, ML and ML_2 model, as well as the MLH, ML, ML_2 and ML_3

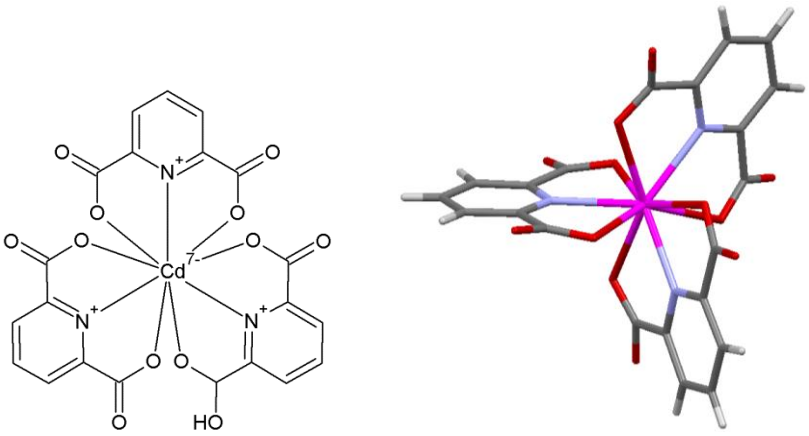


Figure 5.19 The structure of the ML_3 Cd-dipicolinic acid crystal found by Li, Wang, Fu and Chen (2005) and Fu, Wang and Liu (2004).

model, were both considered for solving formation constants for the remaining [L]:[M] ratio experiments. Our data certainly suggests that the ML and ML_2 complexes are not the only complexes in solution as previously found by other authors. Figure 5.20 shows the model containing the MLH, ML and ML_2 complexes fitted to the experimental data for [DIPIC]:[Cd] of 21, 41 and 52. The experimentally obtained potential shift (ECFC vs. pH) increases gradually with the increase in the ligand concentration, as expected.

Below pH 1 for each dataset the model does not fit the experimental data well, as previously discussed. Throughout the rest of the pH range this model seems to describe the data very well, as indicated by the magnitude of the overall fit in Table 5.5.

Formation constants could not be refined for the [DIPIC]:[Cd] = 41 dataset when the ML_3 species was included in the model. This most likely means that if the ML_3 species is present in solution it is only in very small amounts. Results are given in Table 5.6 for the remaining two datasets where ML_3 could be included, which

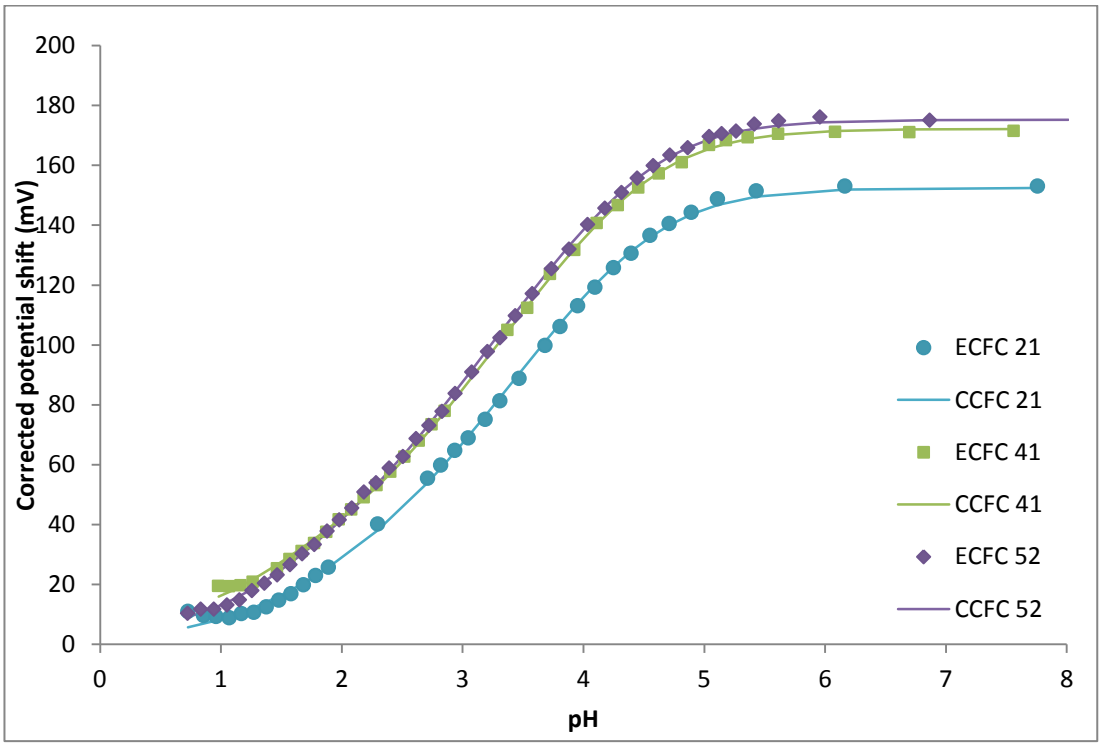


Figure 5.20 ECFC and CCFC fitted with the MLH, ML and ML_2 model for each [DIPIC]:[Cd] ratio at 25 °C.

showed slightly improved overall fits. The corresponding CCFC and ECFC are plotted vs. pH in Figure A5.3 in Appendix A.

Table 5.5 Formation constants determined for each [DIPIC]:[Cd] ratio at 25 °C using the MLH, ML and ML_2 model.

Complex	[L]:[M] = 21		[L]:[M] = 41		[L]:[M] = 52		AVERAGE	
	Log *β*	Std Dev	Log *β*	Std Dev	Log *β*	Std Dev	Log *β*	Std Dev
MLH	8.43	0.02	8.58	0.02	8.28	0.02	8.4	0.1
ML	6.44	0.03	6.65	0.03	6.63	0.02	6.6	0.1
ML_2	11.19	0.01	11.23	0.01	11.13	0.01	11.18	0.05
OVERALL FIT	2.39		0.99		0.77			

Table 5.6 Formation constants used in calculating the CCFC for [L]:[M] = 21 and 52 using the MLH, ML, ML_2 and ML_3 model.

Complex	[L]: [M] = 21		[L]: [M] = 52		AVERAGE	
	Log β	Std Dev	Log β	Std Dev	Log β	Std Dev
MLH	8.40	0.03	8.24	0.03	8.3	0.1
ML	6.51	0.03	6.67	0.02	6.6	0.1
ML_2	11.11	0.02	11.08	0.02	11.10	0.02
ML_3	13.8	0.1	13.1	0.1	13.5	0.5
OVERALL FIT	1.82		0.41			

Since a species distribution diagram "is a powerful tool for the assessment of the concentrations of the species present as a function of p[H]" (Martell and Hancock, 1996), one was plotted here using the average formation constants in Table 5.5 (Figure 5.21). It is seen that the ML_3 complex is not the major species in solution and only reaches a maximum of 30% for these conditions between pH 6 and 12. The prevalence of the ML_2 complex strongly overshadows that of the ML_3 complex in this region which could explain the difficulty in obtaining a formation constant for it. This all is affected though by the uncertainties which still remain: i) whether ML_3 definitely is in solution and ii) whether the magnitudes of the formation constants are accurate.

If the ML_3 species does exist in solution and is not incorporated into the model, the log β value for the ML_2 complex is slightly larger, but that for the other species remain unaffected. The SDD also only changes by increasing the ML_2 concentration since ML_3 is a minor species in the pH region where ML_2 is dominant in solution, if it is present (see Figure 5.22).

Even though one of the datasets did not allow inclusion of the ML_3 complex, its presence in the solid state supports the idea that it can be formed in solution. When growing the crystals, high temperatures were required to improve the solubility of

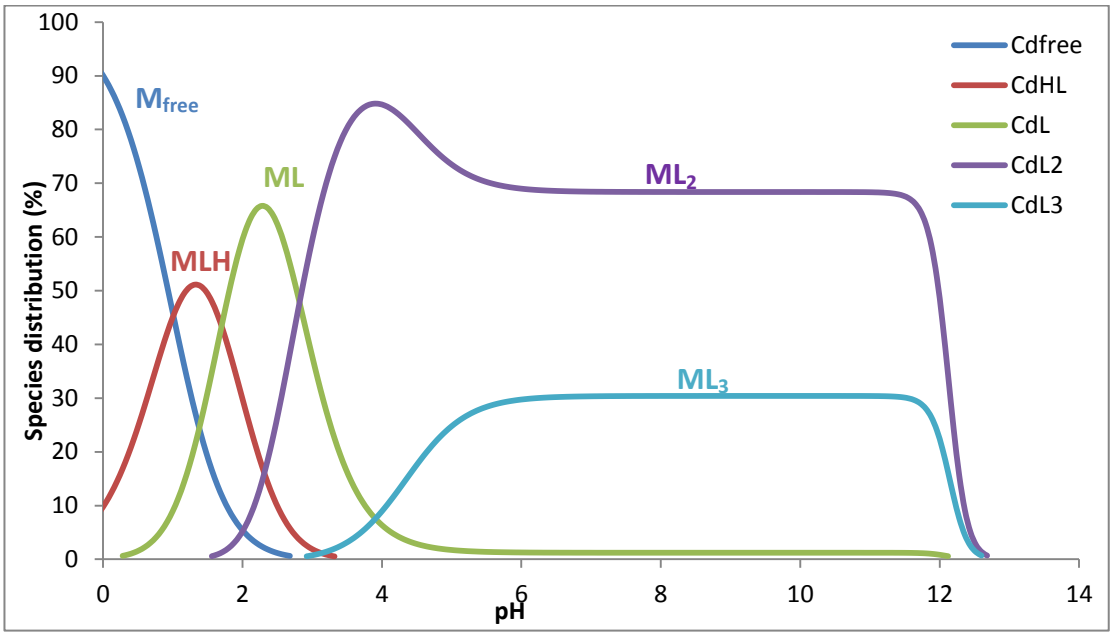


Figure 5.21 Species distribution diagram including ML_3 and MLH for [DIPIC]:[Cd] = 21 using log β values from Table 5.5. The hydroxide complexes have been omitted from the plot for clarity.

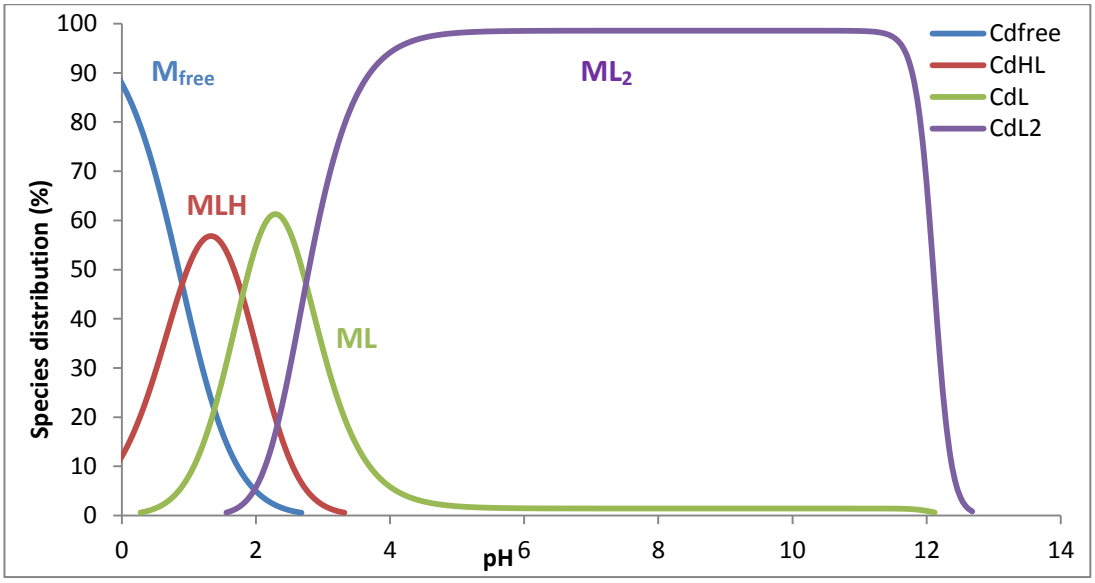


Figure 5.22 Species distribution diagram excluding the ML_3 complex for [L]:[M] = 21 using log β values from Table 5.6. The hydroxide complexes have been omitted from the plot for clarity.

the dipicolinic acid (Li, Wang, Fu and Chen, 2005), but do these high temperatures also possibly promote the formation of the ML_3 complex? The use of ammonia or other solvents may also have played a role in forming this crystalline species. The cadmium(II)-dipicolinic acid system was thus studied at elevated temperatures (32 and 40 °C) in aqueous solution to investigate whether the ML_3 species is formed in solution or not.

5.4.2 The van't Hoff equation and Adjustment of Protonation Constants

Since formation constants are temperature dependent, it is expected that their values increase for endothermic reactions and decrease for exothermic reactions when studied in solutions at higher temperatures. Literature does not provide extensive results at temperatures other than 20 and 25 °C, as well as occasionally 37 °C (body temperature) for biological studies. The van't Hoff equation expresses an equilibrium constant as a function of temperature through the slope of a plot. The equation is given as:

$$\frac{d \ln K}{d\left(\frac{1}{T}\right)} = -\frac{\Delta H^{\circ}}{R} \tag{5.2}$$

where $\Delta H°$ represents the standard reaction enthalpy, K an equilibrium constant, R the gas constant and T the temperature in Kelvin. A plot of ln K vs. $1/T$ has a slope of $-\Delta H°/R$. If the slope is positive, the reaction is exothermic and if it's negative the reaction is endothermic. Equation 5.2 can be written as:

$$\log K_2 = \log K_1 - \frac{\Delta H^{\circ}}{2.303R} \times \left[\frac{1}{T_2} - \frac{1}{T_1}\right] \tag{5.3}$$

which is used to obtain an equilibrium constant at temperature T_2, if the assumption is made that $\Delta H°$ does not vary significantly over the temperature range of interest. Log K_1 and log K_2 are the formation constants at temperatures T_1 and T_2 respectively.

The wider the temperature range examined when using the van't Hoff equation to solve formation constants, the greater the uncertainty in the values ((Kiss, Sóvágó and Gergely, 1991) and (Sóvágó, Kiss and Gergely, 1993)). Kiss, Sóvágó and Gergely (1991) do not give a magnitude of what is meant by "wide" but this is obviously specific to each reaction. They reviewed many different articles and compared Δ*H* values obtained calorimetrically for metal-glycine complexes at three different temperatures and found considerable variation (0.5-1.5 kJ/mol per 10 degrees). Izatt, Johnson and Christensen (1972) have also used calorimetric titration data to show that the assumption that Δ*H*° does not vary is often unfounded. In forming a cadmium(II)-glycine ML complex, the Δ*H*° value varies from -8.9 ± 0.2 kJ/mol at 25 °C to -8.2 ± 0.4 kJ/mol at 40 °C (Izatt, Johnson and Christensen, 1972). Unfortunately though, up until now there has been no such data published for dipicolinic acid.

There are no formation or protonation constants for the cadmium(II) hydroxide species and dipicolinic acid, respectively, at the temperatures studied. The van't Hoff equation (Equation 5.3) was used to adjust protonation constants, to represent their magnitudes at 32 and 40 °C (Table 5.7).

Table 5.7 Enthalpy and protonation constants for dipicolinic acid at 25 °C (Martell, Smith and Motekaitis, 2004) and protonation constants calculated at 32 and 40 °C using the van't Hoff equation.

Compound	**Δ*H*° (kJ/mol)**	**25 °C**	**32 °C**	**40 °C**
DIPIC-H	0.8	4.51	4.54	4.58
DIPIC-H_2	-4.6	2.05	2.03	2.01

The cadmium hydroxide formation constants were not adjusted, due to the difficulty in obtaining enthalpy values for the formation of each of the six complexes. The effect this would have could be reflected in the formation constants because the hydroxide stability constants are used in calculating the CCFC. How large the effect

would be though cannot be stated as experimentation has not before been conducted at 32 or 40 °C for this system. Reaction enthalpies for only three cadmium(II) hydroxide species were found (Martell, Smith and Motekaitis, 2004) and these were used to predict their log *K* values at 32 and 40 °C using the van't Hoff equation. Once again it was assumed that Δ*H* remains unchanged in the temperature range studied. The results (Table 5.8) show that the predicted log *K* values are not much different to those at 25 °C and so we have elected to use the standard values given in the NIST database that are quoted at 25 °C (and 3 M ionic strength, which is already introducing some error). The cadmium(II) hydroxide species only form in aqueous solution at high pH (pH > 8), and so should therefore not affect the formation constant values calculated for the cadmium(II)-dipicolinic acid species anyway.

Table 5.8 Some adjusted cadmium(II)hydroxide stability complexes at 32 and 40 °C using the van't Hoff equation.

Compound	**Δ*H* (kJ/mol)**	**25 °C**	**32 °C**	**40 °C**
CdOH	-1	4.0	4.0	4.0
$Cd_2(OH)$	-10	5.06	5.02	4.98
$Cd_4(OH)_4$	-54	23.7	23.5	23.2

5.4.3 Cadmium(II)-Dipicolinic Acid Formation Constants at 32 °C

Three experiments containing only cadmium(II) and thallium(I) were conducted at 32.0 ± 0.1 °C. These experiments were important for measuring the diffusion junction potential and creating a new Compensation Model, specific to the system at 32 °C. It was necessary for a new model to be created as the potential difference varies differently for cadmium(II) and thallium(I) with a change in temperature. Polarograms were fitted using Equation 2.2, except the Nernst slope was now 0.06055 V per electron transferred, since it is temperature dependent.

The value of delta in Equation 2.2 was found to be 1.0 ± 0.1 for both thallium(I) and cadmium(II) throughout the pH range, indicating full reversibility of the reduction process.

The model representing the difference between the half-wave potentials of thallium(I) and cadmium(II) at 32 °C when no complexes are being formed was generated (Figure 5.23). The same approach of first fitting the thallium(I) and cadmium(II) potential vs. pH data was done for the two metal ions before calculating the differences in half-wave potentials (as in Chapter Three, Section 3.2). Curves and Points models were compared and again the Curves model best described the data.

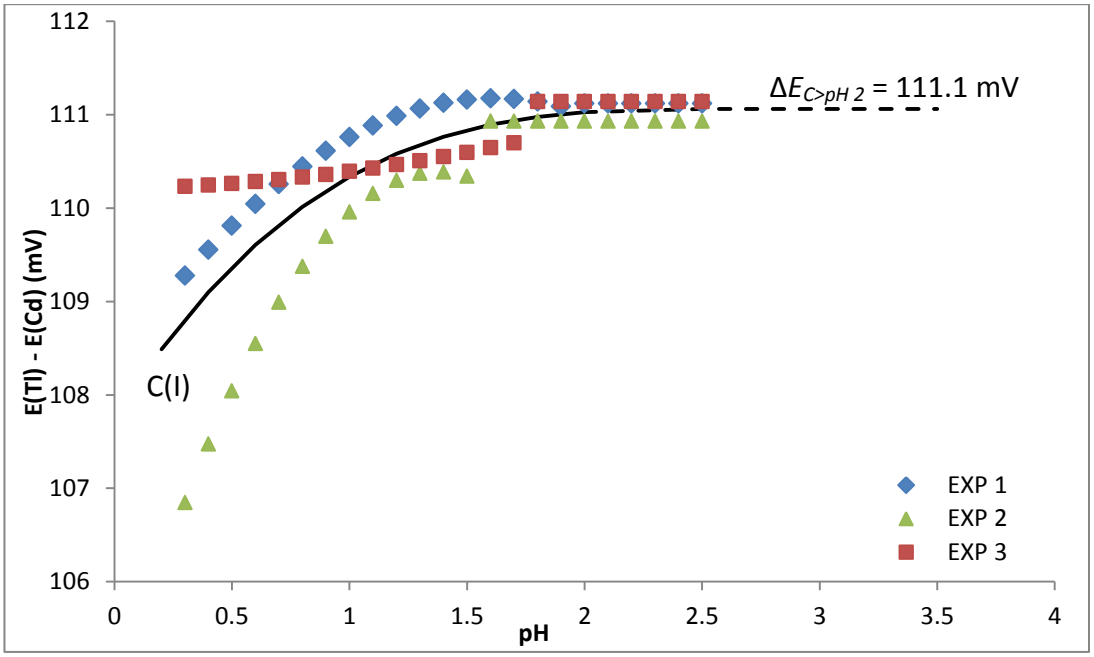


Figure 5.23 Compensation model (C(I)) formed using the difference in half-wave potentials of thallium(I) and cadmium(II), using all three datasets obtained at 32 °C.

The three datasets look very different below pH 2, but all three reach a similar potential above pH 2 which is described by the small standard deviation of the

$\Delta E_{C>pH\ 2}$ value (111.1 ± 0.1 mV). The difference between the thallium(I) and cadmium(II) half-wave potentials for Experiment 3 gave the oddest set of data, but it was not eliminated from the fitting of the average behaviour because the raw data of half-wave potential vs. pH for each metal ion contained nothing suspect. The fitting of the curves was also analyzed and found to be a close match to the raw data points (see Figure A5.4, Appendix A) and the calculated E_j was similar to what the Henderson equation predicts, so there was no good reason to exclude this experiment from our Compensation model. Additionally, the compensation model was only applied to data above pH 1 (unresolved waves prevented the use of data below that) and in this pH region the deviations between the three plots were significantly smaller. A polynomial of degree three was fitted to the data below pH 2 supplied by all three experiments to obtain an equation for the compensation model: $y = 0.2204x^3 - 1.603x^2 + 3.9586x + 107.76$. The variation in the difference of each experiment below pH 2 is caused by the fitting of the potential vs. pH data for each metal ion, which in turn is affected by the magnitude of the diffusion junction potential and also the changing ionic strength which affects thallium(I) and cadmium(II) differently. Although the three experiments making up the model look so different together they form an average behaviour which describes the potential difference between the two metal ions.

Ligand experiments were conducted at three [L]:[M] ratios of 20, 38 and 49 at 32 °C. Compensation of the diffusion junction potential was done as described before, but using the model specific to 32 °C data. Protonation constants used in the 3D-CFC program were those that had been adjusted using the van't Hoff equation (Table 5.8). Fitting all three datasets with an MLH, ML and ML_2 species produced formation constants as shown in Table 5.9 and the plot of the ECFCs and CCFCs are given in Figure 5.24

Table 5.9 Formation constants obtained for each [L]:[M] ratio at 32 °C incorporating MLH, ML and ML2 in the species model.

COMPLEX	[L]:[M] = 20		[L]:[M] = 38		[L]:[M] = 49		AVERAGE	
	Log *β*	Std Dev	Log *β*	Std Dev	Log *β*	Std Dev	Log *β*	Std Dev
MLH	8.33	0.02	8.34	0.02	7.95	0.03	8.2	0.2
ML	6.43	0.02	6.47	0.02	6.25	0.02	6.4	0.1
ML_2	11.092	0.009	10.898	0.008	10.710	0.007	11.0	0.1
OVERALL FIT	1.33		1.04		2.47			

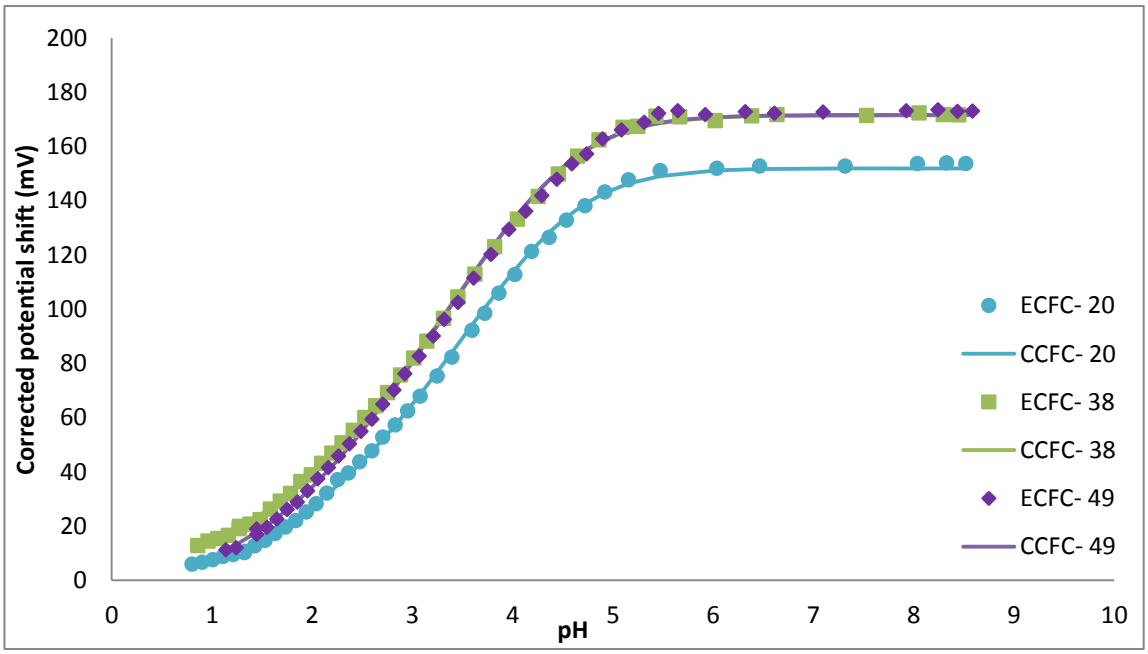


Figure 5.24 ECFC and CCFC calculated using the MLH, ML and ML_2 species model at each [L]:[M] ratio.

The CCFC and ECFC overlap well and the overall fit is below 2.5 for all three experiments. The standard deviation of the average formation constant for the MLH complex is higher than that for the other species, which is understandable due to it existing in the pH region where E_j was corrected. Incorporating the ML_3 species into the model substantially improves the overall fit for all three experiments (Table

5.10). Also visually the CCFC more closely matches the ECFC at high pH (Figure 5.25). The values of the formation constants for MLH and ML remain unchanged and that of ML_2 decreases slightly to account for the formation of the ML_3 complex; however the difference between including and excluding ML_3 is still small.

Table 5.10 Formation constants obtained for each [L]:[M] ratio at 32 °C incorporating MLH, ML, ML_2 and ML_3 in the species model.

COMPLEX	[L]:[M] = 20		[L]:[M] = 38		[L]:[M] = 49		AVERAGE	
	Log *β*	Std Dev	Log *β*	Std Dev	Log *β*	Std Dev	Log *β*	Std Dev
MLH	8.29	0.03	8.32	0.02	7.85	0.04	8.2	0.3
ML	6.50	0.02	6.51	0.02	6.36	0.02	6.4	0.1
ML_2	10.97	0.02	10.83	0.02	10.58	0.02	10.8	0.2
ML_3	13.76	0.07	12.9	0.1	12.85	0.05	13.2	0.5
OVERALL FIT	0.34		0.66		0.69			

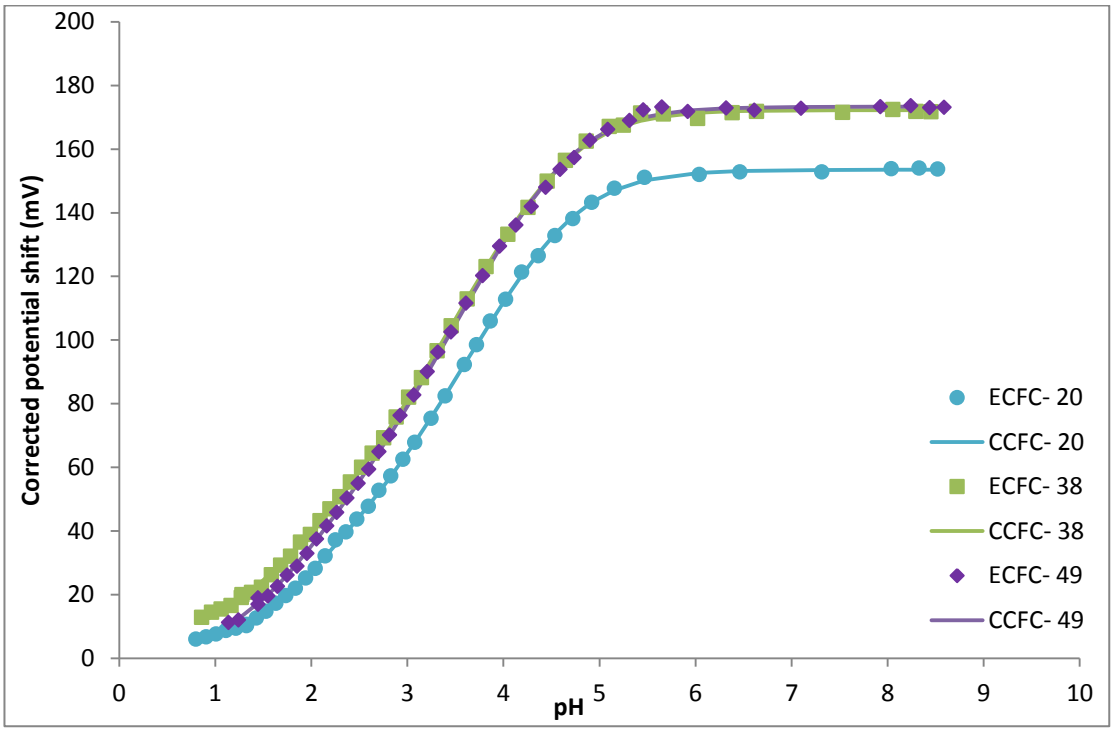


Figure 5.25 ECFC and CCFC calculated using MLH, ML, ML_2 and ML_3 species model at each [L]:[M] ratio.

For interest, formation constants were calculated employing these data using the protonation constants at 25 °C. (A discussion of these data is given in Appendix A, in Section A.5.1, and only some of the figures and tables within this section have been referred to here, hence the sporadic numbering.) Comparing the results for the three-complex model (MLH, ML and ML_2) using protonation constants at 25 °C and those adjusted to 32 °C, the formation constant for ML complex was slightly smaller (6.3 ± 0.1) when using the protonation constants at 25 °C, otherwise everything else remained constant (see Table A5.4, and corresponding figure, Figure A5.4). For the four-complex system (MLH, ML, ML_2 and ML_3) there is a slight decrease in the MLH (8.1 ± 0.3) and ML_2 (10.7± 0.2) values and a slight increase in the ML (6.4 3± 0.09) and ML_3 (13.3 ± 0.5) values when using the protonation constants at 25 °C (see Table A5.3, and corresponding figure, Figure A5.5). All but one of the standard deviations of the average remained the same.

It can be deduced that the adjusted protonation constants did not affect the formation constants significantly for this particular metal-ligand system. If the enthalpy of the reaction for the protonation of the ligand was larger, then a difference in the values would have been observed.

5.4.4 Cadmium(II)-Dipicolinic Acid Formation Constants at 40 °C

Polarographic data for the two metal ions in solution where ligand was not present was collected at 40.0 ± 0.1 °C for three separate experiments. Fitting of the polarographic waves again required an adjustment of the Nernstian slope in Equation 2.2 to a value of 0.06214 V per electron transferred at 40 °C. The Compensation model was built in the same way as was done for the 32 °C data (Figure 5.26).

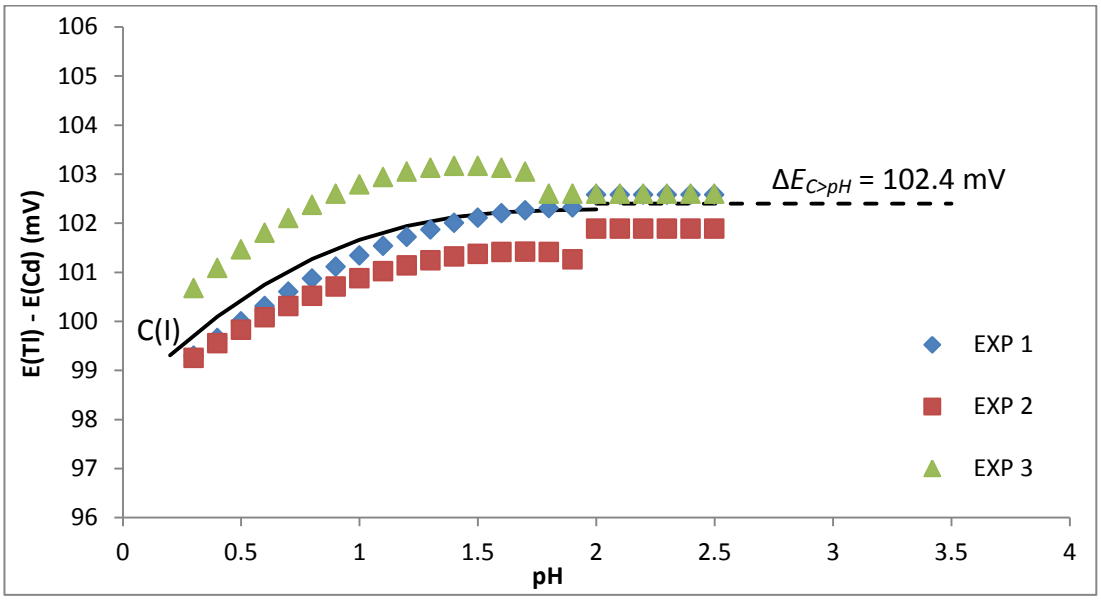


Figure 5.26 Compensation model (C(I)) determined using the difference in half-wave potentials of thallium(I) and cadmium(II), using all three datasets obtained at 40 °C.

A polynomial (degree four) best fitted the potential data below pH 2. The data differed by a maximum of 1.5 mV throughout the pH range. Above pH 2 the average difference between the thallium(I) and cadmium(II) half-wave potentials for this system was 102.4 ± 0.4 mV.

It was interesting to compare the three compensation models that were produced at each temperature studied for the cadmium(II)-dipicolinic acid system. Each Compensation model was plotted on a single graph (Figure 5.27) to see if and how they relate to each other. It was found that the higher the temperature, the smaller were the difference in potential between the reduction half-wave potentials for thallium(I) and cadmium(II) (Table 5.11), indicating that the reduction waves of the metal ions were moving towards each other. Considering a ratio of the change in temperature and average ΔE values a pattern was identified (Table 5.11). The

decrease in the average ΔE value almost follows a geometric sequence which could be calculated more accurately if the change in temperature was constant.

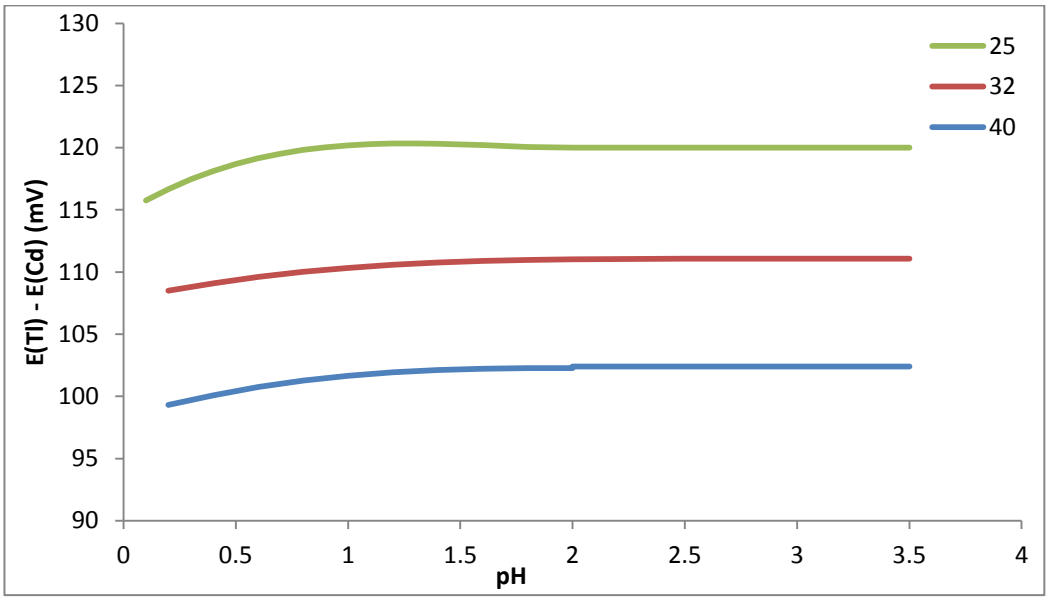


Figure 5.27 Comparison of the C(I) Compensation models for each temperature.

Table 5.11 The average difference in half-wave potentials for thallium(I) and cadmium(II) above pH 2 ($\Delta E_{C>pH}$) for each temperature.

Temperature (°C)	Number of datasets	Average $\Delta E_{C>pH}$ (mV)	Ratio T_n:T_{n-1}	Ratio ΔE_n: ΔE_{n-1}
25	5	120.0 ± 0.5	-	-
32	3	111.1 ± 0.1	1.28	1.080
40	3	102.4 ± 0.4	1.25	1.085

In order to understand these results better, a plot of the polarograms collected at pH 0.3 at each temperature were compared. The data were manipulated so that the base of the thallium(I) waves overlapped (Figure 5.28). This plot highlights the change in the diffusion limited current (i_d) as well as the shifting of reduction potentials with temperature.

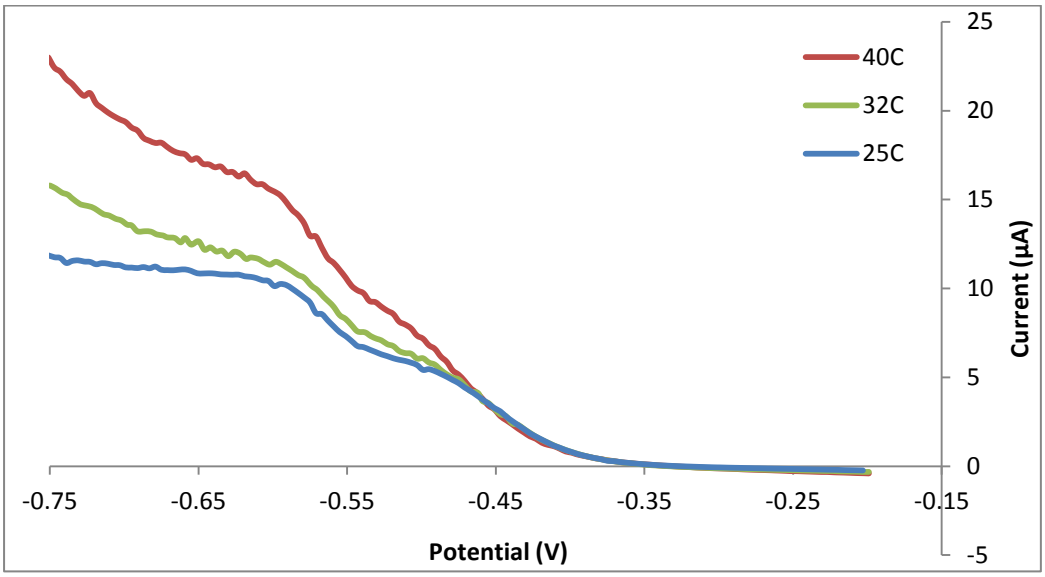


Figure 5.28 Overlap of the polarograms at pH 0.3 collected at each temperature. [Cd] = 1.00 x 10^{-4} M and [Tl] = 2.00 x 10^{-4} M.

The diffusion limited current (i_d) is described by the Ilkovic equation:

$$i_d = 70.8n\, D^{\frac{1}{2}}\, m^{\frac{2}{3}}\, t_D^{\frac{1}{6}}\, c_s \qquad (5.4)$$

where the diffusion limited current (in Amperes) is affected by the mass flow rate of mercury (m), the drop time (t_D), the concentration (c_s) and diffusion coefficient (D) of the analyte, and the number of electrons (n) that react with each molecular unit of the analyte. In these experiments the capillary characteristics (m and t_D), analyte concentration and number of reacting electrons were constant for each experiment. It was therefore the increased diffusion coefficient that caused the diffusion limited current to increase. An increase in temperature causes a decrease in the viscosity of the solution which in turn affects the diffusion coefficient and hence the diffusion current (Thomas and Henze, 2001). According to Thomas and Henze (2001) diffusion coefficients increase with temperature by 1-2% per degree Kelvin. Riches (1948) suggests incorporating thallium ions into the supporting electrolyte as its step height in particular polarograms can be used to apply a correction for slight

temperature changes. This is not necessary in this work because the temperature is well-regulated and monitored throughout a titration experiment. As long as the temperature is constant throughout an experiment, the actual magnitude of the current is not that important as it is the current ratio (I_{comp}/I_{free}) that is used in calculations.

Considering the actual free metal ion potentials for the reduction of thallium(I) and cadmium(II) (given in Table 5.12) was not very useful since slight variations in the reduction potentials occur from one experiment to another due to slight variations in the reference system, the amount of gelatin added and so on. In general, we cannot average the $E(M_{free})$ values due to known variation in the reference system between experiments, but the average is shown in Table 5.12 as it does seem to indicate a rough trend.

Table 5.12 Free metal ion potentials for thallium(I) and cadmium(II) for each ligand-free experiment. The average $\pm$ the standard deviation is shown in italics due to the large uncertainty associated with these values.

EXP	**25 °C**		**32 °C**		**40 °C**	
	E(Tl$_{free}$)	***E(Cd$_{free}$)***	***E(Tl$_{free}$)***	***E(Cd$_{free}$)***	***E(Tl$_{free}$)***	***E(Cd$_{free}$)***
`1	-420.18	-540.88	-425.01	-536.13	-428.81	-531.39
2	-422.63	-542.57	-430.36	-541.29	-434.96	-536.85
3	-425.69	-545.94	-433.39	-544.53	-422.99	-525.59
4	-429.45	-548.96				
5	-422.22	-541.86				
Average	*424 $\pm$4*	*544 $\pm$3*	*430 $\pm$4*	*541 $\pm$4*	*429 $\pm$4*	*531 $\pm$6*

The potential of the reference electrode is temperature dependent (see Table A5.1, Appendix A); as the temperature increases so its potential decreases. If this is the only factor to be considered then it is expected that the potential for both thallium(I) and cadmium(II) would be affected in the same way. According to the

results shown in Table 5.11 this was not observed, which means that there is something other than the decreased potential of the reference system that is responsible for the changing half-wave potentials. On inspection of the glass electrode calibration curves a definite pattern was observed: at higher temperatures the x and y-intercepts (pH and potential, respectively) both got larger (see Table A5.2), which was expected (Metrohm, 2012). Figure A5.8, Appendix A demonstrates this using a single calibration at each temperature (25, 32 and 40 °C), and Table A5.8 supports this finding as it shows the results of the x and y-intercepts when considering two further calibration curves for each temperature.

The results in Table 5.12 really highlight the necessity of incorporating the witness ion into each and every experiment. Even though an experiment is conducted under the same conditions, using the same concentrations and temperature, certain factors do affect the reduction half-wave potentials and is therefore specific to each experiment. Incorporating the witness ion therefore allows for high accuracy in calculating the diffusion junction potential because it is monitored in-situ for each experiment.

Since the $E(M_{free})$ values cannot be averaged (as discussed) and we are trying to establish which metal ions' reduction potential (thallium(I) or cadmium(II)) is most affected by the change in temperature, we used an approach involving Dixon's statistical Q-test for outliers (Rorabacher, 1991). A rough test was done to see if the point with the most different $E(M_{free})$ value (at either 32 or 40 °C) (as compared to the average $E(M_{free})$ value at 25 °C) was considered an outlier of the $E(M_{free})$ values obtained at 25 °C. Firstly the 40 °C $E(Tl_{free})$ point of experiment 2 (-434.96 mV) was found not to be an outlier at the 95% confidence interval, however, for cadmium(II) the 40 °C data point of experiment 3 (-525.59 mV) was found to be an outlier at this same confidence level. From this we can speculate that the cadmium(II) reduction half-wave potentials vary more significantly with temperature than those for

thallium(I). It should also be highlighted that it appears that the waves are moving in opposite directions with increasing temperature (in a negative direction for thallium(I) and in a positive direction for cadmium(II)), thus leading to the smaller $\Delta E_{C>pH}$ value as given in Table 5.11. To answer the question of why we see this, literature was inspected.

Janik and Sommer (1973) studied polyadenylic acid using DC polarography and examined the effect of pH, concentration, temperature and other factors on the shape of the polarogram. An increase in the temperature caused an increase in the diffusion limited current throughout the temperature range studied, as was expected. They also found that the reduction potential shifted in a positive direction between 2.8 and 48.1 °C, and then in a negative direction for the increase of the temperature from 48.1 to 79.0 °C. A diagram from Janik and Sommer's article depicting these changes can be seen in Figure 5.29.

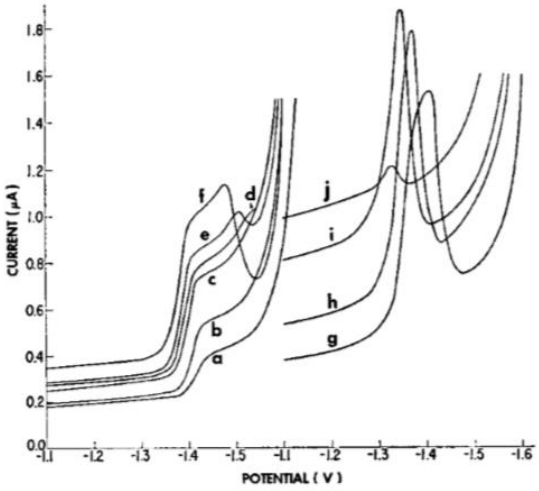


FIGURE 2 Effect of temperature on the shape of DC polarographic curves of 0.2 mM poly A ($49 \cdot 10^4$ daltons) at pH 5.9 in 0.4 M NaCl and phosphate buffer (I = 0.1 M). Temperature (°C): 2.8 (*a*), 6.7 (*b*), 14.5 (*c*), 17.5 (*d*), 22.0 (*e*), 29.5 (*f*), 48.1 (*g*), 59.0 (*h*), 68.8 (*i*), and 79.0 (*j*). The mercury column height was 64 cm. Potentials are against saturated calomel electrode which was held at the temperature indicated. The pH of the solution remained constant within about 0.1 pH over the entire range of temperatures employed.

Figure 5.29 The change in shape of a DC polarogram when the temperature is increased from 2.8 to 79.0 °C, by Janik and Sommer (1973).

Kovács and Kékedy (1975) did a similar study to Janik and Sommer (1973) (on the changing shape of the DC polarogram) but they looked at xanthates. They too observed that the half-wave potentials were dependent on temperature, showing a positive shift with an increase in temperature. Unfortunately the temperature range studied was not communicated in their published article.

Other authors looked at temperature coefficients and used this to describe potential shifting. Samota, Garg and Pandey (2010) did research on an antidepressant, Bupropion, and found that the temperature coefficients of the half-wave potentials were 10-15 mV per degree (indicating the irreversibility of the electrode reaction). At the same time Samota also commented on the linear temperature dependence on the diffusion current. Zutshi (2006) stated that a temperature coefficient of the half-wave potential for a reversible wave is usually between -2 and +2 mV per degree, which is the range in which we found our dE/dT values to be. In a paper entitled "Temperature Coefficients of Half-wave Potentials and Entropies of Transfer of Cations in Aprotic Solvents" Gritzner and Lewandowski (1991) measured the temperature coefficients of several mono- and divalent metal ions (including thallium(I) and cadmium(II)) in non-aqueous solvents. Experiments were conducted between 15 and 65 °C (in 10 °C intervals) using pulse and direct current polarography. Liquid junction potentials were avoided by using the same electrolyte solution in the reference and measuring half-cell. The temperature dependence of the half-wave potential values was analyzed by linear regression, and it was checked that the potential of the reference cell did not change throughout any of the experiments. Four different solvents were used for these experiments and the overall results were rather similar for each of these, for both thallium(I) and cadmium(II). The temperature coefficient (dE/dT) for cadmium(II) was higher than that for thallium(I) in each solvent, with the cadmium(II) to thallium(I) temperature coefficient ratios being in the range of 2.2 to 2.7. These data support what we

found, as they show that the cadmium(II) reduction half-wave potential is far more sensitive to temperature change than that of thallium(I).

Experiments of [L]:[M] ratios of 20, 40 and 49 performed at 40 °C were analyzed using the adjusted values for the protonation constants, even though we showed that the difference between the two was not significant. Solving formation constants without the ML_3 complex was possible for each ratio and Table 5.13 shows their values. The overall fit was however extremely poor for each ratio and the plots (Figure 5.30) of the CCFC and ECFC for each experiment demonstrated this. The CCFCs showed that the species model was incomplete and therefore the ML_3 species should possibly have been incorporated. The largest deviations occurred for the experiments with higher ligand ratios, which were expected if it was the ML_3 species that was missing from the species model as complex formation is promoted when a larger concentration of ligand is available. The ML_2 formation constant appeared to be inflated to compensate for the absence of the ML_3 species, and this was seen in the CCFC which lies above the ECFC between pH 3 and 5. At higher pH the CCFC was not large enough and indicated an additional species existing in the solution. When ML_3 is incorporated into the species model, the CCFC fitted the ECFC between about pH 4.5 to 8.5 much better for all ratios. (Figure 5.31 and Table 5.14).

Table 5.13 Formation constants obtained for each [L]:[M] ratio at 40 °C using the species model containing an MLH, ML and ML_2 species.

COMPLEX	[L]:[M] = 20		[L]:[M] = 40		[L]:[M] = 49		AVERAGE	
	Log β	Std Dev	Log β	Std Dev	Log β	Std Dev	Log β	Std Dev
MLH	8.24	0.03	8.1	0.03	8.17	0.02	8.17	0.07
ML	6.34	0.02	6.23	0.03	6.06	0.03	6.2	0.1
ML_2	11.028	0.008	10.951	0.07	10.818	0.006	10.9	0.1
OVERALL FIT	5.72		19.76		20.79			

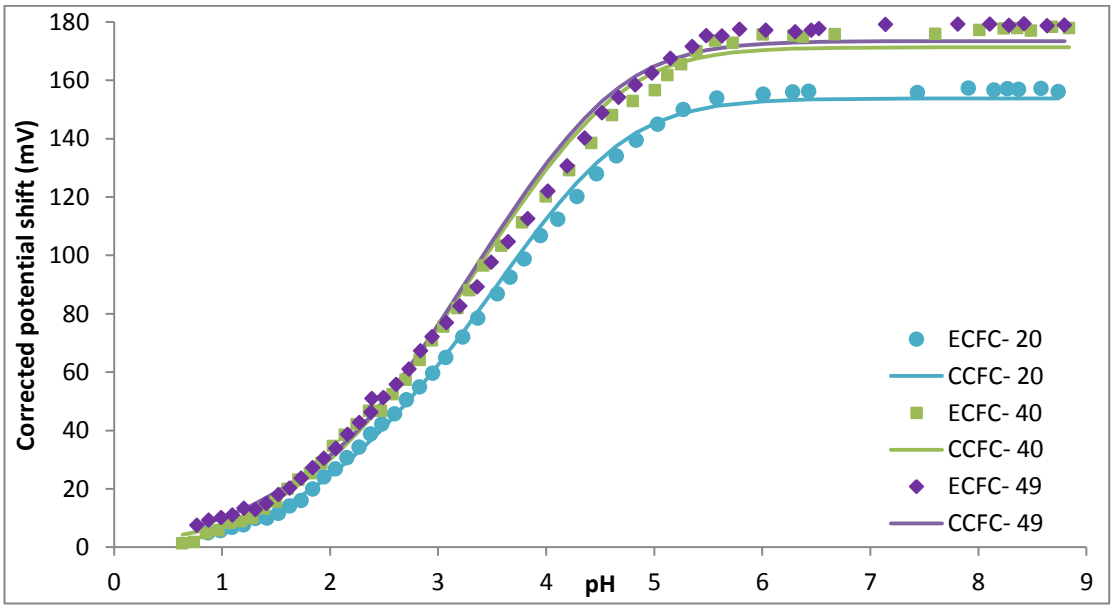


Figure 5.30 ECFC and CCFC fitted using an MLH, ML and ML_2 model for each [DIPIC]:[Cd] ratio at 40 °C.

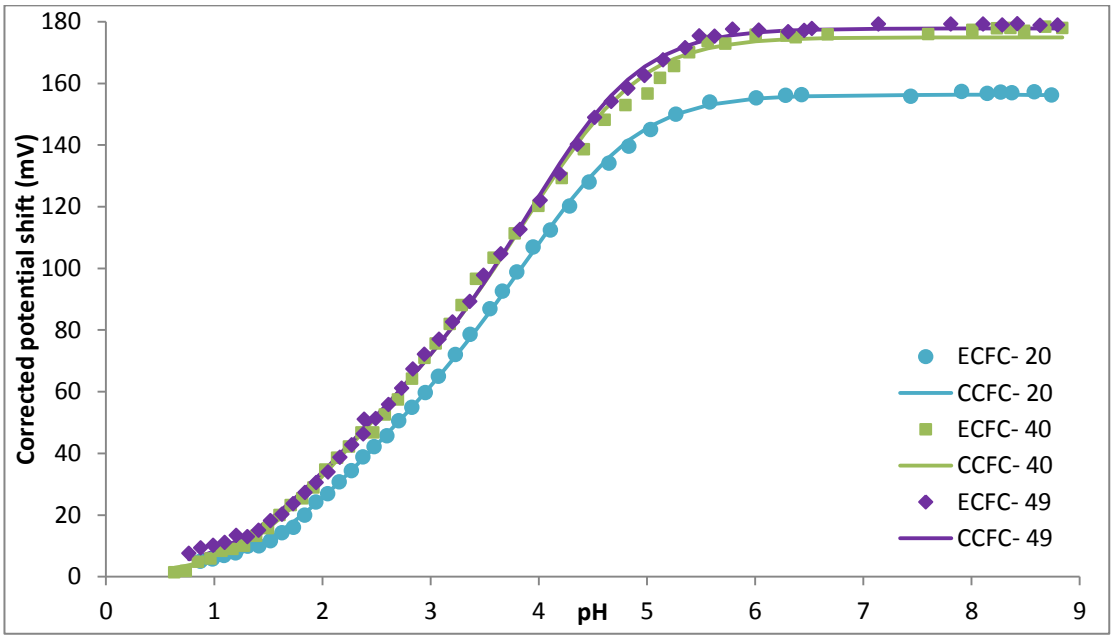


Figure 5.31 ECFC and CCFC fitted using the MLH, ML, ML_2 and ML_3 model for each [L]:[M] ratio at 40 °C.

Table 5.14 Formation constants for each [DIPIC]:[Cd] ratio using the species model containing MLH, ML, ML_2 and ML_3.

COMPLEX	[L]:[M] = 20		[L]:[M] = 40		[L]:[M] = 49		AVERAGE	
	Log *β*	Std Dev	Log *β*	Std Dev	Log *β*	Std Dev	Log *β*	Std Dev
MLH	8.12	0.04	7.86	0.04	7.99	0.03	8.0	0.1
ML	6.49	0.02	6.5	0.02	6.39	0.02	6.46	0.06
ML_2	10.72	0.03	10.45	0.03	10.23	0.04	10.5	0.2
ML_3	13.99	0.03	13.7	0.02	13.51	0.01	13.7	0.2
OVERALL FIT	0.85		6.37		2.76			

Testing the importance of incorporating the MLH complex (at 40 °C) was done by refining formation constants using only the ML, ML_2 and ML_3 species. Figure 5.32 illustrates the very poor fit below pH 2 when the MLH complex is omitted, thereby providing good evidence for its presence in solution. The log *β* value for the ML complex increases (to 6.59 ± 0.04) to compensate for the missing MLH species.

A quick comparison of the effect of eliminating the MLH species from the data obtained at lower temperatures showed that at 25 °C the MLH species has a larger effect on the results because the log *β* value of the ML species increased more than that at 40 °C and also the values of the overall fit increased far more at 25 °C in relation to that at 40 °C. On the other hand, the exclusion of the ML_3 species has a larger effect on the results obtained at 40 °C as opposed to those at 25 °C.

As an aside it should be mentioned that during experimentation at higher temperatures it was noted that some evaporation and condensation started occurring in the cell during the polarographic measurements. To test whether this had an effect on the results (affecting volume and hence concentration) a comparison was made of the expected current and the measured current throughout the polarographic experiment where no ligand was present. The 40 °C data were used for this comparison as it would have been affected the most.

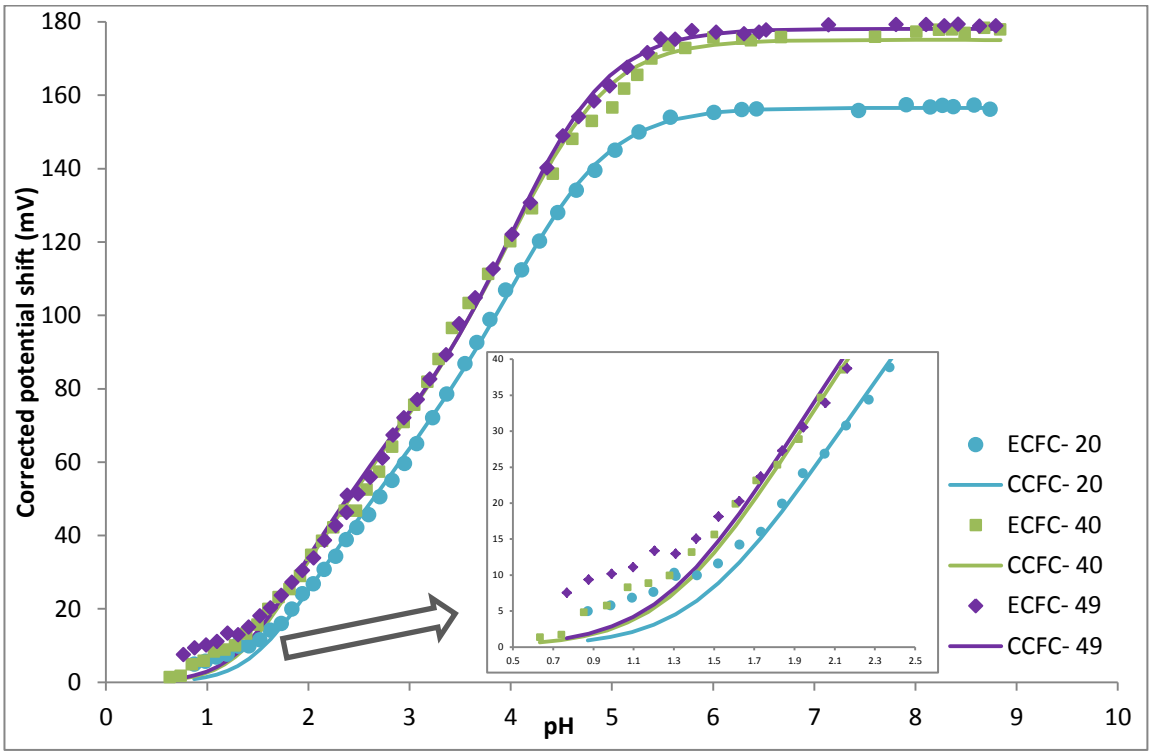


Figure 5.32 ECFC and CCFC for each [L]:[M] ratio (at 40 °C) fitted with the ML, ML_2 and ML_3 model.

Diffusion current is described by the Ilkovic equation (Equation 5.4). By keeping the temperature and drop characteristics constant the variation in *D*, *m* and *t* is eliminated and for a single experiment the number of electrons transferred will be constant, and therefore the only factor affecting the diffusion current is that of concentration (Harris, 1998). The expected current was calculated by using the initial current reading obtained before titration with KOH began, and then projecting currents taking dilution into account. When comparing this calculated current with that measured for an experiment where no ligand was present, it was seen that the currents were very similar (see Figure 5.33). This proves that the slight evaporation and condensation did not have an effect on the results. The standard deviation between measured and predicted currents was around 0.03 for each point throughout, which is within experimental error (relative standard deviation = 0.04).

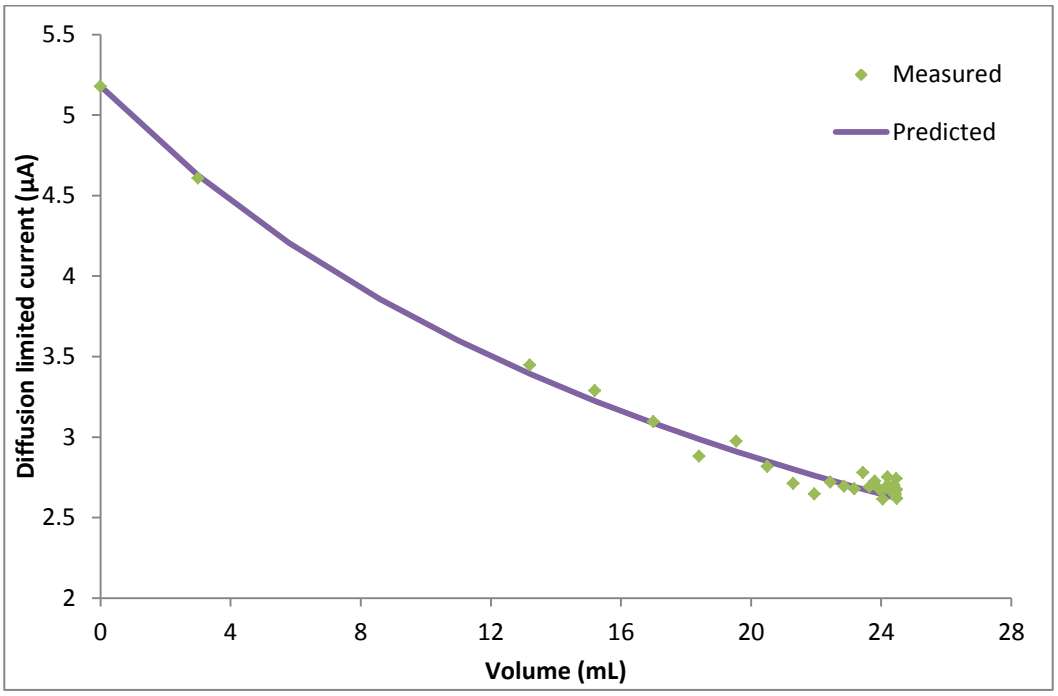


Figure 5.33 Comparison of the predicted current (due to dilution) and that measured during experimentation at 40 °C, where no ligand is present.

5.5 COMPARISON OF RESULTS

Table 5.15 is a summary of the log β values obtained with and without the ML_3 complex in the model. All the data used for the 32 °C and 40 °C experiments were analyzed using adjusted protonation constants. Including ML_3 had a significant effect on the overall fit for data collected at 40 °C, but there was only a small difference at 32 and 25 °C.

From Table 5.15 it is seen that complex formation of the MLH, ML and ML_2 complexes is exothermic because as the temperature increases so the log β values decrease. Formation of the ML_3 complex seems to be endothermic. This is in line

Table 5.15 Average formation constants calculated by excluding and including the ML_3 complex at each temperature.

TEMP	MLH		ML		ML_2		ML_3	
	log *β*	Std Dev	log *β*	Std Dev	log *β*	Std Dev	log *β*	Std Dev
25 °C	8.43	0.15	6.57	0.12	11.18	0.05	-	-
	8.4	0.2	6.61	0.08	11.14	0.08	13.4	0.5
32 °C	8.21	0.22	6.38	0.12	10.9	0.19	-	-
	8.2	0.3	6.46	0.08	10.8	0.2	13.2	0.5
40 °C	8.17	0.07	6.21	0.14	10.93	0.11	-	-
	8.0	0.1	6.46	0.06	10.5	0.3	13.7	0.2
Reaction	Exothermic		Exothermic		Exothermic		-	
	Exothermic		Exothermic		Exothermic		Endothermic	

with the deductions made about the effect of the inclusion or exclusion of the ML_3 species at high or low temperatures.

Using the formation constants calculated in this work the van't Hoff equation was used to calculate ΔH. The slope of the plot of log *β* vs. 1/T is equal to $-\Delta H/2.303R$ (Figure 5.34). Since only three data points are plotted the enthalpy values are by no means accurate, but rather just an indication of whether a reaction is exothermic or endothermic.

The 25 °C data were not incorporated when finding ΔH for the ML_3 complex due to the uncertainty of its existence (or its existence as a minor species) and hence there was a large uncertainty in the log *β* determined. If the log *β* value for ML_3 at 25 °C is included, the ΔH value decreases from 114 to 37 kJ/mol (see Table 5.16). For the ML complex various permutations of excluding a point was considered and the results are shown in Table 5.16. These data clearly show that the formation of ML_3 is endothermic, while the formations of the other species are all exothermic.

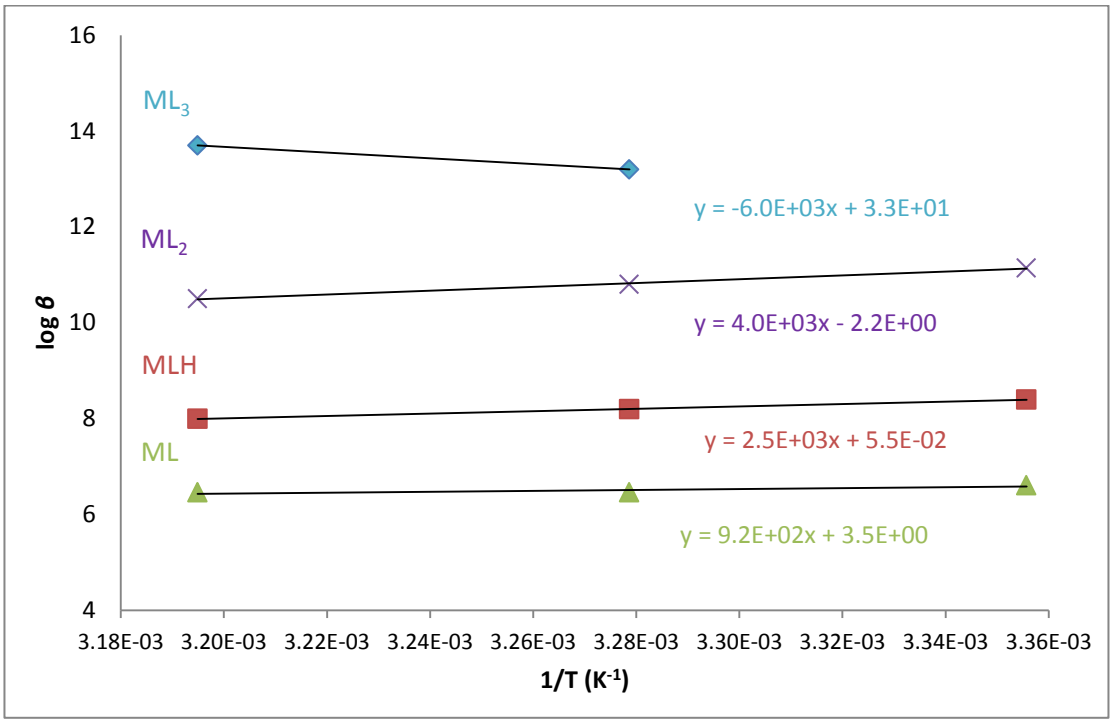


Figure 5.34 van't Hoff plot for the calculation of ΔH values for the formation of the MLH, ML, ML_2 and ML_3 complexes.

Table 5.16 Approximate values for the enthalpy associated with each complexation reaction.

Complex	Included data (°C)	$-\Delta H/2.303R$	ΔH (kJ/mol)
MLH	25, 32, 40	2485.8	-48
ML	25, 32, 40	919.08	-18
	25, 40	932.74	-18
	25, 32	1947.6	-37
ML_2	25, 32, 40	3973.8	-76
ML_3	25, 32, 40	-1925.5	37
	32, 40	-5966.6	114

As mentioned previously there are no enthalpy values available in literature for the cadmium(II)-dipicolinate system, so a quick comparison was made between the enthalpy values we calculated with that of copper(II)- and nickel(II)-dipicolinate

complexes. The ML and ML_2 values for Cu(II) were -11 and -41 kJ/mol respectively (at 25 °C and ionic strength of 0.1 M) and for Ni(II) -12 and -26 kJ/mol respectively (at 25 °C and ionic strength of 1.0 M) (Martell, Smith and Motekaitis, 2004), which provide us with some confidence of the range in which our values fall. In contrast, the ΔH values for the MLH complex differ considerably where that of Cu(II) is even endothermic having an enthalpy value of 29 kJ/mol (Martell, Smith and Motekaitis, 2004).

Species distribution diagrams including and excluding the ML_3 species at 25 °C indicates why this species was initially not speculated in solution under the conditions studied (Figure 5.35). The large concentration of the ML_2 species present overshadows the minor ML_3 species, so it is not clear whether ML_3 is definitely present or not. The remaining cadmium(II)-dipicolinic acid complexes remain largely unaffected. Prediction of species is easiest when a single complex exists over a certain pH range. For the 32 and 40 °C data the ML_3 complex is easily incorporated into the model because under these conditions it is more prominent in solution, as Figure 5.36 shows.

Comparative SDDs have been plotted in Figures 5.37 and 5.38 at the three different temperatures studied where the ML_3 species has been excluded and included, respectively. Table 5.17 gives a summary of the maximum percentage of each species produced at the different temperatures as given in Figure 5.38. For MLH the distribution decreases from 59% to 35% as the temperature is increased, whereas for ML_3 the distribution increases from 25% to 75%. This again points to the fact that the ML_3 species is formed by an endothermic reaction and hence is promoted in solution at higher temperatures.

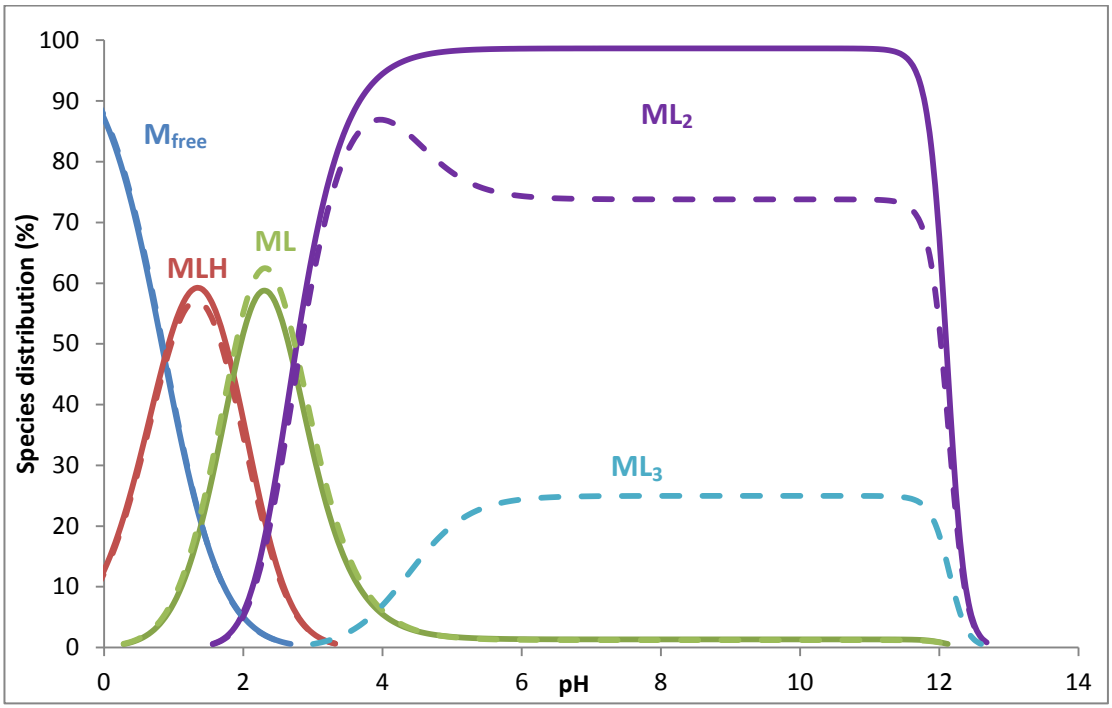


Figure 5.35 Comparison of two SDDs at 25 °C plotted using formation constants where the ML_3 complex was excluded (solid lines) and included (dashed lines) in the model. [Cd] = 1 x 10^{-4} M and [DIPIC] = 2 x 10^{-3} at 0.5 – 0.25 M ionic strength.

The MLH and ML_2 percentage distributions decrease with an increase in temperature, while that of ML and ML_3 increase with an increase in temperature. It would be expected that the ML species behaves like that of MLH and ML_2 because they are all exothermic species, however, the distribution of all species are not governed solely by this, but rather by the sensitivity of the formation of each species to temperature change (i.e. the magnitude of their $\Delta H°$ values). According to our calculations of ΔH (Table 5.16) the ML complex would be least affected by temperature change and would thus increase or decrease in concentration to accommodate changes due to species in a similar pH region that do change with temperature.

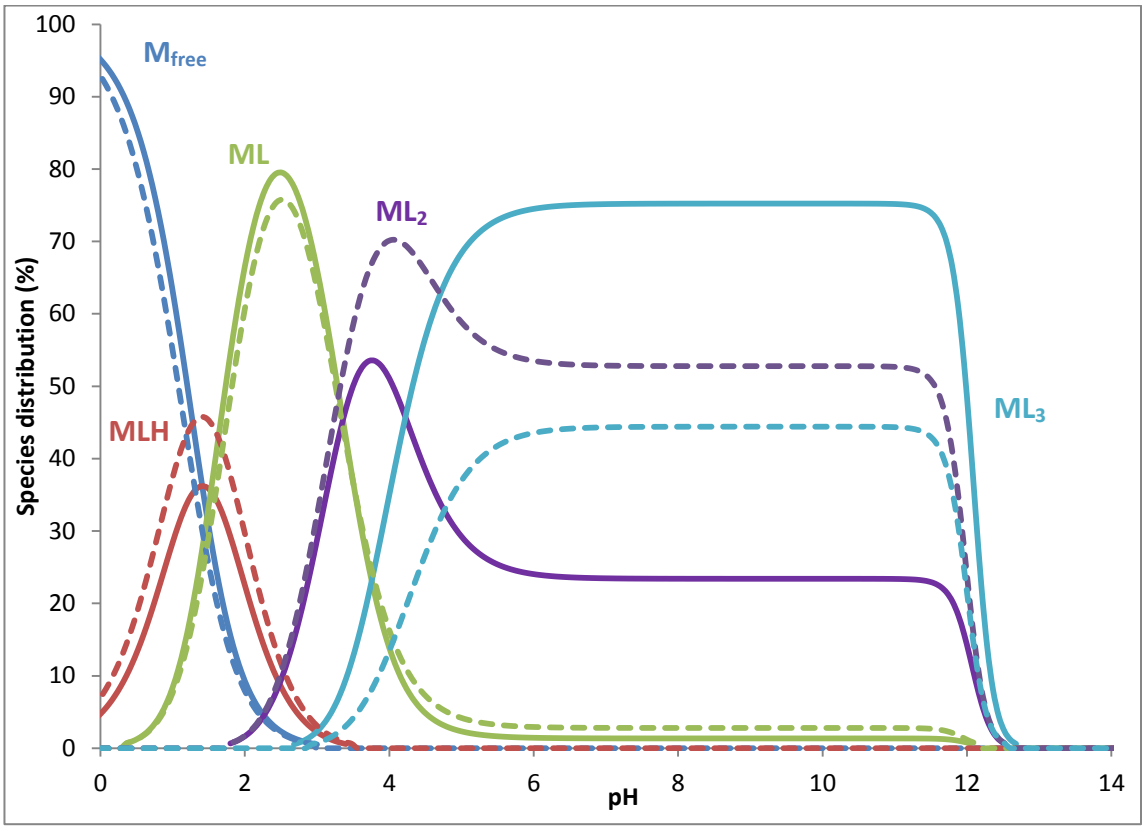


Figure 5.36 Comparison of the SDDs plotted using a MLH, ML, ML_2 and ML_3 species model for the 32 °C (dashed lines) and 40 °C (solid lines) data. [Cd] = 1 x 10^{-4} M and [DIPIC] = 2 x 10^{-3} M at 0.5 - 0.25 M ionic strength.

Table 5.17 Maximum percentage distribution of species at respective pH or pH ranges, corresponding to the SDDs plotted in Figure 5.38.

Complex	25 °C		32 °C		40 °C		Trend
	Distribution (%)	pH	Distribution (%)	pH	Distribution (%)	pH	As T increases:
MLH	59	1.3	46	1.4	36	1.2	Decreases
ML	61	2.2	76	2.5	79	2.4	Increases
ML_2	87 74	3.9 6-12	70 52	4 6-12	54 25	3.8 5.6-12	Decreases
ML_3	25	6-12	44	6-12	75	5.6-12	Increases

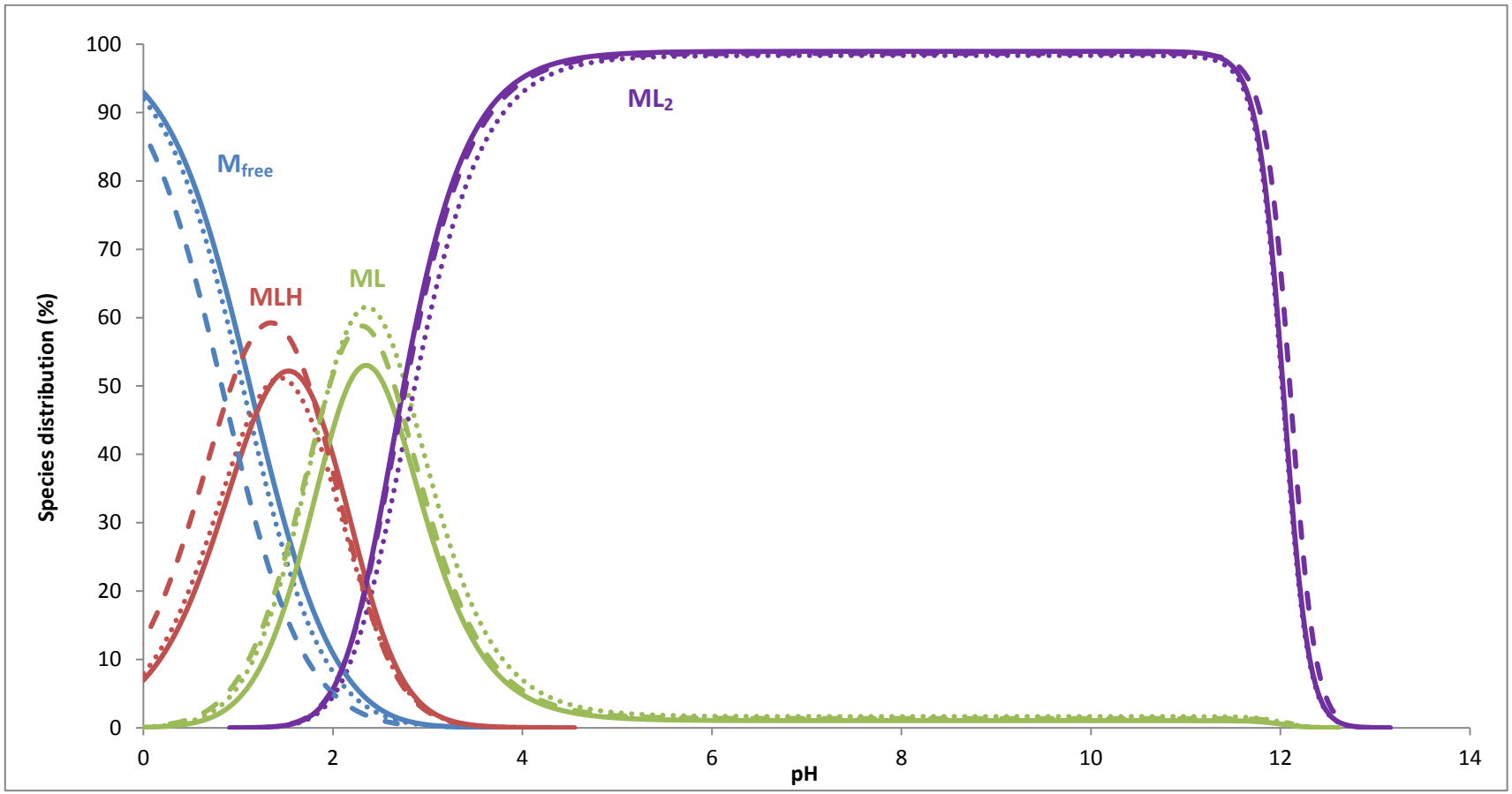


Figure 5.37 Comparison of SDDS at different temperatures plotted using an MLH, ML and ML_2 complex model. 25 °C is represented with solid lines, 32 °C with dotted lines and 40 °C with dashed lines. [Cd] = 1 x 10^{-4} M and [DIPIC] = 2 x 10^{-3} at an ionic strength of 0.25M to 0.5 M.

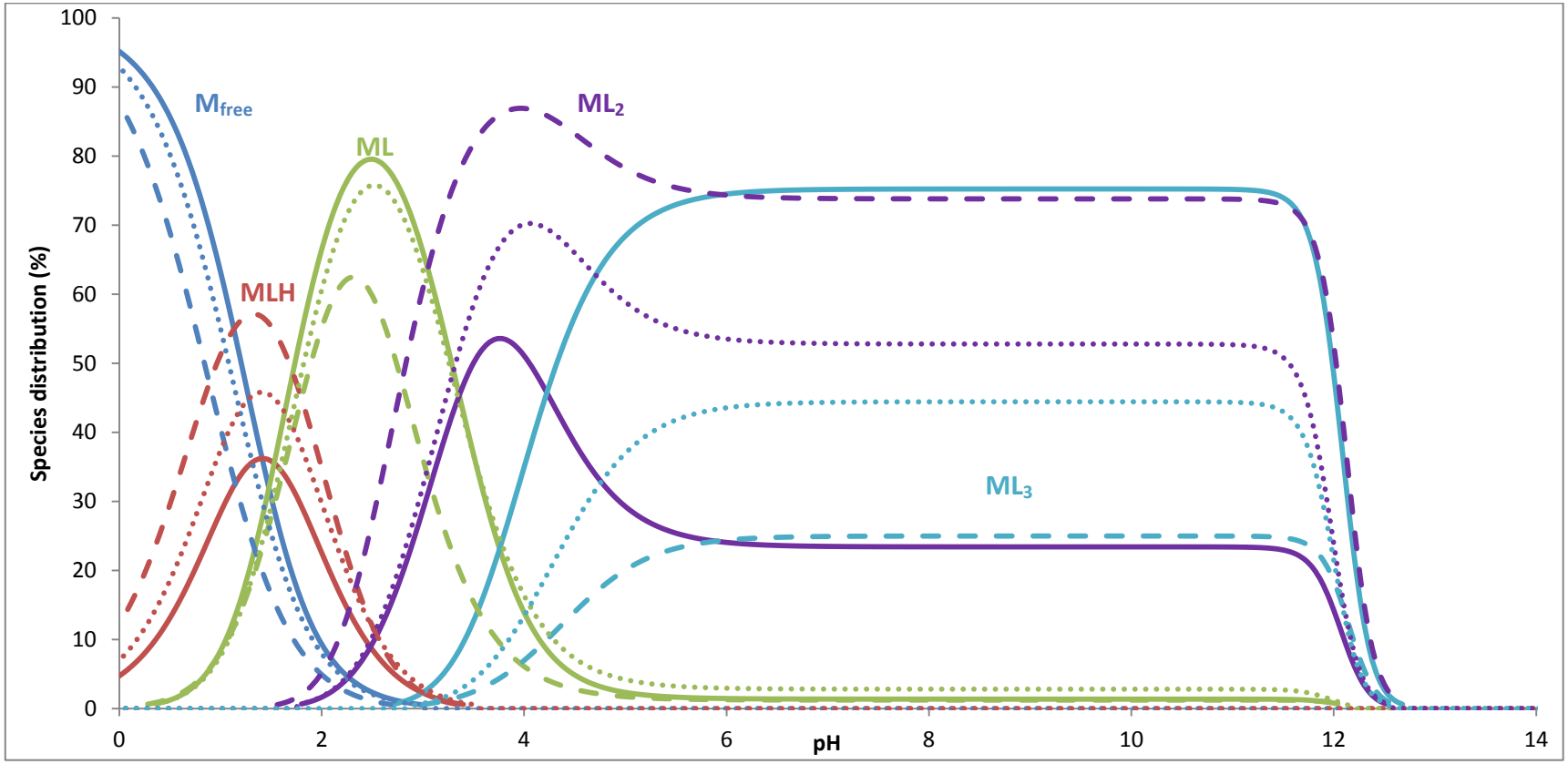


Figure 5.38 Comparison of SDDS at different temperatures plotted using an MLH, ML, ML_2 and ML_3 complex model. 25 °C is represented with solid lines, 32 °C with dotted lines and 40 °C with dashed lines. [Cd] = 1 x 10^{-4} M and [DIPIC] = 2 x 10^{-3} at an ionic strength of 0.25M to 0.5 M.

5.6 CONCLUSIONS

Two novel species were found to exist in solution, namely the MLH species (which exists at low pH) and the ML_3 species (which exists at higher pH and higher temperatures). Complex formation of the cadmium(II)-dipicolinic acid system was studied at low pH (from approximately pH 1) where glass electrode potentiometry is not useful. If the reduction potential of dipicolinic acid had not interfered with that of cadmium(II), data from a pH as low as 0.3 would have been acquired. The data obtained from pH 1 was sufficient though and, together with the compensation of the E_j made, the detection of the MLH species possible.

Without conducting studies of solution species at elevated temperatures the ML_3 complex would not have been identified as it is an endothermic species which requires heat in order for it to be formed in reasonable amounts. This temperature dependent work has shown the importance of conducting experiments at elevated temperatures for the elucidation of particularly endothermic species which are perhaps only present as minor species at lower temperatures and therefore may never be identified as their inclusion in data fitting procedures has no real significance.

Norkus, Stalnioniene and Crans (2002) made the following statement: *"In solution with excess of ligand Cu(II), Pb(II) and Cd(II) form 1:2 complexes with the tridentate dianion of pyridine-2,6-dicarboxylic acid ($dipic^{2-}$) from weak acid to alkaline solutions."*

We have found that this statement is correct as shown by the species distribution diagrams, however the ML_3 complex has not been identified in solution up until now and so their statement is not totally applicable to solutions at elevated temperature (although ML_2 does exists from pH 2 – 12 up to 40 °C it is not the only species present). The reaction enthalpy associated with forming each complex gives an

indication as to the magnitude of the effect that temperature has on the formation of each species.

Finally we can also conclude that the reduction of the cadmium(II) ion is far more sensitive to temperature change than that of thallium(I). We witnessed the reduction potentials of the two ions moving towards each other with an increase in temperature, and this movement was due to changes in the reduction potential of the cadmium(II) ion.

5.7 REFERENCES

Allen, F. H., 2002. Acta Crystallographica, B58, pp 380-388. Cambridge Structural Database. Version 5.31, November 2008 update.

Anderegg, G., 1960. Pyridinderivate als Komplexbildner I. Pyridincarbonsäuren. *Helvetica Chimica Acta,* 43 (1)**,** pp 414-424.

Billing, C. 2012. *Study of bismuth chemistry toward medicinal applications.* Doctor of Philosophy, University of the Witwatersrand.

Calí, R., Rizzarelli, E., Sammartano, S. and Pettit, L. D., 1980. Thermodynamics of protonation of some dicarboxylic acids containing heteroatoms from group 6B. *Thermochimica Acta,* 35 (2)**,** pp 169-179.

Cukrowski, I., 2000. 3D Complex Formation Curves. 5.00 ed.

Cukrowski, I. and Loader, S. A., 1998. Evaluation of a Peak Potential of an Uncomplexed Metal Ion in Speciation Study of Labile Metal–Ligand Systems by Polarography. Stability Constant Determination of Cd^{II} and Pb^{II} with Picolinic Acid at a Fixed L_T:M_T Ratio and Varied pH. *Electroanalysis,* 10 (13)**,** pp 877-885.

Doi, R. H. and Halvorson, H., 1961. Mechanism of Dipicolinic Acid Stimulation of the Soluble Reduced Diphosphopyridine Nucleotide Oxidase of Spores. *Journal of Bacteriology,* 81 (4)**,** pp 642–648.

Evtimova, B., Scharff, J.-P. and Paris, M. R., 1969. *Bulletin de la Societe Chimique de France* pp 81.

Fu, A.-Y., Wang, D.-Q. and Liu, A.-Z., 2004. Bis(ethylenediammonium) tris(pyridine-2,6-dicarboxylato-κ_3O,O',N)cadmium(II) hexahydrate. *Acta Crystallographica Section E,* 60 (10)**,** pp m1372-m1373.

Gritzner, G. and Lewandowski, A., 1991. Temperature coefficients of half-wave potentials and entropies of transfer of cations in aprotic solvents. *Journal of the Chemical Society, Faraday Transactions,* 87 (16)**,** pp 2599-2602.

Hachisuka, Y., Tochikubo, K. and Murachi, T., 1965. Inhibitory effect of dipicolinic acid on the anaerobic oxidation of glucose by the cell-free extract from vegetative cells of b. Subtilis. *Nature,* 207**,** pp 220 – 221.

Harrell, W. K. and Mantini, E., 1957. Studies on dipicolinic acid in spores of Bacillus cereus var. terminalis. *Canadian Journal of Microbiology,* 3 (5)**,** pp 735-739.

Harris, D. C., 1998. *Quantitative Chemical Analysis,* New York, W.H. Freeman and Company.

Izatt, R. M., Johnson, H. D. and Christensen, J. J., 1972. Log K_i, $\Delta H°_i$, and $\Delta S°_i$ Values for the Interaction of Glycinate Ion with H^+, Mn^{2+}, Fe^{2+}, Co^{2+}, Ni^{2+}, Cu^{2+}, Z n^{2+}, and Cd^{2+} at 10, 25, and 40 °C. *Journal of the Chemical Society, Dalton Transactions,* 0 (11)**,** pp 1152-1157.

Janik, B. and Sommer, R. G., 1973. Polarography of Polynucleotides: III. Polyadenylic Acid: The Electrode Process and Interaction with Polyamines. *Biophysical Journal,* 13 (5)**,** pp 449-461.

Kalle, G. and Khandekar, P., 1983. Dipicolinic acid as a secondary metabolite in Penicillium citreoviride. *Journal of Biosciences,* 5 (1)**,** pp 43-52.

Kang, Y., Zhang, J., Li, Z.-J., Cheng, K.-K. and Yao, Y.-G., 2006. Syntheses, structures, and photoluminescent properties of four d^{10} metal-quinolinato coordination polymers with similar rod-like SBUs. *Inorganica Chimica Acta,* 359**,** pp 2201–2209.

Kiss, T., Sóvágó, I. and Gergely, A., 1991. Critical Survey of Stability Constants of Complexes of Glycine. *Pure and Applied Chemistry,* 63 (4)**,** pp 597-638.

Kovács, I. and Kékedy, L., 1975. Contribution to the polarographic behaviour of xanthates. *Fresenius' Journal of Analytical Chemistry,* 274 (1)**,** pp 27-28.

Lainé, P., Gourdon, A., Launay, J. P. and Tuchagues, J. P., 1995. Chemistry of Iron with Dipicolinic Acid. 3. Heptacoordinated Iron in [(dipicH) 2FeII (OH2)] and [(dipic) 2FeII2 (OH2) 6]. cntdot. 2dipicH2. *Inorganic Chemistry,* 34 (21)**,** pp 5150-5155.

Li, M., Xiang, J., Yaun, L., Wu, S., Chen, S. and Sun, J., 2006. Syntheses, Structures and Photoluminescence of Three Novel Coordination Polymers Constructed from Dimeric d Metal Units. *Crystal Growth and Design,* 6 (9)**,** pp 2036-2040.

Li, Z.-X., Wang, D.-Q., Fu, A.-Y. and Chen, D.-H., 2005. Crystal structure of tetraammonium tris(pyridine-2,6-dicarboxylato-O,N,O')cadmate(II) hexahydrate, $(NH_4)_4[Cd(C_7H_3NO_4)_3] \cdot 6H_2O$. *Zeitschrift für Kristallographie,* 220**,** pp 481-482.

Martell, A. E. and Hancock, R. D., 1996. *Metal Complexes in Aqueous Solutions*, New York, Plenum Press.

Martell, A. E., Smith, R. M. and Motekaitis, R. J., 2004. NIST Standard Reference Database 46. 8.0 ed. Gaithersburg, USA: U.S Department of Commerce, National Institute of Standards and Technology.

Mendoza-Díaz, G., Rigotti, G., Piro, O. E. and Sileo, E. E., 2005. Solid-state ^{111}Cd NMR studies on cadmium(II)-2,*x*-pyridinedicarboxylates. Crystal structure of 2, 4-pyridinedicarboxylato triaqua cadmium(II) hemihydrate: [Cd(II)(2, 4-pydc)$(H_2O)_3$]·1/2H_2O. *Polyhedron,* 24 (7)**,** pp 777-783.

Metrohm, 2012. Metrosensor electrodes 2012. Metrohm Ltd.

Norkus, E., Stalnioniene, I. and Crans, D. C., 2002. Cu(II), Pb(II) and Cd(II) complex formation with pyridine-2,6-dicarboxylate and 4-hydroxypyridine-2,6- dicarboxylate in aqueous solutions. *Chemija (Vilnius),* 13**,** pp 194-202.

Park, H., Lough, A. J., Kim, J. C., Jeong, M. H. and Kang, Y. S., 2007. Different coordination modes of Hdipic and dipic ligands to nickel(II) ions in a same environment (dipic = 2,6-pyridinedicarboxylate, dipicolinate). *Inorganica Chimica Acta,* 360 (8)**,** pp 2819-2823.

Riches, J., 1948. An Introduction to Polarographic Methods and Their Application to the Analysis of Plant Material. *New Phytologist,* 47 (1)**,** pp 1-16.

Rorabacher, D. B., 1991. Statistical treatment for rejection of deviant values: critical values of Dixon's "Q" parameter and related subrange ratios at the 95% confidence level. *Analytical Chemistry,* 63 (2)**,** pp 139-146.

Samota, S., Garg, A. and Pandey, R., 2010. The Polarographic Reduction and Electrode Kinetics of Anti-depressant Drug Bupropion Hydrochloride. *Portugaliae Electrochimica Acta,* 28 (2)**,** pp 87-94.

Sóvágó, I., Kiss, T. and Gergely, A., 1993. Critical Survey of the Stability Constants of Complexes of Aliphatic Amino Acids. *Pure and Applied Chemistry,* 65 (5)**,** pp 1029-1080.

Suzuki, K. and Yamasaki, K., 1957. Stabilities of Dipicolinic Acid Complexes with Bivalent Metals. *Die Naturwissenschaften,* 44**,** pp 396.

Thomas, F. and Henze, G., 2001. *Introduction to voltammetric analysis: theory and practice,* Collingwood, Csiro Publishing.

Zutshi, K., 2006. *Introduction to Polarography and Allied Techniques,* New Delhi, New Age International Publishers.

Chapter Six

Cadmium(II)-Dipicolinic Acid Crystalline Complexes

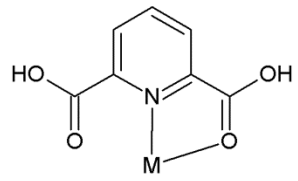
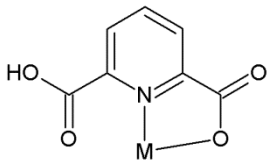
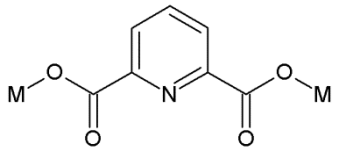
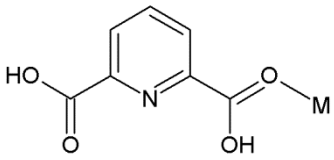
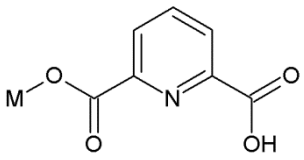
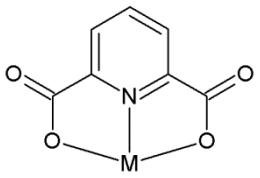
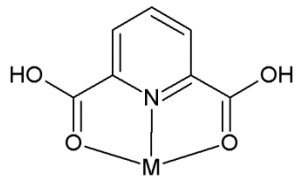
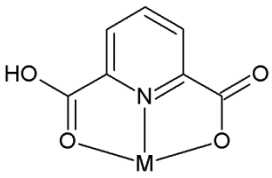
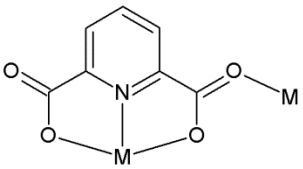
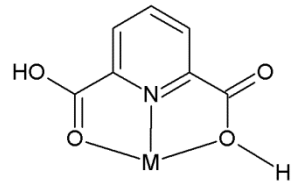
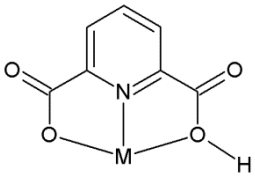
6.1 INTRODUCTION

Cadmium(II) is a soft metal ion that has a high degree of covalency in its coordination bonds and therefore prefers bonding to soft donors. A soft donor atom is one which has low electronegativity and high polarizability, like sulfur or phosphorus. Cadmium(II) is a relatively large ion, having a radius of 0.95 Å, and it chelates well to neutral oxygen donors (Martell and Hancock, 1996) as oxygen is highly electronegative. The relatively large ionic radius of this metal ion allows for high coordination numbers. A six coordinate geometry is common for cadmium(II) (Odoko, Kusano and Okabe, 2002).

Table 6.1 shows the possible coordination modes of dipicolinic acid (DIPIC) bonding to some transition metal (M), which were identified by (Park *et al.*, 2007), but have been arranged here depending on the extent of protonation of the ligand. These levels of protonation indicate the dominant form in which the ligand exists in the given pH range, but competition between the metal ion and the proton can lead to these complexes being found at any pH. A large variety of coordination complexes involving this ligand have been identified due to the many coordination modes it can bind by.

A comprehensive search of the Cambridge Structural Database (CSD) (Allen, 2002) was conducted in order to find information on the structural features of Cd(II)-dipicolinic acid complexes that occur in single-crystal structures. In total, twenty eight structures containing dipicolinic acid bonded to cadmium were found. Of these structures, twenty five showed tridentate coordination of

Table 6.1 Coordination modes of dipicolinic acid (Park *et al.*, 2007) which depend on the protonated form of the ligand.

LH_2	LH^-	L^{2-}
 *i*	 *v*	 *ix*
 *ii*	 *vi*	 *x*
 *iii*	 *vii*	 *xi*
 *iv*	 *viii*	

dipicolinic acid to the cadmium centre, and the remaining three showed tridentate bonding to another metal centre (a different metal ion - other than cadmium) together with it being monodentately bound to cadmium. This indicates that in the crystalline phase dipicolinic acid favours tridentate coordination to cadmium.

In only three of the twenty eight structures was dipicolinic acid in a protonated form, and in each case it was singly protonated and still displayed tridentate bonding (as shown by coordination mode *vii* in Table 6.1). The remaining twenty

five structures contained the fully deprotonated ligand of which seventeen structures had coordination mode *x* (Table 6.1), two had coordination mode *x* but where M represents cerium while the cadmium ion coordinates elsewhere within the structure (DOCQIW and DOCQOC), and the remaining six complexes (GETYOU, IDIFIK, IDIFIK01, QUGCEB, SEFSIG, UQAKED) had coordination mode *x* but are dinuclear bridged structures as depicted in Figure 6.1 below.

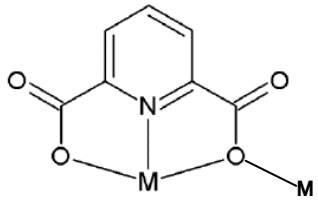


Figure 6.1 Coordination mode *x* with dinuclear bridging.

Of all the structures, ten contained only dipicolinic acid as a coordinated ligand to cadmium. Of these eight were ML_2 complexes and two were ML_3 (CEBPEF and OBUZOB) complexes. This shows a definite preference for structures with a L:M ratio of 2:1 where tridentate coordination occurs, and mostly when the ligand is fully deprotonated. Interestingly, this same deduction about the preference of complexes forming in the 2:1 ratio was made for solution species of cadmium(II) in an excess of dipicolinic acid, by Norkus, Stalnioniene and Crans (2002).

The reported experimental methods used to grow these ten crystals were investigated. Both ML_3 crystals were obtained at an elevated temperature of 60 °C, using ammonia and ethylenediamine as solvents for CEBPEF and OBUZOB, respectively. More than half of the eight ML_2 complexes did not require organic solvents in order to grow single crystals. However, compounds such as piperazine (CONXEJ - Aghabozorg *et al.* (2009)), an imidazole (ETUVAR – Dong *et al.* (2011)) or triazine (MELYOS - Aghabozorg, Aghajani and Sharif (2006)), to mention but a few, were used in some cases to aid either dissolution or crystallization. Many of these crystals were grown at room temperature, but the assisting compound often crystallized together with the ML_2 cadmium(II)-

dipicolinic acid complex. Interestingly, in the case of NOJDOG (Tabatabaee *et al.*, 2008) the solution, containing cadmium(II) nitrate and a charge transfer compound (butane-1,4-diamine) together with the ligand, was prepared at 0 °C. The crystals only formed after 2 months at room temperature. Kukovec and Oliver (2012) did a similar review of each cadmium(II)-dipicolinate complex found on the CSD and documented the counterions used in forming each crystal complex. In this work the focus is primarily on the M-L ratio of each complex and whether or not it can be grown in aqueous solution. There is a small discrepancy in the number of mononuclear cadmium dipicolinate complex anions of the form $[Cd(DIPIC_2)]^{2-}$ found by Kukovec and Oliver (2012) (six) and that was found here (eight). It may be that the two ML_2 complexes, ETUVAR (Dong *et al.*, 2011) and ETUYUO (Aghabozorg *et al.*, 2011), had been left out of the Kukovec and Oliver (2012) article since they were only published in 2011.

6.2 AIMS

Since we found two novel solution species for this metal-ligand system, it was decided that being able to produce them in their crystalline form would give greater confidence in their existence. The MLH complex would need to be grown at low pH, and the ML_3 complex at higher pH and most likely at elevated temperatures, both in purely aqueous solutions. Species distribution diagrams were then plotted with formation constants obtained at each temperature and the growth of a specific species was attempted according to the temperature, [L]:[M], concentration and pH conditions provided by the SDD. The structures of any crystals grown were determined by SCXRD. These crystalline complexes were then compared to their respective solution species that were identified in Chapter Five, to further investigate the link between the two phases.

6.3 EXPERIMENTAL

Crystals of cadmium(II)-dipicolinic acid were generally grown from aqueous solutions at elevated temperatures, and in some cases water-methanol mixtures were used, due to the low solubility of dipicolinic acid. As in the case of the cadmium-picolinic acid complexes, all pH adjustments were done using KOH or HNO_3 and pH was monitored using a glass electrode (LL Biotrode). For this work the glass electrode was calibrated at the specific temperature at which a pH measurement was taken.

The solution compositions for crystallization experiments compared to those for solution studies are quite different. High concentrations are required for crystal growth to occur in a reasonable period of time and small [L]:[M] (of around 1 to 5) are needed to prevent an excess of one component crystallizing without the other. Temperatures of 50 °C or above were needed to dissolve the high concentrations of dipicolinic acid. Details of some of the crystallization experiments attempted are discussed below. Particulars of concentrations, ligand-metal ratios and heating temperatures and duration have been included as far as possible for each experiment since all these factors play an important role in the type of compound formed, just as the SDD predicts and also as Kukovec and Oliver (2012) so clearly highlight.

6.3.1 Crystal growth of hexa-aqua-bis(μ_2-pyridine-2,6-dicarboxylato-N,O,O,O')-di-cadmium(II) bis(pyridine-2,6-dicarboxylic acid)

A 1:1 [L]:[M] (at 0.03 M) solution was made and heated and stirred for 12 hours at about 70 °C, but the ligand wouldn't dissolve. This solution was only further used for a rough test. It was diluted with about 100 mL of deionized water and the beaker was left open. When all the water had evaporated, colourless, striated, rod-shaped crystals were left at the bottom of the beaker. SCXRD was used to identify the crystals, which were found to be crystals of $Cd_2DIPIC_2 \cdot DIPIC\text{-}H_2$. Unfortunately the pH of the solution was not measured at any stage.

Crystallization at low pH was attempted in the hope of finding an MLH complex which would support its postulated existence in solution. The SDDs were plotted at 25 and 40 °C, at [L]:[M] = 1:1 where [Cd] = 0.01 M (Figure 6.2). The MLH species distribution is larger at lower temperatures but because dissolution of the ligand is a problem, high temperatures needed to be used. The aim was therefore to adjust the pH to between 0.9 and 1.5. Two slow-cooling experiments containing dipicolinic acid and cadmium(II) nitrate tetrahydrate at a dipicolinic acid concentration of 0.01 M, where [L]:[M] = 1:1 and 2:1 adjusted to pH 1.02 and 1.09 using nitric acid, respectively, were carried out from 55 °C to 25 °C cooling at 1 °C/hr. By 32°C colourless, block-shaped crystals were apparent on the base of the vials as well as floating on the solution surface. The pH of the solutions was not measured over again since the crystals formed so soon. The crystals produced from the higher [L]:[M] ratio appeared to be larger than those from the lower ratio. Upon identification of these crystals it was found that some of them were the same as those produced in the dry beaker ($Cd_2DIPIC_2 \cdot DIPIC\text{-}H_2$), while others were of free dipicolinic acid.

After these experiments, only one type of crystal turned out to be of a metal-ligand complex formed by dipicolinic acid and cadmium(II). Although many other experiments were conducted none were successful in forming cadmium(II)-dipicolinate complexes, and these attempts are discussed below.

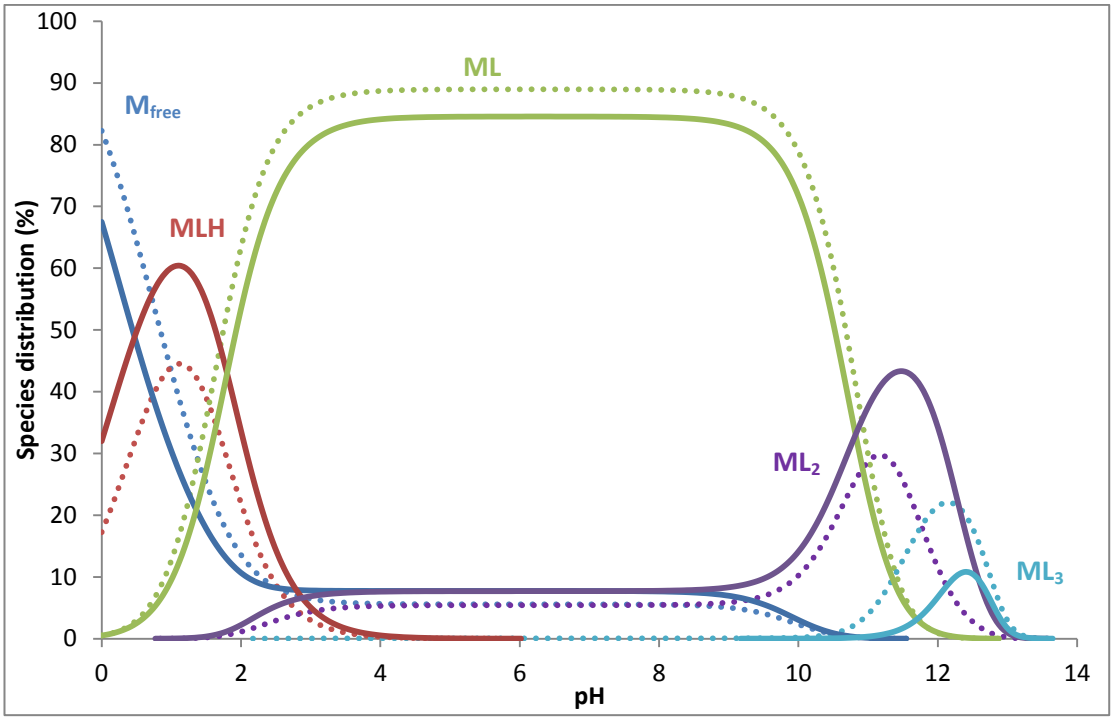


Figure 6.2 SDD plotted using MLH, ML, ML_2 and ML_3 formation constants calculated at 25 (solid lines) and 40 °C (dotted lines), where [L]:[M] = 1 and [Cd] = 0.01 M.

6.3.2 Other Attempts at Crystallization of Cadmium(II)-Dipicolinic acid Complexes

The ML_2 or ML_3 complexes portrayed in the species distribution diagram (Figure 6.2) exist in solution between pH 2 and 14 at temperatures of between 25 and 40 °C. These complexes were targeted for crystal growth because of the deliberation around the existence of the ML_3 complex. The aim was to have the ligand fully deprotonated in solution to assist the chelation of the cadmium(II) ion. Three experiments were done at a DIPIC concentration of 0.01 M having [L]:[M] ratios of 1:1, 2:1, and 3:1, all conducted at 50 °C. When the pH of the 1:1 solution was adjusted to pH 7.4, rapid precipitation of a powder occurred. This vial was left open and after a month a few minute crystals had formed within the powder, but they were too small to be analyzed. The solution with a [L]:[M] of 2:1 was adjusted to pH 9.4 and that of [L]:[M] = 3:1 was adjusted to pH 6.8, and

both vials were left in the oil bath (which was then switched off) to cool from 50 °C to room temperature. The vials remained closed at room temperature and after six weeks no crystals had formed. The vials were then left open to the atmosphere. A month later large, clear, colourless crystals had formed for the 2:1 ratio and the small unit cell obtained for these crystals (Table 6.2) indicated that a simple salt or a hydroxide had crystallized. The solution of [L]:[M] = 3:1 formed large, rectangular, striated and almost glassy-looking crystals. These crystals proved to have the same unit cell as those crystals found in the [L]:[M] = 2:1 liquor. pH was not re-measured for either of the vials as the liquor had completely evaporated once crystals had formed.

Table 6.2 Unit cell data for the salt, obtained by SCXRD.

Characteristic		**Measure**
Space group		Pnma
Length (Å)	a	5.407(1)
	b	6.326(1)
	c	9.157(2)
Angles (°)	α	90
	β	90
	γ	90

A slow-cooling experiment with a solution of 0.01 M concentration and [L]:[M] = 1:1, with pH adjusted to approximately 9.4, conducted from 50 °C to 25 °C at a rate of at 1 °C/hr., immediately formed an emulsion upon addition of the strong base. Once the temperature had reached 31 °C the emulsion turned into a cloudy gel at the base of the vial. Ten days later the gel had formed several tiny needle-like crystal outgrowths. After a further ten days the cloudiness had disappeared and only small, non-crystalline fragments were found on the base of the vial. The same results were found for similar experiments where solutions

had [L]:[M] ratios of 2:1 and 3:1. SCXRD could not be used to characterize the fragments because they were not crystalline.

In another attempt, a solution of an approximate concentration of 0.03 M and [L]:[M] = 1:1 was set up by initially dissolving the dipicolinic acid in deionized water in a closed vial at 55 °C. Once all was dissolved (after a number of hours) a solution of slightly acidified cadmium(II) nitrate was added to the dipicolinic acid solution and shaken. Immediately, a white powder precipitated out of solution. The same conditions were used for a second experiment, but this time it was not shaken upon addition of the metal ion solution. After about ten minutes, tiny particles – more crystalline than the powder previously obtained, precipitated out of solution very slowly. This liquor was quickly transferred to be slow-cooled in the hope that the crystal size would increase due to the slower rate of crystallization, but this was unsuccessful.

Another method reported in the literature used methanol to dissolve dipicolinic acid and Cd(II) at room temperature (Wu, Chen and Du (2007)). Solutions of 25%, 50% and 75% methanol-water were prepared in order to attempt crystallization in the same way (with small amounts of HNO_3 or KOH for pH adjustments). These experiments were carried out at room-temperature as well as by the slow-cooling technique. The pH of liquors, used in slow-cooling experiments, was adjusted to below 1 using HNO_3 in an attempt to grow crystals of a protonated complex (MLH for example). The temperature was regulated from 53 °C to 32 °C at a rate of 0.5 °C/hr. and then kept at 32 °C for a week. Unfortunately none of these experiments, slow-cooled or room temperature, yielded suitable crystals.

Growing crystals of metal complexes with dipicolinic acid was more difficult than anticipated. This difficulty was also experienced by Lainé, Gourdon and Launay (1995) who conducted research on the synthesis of dipicolinic acid derivatives and observed gel formation when an aqueous solution of NaOH was added to a boiling suspension of dipicolinic acid. They found that thickening of the solution

occurred at pH 3.30, 4.85 and 5.30, and between these values the gel liquefies progressively. Above pH 5.3 the solution was completely clear. They used these findings to prove the strong aggregation of dipicolinic acid in solution, describing three network structures created by hydrogen bonding and electrostatic interactions that are responsible for the gel formation.

Peral and Gellago (2000) found that dipicolinic acid had a tendency to undergo dimerization (the chemical union of two identical molecules) in aqueous solutions. They did experiments that showed that the mode of dimer formation could change depending on the pH of the solution, again due to the level of protonation of the ligand. They showed that the ML_2 zwitterions and the fully deprotonated dipicolinic acid species ($DIPIC^{2-}$) displayed hypochromic effects which indicated that their most likely mode of dimerization was the vertical stacking of the pyridine rings by $\pi \rightarrow \pi^*$ interactions. The singly deprotonated species ($DIPIC\text{-}H^-$), on the other hand, showed a hyperchromic effect that could indicate dimer formation by a collinear arrangement of hydrogen bonds (Peral and Gallego, 2000). Hypochromism or hyperchromism is observed when there is a decrease or increase, respectively, in the intensity of an absorption band of a chromophore depending on the relative orientation of the transition dipole moment interacting with the induced dipole of the adjacent molecule. This phenomenon could possibly be used to further rationalize why gels are produced in specific pH regions.

Laine, Gourdon and Launay (1995) obtained a sodium salt of dipicolinic acid by slow-cooling a pH 3.5 solution, which was prepared by adding excess base to a dipicolinic acid suspension until it dissolved, and then acidifying it with concentrated HCl. In order to obtain a metal-ligand complex of the form $[(DIPIC)_2M]^{n+}$ they suggest neutralizing the protonated dipicolinic acid in water and then adding the metal salt (this works best for the salts of alkaline and alkaline earth metals) so that the product precipitates out. This idea was used in another crystallization attempt in which we dissolved the ligand in a potassium

hydroxide solution. The metal ion (in three different [L]:[M] ratio experiments) was then added to the solution. Everything dissolved and the solution remained clear, yet no suitable crystals were formed.

It was also attempted to add an excess of the metal ion in relation to the ligand ([L]:[M] = 0.25 and 0.125 at a cadmium concentration of 0.08 M). Solid dipicolinic acid was added to the solution together with deionized water. However, it would not dissolve, even at elevated temperatures with stirring over a number of hours.

6.3.3 Crystallographic Data collection, structure solution and refinement

SCXRD data were collected on the Bruker SMART diffractometer at -100 °C. The structure was solved by direct methods using *SHELX-97 (Sheldrick, 2008)*. *SAINT+,* version 6.02 was used for data reduction, and multi-scan absorption corrections were done with SADABS 2008/1. Absorption corrections are necessary when the intensity of the x-ray beam is lowered due to absorption as it passes through the crystal, which often depends on the crystals shape and orientation (de Meulenaer and Tompa, 1965). Non-hydrogen atoms were first refined isotropically, followed by anisotropic refinement by full matrix least-squares calculations based on F^2 using *SHELX-97.* All hydrogen atoms were positioned geometrically and allowed to ride on their respective parent atoms. The crystallographic data are given in Table 6.3 and will be discussed in section 6.4.1 of this chapter.

Table 6.3 Crystal data and structure refinement for hexa-aqua-bis(μ_2-pyridine-2,6-dicarboxylato-N,O,O,O')-di-cadmium(II) bis(pyridine-2,6-dicarboxylic acid).

Identification code	$Cd_2DIPIC_2 \cdot DIPIC\text{-}H_2$	
Empirical formula	$C_{28}H_{28}Cd_2N_4O_{22}$	
Formula weight	997.34	
Temperature	173(2) K	
Wavelength	0.71073 Å	
Crystal system	Monoclinic	
Space group	P2(1)/c	
Unit cell dimensions	a = 9.1140(5) Å	α = 90°
	b = 14.7316(8) Å	β = 98.244(4)°
	c = 12.2439(7) Å	δ = 90°
Volume	1626.93(16) $Å^3$	
Z	2	
Density (calculated)	2.036 Mg/m^3	
Absorption coefficient	1.413 mm^{-1}	
F(000)	992	
Crystal size	0.50 x 0.30 x 0.16 mm^3	
Theta range for data collection	2.18 to 28.00°	
Index ranges	$-12 \leq h \leq 12$, $-19 \leq k \leq 19$, $-16 \leq l \leq 16$	
Reflections collected	31682	
Independent reflections	3916 [R(int) = 0.0283]	
Completeness to theta = 28.00°	100.0%	
Absorption correction	Semi-empirical from equivalents	
Max. and min. transmission	0.8055 and 0.5385	
Refinement method	Full-matrix least-squares on F^2	
Data / restraints / parameters	3916 / 0 / 291	
Goodness-of-fit on F^2	1.077	
Final R indices [I>2sigma(I)]	R_1 = 0.0176, wR_2 = 0.0438	
R indices (all data)	R_1 = 0.0207, wR_2 = 0.0450	
Largest diff. peak and hole	0.410 and -0.468 $e.Å^{-3}$	

6.4 RESULTS AND DISCUSSION

6.4.1 Hexa-aqua-bis(μ_2-pyridine-2,6-dicarboxylato-N,O,O,O')-di-cadmium(II) bis(pyridine-2,6-dicarboxylic acid)

6.4.1.1 Analysis of the Crystal Structure

$Cd_2DIPIC_2 \cdot DIPIC\text{-}H_2$, $[Cd_2(C_7H_3NO_4)_2(H_2O)_6] \cdot 2C_7H_5NO_4$, crystallized in a monoclinic crystal system, space group of *P2₁/c*. The asymmetric unit contains half the dinuclear metal-ligand complex and a single dipicolinic acid ligand molecule. The ratio of dinuclear Cd(II) complexes to uncomplexed ligand is 1:2. The dinuclear structure is arranged by two bifurcated coordination bonds that bridge two metal centres through the carboxylate oxygen atoms on two adjacent ligand molecules (see Figure 6.3). The cadmium ions are related by a centre of inversion. The entire dinuclear structure is almost planar (see inset of Figure 6.3), with only four H_2O molecules (two per metal centre) as axial ligands.

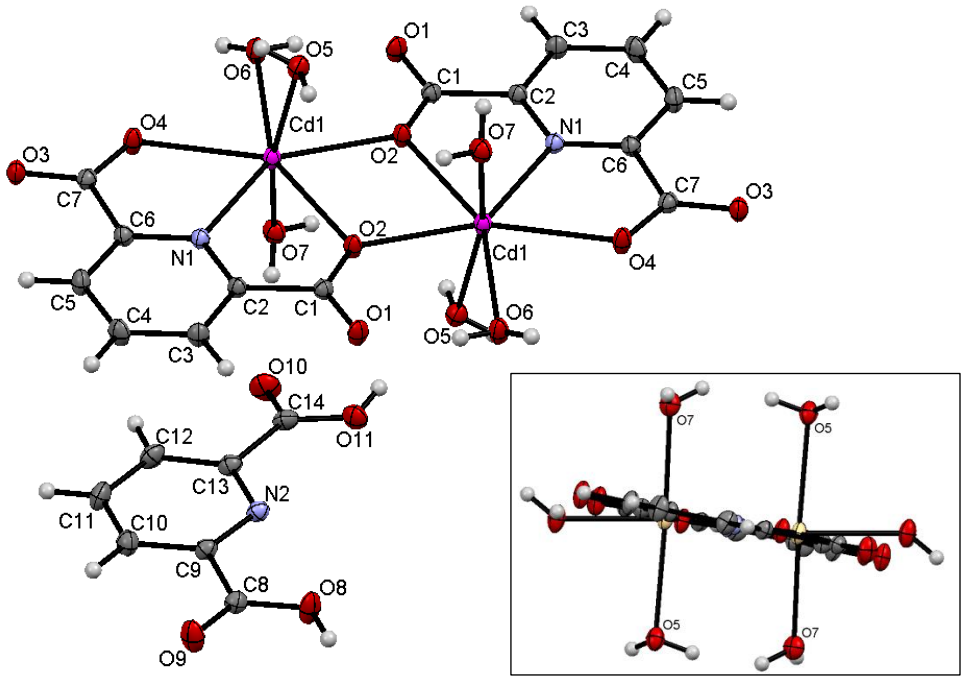


Figure 6.3 ORTEP diagram showing the structure of $Cd_2DIPIC_2 \cdot DIPIC\text{-}H_2$ at the 50% probability level. The inset highlights the planarity of the dinuclear portion of the structure.

Each cadmium(II) metal centre is seven coordinate. The dipicolinic acid acts as a tridentate ligand bonding to the metal centre via one oxygen from each carboxylate group and via the pyridyl nitrogen. Three water molecules are coordinated to the cadmium(II) via their oxygen atoms and the remaining coordination site is taken up by an oxygen atom of a carboxylate group from an adjacent dipicolinic acid. The metal centre demonstrates distorted pentagonal bipyramidal geometry. Figure 6.4 shows the pentagonal symmetry of the coordinated atoms, with angles that deviate slightly from the ideal angle of 72°.

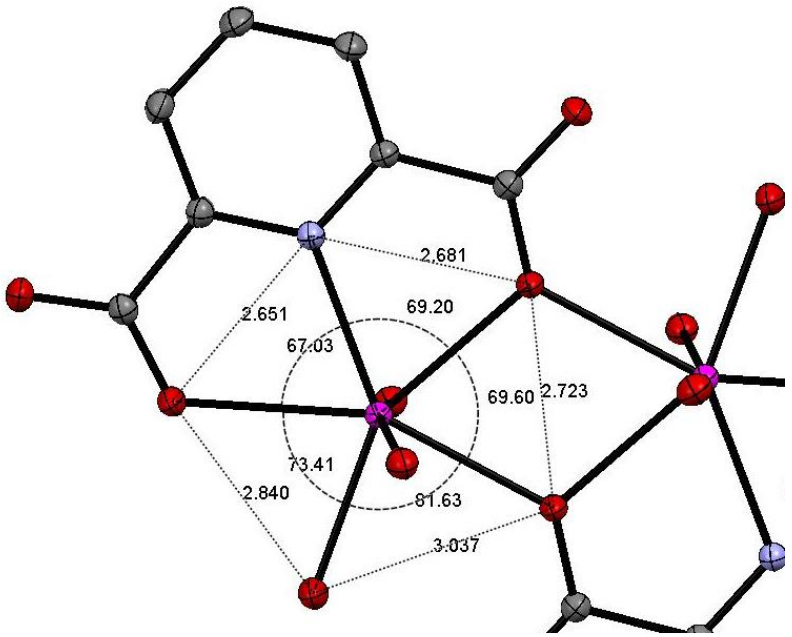


Figure 6.4 ORTEP diagram of $Cd_2DIPIC_2 \cdot DIPIC\text{-}H_2$, showing the distorted pentagonal bipyramidal geometry around the cadmium(II) centre.

According to Odoko, Kusano and Okabe (2002) a seven coordinate cadmium(II) is unusual, since cadmium(II) typically has a coordination number of six, with an octahedral d^2sp^3-hybridized geometry. Interestingly, we have also found cadmium(II) to exhibit a coordination of seven in a cadmium(II)-picolinic acid structure that was discussed in Chapter Four. The central cadmium(II) ion bonds to a picolinic acid ligand bidentately, two nitrates – one monodentately and the other bidentately, and two water molecules. However, the intraligand (O3…O4) distance of the bidentate nitrate is found to be smaller than 2.2 Å (2.162(2) Å),

thus resulting in a reduction of the coordination number of seven to six. A search of the CSD showed that a number of structures have been reported where cadmium(II) has a coordination number of seven. This will be discussed in section 6.4.2.

Each fully deprotonated dipicolinic acid ligand chelates tridentately with the metal cation, creating two 5-membered chelate rings. This mode of coordination is common for cadmium(II)-dipicolinic acid complexes and is described by coordination mode *x* where bridging also takes place (Table 6.1).

Hydrogen bonding occurs between two dinuclear complexes, as well as between a dinuclear complex and an unbound ligand (see Figure 6.5). Intramolecular hydrogen bonding takes place between the hydrogens of the equatorial water molecule and the uncomplexed carboxylate oxygen of the adjacent dipicolinic acid. Intermolecular hydrogen bonding occurs between all the hydrogen atoms of the axial water molecules (H-bond donors) and the carboxylate oxygens and pyridyl nitrogen (H-bond acceptors) of the uncomplexed ligand. The uncomplexed dipicolinic acid is responsible for linking two dinuclear complexes together via hydrogen bonding. Dinuclear complexes are hydrogen bonded to each other via the hydrogens of the axial water molecules and a free carboxylate oxygen of the complexed ligand.

Looking down the b-axis shows that there are dinuclear complexes and ligand molecules alternating in the a-direction, as shown by Figure 6.6. In the c-direction there is a row of dinuclear complexes, all linked to each other via hydrogen bonding, and directly above and below this row is a row of ligand molecules. Two dipicolinic acid molecules related to each other via the centre of inversion are linked by a hydrogen bond between their carboxylate groups. This set of dipicolinic acid molecules and the next set (created by the 2-fold screw axis) only interact with each other by weak Van Der Waals forces. These

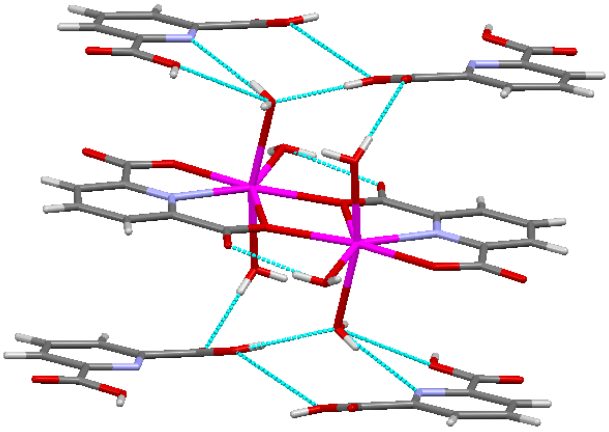


Figure 6.5 Intra- and inter-molecular hydrogen bonding within the crystal structure of $Cd_2DIPIC_2 \cdot DIPIC\text{-}H_2$.

dipicolinic acid molecules are held in place mainly by the hydrogen bonding donated by the axial water groups of the dinuclear complex above and below it.

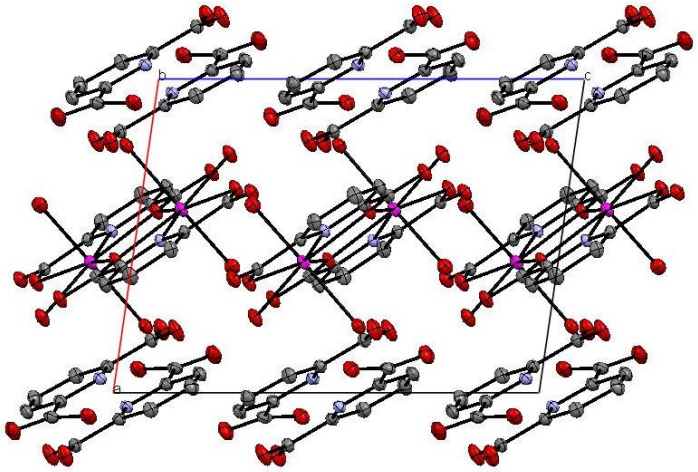


Figure 6.6 ORTEP diagram showing the packing of a unit cell as seen down the b-axis.

6.4.1.2 A Comparative Study with Literature Structures

This structure was published in 2002 by Odoko, Kusano and Okabe (Odoko, Kusano and Okabe, 2002) who grew the crystal for the purpose of clarifying the coordination mode of this ligand with divalent metal ions, thereby having no

need to measure the pH at which crystallization occurred. Now that we have measured the pH at which crystallization occurs (1.02 and 1.09 for the [L]:[M] ratio of 1 and 2, respectively) we can try to relate this complex to solution species identified in our polarographic experiments. Even though we obtained the exact same unit cell, space group and structure as Odoko, Kusano and Okabe (2002) there are still a number of differences in the experimental procedures used and the crystals produced. Odoko, Kusano and Okabe (2002) obtained colourless, plate-shaped crystals by slow evaporation at room temperature from a 70% methanol-water solution that contained dipicolinic acid and cadmium chloride in a 1:4 molar ratio. Their single crystal x-ray diffraction data were collected at 296.2 K. We obtained the same crystal structure from colourless, block-shaped crystals grown by a slow-cooling method. Crystal formation occurred between 55 and 32 °C from a purely aqueous solution. Diffraction data were obtained at a lower temperature (173 K) to that of Odoko, Kusano and Okabe (2002) and the R-factor (1.72%) in this study is considerably better than that reported by them (3.71%). The fact that the crystals can be grown from a purely aqueous solution has environmental advantages. Table 6.4 is a comparative summary of the crystal data that were determined in this research and that by Odoko, Kusano and Okabe (2002).

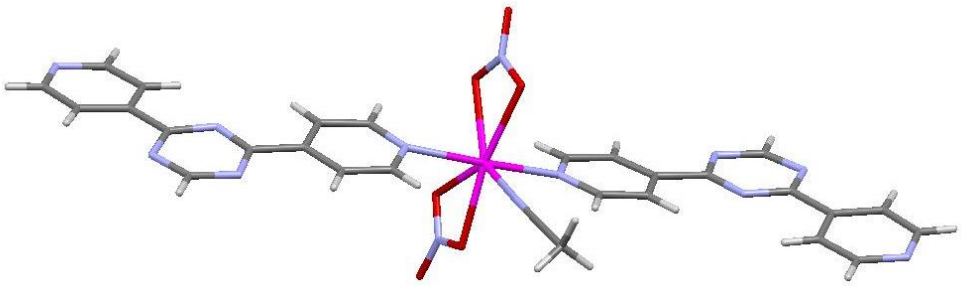
A search of the CSD showed that there are a number of cadmium(II) complexes that are seven coordinate. A coordination number of seven is only rare when considering a reduced coordination mode due to a short intraligand distance exhibited by a nitrate ion. A number of these have been reported in literature, and a few selected structures are discussed here. Barnett *et al* (2001) produced a discrete seven coordinate cadmium(II) molecular complex (REFCODE: XESHUY), where the metal centre is coordinated to two 2,4-bis(4-pyridyl)-1,3,5-triazine ligands, two nitrate anions bidentately and a MeCN molecule (Figure 6.7a)). The nitrate intraligand distances measured 2.161 Å (O4···O5) and 2.143 Å (O1···O2), which once again are smaller than 2.2 Å (Figure 6.7 b)), and therefore the

coordination number is reduced. The geometry can now be described as distorted trigonal bipyramidal.

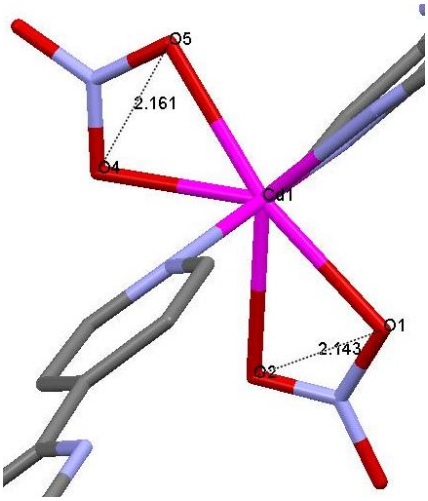
Table 6.4 Comparison of the crystallographic data for the Cd(II)-dipicolinic acid crystal, $Cd_2DIPIC_2 \cdot DIPIC\text{-}H_2$, from this work and that of Odoko, Kusano and Okabe (2002).

Characteristic		**This Work**	**Literature**
Space group		$P2_1/c$	$P2_1/c$
Length (Å)	a	9.1140(5)	9.222(3)
	b	14.7316(8)	14.768(3)
	c	12.2439(7)	12.239(3)
Angles (°)	α	90	90
	β	98.244(4)	97.70(2)
	γ	90	90
Cell Volume		1626.93	1651.81
Z, Z'		2, 0.5	2, 0.5
R factor		1.72	3.71
Temperature (K)		173	296.2
Recryst. Solvent		water	70% methanol-water

In the same article (Barnett *et al.*, 2001) two other seven coordinate structures (REFCODES: XESHOS and XESHUY) are described, both of which are polymeric. XESHOS has a seven coordinated cadmium(II) ion bonding to two pyridyl nitrogens of the ligand monodentately, two bidentate nitrates and then polymerizes to an adjacent ligand again through the pyridyl nitrogen. The two coordinating nitrate groups have intraligand distances of 2.169 Å (O7···O8) and 2.159 Å (O10···O11) (Figure 6.8), resulting in the coordination number of the metal centre being reduced by 2 and creating a geometry more correctly described as trigonal bipyramidal.



a)



b)

Figure 6.7 a) The distorted trigonal bipyramidal geometry, and b) the intraligand distances of the nitrate anions, in the structure of XESHUY.

In XESJAG cadmium(II) bonds to two pyridyl nitrogens of two separate ligands, two nitrate anions bidentately and an ethanol molecule (Figure 6.9). The two nitrate groups have intraligand distances of 2.161 Å (O1···O2) and 2.158 Å (O4···O5) thus reducing the coordination of the metal centre by 2, as before, to give a coordination number of five.

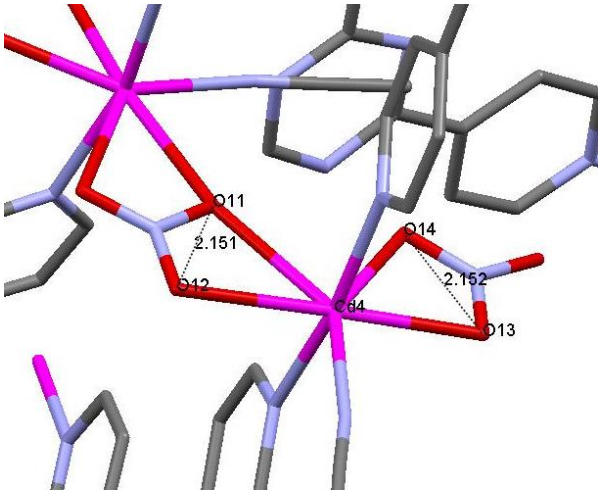


Figure 6.8 A portion of the structure of XESHOS with seven coordinate geometry around the cadmium ion, showing the intraligand distances of the nitrate anions.

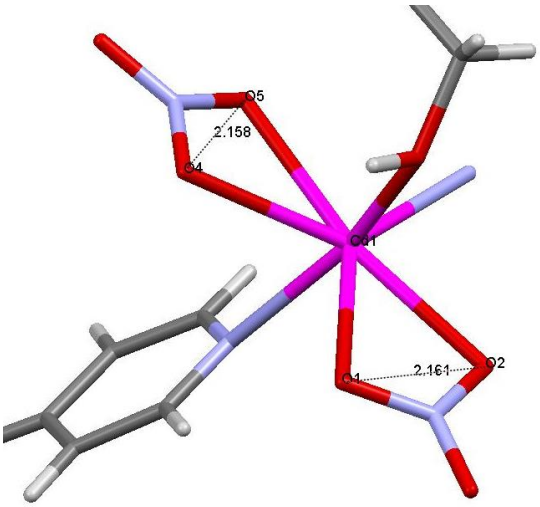
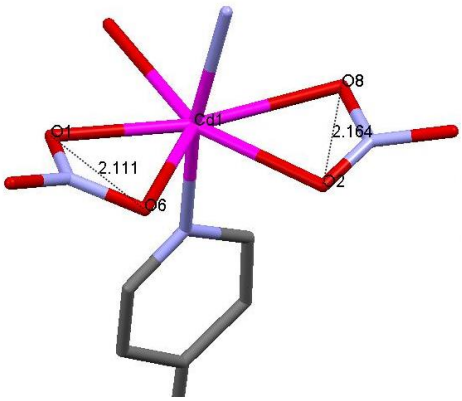


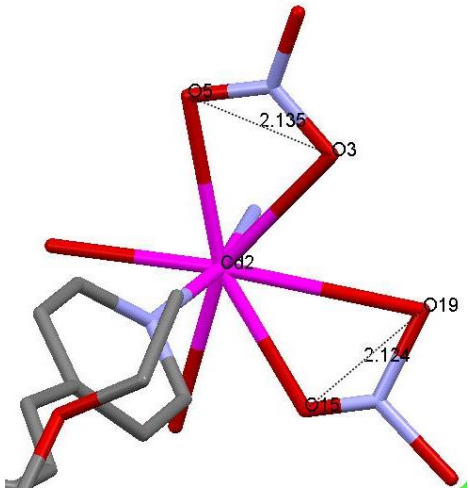
Figure 6.9 The structure of XESJAG with seven coordinate geometry around the cadmium ion, showing the intraligand distances of the nitrate anions.

Wu, Zhang and Lin (2006) produced a polymeric structure (REFCODE: DEQDIN) comprising two cadmium(II) molecules that adopt different coordination environments. The first cadmium(II) metal centre is seven coordinate and bonds to two pyridine-type ligands through the pyridyl nitrogen, two bidentate nitrate anions, and one water molecule (Figure 6.10a)). The second metal centre is eight

coordinate and bonds to two pyridyl nitrogens of two ligands, two water molecules and bidentately to two nitrate anions (Figure 6.10b)). Intraligand nitrate distances of the first metal centre were measured to be 2.164 Å and 2.111 Å, and on the second metal centre 2.124 Å and 2.135 Å, therefore reducing the coordination to 5 and 6 respectively.



a)



b)

Figure 6.10 Portions of the structure of DEQDIN with seven coordinate geometry around the cadmium ions, showing intraligand distances of the nitrate anions around a) Cd1 and b) Cd2.

All of these examples highlight that cadmium(II) seems to prefer lower coordination numbers - where a coordination number of five also seems to be quite prevalent.

6.4.2 Analysis of Doubly Protonated Dipicolinic acid (DIPIC-H_2)

From the pH-regulated crystallization experiments where the $Cd_2DIPIC_2 \cdot DIPIC\text{-}H_2$ crystal was found, crystals of the free ligand were also isolated. The unit cells of these crystals matched those of a previously determined structure by Tellez, Gaytan, Bernes and Vergara (2002) (REFCODE: AFEBUI). They obtained this crystal by the slow cooling of a hot, saturated aqueous solution of dipicolinic acid. The ligand crystallized in the monoclinic space group ($P2_1/m$), with a molecular formula of $C_7H_5NO_4$, implying that it is the doubly protonated form of dipicolinic acid seen in Figure 6.11. The hydrogen atom of the carboxylate, labeled *H4?* (by Tellez, Gaytan, Bernes and Vergara (2002)), is disordered over two positions.

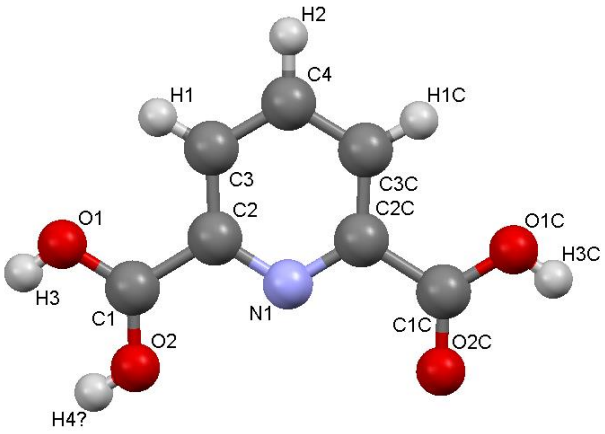


Figure 6.11 Structure of AFEBUI showing the disordered hydrogen atom.

Since our main aim was the formation of metal-ligand complexes, not too much time was spent on investigating this species. However, its formation and identification was of interest since it may be useful in studying the possible link between solution and crystalline species.

6.4.3 Analysis of the Salt Crystal

The liquors of the two experiments that produced this salt or hydroxide had [L]:[M] ratios of 2:1 and 3:1, with respective pH values of 9.4 and 6.8 at the start

of the experiment. High temperatures were used for preparation of both the solutions and the crystals were formed at room temperature by complete evaporation of the liquor. The Inorganic Single Crystal Database (ICSD) (Belsky, Hellenbrandt, Karen and Luksch, 2002) was searched using the unit cell data together with the possible atoms (Cd, H, O and N) that may be present in the crystal, but no matches were found for these search criteria. By omitting cadmium from the search criteria and taking the large concentration of KOH into account, the unit cell of the salt was matched to a structure on the ICSD, which was compared to our crystal data in Table 6.5. The ICSD structure is that of potassium nitrate (KNO_3).

Table 6.5 Comparison of the crystal data found in this work and that for KNO_3 found in the ICSD.

Characteristic		**This work**	**ICSD (Holden and Dickinson, 1975)**
Space group		Pnma	Pnma
Length (Å)	a	5.407(1)	6.458
	b	6.326(1)	5.444
	c	9.157(2)	9.211
Angles (°)	α	90	90
	β	90	90
	γ	90	90

Finding a crystal structure of this nature from our solution between pH 6.8 and 9.4 was highly likely because of the KOH that was added to the liquor to increase the pH. The structures of the salt by Holden and Dickinson (1975) Figure 6.12.

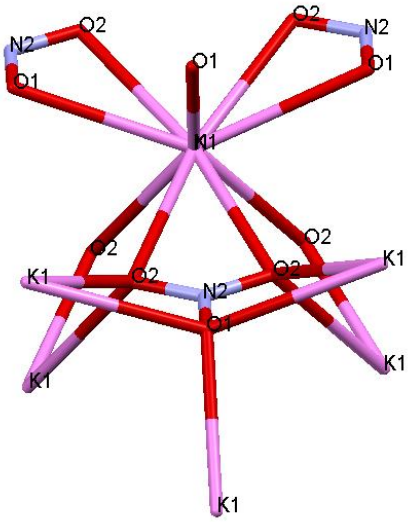


Figure 6.12 KNO_3 salt structure by Holden and Dickinson (1975).

6.5 RELATING SOLUTION SPECIES TO CRYSTALLINE COMPLEXES

The metal-ligand crystal structure of $Cd_2DIPIC_2 \cdot DIPIC\text{-}H_2$ has a L:M ratio of 1:1 which corresponds to an ML species in solution, or it could represent the dinuclear structure of M_2L_2 in solution as formed in the solid state. The crystallized solid also contains uncomplexed ligand where both carboxylates are protonated. The crystals of $Cd_2DIPIC_2 \cdot DIPIC\text{-}H_2$ and $DIPIC\text{-}H_2$ were therefore produced at an approximate pH of 1.02 and 1.09 and between 32 and 50 °C. Species distribution diagrams plotted at both 32 °C and 40 °C, utilising the initial concentrations of the solutions from which crystals were grown , were compared (Figure 6.13). The concentration of the solutions would have remained relatively constant for these experiments because the vials were closed and the crystals grew within 23 hours. Also indicated on the diagram is the LH_2 complex, plotted in terms of percentage dipicolinic acid, at 32 °C (dashed lines). (The LH_2 species at 40 °C is not shown on the SDD to avoid confusion, and also its distribution did not change very much between the two temperatures as the protonation constants were almost the same.) Figure 6.13 shows that the higher the temperature, the greater the chance of forming the ML species in preference to

the MLH species in the lower pH region. At pH 1 (at 32 or 40 °C) the MLH species is dominant in solution, but crystals of the ML and LH_2 species were obtained. Although the crystals were observed at 32 °C they may have started growing at some stage through the night at a higher temperature.

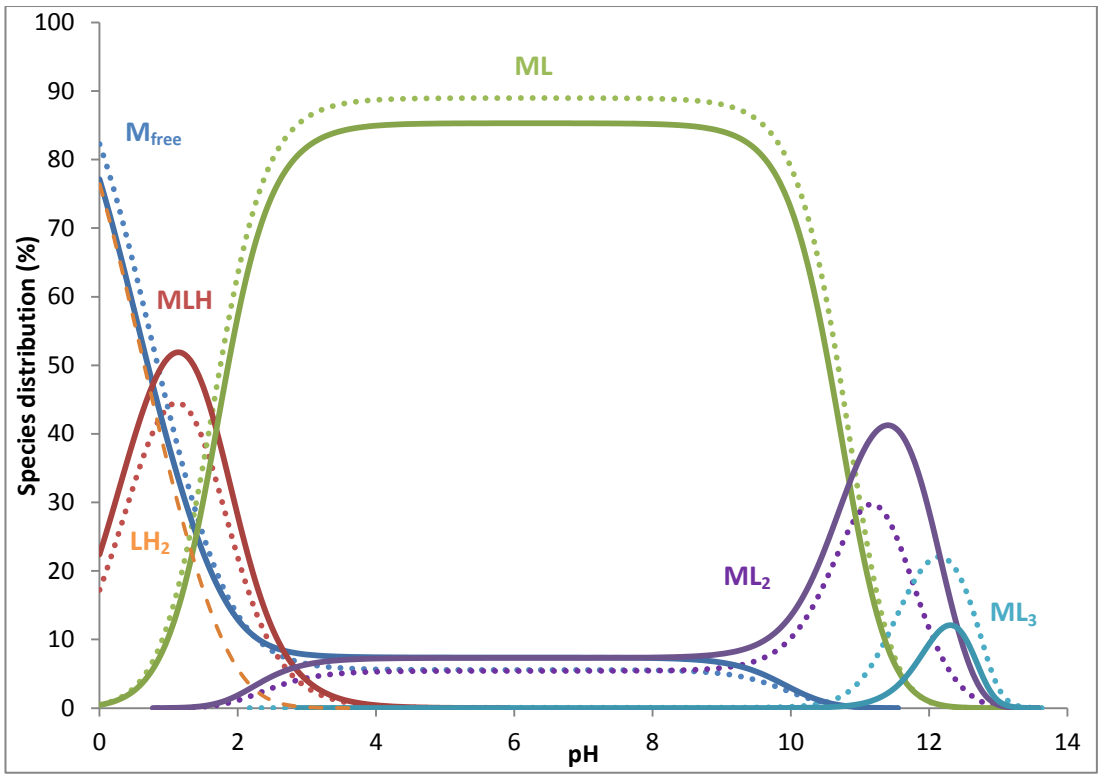


Figure 6.13 SDD plotted using MLH, ML, ML_2 and ML_3 formation constants calculated at 32 °C (solid lines) and 40 °C (dotted lines), where [L]:[M] = 1 and [Cd] = 0.01 M. LH_2 is represented by the dashed line. Cadmium(II) hydroxide species were omitted for clarity.

The same crystals were also obtained at a higher [L]:[M] ratio of 2:1 and according to the corresponding SDD (Figure 6.14) there is a slightly higher chance of obtaining the ML crystal at lower pH values. However, considering the very narrow pH range where MLH is dominant in solution and that ML is formed to a larger extent in solution, it is not surprising that the ML species (or more correctly M_2L_2) crystalized from the solution, especially since dipicolinic acid was also present to consume the protons and form LH_2.

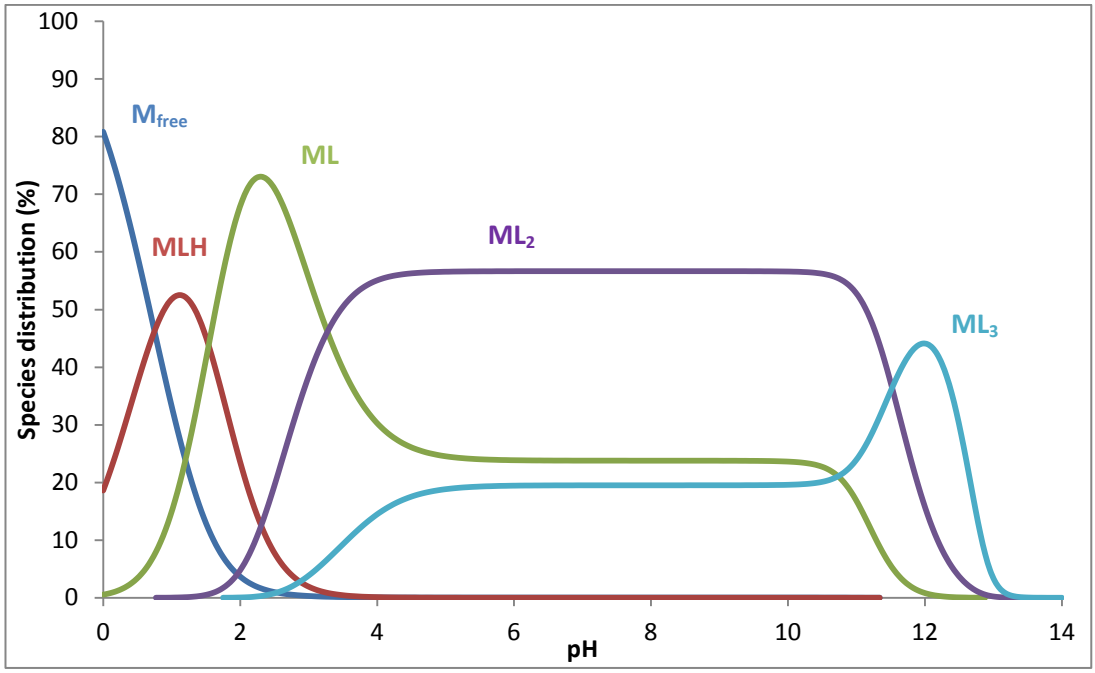


Figure 6.14 SDD plotted using MLH, ML, ML_2 and ML_3 formation constants calculated at 40 °C, where [L]:[M] = 2:1 and [Cd] = 0.005 M. Cadmium(II)hydroxide species have been omitted for clarity.

It was attempted to calculate formation constants for the [L]:[M] ≈ 50 datasets at each temperature by incorporating the M_2L_2 species into the final species set (MLH, ML, ML_2 and ML_3). In each case the formation constants would not refine, but it was found that the pH range (about pH 1.0 – 4.0) where this species affected the CCFC correlated to that at which the crystal structure was grown. (The other [L]:[M] ratios were not used to attempt calculation of formation constants as it was clear from the [L]:[M] ≈ 50 data that this species could not be incorporated in the species set.) The chances of forming polynuclear species increases with increasing concentrations, so it is not surprising to find the M_2L_2 species in the crystal, but the ML species in solution where the concentrations were significantly lower.

The free ligand crystals were obtained at high temperatures in our experiment as well is in literature (Tellez, Gaytan, Bernes and Vergara, 2002) and so an SDD using the 40 °C data was plotted using concentration and ratio conditions used

for the respective crystal growth experiment (Figure 6.15). This SDD shows only the uncomplexed ligand species and predicts the existence of the LH_2 species in solution from below pH 0 up to approximately pH 2.1, which coincides with the pH at which the crystals were harvested. (Plotting this SDD at 32 °C gave almost identical results.) The chances of finding the monoprotonated dipicolinic acid species free in solution is small as it is charged and therefore easily interacts with the metal ions to form neutral species.

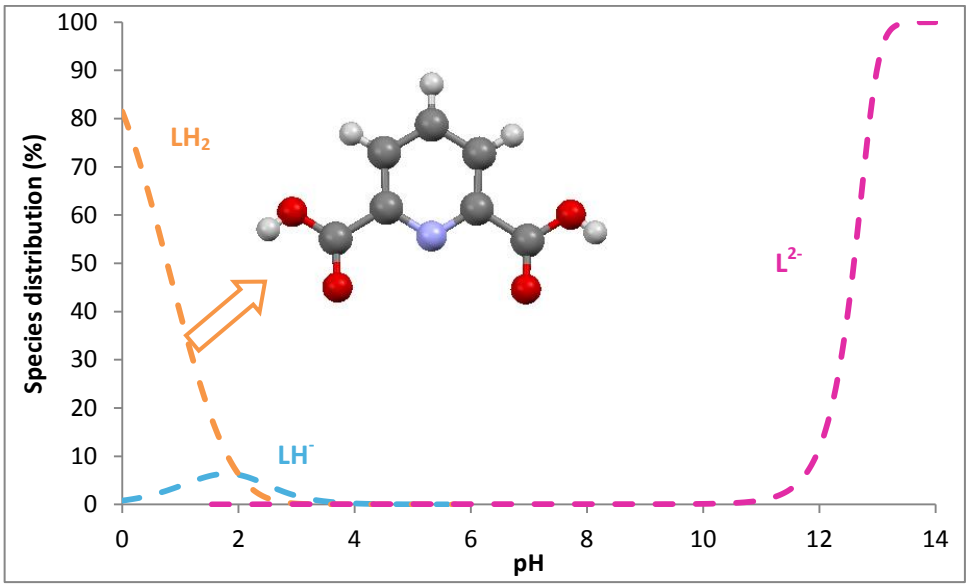


Figure 6.15 SDD plotted in terms of the remaining uncomplexed dipicolinic acid at 40 °C where [L]:[M] = 1 and [Cd] = 0.01 M.

6.6 CONCLUSION

Obtaining formation constants at various temperatures proved useful in this study since crystal formation at room temperature was not possible. Plotting SDDs at the various temperatures using the same concentrations shows the fluctuation in distribution of the predicted species in solution. Interestingly, at the small [L]:[M] ratios used for crystal growth, the fluctuations due to temperature were not as significant as those in experiments using higher [L]:[M] ratios.

The ML dinuclear crystal species that was formed seems to be the most stable complex (in its mononuclear form) in a solution where [L]:[M] = 1:1 and [Cd] = 0.01 M (inferred from an SDD plotted at these conditions, due to the high concentrations of the ML species which occurs over a wide pH range). The pH at which the solution for crystal growth was prepared at does not correlate exactly to the formation of only the ML species in solution. According to the prediction of the SDD it definitely can be found in solution at pH 1.1, but it is actually the MLH species that is dominant here. Since the M_2L_2 species existed in conjunction with the H_2L species in the crystal, it may be that the dipicolinic acid sequestered protons which led to the formation of the ML dinuclear species as opposed to the MLH species.

Elevated temperatures were necessary in order to get crystalline complexes of cadmium(II)-dipicolinic acid. The question as to whether the high temperatures in these experiments were used simply to dissolve the ligand or to actually aid in the crystallization process could not be answered. Kukovec and Oliver (2012) explained that in their work, the duration of heating solutions for crystal growth directly influenced the cadmium(II)-dipicolinate crystal complex that was produced.

The difficulty faced in crystallizations attempted in less acidic solutions was mainly the formation of gels. Hydrogen bonding and electrostatic interactions are the primary reason for the formation of gels (Laine, Gourdon and Launay, 1995). The low solubility of dipicolinic acid in solutions of moderate to high pH affected our chances of obtaining a ML_2 or ML_3 crystalline complex. However, the fact that crystals for ML_3 have been obtained before (Fu, Wang and Liu, 2004, Li, Wang, Fu and Chen, 2005) and were grown from solutions at elevated temperatures (60 °C) certainly gives us confidence that our observation of the ML_3 species forming in solution at 32 and 40 °C is not unfounded.

6.7 REFERENCES

Aghabozorg, H., Aghajani, Z. and Sharif, M., 2006. Bis (2, 4, 6-triamino-1, 3, 5-triazin-1-ium) bis (pyridine-2, 6-dicarboxylato-κ^3O,N,O')cadmate(II). *Acta Crystallographica Section E: Structure Reports Online,* 62 (8)**,** pp m1930-m1932.

Aghabozorg, H., Khazaie, Z., Agah, A. A., Saemi, M. and Notash, B., 2011. Propane-1,2-diaminium bis(pyridine-2, 6-dicarboxylato-κ^3O^2,N,O^6)cadmate dihydrate. *Acta Crystallographica Section E: Structure Reports Online,* 67 (7)**,** pp m982-m982.

Aghabozorg, H., Manteghi, F., Ghadermazi, M., Mirzaei, M., Salimi, A. R., Shokrollahi, A., Derki, S. and Eshtiagh-Hosseini, H., 2009. A novel supramolecular compound of cadmium(II): Synthesis, characterization, crystal structure,*ab initio HF, DFT* calculations and solution study. *Journal of Molecular Structure,* 919 (1)**,** pp 381-388.

Allen, F. H., 2002. Acta Crystallographica, B58, pp 380-388. Cambridge Structural Database. Version 5.31, November 2008 update.

Barnett, S. A., Blake, A. J., Champness, N. R., Nicolson, J. E. B. and Wilson, C., 2001. Synthesis and structural characterisation of cadmium(II) and zinc(II) coordination polymers with an angular dipyridyl bridging ligand: parallel interpenetration of two-dimensional sheets with 4.8^2 topology. *Journal of the Chemical Society, Dalton Transactions,* (5)**,** pp 567-573.

Belsky, A., Hellenbrandt, M., Karen, V. L. and Luksch, P., 2002. Acta Crystallographica, B58, pp 364-369. Inorganic Crystal Structure Database.

de Meulenaer, J. and Tompa, H., 1965. The absorption correction in crystal structure analysis. *Acta Crystallographica,* 19 (6)**,** pp 1014-1018.

Dong, G.-Y., Liu, T.-F., He, C.-H., Deng, X.-C. and Shi, X.-G., 2011. Bis(2-propyl-1H-imidazol-3-ium) bis(pyridine-2,6-dicarboxylato-κ^3O^2,N,O^6)cadmate(II). *Acta Crystallographica Section E: Structure Reports Online,* 67 (7)**,** pp m1007.

Fu, A.-Y., Wang, D.-Q. and Liu, A.-Z., 2004. Bis(ethylenediammonium) tris(pyridine-2,6-dicarboxylato-κ_3O,O',*N*)cadmium(II) hexahydrate. *Acta Crystallographica Section E,* 60 (10)**,** pp m1372-m1373.

Holden, J. R. and Dickinson, C. W., 1975. Crystal structures of three solid solution phases of ammonium nitrate and potassium nitrate. *The Journal of Physical Chemistry,* 79 (3)**,** pp 249-256.

Kukovec, B.-M. and Oliver, C. L., 2012. Unique cadmium(II) dipicolinate coordination tetramers with different Cd(II) coordination environments and number of halide ions (Cl, Br). *Polyhedron,* 34 (1)**,** pp 46-55.

Laine, P., Gourdon, A. and Launay, J.-P., 1995. Chemistry of iron with dipicolinic acid. 1. Mononuclear complexes of iron(II) or iron(III). *Inorganic Chemistry,* 34 (21)**,** pp 5129-5137.

Li, Z.-X., Wang, D.-Q., Fu, A.-Y. and Chen, D.-H., 2005. Crystal structure of tetraammonium tris(pyridine-2,6-dicarboxylato-O,N,O')cadmate(II) hexahydrate, $(NH_4)_4[Cd(C_7H_3NO_4)_3] \cdot 6H_2O$. *Zeitschrift für Kristallographie,* 220**,** pp 481-482.

Martell, A. E. and Hancock, R. D., 1996. *Metal Complexes in Aqueous Solutions*, New York, Plenum Press.

Norkus, E., Stalnioniene, I. and Crans, D. C., 2002. Cu(II), Pb(II) and Cd(II) complex formation with pyridine-2,6-dicarboxylate and 4-hydroxypyridine-2,6-dicarboxylate in aqueous solutions. *Chemija (Vilnius),* 13**,** pp 194-202.

Odoko, M., Kusano, A. and Okabe, N., 2002. Hexaaquabis(μ-pyridine-2,6-dicarboxylato-O,N,O':O)-dicadmium(II)-pyridine-2,6-dicarboxylic acid (1/2). *Acta Crystallographica,* E58 (1)**,** pp m25-m27.

Park, H., Lough, A. J., Kim, J. C., Jeong, M. H. and Kang, Y. S., 2007. Different coordination modes of Hdipic and dipic ligands to nickel(II) ions in a same environment (dipic = 2,6-pyridinedicarboxylate, dipicolinate). *Inorganica Chimica Acta,* 360 (8)**,** pp 2819-2823.

Peral, F. and Gallego, E., 2000. Self-association of pyridine-2,6-dicarboxylic acid in aqueous solution as determined from ultraviolet hypochromic and hyperchromic effects. *Spectrochimica Acta Part A: Molecular and Biomolecular Spectroscopy,* 56 (11)**,** pp 2149-2155.

Sheldrick, G. M., 2008. A short history of *SHELX*. *Acta Crystallographica,* A64**,** pp 112–122.

Tabatabaee, M., Aghabozorg, H., Nasrolahzadeh, R., Roshan, L. and Firoozi, N., 2008. Butane-1,4-diammonium bis(pyridine-2,6-dicarboxylato-κ^3O^2,N,O^6)cadmate(II) dihydrate. *Acta Crystallographica Section E: Structure Reports Online,* 64 (10)**,** pp m1290-m1290.

Tellez, V. C., Gaytan, B. S., Bernes, S. and Vergara, E. G., 2002. The supramolecular structure of pyridine-2,6-dicarboxylic acid. *Acta Crystallographica Section C,* 58 (4)**,** pp o228-o230.

Wu, C.-D., Zhang, L. and Lin, W., 2006. 1D and 2D Homochiral Metal-Organic Frameworks Built from a New Chiral Elongated Binaphthalene-Derived Bipyridine. *Inorganic Chemistry,* 45 (18)**,** pp 7278-7285.

Wu, H.-F., Chen, X.-D. and Du, M., 2007. A one-dimensional Cd^{II} coordination polymer: poly[[[bis[methanolcadmium(II)]-μ_2-aqua]-bis-(μ_3-pyridine-2,6-dicarboxylato-κ^5O:O,N,O':O')]. *Acta Crystallographica,* E63**,** pp m126-m128.

Chapter Seven

Complex Formation of Cadmium(II)-Quinolinic Acid

7.1 INTRODUCTION

Quinolinic acid is a metabolite of tryptophan (an essential amino acid) and is a well-known precursor of nicotinamide adenine dinucleotide (NAD^+) (Mawatari, Oshida, Iinuma and Watanabe, 1995) (Grant, Coggan and Smythe, 2009). NAD^+ is a coenzyme that is vital in all living cells as its function is to transport electrons for the completion of metabolite redox reactions. An over production of quinolinic acid does have detrimental effects in the brain – often being related to psychiatric disorders like autism, schizophrenia, severe depression, Alzheimer's disease, Huntington's' disease, and Parkinson's disease (Myint, 2012). Raised levels of quinolinic acid in HIV or AIDS patients has been linked to subcortical dementia which is characterized by cognitive, motor and even behavioural abnormalities (Valle *et al.*, 2004). The quinolinic acid causes cell death and damage to the myelin sheath of neurons thereby destroying the conduction of signals through the nervous system.

Quinolinic acid is used in the production of imazapyr, a herbicide, and also nicotinic acid. Imazapyr is a chemical that functions by disrupting protein synthesis. It enters the environment when used to treat plants and therefore exists in the soil and water.

Quinolinic acid is mainly found as a zwitterion in nature. Research shows that quinolinic acid often prefers to behave more like picolinic acid than dipicolinic acid, even though it is an isomer of the latter (Li *et al.*, 2006a) (Yen, Chen and Shiu, 2007).

The structure of this pyridinedicarboxylic acid can be seen in Figure 7.1. The stepwise protonation constants of quinolinic acid quoted as log *K* values are 4.58, and 2.3 (at 25°C and 0.5 M ionic strength) (Martell, Smith and Motekaitis, 2004) which indicates the form in which the ligand exists in solution. Figure 7.2 shows the extent of protonation of the ligand under different pH conditions. Quinolinic acid has been found to chelate through the nitrogen and the oxygen of the carboxylate group in the *ortho* position forming a 5-membered ring. That same carboxylate group can also undergo decarboxylation transforming it into nicotinic acid (pyridine-3-carboxylic acid) (Li *et al.*, 2006a), an isomer of picolinic acid. In cases where chelation occurs between the nitrogen and oxygen of the *ortho* carboxylate, the second carboxylate (*meta*) will either remain unbound (or protonated), or the oxygen atoms can bind monodentately or bidentately by bridging in another plane (Yen, Chen and Shiu, 2007). Various published coordination modes between this ligand and various metal ions (M) have been organized in terms of the level of protonation of the ligand and displayed in Table 7.1. In the case of polymeric structures, only the monomer was considered when drawing the coordination mode.

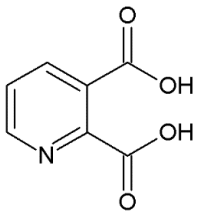


Figure 7.1 Chemical structure of quinolinic acid (pyridine-2,3-dicarboxylic acid).

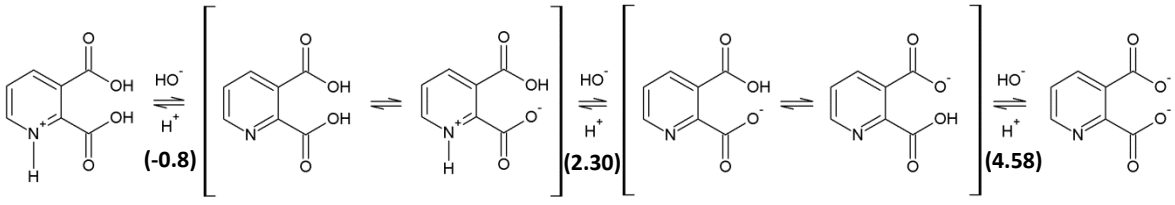
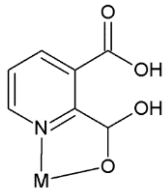
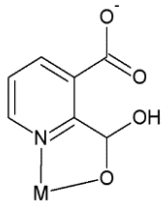
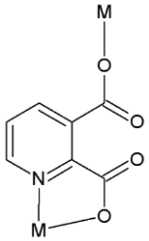
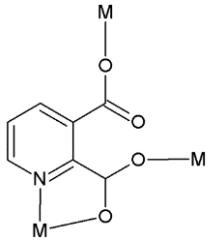
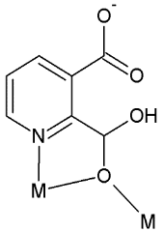
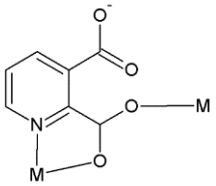
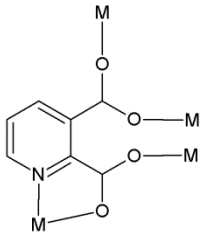
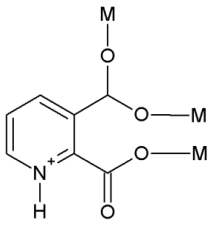
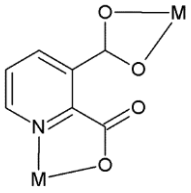
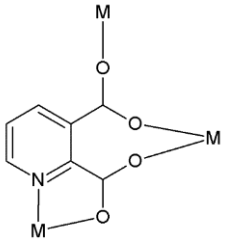
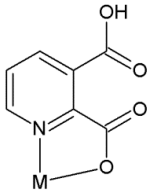
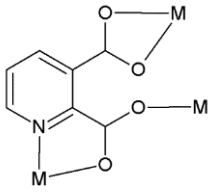
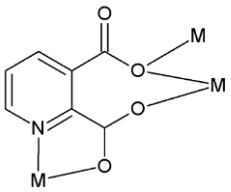
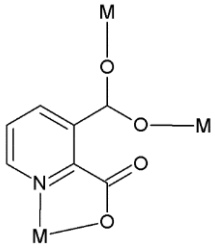
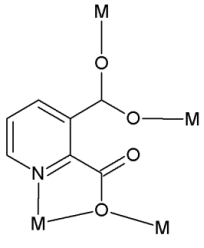


Figure 7.2 Deprotonation equilibria of quinolinic acid with stepwise protonation constants given in brackets and quoted as log *K* values.

Table 7.1 Coordination modes of quinolinic acid with various metal ions, M, as found in literature.

LH_2	LH^-	L^{2-}	
 *i*	 *ii*	 *vi*	 *xi*
	 *iii*	 *vii*	 *xii*
	 *iv*	 *viii*	 *xiii*
	 *v*	 *ix*	 *xiv*
		 *x*	 *xv*

7.1.1 Crystalline Complexes for the Cadmium(II)-Quinolinic Acid System

A CSD search of quinolinate complexes containing specifically the cadmium ion produced 20 hits (April 2013), all of them being reported more recently than 2005 surprisingly. Of the twenty structures there were eleven different modes of coordination, with *vi* (see Table 7.1) occurring the most frequently. There were no cadmium complexes exhibiting the *iv* coordination mode (Table 7.1), however two structures with calcium (REFCODES: DOZDEC and TUXLAA) were found to have the pyridyl nitrogen of the quinolinic acid protonated. This is most likely due to the fact that the calcium(II) cation is a hard acid and therefore prefers bonding with hard donor atoms. Oxygen is more electronegative than nitrogen and not much more polarizable than nitrogen, making it a harder donor than nitrogen. Calcium(II) would therefore preferentially bind to the oxygen. On the other hand, cadmium(II) is a softer metal ion and preferentially binds to the softer donor atoms. Only one cadmium structure (REFCODE: TUXLEE) contained the ligand in a protonated form, mode *v* (Table 7.1), which up until now was a rare coordination mode for quinolinic acid. Most of the twenty cadmium structures from the CSD are solvates, incorporating molecules of the organic solvent into the crystal.

7.1.2 Solution Complexes for the Cadmium(II)-Quinolinic Acid System

There are no formation constants for the cadmium(II)-quinolinic acid system given in the NIST database (Martell, Smith and Motekaitis, 2004). If values have been published in the literature either they did not meet the criteria to be included in the database or they were published after the NIST database was compiled (2004). Only one publication was found where the cadmium(II)-quinolinate system was studied for the purpose of obtaining stability constants. Yasuda and Yamasaki (1958) conducted pH titrations at 25 °C in a background solution of 0.1 M KNO_3. They suggested the presence of two complexes (ML and ML_2) for this metal-ligand system with overall formation constants (log β values) of 4.1 and 7.0 respectively. What is

important to note about this study is that they specifically started their pH titrations from above pH 3.5 in order to avoid the metal ion from chelating to a protonated ligand. It therefore raises the question whether a complex with the protonated ligand can form at lower pH and if so, what is the stability constant for this complex.

7.2 AIMS

Complex formation between cadmium(II) and quinolinic acid was studied in solution and the solid state. All solution species existing between pH 0.3 and 7 were identified and their formation constants calculated. These data were presented using species distribution diagrams where particular species could be targeted for crystal growth. In order to ascertain whether new species could be identified in the solid state, crystalline complexes were grown from aqueous solutions set at specific conditions. The structure of all crystals was determined using SCXRD which were then used to examine the potential link between solution and crystalline species.

A comparative study of the elucidated species sets and the coordination modes of picolinic acid, dipicolinic acid and quinolinic acid were made based upon the results obtained in Chapters Four, Five, Six and the work done here. Any relationships found between solution and solid state species for each of these metal-ligand systems are collated in the conclusion.

7.3 RESULTS AND DISCUSSION

The Results and Discussion section has been split into Parts A and B since studies on complex formation in both solution and the solid state were accomplished for this metal-ligand system.

Part A: Solution Complex Formation

Complex formation between quinolinic acid and cadmium(II) was studied at 25.0 ± 0.1 °C at an initial ionic strength of 0.5 M. Four experiments were done where the ligand was present in 21, 56, 101 and 196 times the concentration of cadmium(II). The C(I) Compensation Model discussed in Chapter Three is the model that was used to account for E_j and to determine the free cadmium(II) potential throughout this chapter.

The same general procedure for obtaining formation constants as was used for the dipicolinic acid system was applied here for the quinolinic acid system. The half-wave potential vs. pH data for thallium(I) above pH 2 obtained during a complex formation experiment was used to firstly calculate the free thallium(I) potential, and secondly determine the free cadmium(II) potential as before. The same challenges as experienced with the dipicolinic acid arose: (i) the reduction wave of the quinolinic acid overlapped that of cadmium(II) at very low pH and (ii) the witness ion (thallium(I)) formed complexes with the ligand from pH 3.5.

7.3.1 Interference from Ligand Reduction at Low pH

The reduction potential for quinolinic acid overlaps with that of cadmium(II) at low pH. Selected polarograms between pH 0.3 and 1.3 were plotted (Figure 7.3) to illustrate this as well as the shift in the reduction potentials to more negative values with increasing pH. Needless to say, the interference from the ligand was worst for the experiment containing the highest concentration of ligand (i.e. [L]:[M] = 196) and so these data were used to demonstrate the finding. As the pH increases so the ligand's reduction potential shifts quite considerably to more negative potentials.

From pH 0.932 the cadmium(II) and quinolinic acid waves were sufficiently resolved, which resulted in the experimental data only being analyzed from this pH onwards.

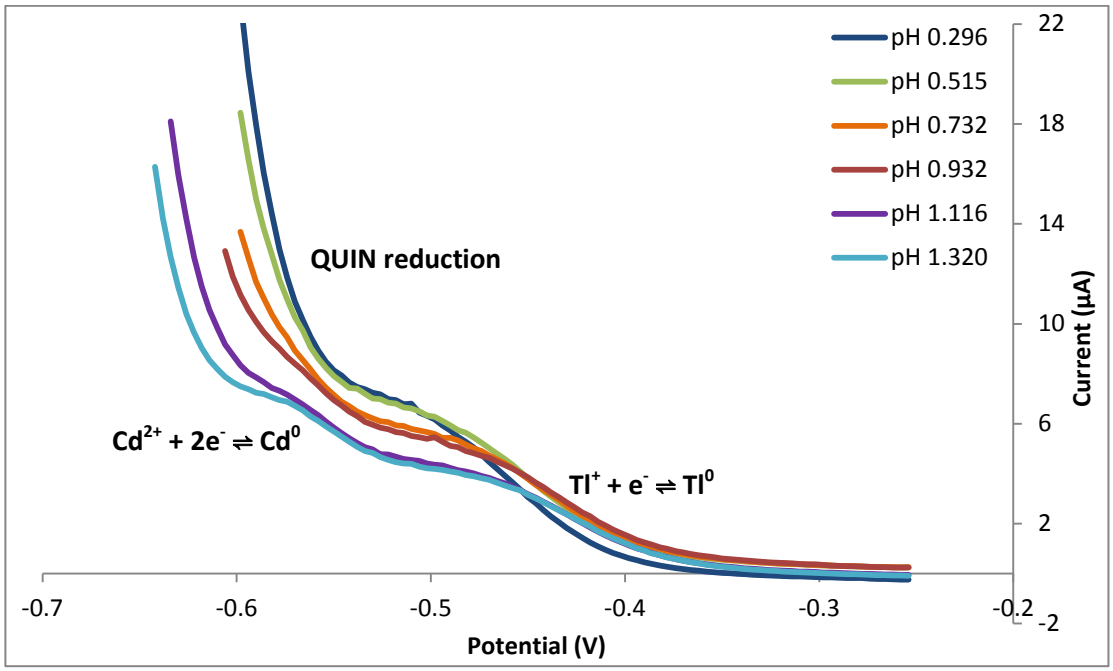


Figure 7.3 Selected polarograms from pH 0.3 to 1.3 showing the overlap of quinolinic acid and cadmium(II) reduction waves and highlighting the shift of the quinolinic acid wave as the pH is increased ([L]:[M] = 196 data).

At lower [L]:[M] ratios the pH from which the cadmium(II) data could be used was generally slightly lower (except that for [L]:[M] = 101, surprisingly).

7.3.2 Complex Formation with the In-situ Witness Ion, Thallium(I)

A plot of half-wave potential for thallium(I) versus pH for each [L]:[M] ratio can be seen in Figure 7.4. The only region where a potential shift is expected for an ideal in-situ witness is below pH 2 where the E_j is changing. From the figure below it is clear that there is a shift in the potential below pH 2 as well as above pH 3.5. The shifting above pH 3.5 therefore has to be due to complexation between the quinolinic acid and thallium(I).

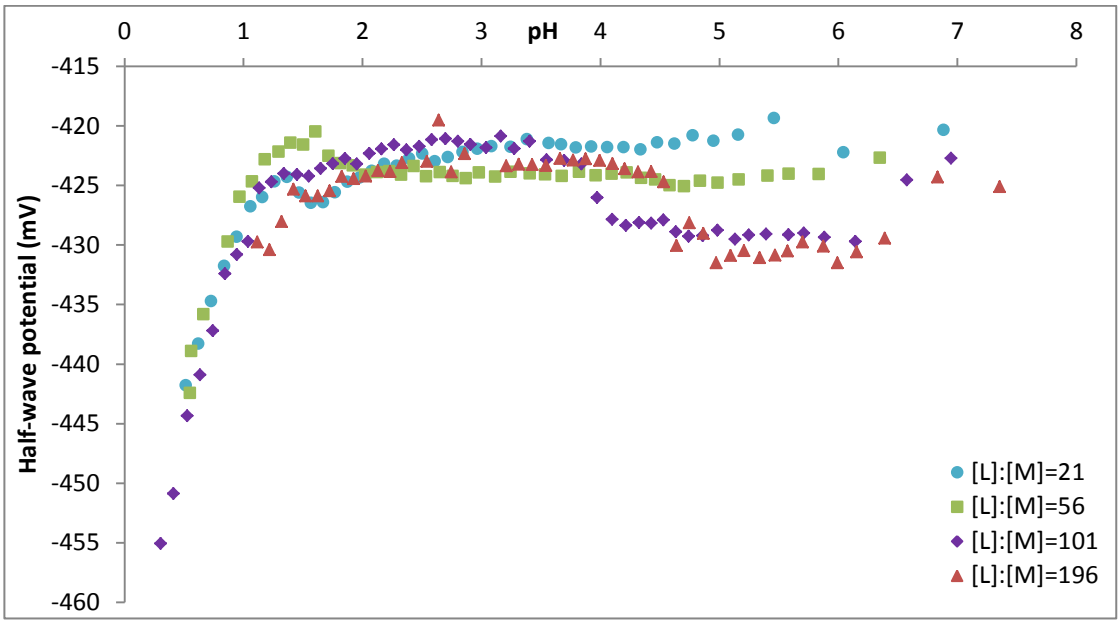


Figure 7.4 Comparison of the half-wave potential data for thallium(I) at different [L]:[M] ratios.

The pH from where complexation starts to occur between the thallium(I) and quinolinic acid differs for experiments containing different concentrations of the ligand. The thallium(I) data for each [L]:[M] ratio had to be scrutinized individually in order to check its feasibility for obtaining an accurate free metal ion potential. (For the [L]:[M] = 196 data there is a definite outlier at pH 2.64 (-419.52 mV) and so it was removed from the dataset in subsequent analyses.)

For the dipicolinic acid data we showed that the free metal ion potential could be calculated using data above pH 2 and below the pH where complex formation started occurring. This same method was used for the quinolinic acid data, averaging the maximum potential values between pH 2 and approximately 3.5 (depending on the experiment). For easier comparison the half-wave potential of each polarogram was subtracted from the respective $E(Tl_{free})$ values determined and plotted in Figure 7.5.

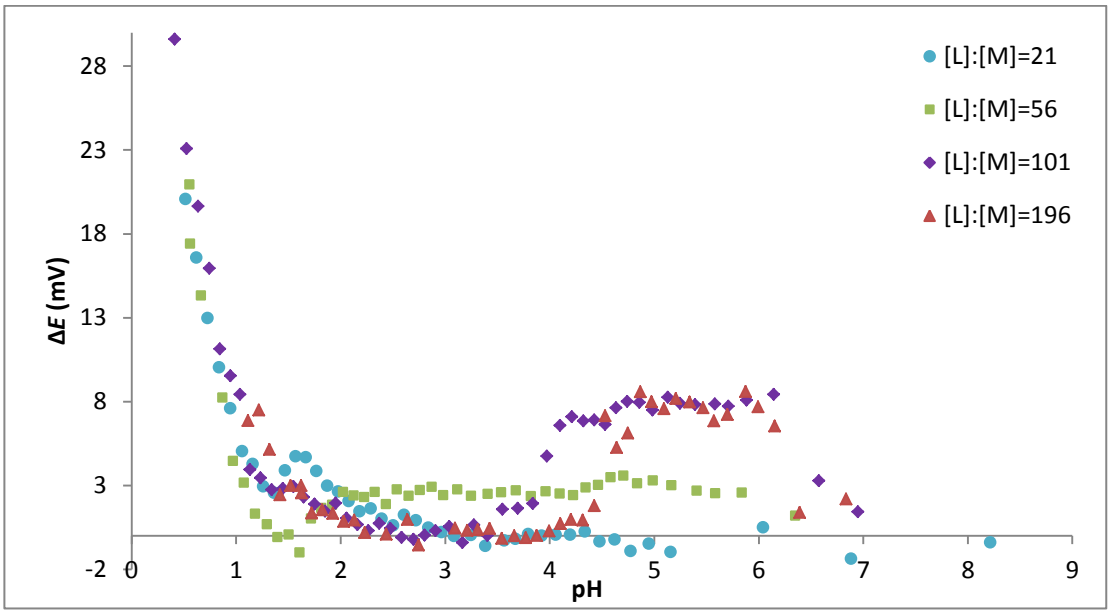


Figure 7.5 Difference between $E(Tl_{free})$ (averaged between approximately pH 2 and 3.5) and the half-wave potentials for thallium(I) at each pH.

Figure 7.5 shows that complex formation for the low [L]:[M] ratios is negligible, but is evident for the [L]:[M] = 101 and 196 data. Comparing these data to that for dipicolinic acid (see Figure 5.10) it can be seen that for dipicolinic acid complex formation with thallium(I) started at pH 2.9 already for the lowest [L]:[M] ratio (50), but for quinolinic acid only at pH 4 for the highest [L]:[M] ratio (196). This difference indicates the strong complexing ability of dipicolinic acid in comparison to its isomer – quinolinic acid. This is due to the position of the second carboxylic acid group which in quinolinic acid often is not involved in chelating to metal ions and therefore shows complexing abilities more similar to picolinic acid, as mentioned in the introduction.

7.3.3 Cadmium(II)-Quinolinic Acid Formation Constants

Obtaining an accurate $E(Tl_{free})$ value is very important as $E(Cd_{free})$ is calculated relative to it. Figure 7.5 indicates that each experiment reaches a similar value

between pH 2 and 3.5, except the [L]:[M] = 56 data. When this graph is plotted in its usual fashion, having half-wave potential vs. pH, the points between pH 2 and 3 are those at a maximum and are used to determine $E(Tl_{free})$. Beyond pH 3.5 the half-wave potentials decrease for the [L]:[M] = 101 and 196 data, which is a characteristic of complex formation. According to these plots, complex formation starts at lower pH for the 101 ratio data in comparison to that of the 196 ratio data, which cannot really be the case. For the [L]:[M] = 21 data no complex formation is evident. The 56 ratio data show a shift in half-wave potentials from pH 1.5 onwards which must be an error in the data and most certainly not complex formation. The [L]:[M] = 21 half-wave potential data have a dip between pH 1 and 2.5 which again is erroneous data, but fortunately the data are stable from pH 3 onwards and so calculating the free metal ion potential for thallium(I) is straight forward. However, for the [L]:[M] = 56 data it is not clear how to go about calculating the free metal ion potential for thallium(I) – data could be used either between pH 1.3 and 1.8 ("the maximum") or data beyond pH 1.8 ("the plateau").

The free thallium(I) potential was obtained for each [L]:[M] ratio by averaging the maximum half-wave potential points (see Figure 7.6). $E(Tl_{free})$ for [L]:[M] = 101 was calculated by an average of four points between pH 2.583 to pH 2.908, and for [L]:[M] = 196 using an average of five points between pH 3.661 to pH 4.102. For [L]:[M] = 21 this was an average of a number of points between pH 2.186 and pH 5.618, and for [L]:[M] = 56 this was an average of only four points between pH 1.390 and 1.716. This is in the pH range where the E_j is generally large and changing, which will result in a smaller $E(Tl_{free})$ value. In turn this will decrease the magnitude of the calculated E_j and $E(Cd_{free})$, which will affect shifts ascribed to complex formation and hence the formation constants. So it was decided to also calculate a free metal ion potential using the "plateau" between pH 1.8 and 6. The E_j values calculated using the Henderson equation was then compared to the values

determined using both the “maximum” value and the “plateau” value (see Figure 7.7).

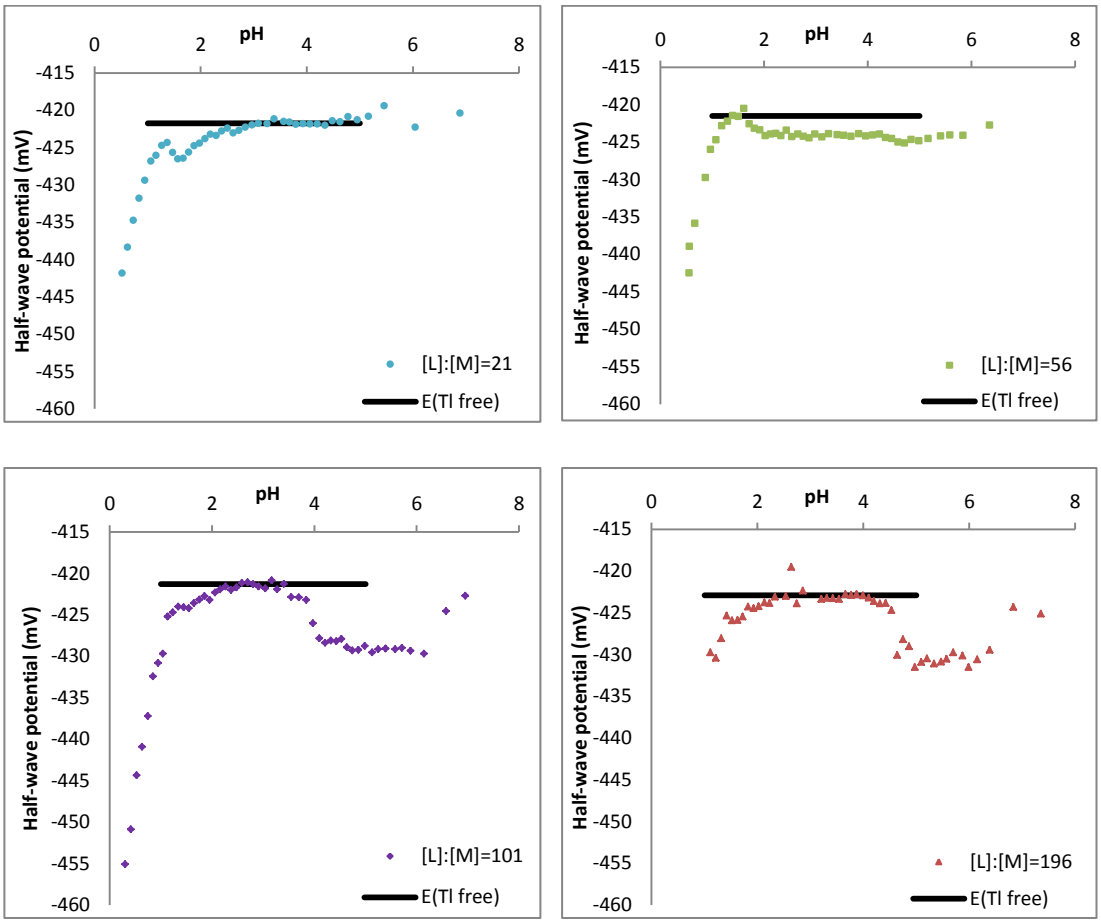


Figure 7.6 Thallium(I) half-wave potential vs. pH plots showing $E(Tl_{free})$ for each dataset.

To test the compensation method for the E_j and hence the predicted value of $E(Tl_{free})$ the magnitude of the E_j for each dataset was calculated using the Henderson equation (Equation 3.3) and then compared to that calculated using the witness ion (Figure 7.7). Although the [L]:[M] = 21 dataset is not ideal, it is the [L]:[M] = 56 dataset that is most problematic. From the figure it is not possible to make a decision as to which $E(Tl_{free})$ value is better to use for the [L]:[M] = 56 dataset; the “maximum” and “plateau” values give equally unreliable diffusion junction potential

predictions. Additionally, if the witness ion data are questionable, how reliable are the data of the cadmium(II) species reduction in this same experiment?

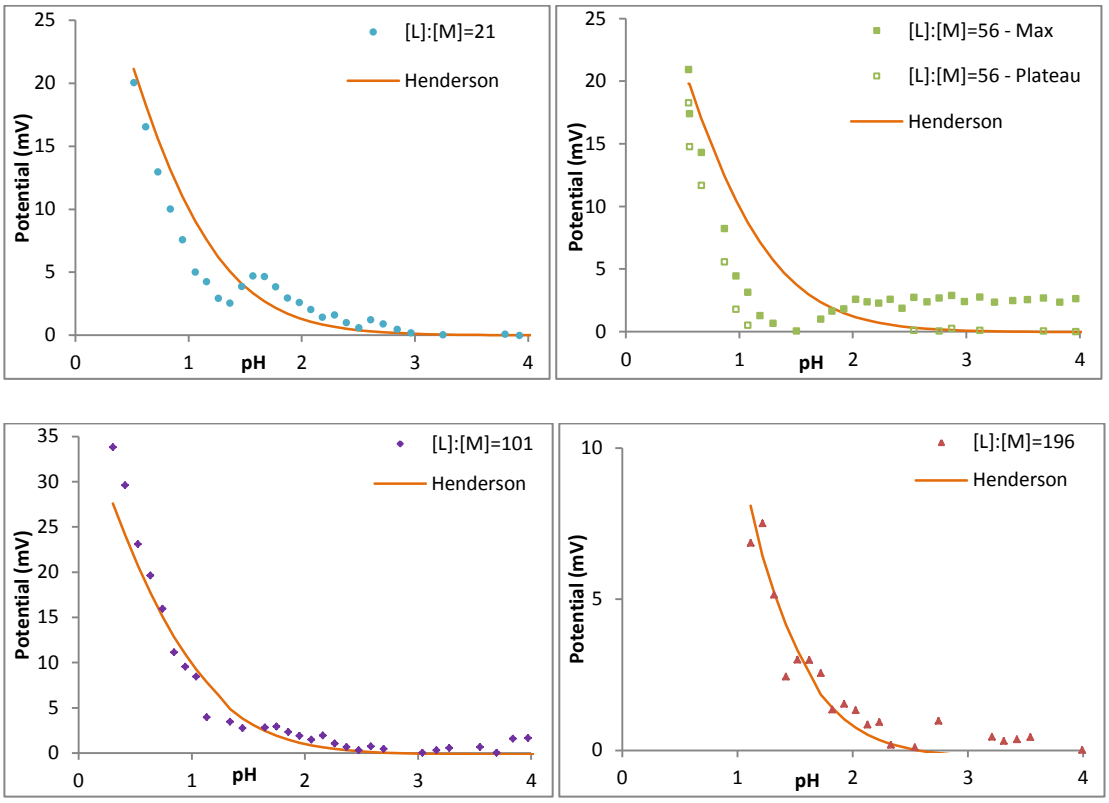


Figure 7.7 Comparison of the diffusion junction potential calculated using the Henderson equation with that determined from thallium(I) for each dataset.

The free metal ion potential for thallium(I) and the C(I) Compensation model were used to calculate the free metal ion potential for cadmium(II). The shifts due to the diffusion junction potential were also compensated for on the cadmium(II) data using the compensation model. The remaining shifts in the compensated cadmium(II) potential data should therefore be due only to complex formation between quinolinic acid and cadmium(II). When using the "plateau" to calculate $E(Tl_{free})$ for the [L]:[M] = 56 dataset the initial data points of the ECFC were negative values which shows a positive shift in potential which is not possible. Hence, the

"maximum" $E(Tl_{free})$ value was used for determining $E(Cd_{free})$. These data were then used to calculate formation constants of species that were speculated in solution, as was done in Chapter Five.

The ML and ML_2 complexes which are described by Yasuda and Yamasaki (1958) were fitted to our data (Figure 7.8). Above pH 3.5 the fit of the lower ratio experiments looked good which explains why these two complexes were sufficient in describing the data collected by Yasuda and Yamasaki (1958). However, the fit in the low pH region is really poor especially for the data obtained at higher [L]:[M] ratios, which clearly indicates missing species from the model that was used to calculate the CCFC. This was advocated by the statement made by Yasuda and Yamasaki (1958) about protonated ligands forming complexes at low pH.

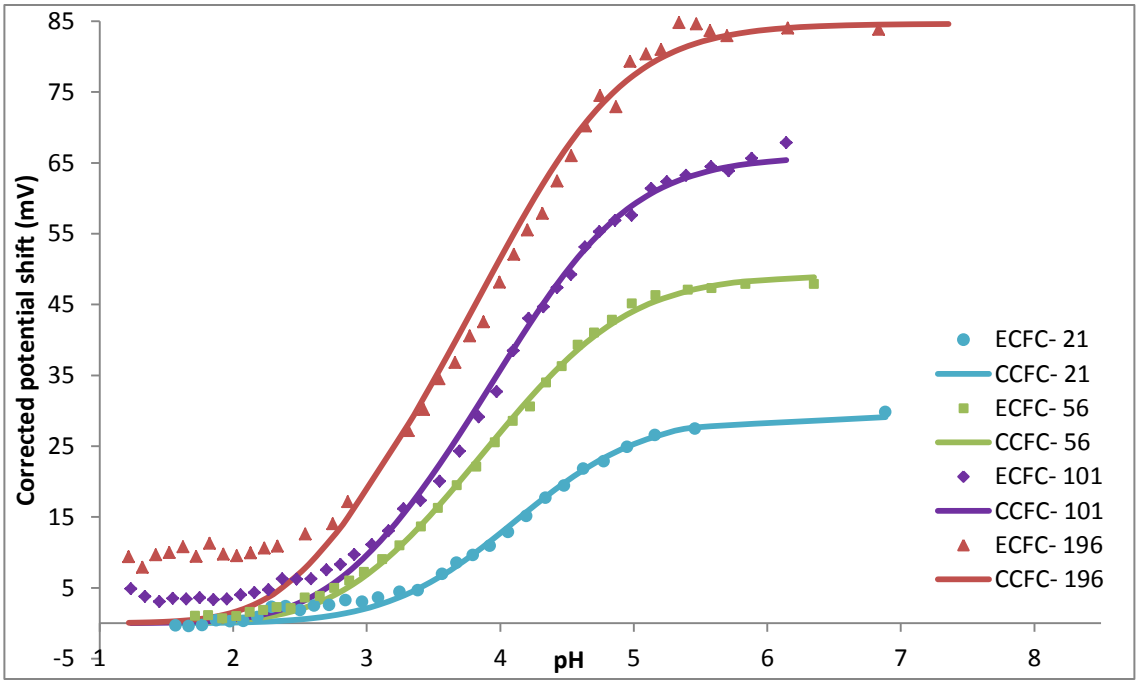
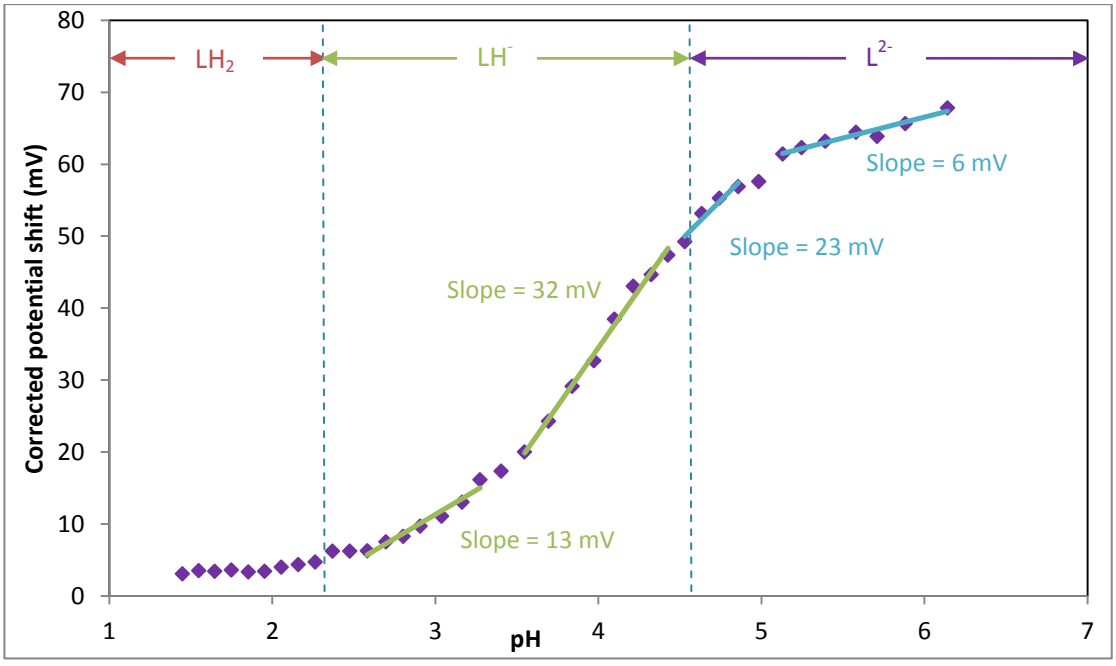


Figure 7.8 ECFC and CCFC calculated using the ML and ML_2 complex for each [L]:[M] ratio for the cadmium(II)-quinolinate system.

In order to speculate what the missing species could be, slope analysis was performed. Figures 7.9 a) and b) show the different slopes for each part of the ECFC for the [L]:[M] = 101 and 21 data, respectively. Table 7.2 shows the possible reactions that could be occurring, together with the calculated slope.

Below pH 2 in each figure the slope is close to zero and the zero shift for the [L]:[M] = 21 data indicates no real complex formation, while the 3-4 mV shifts for the [L]:[M] = 101 shows that some complex formation is starting. The very small slope at the start of the second pH region could represent a combination of ML and a protonated species such as MLH, $M(LH)_2$ or $M(LH)_3$. The main slope of 32 mV in the [L]:[M] = 101 dataset between pH 2.30 and 4.58 most likely represents the ML complex. For the [L]:[M] = 21 dataset the main slope in this region is much smaller (14 mV) and could still represent a mixture of two species such as ML and a protonated species, or even uncomplexed metal ion. The decreasing slopes in the region above pH 4.58

a)



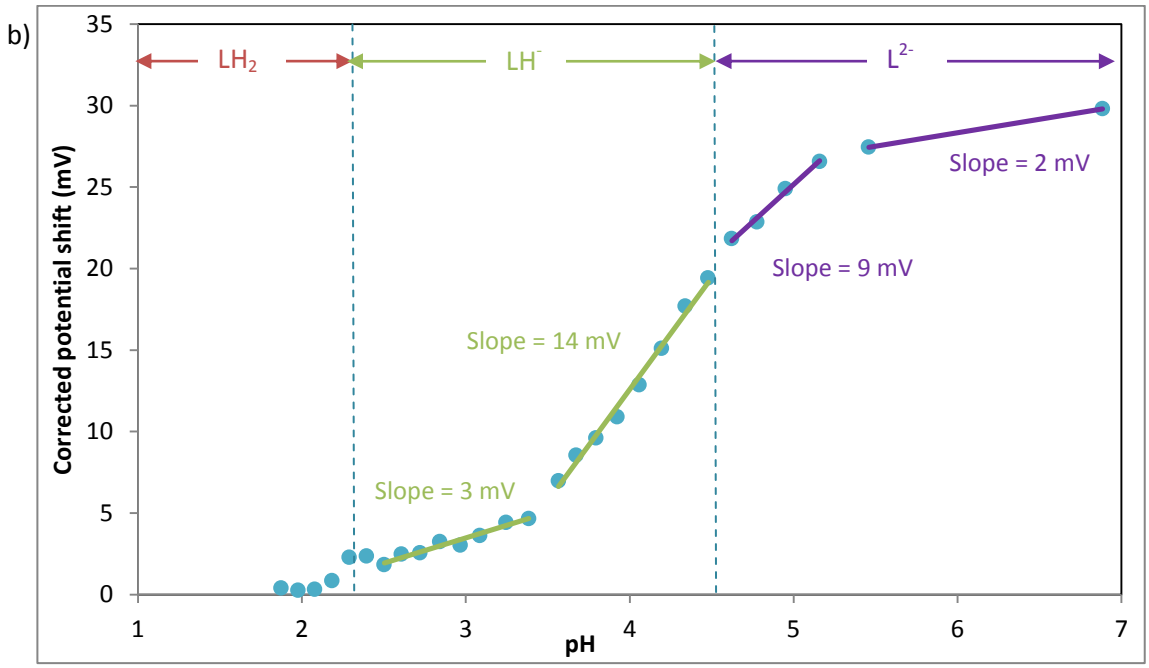


Figure 7.9 Slope analysis performed on the ECFC for [QUIN]:[Cd] of a) 101 and b) 21.

Table 7.2 Reduction reactions with their respective calculated slopes given for possible species in solution.

pH range	Possible reduction reactions	Calculated slope
pH < 2.30	$CdLH_2^{2+} + 2e^- \rightleftharpoons Cd^0 + H_2L$	0
	$CdLH^+ + 2e^- + H^+ \rightleftharpoons Cd^0 + H_2L$	30
	$CdL + 2e^- + 2H^+ \rightleftharpoons Cd^0 + H_2L$	60
2.30 < pH < 4.58	$CdLH^+ + 2e^- \rightleftharpoons Cd^0 + HL^-$	0
	$CdL + 2e^- + H^+ \rightleftharpoons Cd^0 + HL^-$	30
	$CdL_2^{2-} + 2e^- + 2H^+ \rightleftharpoons Cd^0 + 2HL^-$	60
	$CdL_3^{4-} + 2e^- + 3H^+ \rightleftharpoons Cd^0 + 3HL^-$	90
pH > 4.58	$CdL_2^{2-} + 2e^- \rightleftharpoons Cd^0 + 2L^{2-}$	0
	$CdL_3^{4-} + 2e^- \rightleftharpoons Cd^0 + 3L^{2-}$	0

are due to L^{2-} being the dominant ligand species and the reduction reactions no longer involve protons, so slope analysis cannot be used to determine whether a complexed species such as ML_2 is present.

The low pH region is where the largest deviation between the ECFC and CCFC was occurring. The most obvious species to try include in the model to improve the fit in this pH region was MLH. This inclusion improved the overall fit of the CCFC not only in the low pH region but throughout the pH range (Figure 7.10). The log β values (Table 7.3) are also in far greater agreement with each other having similar standard deviations for each complex.

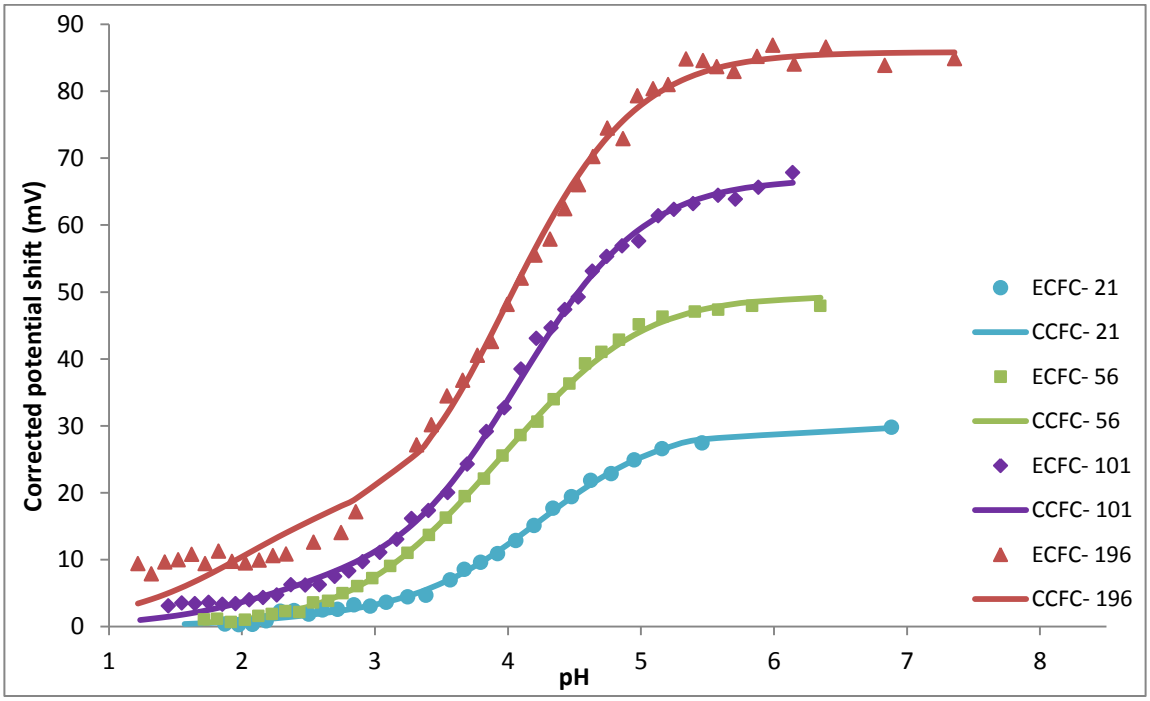


Figure 7.10 ECFC and CCFC calculated using the MLH, ML and ML_2 complex for each [L]:[M] ratio for the cadmium(II)-quinolinate system.

However, for the two highest [L]:[M] ratios there is still significant deviation between the ECFC and CCFC in the low pH region (see Figure 7.10). At low pH the CCFC of the [L]:[M] = 196 dataset does not fit the ECFC at all.

Table 7.3 Formation constants for each [QUIN]:[Cd] ratio using MLH, ML and ML_2 complexes in the model.

Complex	[L]:[M] = 21		[L]:[M] = 56		[L]:[M] = 101		[L]:[M] = 196		AVERAGE	
	Log β	Std Dev	Log β	Std Dev	Log β	Std Dev	Log β	Std Dev	Log β	Std Dev
MLH	6.8	0.1	6.3	0.1	6.83	0.04	7.14	0.02	6.8	0.3
ML	3.81	0.04	4.03	0.02	3.74	0.04	3.55	0.08	3.8	0.2
ML_2	6.4	0.2	6.37	0.07	6.81	0.02	6.93	0.01	6.6	0.3
OVERALL FIT	0.237		0.231		1.309		5.738			

All pyridinedicarboxylic acids have three protonation constants of which two are generally only ever mentioned. Protonation of the third electron rich site occurs at very low pH. Most research for obtaining formation constants has been done from about pH 2 onwards where the ligand is either doubly, singly or not protonated, and so the third protonation constant has not been used extensively. However, the third protonation may affect our analysis because we analyze data from approximately pH 1. This may explain why the fit of the CCFC is so poor at low pH. This third protonation constant was therefore incorporated to assess whether it would play a role in improving the fit. The NIST database (Martell, Smith and Motekaitis, 2004) gives no data for this value. A search of the IUPAC Stability Constants Database (Powell and Pettit, 1997) yielded a log K_3 value of -0.8 is given by Chiacchierini *et al.* (1977), which was determined spectrophotomerically at 25 °C and 0.5 M ionic strength. No other values could be found and so precision of this value cannot be commented on, although in general protonation constants at such low pH are not very accurate. Measuring the concentration of protons dissociating from the ligand in exceptionally acidic solution is extremely difficult because of all the H^+ ions that are already present in solution. Spectrophotometry was therefore used, although a measure of the pH is still required.

Looking at the ranges of the log K_3 values of other pyridinedicarboxylic acids (Table 7.4) which have been determined by several authors using various techniques, may give insight into the precision of the values for quinolinic acid.

Table 7.4 Log K_3 values for quinolinic acid and its isomers as found in literature (at 25 °C).

Compound Name	log K_3	μ (M)	Author
Quinolinc acid (pyridine-2,3-dicarboxylic acid)	−0.8**	0.5	Chiacchierini *et al.* (1977)
Lutidinic acid (pyridine-2,4-dicarboxylic acid)	0.8*	1.0	Chiacchierini *et al.* (1977)
	0.9**	0.5	Chiacchierini *et al.* (1977)
	1.6**	dilute	Ooi and Magee (1970)
Isocinchomeronic acid (pyridine-2,5-dicarboxylic acid)	1.0**	0.5	Chiacchierini *et al.* (1977)
	1.5**	1.0	Ooi and Magee (1970)
Dipicolinic acid (pyridine-2,6-dicarboxylic acid)	0.49**	1.0	Funahashi, Haraguchi and Tanaka (1977)
	0.6**	0.4	Crans, Yang, Jakusch and Kiss (2000)
	−1.0**	0.5	Chiacchierini *et al.* (1977)
	< 0.5**	0	Faucherre, Petitfaux and Charlier (1967)
Cinchomeronic acid (pyridine-3,4-dicarboxylic acid)	0.6*	1.0	Chiacchierini, D'Ascenzo and De Angelis (1976)
Dinicotinic acid (pyridine-3,5-dicarboxylic acid)	1.1*	1.0	Chiacchierini *et al.* (1977)

* Critically assessed - found on the NIST database (Martell, Smith and Motekaitis, 2004).
** IUPAC Stability Constants Database (Powell and Pettit, 1997).

Due to the variation in the ionic strengths at which the log K_3 values were measured a direct comparison could not be made. Considering the values obtained for dipicolinic acid it can be seen that the value calculated by Chiacchierini *et al.* (1977) is significantly lower than the others. The only value that was found for quinolinic acid was produced by Chiacchierini *et al.* (1977) too. Therefore to account for the possibility that this value may also be too low, two values of log K_3, −0.8 and +0.8, were used in determining formation constants. This range also serves to show the effect of the magnitude of this protonation constant on the log β values calculated. A SDD (Figure 7.11) of the protonation of quinolinic acid using the two different log

K values for the LH_3^+ species shows that the distribution of LH_3^+ at pH 1 will vary from 1.6% to 38.7% depending on the magnitude of log K_3 (if $-0.8 < \log K_3 < 0.8$).

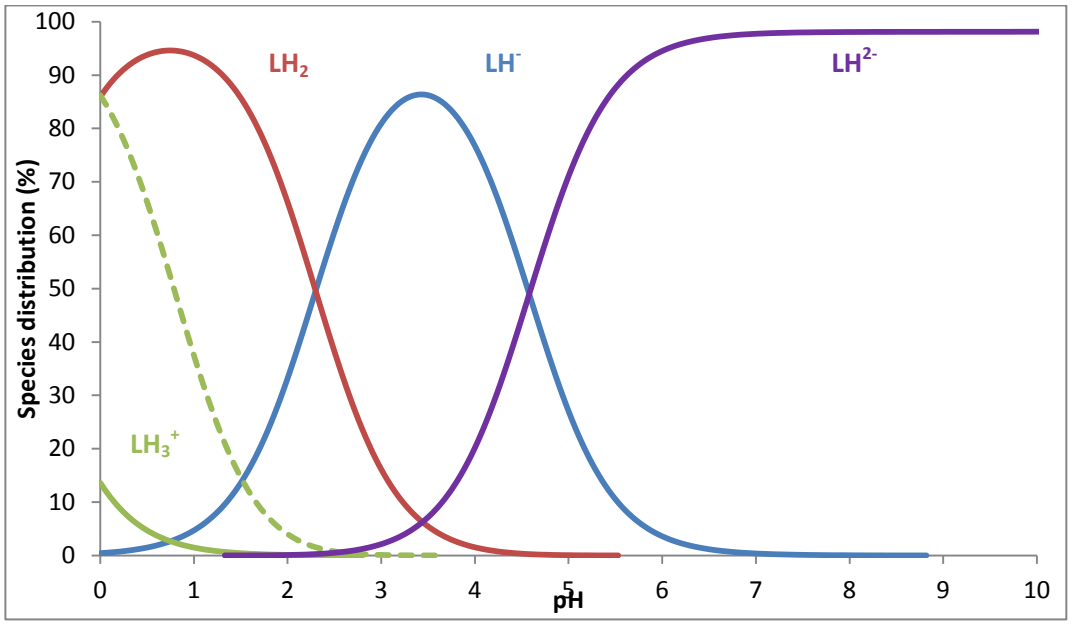


Figure 7.11 SDD for the protonation of quinolinic acid: LH^-, LH_2 and LH_3^+ where log K_3 is –0.8 (solid green line) and where log K_3 is +0.8 (dashed green line).

Formation constants were calculated using log K_3 as –0.8 implying that the doubly protonated ligand predominates between pH -0.8 and 2.3 The MLH_2 species was thus incorporated into the model because it could possibly exist at lower pH values than the ML and MLH species and may improve the fitting in the low pH region. The actual fit of the CCFC did improve significantly for the two higher [L]:[M] ratios at low pH, as illustrated in Figure 7.12 and as seen by the overall standard deviation of fitting (Table 7.5).

The standard deviation for the MLH_2 complex for the [L]:[M]= 56 data is very large (8 ± 1) for unknown reasons. The log β values for [L]:[M] = 56 are generally lower than the other formation constants, as was expected, and so this dataset was omitted (as

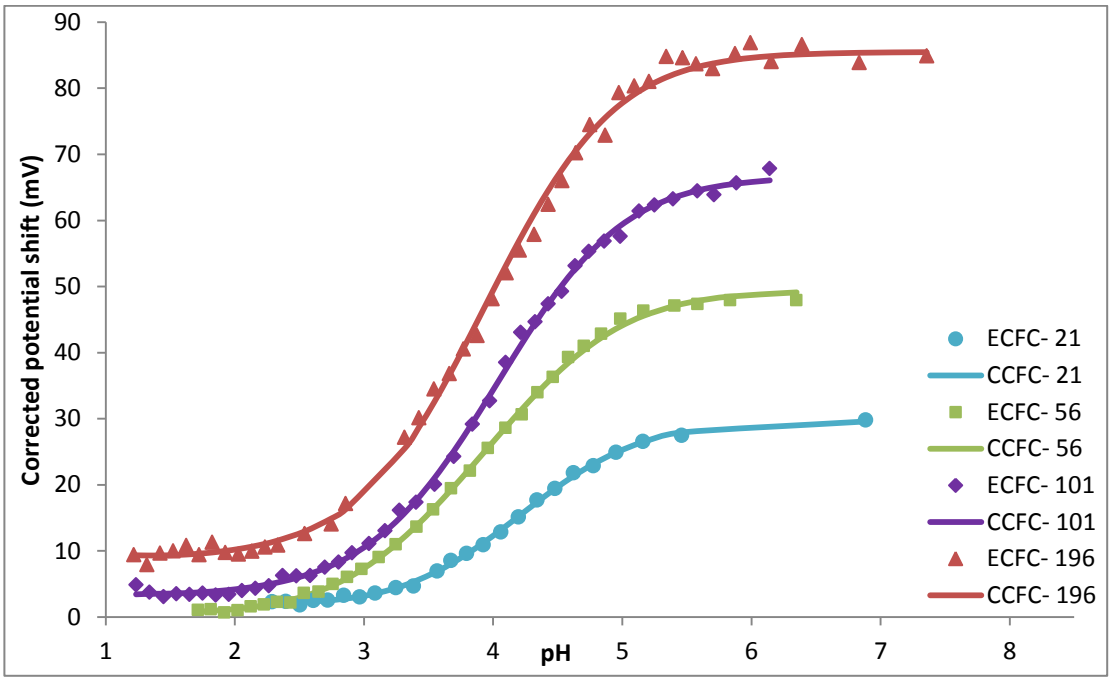


Figure 7.12 ECFC and CCFC calculated using the MLH_2, MLH, ML and ML_2 complex for each [L]:[M] ratio for the cadmium(II)-quinolinate system.

Table 7.5 Formation constants for each [QUIN]:[Cd] ratio using the MLH_2, MLH, ML and ML_2 complex model and log K_3 = –0.8

Complex	[L]:[M] = 21		[L]:[M] = 56		[L]:[M] = 101		[L]:[M] = 196		AVERAGE	
	Log β	Std Dev	Log β	Std Dev	Log β	Std Dev	Log β	Std Dev	Log β	Std Dev
MLH_2	9.2	0.3	7.9	1.0	8.58	0.08	8.85	0.04	8.6	0.5
MLH	6.6	0.3	6.3	0.2	6.60	0.08	6.78	0.06	6.6	0.2
ML	3.83	0.05	4.04	0.03	3.83	0.04	3.85	0.04	3.9	0.1
ML_2	6.4	0.2	6.36	0.08	6.78	0.02	6.9	0.01	6.6	0.3
OVERALL FIT	0.091		0.225		0.544		2.061			

even the witness ion data were problematic for this experiment) in order to see the effect on the overall standard deviation of the average log β values for the remaining ratios (Table 7.6). The standard deviation improved for each complex

except for that of ML_2 which remained the same and the ML complex shows a marked improvement.

Table 7.6 Average formation constants for the [QUIN]:[Cd] = 21, 101 and 196 data using the MLH_2, MLH, ML and ML_2 complex model.

Complex	AVERAGE	
	Log β	Std Dev
MLH_2	8.9	0.3
MLH	6.7	0.1
ML	3.84	0.01
ML_2	6.7	0.3

Due to the unknown accuracy of the third protonation constant, formation constants were recalculated for log K_3 = +0.8 (see Table A7.1 in Appendix A). The only effect using the different log K_3 value had was to decrease the MLH_2 formation constant from 8.7 ± 0.5 to 8.6 ± 0.5, and the overall standard deviation of fitting improved only slightly for three of the four ratios. Otherwise, all the other data remained the same as indicated in Figure 7.13 which shows a comparison of SDDs plotted using formation constants when log K_3 is –0.8 and +0.8.

As expected the effect of the varied log K_3 value occurs at low pH, affecting mainly the MLH_2 complex which in turn affects the amount of free metal ion present in solution. Data obtained using log K_3 as -0.8 will be used in further discussion (since it was the value reported in literature). The log K values we obtained with this model for ML and ML_2 were 3.8 and 2.9 respectively (when data for [L]:[M] = 56 was excluded). In comparison with those of Yasuda and Yamasaki (1958) (4.1 and 2.9, respectively) only the ML formation constant was different, being only slightly smaller. At the [L]:[M] ratio used to plot the SDD in Figure 7.13, the MLH species is still present in solution at pH 3.5. If Yasuda and Yamasaki (1958) performed their titration at a similar concentration and ratio, the MLH species would be present in

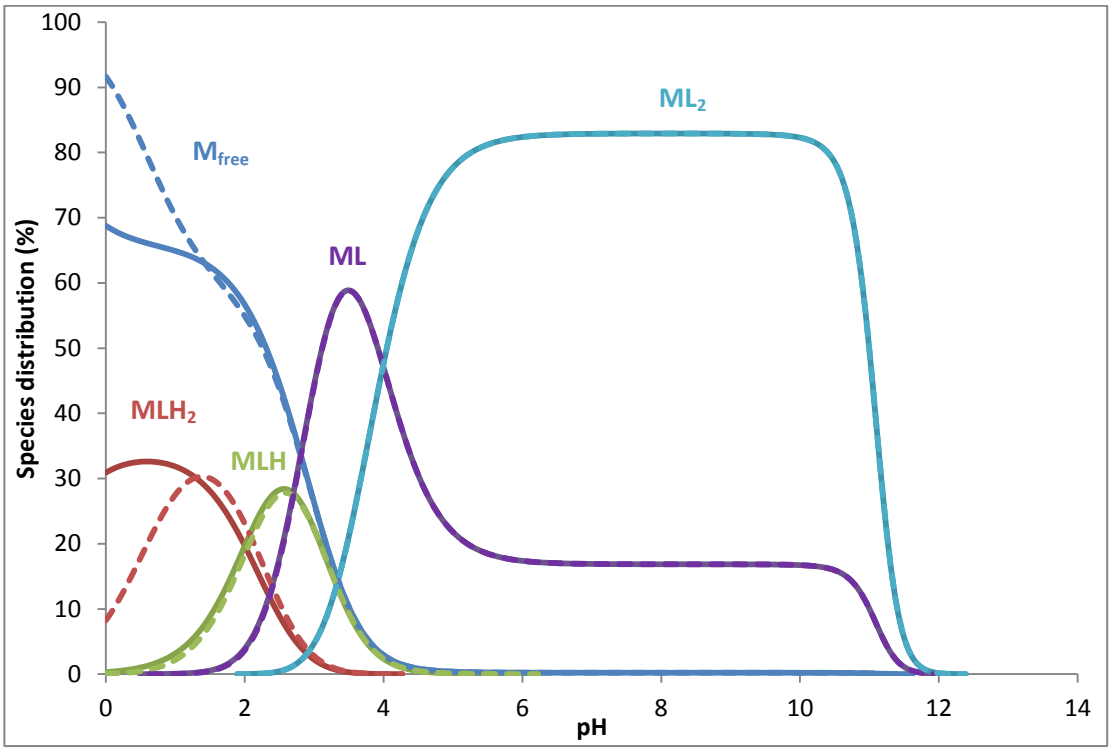


Figure 7.13 Comparative SDD showing the variation in species distribution when the value of log K_3 is –0.8 (solid lines) or +0.8 (dashed lines), [L]:[M] = 100 where [Cd] = 1 x 10^{-4} M.

their solution which could cause the value of the ML formation constant to be somewhat inflated (concentration or ratio particulars were not given in their article). The values determined by Yasuda and Yamasaki (1958) were at 0.1 M ionic strength which would also introduce slight discrepancies.

Part B: Crystalline Complex Formation

7.3.4 Experimental Overview

Crystal growth of cadmium(II)-quinolinate complexes was attempted from aqueous solutions under ambient temperature, using the pH where a particular species was

dominant in solution. Many crystallizations were attempted - some were successful in obtaining metal-ligand crystalline complexes, while others were not - but each one is important in investigating the link between solution and crystalline complexes.

A 0.05 M solution was made with acidified cadmium(II) nitrate solution and solid quinolinic acid where [L]:[M] = 1. The ligand dissolved upon heating to 65 °C for an hour and a half, with shaking in between. The solution was left in the closed vial in the water bath overnight to cool to room temperature and in the morning its pH was recorded (pH 1.48). The vial was then opened for evaporation to occur. After two weeks, angular crystals with well-defined faces formed. Some crystals were harvested and the pH of the mother liquor was measured to be 1.24. The vial was left open for further crystallisation to possibly occur. After two weeks several more crystals appeared and the pH had decreased to 0.79. Some of these crystals were colourless blocks and others were prisms. SCXRD analysis showed that a Cd(QUIN-H)$_3$ complex had formed.

A 0.05 M cadmium(II)-quinolinate solution was prepared as above but with the ratio of [QUIN]:[Cd] = 2. The initial pH measured 1.37 and the vial was left open for evaporation to occur. Prismatic crystals formed in three days and the pH was measured to be 1.32. The vial was left open and more crystals grew over the following month - some on top of the solution and others on the base of the vial. Crystals were again harvested from the solution which now had a pH of 0.85. Both the top and bottom layer contained the Cd(QUIN-H)$_3$ complex and also quinolinic acid (QUIN).

A solution with [QUIN]:[Cd] = 3 was produced as above, at a cadmium(II) concentration of 0.05 M. Again the solution was heated and once all was dissolved the vial was left closed and in the water bath to reach room temperature overnight.

After 12 hours the ligand had all precipitated out of solution and so the mixture was again heated until it all dissolved. The solution was allowed to cool again overnight and by the next morning crystals had formed. Some were fine, individual needle-like crystals while others formed in large clusters. Some of the fine crystals were harvested and found to be $Cd(QUIN\text{-}H)_3$ and others quinolinic acid (QUIN). The pH of the solution was measured to be 1.27. The vial was then closed and within the next three days a large, pale yellow, crystalline cluster was produced. The pH was now 1.29. The crystals were again found to be a mixture of quinolinic acid (QUIN) and $Cd(QUIN\text{-}H)_3$.

A similar experiment was attempted but at a higher concentration of 0.5 M where [QUIN]:[Cd] = 1. The solution was heated for 8 hours but it would not dissolve. Experiments like these were not pursued due to the difficulty with dissolving large amounts of the ligand.

A solution of quinolinic acid and cadmium(II) in a 1:1 concentration ratio, where [Cd] = 0.1 M (from a slightly acidified solution) was set up. The solution was heated for 4 hours at about 64 °C and no pH adjustments were made. Large hexagonal crystals formed overnight (Figure 7.14 a)) and the solution pH was measured to be 1.03 upon harvesting of some of these crystals. The vial was left open again overnight and many smaller crystals formed. A photo of these crystals was taken 26 hours after the original harvesting of the some of the larger crystals (Figure 7.14 b)). SCXRD showed that again a mixture of crystalline $Cd(QUIN\text{-}H)_3$ and QUIN had formed.

A number of experiments were conducted at higher pHs of between 3 and 4 so that this region could also be investigated. Different [L]:[M] ratios ranging between 1:1 and 8:1 were used and the concentration of cadmium(II) was set between 0.05 M

and 0.08 M. However, with the pH adjustments using KOH, the solutions either went cloudy or immediately formed insoluble precipitates.

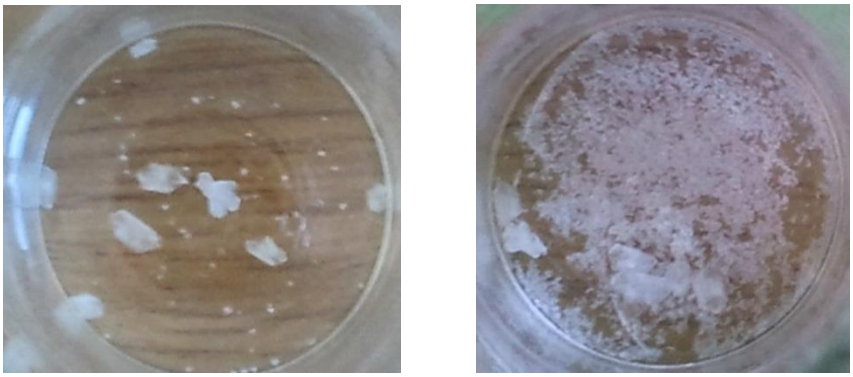


Figure 7.14 a) The start of crystal formation, and b) the formation of many more crystals within the following 26 hours. ([Cd] = 0.1 M, [QUIN]:[Cd] = 1)

Lower concentration experiments of 0.005 M were attempted where [QUIN]:[Cd] = 1:1. (The cadmium(II) solution was again slightly acidified.) The pH measured 2.10 and was adjusted to 4.08 using KOH. The vial was left open and overnight a few crystals formed that resembled dandelion seeds (see Figure 7.15). These fine crystals were identified by SCXRD to be a Cd(QUIN) complex (ML).



Figure 7.15 The fine Cd(QUIN) (ML) crystals, that resembled dandelion seeds, as viewed under a microscope using polarized light.

Another solution was set up at double the concentration (0.01 M) of the previous experiment and this time at a slightly lower pH of 3.24. Overnight a large number of dandelion crystals were formed in the open vial. There were two clusters floating on the solution and many on the base of the vial. Again the Cd(QUIN) complex which the fine, dandelion-like crystals indicated, were present in the sample solution.

An experiment was conducted at a cadmium(II) concentration of 0.005 M where [QUIN]:[Cd] = 2:1. The solution was heated for 45 minutes at about 56 °C and then allowed to cool naturally to room temperature. The clear solution was then adjusted to a pH of 2.81 using 25% KOH and the vial was left open. Overnight small dandelion crystals formed upon the top of the solution and they were left there for another day to hopefully increase in size. The crystals, which were identified as the Cd(QUIN) complex again, did increase in size and number, and so some of these were harvested at a solution pH of 2.61.

A summary of the experiments that successfully formed crystals is given in Table 7.7. SCXRD and structure determination of various crystals showed that the complexes were either of the ligand (QUIN) alone, Cd(QUIN) or Cd(QUIN-H)$_3$. In two cases the pH was not remeasured when the crystals were harvested because it was so soon after the pH adjustment. The pH should not have changed significantly over such a short period. Cd(QUIN) and Cd(QUIN-H)$_3$ correspond to an ML and an M(LH)$_3$ species in solution. The identification of the novel M(LH)$_3$ species was used to re-evaluate the species that had been speculated to exist in solution for the Cd(II)-quinolinic acid system (which will be discussed in Section 7.4).

Table 7.7 Crystals produced using Cd(II) and quinolinic acid and their associated experimental conditions.

[L]:[Cd]	[Cd] (M)	Temp (°C)	pH Adj	Vial	Duration	Harvest pH	Structure
1:1	0.05	65	none	open open	2 weeks 2 weeks	1.24 0.79	$Cd(QUIN\text{-}H)_3$
2:1	0.05	65	none	open open	3days 1 month	1.32 0.85	$Cd(QUIN\text{-}H)_3$ $Cd(QUIN\text{-}H)_3$ & QUIN
3:1	0.05	65	none	closed closed	1 day 3 days	1.27 1.29	$Cd(QUIN\text{-}H)_3$ & QUIN QUIN & some $M(LH)_3$
1:1	0.1	64	none	open	1 day	1.03	Hexagons - $Cd(QUIN\text{-}H)_3$ Prisms - QUIN
1:1	0.005	room	4.08	open	1 day	not remeasured	Cd(QUIN)
1:1	0.01	room	3.24	open	1 day	not remeasured	Cd(QUIN)
2:1	0.005	56	2.81	open	1 day	2.61	Cd(QUIN)

7.3.5 Crystallographic Data Collection, Structure Solution and Refinement

The polymeric Cd(QUIN) crystal structure has been published before by Aghabozorg *et al*. (2008), who obtained this structure from aqueous solution using an organic proton transfer compound – piperazine. We reproduced this structure using different methods, focusing on purely aqueous solutions and particular pH values. The $Cd(QUIN\text{-}H)_3$ crystal structure was also grown under similar conditions, but at lower pH. During the progress of our research the structure was reported by Barszcz *et al.* (2010) (who grew the structure using aqueous solution at room temperature).

Intensity data were collected on a Bruker SMART CCD area detector diffractometer with graphite monochromated Mo Kα radiation (50 kV, 30 mA). The collection method involved ω-scans of width 0.3 °. Data reduction was carried out using the program *SAINT+,* version 6.02 *(Bruker smart and Saint (Bruker, 1999)).* Empirical absorption corrections were made for $Cd(QUIN\text{-}H)_3$ using the program SADABS. No absorption corrections were carried out for crystals of Cd(QUIN) since this increased

the internal R-factor. All crystals were studied at -100 °C (173.15 K) and structures were solved by direct methods using *SHELX-97* (Sheldrick, 1997). Non-hydrogen atoms were first refined isotropically followed by anisotropic refinement by full matrix least-squares calculations based on F^2 using *SHELX-97*. All hydrogen atoms were positioned geometrically and allowed to ride on their respective parent atoms, except those of H5 and H6 in Cd(QUIN-H)$_3$ which were placed according to electron density and then refined freely. A summary of the crystallographic data for both structures is given in Table 7.8.

Table 7.8 Crystal data and structure refinement for Cd(QUIN) and Cd(QUIN-H)$_3$.

Complex	Cd(QUIN)	Cd(QUIN-H)$_3$
Empirical formula	$C_7H_9CdNO_7$	$C_{42}H_{36}Cd_3N_6O_{30}$
Formula weight	331.55	1441.97
Temperature	173(2) K	173(2) K
Wavelength	0.71073 Å	0.71073 Å
Crystal system	Orthorhombic	Trigonal
Space group	Pca2(1)	P-3
A	16.8273(10) Å	14.7806(2) Å
B	6.8169(4) Å	14.7806(2) Å
C	8.6766(5) Å	6.34040(10) Å
A	90	90
B	90	90
Δ	90	120
Volume	995.29(10) Å^3	1199.59(3) Å^3
Z	4	1
Density (calculated)	2.213 Mg/m^3	1.996 Mg/m^3
Absorption coefficient	2.216 mm^{-1}	1.429 mm^{-1}
F(000)	648	714
Crystal size	0.31 x 0.04 x 0.02 mm^3	0.44 x 0.41 x 0.36 mm^3
Theta range for data collection	2.42 to 27.99°	1.59 to 27.99°
Index ranges	-21≤h≤22, -9≤k≤9, -11≤l≤11	-19≤h≤19, -19≤k≤19, -8≤l≤8
Reflections collected	12315	19262
Independent reflections	2399 [R(int) = 0.0914]	1945 [R(int) = 0.0235]
Completeness to theta	100.00%	100.00%
Absorption correction	None	Empirical
Max. and min. Transmission	0.9570 and 0.5467	0.6273 and 0.5721
Refinement method	Full-matrix least-squares on F^2	Full-matrix least-squares on F^2
Data/ restraints/ parameters	2399 / 31 / 145	1945 / 0 / 132
Goodness-of-fit on F2	0.987	1.259
Final R indices [I>2sigma(I)]	R_1 = 0.0381, wR_2 = 0.0525	R_1 = 0.0228, wR_2 = 0.0630
R indices (all data)	R_1 = 0.0673, wR_2 = 0.0586	R_1 = 0.0233, wR_2 = 0.0633
Absolute structure parameter	0.01(4)	
Largest diff. peak and hole	0.674 and -0.648 e.Å^{-3}	0.429d -2.079 e.Å^{-3}

7.3.6 Analysis of the Crystal Structure of catena-[(μ_2-Pyridine-2,3-dicarboxylato-κ^3N,O,O')-triaqua-cadmium(II)] or catena-Poly[[triaquacadmium(II)]-μ-pyridine-2,3-carboxylato-κ^3N,O^2:O^3]

Cd(QUIN), $[Cd(H_2O)_3(C_5H_3NC_2O_4)]_n$, crystallized in the $Pca2_1$ space group with an orthorhombic unit cell, having four molecules in the asymmetric unit. Its structure and numbering scheme can be seen in Figure 7.16. It is a polymeric structure where the ligand binds to two metal centres, each in a different way. There is (i) an N,O bidentate bond to the cadmium(II) ion and (ii) a monodentate bond bridging the ligand to a second cadmium ion which occurs through an oxygen of the *meta* carboxylate group. The metal centre then also coordinates to three water molecules. The ligand is fully deprotonated and the repeating unit of the polymer is an ML species.

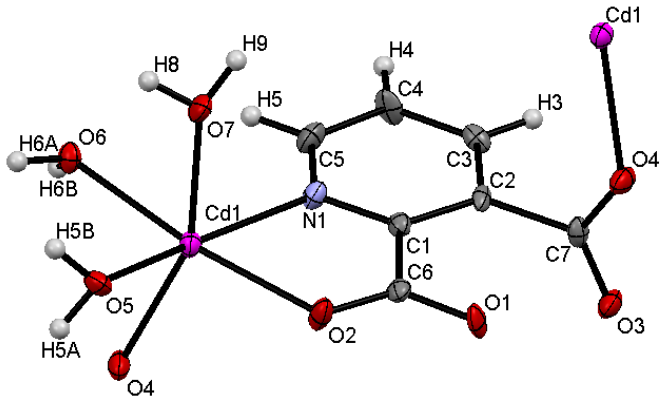


Figure 7.16 The molecular structure of Cd(QUIN) with displacement ellipsoids drawn at the 50% probability level.

The coordination mode of the cadmium centre corresponds to *vi* in Table 7.1, the most common mode of coordination for crystalline cadmium-quinolinic acid complexes. The cadmium(II) ion has a coordination number of six where the metal centre has a distorted octahedral geometry, as shown by Figure 7.17. Selected bond

lengths and angles are given in Table 7.9. The axial ligands are not quite linear, with an O4-Cd1-O7 angle of 156.89 °. There is also distortion in the equatorial plane which is caused by the small N,O bidentate bond angle to the quinolinic acid ligand (72.9(2)°). This coordination is comparable to that of the same crystal structure published in literature, REFCODE GISJUO (73.3(1)°), as well as two other similar cadmium(II)-quinolinic acid structures - PEPXOY (73.00(6)°) (Li *et al.*, 2006b) and TUXLEE (72.27(7)°) (Barszcz *et al.*, 2010). Four other structures having the same coordination mode to cadmium were found to have only slightly smaller N-Cd-O bond angels, with the smallest being 70.02(5) ° (REFCODE: AGUBEK) (Li, Ha, Chang and Yuan, 2008).

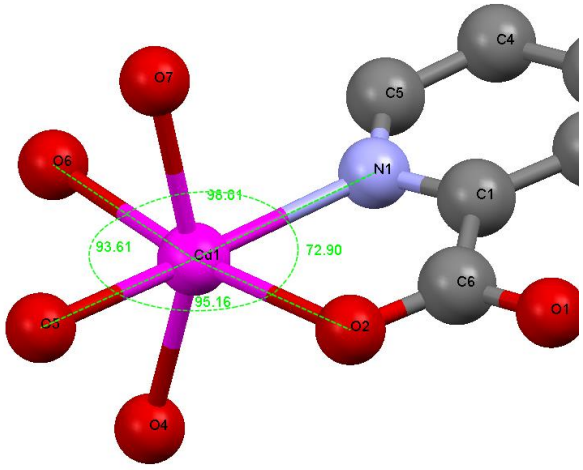


Figure 7.17 Distorted octahedral geometry of the cadmium(II) metal centre in Cd(QUIN).

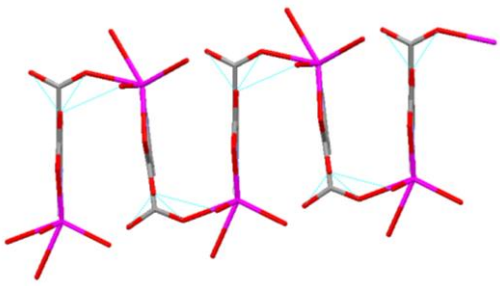
The N1-Cd1 and O2-Cd1 bond lengths are 2.296(5) and 2.260(3) Å, respectively. These bond lengths compare well to those found in similar structures and are almost identical to those in the structure by Aghabozorg *et al*. (2008) (REFCODE: GISJUO). The carboxylate group in the *ortho* position which is coordinated to the cadmium(II) ion, is almost planar with the pyridine ring. Polymerization occurs by the twisting of the *meta*-position carboxylate group which enables this process to occur with

Table 7.9 Selected bond lengths [Å] and angles [°] for Cd(QUIN).

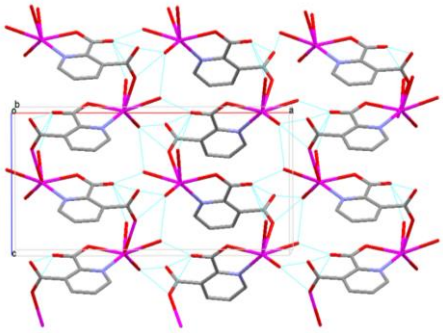
Cd(QUIN)			
N(1)-Cd(1)	2.295(5)	Cd(1)-O(7)-H(8)	117.9
O(2)-Cd(1)	2.260(4)	Cd(1)-O(7)-H(9)	130
O(4)-Cd(1)#1	2.281(4)	O(5)-Cd(1)-O(2)	95.15(14)
O(5)-Cd(1)	2.255(4)	O(5)-Cd(1)-O(7)	80.95(14)
O(6)-Cd(1)	2.385(4)	O(2)-Cd(1)-O(7)	97.79(13)
O(7)-Cd(1)	2.267(4)	O(5)-Cd(1)-O(4)#2	85.40(14)
Cd(1)-O(4)#2	2.281(4)	O(2)-Cd(1)-O(4)#2	101.95(14)
		O(7)-Cd(1)-O(4)#2	156.89(13)
		O(5)-Cd(1)-N(1)	163.62(16)
C(5)-N(1)-Cd(1)	126.8(4)	O(2)-Cd(1)-N(1)	72.92(15)
C(1)-N(1)-Cd(1)	114.7(4)	O(7)-Cd(1)-N(1)	89.43(15)
C(6)-O(2)-Cd(1)	117.6(4)	O(4)#2-Cd(1)-N(1)	107.72(16)
C(7)-O(4)-Cd(1)#1	136.1(4)	O(5)-Cd(1)-O(6)	93.61(14)
Cd(1)-O(5)-H(5A)	118.5	O(2)-Cd(1)-O(6)	170.91(13)
Cd(1)-O(5)-H(5B)	127.9	O(7)-Cd(1)-O(6)	81.18(13)
Cd(1)-O(6)-H(6A)	109.8	O(4)#2-Cd(1)-O(6)	81.17(13)
Cd(1)-O(6)-H(6B)	120.1	N(1)-Cd(1)-O(6)	98.02(15)

#1 and #2 refer to two symmetry related molecules

limited steric hindrance. The polymer is formed by joining the monomeric ML units together in a head-to-tail fashion (Figure 7.18 a)). Looking down the b-axis shows how the head-to-tail chain propagates in the c-direction (Figure 7.18 b)).



a)



b)

Figure 7.18 Polymeric head-to-tail chains a) as viewed down the c-axis and b) down the b-axis. Hydrogen atoms omitted for clarity.

The packing of the structure is created by strong, directional hydrogen bonds forming a zigzag pattern which extends in the b-direction. Identical zigzag layers then lie directly above each other going in the c-direction, as Figure 7.19 illustrates.

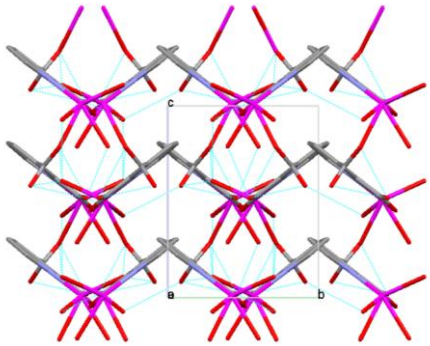


Figure 7.19 View down the a-axis showing a zigzag pattern. Hydrogen atoms omitted for simplicity.

There is extensive hydrogen bonding within this crystal structure due to the presence of the three water molecules bound to the cadmium centre, but numerous shorter contacts also play a role in maintaining the packing of this solid structure. The adjacent polymeric units hydrogen bond to each other via a water molecule and carboxylate oxygen of the *ortho* carboxylate group (Figure 7.20).

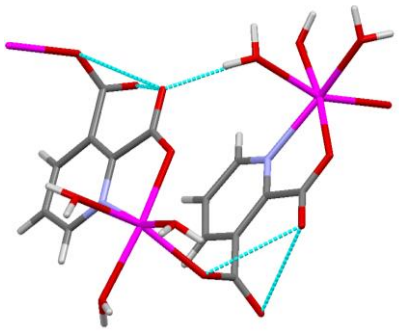


Figure 7.20 Hydrogen bonded monomers forming the polymeric chain.

The *ortho* carboxylate oxygen atom forms intermolecular hydrogen bonds to another ML unit via a water molecule. Between the same two ML units a third hydrogen bond is present between another water molecule and the *meta* carboxylate group. This *meta* carboxylate group then also hydrogen bonds through its other oxygen atom to the third water molecule (Figure7.21).

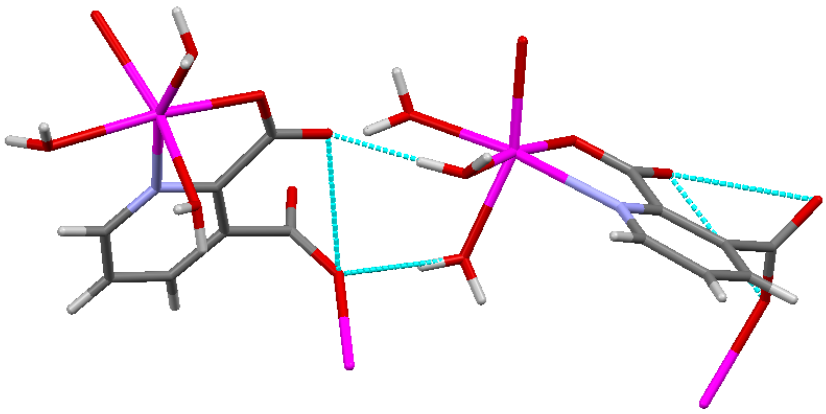


Figure 7.21 Intermolecular hydrogen bonding in Cd(QUIN).

7.3.6.1 A Comparative Study with Literature Structures

Aghabozorg *et al.* (2008) (REFCODE: GISJUO) prepared the same polymeric Cd(QUIN) crystal structure by reacting cadmium(II) nitrate hexahydrate with $(pipzH_2)(QUIN^{2-})$ (where pipz is piperazine) in a 1:2 molar ratio. The anionic piperazine portion of the

ligand was used as a charge transfer agent and it did not feature in the final structure. A comparison of crystal data in Table 7.10 demonstrates that this structure is almost identical to ours.

Table 7.10 Comparison of our ML crystal characteristics with that by Aghabozorg *et al*. (2008).

Characteristic		**This Research**	**Literature (GISJUO) Aghabozorg *et al.* (2008)**
Space group		*Pca*2_1	*Pca*2_1
Unit cell		orthorhombic	orthorhombic
Length (Å)	**a**	16.827(1)	16.820(3)
	b	6.8169(4)	6.808(1)
	c	8.6766(5)	8.666(2)
Cell Volume (Å^3)		995.293	992.267
Z		4	4
R factor (%)		3.81	2.86
Temperature (K)		173	100
Recryst. Solvent		water	water
Recryst. Temp		room temp	room temp

Li *et al.* (2006b) produced a similar compound, catena-((μ3-Pyridine-2,3-dicarboxylato)-diaqua-cadmium), by the hydrothermal reaction of quinolinic acid with cadmium oxide (REFCODE: PEPXOY). In their study a 10 ml solution containing the ligand, cadmium(II) oxide and La_2O_3 were stirred in air and then transferred to a sealed container in which the solution was heated to 120 °C and allowed to react over 3 days. The resulting solution was then slow-cooled at 5 °C/hr to room temperature and colourless crystals then emerged. Structural studies of the complex show a one-dimensional coordination polymer where the quinolinic acid

acts as a bridging ligand. (Interestingly the lanthanum does not crystallize out which may imply that there is a competitive reaction occurring between the cadmium(II) and La(III)). When the La_2O_3 was omitted from their experimental procedure the same structure resulted but its crystallinity was not as good as when it was prepared with the La_2O_3 (Li *et al.*, 2006b)). The cadmium ion is bound to the ligand through a nitrogen atom and an oxygen from the ligands *ortho* carboxylate group, as coordination mode *vi* depicts (when considering the coordination of a single monomer). It further coordinates to two other carboxylate oxygens from two separate ligands, as well as to two water molecules (see Figure 7.22). This arrangement leads to a distorted octahedral geometry, similar to that occurring in our structure.

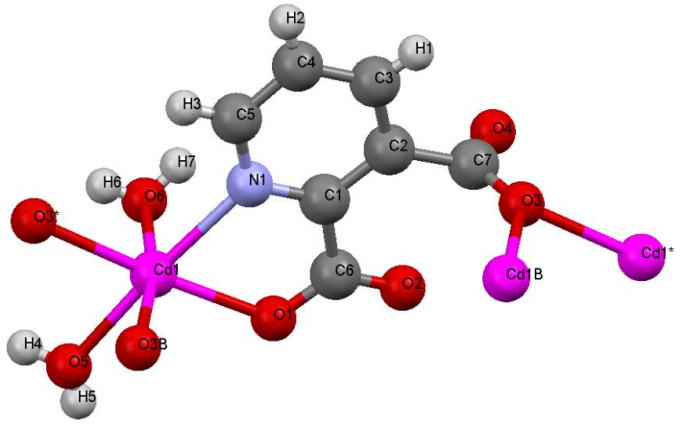


Figure 7.22 Ball and stick representation of catena-((m3-Pyridine-2,3-dicarboxylato)-diaqua-cadmium) (REFCODE: PEPXOY) (Li et al., 2006b).

The coordination mode employed by PEPXOY, GISJUO, our structure and many others reinforce the point that Li *et al.* (2006b) made by stating that quinolinic acid prefers to act more like picolinic acid. All three structures show quinolinic acid acting as a bidentate ligand bonding through the nitrogen of the pyridyl ring and only one of the carboxylate oxygen atoms. Due to polymerisation the next ligand

molecule bonds monodentately to the cadmium atom. All twenty of the CSD literature structures with cadmium and quinolinic acid coordinate via the N,O bidentate mode.

Barszcz *et al.* (2010) published an article where they discuss the protonation of quinolinic acid being dependent on the hydrothermal or non-hydrothermal methods that are used in preparing the complexes and said: "Preparation of metal complexes of 2,3-pydcH_2 by hydrothermal reaction with $Cd(NO_3)_2 \cdot 4H_2O$ or $Mn(NO_3)_2 \cdot 6H_2O$ under basic conditions (NaOH) led to coordination polymers in which the doubly deprotonated dicarboxylate anions acts as tetra-donating and penta-donating ligands" (as illustrated by coordination modes *ix, x, xi, xii, xiii, xv* and *xiv* in Table 7.1). They further this by saying that "An examination of the literature data shows that the coordination ability of pyridine-2,3-dicarboxylic acid towards metal ions depends on the hydrothermal or non-hydrothermal methods used to prepare the complexes."

In their work they describe the synthesis of two different cadmium-quinolinic acid complexes (which are the same structures as we produced – $Cd(QUIN\text{-}H)_3$ and Cd(QUIN), which we will refer to as Complex A and B, respectively. Barszcz *et al.* (2010) report that these complexes were obtained by non-hydrothermal methods where the ligand was doubly deprotonated for complex B and singly protonated for complex A. However, in their description of the synthesis of each of these complexes they clearly state using high temperatures of 80 °C in the preparation of complex A while complex B was prepared at room temperature. They attempted to relate the degree of protonation of the coordinated ligand to the reaction conditions used in preparing the coordination compounds. However, it should be noted that other experimental conditions were not kept constant. In their study both the concentration ratios and the metal counterions were altered. The source of cadmium(II) for complex A was cadmium(II) nitrate tetrahydrate and that for

complex B was cadmium(II) carbonate. The anion in solution may affect the pH; carbonate will increase the pH whereas the nitrate wouldn't alter it significantly. The concentration and concentration ratio could also have an impact on what species would form, as we have illustrated before using species distribution diagrams. Many factors were varied in their experiments, making it difficult to attribute different coordinating abilities or degree of protonation of the ligand to the experimental method alone.

In this work the same crystal of complex B (Cd(QUIN)) was grown a number of times, both with and without heating, as Table 7.7 shows. Also, Aghabozorg *et al*. (2008) produced the same crystal structure without heating. This demonstrates that the N,O-bidentate and O-monodentate (of the *meta* carboxylate group) combination coordination mode can be achieved by using either hydrothermal or non-hydrothermal techniques. Also, it is not expected that the extent of protonation of the ligand be significantly changed by the temperature of the solution. Unfortunately no literature enthalpy values for cadmium(II)-quinolinic acid complexes could be found and so the dependence of complex formation on temperature could not be quantified. Very minimal changes in the magnitudes of protonation constants calculated at various temperatures (using the van't Hoff equation), as found for dipicolinic acid, may indicate the small effect of temperature. However, the formation constants of the metal-ligand complexes were found experimentally to differ at higher temperatures for the cadmium(II)-dipicolinic acid system.

More significantly, the pH of the solution dictates the extent of protonation of the species. The reason that Barszcz *et al.* (2010) found the ligand binding in different ways for complex A and B was due to the degree of protonation of the ligand, which is brought about by the pH of the solution as a direct consequence of using nitrate and carbonate, respectively, as the counterions. (They found the deprotonated

species (Cd(QUIN)) formed when carbonate was used.) A better comparison could have been made by using the same cadmium(II) salt in the preparation of the complexes.

7.3.7 Analysis of the Crystal Structure of Tri(quinolinato-N,O)-cadmium(II)) hexa-aqua-cadmium

$Cd(QUIN\text{-}H)_3$, $[Cd(C_5H_3NC_2O_4H)_3]\cdot[Cd(H_2O)_6]$, crystallized in the trigonal crystal system and P-3 space group, where Z = 1. The cadmium metal is coordinated bidentately to three quinolinic acid ligands (Figure 7.23), each through an oxygen atom of the *ortho* carboxylate group and the nitrogen atom of the pyridine ring. The second carboxylate group on each ligand remains unbound and is protonated. The coordination mode for this particular structure is the only one of its kind so far for this specific metal-ligand system. The geometry around the metal centre is distorted octahedral, having a bite angle (O-Cd-N) of 72.48(5)°. The counter ion in the asymmetric unit is a hexaaqua cadmium(II) ion. Despite the different ligand and counter ion, this structure is similar to the $Cd(PIC\text{-}H)_3$ structure described in Chapter Six and previously published in literature (Billing, Levendis and Vieira, 2011).

The $Cd(H_2O)_6$ ion occupies the special position at (0,0,0), with a three-fold rotation-inversion site symmetry. The unit cell contains two different 3-fold rotation axes – the tri-quinolinate complex occupies the (0.6667, 0.3333, z) and (0.3333, 0.6667, z) special positions. The two tri-quinolinate complexes in the unit cell are related to each other by a centre of inversion (Figure 7.24). The Cd-O distances in the quinolinate complex and the hexaaqua cation are identical (Cd1-O1 is 2.262 (1) Å and Cd2-O5 is 2.260 (1) Å). Charge balance is attained when each tris complex (overall charge of -4) is associated with two hydrated metal centres (each with a +2 charge).

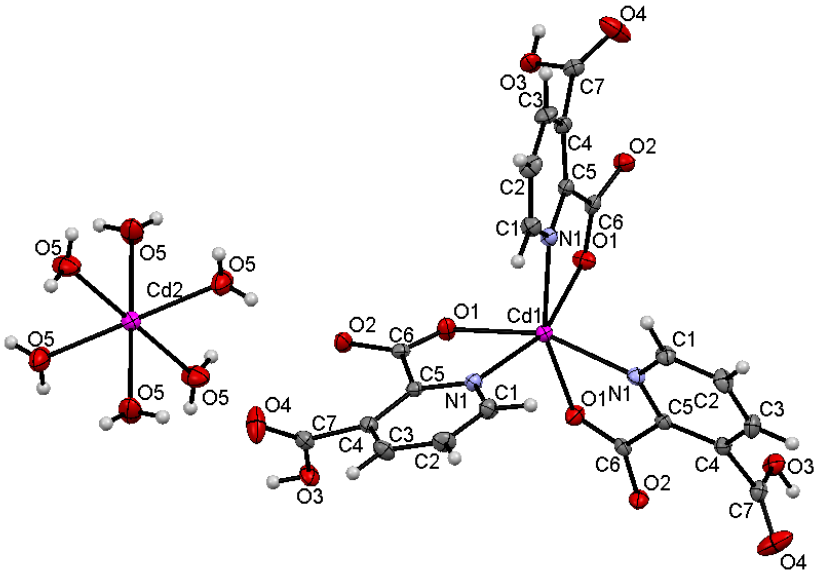


Figure 7.23 ORTEP diagram of the molecular structure of $Cd(QUIN\text{-}H)_3$. Displacement ellipsoids are drawn at the 50% probability level.

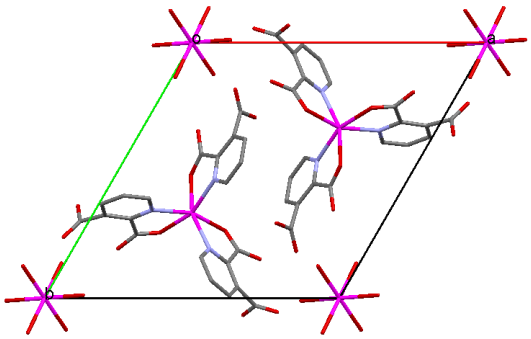


Figure 7.24 The unit cell of $Cd(QUIN\text{-}H)_3$ as viewed down the c-axis.

This complex packs in such a way that when viewed down the *c*-axis (Figure 7.25) it shows channels of the hydrated metal cation that are surrounded by tris complexes in a circular arrangement. This arrangement is maintained by strong hydrogen bonds between the cationic hydrate and pairs of Cd(II)-quinolinate complexes. The hydrated metal centre is hydrogen bonded through a water molecule to an adjacent metal-ligand complex in two ways: i) via the uncomplexed carboxylate oxygen atom

(O5-H5…O4) and ii) via the complexed carboxylate unbound oxygen atom (O5-H6…O2) (see Figure 7.26 a)). The two Cd(II)-quinolinate complexes per unit cell, related by a centre of inversion, are hydrogen bonded by the non-complexing protonated carboxylate oxygen and the adjacent carboxylate oxygen of the coordinating carboxyl group (O3-H4…O2 having a distance of 1.776(2) Å) (see Figure 7.26 b)).

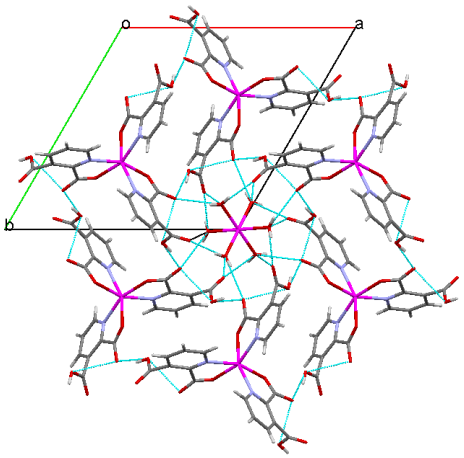
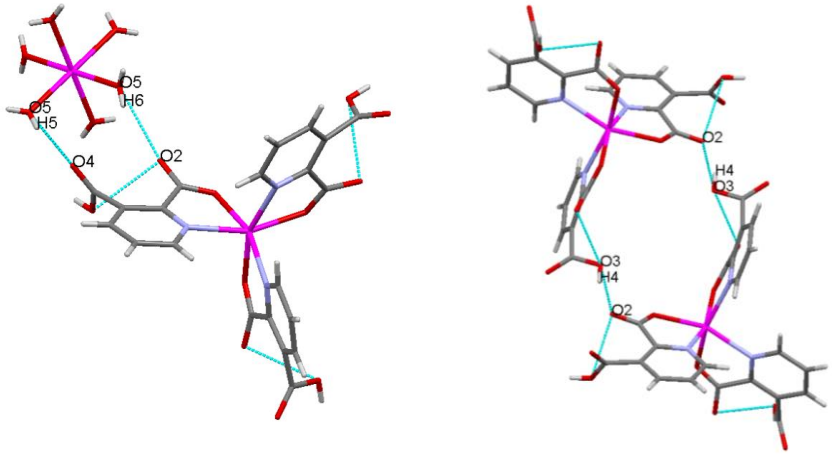


Figure 7.25 Packing diagram of Cd(QUIN-H)$_3$, as seen down the c-axis showing the hydrate down the channels of the hydrogen bonded cadmium complexes.



a) b)

Figure 7.26 Diagram highlighting the hydrogen bonding shown in Figure 7.25. Hydrogen bonding between a) the hydrate and the tris complex ($Cd(QUIN\text{-}H)_3$) and b) two adjacent $Cd(QUIN\text{-}H)_3$ complexes.

Table 7.11 Selected bond lengths [Å] and angles [°] for $Cd(QUIN\text{-}H)_3$.

$Cd(QUIN\text{-}H)_3$	
Cd(1)-O(1)#1	2.2621(13)
Cd(1)-O(1)#2	2.2621(13)
Cd(1)-N(1)#1	2.3371(15)
Cd(1)-N(1)#2	2.3371(15)
Cd(2)-O(5)	2.2600(16)
O(1)#1-Cd(1)-O(1)	93.03(5)
O(1)-Cd(1)-N(1)#1	159.39(5)
O(1)#1-Cd(1)-N(1)	102.10(5)
O(1)-Cd(1)-N(1)	72.48(5)
N(1)#1-Cd(1)-N(1)	95.81(5)
O(5)#5-Cd(2)-O(5)#7	84.81(7)
O(5)#5-Cd(2)-O(5)	95.19(7)
O(5)#7-Cd(2)-O(5)	180.00(9)

#1 and #2 refer to two symmetry related molecules

7.3.7.1 A Comparative Study with Literature Structures

A search of the CSD (Allen, 2002) produced only five hits of transition metal tris-quinolinate complexes, which were of manganese (HAZSIK), cadmium (TUXLEE) and three of zinc (WABJUG, IRADAH and LEHCEI). The counterions in the structures of IRADAH and LEHCEI are organic cations and are therefore not comparable to Cd(Quin-H)$_3$. During the course of our research the structure of Cd(QUIN-H)$_3$ was published as TUXLEE (REFCODE) by Barszcz *et al.* (2010). In the CSD this is the only Cd(II)-quinolinic acid structure where the ligand is protonated.

We have identified two structures in literature that are isomorphous to our Cd(QUIN-H)$_3$ structure - meaning they contain different molecules but have the same space group and unit cell (HAZSIK and WABJUG). Complex II of Billing, Levendis and Vieira (2011) (which is Cd(Pic-H)$_3$, reported in this work), also crystallises in the trigonal space group P-3 with similar unit cell parameters, even though the ligand is picolinic acid and the counterion is NO_3^-). All four structures can be described as M(LH)$_3$ complexes and are compared in Table 7.12.

The unit cell volume of HAZSIK and WABJUG are very similar to that of our Cd(QUIN-H)$_3$ complex. The ionic radii of Cd(II), Mn(II) and Zn(II) is 1.48 Å, 1.39 Å and 1.31Å (Brown, LeMay and Bursten, 2000) respectively, which would explain the trend of the decreasing cell volumes for the three quinolinic acid complexes. HAZSIK (Goher, Youssef, Zhou and Mak, 1993) has identical hydrogen bond patterns to our structure, the only difference is the shift in origin (Figure 7.27). Hydrogen bonding occurs between the hydrate and the tris complex, and also between the hydrogen atoms of two tris complexes. The respective hydrogen bond distances are 2.877 Å (O9-H8…O8B) and 2.597 Å (O2…H12-O7) for the manganese structure and similarly 2.812 Å and 2.582Å for our structure.

Table 7.12 Comparison of Cd(QUIN-H)$_3$ with two isomorphous structures and a similar picolinate complex (Cd(Pic-H)$_3$).

Characteristic	**Cd(Quin-H)$_3$** This work	**Mn(Quin-H)$_3$** (Goher, Youssef, Zhou and Mak, 1993)	**Zn(Quin-H)$_3$** (Gharagozlou, Langer and Nemati, 2010)	**Cd(Pic-H)$_3$** (Billing, Levendis and Vieira, 2011)
REFCODE	(like TUXLEE)	HAZSIK	WABJUG	-
a (Å)	14.7806(2)	14.633 (3)	14.470(4)	14.0290(5)
b (Å)	14.7806(2)	14.633 (3)	14.470(4)	14.0290(5)
c (Å)	6.34040(10)	6.349 (2)	6.284(2)	5.6564(2)
α	90	90	90	90
β	90	90	90	90
γ	120	120	120	120
Volume (Å^3)	1199.59	1177.3	1139.473	964.10(6)
Space group	P-3	P3	P-3	P-3
Unit cell	Trigonal	Trigonal	Trigonal	Trigonal

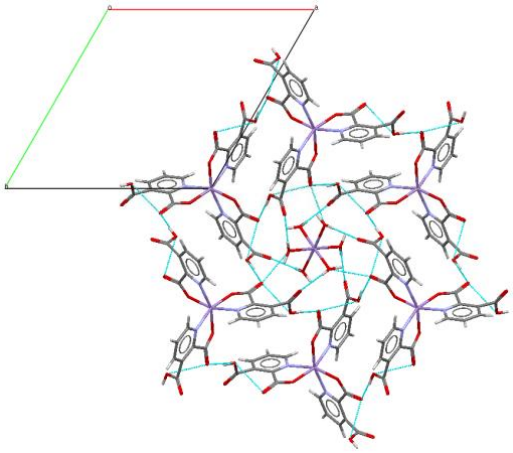


Figure 7.27 Packing diagram as seen down the *c*-axis showing the hydrate down the channels of the hydrogen bonded manganese complexes (REFCODE: HAZSIK).

The structure by Billing, Levendis and Vieira (2011) is also a cadmium complex but the coordinating ligand is picolinic acid. The Cd – O bond distance (2.321(2) Å) and Cd – N bond distance (2.295(2) Å) are both comparable to the values within our tri-quinolinate complex (2.262(1) Å and 2.337(2) Å respectively). This shows that the *meta* carboxylate group does not significantly affect the molecular structure. The hydrogen bond pattern differs slightly as there are no hydrogen bonds to the hydrate (only shorter contacts) because of the absence of a second carboxylate group (Figure 7.28).

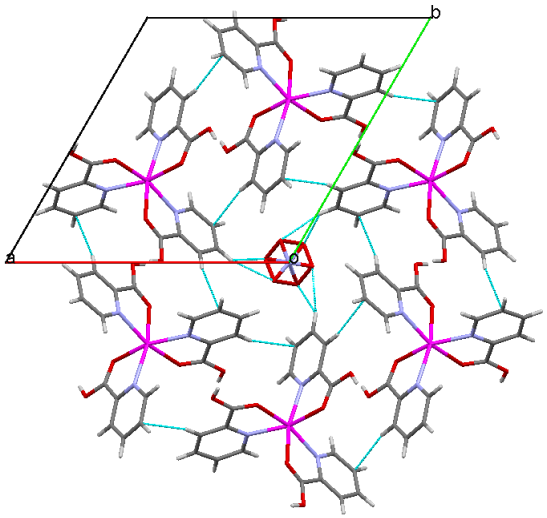


Figure 7.28 Packing diagram of $Cd(Pic\text{-}H)_3$ as seen down the c-axis showing the disordered nitrate ions down the channels of the hydrogen bonded cadmium complexes (Billing, Levendis and Vieira, 2011).

Goher, Youssef, Zhou and Mak (1993) compare $Mn\text{-}N_{pyridyl}$ bond lengths found in their Mn(II)-triquinolinate structure (HAZSIK) with a Mn(III)-tripicolinate structure (PYCXMN) (Figgis, Raston, Sharma and White, 1978) and found that the $Mn\text{-}N_{pyridyl}$ distances were shorter in the picolinate structure than in the quinolinate structure. This phenomenon may be due to the difference in oxidation states of the

manganese, as we do not see the same trend when comparing Cd(II)-triquinolinate with Cd(II)-tripicolinate Cd-$N_{pyridyl}$ bond lengths.

7.3.8 Analysis of the Crystal Structure of Pyridine-2,3-dicarboxylic Acid

Crystallization experiments yielded crystals of the pure ligand, pyridine-2,3-dicarboxylic acid, which had been previously published by Kvick, Koetzle, Thomas and Takusagawa (1974). Analysis of the crystals using SCXRD produced a matching unit cell and space group which was sufficient proof that the doubly protonated form of quinolinic acid had been crystallized. The ligand was found to crystallize in its zwitterionic form, having a structure depicted by Figure 7.29. The one hydrogen atom is shared between the two carboxylate groups while the other remains bound to the pyridyl nitrogen (Kvick, Koetzle, Thomas and Takusagawa, 1974). No further analysis is given here.

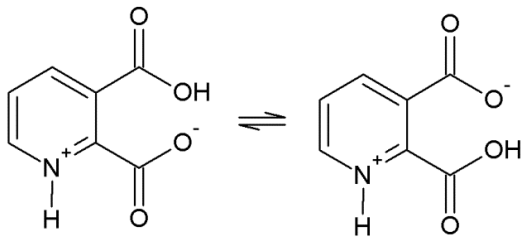


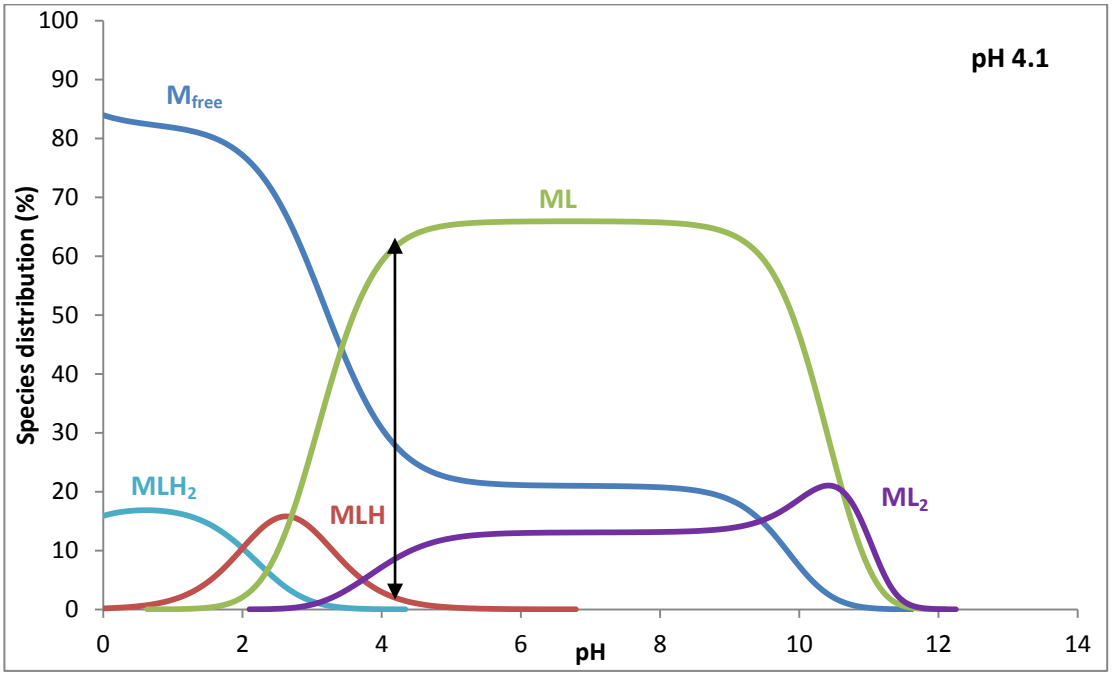
Figure 7.29 Tautomeric diagram illustrating the structure of the doubly protonated quinolinic acid crystals.

7.4 RELATING SOLUTION SPECIES TO CRYSTALLINE COMPLEXES

Species found in solution experiments were re-evaluated by considering the crystalline metal-ligand complexes that were successfully grown and analysed. We found the ML species to exist in solution, as did Yasuda and Yamasaki (1958). Does the pH at which the crystals formed relate to that which a SDD predicts when

plotted using the conditions of the experiment for crystal growth? This can be answered in relation to two different experiments where crystals were formed - pH 4.1 and 2.61 (refer to Table 7.7 for a summary of the experimental details). SDDs plotted using the conditions for each of these two experiments are given in Figure 7.30 a) and b). In each case the final set of formation constants, where the third protonation constant (log K_3 = –0.8) and the MLH_2 species was included, was used. At pH 4.1 the SDD shows that the ML species is the dominant species in solution under the corresponding conditions used for crystal growth. According to the SDD in Figure 7.30 b) the MLH and ML species are both present at pH 2.61 under the corresponding conditions. Perhaps if more crystallites from this specific batch were examined a MLH species may too have been identified. A PXRD pattern may also have been useful for this same reason.

a)



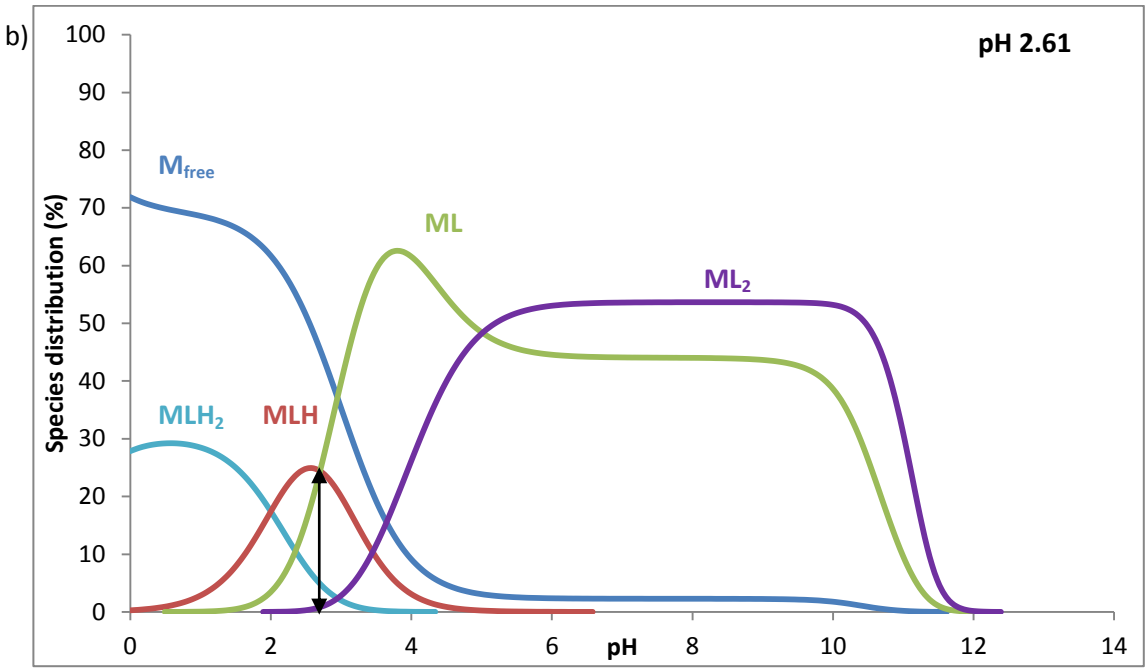
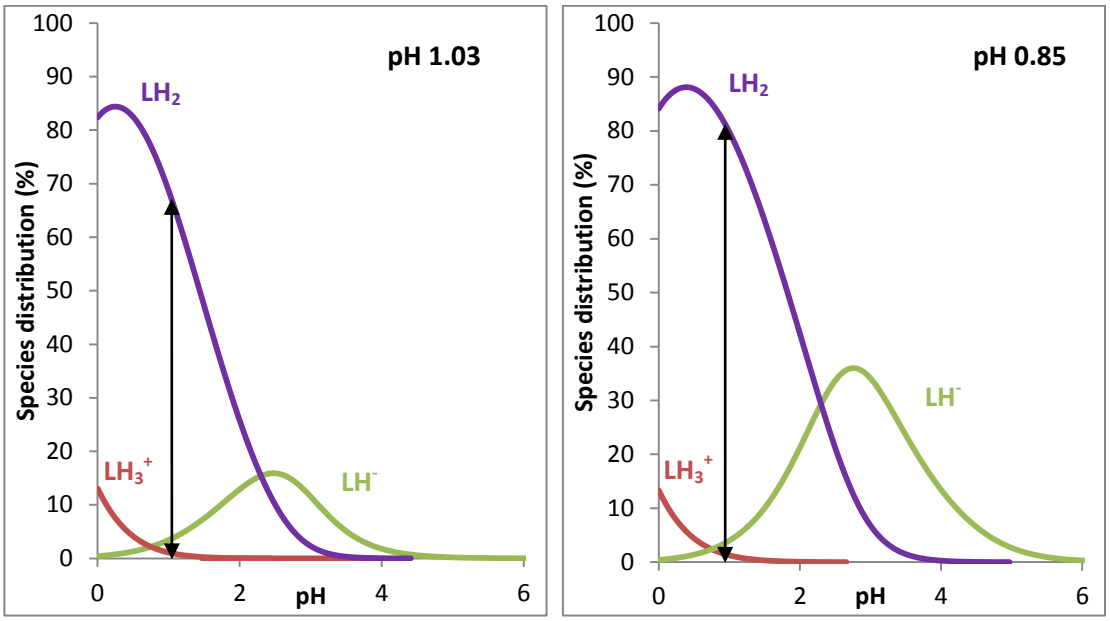


Figure 7.30 SDDs plotted under solution conditions from which crystals of the ML complex was formed: a) a [L]:[M] of 1, where [Cd] = 0.005 M and b) a [L]:[M] of 2:1, where [Cd] = 0.005 M. The pH of the solution is also indicated. (Log $\beta(MLH_2)$ = 8.6, log β(MLH) = 6.6, log β(ML) = 3.9 and log $\beta(ML_2)$ = 6.6 when log K_3 = -0.8.)

Plotting a SDD using the conditions from an experimental liquor that produced QUIN-H_2 crystals shows that the doubly protonated quinolinic acid is the predominant form of the ligand in solution (Figure 7.31 a)). At pH 1.03, the pH at which these ligand crystals were harvested, correlates to that predicted by the SDD (Figure 7.31a)). Also, these crystals were formed in a single day and so the solution concentration would not have changed to a large extent due to evaporation. The QUIN-H_2 crystals were formed from several solutions prepared at different conditions. Again using the final formation constants a SDD was plotted using the liquor conditions of a different experiment and only the uncomplexed form of the ligand is shown. A direct correlation was found between the pH value at which the crystals were harvested and where this species exists in solution (Figure 7.31 b)).



a) b)

Figure 7.31 Partial SDD showing the different protonated forms of ligand available in solution using under the following conditions: a) [L]:[M] = 1 where [Cd] = 0.1 M and b) where [L]:[M] = 2 and [Cd] = 0.05 M.

The formation of the $M(LH)_3$ crystal structure was unexpected as this species has, to our knowledge, not previously been observed in solution. The crystallization of this species suggests that it may also exist as a minor species in solution. It was thus investigated to see if this $M(LH)_3$ species could be incorporated when calculating formation constants. Initially this species together with ML and ML_2 only, was considered for each of the four [L]:[M] ratio experiments. Formation constants could be refined for all species and the $M(LH)_3$ species affected the CCFC to a small extent at low pH, as anticipated. The correlating ECFC/CCFC plots for each experiment are shown in Figure 7.32, which clearly indicates that this species model is still incomplete, especially for the higher [L]:[M] ratios. For these plots the log β for $M(LH)_3$ was 21.2 $\pm$ 0.7. This value may be an overestimation as the CCFC lies above the ECFC in the pH region where this species affected the data.

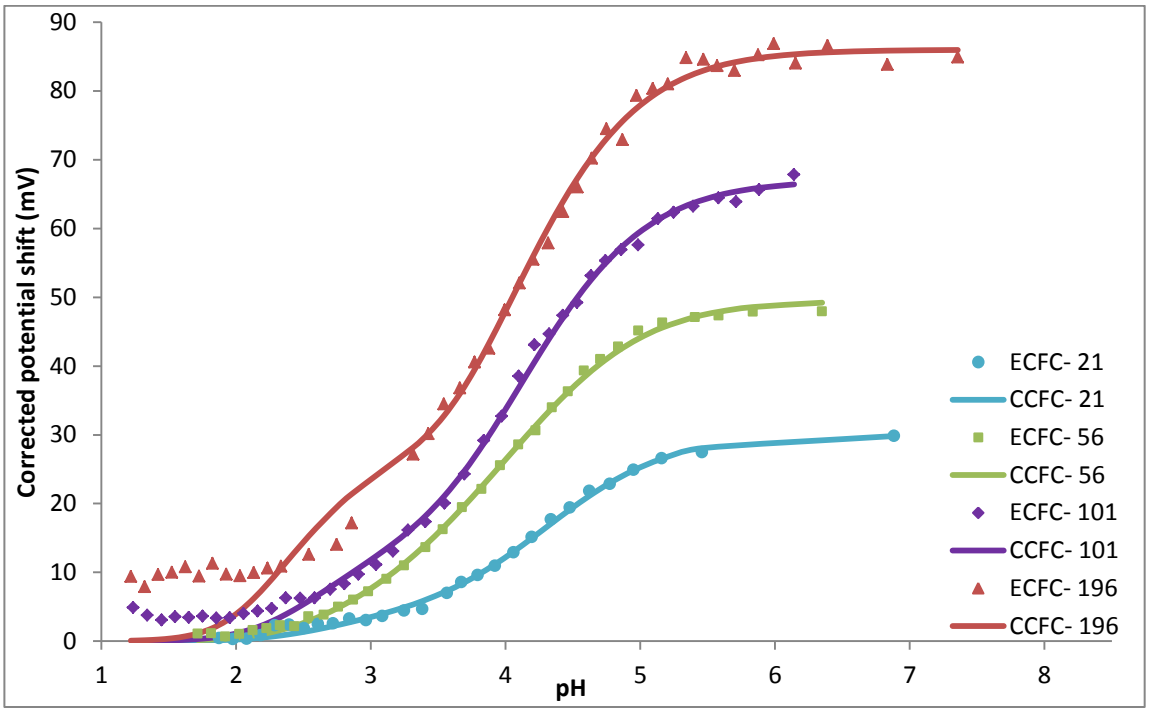


Figure 7.32 ECFC and CCFC calculated using the $M(LH)_3$, ML and ML_2 complex for each [L]:[M] ratio for the cadmium(II)-quinolinate system.

For interest, a SDD was plotted using the conditions of a crystal experiment where the $M(LH)_3$ complex was found, together with the average log *β* value determined. At pH 1.2 the $M(LH)_3$ complex is shown to be dominant under these conditions, however, for a SDD plotted using the conditions of a polarographic experiment ([L]:[M] = 20 and [Cd] = 1 x 10^{-4} M for example), the distribution of the $M(LH)_3$ species decreases substantially (Figure 7.33). This explains why incorporating it into the CCFC did not make a considerable improvement on the fit. It seems that the presence of this complex in the crystal form is driven by the higher concentrations of the solution. From Figure 7.30 it can be seen that MLH exists in the same pH region as in which the $M(LH)_3$ species was predicted.

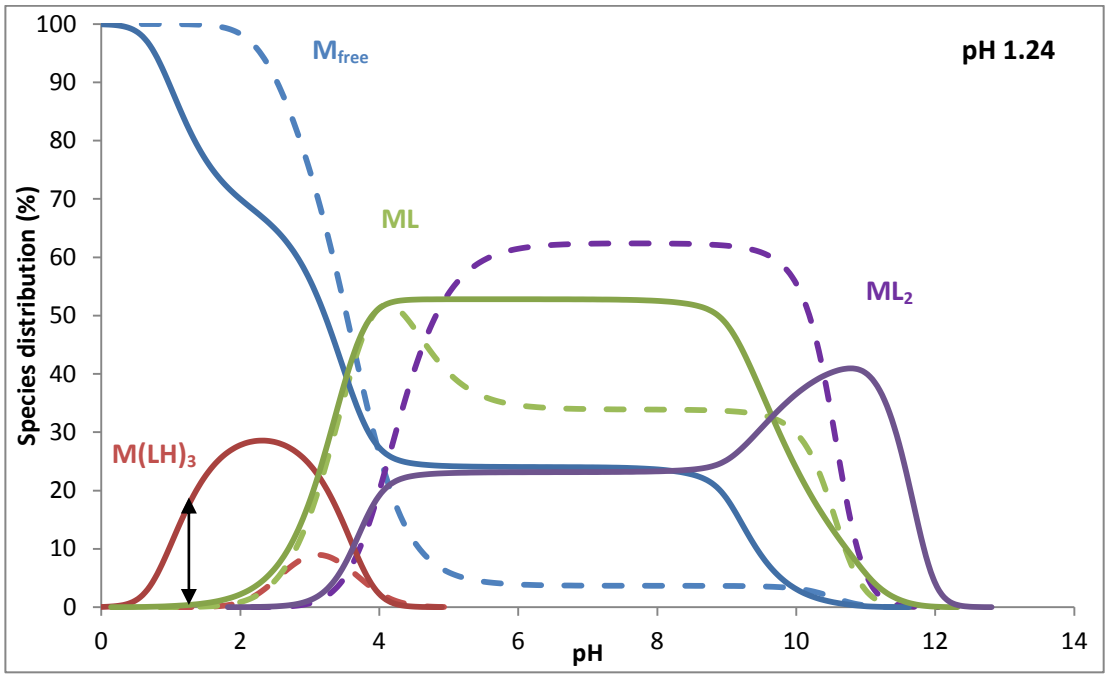


Figure 7.33 Comparison of SDDs plotted at an [L]:[M] of 1 where [Cd] = 0.05 M (solid lines) and at an [L]:[M] of 20 where [Cd] = 1 x 10^{-4} M (dashed lines), using average formation constants of log $\beta(M(LH)_3)$ = 21.2, log $\beta(ML)$ = 3.7 and log $\beta(ML_2)$ = 6.7.

An attempt was made to calculate formation constants by including the $M(LH)_3$ species in the model with the MLH_2, MLH, ML and ML_2 species, but the data could not be refined, indicating that if the $M(LH)_3$ species was present in solution under those conditions, it was at very low concentrations. It is not completely surprising that MLH predominates in solution while $M(LH)_3$ is more stable in the solid state since different concentrations and [L]:[M] ratios were used in solution and solid state experiments.

7.5 CONCLUSIONS

This research shows that there is a link between solution species and crystalline complexes for the ML and QUIN-H_2 species. However, with the $M(LH)_3$ complex the link is more tenuous since minor species in solution could be major species in the liquors for crystal growth, and vice versa. The species distribution diagrams corroborate this point. There definitely seems to be a direct correlation between the extent of protonation of the ligand in the complex in solution and in crystal form.

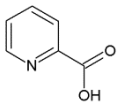
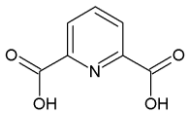
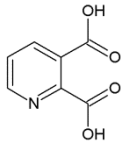
The QUIN-H_2 complex readily crystallized from solutions of pHs below approximately 1.3. This shows why there are so few crystalline complexes (or coordination modes) for this ligand when it is doubly protonated as it prefers to remain uncomplexed at low pH. When there is sufficient singly protonated ligand in solution the extent of complexation increases, and again this is indicated by the number of coordination modes found for singly protonated quinolinic acid.

The final solution species model and respective formation constants, as log β values, for the cadmium-quinolinic acid system, at 25 °C and ionic strength of 0.5 - 0.25 M, are as follows: $MLH_2 = 8.6 \pm 0.5$, $MLH = 6.6 \pm 0.2$, $ML = 3.9 \pm 0.1$ and $ML_2 = 6.6 \pm 0.3$. Having studied this work from low pH values (approximately pH 1) the previously undetected species of MLH_2 and MLH could be identified. The fact that a protonated species ($M(LH)_3$) was crystallized at low pH supports the inclusion of protonated species in solution. This $M(LH)_3$ species may very well be present in solution, but as a minor species under these specific conditions. Considering the third protonation constant for this work was important since complexes were formed at such low pH. The problem with working in the low pH region is that protonation constants are generally not very accurate, however, in this case using log K_3 values between -0.8 and $+0.8$ did not affect the results significantly.

When comparing the coordination modes and formation constants of quinolinic acid with dipicolinic acid (an isomer) (Table 7.13) it becomes clear how the actual structure of the ligand affects the manner in which it complexes to a metal ion. Dipicolinic acid forms stronger bonds than quinolinic acid due to the tridentate and bidentate (if protonated) nature it adopts when binding to a metal ion. The cadmium(II)-quinolinic acid system more easily forms polymers because the *meta* carboxylate group on the ligand is not in a position which allows for a tridentate N, O, O' bond to form. In fact, the formation constants of quinolinic acid are more similar to those of picolinic acid for the MLH, ML and ML_2 species (see Table 7.13) which points to a similar mode of coordination.

One could speculate on a coordination mode for the MLH_2 species with quinolinic acid based on what was observed for the MLH complex that was formed with picolinic acid. The envisaged MLH_2 complex is illustrated in Figure 7.34. The tautomeric diagram (Figure 7.29) supports the coordination mode which was suggested because it shows that the hydrogen bonded to the pyridyl nitrogen is fixed. The carboxylate's proton is shared and therefore moves between the two

Table 7.13 Comparison of the formation constants of picolinic acid, dipicolinic acid and quinolinic acid at 25 °C and ionic strength 0.5 – 0.25 M.

Species	**Picolinic Acid** 	**Dipicolinic Acid** 	**Quinolinic Acid** 
MLH_2	-	-	8.6 ± 0.5
MLH	6.27 ± 0.07	8.4 ± 0.2	6.6 ± 0.2
ML	4.23 ± 0.01	6.61 ± 0.08	3.9 ± 0.1
ML_2	7.81 ± 0.09	11.14 ± 0.08	6.6 ± 0.3
ML_3	10.53 ± 0.08	13.4 ± 0.5	-

carboxylate groups, thereby making it easier for a competing metal ion to occupy one of these sites before the proton reattaches itself to a carboxylate group.

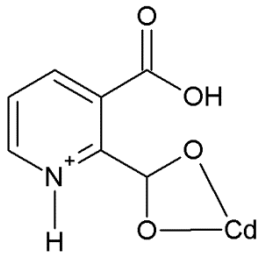


Figure 7.34 Suggested coordination mode for a MLH_2 crystal complex.

From Table 7.13 it is also noted that a ML_3 species was not identified in the case of cadmium(II)-quinolinic acid, whereas it was found for the picolinic and dipicolinic acid systems. If the dipicolinic acid ligand was able to form this complex by binding tridentately to the cadmium(II) ion then sterically this species should be able to form with quinolinic acid too. The formation of this species with the picolinic acid ligand also proves that the bidentate bond which would be produced with the quinolinic acid would be sufficiently strong for the complex to exist. It can therefore be speculated that this species may not have been identified in solution simply because the experimental data that were obtained was only analysed up to an average pH of about 6.4, whereas for the dipicolinic acid system data were analysed up until pH 7.8 (at least). According to the slope analysis and predicted calculated slopes this suggestion seems viable. Another possibility is the likelihood that the *meta* carboxylate group, which would be deprotonated at this higher pH, could interact with other solution species resulting in polymeric species rather than forming the ML_3 species.

7.6 REFERENCES

Aghabozorg, H., Motyeian, E., Khadivi, R., Ghadermazic, M. and Manteghi, F., 2008. catena-Poly[[triaquacadmium(II)]-μ-pyridine-2,3-dicarboxylato-$\kappa^3N,O^2:O^3$]. *Acta Crystallographica,* E64**,** pp m320-m321.

Allen, F. H., 2002. Acta Crystallographica, B58, pp 380-388. Cambridge Structural Database. Version 5.31, November 2008 update.

Barszcz, B., Hodorowicz, M., Jabłońska-Wawrzycka, A., Masternak, J., Nitek, W. and Stadnicka, K., 2010. Comparative study on Cd(II) and Ca(II) model complexes with pyridine-2,3-dicarboxylic acid: Synthesis, crystal structure and spectroscopic investigation. *Polyhedron,* 29 (4)**,** pp 1191-1200.

Billing, C., Levendis, D. C. and Vieira, V. L., 2011. The crystal structures of two novel cadmium-picolinic acid complexes in relation to the solution species. *South African Journal of Chemistry,* 64**,** pp 38-41.

Brown, T. L., LeMay, H. E. and Bursten, B. E., 2000. *Chemistry: The Central Science,* New Jersey, Prentice Hall.

Bruker, S. a. S., 1999. Ver. 6.02 (including XPREP) ed. Madison, WI, USA.: Bruker AXS Inc.

Chiacchierini, E., D'Ascenzo, G. and De Angelis, G., 1976. *Gazzetta Chimica Italiana,* 106**,** pp 19.

Chiacchierini, E., d'Ascenzo, G., de Angelis, G., Magri, A. L. and Petrone, V., 1977. *Annali di Chimica (Rome),* 67**,** pp.

Crans, D. C., Yang, L., Jakusch, T. and Kiss, T., 2000. Aqueous chemistry of ammonium (dipicolinato)oxovanadate(V): the first organic vanadium(V) insulin-mimetic compound. *Inorganic Chemistry,* 39 (20)**,** pp 4409-4416.

Faucherre, J., Petitfaux, C. and Charlier, B., 1967. *Bulletin de la Societe Chimique de France***,** pp 1091.

Figgis, B., Raston, C., Sharma, R. and White, A., 1978. Crystal structure of Tris (pyridine-2-carboxylato) manganese(III) monohydrate. *Australian Journal of Chemistry,* 31 (11)**,** pp 2545-2548.

Funahashi, S., Haraguchi, K. and Tanaka, M., 1977. Reactions of hydrogen peroxide with metal complexes. 2. Kinetic studies on the peroxo complex formation of

nitrilotriacetatodioxovanadate (V) and dioxo (2,6-pyridinedicarboxylato) vanadate (V). *Inorganic Chemistry,* 16 (6)**,** pp 1349-1353.

Gharagozlou, M., Langer, V. and Nemati, A., 2010. Hexaaquazinc(II) bis[tris (3-carboxypyridine-2-carboxylato)zincate(II)]. Acta Crystallographica Section E: Structure Reports Online, 66 (12), pp m1606-m1607.

Goher, M. A. S., Youssef, A. A., Zhou, Z.-Y. and Mak, T. C. W., 1993. Synthesis and characterization of some metal(II) complexes of quinolinic acid (H_2-Quin) and X-ray crystal structures of $[Ni(H\text{-}Quin)_2(H_2O)_2]$ and $[Mn(H_2O)_6][Mn(H\text{-}Quin)_3]_2$. *Polyhedron,* 12 (15)**,** pp 1871-1878.

Grant, R. S., Coggan, S. E. and Smythe, G. A., 2009. The Physiological Action of Picolinic Acid in the Human Brain. *International Journal of Tryptophan Research,* 2**,** pp 71.

Kvick, Å., Koetzle, T. F., Thomas, R. and Takusagawa, F., 1974. Hydrogen bond studies. 85. A very short, asymmetrical, intramolecular hydrogen bond: A neutron diffraction study of pyridine-2, 3-dicarboxylic acid (CHNO). *The Journal of Chemical Physics,* 60**,** pp 3866.

Li, M., Ha, W., Chang, L. and Yuan, L., 2008. catena-Poly [[[aqua(1,10-phenanthroline-κ^2N,N')cadmium(II)]-μ-pyridine-2,3-dicarboxylato-$\kappa^4N,O^2:O^3,O^{3'}$] dihydrate]. *Acta Crystallographica Section E: Structure Reports Online,* 64 (12)**,** pp m1554-m1555.

Li, M., Xiang, J., Yaun, L., Wu, S., Chen, S. and Sun, J., 2006a. Syntheses, Structures and Photoluminescence of Three Novel Coordination Polymers Constructed from Dimeric d Metal Units. *Crystal Growth and Design,* 6 (9)**,** pp 2036-2040.

Li, M., Xiang, J., Yuan, L., Wu, S., Chen, S. and Sun, J., 2006b. Syntheses, Structures, and Photoluminescence of Three Novel Coordination Polymers Constructed from Dimeric d^{10} Metal Units. *Crystal Growth and Design,* 6 (9)**,** pp 2036-2040.

Martell, A. E., Smith, R. M. and Motekaitis, R. J., 2004. NIST Standard Reference Database 46. 8.0 ed. Gaithersburg, USA: U.S Department of Commerce, National Institute of Standards and Technology.

Mawatari, K., Oshida, K., Iinuma, F. and Watanabe, M., 1995. Determination of quinolinic acid in human urine by liquid chromatography with fluorimetric detection. *Analytica Chimica Acta,* 302**,** pp 179-183.

Myint, A. M., 2012. Kynurenines: from the perspective of major psychiatric disorders. *The Federation of European Biochemical Societies Journal,* 279 (8)**,** pp 1375-1385.

Ooi, G. and Magee, R., 1970. Studies on some monomethyl esters of pyridine dicarboxylic acids. *Journal of Inorganic and Nuclear Chemistry,* 32 (10)**,** pp 3315-3320.

Powell, K. and Pettit, L., 1997. IUPAC Stability Constants Database. *Academic Software, Otley (UK).*

Valle, M., Price, R. W., Nilsson, A., Heyes, M. and Verotta, D., 2004. CSF quinolinic acid levels are determined by local HIV infection: cross-sectional analysis and modelling of dynamics following antiretroviral therapy. *Brain,* 127 (5)**,** pp 1047-1060.

Yasuda, M. and Yamasaki, K., 1958. Stabilities of chelates of quinolinic and lutidinic acids with bivalent metals. *Naturwissenschaften,* 45 (4)**,** pp 84-84.

Yen, C.-H., Chen, C.-Y. and Shiu, K.-B., 2007. Hydrothermal Synthesis and X-Ray Structural Characterization of Manganese, Nickel, and Cadmium Coordination Polymers Containing 2,3-Pyridinedicarboxylate as Multidentate Ligands. *Journal of the Chinese Chemical Society,* 54**,** pp 903-910.

Chapter Eight

Bismuth(III)-Quinolinic Acid Crystalline Complexes

8.1 INTRODUCTION

"Although it has been used for centuries, bismuth remains one of the least understood elements in the periodic table."

(Yang and Sun, 2011)

The introductory chapter (Chapter One) gave a short description of the uses of bismuth(III) in medicine, but this is not the only field where it is valuable and indispensable. This ion is used in pigments, pearlescent cosmetics, ammunition, alloys and solders (Yang and Sun, 2011). Due to its low toxicity to both humans and the environment its usage has increased tremendously, mostly replacing the more harmful element lead in solders used in food processing equipment, valves in systems for potable water, fishing sinkers and even in some ammunition.

Even though this element has a wide variety of uses its chemistry has not been well documented. Separate CSD searches (Allen, 2002) of any crystal structure containing bismuth, cadmium, zinc or copper were done using the 2008 version 5.3 CSD database as an indication of the amount of research that has been conducted on bismuth, in comparison to the other metals. The same searches were repeated again in 2012 (Allen, 2002) which showed the same trend. Table 8.1 shows the actual number of crystal structures containing these ions, as well as the results of calculating the percentage increase in the number of structures containing each metal ion over the four year period. These percentages are largely on par for each

ion which shows that interest in complexation of bismuth has definitely grown in the last few years.

Table 8.1 Comparison of number of crystal structures for various metal ions.

Metal Ion	2008	2012	Percentage Increase
Bismuth	1 804	2 257	20
Cadmium	6 557	9 642	32
Zinc	14 424	20 301	29
Copper	35 867	45 887	22

We have previously introduced quinolinic acid (in Chapter Seven) and looked at its properties and possible applications. Studying complex formation of this metal-ligand system may produce some information on the interaction of bismuth(III) used in medical treatments with quinolinic acid which is produced in the human body. In Chapter Seven the possible coordination modes of quinolinic acid were considered, of which there were many. Remarkably, a search of the CSD (Allen, 2002) showed that there have been no published structures where quinolinic acid is bonded to bismuth. This is most likely due to the complexity of preparing a solution at a low enough pH where bismuth(III) does not precipitate out of solution and where it does not preferentially bind to another ligand, such as hydroxide or other anions such as nitrate, chloride or perchlorate. According to Andrews *et al.* (2006) crystal structure determinations of bismuth carboxylates are rare due to their general insolubility and their tendency to undergo slow hydrolysis. Summers, Abboud, Farrah and Palenik (1994) produced bismuth(III) crystal complexes with EDTA (ethylenediaminetetraacetic acid) and NTA (nitrilotriacetic acid), using bismuth subcarbonate ($Bi_2O_2CO_3$) as their bismuth(III) source. They found that this metal ion source was not suitable for forming metal-ligand complexes when the ligand is weakly acidic "such as picolinic acid or dipicolinic acid", having a pK_a of approximately 5. The first pK_a (deprotonation constant) of quinolinic acid lies

between that of picolinic acid and dipicolinic acid, which may be a further indication as to why there are no reported structures of this ligand with bismuth.

Billing (2012) conducted solution studies on the bismuth(III)-quinolinic acid system at 25 °C and ionic strength ranging from 0.5 to 0.25 M, using the same polarographic experimental technique for data collection that has been described in this thesis. However, the procedure that was used for analyzing these data was somewhat different for two specific reasons: firstly because the bismuth(III) ion undergoes hydrolysis at low pH and secondly due to complex formation between bismuth(III) and the nitrates present at high concentrations in the background solution.

Hydrolysis is the splitting of water, and in this case we are referring to the reaction of hydrated bismuth(III) with water to liberate protons and produce oxy or hydroxy complexes in solution, some of which are insoluble. For example, the first step in the hydrolysis of metal ion M that is coordinated by *n* waters would be:

$$M(H_2O)_n \rightleftharpoons M(OH)(H_2O)_{n-1} + H^+$$

The species that are formed are governed by the hardness of the metallic cation, its size and charge (Mesmer and Baes, 1990), as well as its concentration in solution. The charge, size and hardness of the ion affect its ability to hold onto the sphere of hydrated water which surrounds it in solution. Since bismuth(III) readily hydrolyses and precipitates at low pH, its concentration was kept as low as possible in the polarographic pH titrations to delay precipitation to the higher the pH and also to reduce the likelihood of forming polynuclear species.

Over the past one hundred years hydrolysis of bismuth has been a topic of interest and many authors have published a range of different species that they have found to be in solution. A review by Granér and Sillén (1947) explains that initially (in 1923) it was thought that only BiO^+, $BiOH^{2+}$ and $Bi(OH)_2^+$ existed in solution, until 1936 when Holmqvist (1936) , and Prytz and Nagel (1936) concluded that

polynuclear bismuth ions were also present in solution. Prytz and Nagel (1936) used the rate of diffusion of species in bismuth perchlorate solutions to explain that at low pH smaller molecules are found in solution, but then as pH increased so did the molecular weight of the molecules. This gave an indication that polynuclear species were forming in solution as the pH became less acidic. Later on, studies of the hydrolytic behaviour of bismuth(III) in perchloric acid medium by x-ray diffraction of the liquid sample produced the structure of the $Bi_6(OH)_{12}^{+6}$ ion (Levy, Danford and Agron, 1959), giving evidence of a polynuclear species.

More recently a comprehensive study of the bismuth hydroxide, bismuthoxynitrate and bismuthoxyperchlorate species was done by Kragten, Decnop-Weever and Gründler (1993). The bismuth hydroxide species identified included Bi^{3+}, $Bi(OH)^{2+}$, $Bi(OH)_2^{+}$, $Bi(OH)_3$, $Bi(OH)_4^{-}$, and $Bi_6(OH)_{12}^{6+}$ and only one precipitate ($Bi(OH)_3$) had formed. If the concentration of the background nitrate solution was increased (they did studies at 1.00 ± 0.01 M ionic strength at 23 ± 0.5 °C) a second crystalline precipitate also formed which is a mixed hydroxide (as shown in Figure 8.1 where A represents nitrate (or perchlorate or chloride)) and it forms at lower pH than the $Bi(OH)_3$ precipitate. Bismuth can also form nitrate species as has been included in a schematic diagram by Kragten, Decnop-Weever and Gründler (1993). The neutral $Bi(OH)_2NO_3$ (also written as $BiONO_3$) has been identified in solution and has limited solubility, thereby easily forming a precipitate.

Many authors studying the hydrolysis of bismuth have given conflicting evidence of different species, understandably so due to the difficulty faced with studying such a complicated system. The products of bismuth hydrolysis that are generally accepted as being present in solution as presented by the NIST database (Martell, Smith and Motekaitis, 2004) are therefore provided in Table 8.2. A separate table (Table 8.3) also provides formation constants for the bismuth nitrate species. In each case the

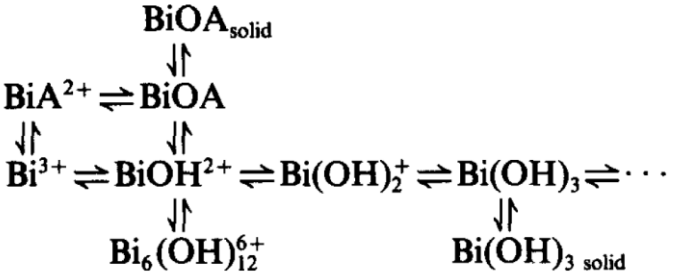


Figure 8.1 Schematic representation by Kragten, Decnop-Weever and Gründler (1993) which shows how the solution species and precipitates are formed from various equilibrium reactions taking place in solution. A symbolizes NO_3^- (or ClO_4^- or Cl^-).

log *β* values included in the tables were selected in terms of the temperature and ionic strength being as close as possible to our experimental conditions of 25°C and 0.5 – 0.25 M respectively. Also, in Table 8.2, log *β* values for the hydroxides that were recalculated for 0.5 M ionic strength by Cukrowski, Hancock and Luckay (1996) are included. Using the formation constants marked with an asterisk in Table 8.2 and 8.3 a SDD (Figure 8.2) was plotted to show an example of the pH range in which these complexes are formed. Since a protonation constant for nitrate is required by the software, it was set to -5 because HNO_3 is a very strong acid and deprotonates immediately in solution.

Bismuth(III) nitrate species are found to exist at very low pH and the formation of hydroxides start at about pH 0 in 0.5 M nitrate. As the pH increases the degree of hydrolysis also increases. The formation of polynuclear species increases with higher concentrations of bismuth(III), but at the concentrations at which our work was done, relatively low concentrations of these species are present.

Since bismuth(III) never appears merely as the hydrated species in solution (only 15% is present as Bi^{3+} in Figure 8.2), the free metal ion potential cannot be measured and thus procedures were developed to determine this potential. Due to the

Table 8.2 The overall stability constants for bismuth hydroxide species at 25 °C.

Bismuth hydroxide	**Log *β***	**Ionic strength (M)** (Martell, Smith and Motekaitis, 2004)	**Log *β* at 0.5 M ionic strength** (Cukrowski, Hancock and Luckay, 1996)
$Bi(OH)^{2+}$	12.4	0.1	12.42*
$Bi(OH)_2^{+}$	23.5	1.0*	-
$Bi(OH)_3$	31.9	0.1	31.88*
$Bi(OH)_4^{-}$	33.6	1.0	32.98*
$Bi_6(OH)_{12}^{6+}$	165.3	1.0	162.78*
$Bi_9(OH)_{20}^{7+}$	23.9	0.1	266.92*
$Bi_9(OH)_{21}^{6+}$	10.6	0.1	276.76*
$Bi_9(OH)_{22}^{5+}$	11.1	0.1	287.30*

* Log *β* values used in this work

Table 8.3 The overall stability constants for bismuth nitrate species at 25 °C as given by the NIST database (Martell, Smith and Motekaitis, 2004).

Bismuth nitrate	**Log *β***	**Ionic strength (M)**
$Bi(NO_3)^{2+}$	0.72*	0.5
$Bi(NO_3)_2^{+}$	0.94*	0.5
$Bi(NO_3)_3$	0.7*	1.0
$Bi(NO_3)_4^{-}$	0.6*	2.0

* Log *β* values used in this work

complex formation with the background nitrate ions as well as hydrolysis occurring, Billing (2012) had to adjust the procedure used for obtaining the free bismuth(III) potential. Data analysis of the ligand-free titration experiments is more complicated for the bismuth(III) systems as compared to the cadmium(II) systems, as now the formation of complexes with hydroxide and nitrate also had to be considered and

precipitation took place at about pH 2 already. Thallium(I) reduction potentials alone were used to determine the diffusion junction potentials and this magnitude was applied to the bismuth(III) reduction data to compensate for it. The expected shift due to complex formation with nitrates and hydroxides was calculated using

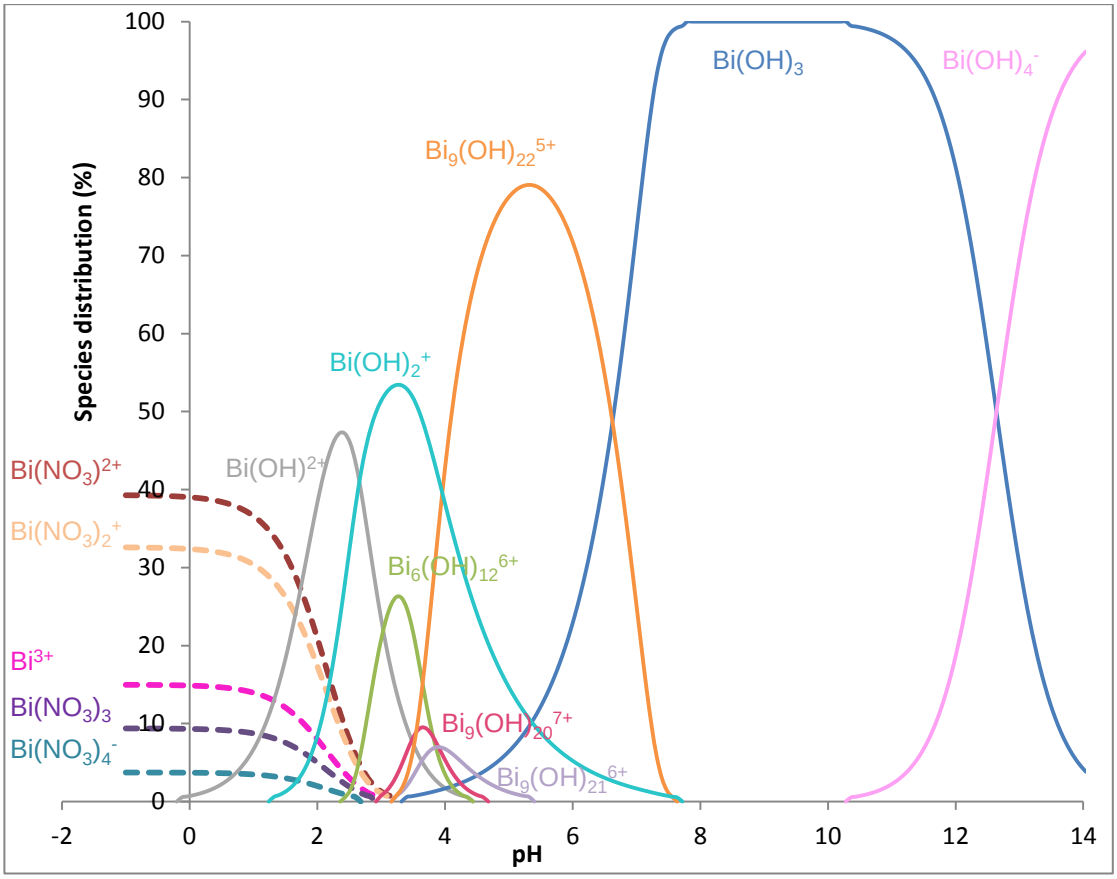


Figure 8.2 SDD showing the possible bismuth(III) nitrate and hydroxide species found in solution when $[NO_3^-]$ = 0.5 M and [Bi] = 5 x 10^{-5} M, using log *β* values given in Table 8.2 and 8.3.

the 3D-CFC program, where

$$\Delta E = \frac{RT}{nF} ln \frac{[M_T]_i}{[M_{free}]_i} \qquad (8.2)$$

which is derived from Cukrowski's equation (Equation 2.5) by the assumption that $I(M_{comp})_{pH} = I(M_{free})_{pH}$ and $ln1 = 0$. In this case all log *β* values from Tables 8.2 and 8.3

were entered and ΔE calculated. This shift in potential was then applied as a further compensation to the bismuth(III) data, and provides the value of the totally free bismuth(III) potential ($E(Bi_{free})_T$). The 3D-CFC program also gives the percentage of each bismuth(III) hydroxide species that is present at each pH, which allows for calculation of a further free bismuth(III) potential ($E(Bi_{free})_{OH}$), which accounts for only the shifts due to the formation of hydroxide species in the presence of the nitrates. In Chapter Nine the actual calculation of these shifts will be described fully and all compensations will be presented graphically. The reason that two different free metal ion potential values were considered is due to the limitations of the 3D-CFC program (I. Cukrowski, 2000) used to refine the formation constants. This software can only take into account complexation with one ligand besides hydroxide. This means that complex formation between bismuth(III) and nitrates cannot be accounted for while simultaneously determining that of bismuth(III) and quinolinic acid. At this stage, the only way to account for any shift due to nitrate complex formation is to incorporate it in the magnitude of the free metal ion potential of bismuth(III), bearing in mind that competition between nitrate and quinolinic acid should only occur in the low pH region where bismuth(III) nitrate species exist.

Billing (2012) performed three experiments for the calculation of formation constants at ligand-to-metal concentration ratios of 47, 75 and 102. Higher concentrations could not be used because the reduction wave of quinolinic acid overlapped with that of thallium(I), as was seen in this work in Chapter Seven. Titration data were collected between pH 0.3 and approximately pH 5; above this pH precipitation started to occur. Once E_j was compensated for, at low pH (below 2) only small shifts in potential from $E(Bi_{free})_{OH}$ were observed, so it was assumed that bismuth(III) nitrate species were still in solution and negligible complexation with quinolinic acid occurred. Data were therefore analyzed using both free metal ion potentials – $E(Bi_{free})_T$ and $E(Bi_{free})_{OH}$, and the respective log β values determined are

given in Table 8.4. The final species model was not definitive, so using $E(Bi_{free})_T$ the log β values for two species models were calculated, namely: (i) MLH, ML, ML_2 and ML_2OH and (ii) MLH, ML, ML_2, ML_3 and ML_3OH. The MLH species was not needed when using the $E(Bi_{free})_{OH}$ value to calculate the CCFC and only log β values for ML and ML_2 are quoted (other species formed at higher pH would not have been affected by competing bismuth(III) nitrate species so values determined using $E(Bi_{free})_T$ would give the best results). Billing (2012) also calculated formation constants using virtual potentiometry (VP) where polarographic data are converted to pseudo-potentiometric data. Software used to analyze potentiometric data can then be used and this allows for a second ligand to be incorporated as a competing species. This meant that the $E(Bi_{free})_T$ was necessary for calculating the formation constants.

Table 8.4 Average log β values calculated by Billing (2012) using $E(Bi_{free})_T$ and $E(Bi_{free})_{OH}$.

	$E(Bi_{free})_T$			$E(Bi_{free})_{OH}$
	Species Set 1	**Species Set 2**	**VP**	**Species Set 1**
MLH	9.7 ± 0.2	9.7 ± 0.2	9.3 ± 0.2	
ML	7.7 ± 0.1	7.7 ± 0.1	7.50 ± 0.07	7.2 ± 0.1
ML_2	13.19 ± 0.06	13.19 ± 0.06		12.54 ± 0.06
ML_2OH	22.90 ±0.02	-		
ML_3		16.8 ± 0.4		
ML_3OH		26.6 ± 0.1		

The best estimates for the formation constants of species formed at low pH would be those obtained by VP. The magnitude of their values are between those calculated using $E(Bi_{free})_T$ and $E(Bi_{free})_{OH}$ which are over- and under-estimated values, respectively. Data only up until approximately pH 2.4 could be fitted when determining the formation constants by VP and so unfortunately formation constants of species found at higher pH values could not be determined in this way.

8.2 AIMS

For this section of work the sole aim was to investigate if species of the bismuth(III)-quinolinic acid system, that had previously been identified by Billing (2012) in solution, could be produced as a crystalline complex. Due to the inconclusive species model it would have been useful to see if information gained from crystal structures could assist in deciding which model was more probable. Additionally, no crystal structures of bismuth(III)-quinolinic acid complexes were found in literature, and so obtaining any crystalline complex of this system would be interesting in order to investigate the bonding interactions.

8.3 EXPERIMENTAL

Species distribution diagrams were plotted using the log β values calculated by Billing (2012) using conditions plausible for crystal growth. Due to the uncertainty of which model best represents the solution a comparison of SDDs (Figure A8.1, Appendix A) was plotted using the same conditions to show the differences in the distributions of species predicted by species set 1 and 2 ($E(Bi_{free})_T$) (Table 8.4). The main difference between these SDDs is from pH 3 where either the formation of the ML_3 and ML_3OH species would occur, or that of ML_2OH. These species exist in approximately the same broad pH range (pH 3 to 8) and so using the SDD of a single species set would be sufficient when targeting species for crystal growths, as the result of the structure would then indicate which species set to correlate the crystalline complex with. We have elected here present the SDDs that were plotted using species set 2 (MLH, ML, ML_2, ML_3 and ML_3OH). Table 8.5 shows the experimental conditions that could be used for targeting the growth of specific species, and it was drawn up by using a summary of the information provided by

three SDDs (see Figure 8.3) and working on a total solution volume of 20 mL. By using specific conditions (i.e. particular [L]:[M] ratios, concentrations and adjusting pH) means that different species could be targeted. The information given in Table 8.5 was used in setting up some experiments to aim at producing crystal structures of particular species. The highlighted rows show which species are present exclusively over a pH range or are present at significantly higher concentrations than the other species and therefore theoretically show the most promise in targeting that specific species. A 0.54 M bismuth(III) stock solution was prepared by dissolving $BiONO_3$ (Fluka, ≥ 98.0%) in deionized water and concentrated HNO_3 (approximately 5 M in concentration in the final stock solution).

Table 8.5 Experimental conditions used when trying to grow specific bismuth(III)-quinolinic acid species in an initial solution volume of 20 mL.

From Fig. 8.3	Targeted Species	[Bi] (M)	[QUIN] (M)	pH Adj	Vol Bi (mL)	Mass QUIN (g)
Solid lines	MLH	0.05	0.05	0-2	1.85	0.16712
	ML	0.05	0.05	1.8	1.85	0.16712
	ML_2	0.05	0.05	3	1.85	0.16712
	ML_3	0.05	0.05	3.8	1.85	0.16712
	ML_3OH	0.05	0.05	5-8	1.85	0.16712
Dashed lines	MLH	0.05	0.1	0-2	1.85	0.33424
	ML	0.05	0.1	1.7	1.85	0.33424
	ML_2	0.05	0.1	2.5	1.85	0.33424
	ML_3	0.05	0.1	4	1.85	0.33424
	ML_3OH	0.05	0.1	5-8	1.85	0.33424
Dotted lines	MLH	0.05	0.15	0-1.5	1.85	0.50136
	ML	0.05	0.15	1.2	1.85	0.50136
	ML_2	0.05	0.15	2	1.85	0.50136
	ML_3	0.05	0.15	3.2	1.85	0.50136
	ML_3OH	0.05	0.15	5-8	1.85	0.50136

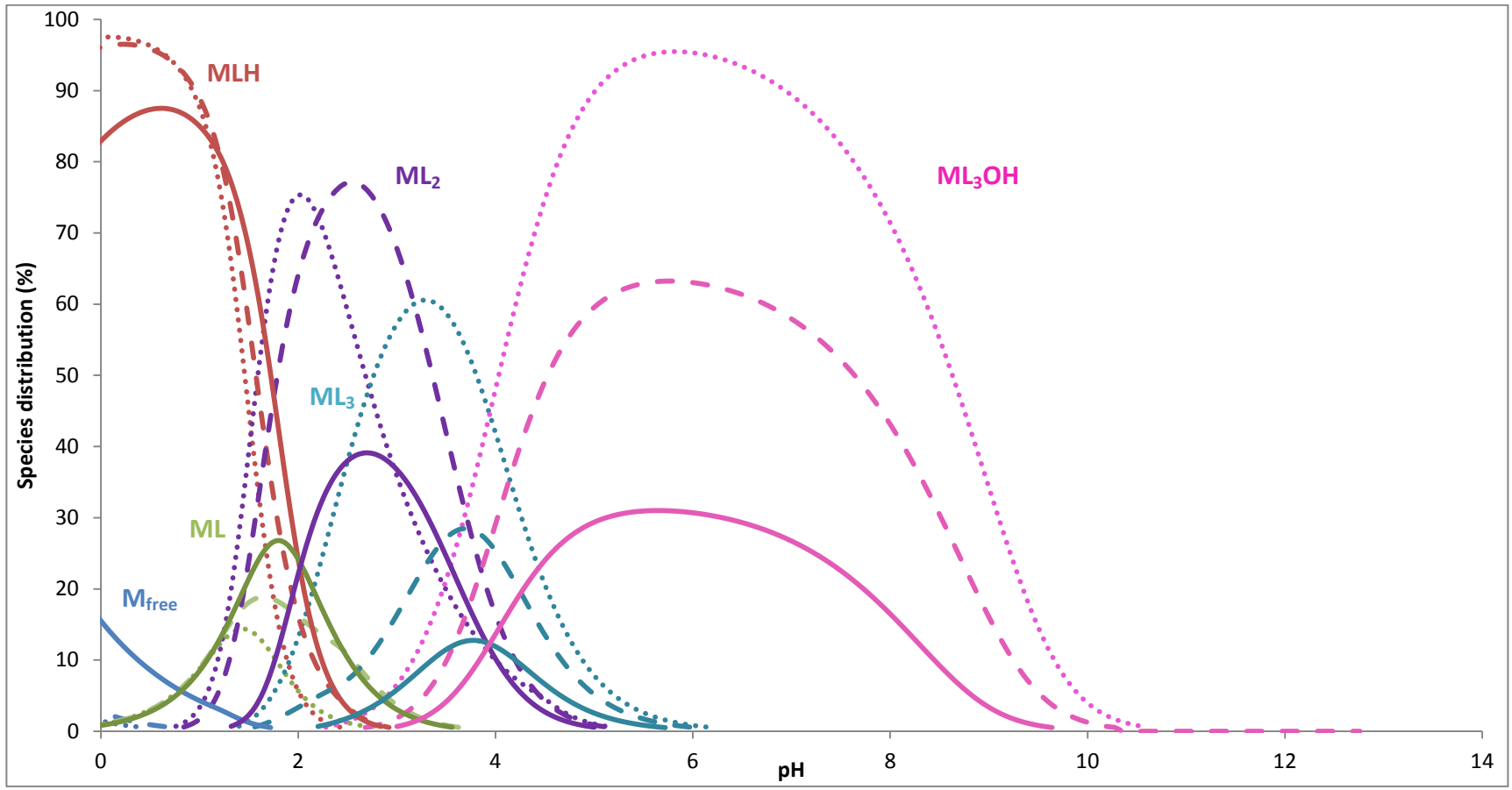


Figure 8.3 SDDs plotted using the MLH, ML, ML_2, ML_3 and ML_3OH species model where [Bi] = 0.05 M. Solid lines represent [L]:[M] = 1:1,dashed lines represent [L]:[M] = 2:1 and dotted lines represent [L]:[M] = 3:1. All hydroxides have been omitted for clarity.

Figure 8.3 clearly shows that these conditions would not be used to target the ML species. Its percentage distribution is very low and it is overshadowed by other species existing in much higher concentrations at the same pH. The ML_2 species is more dominant and exists over a slightly wider pH range where [L]:[M] = 2:1.

Aiming to investigate the competition between the MLH and ML species (see Table 8.5), a solution of [L]:[Bi] = 1:1 at a concentration of 0.05 M was prepared using the stock solution (and the pH was adjusted to about 1.5). Upon adjustment of the pH using KOH, the solution fizzed and went murky. A jelly like substance slowly sank to the bottom of the vial and at this point the pH was only 0.84. After several unsuccessful attempts at adjusting the pH of a few of the experiments outlined in Table 8.5 it was decided to use a bismuth(III) stock solution that was less acidic.

In preparing a new stock solution, $BiONO_3$ was again dissolved using concentrated HNO_3 but now using smaller additions of the acid and allowing a longer period of time for the salt to dissolve. The resulting bismuth(III) concentration was 0.46 M and that of HNO_3 was approximately 2.7 M. The same initial crystallization experiment was again attempted, but unfortunately by pH 0.86 gel clouds had already formed in the solution.

In making up the stock solution the bismuth(III) salt did not easily dissolve unless the pH of the solution was very low, which was also experienced by Wibowo, Vaughn, Smith and zur Loye (2010). The main problem was that the pH could not be adjusted high enough before precipitation occurred. All species except MLH were predicted to form above pH 0.8 and since adjustment above this value was not possible it was decided not to adjust pH at all. This was unfortunate as the pH range between 3 and 8 needed to be investigated in order to gain insight into which species set was more probable.

The solution was prepared using solid quinolinic acid and bismuth(III) (stock solution = 0.46 M) at a [L]:[M] of 3:1, where [Bi] = 0.05 M. The solution was heated at 40 °C until the ligand had dissolved (approximately 20 minutes) and was then left to cool at room temperature. No pH adjustments were done and the vial was left closed. After five days there was no change in the contents of the vial, so it was opened and the following day crystals formed. Some small, colourless crystals were floating on the solution surface, while others formed a solid mass at the base of the vial. These crystals were harvested separately and the solution pH was measured to be −0.20. The vial was left open with the remaining solution and crystals. Interestingly, after about 2 weeks all the crystals had redissolved and the pH at this point was −2.20. After a month with the vial open, no crystals formed again.

Under the microscope it was found that what had formed on the surface of the solution was a solid amorphous mass with tiny needle-like crystals around the edges. They extinguished polarized light under the microscope but unfortunately were too small for a data collection. On the bottom of the vial slightly bigger needles and a few block-shaped crystals could be obtained from the solid mass. One of the needles was just large enough to be analyzed using SCXRD; its dimensions were 0.04 x 0.01 x 0.20 mm. Due to the poor crystal quality and small size, the crystal structure was solved yielding a R1 = 15%. Nevertheless the structure is reported here due to the scarcity of such structures in literature.

8.3.1 Crystallographic Data Collection, Structure Solution and Refinement

SCXRD performed on the Bruker X8 PROTEUM x-ray diffractometer equipped with a Microstar copper rotating anode generator, Montel Optics, a PLATINUM 135 CCD detector, allowed for structure determination of the crystal at -100 °C by the aid of an Oxford Cryostream Plus system. The structure was solved by direct methods using *SHELX-97 (Sheldrick, 2008)*. *SAINT+,* version 6.02 was used for data reduction,

and multi-scan absorption corrections were done with SADABS 2008/1. All atoms were made isotropic. The crystallographic data is given in Table 8.6.

Table 8.6 Crystallographic data for the bismuth(III)-quinolinate structure.

Space group		$P2_1/c$
Unit Cell Parameters (Å and °)	a	15.380(5)
	b	19.234(5)
	c	10.000(5)
	α	90
	β	92.369(5)
	γ	90
Unit Cell Volume ($Å^3$)		2955.66
R factor		15%
Temperature (K)		173

8.4 RESULTS AND DISCUSSION

8.4.1 Structure Analysis of the Bismuth(III)-Quinolinate Crystal Complex

The complex crystallized in a monoclinic crystal system, space group $P2_1/c$. The bismuth(III) metal ion is found to exist in two different coordination modes. Bi1 is 7 coordinate and bonds to five separate quinolinate ligands, as shown in Figure 8.4 a). Three of these bond to bismuth(III) monodentately through the oxygen of the *ortho* carboxylate and the remaining two ligands bond bidentately, one via N,O and the other O,O to the *meta* carboxylate. Bi2 is 9 coordinate and is associated with two separate quinolinic acid molecules and two nitrates which are all bound bidentately to bismuth(III), as shown in Figure 8.4 b). The ninth coordination site is occupied by a water molecule. Bi1 and Bi2 are linked via a common quinolinate ligand (which is

shaded in grey) and the entire structure has been presented in Figure 8.4 c). These high coordination numbers are common for bismuth(III), which can achieve coordination numbers of up to 10, due to its highly acidic nature (Stavila et al., 2011).

Due to the complexity of the structure a three-dimensional figure using SCHAKAL (a graphic program for representing molecular and solid-state structures (Keller, 1999)) was drawn to show the structure of the polymeric complex (Figure 8.5). This view of the polymeric chain allows the structure and the bonding around the metal centre to be seen clearly.

Some of the carboxylate groups in the *meta* position on the quinolinic acid molecules appear to be protonated (due to the quality of the data there is a large uncertainty in the location of hydrogen atoms). This is not surprising since the pH of the solution from which the crystal was grown was extremely low. Despite the poor resolution of the data (R-factor of 15%) it was possible to discern the main features of the packing in the structure, as shown in Figure 8.6. The water molecules, the nitrates and the carboxylate groups of the ligand are responsible for hydrogen bonding. Viewing the structure along the b-axis shows clusters of molecules that are linked by these hydrogen bonds (Figure 8.6). Within a cluster there are four distinct rows, each consisting of only one of the two types of bismuth coordination spheres. The rows made up of Bi2 spheres are found at the top and bottom of the clusters with two rows of Bi1 spheres sandwiched between, making a pattern of Bi2, Bi1, Bi1, Bi2. Solvent molecules are visible when the structure is viewed down the c-axis as in Figure 8.7, where only the oxygen atoms of the water molecules are shown.

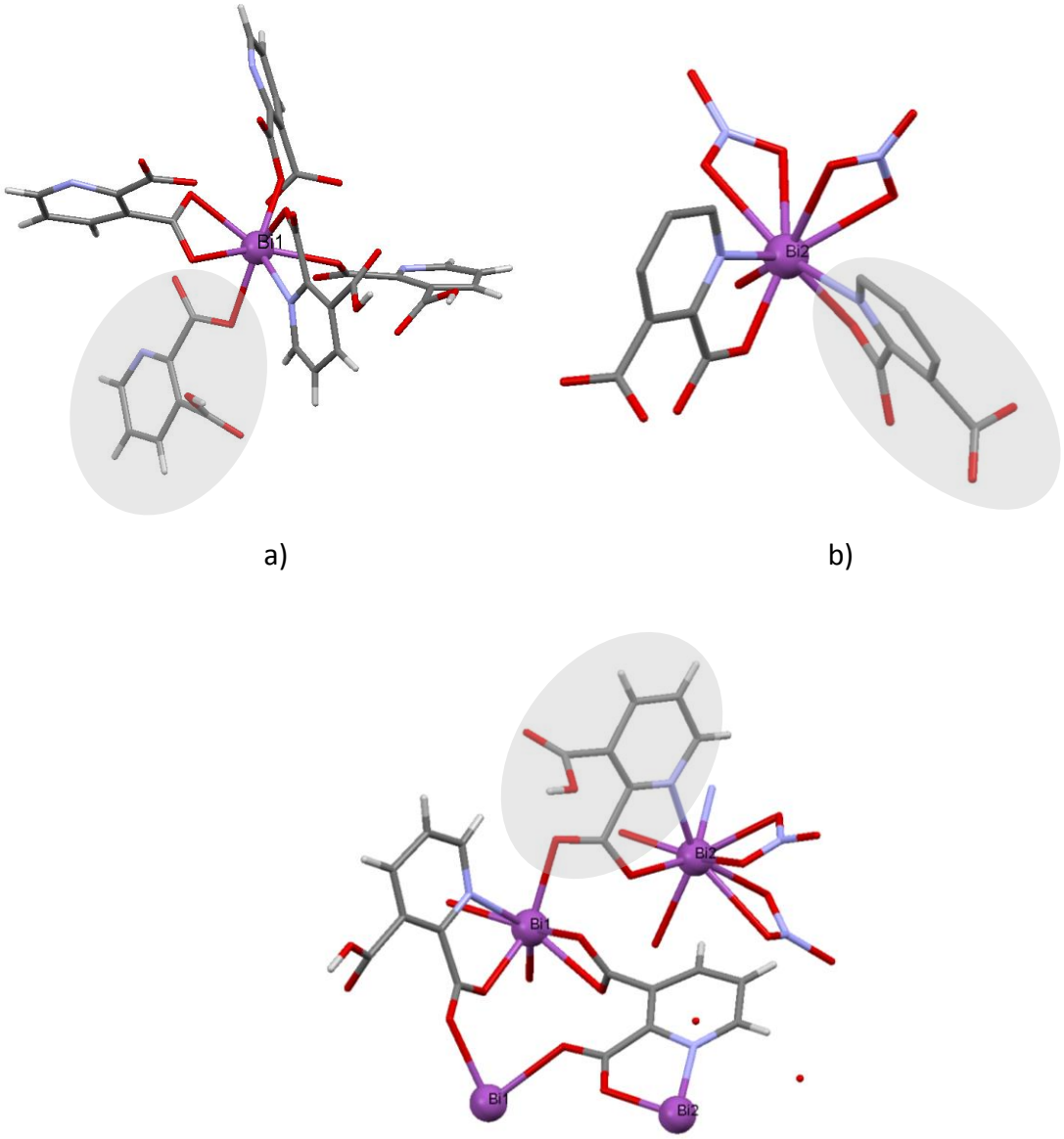


Figure 8.4 The coordination modes for Bi1 and Bi2 have been shown in a) and b), respectively, where the shaded region indicates the ligand which is common to both illustrations. The overall view of the structure is given in c).

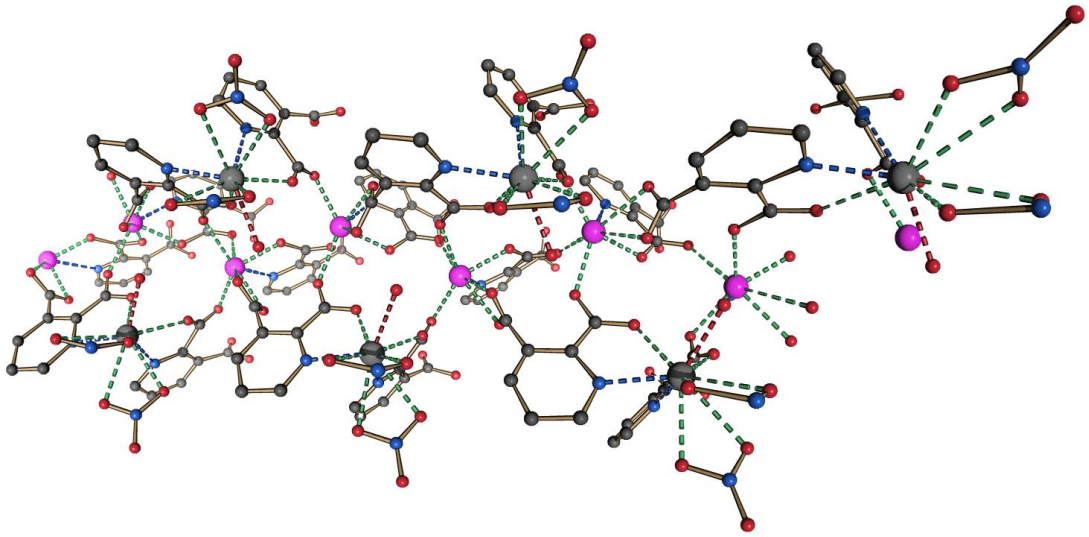


Figure 8.5 Extended structure of the bismuth(III)-quinolinic acid complex generated using the program Schakal. The pink balls represent Bi1 and the large grey balls Bi2. Solvent molecules were omitted for clarity.

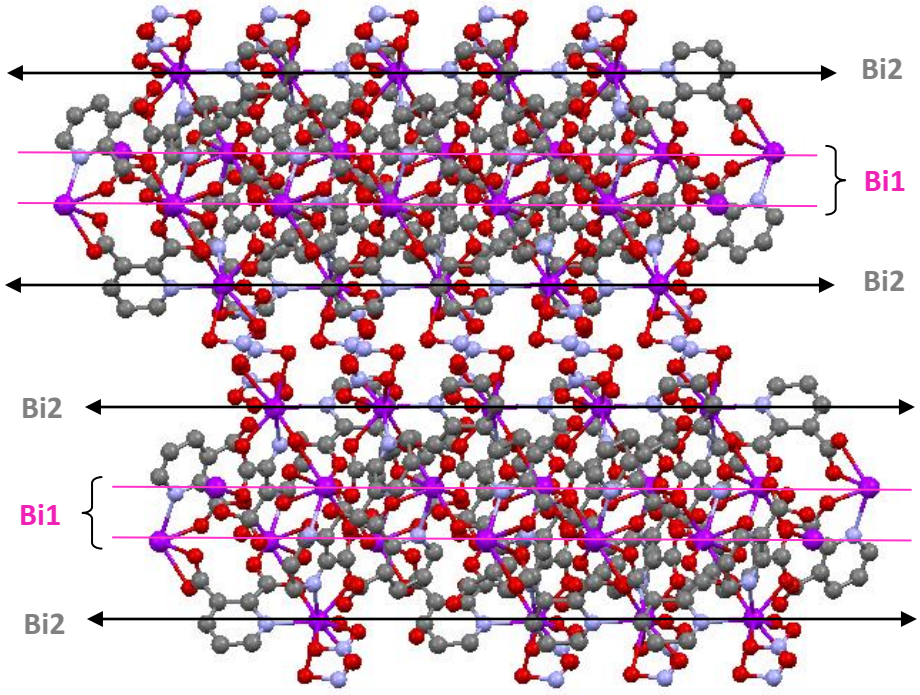


Figure 8.6 Packing diagram seen down the b-axis, created by an extensive hydrogen bond network, which forms clusters of molecules in the a-direction.

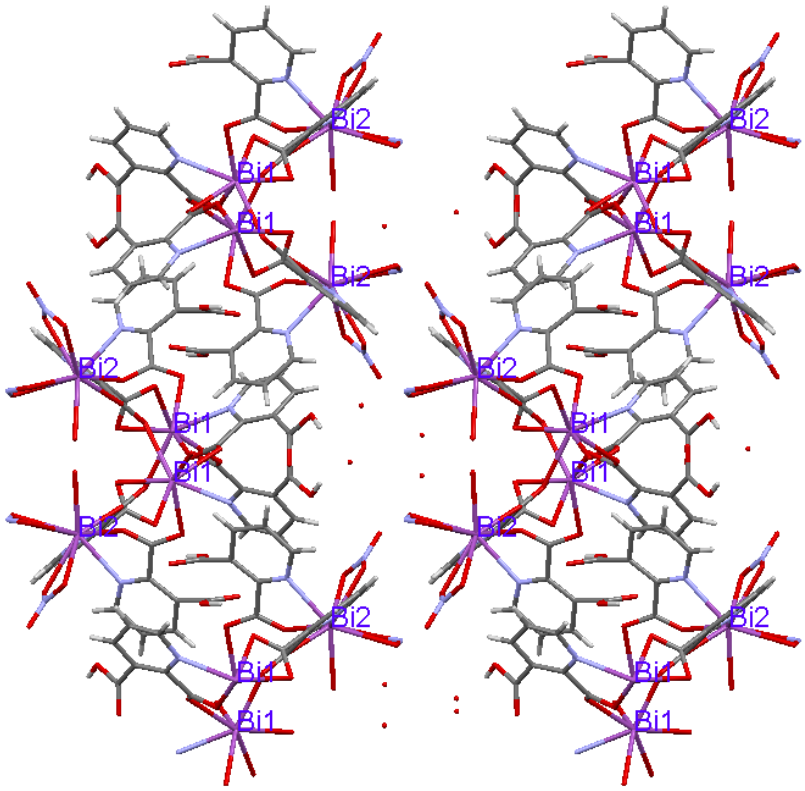


Figure 8.7 A view down the c-axis which shows the solvent molecules of water present in the structure.

This is the first reported structure of a bismuth(III)-quinolinate complex. Andrews *et al*. (2006) comment on the difficulty in fully characterizing such structures. In this case the difficulty was caused by the poor diffraction pattern and so regrowing crystals that are larger in size may in fact allow for the structure to be solved more completely in future. However, Andrews *et al*. (2006) have noted that carboxylate chemistry of bismuth in general has its problems which arise from the acidity and size of the metal centre which results in polymer formation, ligand lability and thermodynamic instability in water or organic solvents. Also, the bismuth(III) ion has a lone pair which could be stereochemically active and according to Summers, Abboud, Farrah and Palenik (1994) this introduces further complication. Upon formation of a bond between a multidentate ligand and a metallic ion there must be

a compromise between the steric interactions of the ligand, and the steric and electronic requirements of the metal ion. It is these characteristics which lead to the various geometries that this type of metal ion can exhibit (Anjaneyulu, Maddileti and Swamy, 2012), as was shown in the structure described here.

Considering the actual structure of this crystalline complex with its large channels containing solvent molecules (water), it is expected that it may have an application in the molecular organic framework field.

8.4.2 A Comparative Study with Literature Structures

Since there are no reported structures of the metal-ligand system under investigation, a discussion of the coordination of similar pyridinecarboxylic acid ligands has been included. A search of the CSD (Allen, 2002) rendered twenty seven structures in which dipicolinic acid is coordinated to bismuth(III) and only four structures in which picolinic acid is coordinated to bismuth(III). As discussed before, the coordination of quinolinic acid to metal ions is more similar to that of picolinic acid as opposed to dipicolinic acid. Hence, the coordination of the four picolinate structures (REFCODES: GERGOA, YIZVAF, YIZVEJ and YIZVEJ01) have been considered for comparison. The picolinic acid in each crystal complex was deprotonated and all were bonded to the bismuth(III) metal centre by a N,O bidentate bond. The coordination of bismuth(III) for GERGOA was six (see Figure 8.8), where three picolinic acid ligands were bonded to the metal centre, two N,O-bidentately and the third monodentately through the carboxylate oxygen. This structure was interesting because four of these bismuth(III) metal centres link together by shared picolinic acid ligands to produce a ring, as shown by Figure 8.8.

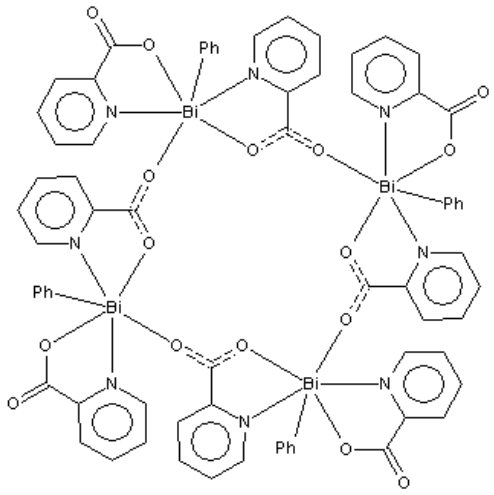


Figure 8.8 Structural diagram showing the coordination of the bismuth(III) ion when complexed by picolinic acid, and the ring formation it forms (REFCODE: GERGOA).

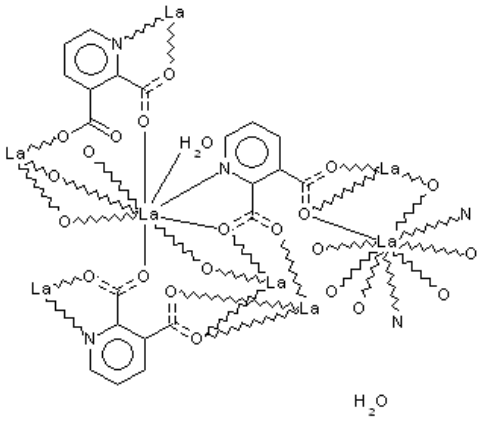
YIZVAF is the structure of an ML_4 species, where the metal centre is eight coordinate which is common for bismuth(III). YIZVEJ (and YIZVEJ01) are polymeric structures where the monomeric unit is an ML_3 species, and the coordination of the bismuth(III) in each of these structures is 8 and 9 respectively.

The considerably larger number of structures containing bismuth(III) with dipicolinic acid as the coordinating ligand, as opposed to picolinic acid and quinolinic acid, indicate the relative stabilities of the complexes that are formed which is due to the ability of dipicolinic acid to chelate tridentately to metal ions.

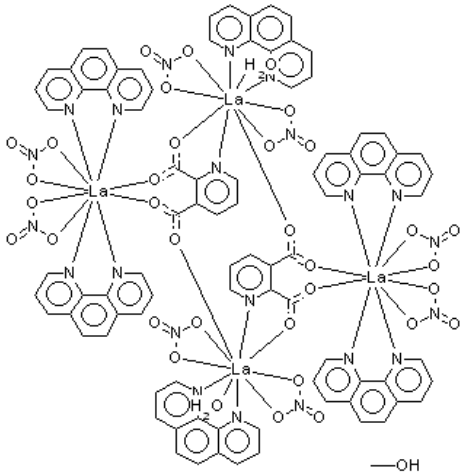
As mentioned by Andrews *et al.* (2006) carboxylate chemistry with bismuth(III) is not straight forward due to the nature of the metal ion, as well as due to the tendency of these complexes to polymerize. Forming structures with lanthanum(III) would have possibly involved similar issues since its radius is even larger than that of bismuth and its ion also behaves as a Lewis acid in solution. The complexity of lanthanum(III)-quinolinic acid structures is evident from literature. The CSD (Allen,

2002) has seven structures reported for this system, of which four were additionally bonded to other metal ions. Structural diagrams for the three remaining structures (CEXWEI, ILEJUF and NOCPUR) are given in Figure 8.9. In each of these structures the quinolinic acid ligand binds N,O bidentately and O monodentately to the metal ion, in a similar manner to the coordination to bismuth(III) reported in this work. High coordination numbers are evident in these structures with 9 being most frequent - as was seen for bismuth(III), and again, as found in our structure, polymerization occurs in both CEXWEI and NOCPUR too.

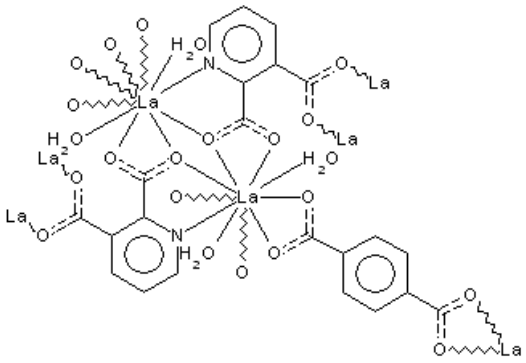
Similar structures of lead(II) were considered as bismuth(III) and lead(II) have similar ionic radii and so it is expected that they may have similar coordination abilities. Also, bismuth(III) is known to replace lead(II) in many products, like paint, cosmetics and solders for example, also showing that they have similar properties. The CSD contained only two structures where quinolinic acid was bonded to lead – REFCODES: IJIYOQ (and the same structure published by different authors, IJIYOQ01) and REMJOJ (and the same structure published by different authors, REMJOJ01) – having coordination numbers of eight and six, respectively, slightly lower than that found for bismuth(III). Both structures were polymeric, but were far less complicated than those of the M(III) ions (where M represents a metal ion) discussed above.



a)



b)



c)

Figure 8.9 Structural diagrams showing the complexity of lanthanum(III)-quinolinic acid complexes: a) CEXWEI, b) ILEJUF and c) NOCPUR.

8.5 CONCLUSIONS

Due to the complexity of the crystal structure determined in this work, a comparison with solution species could not be considered. The problem arose with trying to designate both metal centres of the crystal structure using the simplified $M_xL_yH_z$-

type ratio, and additionally the exact extent of protonation is not clear. The only conclusion that can be drawn between the solution and solid state is that the crystal produced at low pH (approximately -0.2) contained some protonated ligand, which relates to the solution species in that they, too, are often protonated at these low pHs. Billing (2012) speculated only one protonated species (MLH) which is found to exist below pH 2 and in quite high concentrations (using solution conditions for crystal growth).

The difficulty faced when trying to make up liquors to grow crystals at specified pH values, was due to the hydrolysis of bismuth(III). At the higher concentrations used for crystal growth experiments, the formation of both polynuclear hydroxide species and insoluble mixed bismuth hydroxide-nitrate complexes are promoted. At high pHs where the two species sets suggested by Billing (2012) could be differentiated (Figure A10.1), no crystals could be formed due to hydrolysis that occurred at pH 0.8 already. It was thus not possible to deduce which species set was more plausible.

Hydrothermal techniques (which use a bomb to induce high pressures) may be useful for growth of crystalline bismuth(IIII)-quinolinate complexes, as was found by Wibowo, Vaughn, Smith and zur Loye (2010) who were successful at producing crystals of bismuth(III)-pyridine-2,5-dicarboxylic acid in this way. It should be mentioned though that one of the three pyridine-2,5-dicarboxylic acid ligands within this structure was protonated which indicates that this bismuth(III) complex was most likely also formed at very low pH.

8.6 REFERENCES

Allen, F. H., 2002. Acta Crystallographica, B58, pp 380-388. Cambridge Structural Database. Version 5.31, November 2008 update.

Andrews, P. C., Deacon, G. B., Junk, P. C., Kumar, I. and Silberstein, M., 2006. Synthetic and structural comparisons of bismuth(III) carboxylates synthesised under solvent-free and reflux conditions. *Dalton Transactions,* (40)**,** pp 4852-4858.

Anjaneyulu, O., Maddileti, D. and Swamy, K. K., 2012. Structural motifs in phenylbismuth heterocyclic carboxylates–secondary interactions leading to oligomers. *Dalton Transactions,* 41 (3)**,** pp 1004-1012.

Billing, C. 2012. *Study of bismuth chemistry toward medicinal applications.* Doctor of Philosophy, University of the Witwatersrand.

Cukrowski, I., Hancock, R. D. and Luckay, R. C., 1996. Formation constant calculation for non-labile complexes based on a labile part of the metal-ligand system. A DPP study at a fixed ligand to metal ratio and varied pH. Application to polarographically inactive complexes. *Analytica Chimica Acta,* 319**,** pp 39 - 48.

Granér, F. and Sillén, L. G., 1947. On the Hydrolysis of Bi^{3+} Ion. Repeated Oxygen Bridging: A new Type of Ionic Equilibrium. *Nature,* 160 (4073)**,** pp 715.

Holmqvist, A., 1936. *Svensk Kemisk Tidskrift,* 48**,** pp 106.

I. Cukrowski, 2000. 3D-CFC10. 5.0 ed.

Keller, E., 1999. SCHAKAL-99. . University of Freiburg: Freiburg im Breisgau, Germany.

Kragten, J., Decnop-Weever, L. G. and Gründler, P., 1993. Mixed hydroxide complex formation and solubility of bismuth in nitrate and perchlorate medium. *Talanta,* 40 (4)**,** pp 485-490.

Levy, H. A., Danford, M. D. and Agron, P. A., 1959. X-Ray Diffraction Study of Bismuth Polymer in Aqueous Perchlorate Solution. *The Journal of Chemical Physics,* 31 (6)**,** pp 1458-1461.

Martell, A. E., Smith, R. M. and Motekaitis, R. J., 2004. NIST Standard Reference Database 46. 8.0 ed. Gaithersburg, USA: U.S Department of Commerce, National Institute of Standards and Technology.

Mesmer, R. E. and Baes, C. F., 1990. *Review of Hydrolysis Behavior of Ions in Aqueous Solutions*.

Prytz, M. and Nagel, P., 1936. Über amphotere Oxydhydrate, die Lösungen ihrer hydrolysierenden Salze und ihre hochmolekularen Verbindungen. Über die Hydrolyse und die Eigenschaften der Wismutperchlorate. *Zeitschrift für Anorganische und Allgemeine Chemie,* 227 (1)**,** pp 65-80.

Sheldrick, G. M., 2008. A short history of *SHELX*. *Acta Crystallographica,* A64**,** pp 112–122.

Stavila, V., Bulimestru, I., Gulea, A., Colson, A. C. and Whitmire, K. H., 2011. Hexaaquacobalt(II) and hexaaquanickel(II) bis(μ-pyridine-2,6-dicarboxylato) bis[(pyridine-2,6-dicarboxylato)bismuthate(III)] dihydrate. *Acta Crystallographica Section C,* 67 (3)**,** pp m65-m68.

Summers, S. P., Abboud, K. A., Farrah, S. R. and Palenik, G. J., 1994. Syntheses and structures of bismuth(III) complexes with nitrilotriacetic acid, ethylenediaminetetraacetic acid, and diethylenetriaminepentaacetic acid. *Inorganic Chemistry,* 33 (1)**,** pp 88-92.

Wibowo, A. C., Vaughn, S. A., Smith, M. D. and zur Loye, H.-C., 2010. Novel Bismuth and Lead Coordination Polymers Synthesized with Pyridine-2,5-Dicarboxylates: Two Single Component “White” Light Emitting Phosphors. *Inorganic Chemistry,* 49 (23)**,** pp 11001-11008.

Yang, N. and Sun, H., 2011. Bismuth: environmental pollution and health effects. *Encyclopedia of Environmental Health. Edited by Nriagu JO. Elsevier***,** pp 414-420.

Chapter Nine

Complex Formation of Bismuth(III)-EDTA

9.1 INTRODUCTION

Ethylenediaminetetraacetic acid (EDTA) is a common ligand due to its remarkable ability to chelate to almost any metal ion, regardless of its valency. This ligand has been well studied and is therefore often used as a model for understanding other metal complexes (https://www.bhsu.edu/Portals/91/AnalyticalChemistry/StudyHelp/LectureNotes/Chapter13.pdf). It is a multidentate ligand having six electron pairs that are available for bonding; its structure is shown in Figure 9.1. From the structure it is evident that EDTA is an amino acid compound. The human body assimilates EDTA, which is found in many of our daily foodstuffs and beverages, where it functions mainly to protect us from harmful metals by removing them from our bodies by chelation. EDTA is used in canned beans to remove the metallic taste, in beer to prevent gushing (fizziness), in condensed milk to prevent thickening, as well as in frozen desserts and salad dressings to prevent catalyzation of decomposition reactions (Brown, LeMay and Bursten, 2000). Industrial grade EDTA is often added to batteries to restore and prolong their use by stripping sulfate off the electrode plates. Pharmaceutical grade EDTA, known as a sequestering agent, is used to remove toxic metal ions such as mercury, arsenic, cadmium and lead (to name a few) from organs and the cardiovascular system. As described, this ligand has many applications and is valuable to humans; however, it was banned from use in detergents as it is not biodegradable and can be an environmental hazard.

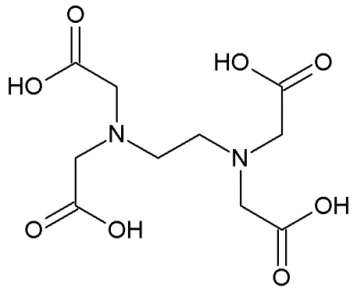


Figure 9.1 Chemical structure of EDTA (ethylenediaminetetraacetic acid).

This ligand is often used in complexometric titrations due to the thermodynamic stability of its complexes (Stavila, Davidovich, Gulea and Whitmire, 2006). When EDTA is fully protonated it is designated as H_6Y^{2+} and its complexing ability is greatest when it is completely deprotonated (Y^{4-}), which occurs at high pH. Figure 9.2 shows the extent of protonation of the ligand in aqueous solution at various pHs.

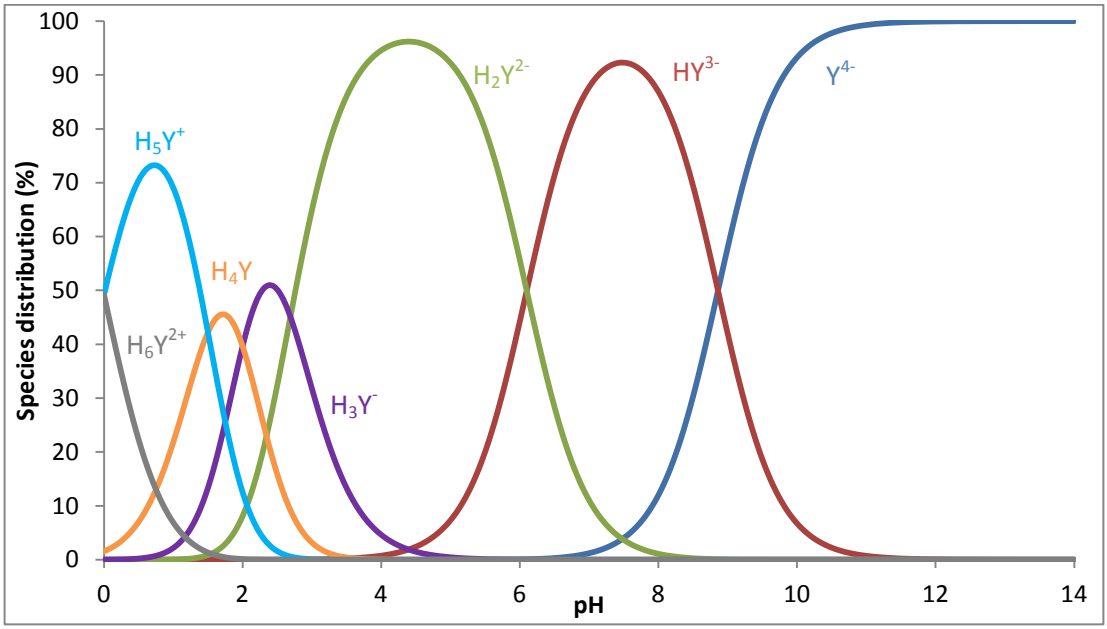


Figure 9.2 SDD showing the percentage distribution of the EDTA species that predominate in specific pH regions in aqueous solution at 25°C.

Bismuth(III) is known to have a high affinity for multidentate ligands containing O and N donor atoms because of its borderline characteristic in terms of Pearson's

hard-soft acid-base theory (Stavila, Davidovich, Gulea and Whitmire, 2006). Multidentate ligands such as EDTA have stronger binding constants than the equivalent unidentate ligands because the change in entropy associated with the former is smaller; and also, once the multidentate ligand has been bound at one site, other binding sites are in close proximity and therefore can bind almost immediately. This is all described by the chelate effect (Martell and Hancock, 1996). All six donor atoms can be used during chelation but, according to Brown, LeMay and Bursten (2000), EDTA often acts as a pentacoordinate ligand – occupying 5 coordination positions with one of the acetate groups dangling free. Even though Bi(III) easily hydrolyzes, according to Bottari and Anderegg (1967) (in Stavila, Davidovich, Gulea and Whitmire (2006)) its complexes with strongly chelated ligands are stabilized up to pH 10. Bismuth(III) has been found to form stable complexes with Y^{4-} and it is a system that is well documented in literature. Stavila, Davidovich, Gulea and Whitmire (2006) have reviewed this M-L system which has been studied by several different techniques, namely: spectrophotometry, IR, NMR, potentiometry, polarography (Kornev and Trubachev, 1987, Sochevanov and Volkova, 1969, Miklos and Szeged, 1961), SCXRD and PXRD.

9.1.1 Solution Complexes for the Bismuth(III)-EDTA System

Bhat and Iyer (1966) obtained formation constants spectrophotometrically at 25 ± 1 °C and 1 M sodium perchlorate to maintain the ionic strength. They used pH vs. absorbance curves to solve the molar absorbance of the species, as well as that of the free metal ions from corresponding perchlorate solutions. These experiments were performed at four different pH values (0.22, 0.4, 0.7 and 1) which were measured using a calibrated glass electrode. The ML species (Bi(EDTA)) was found to have an average formation constant (log *K* value) of 26.47.

Other spectrophotometric studies by Karadakov and Ivanova (1973) (in Stavila, Davidovich, Gulea and Whitmire (2006)), done at 25 °C and 1.0 M ionic strength,

showed the formation of a protonated species (Bi(EDTA-H)) with a log *K* value of 17.73 existing between pH 0.6 and 1.4, and the Bi-EDTA complex with a log *K* value of 25.68 existing between pH 1.5 and 10. At higher pHs bismuth hydroxide was present in solution. The value of their log *K* for Bi-EDTA is somewhat lower than that given by Bhat and Iyer (1966) whose value more closely resembles that found polarographically by Kornev and Trubachev (1987) (log *K* = 26.41). Table 9.1 gives a summary of the formation constants for the MLH and ML species and the values that were critically assessed by Martell, Smith and Motekaitis (2004) are indicated with an asterisk. According to results found on the IUPAC Stability Constants Database (Powell and Pettit, 1997) Karadakov and Ivanova (1973) also measured the log *K* value (0.9) for the Bi(EDTA-H) complex by the protonation of Bi(EDTA). The log *K* value of 17.73 for the Bi(EDTA-H) quoted in Stavila, Davidovich, Gulea and Whitmire (2006) as determined by Karadakov and Ivanova (1973) was therefore unrealistic and has been left out of the tabulated data. Interestingly, below pH 1 Bhat and Iyer (1966) found the ML species in solution whereas Karadakov and Ivanova (1973) found the MLH species, even though the experiments were done under the same conditions and using the same technique.

Table 9.1 Formation constants for Bi-EDTA complexes from literature.

Species reaction	Log *K*	Author	Temp, μ	Method
ML + H ⇌ MLH	(1.4)*	NIST Martell, Smith and Motekaitis (2004)	25 °C, 0.1 M	-
	1.7	Bottari and Anderegg (1967)	20 °C, 1.0 M	Potentiometry
	0.9[b]	Karadakov and Ivanova (1973)	25 °C, 1.0 M	Spectrophotometry
M + L ⇌ ML	25.68[a, b]			
	26.47 ≈(26.5*)	Bhat and Iyer (1966)	25 °C, 1.0 M	Spectrophotometry
	26.41[a, b]	Kornev and Trubachev (1987)	25 °C, 1.0 M	Polarography
	26.7[b]	Bottari and Anderegg (1967)	20 °C, 1.0 M	Potentiometry
	27.93[a, b]	Sochevanov and Volkova (1969)	3.60 M	Polarography
	27.94[a, b]	Miklos and Szeged (1961)	20 °C, 0.1 M	Polarography

*NIST, (NIST was unsure of the value of 1.4 because protonation is below pH 2).
[a]Values from Stavila, Davidovich, Gulea and Whitmire (2006).
[b]Values from the IUPAC Stability Constants Database (Powell and Pettit, 1997).

9.1.2 Crystalline Complexes for the Bismuth(III)-EDTA System

According to Stavila, Davidovich, Gulea and Whitmire (2006), as well as Summers, Abboud, Farrah and Palenik (1994), the Bi(III) metal ion exhibits coordination numbers of between seven and ten, with eight being the most frequent. A search of the CSD for Bi-EDTA complexes produced 44 hits. Of these 82% had a coordination number of eight and none of them had a coordination number of ten. EDTA is known to form monomers, dimers or polymeric arrays (Stavila, Davidovich, Gulea and Whitmire, 2006) and it was found that 27 structures formed polymeric arrays of which 5 were also dimeric. Of all the 44 structures 11 of them were dimeric. EDTA is known to form 1:1 complexes with metal ions of any charge (Harris, 1998), due to the way in which the EDTA forms a cage around the metal centre. For all 44 Bi(III)-

EDTA structures the metal-ligand stoichiometry was 1:1 (or 2:2 for bridged complexes), but interestingly a neodymium-EDTA complex was found to have a metal-ligand stoichiometry of 1:2 (REFCODE: FAFSAH) (the structural diagram of FAFSAH is given in Figure A9.1, Appendix A).

By 1948 the protonated species Bi(EDTA-H) in the solid state had been identified by Brintzenger and Munkelt (1948). Bhat and Iyer (1966) then grew a crystalline complex of this same species (determined using PXRD), from an aqueous solution containing equimolar amounts (0.1 M) of $Bi(NO_3)_3$ and EDTA. According to their elemental analysis the structure was found to be the hydrated form, Bi(EDTA-H)·H_2O. The complex had to be kept over calcium chloride in order to maintain its stability. By the late 1980's there was proof of the Bi(EDTA-H) and Bi(EDTA-H)·$2H_2O$ crystal species determined using IR and PXRD (Stavila, Davidovich, Gulea and Whitmire, 2006). No structural information was given for any of these crystals.

Stavila, Davidovich, Gulea and Whitmire (2006) were able to obtain the Bi(EDTA-H) complex by fast crystallization from a hot aqueous solution or by dehydration of the dihydrate (Bi(EDTA-H)·$2H_2O$). The dihydrate was obtained by crystallization from dilute solutions at room temperature.

Summers, Abboud, Farrah and Palenik (1994) aimed to grow crystals of bismuth(III) with three different ligands, one of which was EDTA. Even though crystals of Bi(EDTA) and Bi(EDTA-H) species had been grown before (by Brintzenger and Munkelt (1948) and Shchelokov, Mikhailov, Mistryukov and Sergccv (1987), respectively) they aimed to grow crystalline species of the Bi(III)-EDTA system and supply structural data which had not been published before. They prepared and heated an aqueous solution of EDTA and upon boiling added $(BiO)_2CO_3$ in small amounts over half an hour. The solution was then filtered and crystals of Bi(EDTA-H)·$2H_2O$ formed upon evaporation of the solution. The structure of this complex

was determined using SCXRD and is shown in Figure 9.3, but unfortunately the pH at which it was grown was not determined.

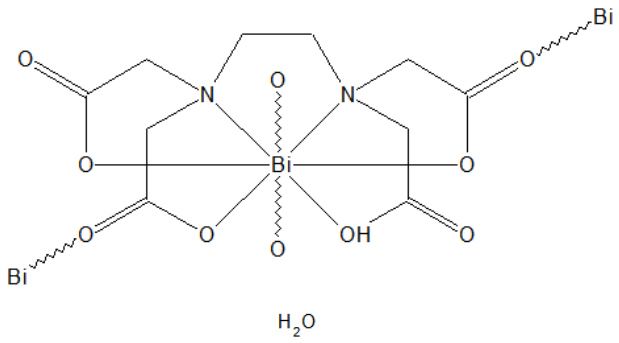


Figure 9.3 Structural diagram of HAYPEC (Summers, Abboud, Farrah and Palenik, 1994).

Wullens, Bodart and Devillers (2002) studied the complexation of M(III) (where M represents any metal ion) with polyaminocarboxylate ligands which included EDTA. Their paper reports the preparation and characterization by Fourier transform infrared spectrometry (FTIR) and thermogravimetric analysis (TGA) of new complexes of Bi(III), La(III) and Pr(III) with EDTA as well as other ligands. Elemental analyses are provided for each of them. The various complexes were characterized by thermogravimetry under air in order to determine the water content, to validate the assumed stoichiometry on the basis of the total weight loss up to the oxide stage, to determine their final decomposition temperature and to investigate their thermal degradation scheme. They synthesized their Bi(III)-polyaminocarboxylate complexes using the procedure described by Summers, Abboud, Farrah and Palenik (1994). The ligand was introduced in its ionized form in boiling water where it dissolved. $Bi_2O_2CO_3$ (Bi(III)oxocarbonate) was added to the aqueous solution which formed a white suspension. Heating and stirring was necessary until the solid disappeared. Any excess $Bi_2O_2CO_3$ was filtered off and the remaining solution was

allowed to evaporate which led to the formation of either a white powder or crystals which were of the Bi(EDTA-H) complex.

9.2 AIMS

The initial aim of this part of the project was to test the accuracy of the method described by Billing (2012) for calculating formation constants. This system was thought to be ideal because: "Bismuth complexes with anions of ethylenediaminetetraacetic acid (H_4EDTA) are far the most widely investigated of the diaminocarboxylates because the acid and its disodium salt are readily available and form stable complexes with the bismuth(IIII) ion in aqueous solution" (Stavila, Davidovich, Gulea and Whitmire, 2006). Unfortunately, upon experimentation it was found that the reduction process of the Bi(III)-EDTA complexes was irreversible when studied using polarography and several methodologies for analyzing the experimental data are attempted.

The formation of crystalline complexes from aqueous solutions was attempted. Even though the structures of the Bi(EDTA) and Bi(EDTA-H) species are well-known, we were interested in relating the pH of the solution to the type of species that is formed in the crystal.

9.3 EXPERIMENTAL

9.3.1 Solution Complex Formation

Polarographic experiments were conducted in the same way as described before in chapters Three and Five - first without ligand present and then with the ligand. Three experiments containing Bi(III) and Tl(I) without the ligand were obtained in

order to study the diffusion junction potential. pH titrations were run between pH 0.3 and 7, and polarograms were recorded in the potential range from 180 to -700 mV. The E_j cannot be compensated for in the same way as described for the cadmium(II)-ligand systems and so the method will be clearly outlined under Results and Discussion (Section 9.4). An experiment was then conducted with added EDTA-disodium salt ligand where [L]:[Bi] = 100. Due to the high stability of the Bi-EDTA complexes, it was found that the reduction wave of the complexed Bi(III) metal ion shifted in the negative direction (as the pH was increased) to such an extent that it started to overlap with the reduction wave of thallium(I). To avoid the overlap it was decided to perform an experiment with only Bi(III) and the EDTA disodium salt ([L]:[M] = 100). As previously discussed, the problem when doing this experiment without the in-situ witness ion present is that the magnitude of the diffusion junction potential will not be measured and the compensation will only be an estimate of the diffusion junction potential.

9.3.2 Crystalline Complex Formation

9.3.2.1 Crystal Growth of catena((m3-hydrogen-ethylenediaminetetra-acetato)-bismuth(III)) dihydrate

From the 0.54 M Bi(III) stock solution described in Chapter Eight, 0.185 mL and 0.03743 g of the disodium salt of EDTA was added to deionized water in order to make a 1:1 [L]:[M] ≈ 0.01 M solution. The solution was heated at 40 °C and all the solid dissolved within twenty minutes. The closed vial was left to cool naturally to room temperature. After five days the vial was opened and within a month three large colourless, block-shaped crystals formed in solution and the pH was measured to be 0.380. When studying these crystals under the microscope some were found to be triangular plates and others block-like in shape. The structure of the triangular plate crystal was solved and found to be the Bi(EDTA-H)·2H_2O complex, which matched HAYPEC (Summers, Abboud, Farrah and Palenik, 1994) in the CSD.

9.3.2.2 Crystallographic Data Collection, Structure Solution and Refinement of catena((m3-Hydrogen-ethylenediaminetetra-acetato)-bismuth(III)) dihydrate

Intensity data were collected on a Bruker SMART CCD area detector diffractometer with graphite monochromated Mo Kα radiation (50 kV, 30 mA). The collection method involved ω-scans of width 0.3 °. Data reduction was carried out using the program *SAINT+,* version 6.02 (Bruker, 1999). Empirical absorption corrections were made using the program XPREP. The triangular plate crystal was studied at -100 °C (173.15 K) and structures were solved by direct methods using *SHELX-97* (Sheldrick, 2008). Non-hydrogen atoms were first refined isotropically followed by anisotropic refinement by full matrix least-squares calculations based on F^2 using *SHELX-97*. As far as possible proton positions were found from the difference Fourier map, while the positions of remaining H atoms were deduced from H-bonding pattern and added geometrically. A summary of the crystallographic data for the Bi(EDTA-H) structure can be seen in Table 9.2.

Table 9.2 Crystal data and structure refinement for Bi(EDTA-H).

Identification code	Bi(EDTA-H)	
Empirical formula	$C_{10}H_{17}BiN_2O_{10}$	
Formula weight (g/mol)	267.12	
Temperature	173(2) K	
Wavelength	0.71073 Å	
Crystal system	Monoclinic	
Space group	Cc	
Unit cell dimensions	a = 17.0460(8) Å	α= 90°
	b = 6.8367(3) Å	β = 105.637(1)°
	c = 13.2314(6) Å	δ= 90°
Volume	1484.9(1) $Å^3$	
Z	4	
Density (calculated)	2.390 Mg/m^3	
Absorption coefficient	11.931 mm^{-1}	
F(000)	1016	
Crystal size	0.46 x 0.35 x 0.13 mm^3	
Theta range for data collection	2.48 to 27.99°	
Index ranges	-22≤h≤22, -9≤k≤9, -16≤l≤17	
Reflections collected	8822	
Independent reflections	3146 [R(int) = 0.0560]	
Completeness to theta = 27.99°	100.0%	
Max. and min. transmission	0.3061 and 0.0731	
Refinement method	Full-matrix least-squares on F^2	
Data / restraints / parameters	3146 / 90 / 204	
Goodness-of-fit on F^2	1.112	
Final R indices [I>2sigma(I)]	R_1 = 0.0267, wR_2 = 0.0670	
R indices (all data)	R_1 = 0.0285, wR_2 = 0.0675	
Absolute structure parameter	-0.020(11)	
Largest diff. peak and hole	0.598 and -2.761 e.$Å^{-3}$	

9.4 RESULTS AND DISCUSSION

9.4.1 Solution Studies

Usually a discussion of the ligand-free experiments is done up front as this data is important for studying the diffusion junction potential, which is then applied to compensate the data obtained from a complexation experiment. For this chapter it has been presented slightly differently because of the overlap of the reduction waves for bismuth(III) and thallium(I) in the initial complexation experiment. Firstly, the data with the overlapping waves will be dealt with, using a method described by Ružić and Branica (1969) for analyzing composite waves of an irreversible system. This section is quite brief because the analysis was unsuccessful. Secondly, the analysis of the ligand-free experiments for determining the magnitude of the diffusion junction potential and the free bismuth(III) potential is presented and then thirdly, the complexation experiment containing only Bi(III) with EDTA is analyzed. A new procedure is put forward for obtaining $E_{½}$ values at a fixed degree of reversibility, which was adapted from a method described by Cukrowski and Zhang (2004).

9.4.1.1 Analysis of Composite Waves where the Reduction of Bismuth(III) is Irreversible

When running complex formation experiments with both bismuth(III) and thallium(I) in the same solution (together with EDTA), it was found that the two reduction waves started to overlap just before the solution reached pH 2. Figure 9.4 shows that the waves were initially resolved and could be fitted as before (using Equation 2.2) up to pH 1.8. The large negative shift in the reduction potential of Bi(III) with increasing pH resulted in the two waves overlapping totally. The polarogram that was collected just before EDTA was added to the solution has been plotted in Figure 9.4 to highlight the large shift due to complex formation of Bi-EDTA species.

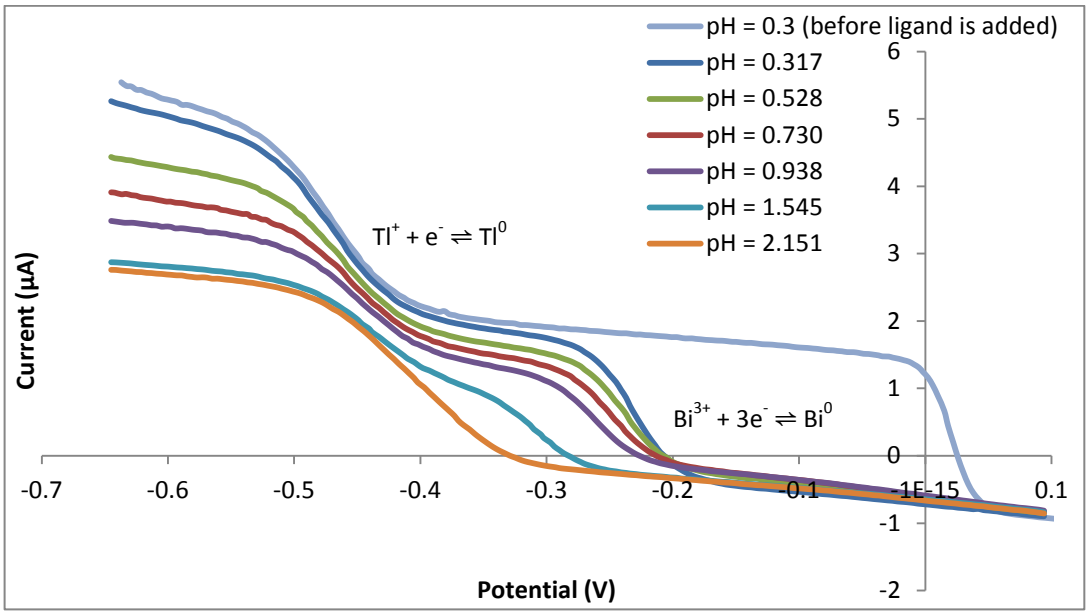


Figure 9.4 Polarograms showing negative shifts in Bi(III) reduction potential due to complex formation as pH is increased. (The small positive shift in the reduction potentials for Tl(I) is due to E_j.) [EDTA]:[Bi] = 100 at 25 °C.

The data that were collected up to pH 1.85 showed that the complexation of bismuth(III) was not a reversible process, having an average delta value (as given in equation 2.1) of 0.52 ± 0.02. Cukrowski *et al.* (2007) found that for the application of determining formation constants, the value delta (δ) could be used to classify the kinetics of the reduction process. For δ = 0.9 – 1 the process was considered to be fully reversible, δ = 0.5 – 0.9 the process was considered to be quasi-reversible and irreversible for δ < 0.5. According to this description, the reduction of the Bi-EDTA species was considered as irreversible. An irreversible reduction is one in which electron transfer proceeds so slowly that it does not attain equilibrium during the lifetime of each mercury drop. The electron transfer rate is slower than the rate of mass transport (diffusion in this case). Upon inspection of the literature, it was found that irreversibility is common when using polarographic techniques for

studying metal ions with an oxidation state of three in non-complexing media (Moussa and Sammour, 1960, Randles and Somerton, 1952, Bauer and Elving, 1960). However, in the presence of halides (except fluoride (Bond, 1969)) and some pseudohalides (such as nitrate) the reduction of Bi(III) becomes reversible. It therefore seems more likely that the chelation by EDTA, which is large, can form up to six bonds with the metal ion and forms a cage-like structure around the metal center, is responsible for the slow reduction rate.

Even though significant complex formation had already taken place between bismuth(III) and EDTA at pH 1.85, these data still could not simply be analyzed for two reasons: (i) the reduction of bismuth(III) was not fully reversible (a requirement to apply Equation 2.5 to determine stability constants) and (ii) the half-wave potentials for thallium(I) were required above pH 2 as they are used to calculate the magnitude of E_j as well as the free bismuth(III) potential.

In order to obtain data above pH 2, it was decided to apply a procedure described by Ružić and Branica (1969) which used logarithmic analysis of a composite DC wave (for reversible or totally irreversible processes) to evaluate the half-wave potentials and diffusion limited currents for the separate reductions. A composite wave is defined as one which contains two waves that are so close together that the first wave reaches its limiting current in the potential region where the second wave begins. Their procedure involved plotting the log of the current ratio ($i/(i_d-i)$) vs. the potential (E) according to the following equation, for each composite polarogram:

$$\log x = -a'E + logA \qquad 9.1$$

where x = $i/(i_d-i)$, a' = (nF/RT)log e and $A = 10^{a' E½}$. Since the linear additivity of currents must be fulfilled at each point analyzed, the sum of the currents of the two overlapping waves is expressed as:

$$x = \frac{mx_1(1+x_2)+ x_2(1+x_1)}{m(1+x_2)+1+x_1} \qquad 9.2$$

where $x_k = i_k/(i_{dk}-i_k)$ and k represents either wave 1 or 2, and m is the ratio of diffusion currents (i_{d1}/i_{d2}) and is evaluated using the point of inflection on the plot. At the foot of the wave (i.e. at sufficiently positive potentials), $x_1 \leq 1$ and $x_2 \leq 1$ which implies that $1 + x_1 \approx 1$ and $1 + x_2 \approx 1$, therefore

$$x = \frac{mx_1 + x_2}{m+1} = x_1^* \qquad 9.3$$

At the top of the wave (i.e. at sufficiently negative potentials), $x_1 \geq 1$ and $x_2 \geq 1$, which means that $1 + x_1 \approx x_1$ and $1 + x_2 \approx x_2$, therefore

$$x = \frac{mx_1x_2 + x_2x_1}{mx_2+x_1} = \frac{(m+1)x_1x_2}{mx_2+x_1} = x_2^* \qquad 9.4$$

Tangents to the plot of log x vs. E close to the foot and top of the wave are drawn and extrapolated to the x-axis to give values of E_1 and E_2, respectively, as shown in Figure 9.5.

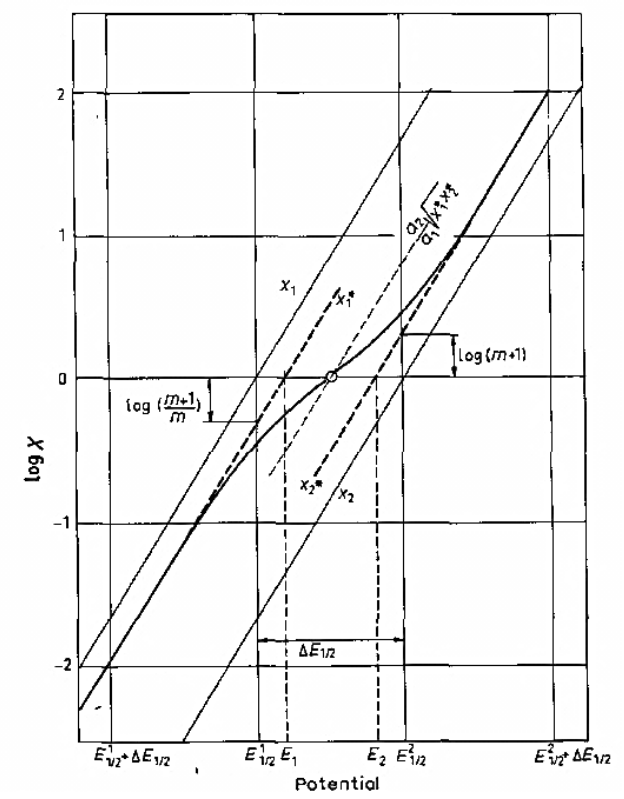


Figure 9.5 An illustration of the log analysis plot from Ružić and Branica (1969). It should be noted that the log analyses described in the article by Ružić and Branica (1969) were done on theoretical polarograms and the procedure was not applied to experimental data as done in this work.

In order to determine $E_{½,1}$ and $E_{½,2}$, a shift in potential from E_1 and E_2, respectively, is calculated. If the condition that $x_1 \geq x_2$ for all potentials holds, then the shifts are calculated using the following:

$$shift_1 = \frac{1}{a_1'} log\left[\frac{m+1}{m}\right] \quad 9.5$$

$$shift_2 = \frac{1}{a_2'} log[m+1] \quad 9.6$$

where $1/a' = 0.05916/n$ at 25 °C. The half-wave potentials are then calculated using:

$$E_{\frac{1}{2},k} = E_k + shift_k \quad 9.7$$

However, when consulting the graph given in Figure 9.5, it appears that the shift for the first wave is negative and hence equation 9.5 should rather be:

$$shift_1 = -\frac{1}{a_1'} log\left[\frac{m+1}{m}\right] \quad 9.8$$

If the stipulation that $x_1 \geq x_2$ is not satisfied, then more elaborate procedures are required for calculating these shifts and these are dependent on the ratio of the slopes of the individual polarograms.

As an example, the first unresolved polarogram (at pH 1.95) was analyzed using the log analysis procedure. The polarograms measured at pH 1.85 and at 1.95 are shown in Figure 9.6, together with the log plot for the polarogram at pH 1.95. To find the value of i_d of the composite wave in order to calculate log *x*, the composite polarogram was fitted as a single wave using Equation 2.1, and the average number of electrons transferred (n (average) = 2 since bismuth(III) has n = 3 and thallium(I) has n = 1) was used. This was not the best fit, as could be expected, but it gave a reasonable i_d value.

It was initially thought that the tangents at the foot and top of the wave were to be drawn as indicated in Figure 9.6, but this produced meaningless results. It was difficult to decide where exactly to draw these tangents because no guidelines were given by Ružić and Branica (1969); these tangents were therefore drawn as shown in Figure 9.7. Using the tangents indicated in red (in Figure 9.7) the intercepts of the tangents with the x-axis, which represent the E_1 and E_2 values, were as follows: E_1 = 0.4056 V and E_2 = 0.4552 V.

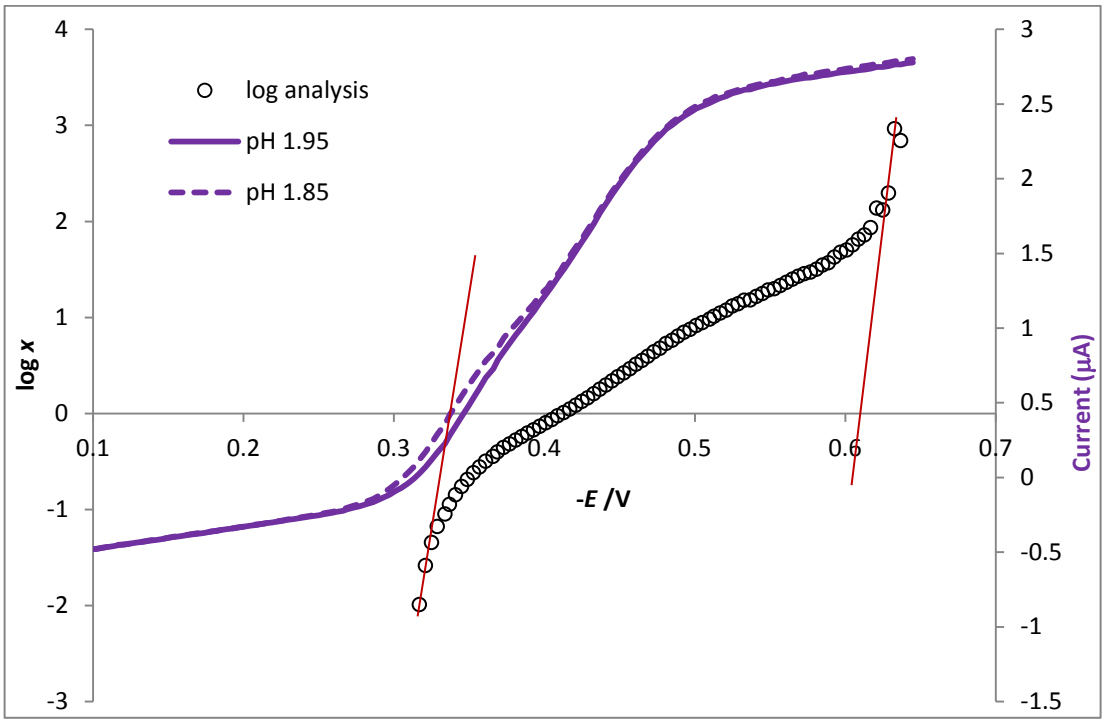


Figure 9.6 Comparison of the polarograms collected at pH 1.85 and 1.95, with the log plot drawn for that obtained at pH 1.95.

The ratio of diffusion currents, $m = i_{d1}/i_{d2}$, had to be evaluated from the point of inflection. In the paper by Ružić and Branica (1969) they suggest initially estimating the inflection point visually and then refining it through several iterations. It certainly was impossible to determine the inflection point as the point where the second derivative crosses the x-axis, as the values determined for the second derivative were all close to zero and fluctuated between positive and negative values in almost the entire potential range (0.35 to 0.62 V). The value of log *x* at the inflection point was visually estimated to be 1.18 (the purple point in Figure 9.7), thus m = 15.1. Since the values of i_d for both bismuth(III) and thallium(I) were known from the polarogram at pH 1.85 , it was decided to rather use those values to calculate m. This should be a good estimate for the polarograms at pH 1.95 since the ratio of the currents would not be affected by dilution and the diffusion rate of the species in solution should not change significantly. Therefore m = 0.904/ 1.637 =

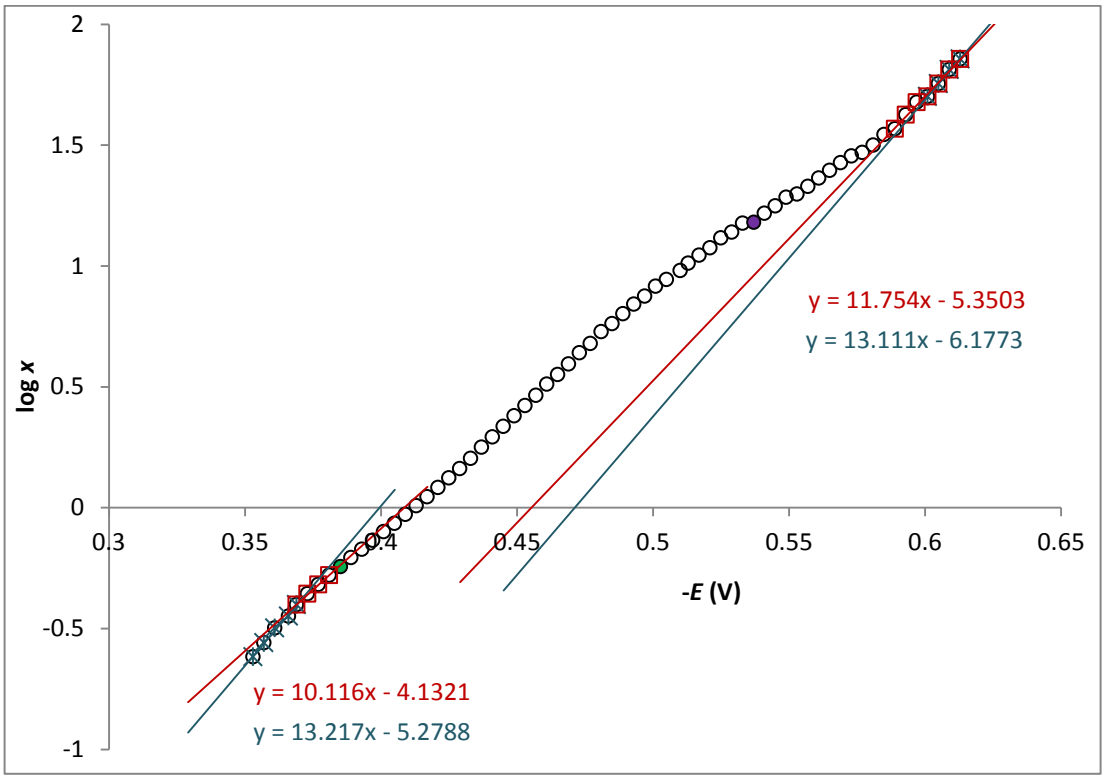


Figure 9.7 Log plot for the polarogram measured at pH 1.95 showing the tangents drawn using different data points, which were extrapolated to the x-axis to obtain E_k values.

0.55 and log m = -0.25, which corresponds approximately to the green point in Figure 9.7. Thus two very different results for m were found, with the latter value being more believable when looking at its position on the composite polarogram itself.

Substituting equation 9.6 or 9.8 into equation 9.7 and using m = 0.55, the $E_{1/2,k}$ values were determined as follows:

$$E_{\frac{1}{2},1} = E_1 - \frac{1}{a_1'} log\left[\frac{m+1}{m}\right] = 0.4056 - \frac{0.05916}{3}\log(2.82) = 0.3967\ V$$

$$E_{\frac{1}{2},2} = E_2 + \frac{1}{a_2'} log[m+1] = 0.4552 + \frac{0.05916}{1}\log(1.55) = 0.4665\ V$$

This determination of $E_{1/2,k}$ values only applies if the condition that $x_1 \geq x_2$ for all potentials holds, which would not be the case here. The slopes of the two waves then become a factor in the process used to calculate the $E_{½}$ values. If it is assumed that the slope of the bismuth wave (the first wave) is greater than the slope of the thallium wave (the second wave), then $E_{½,2}$ is still calculated as above. Taking into account that the slope of a polarogram is proportional to $n\delta$ and for the bismuth(III) wave $n\delta \approx 3 \times 0.5$ and for the thallium wave $n\delta \approx 1 \times 1$, this is a valid assumption. From the publication, it was never deduced how to calculate $E_{½,1}$ for these conditions. Plotting the graph of potential vs. pH for thallium(I) shows that the result obtained here (the red data point in Figure 9.8) did not follow the expected trend at all. This process was therefore aborted and a different approach was used to avoid the overlap of the two reduction waves.

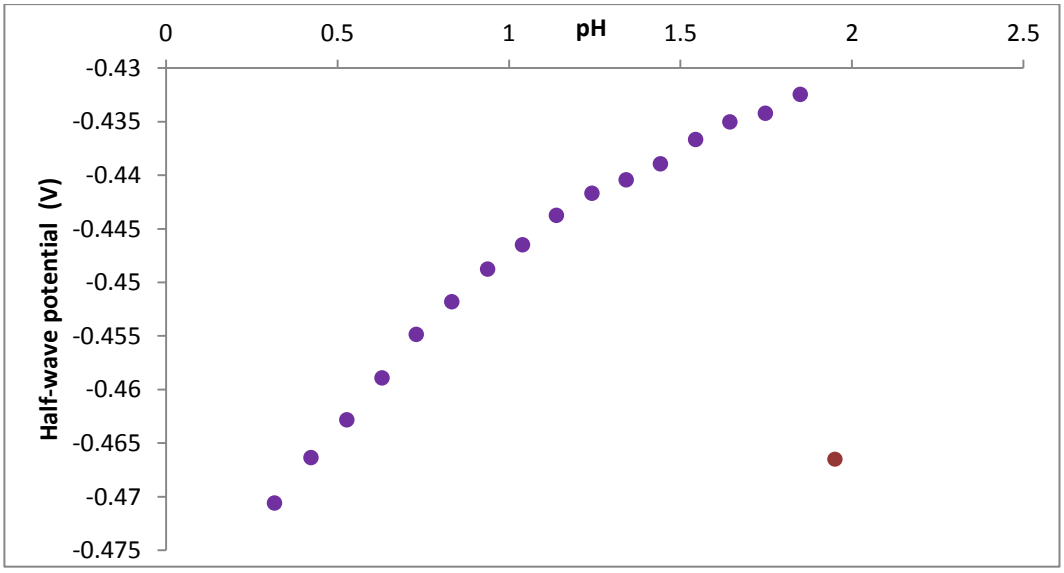


Figure 9.8 Half-wave potential vs. pH plot for thallium(I) obtained for resolved waves. The red data point indicates the next point in the series according to calculation based on the log analysis.

9.4.1.2 Determination of the Diffusion Junction Potential

Three separate experiments were conducted where bismuth(III) and thallium(I) were present but no ligand was added. These experiments were used to quantify and average the magnitude of the diffusion junction potential, which would be applied to the complexation experiments to compensate for E_j. Only the thallium(I) data were considered when calculating the diffusion junction potential in these experiments. The bismuth(III) ion has a high affinity for hydroxides and nitrates (affected by the large concentration of NO_3^- compared to Bi(III)), so shifts in the reduction potential of bismuth(III) with changing pH are not only due to changes in E_j, but also due to the constituents in the background electrolyte forming complexes with bismuth(III). The diffusion junction potential was calculated by subtracting each half-wave potential value for thallium(I) of smoothed (fitted) data below approximately pH 2, from the free metal ion potential for thallium ($E(Tl_{free})$). This difference was plotted vs. pH for each of the three experiments (Figure 9.9) and a polynomial (degree 3) was fitted to the data.

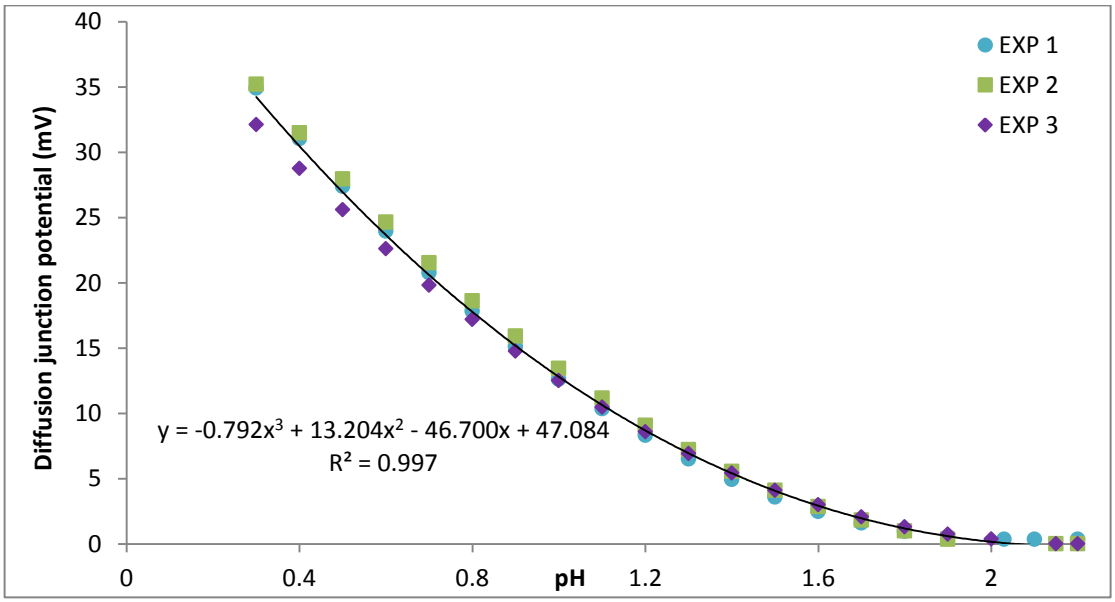


Figure 9.9 The average magnitude of the diffusion junction potential.

Since bismuth(III) already forms complexes in the ligand-free experiments it cannot be used together with the thallium(I) to create a model, as was done for cadmium(II) and thallium(I). In this case it was assumed that shifts due to changing ionic strength for bismuth(III) and thallium(I) were negligible and so the polynomial equation in Figure 9.9 represents the E_j for thallium(I) which is equivalent to that of bismuth(III).

The equation was used to calculate the diffusion junction potential at each pH value for the bismuth(III) data. This magnitude was added to the experimental half-wave potential data for bismuth(III), acquired at each pH to obtain the E_j corrected half-wave potential values.

9.4.1.3 Modelling the Free Bismuth(III) Ion Potential

In order to determine the uncomplexed or free Bi(III) potential, potential shifts due to the formation of complexes with hydroxides and nitrates had to be quantified and compensated for. Two free Bi(III) potentials were considered, one where complex formation with hydroxides is accounted for ($E(Bi_{free})_{OH}$) in solutions containing nitrates, and the other where complex formation with both hydroxides and nitrates is accounted for ($E(Bi_{free})_T$). In the former case both nitrate and hydroxide complexes are considered to form, but the shift due only to the formation of bismuth hydroxides is determined. In the latter case the overall shift due to both nitrate and hydroxide complex formation is determined. Both these values were required to estimate log β values due to limitations in the software used (Cukrowski, 2000) which cannot take competition of bismuth(III)-nitrate formation into account . The exact implications of using these two values will be highlighted in Chapter Ten. Figure 9.10 shows the possible nitrate and hydroxide complexes of bismuth(III) that form in solution. The nitrate complexes form at very low pH and the hydroxides begin forming at about pH 1. The two hydroxide species that form in appreciable amounts before Bi(III) precipitates in our experiments are $Bi(OH)^{2+}$ and $Bi(OH)_2^{+}$.

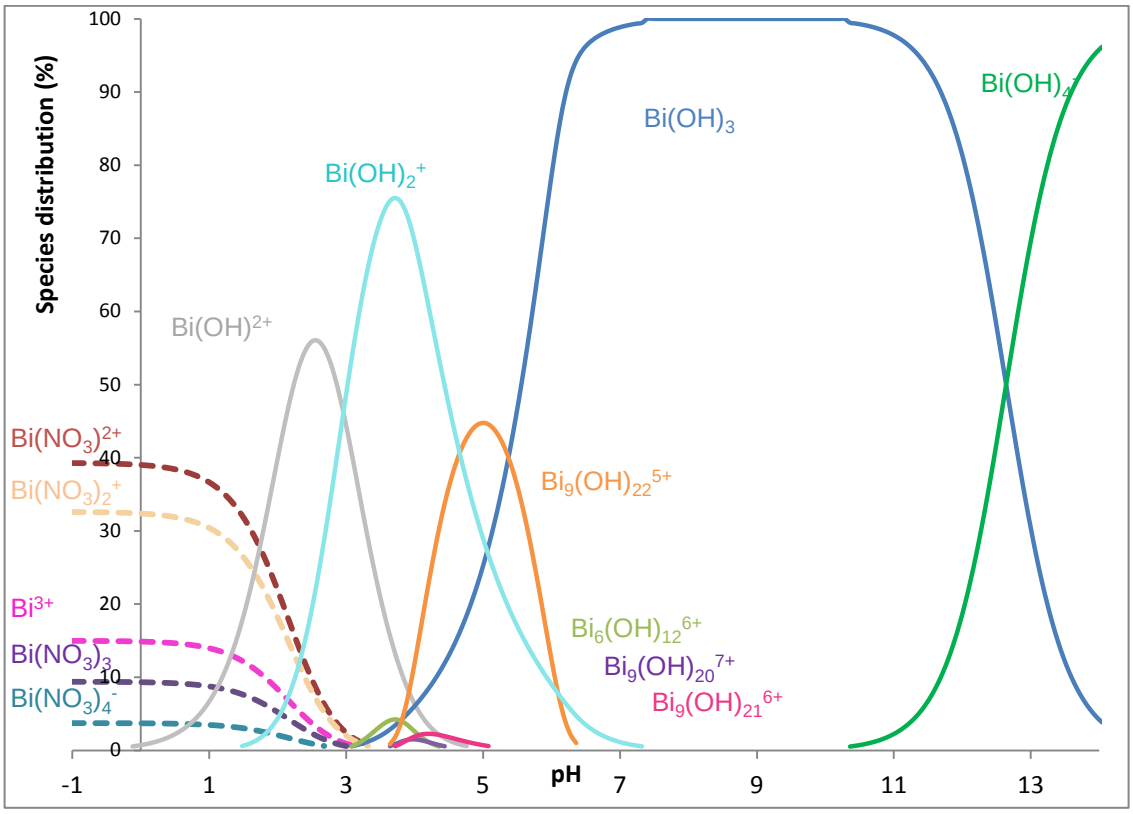


Figure 9.10 SDD showing the possible bismuth(III) nitrate and hydroxide species found in solution when $[NO_3^-]$ = 0.5 M and [Bi] = 1 x 10^{-5} M, using log β values given in Table 8.2 and 8.3. (The protonation constant for nitric acid was set as -5.00).

The 3D-CFC program was used to obtain the shift in potential due to nitrate and hydroxide complex formation with bismuth(III) at each pH at which polarograms were recorded, for each ligand-free experiment. The data required for calculation of these shifts includes: bismuth hydroxide formation constants (Table 8.2), Bi(III)-nitrate formation constants (Table 8.3), protonation constant for nitrate (set as -5), pK_w as 13.74, pH at which each polarogram was recorded (specific to each ligand-free experiment) and the concentration of nitrate and bismuth(III) in solution at the corresponding pHs (to account for dilution and it is specific to each ligand-free experiment).

The shift due to complexation with nitrates and hydroxides at each pH is calculated directly by the 3D-CFC program using equation 8.2. This shift is added to the corrected half-wave potential data to obtain the values which represent $E(Bi_{free})_T$. This data was smoothed by obtaining an average of the greatest number of points that allowed for a standard deviation of the average to be < 1. For some reason the first few points calculated at the lowest pHs are always overestimated compared to the rest and were not used to determine the average (see Figure 9.11). It is not due to an over correction of E_j since this was not seen when determining $E(Bi_{free})_{OH}$. This phenomenon may be due to the change in ionic strength which occurs predominantly below pH 2.

At each pH the 3D-CFC program also produced the percentage of each bismuth(III) hydroxide species present in solution. The concentration of each hydroxide species was then calculated by multiplying the percentage fraction of the hydroxide by the total Bi(III) concentration (taking dilution into account) at each pH. The concentration of all the hydroxides was summed at each pH and then subtracted from the total bismuth concentration (at each pH) in order to obtain the free bismuth(III) concentration, according to the following equation:

$$[Bi_{free}]_i = [Bi]_T - [Bi_x(OH)_y]_i \quad (9.9)$$

The concentration of free and total bismuth(III) at each pH was then used to calculate the shift in potential caused by the formation of hydroxides, using the equation derived by Cukrowski (Equation 2.5) and assuming that $I(Bi_{comp})_i = I(Bi_{free})_I$ since the hydrated and hydrolyzed species should not diffuse at significantly different rates, thus giving:

$$\Delta E_i(OH) = \frac{RT}{nF} ln \frac{[Bi_T]_i}{[Bi_{free}]_i} \quad (9.10)$$

This value was the added to the E_j corrected half-wave potential values for bismuth(III) at each pH to obtain the value of $E(Bi_{free})_{OH}$.

The above mentioned compensations, (i) shifts due to E_j, ii) shifts due to bismuth(III) hydroxide and nitrate formation to give $E(Bi_{free})_T$ and (iii) shifts due to bismuth(III) hydroxide only to give $E(Bi_{free})_{OH}$, have been plotted graphically in Figure 9.11. The very small shifts for hydroxide complexation at low pH can be related to the SDD (Figure 9.10) which shows the small amount of $Bi(OH)^{2+}$ there and then the increase in hydroxide formation with increasing pH. Nitrate and hydroxide complex formation is somewhat larger at low pH and this is due to the nitrate complexes that start forming already before pH 0.

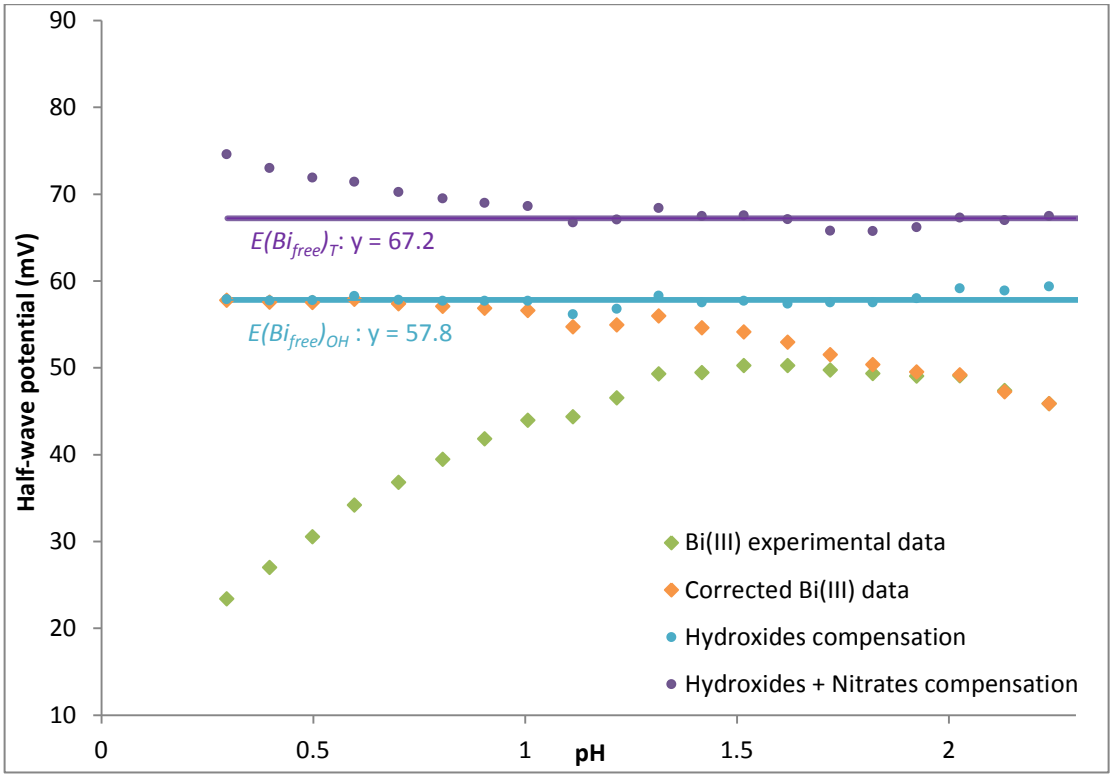


Figure 9.11 Experimental bismuth data and where E_j has been compensated for. The free metal ion potential of bismuth was calculated in two ways: by considering complexation with hydroxides only and by considering complexation with hydroxides and nitrates.

9.4.1.4 Model to Determine the Free Bi(III) Potential in Complexation Experiments

In the case of the cadmium(II)-ligand experiments the average difference between $E(Cd_{free})$ and $E(Tl_{free})$, determined from ligand-free experiments, was added to $E(Tl_{free})$ to determine $E(Cd_{free})$ in complexation experiments. For these data thallium(I) was not incorporated in the same experiment due to the overlap with bismuth(III) waves and thus another approach was devised.

In this case the difference was calculated between the $E(Bi_{free})$ values and the averaged half-wave reduction potential of bismuth(III) for the initial three overlapping waves that were collected before the titration was initiated. An example of how the differences were calculated has been applied to EXP 1 and is shown graphically in Figures 9.12 and 9.13. The differences found in each experiment were then averaged to create a model that could be used to calculate the two $E(Bi_{free})$ values in the ligand experiment.

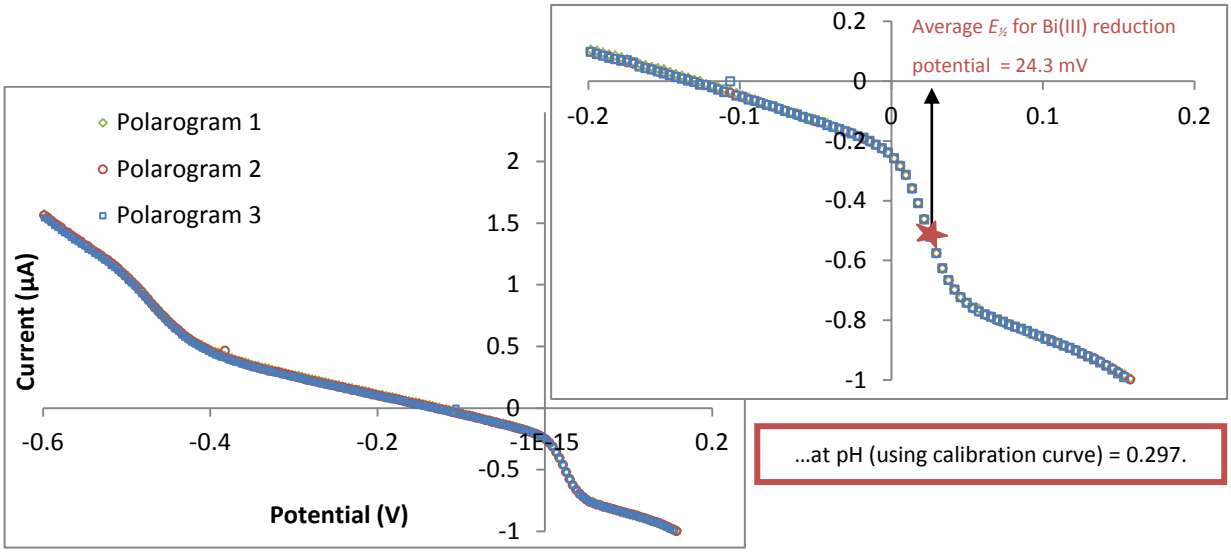


Figure 9.12 Overlap of the three polarograms that were collected manually at the start of EXP 1. The inset shows the average $E_{½}$ value for these three polarograms that were obtained at pH 0.297.

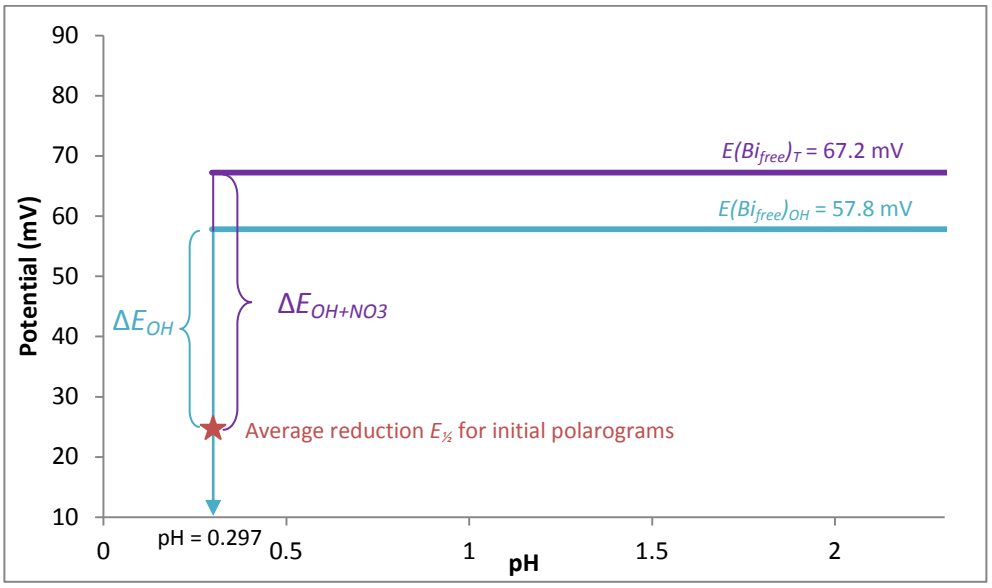


Figure 9.13 Calculation of ΔE_{OH} and ΔE_{OH+NO3} as the differences between $E_{½}$ and $E(Bi_{free})_T$ and $E(Bi_{free})_{OH}$, respectively.

The differences (ΔE_{OH} and ΔE_{OH+NO3}) obtained in each of the three experiments were averaged, as shown by Table 9.3. Even though the standard deviations of both the difference values were within experimental error, they were still not satisfactory. This average is not actually scientifically correct because the pH at which the three overlapping polarograms were recorded, were not the same for each of the three ligand-free experiments and varied by 0.005 pH units. Thus, the extent of E_j as well as complex formation with nitrates and hydroxides will vary slightly. Further error would then also be introduced when this data is related to the ligand experiment which would again have initial polarograms obtained at a different pH. Consequently, to improve upon this method, the experimental half-wave potential vs. pH data for bismuth(III) (for the ligand-free experiments) was fitted with a quadratic function up until a pH of about 1.3, as shown in Figure 9.14 for EXP 1.

Table 9.3 The differences between the free metal ion potentials and the average half-wave potential of Bi(III) from the initial polarograms.

EXP	ΔE_{OH} (mV)	ΔE_{OH+NO3} (mV)
1	33.5	42.9
2	34.7	43.8
3	36.4	44.6
Average	34.9 ± 1.4	43.8 ± 0.9

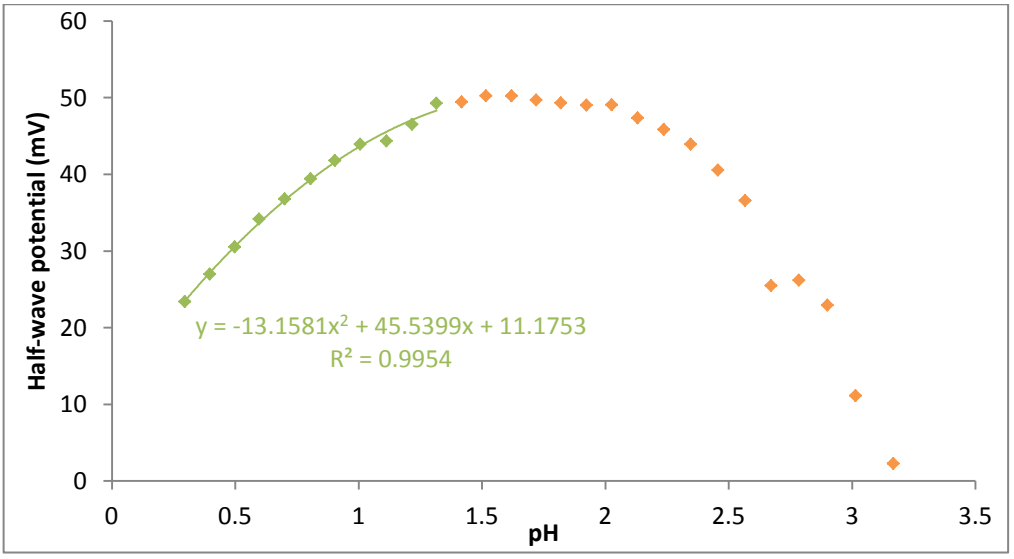


Figure 9.14 The quadratic function obtained when fitting the half-wave potential vs. pH data up until pH 1.3 for EXP 1.

In the complexation experiment it was found that the pH of the solution before ligand was added (where the initial polarograms were collected) was 0.345. Thus using the quadratic equations determined for each ligand-free experiments, the **difference** between the potential at pH 0.345 and both $E(Bi_{free})$ values were then calculated. Table 9.4 shows the values obtained for each of these differences for all three ligand-free experiments. This also meant that values from these three experiments could be averaged meaningfully, which is indicated by the improved standard deviations.

Table 9.4 The calculated $E_{½}$ values at pH 0.345, together with the differences calculated between $E_{½}$ and the free metal ion potentials for each ligand-free experiment. The E_j = 32.5 mV at pH 0.345, according to the quadratic function in Figure 9.9.

EXP	$E_{½}$	ΔE_{OH} (mV)	ΔE_{OH+NO3} (mV)	$E(Bi_{free})_T - E(Bi_{free})_{OH}$ (mV)
1	25.32	32.5	41.9	9.4
2	23.20	31.9	41.0	9.0
3	26.73	33.1	41.4	8.2
	Average	32.5 ± 0.6	41.4 ± 0.5	8.9 ± 0.6

9.4.1.5 Solving for $E(Bi_{free})$ in a Complexation Experiment using the "Difference" Models

The experiment for complex formation with EDTA was conducted with Bi(III) only and the polarograms were fitted using Equation 2.1 and the δ value was allowed to vary. Complex formation was evident by the huge initial potential shifts. The δ value obtained from curve fitting indicated that the reductions were irreversible and that the extent of irreversibility increased with increasing pH (see Figure 9.15).

In order to apply methodologies to determine formation constants, reversible half-wave potentials would need to be determined from these irreversible waves. The half-wave potential is dependent on the degree of reversibility, however the diffusion limited current is not. The method described by Cukrowski and Zhang (2004) for determining reversible half-wave potentials from quasi-reversible waves was attempted on the irreversible waves measured here.

Cukrowski and Zhang (2004) conducted polarographic experiments with cadmium(II) and glycine using similar polarographic experiments as to what we have used. On observation of their fitted data it was found that the δ value of the polarographic

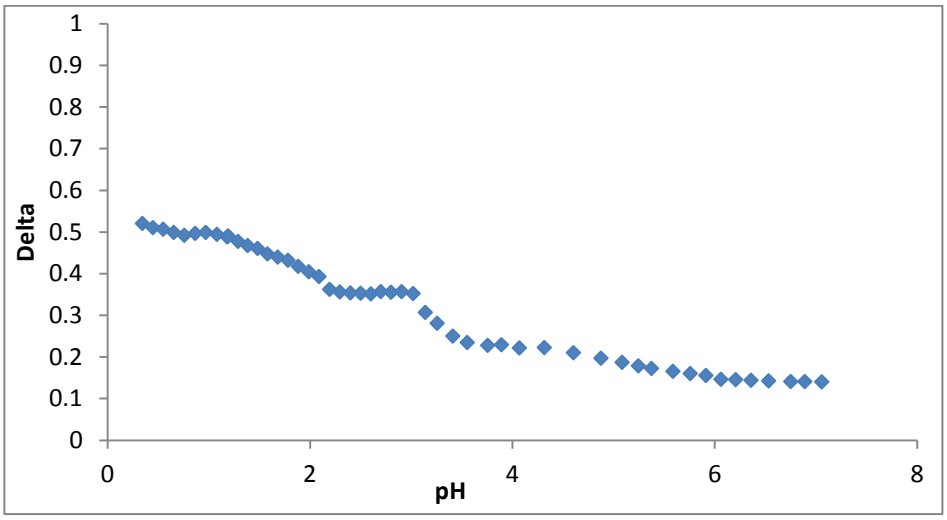


Figure 9.15 The δ value as a function of pH for Bi(III) during a ligand experiment where [L]:[M] = 100.

Cd(II) wave before ligand was added was very close to 1 (0.97), indicating a reversible reduction, but after the ligand was added, the δ value of the cadmium(II) waves decreased to about 0.8, indicating a quasi-reversible reduction process. They therefore aimed to obtain the reversible half-wave potential in the latter case. In order to do this, they initially fitted the quasi-reversible wave as before (using Equation 2.1). They then removed some points along the slope of the wave, leaving the foot of the wave and the top of the wave where i_d had been reached. They then refitted this data by using the value of I_d obtained before and setting the delta value to 0.97 (as for the reversible process before the ligand was added), but allowing the $E_{½}$ values to vary. In this case they found that the difference between the reversible and quasi-reversible $E_{½}$ values was 3 mV. The log β values were determined using these reversible $E_{½}$ values and they were found to be almost identical to those in literature obtained using GEP (glass electrode potentiometry).

It was attempted to see whether a similar strategy could be applied to the irreversible waves here. It was impossible to obtain the fully reversible $E_{½}$ values in

this case, but the idea was to determine $E_{½}$ values at the same value of δ throughout. To determine formation constants it is the shift in half-wave potential ($E(M_{free})$ - $E(M_{Comp})$) that is used, so if these values were all calculated at a fixed δ value then it was then assumed that the shift could be used to obtain formation constants in the same way as before.

All curves were fitted as normal and their curve fitting parameters were recorded. Data points on the slope of the wave were removed and then it was refitted, keeping the I_d value, as well as the background values *a*, *b*, *c* and *d,* constant and fixing δ to 0.4. This value of δ was chosen because it is a rough average of the δ values between pH 0.3 and 3, the pH range before the degree of irreversibility changed too significantly. The half-wave potential was thus allowed to vary in accord with the remaining values that were fixed. Points of the experimental wave were removed in such a way so that the base of the polarogram was still fitting correctly and the diffusion limited current was reached, as suggested by Cukrowski and Zhang (2004) (see Figure 9.16). An example showing the experimental wave taken just before the EDTA was added (which was still reversible and had a delta value of 0.988), and the wave at a fixed δ of 0.4 is shown in Figure 9.16 (the points that were removed are indicated with blue crosses). Once the procedure had been applied to each Bi-EDTA polarogram the E_j could be compensated for (see Figure 9.17). This was done by calculating the magnitude of the E_j at each pH point using the equation of the E_j model (Figure 9.9). Data obtained only up until a pH of 3 has been presented as beyond this pH the degree of irreversibility changes dramatically.

The initial polarograms that were collected before ligand was added were completely reversible (average $E_{½}$ = 30.0 ± 0.2 mV), but in order to be used in conjunction with the new $E_{½}$ values where δ was forced to 0.4, they too had to be fitted in the same way. The average half-wave potential (with δ = 0.4) was

calculated to be –16.4 ± 0.5 mV. The shift due to the change in extent of reversibility is large, differing by 46.4 mV (also shown in Figure 9.16).

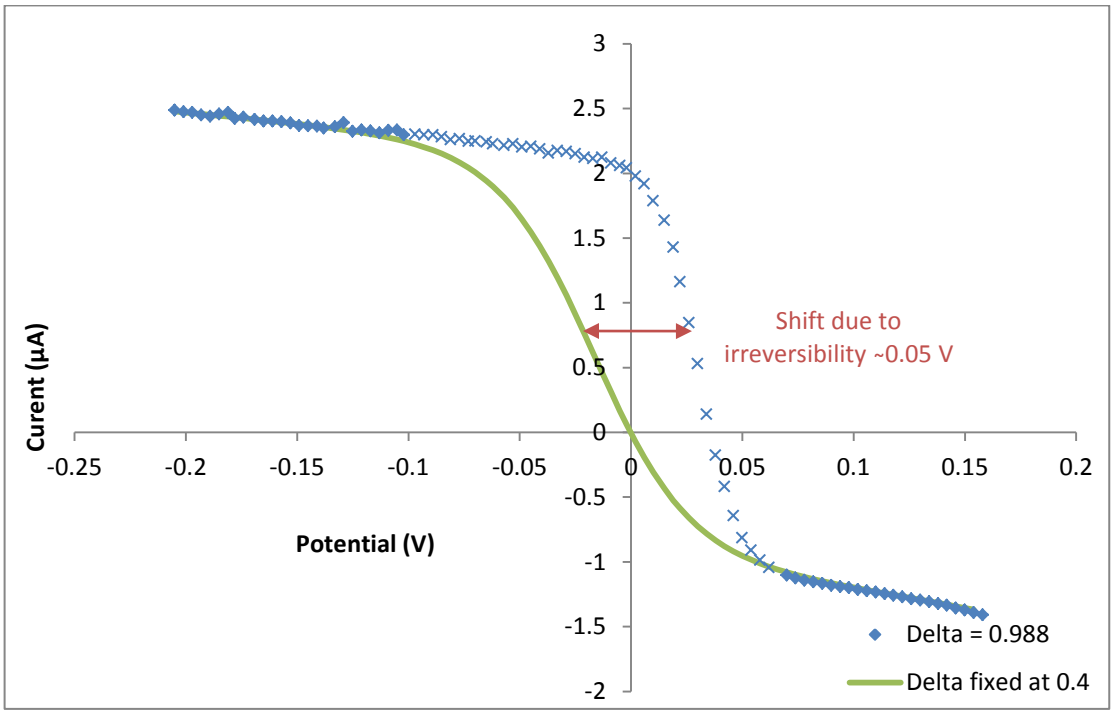


Figure 9.16 Comparison of the experimental polarogram (where δ = 0.988) and the polarograms fitted by forcing δ to 0.4. The blue crosses represent the points that were removed when fixing δ to 0.4.

The next step was to obtain the free metal ion potential for Bi(III) which required the application of the "difference" models. The differences, as determined in Table 9.4, were added to the average reduction half-wave potential of the initial polarograms (–16.4 mV indicated in Figure 9.18 by an orange diamond) to give the two $E(Bi_{free})$ values for this ligand experiment. The resulting free metal ion potentials that are needed for solving formation constants were calculated to be: $E(Bi_{free})_{OH}$ = 16.2 mV and $E(Bi_{free})_{T}$ = 25.1 mV.

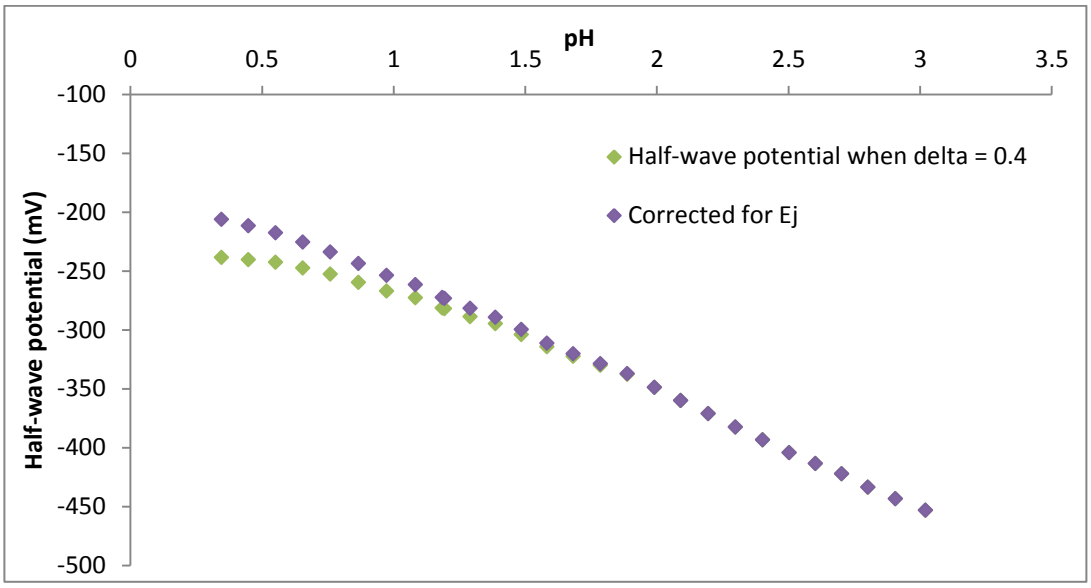


Figure 9.17 Half-wave potential for Bi(III) where δ is fixed at 0.4 throughout the pH range, together with the compensation of E_j.

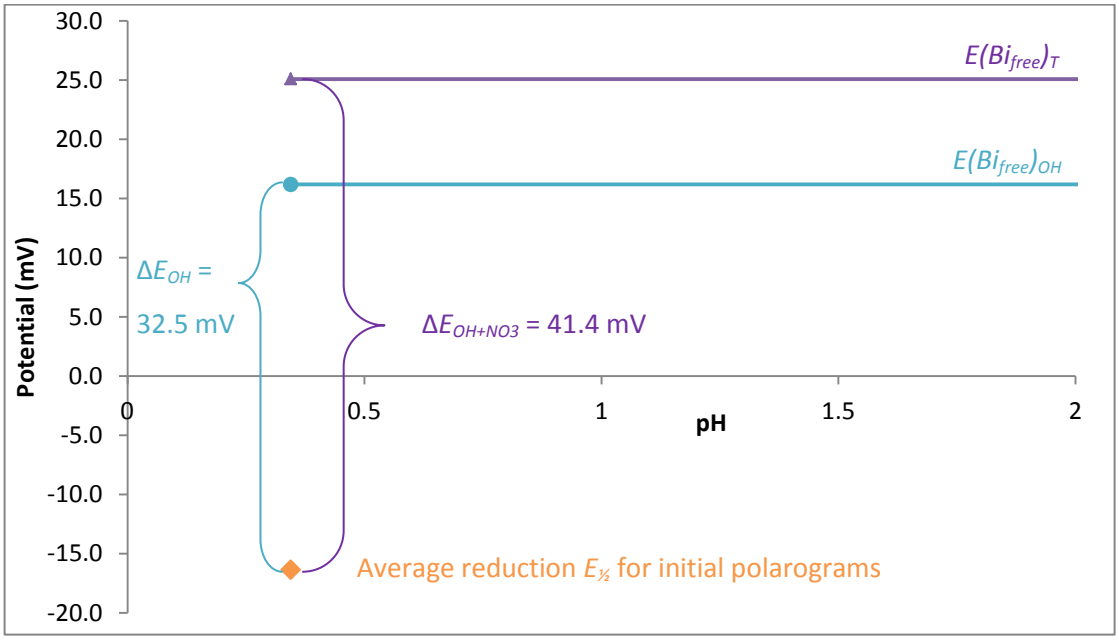


Figure 9.18 Graph showing the calculation of the free bismuth potentials using the difference models determined in Table 9.4.

Immediately after ligand was added to the solution a large shift in potential occurred and after correcting for the E_j it was found that the initial half-wave potential (at pH 0.345) was -206 mV. This means that the shift due to complex formation was 222 mV and 231 mV when using $E(Bi_{free})_{OH}$ and $E(Bi_{free})_T$, respectively. These shifts are huge, which indicate that complexation of Bi(III) with EDTA was very strong, as expected for such a ligand. In this case it can be safely said that there is no chance that nitrate can be a competing ligand and so the $E(Bi_{free})_{OH}$ value can be ignored when calculating formation constants. In order to solve the formation constants the 3D-CFC program was used as before, entering the necessary data (see Table A9.1 in Appendix A for basic experimental conditions). The protonation constants for EDTA given in Table 9.5 and log β values for bismuth(III) hydroxides in Table 8.2 were used. The half-wave potentials at δ = 0.4 were compensated for E_j and the data were entered into the program, and $E(Bi_{free})_T$ was used to calculate formation constants. These data could not be fitted using only the MLH and ML species (species set 1) as literature suggests. The values are given in Table 9.6 and correspond to the graph in Figure 9.19, but these values were not refined. It was necessary to add a complex to the species model in order to improve the fit above pH 2, so even though we know that EDTA would not form a ML_2 complex, it was incorporated into the model so that the log β values could be refined (species set 2). Formation constants for this species set are also given in Table 9.6, and the corresponding CCFC is given in Figure 9.19. In comparison to the log β values in literature (26.5 at 1 M ionic strength (Martell, Smith and Motekaitis, 2004)) the values that were calculated here were too high.

The fact that the ML_2 allows for a refinement does not mean that it is formed in solution. From literature we know that this is extremely rare. Only one example of a ML_2 EDTA crystalline complex, with neodymium, has been reported, (REFCODE: FAFSAH, (Wang, Jin and Zheng, 2000)) and no atomic coordinates were given for this

Table 9.5 Protonation constants of EDTA at 25 °C.

Equilibrium Equation	**Log *K***	**Ionic strength (M)**
[HL]/[H][L]	8.86	0.5
$[H_2L]/[H][HL]$	6.10	0.5
$[H_3L]/[H][H_2L]$	2.69	0.1
$[H_4L]/[H][H_3L]$	2.00	0.1
$[H_5L]/[H][H_4L]$	1.5	0.1
$[H_6L]/[H][H_5L]$	0.0	1.0

Table 9.6 Formation constants for the bismuth(III)-EDTA system when using species set 1 (MLH and ML) and species set 2 (MLH, ML and ML_2) and $E(Bi_{free})_T$. Refinement on species set 1 was not possible thus standard deviations cannot be quoted.

Complex	**Species set 1**		**Species set 2**	
	Log *β*	**Std Dev**	**Log *β***	**Std Dev**
MLH	33.4	-	33.08	0.06
ML	33.05	-	33.28	0.02
ML_2	-	-	47.89	0.02
OVERALL FIT	-		9.40	

structure. The apparent absence of ML_2 crystal structures is probably because of size and shape of the EDTA ligand. A slope analysis of these data between pH 0.3 and 3 was therefore considered and is shown in Figure 9.20. The prediction of the reduction reactions that could occur in each pH range together with the calculated slopes is given in Table 9.7.

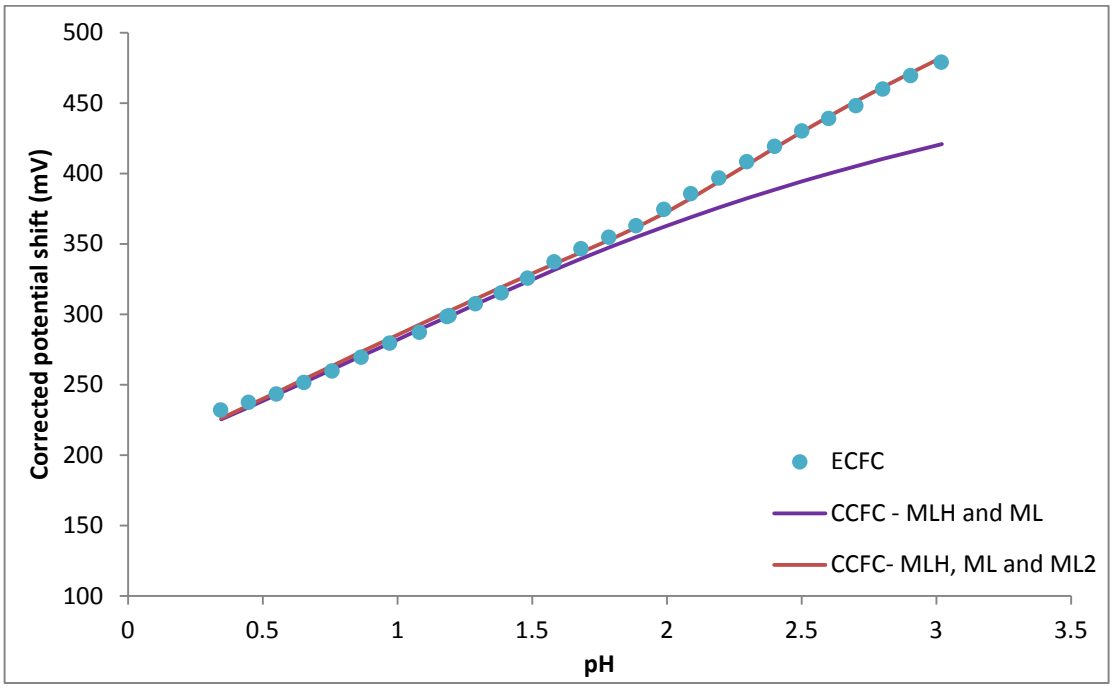


Figure 9.19 Comparison of CCFCs obtained using $E(Bi_{free})_T$ and the MLH and ML species set (purple) and the MLH, ML and ML_2 species set (red). The log β values for the MLH and ML species set (Table 9.6) did not refine.

Table 9.7 Possible reduction reactions in the given pH regions with their respective calculated slopes.

pH range	Possible reduction reactions	Calculated slope
0 < pH < 1.5	$BiLH_2^+ + 3e^- + 3H^+ \rightleftharpoons Bi^0 + H_5L^+$	60
	$BiLH + 3e^- + 4H^+ \rightleftharpoons Bi^0 + H_5L^+$	80
	$BiL^- + 3e^- + 5H^+ \rightleftharpoons Bi^0 + H_5L^+$	100
1.5 < pH < 2.0	$BiL^- + 3e^- + 4H^+ \rightleftharpoons Bi^0 + H_4L$	80
2.0 > pH > 2.69	$BiL^- + 3e^- + 3H^+ \rightleftharpoons Bi^0 + H_3L^-$	60

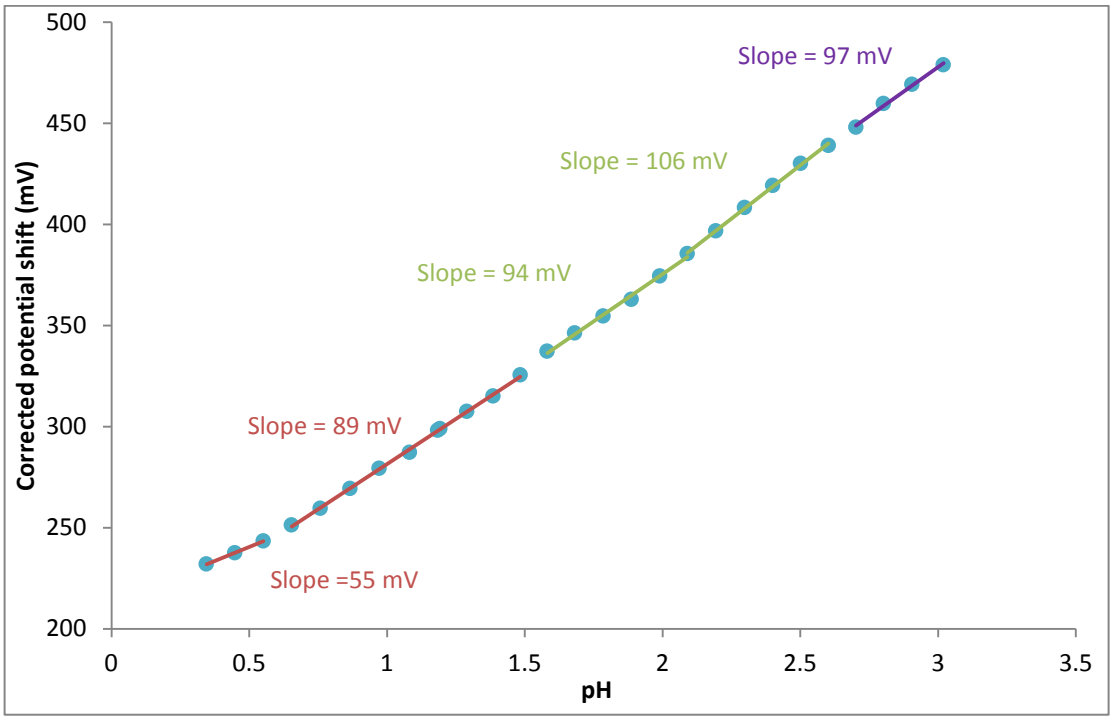


Figure 9.20 Slope analysis performed on the ECFC.

A slope of 89 mV between pH 0.6 and 1.5 would indicate a combination of MLH and ML species in solution. Above pH 2 the slope is expected to steadily decrease if the ML species is present as the extent of protonation of the ligand decreases and the slope is calculated using the ratio of the number of protons to the number of electrons involved in the reduction reaction. From Figure 9.20 the slopes in this region are 106 mV and 97 mV which shows that the shifts are most likely exaggerated.

At pH 2.090 the δ value for the experimental data was 0.40, above this pH the δ value was lower (0.362 - 0.356 for pH 2.194 - 2.906) and below this pH the δ value was higher (0.40 - 0.52 for pH 2.090 - 0.345). This means that when fixing δ to 0.4 for the data above pH 2.090, the $E_{½}$ values were greater than for the actual polarograms and similarly for the data below pH 2.090, the $E_{½}$ values were smaller than for the actual polarograms. Also, obtaining the free metal ion potential

required the $E_{½}$ values from polarograms before ligand was added to the system (where reductions was still reversible) to be calculated. This $E_{½}$ value therefore had to be adjusted from having a δ value of 1 to 0.4.

The huge differences between the half-wave potential vs. pH data and the $E(Bi_{free})_T$ value indicates very high log β values were expected, but those determined here were significantly higher than literature values. To obtain values comparable to literature meant that the potential shift would need to be approximately 140 mV smaller than that observed in our experiment. This raises questions about using irreversible waves to determine potential shifts for calculating formation constants.

It appears that for reduction of these complexes, not only changes to the shape of the wave are apparent, but for such irreversible reductions the onset of the reduction itself is shifted significantly more negative than would be expected for the reversible case. Hence, the method that was adapted from Cukrowski and Zhang (2004) clearly cannot be applied to irreversible processes.

The raw data were considered again as the irreversibility of this Bi(III)-EDTA system seemed to be the route problem. For the system to maintain reversibility, the rate of charge transfer must be high enough to allow the concentrations of reactants and products at the electrode surface to maintain their equilibrium values. This depends on factors like timescale of the experiment, rate of diffusion and the heterogeneous rate constant. A system can have a gradual transition into irreversible behaviour simply due to the timescale of an experiment. (Gileadi, 2011)

Considering the bonding arrangement of the EDTA ligand, the kinetics of the reduction process is most likely the cause. When the bismuth ion is complexed to EDTA and a cage-like structure is formed, it becomes more difficult to transfer electrons to the metal ion centre, especially three electrons simultaneously, and hence the magnitude of the heterogeneous rate constant is small.

A comparison of theoretical polarograms by Gileadi (2011) shows why the method by Cukrowski and Zhang (2004) failed for our data. Gileadi (2011) plotted polarograms calculated for a) different values of the standard heterogeneous rate constant at a fixed measurement rate (Figure 9.21 a) and then b) at a fixed standard heterogeneous rate constant and variable time of measurement (Figure 9.21 b)). As the rate constant in Figure 9.21 a) was decreased so the degree of reversibility decreased, as was found for when the period of time for measurement in Figure 9.21 b) was decreased.

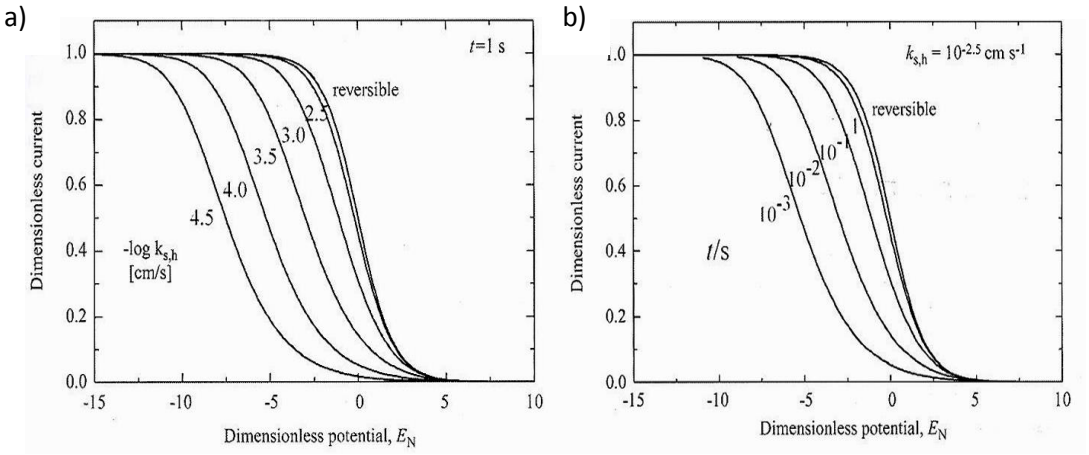


Figure 9.21 Polarograms showing the effect of varying a) the standard heterogonous rate constant and b) the timescale of a measurement on the degree of reversibility of the process. This figure has been reproduced from Gileadi (2011).

From these plots it is seen that the magnitude of the diffusion limited current does not change. Additionally, the current at the foot of the wave for the different polarograms overlap when there is only a slight departure from reversibility (as in the case of Cukrowski and Zhang (2004)). For larger departures from reversibility it is apparent that there is no longer this overlap (as we had assumed) and that the onset of reduction occurs at more negative potentials. Thus the assumptions we

made in fitting the polarograms where δ was fixed to 0.4 were incorrect, which explains the large shifts in potentials and the obscure species model.

9.4.2 Crystallographic Studies

9.4.2.1 Analysis of the Crystal Structure of catena((μ_3-Hydrogen-ethylenediaminetetra-acetato)-bismuth(III)) dihydrate

Bi(EDTA-H) crystallized in the Cc space group, having eight molecules within the asymmetric unit (Z = 4). The defining feature of this polymeric structure is the protonated carboxylate oxygen. Without this proton charge neutrality would not be maintained. One EDTA molecule is bonded to a single bismuth metal ion which represents the monomer within this structure. Two water molecules are associated with each monomer. The molecular structure and numbering scheme are shown in Figure 9.22. The bismuth(III) metal centre has a coordination number of eight which is typical for this large, acidic metal ion. Four carboxylate oxygens and two nitrogens from a single EDTA molecule are bound to the Bi(III) centre, which is then polymerized to a second and third EDTA molecule via O4 and O8. All five of the chelate rings associated with this structure are five-coordinate. Three of the four N,O' bidentate bite angles of the chelate rings are similar, having an average value of 69.2 ± 0.4 °. The fourth N,O' bidentate bite angle (O5-Bi-N2) is significantly smaller (63.80 °) which may be due to the fact that it is this carboxylate that is protonated.

Long chains extending in the b- and c-direction are created by polymerization from O4 and O8 respectively, as shown in Figure 9.23. Hydrogen bonding is responsible for layering these chains in the a-direction. The water molecules act both as hydrogen bond donors and acceptors. They are linked to each other, as well as to two separate carboxylate oxygens. O6 is a H-bond donor to O1W and O3 is a H-bond acceptor of O2W. A view down the b-axis shows how these hydrogen bonds link together rows of polymerized Bi(EDTA-H) molecules, where the orientation of

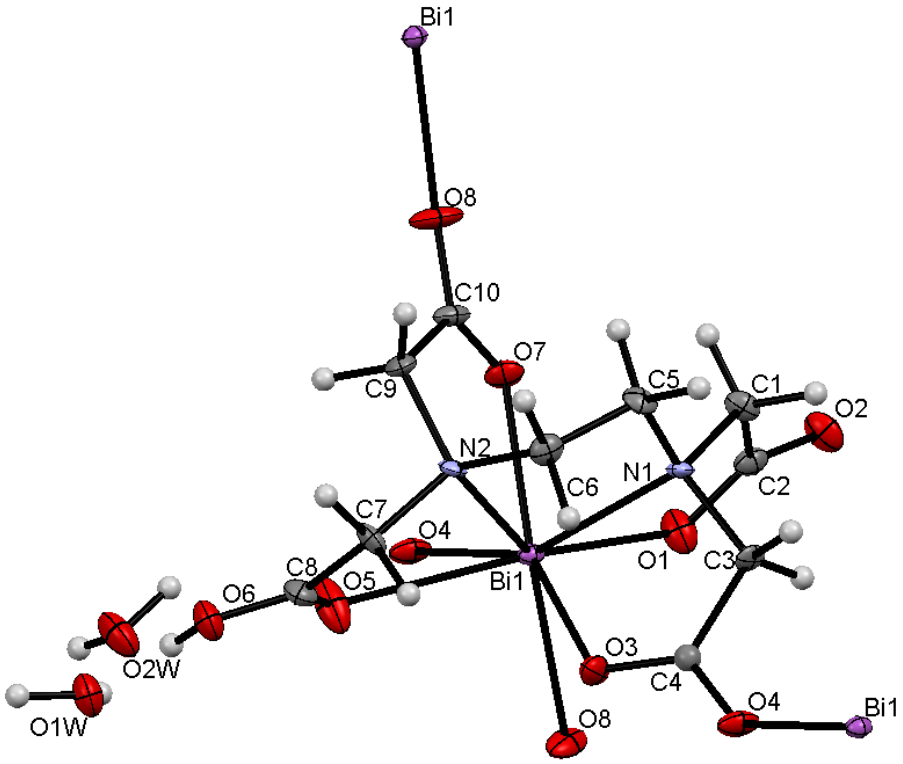


Figure 9.22 ORTEP diagram showing the structure of Bi(EDTA-H) at the 50% probability level. Labels of hydrogen atoms have been omitted for clarity.

each Bi-EDTA molecule is the same in each layer, and each layer is then offset by a quarter of the distance of the unit cell edge of the c-axis (Figure 9.24).

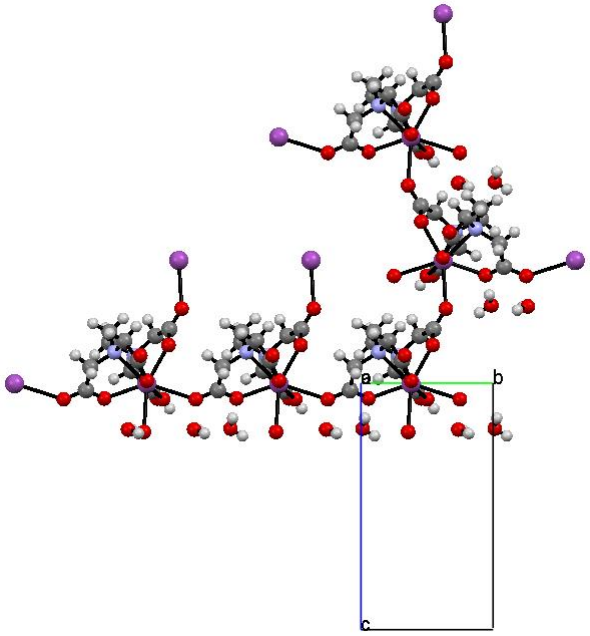


Figure 9.23 Polymerization occurring in two directions (b and c), as seen down the a-axis.

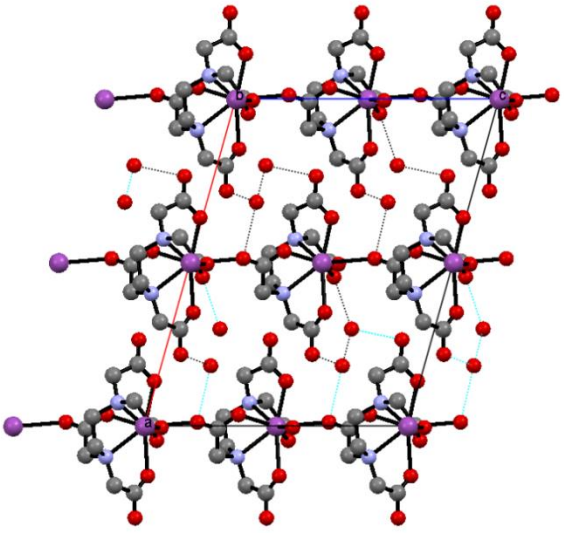


Figure 9.24 Water molecules responsible for linking polymerized chains together by hydrogen bonding in the a-direction, as seen down the b-axis. Hydrogen atoms have been omitted for clarity.

9.4.2.2 A Comparative Study with Literature Structures

As mentioned previously, this crystal structure was determined before by Summers, Abboud, Farrah and Palenik (1994) (REFCODE: HAYPEC). The way in which they obtained crystals was very similar to the way in which we did – heating a mixture of EDTA and water until it dissolved. However, they introduced the Bi(III) ion in the form of $(BiO)_2CO_3$ which was added to the solution in small increments. Another small difference was that they collected the diffraction pattern of their single crystal at room temperature, hence the difference in cell volumes. Table 9.8 shows that the unit cell of HAYPEC and our structure is identical. Included in this table is SBEDTA10 (Shimoi *et al.*, 1980) - an antimony analogue to our Bi(EDTA-H) complex, to highlight the differences in the unit cell parameters. The general formula of $C_{10}H_{13}N_2O_8M{\cdot}2H_2O$ represents all these complexes when M = Sb or Bi. The antimony structure was therefore interesting to use as a comparison to the characteristics found with our structure. Unfortunately hydrogen positions were not determined for SBEDTA10, but another paper which describes the same structure which contained the hydrogen atoms was found (Li and Zhong, 2014). This structure is only 5-coordinate and the protonated carboxylate is the one which is not bound to the metal centre. Li and Zhong (2014) found a pattern in the C-O bond lengths where the coordinated oxygen of a carboxylate group had a longer C-O bond length to that of the uncoordinated oxygen, and according to them it is this coordination that enhances the acidity of the complex. In the structure that we produced with Bi(III) all the C-O bond lengths were similar (even that of the protonated group) with an average of 1.25 ± 0.02 Å. For HAYPEC the same observations were made, with an average C-O bond distance of 1.25 ± 0.03 Å.

The CSD also contained HAYPEC02 (R.L. Davidovich, 1998) which is a polymorph of HAYPEC (and its equivalent HAYPEC01, by other authors (Shkol'nikova *et al.*, 1994)).

The coordination around the bismuth(III) metal centre is equivalent for the polymorphs.

Table 9.8 Comparison of the Bi(EDTA-H) crystal $(C_{10}H_{13}N_2O_8Bi)_n,2(H_2O)_n$ from this work and that grown by Summers, Abboud, Farrah and Palenik (1994). An antimony analogue (SBEDTA10) has been included for comparison.

Characteristic		This Work	Literature (HAYPEC)	SBEDTA10
Space group		C c	C c	P b n 2_1
Length (Å)	a	17.0460(8)	17.196(2)	10.98(2)
	b	6.8367(3)	6.837(1)	18.496(4)
	c	13.2314(6)	13.277(2)	7.341(9)
Angles (°)	α	90	90	90
	β	105.637(1)	105.74(1)	90
	γ	90	90	90
Cell Volume		1484.9	1502.43	1490.85
Z		4	4	4
R factor		2.67	2.24	3.6
Temperature (K)		173	273	
Recryst. Solvent		water	water	

Other similar structures were also found in the CSD where EDTA is chelated to a number of different metal ions, namely, cadmium(II), cobalt(II), lead(II), copper(II), tin(II), nickel(II), gallium(III), gadolinium(III) and terbium(III) to mention a few. Some of these structures were coordinated with only 5 coordination sites of EDTA, but most were with all 6. Of these, none exhibited the protonated oxygen of the carboxylate group binding to the metal centre as in our structure.

9.5 RELATING SOLUTION SPECIES TO CRYSTALLINE COMPLEXES

The protonated bismuth(III)-EDTA complex that was crystallized in this work is equivalent to an MLH species existing in solution. Karadakov and Ivanova (1976) (in Stavila, Davidovich, Gulea and Whitmire (2006)) studied Bi(III)-EDTA complexation spectrophotomerically and found that the MLH species existed between pH 0.6 and 1.4 and the ML species between pH 1.5 and 10. This is very much dependent upon the solution conditions, as we have demonstrated before using SDDs plotted at various conditions. Unfortunately the article by Karadakov and Ivanova (1976) was not available and so the actual experimental conditions are unknown. We produced a crystal structure of the MLH species from a solution at pH 0.38, which is lower than the range predicted by Karadakov and Ivanova (1976), which may be due to differences in the experimental conditions, or perhaps Karadakov and Ivanova (1976) simply did not carry out spectrophotometric studies at a pH value this low.

Unfortunately formation constants for this system were not determined in this work and using the values suggested by the NIST database (Martell, Smith and Motekaitis, 2004) was not so straightforward as the values it provides for the MLH and ML species were not obtained under the same conditions. It was therefore decided to use the log β value for ML of 25.68, together with the MLH log K value of 0.9 (Powell and Pettit, 1997) which were obtained from the same spectrophotometric experiments by Karadakov and Ivanova (1976). Species distribution diagrams were therefore plotted using log β values of 26.58 (= 25.68 + 0.9) and 25.68 for the MLH and ML species, respectively, at conditions used for polarographic experiments and crystal growth experiments. The SDDs are surprisingly very similar, and were plotted together in Figure 9.25 to allow for comparison. The pH at which the MLH crystals were formed (0.38) matches that which the SDD predicts (see Figure 9.25).

The reason for the similarity between the SDDs plotted under solution and crystal growth conditions is due to the phenomenal ability of this ligand to form complexes,

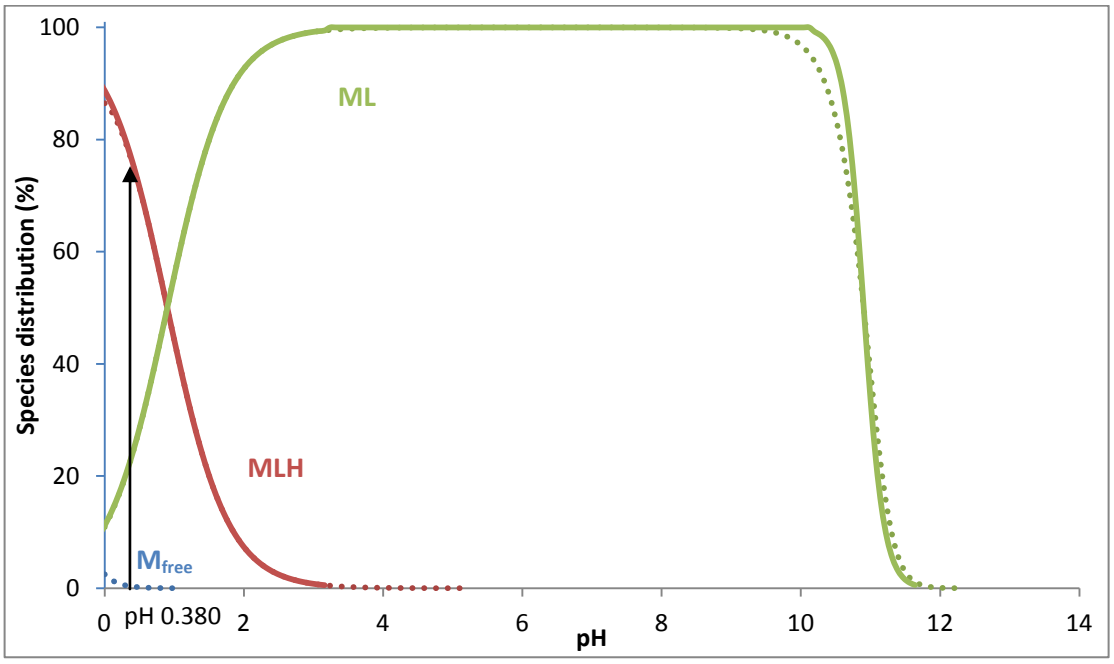


Figure 9.25 SDD was plotted using the MLH and ML species set with log β values of 26.58 and 25.68, respectively. Solid lines represent [L]:[M] = 100 and [Bi] = 5 x 10^{-3} M (polarographic solution conditions) and dotted lines represent [L]:[M] = 1 and [Bi] = 0.1 M (crystal growth conditions). Bismuth(III) hydroxide species have been omitted for clarity.

and also the fact the stoichiometry of the metal-ligand complex is not affected by the [L]:[M] ratio of the solution is due to EDTA forming only 1:1 metal-ligand complexes.

9.6 CONCLUSIONS

Irreversibility of the reduction of the Bi(III)-EDTA complexes was the main hurdle when studying this metal-ligand system by polarography. The fact that the EDTA ligand forms a large cage-like structure which holds the bismuth metal ion at its centre certainly affects the kinetics of the reduction reaction. Although this metal-ligand system was found to be reduced irreversibly in these experiments it does not mean that the process is always irreversible, and the choice of background electrolyte can even play a role here. Kornev and Trubachev (1987), Sochevanov and Volkova (1969) and Miklos and Szeged (1961) all studied this system using polarography (unfortunately they did not publish in English so the conditions they used are unknown). Probably GEP or spectrophotometric methods would be better choices in techniques for obtaining stability constants for this system.

The dependence of the wave-form on the reversibility of the reduction process has been highlighted in this research. The method described by Cukrowski and Zhang (2004) is only applicable to quasi-reversible systems. Perhaps a restriction should be set where this method is to be applied to polarograms with δ value great than a certain magnitude only.

Obtaining a crystal structure for this system was not too difficult because of the high solubility of the EDTA salt that was used in crystal growth experiments and the fact that such stable Bi(III)-EDTA complexes are formed. The crystalline MLH complex was formed in solution at a low pH of 0.38 which matched the pH at which the solution data predicted it to exist. The structure was found to be polymeric in nature which is typical for EDTA being a polydentate chelating agent.

9.7 REFERENCES

Chapter 13: EDTA Titrations [Online]. Black Hills State University. Available: https://www.bhsu.edu/Portals/91/AnalyticalChemistry/StudyHelp/LectureNotes/Chapter13.pdf [Accessed 10 March 2014.

Bauer, H. H. and Elving, P. J., 1960. The polarographic reduction of Bi(III) in the presence of chloride ion. *Electrochimica Acta,* 2 (4)**,** pp 240-247.

Bhat, T. R. and Iyer, R. K., 1966. Antimony(lll) and Bismuth(III) EDTA System. *Zeitschrift für Anorganische und Allgemeine Chemie,* 343 (5-6)**,** pp 329-336.

Billing, C. 2012. *Study of bismuth chemistry toward medicinal applications.* Doctor of Philosophy, University of the Witwatersrand.

Bond, A., 1969. An application of rapid polarographic techniques and the derivation of an equation for the polarographic study of the fluoride complexes of bismuth(III) in acid media. *Journal of Electroanalytical Chemistry and Interfacial Electrochemistry,* 23 (2)**,** pp 269-276.

Bottari, E. and Anderegg, G., 1967. Komplexone XLII. Die Untersuchung der 1: 1:-Komplexe von einigen drei-und vierwertigen Metall-Ionen mit Polyaminocarboxylaten mittels Redoxmessungen. *Helvetica Chimica Acta,* 50 (8)**,** pp 2349-2356.

Brintzenger, H. and Munkelt, S., 1948. Komplexverbindungen und Salze der Äthylendiamintetraessigsäure. III. Mitteilung. *Zeitschrift für Anorganische Chemie,* 256 (1-3)**,** pp 65-74.

Brown, T. L., LeMay, H. E. and Bursten, B. E., 2000. *Chemistry: The Central Science,* New Jersey, Prentice Hall.

Bruker, S. a. S., 1999. Ver. 6.02 (including XPREP) ed. Madison, WI, USA.: Bruker AXS Inc.

Cukrowski, I., 2000. 3D Complex Formation Curves. 5.00 ed.

Cukrowski, I., Marques, H. M., Mkwizu, T. S., Magampa, P. P. and Serge, C., 2007. Influence of electronic and steric effects on stability constants and electrochemical reversibility of divalent ion complexes with glycine and sarcosine: A glass electrode potentiometric, sampled direct current polarographic, virtual potentiometric, and molecular modelling study. *Analytica Chimica Acta,* 590 (2)**,** pp 203-216.

Cukrowski, I. and Zhang, J. M., 2004. Voltammetry as a Virtual Potentiometric Sensor in Modeling of a Metal-Ligand System and Refinement of Stability Constants. Part 1. Polarographic and Glass Electrode Potentiometric Study of a Dynamic Cd-Glycine System. *Electroanalysis,* 16 (8)**,** pp 612-626.

Gileadi, E., 2011. *Physical Electrochemistry: Fundamentals, Techniques and Applications,* Weinheim, Wiley-VCH.

Harris, D. C., 1998. *Quantitative Chemical Analysis,* New York, W.H. Freeman and Company.

Karadakov, B. and Ivanova, H., 1976. Spectrophotometry investigation of complex-formation of bismuth, copper and lead with ethylene-diamine-n, n'-diacetic acid. *Comptes rendus de l'Académie bulgare des sciences: sciences mathématiques et naturelles,* 29 (7-12)**,** pp 999.

Karadakov, B. P. and Ivanova, K. R., 1973. *Zhurnal Analiticheskoi Khimii,* 28**,** pp 525.

Kornev, V. I. and Trubachev, A. V., 1987. Stability of Bismuth(III) Complexones in Aqeuous Solutions. *Zhurnal Neorganicheskoi Khimii,* 32 (10)**,** pp 2433-2437.

Li, D. and Zhong, G.-Q., 2014. Synthesis and Crystal Structure of the Bioinorganic Complex [Sb(Hedta)]·$2H_2O$. *Bioinorganic Chemistry and Applications,* 2014**,** pp 7.

Martell, A. E. and Hancock, R. D., 1996. *Metal Complexes in Aqueous Solutions*, New York, Plenum Press.

Martell, A. E., Smith, R. M. and Motekaitis, R. J., 2004. NIST Standard Reference Database 46. 8.0 ed. Gaithersburg, USA: U.S Department of Commerce, National Institute of Standards and Technology.

Miklos, I. and Szeged, R., 1961. *Acta Chimica Academiae Scientiarum Hungaricae,* 26**,** pp 365.

Moussa, A. and Sammour, H., 1960. 434. Reactivity of anions towards electron transfer in the bismuth [right left harpoons] tervalent bismuth exchange reaction. *Journal of the Chemical Society (Resumed)***,** pp 2151-2157.

Powell, K. and Pettit, L., 1997. IUPAC Stability Constants Database. *Academic Software, Otley (UK).*

R.L. Davidovich, A. B. I., S.-Z. Hu, , 1998. *Kristallografiya,* 43**,** pp 653.

Randles, J. and Somerton, K., 1952. Kinetics of rapid electrode reactions. Part 4. Metal ion exchange reaction at amalgam electrodes. *Transactions of the Faraday Society,* 48**,** pp 951-955.

Ružić, I. and Branica, M., 1969. Logarithmic analysis of two overlapping DC polarographic waves: I. Reversible and totally irreversible processes. *Journal of Electroanalytical Chemistry and Interfacial Electrochemistry,* 22 (2)**,** pp 243-252.

Shchelokov, R. N., Mikhailov, Y. N., Mistryukov, V. E. and Sergccv, A. V., 1987. *Doklady Akademii Nauk SSSR,* 293**,** pp 642-644.

Sheldrick, G. M., 2008. A short history of *SHELX*. *Acta Crystallographica,* A64**,** pp 112–122.

Shimoi, M., Orita, Y., Uehiro, T., Kita, I., Iwamoto, T., Ouchi, A. and Yoshino, Y., 1980. The Structure of (Hydrogen Ethylenediaminetetraacetato) antimony (III) Dihydrate Sb (C 10 H 13 N 2 O 8)· 2H 2 O. *Bulletin of the Chemical Society of Japan,* 53 (11)**,** pp 3189-3194.

Shkol'nikova, L. M., Porai-Koshits, M. A., Davidovich, R. L., Hu, C.-D. and Ksi, D.-K., 1994. *Russian Journal of Coordination Chemistry,* 20**,** pp 593.

Sochevanov, V. and Volkova, G., 1969. *Zhurnal Neorganicheskoi Khimii,* 14**,** pp 118.

Stavila, V., Davidovich, R. L., Gulea, A. and Whitmire, K. H., 2006. Bismuth (III) complexes with aminopolycarboxylate and polyaminopolycarboxylate ligands: Chemistry and structure. *Coordination Chemistry Reviews,* 250 (21)**,** pp 2782-2810.

Summers, S. P., Abboud, K. A., Farrah, S. R. and Palenik, G. J., 1994. Syntheses and structures of bismuth(III) complexes with nitrilotriacetic acid, ethylenediaminetetraacetic acid, and diethylenetriaminepentaacetic acid. *Inorganic Chemistry,* 33 (1)**,** pp 88-92.

Wang, R.-Y., Jin, T.-Z. and Zheng, Z.-P., 2000. *Acta Chimica Sinica,* 58**,** pp 1481.

Wullens, H., Bodart, N. and Devillers, M., 2002. New bismuth(III), lanthanum(III), praseodymium(III), and heterodinuclear Bi–La and Bi–Pr complexes with polyaminocarboxylate ligands. *Journal of Solid State Chemistry,* 167 (2)**,** pp 494-507.

Chapter Ten

Complex Formation of Bismuth(III)-Pyrazinecarboxylic (Pyrazinoic) Acid

10.1 INTRODUCTION

Pyrazinecarboxylic acid - a biologically important ligand - is the active form of the antituberculosis drug pyrazinamide (Zhang *et al.*, 2008). The specific function of this drug is to minimize the period of time that a patient is exposed to the tuberculosis therapy, which is only brought about when the drug is exposed to acidic media where the active form exists in substantial concentrations (Zhang *et al.*, 2003). Not only has the free acid been found to be useful in the medicinal sector, but some metal-ligand complexes have also been screened against bacteria such as *Escherichia coli*, *Salmonella typhi* and *Vibrio cholera* (Premkumar and Govindarajan, 2006). The ability of hydrazinium lanthanide complexes of pyrazinecarboxylic acids to act against the above mentioned bacteria were found to be better than the activity of the free acid, as well as two standard antibiotics (Co-trimoxazole and Carbendazim) (Premkumar and Govindarajan, 2006). Interestingly, it is the mode of chelation (referred to as the Tweedy chelation theory) which has been found to be responsible for this improved action. Tweedy's chelation therapy predicts that the polarity of the central metal ion gets reduced because of sharing its positive charge with donor atoms of the ligand. This causes electron delocalization over the entire pyrazine ring which results in the complex having a more lipophilic character which means the drug can more easily permeate the lipid layers of the bacterial membrane. Bismuth(III) would most likely chelate to this acid by the Tweedy theory too, as was found for lanthanum(III) and other lanthanide elements. With

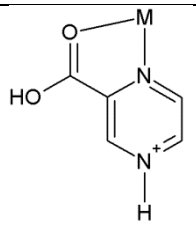
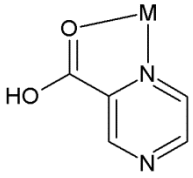
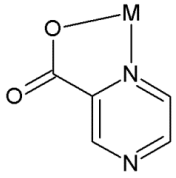
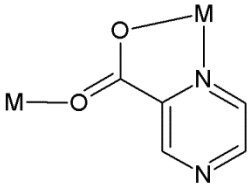
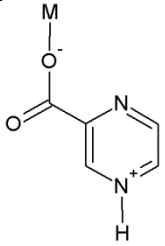
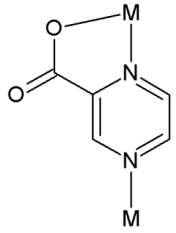
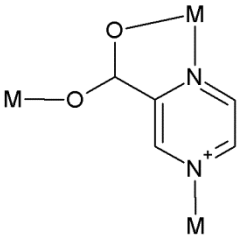
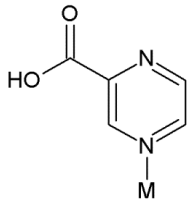
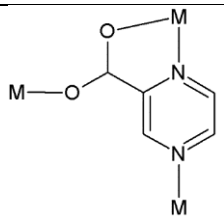
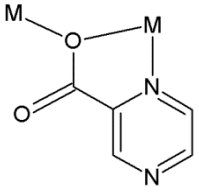
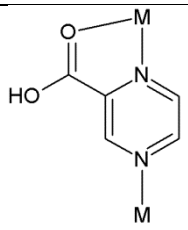
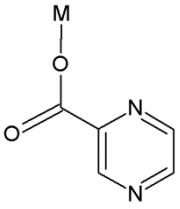
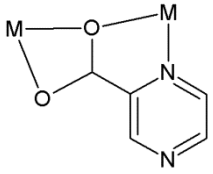
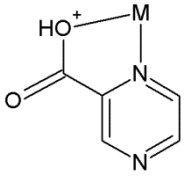
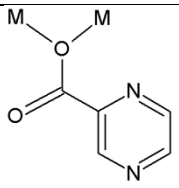
bismuth(III) already having such vast medicinal applications and also acting as an anti-bacterial itself, perhaps studying the complex formation of bismuth(III)-pyrazinecarboxylic acid may lead to knowledge useful in the field of drug design and discovery.

Klein, Majeste, Trefonas and O'Connor (1982) described the potential of ligands containing a combination of the pyrazine base and carboxylate group in the field of magneto-chemistry and electron-transfer research, as both these functionalities easily form bridged structures with metal ions, therefore providing exchange pathways for magnetism or electrons.

According to Martell and Hancock (1996) the pyrazine ligand can exert very high ligand field strengths because the nitrogen is sp^2 hybridized, which leads to greater s character in the orbitals used for bonding to the metal ion and hence more covalent bonding. The numerous different coordination modes found for pyrazinecarboxylic acid have been graphically presented in Table 10.1. Again, the degree of protonation of the ligand was used in separating the modes into the different pH regions which the protonation constants indicate.

About 200 pyrazinecarboxylic acid complexes were found on the CSD of which a majority of these complexes contained the fully deprotonated form of pyrazinecarboxylic acid. Only about 4.6% of all the complexes were formed with a protonated ligand and only a single one of them contained the ligand in it's doubly protonated form, corresponding to coordination mode *i* (REFCODE: NIBLUG). The structure of NIBLUG which is a complex with indium can be seen in Figure 10.1. Barszcz, Masternak, Hodorowicz and Jabłońska-Wawrzycka (2012) suitably mention that this ligand has a wide variety of coordination modes, but go on to illustrate only four different possibilities. Of these four, only examples of two of the modes could

Table 10.1 Coordination modes of pyrazinecarboxylic acid with various metals (M), which depend on the extent of protonation of the ligand.

← LH_2^+ →	← LH →	← L^- →	
 *i*	 *ii*	 *vii*	 *xi*
	 *iii*	 *viii*	 *xii*
	 *iv*	 *ix (O-O delocalized)*	 *xiii*
	 *v*	 *x*	 *xiv*
	 *vi*		 *xv*

be found in the CSD, which correlate to mode *vii* and *xi*. The other two possible modes that they suggest were therefore not included in the above table.

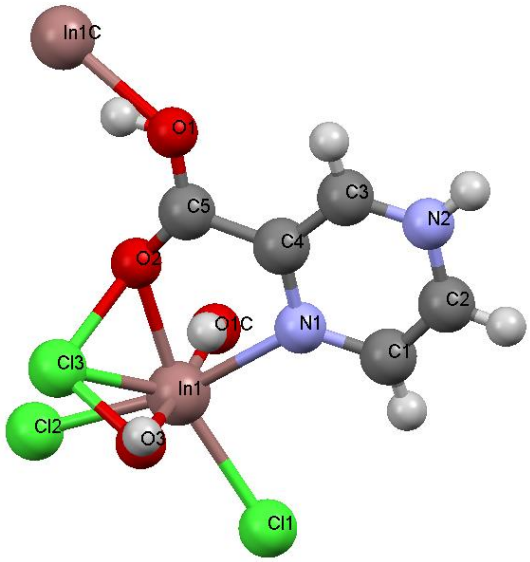


Figure 10.1 Doubly protonated pyrazinecarboxylic acid complex (REFCODE: NIBLUG).

In the CSD (Allen, 2002) there is only one pyrazinecarboxylic acid complex which bonds to Bi(III) and it was published just over a year ago (REFCODE: FAPQUK) by Anjaneyulu, Maddileti and Swamy (2012) (Figure 10.2). The bismuth(III) centre is six coordinate, which they described as a pentagonal prism geometry. What is interesting about this structure is that of the three pyrazinecarboxylic acid ligands bonded to the Bi(III), two are *N,O* bidentate and one is *O* monodentate. This may have occurred due to steric hindrance. The monodentately bonded pyrazinecarboxylic acid ligand is also the only protonated one in this structure and this occurs at the nitrogen in the *meta* position from the carboxylic acid group. Within this structure we find two different coordination modes of the pyrazinecarboxylic acid ligand which correspond to *vii* and *x* in Table 10.1. In the

sixth coordination site there is a monodentately bonded phenyl ring, and the complex is neutral and has a single water molecule associated with it.

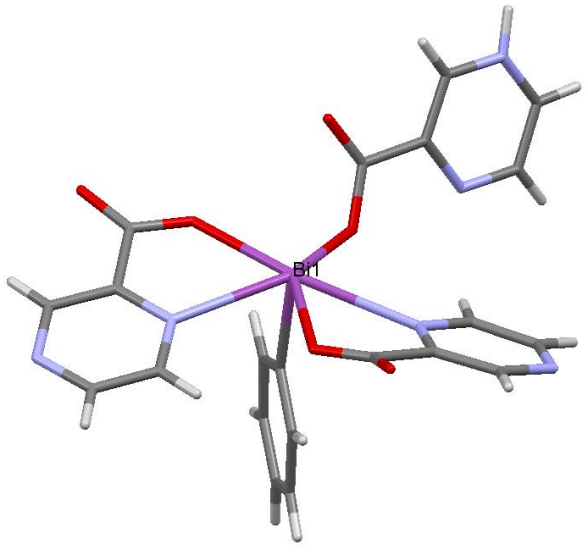


Figure 10.2 Coordination modes of the pyrazinecarboxylic acid ligands around the bismuth(III) centre. (The water molecule was omitted for simplicity.)

Bi(III) has a high affinity for both oxygen and nitrogen functionalities in aqueous solution which is probably due to it being a borderline metal ion (perhaps tending more towards being soft as opposed to hard) in terms of Pearson's Hard-Soft Acid-Base theory (Sun, Li and Sadler, 1997). The protonation constants of pyrazinecarboxylic acid are given in Table 10.2 and were obtained from the NIST database (Martell, Smith and Motekaitis, 2004). Unfortunately the only value for the second protonation constant was given for an ionic strength of 3 M, which is substantially higher than the 0.25-0.5 M range at which our experiments are usually conducted. Also, according to Martell, Smith and Motekaitis (2004) this value does carry some uncertainty. The second protonation constant carries a value of 0.45 at 25 °C and 0.1 M ionic strength according to the IUPAC Stability Constants Database (Powell and Pettit, 1997), and so from this value it seems that using the 0.5 M value

(quoted by NIST) in relation to our data at ionic strengths between 0.25 and 0.5 M should not cause any significant discrepancies.

Table 10.2 Protonation constants for pyrazinecarboxylic acid as quoted by the NIST database (Martell, Smith and Motekaitis, 2004).

Equilibrium Equation	Log K	Ionic strength (M)	Temperature (°C)
[HL]/[H][L]	2.7	0.5	25
$[H_2L]/[H][HL]$	0.5*	3.0	25

*Uncertain value as protonation occurs below pH 2

Complex formation studies on bismuth with pyrazinecarboxylic acid have not been published before. The NIST database (Martell, Smith and Motekaitis, 2004) holds formation constant values for many other 3+ oxidation state metal ions complexed to pyrazinecarboxylic acid, such as lanthanum, neodymium, samarium, europium, gadolinium, terbium, holmium, erbium and lutetium. One of the reasons why bismuth chemistry is rather difficult to study in solution is due to the fact that it precipitates out of solution (mostly as bismuth-oxy nitrates or perchlorates) at really low pH, therefore not allowing a large enough pH range in which complexes can actually form. The conditions used in the electrochemical technique to collect metal-ligand complexation data for Bi(III) need to be carefully selected. The concentration of the metal ion should be low, the [L]:[M] ratio high and the data collection must start before pH 2 to avoid the precipitation of hydroxyl species (Cukrowski and Luckay, 1998).

10.2 AIMS

The aims of this research were to identify the different species that form in solution between bismuth(III) and pyrazinecarboxylic acid starting from pH 0.3. Formation

constants for these species were calculated using the same method that Billing (2012) used for the bismuth(III)-quinolinate system. Challenges specific to studying this metal-ligand system were addressed.

10.3 EXPERIMENTAL

Complex formation between pyrazinecarboxylic acid and bismuth(III) was studied at 25.0 ± 0.1 °C at an initial ionic strength of 0.5 M. For this system three ligand-free and three complexation experiments were run (directly after each other as described below). The initial glass electrode calibration was done, followed by the polarographic ligand-free experiment, and then the final calibration. This then also acted as the initial calibration for the complexation experiment which was done directly after it. A final calibration was then measured. The [L]:[M] ratios for the complexation experiments were 100, 77 and 49, which were directly preceded by the ligand-free experiments labeled as EXP 1, 2 and 3, respectively. Polarograms were collected in the potential range from 180 to -700 mV. Experimental data were collected between pH 0.3 and 10 because it was found that reduction of the ligand overlapped that of thallium(I) and so the waves could only be resolved at much higher pH values. It was necessary to obtain the half-wave potential of free thallium(I) because it was used in calculating the free metal ion potential for bismuth(III).

Polarographic data were separated at a potential of -200 mV so that the thallium(I) and bismuth(III) waves could be fitted separately, using Equation 2.1 for the individual waves. In each case the delta value was allowed to vary and it was found that all the data represented a reversible system.

10.4 RESULTS AND DISCUSSION

As before, the smoothed thallium(I) half-wave potential data of the three ligand-free experiments was used to create a model which represented the average diffusion junction potential. For all three experiments the diffusion junction potential was similar and so the model has high precision (see Figure 10.3). A polynomial of degree three was fitted to these data and was used for compensation of the diffusion junction potential in the complexation experiments. It is assumed that the E_j for bismuth(III) is equal to that of thallium(I), as before. This compensation model only accounts for the shifts due to the diffusion junction and does not consider the effects due to changes in ionic strength (as was the case in the cadmium(II) compensation models).

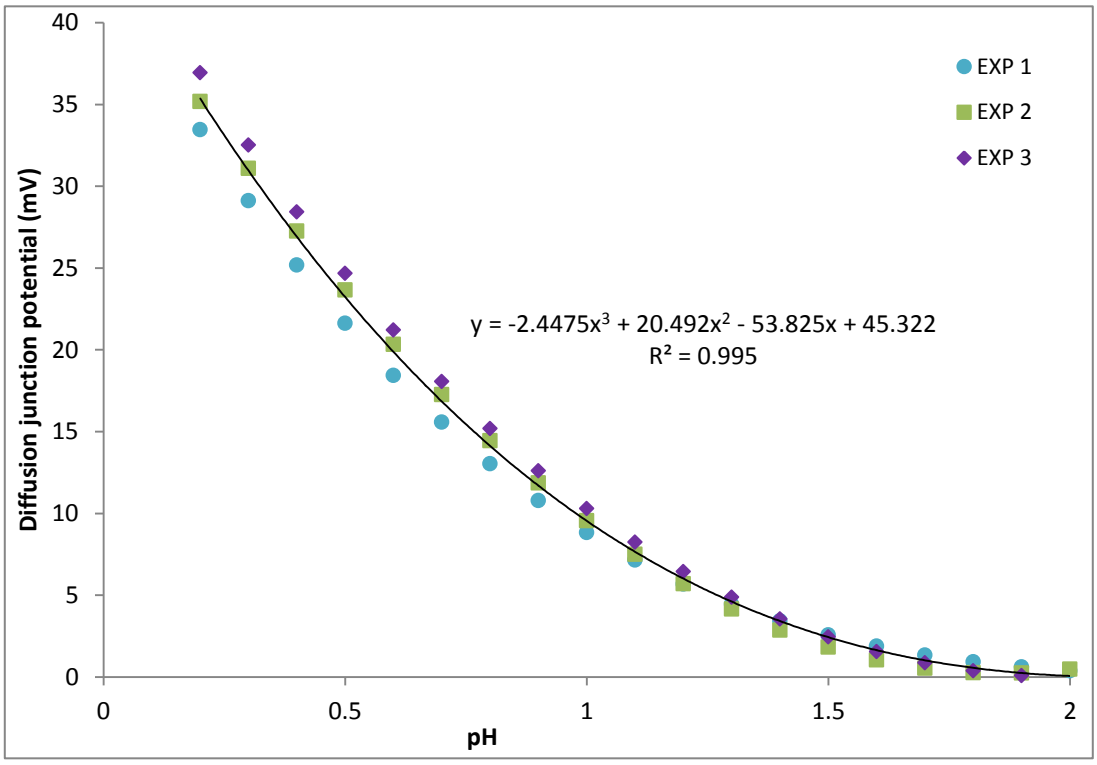


Figure 10.3 The magnitude of the diffusion junction potential as a function of pH.

For the bismuth(III) reduction data, compensation of the E_j as well as potential shifts due to complex formation with hydroxides, as well as both hydroxide and nitrate complexes was done for each ligand-free experiment, as described in Chapter Nine. EXP 3 is used here to illustrate the necessary compensations to obtain the free metal ion potentials for bismuth (Figure 10.4).

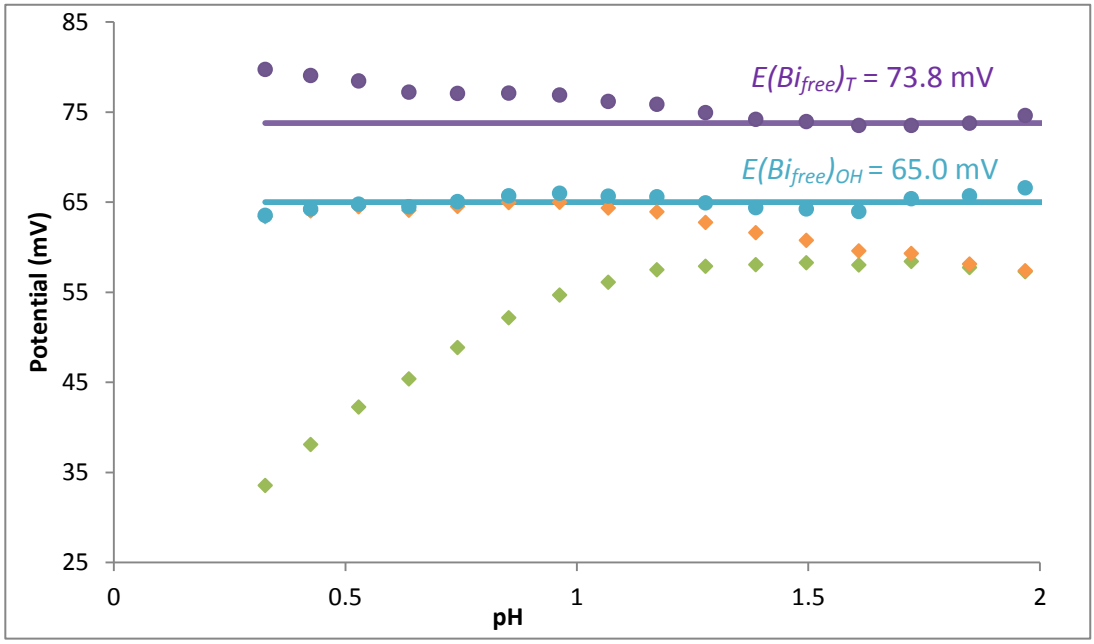


Figure 10.4 Illustration showing the experimental data (green) for bismuth(III) which is compensated for the shifts by E_j (orange) and complex formation with hydroxides (blue) and nitrates + hydroxides (purple).

For these data two approaches for determining the "difference" model, which is used to calculate the free bismuth(III) potential, were considered. It is called a "difference" model since we use the ligand free experiments to find a relationship (in this case it is a difference) between the free bismuth(III) potential and the thallium(I) potential data. In the complex formation experiment this "difference" model together with the thallium(I) potential data is then used to predict the free bismuth(III) potential.

10.4.1 Approach 1

In this approach differences were obtained by subtracting $E(Tl_{free})$ from the $E(Bi_{free})_{OH}$ and $E(Bi_{free})_T$ values obtained for each ligand-free experiment, as shown in Figure 10.5. Thus $\Delta E_{OH} = E(Bi_{free})_{OH} - E(Tl_{free})$ and $\Delta E_{OH+NO3} = E(Bi_{free})_T - E(Tl_{free})$. The value of $E(Tl_{free})$ was obtained by finding the average half-wave potential in the pH region where the junction potential was constant (above approximately pH 2), as before. The results are given in Table 10.3 and the average ΔE_{OH} and ΔE_{OH+NO3} values were determined and used in further calculation.

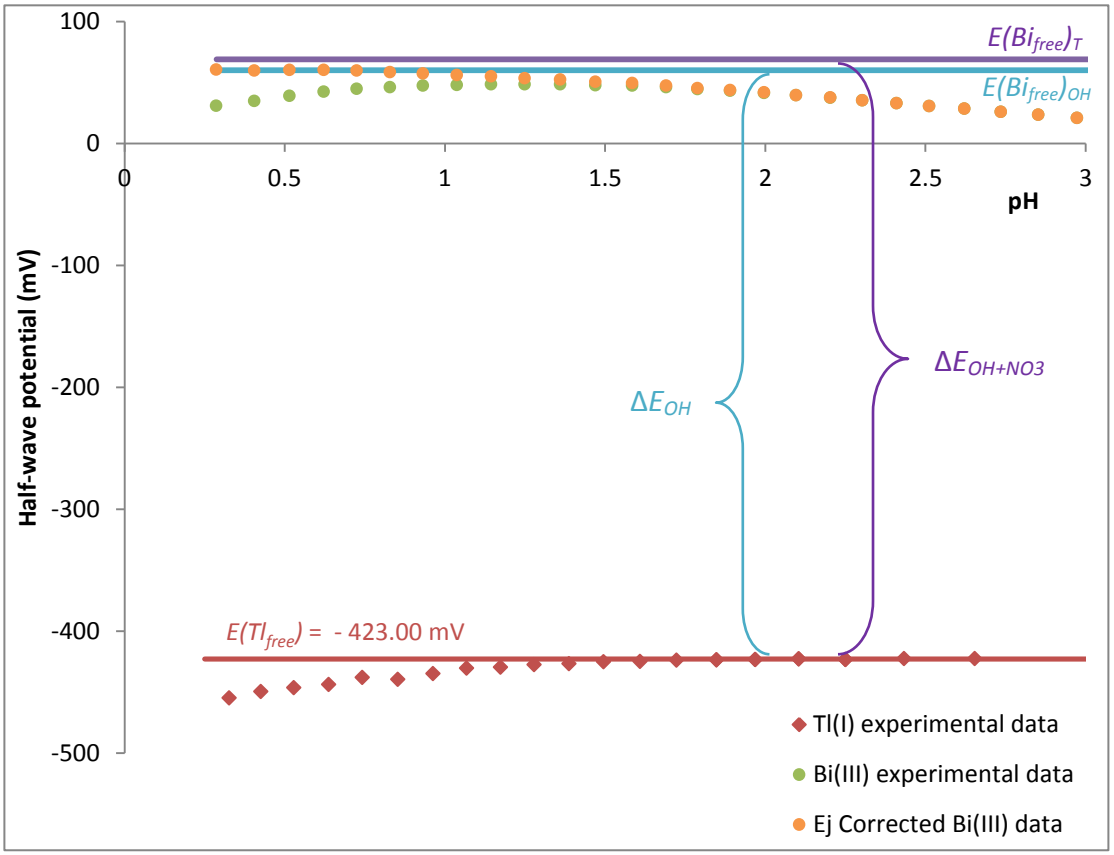


Figure 10.5 Calculation of the difference values ΔE_{OH} and ΔE_{OH+NO3} for EXP 3.

Table 10.3 Differences calculated using Approach 1

EXP	$E(Bi_{free})_{OH}$ (mV)	$E(Bi_{free})_T$ (mV)	$E(Tl_{free})$ (mV)	ΔE_{OH} (mV)	ΔE_{OH+NO3} (mV)
1	67.5	76.4	-421.8	489.3	498.2
2	61.4	70.4	-424.7	486.1	495.0
3	65.0	73.8	-423.0	488.0	496.8
			Average	487.8 ± 1.6	496.7 ± 1.6

In the ligand experiments, the accessible thallium half-wave potential data were limited by the reduction of pyrazinecarboxylic acid itself in a similar potential range (see Figure 10.6). The reduction of the ligand overlapped that of thallium(I) from the start of the experiment (± pH 0.3) until approximately pH 6 (depending on the concentration of the ligand present). Above pH 6 the reduction potential of the ligand had moved more negative and the half-wave potentials for thallium(I) could be obtained. For each experiment these last few data points were averaged to obtain a value for $E(Tl_{free})$. The $E(Tl_{free})$ value for each ligand experiment was then added to the average difference ΔE_{OH} or ΔE_{OH+NO3} (Table 10.3) to determine $E(Bi_{free})_{OH}$ or $E(Bi_{free})_T$, respectively (Table 10.4). For this approach the average diffusion junction potential, as shown in Figure 10.3, was used to compensate the shifts due to E_j in the complexation experiments.

In order to solve the formation constants the 3D-CFC program was used as before, entering the protonation constants for pyrazinecarboxylic acid which are given in Table 10.2, as well as the bismuth(III) hydroxide formation constants (Table 8.2) and the necessary experimental conditions (see Table A9.1 in Appendix A). When determining the formation constants, both the $E(Bi_{free})$ values were considered.

When using the $E(Bi_{free})_{OH}$ value, initially just a ML species was used for refining the formation constants. The fit of the CCFC was found to be poor above pH 2 for

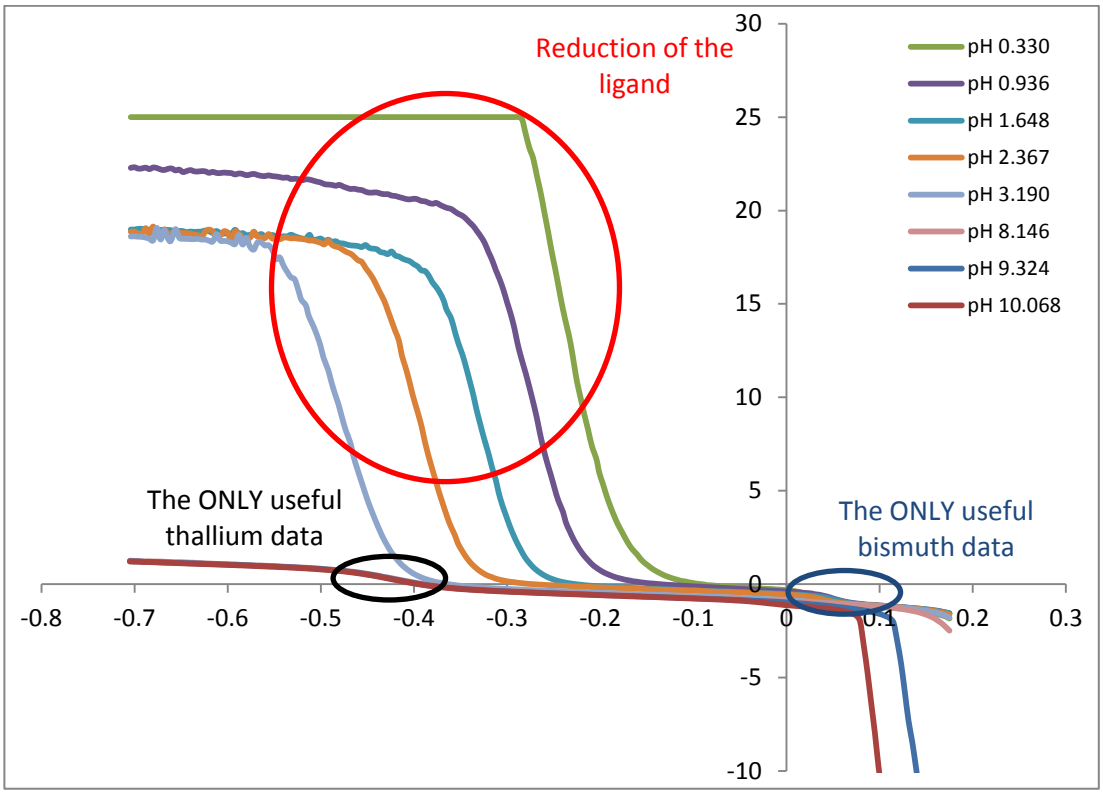


Figure 10.6 Polarograms collected at increasing pH showing the movement in the reduction potential of the ligand, where [L]:[M] = 49. (Note that the current of the polarogram at pH 0.330 is saturated at 25 µA.)

Table 10.4 Values for $E(Bi_{free})$ calculated using Approach 1.

[L]:[M]	$E(Tl_{free})$ (mV)	$E(Bi_{free})_{OH}$ (mV)	$E(Bi_{free})_T$ (mV)
100	-426.3	61.6	70.4
77	-419.6	68.2	77.1
49	-422.7	65.1	74.0

[L]:[M] = 77 and above pH 2.3 for [L]:[M] = 100, but good throughout the pH range for [L]:[M] = 49 (see Figure 10.7). The formation constants for the ML species were similar (Table 10.5). There was no need to incorporate a MLH species in the model because the shifts at low pH were very small.

Table 10.5 Formation constants calculated using Approach 1 and $E(Bi_{free})_{OH}$.

Complex	[L]:[M] = 100		[L]:[M] = 77		[L]:[M] = 49		AVERAGE	
	Log β	Std Dev	Log β	Std Dev	Log β	Std Dev	Log β	Std Dev
ML	4.58	0.04	4.75	0.04	4.80	0.05	4.7	0.1
OVERALL FIT	1.85		8.37		0.54			

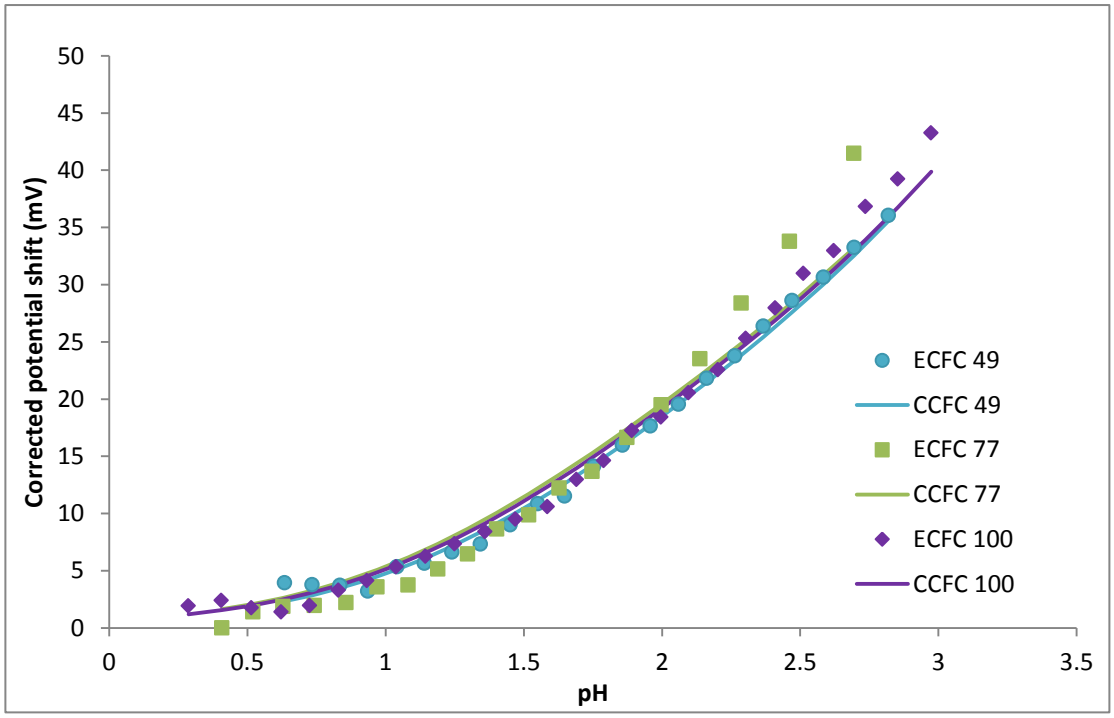


Figure 10.7 ECFC for each [L]:[M] ratio with its corresponding CCFC obtained using the ML species and $E(Bi_{free})_{OH}$.

From Figure 10.7 (as well as the value of the overall fit in Table 10.5) it was evident that the [L]:[M] = 77 dataset did not follow the same trend as the other two ratios as the potential shifts above pH 2 were significantly larger. The original experimental data for these experiments was therefore compared and contrasted. The plots of current vs. pH (Figure 10.8) indicate the pH at which precipitation of bismuth(III) occurs by a sharp decrease in the current. (Corresponding half-wave potentials achieved past this pH were not used for data analysis.) The [L]:[M] = 77 data

showed a more gradual decrease in current from pH 2 already, the pH at which the potential also started increasing significantly more than the other experiments. This decrease in current could not be due to precipitation the change is too gradual and because it would be expected that precipitation for the lower [L]:[M] ratio experiment would occur at lower pH (increasing concentration ratios promote complex formation). Since the [L]:[M] = 77 dataset seems to be problematic, the experimental data before any compensations were done was scrutinized.

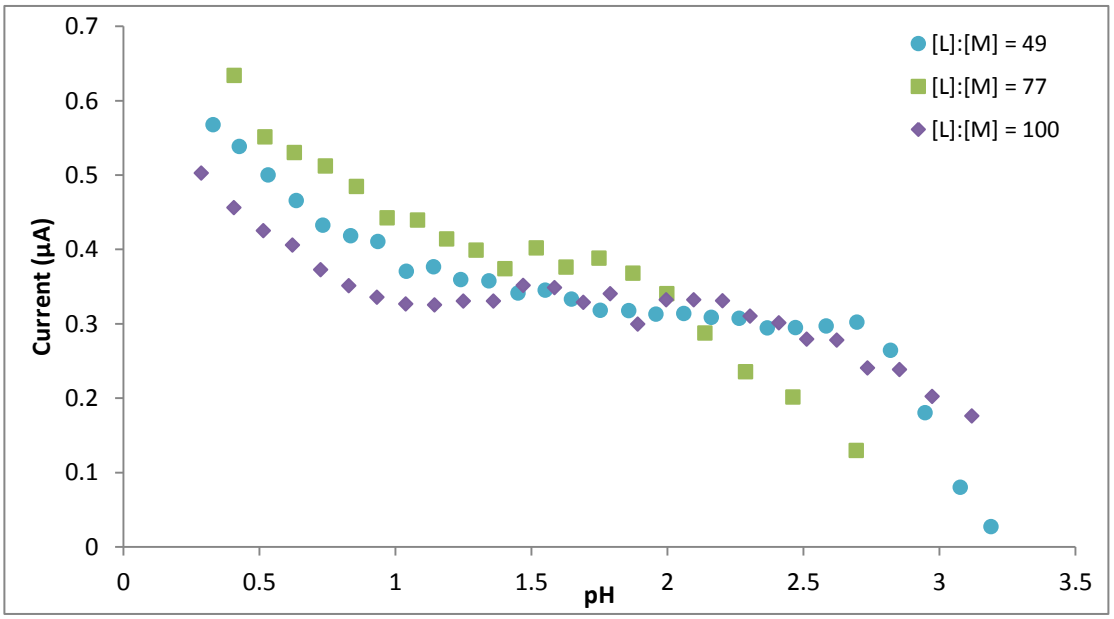


Figure 10.8 The current of bismuth for each complexation experiment which shows the point where precipitation occurs.

The overlapping polarograms that were recorded at the start of the complexation experiments were compared before and just after the ligand was added to the cell solution (see Figure 10.9). For the [L]:[M] = 77 data it was seen that after the ligand was added to the solution, the half-wave potential of the bismuth(III) reduction wave shifted slightly negative and the currents more positive. This was not observed in the other experiments, however, this should not affect the results significantly and was shown to be the case as data in the low pH region (below pH 2)

behaved according to the trend of the other experiments (see Figure 10.7). Another important aspect which Figure 10.9 (a) and b)) highlights is that no complex formation between bismuth(III) and pyrazinecarboxylic acid occurred upon addition of the ligand as the reduction potentials were essentially identical before and after ligand was added.

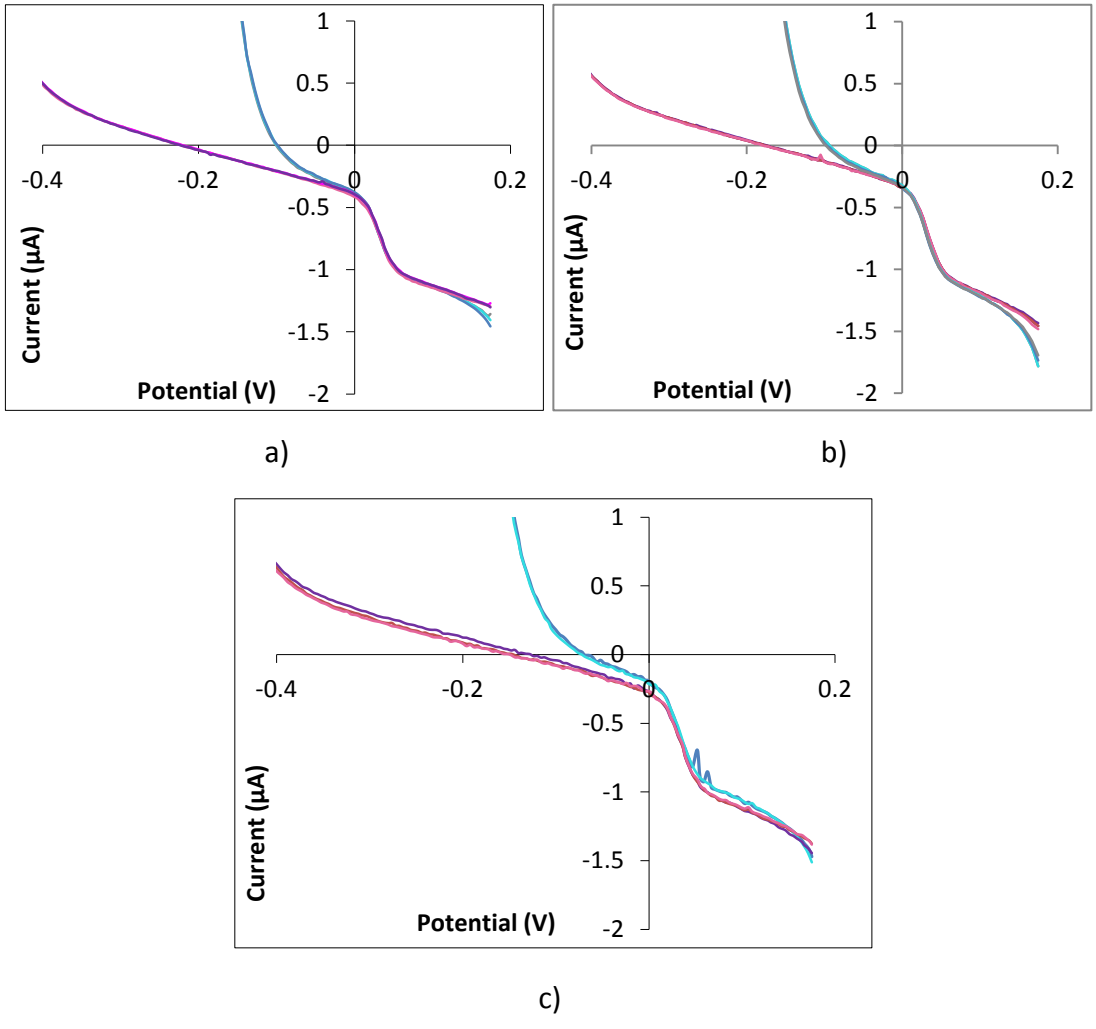


Figure 10.9 Overlapping polarograms recorded before (pink lines) and after (blue lines) the ligand was added to the complexation experiment, where a) [L]:[M] = 100, b) [L]:[M] = 49 and c) [L]:[M] = 77.

Comparing the half-wave vs. pH data for the corresponding ligand-free and complexation experiments could therefore be done by overlapping the initial points since they were equivalent because no complexation had occurred yet (see Figure 10.10). Manipulation of the complexation experiment data was done by adding a small constant (as required for each comparison) to all potential values throughout the titration to force these initial points to overlap. From Figure 10.10 it can be seen that complex formation starts around pH 1 for [L]:[M] = 100 and 49, but only at approximately pH 1.5 for [L]:[M] = 77, which is contrary to what would be expected. Due to these discrepancies in the data, it was decided that the [L]:[M] = 77 dataset would not be used further in calculating formation constants. In some cases log β values for this dataset will still be quoted in italics, but they were not used in calculating the average log β values for the bismuth(III)-pyrazinecarboxylic acid system.

Calculation of formation constants using the $E(Bi_{free})_T$ value required that additional species had to be added to the model. (The ML species on its own was no longer sufficient in describing the potential shifts calculated, as was the case when using $E(Bi_{free})_{OH}$.) The MLH species was introduced to account for the large shifts in the low pH region, but the CCFC still gave a poor fit in the higher pH region. Incorporating a further species, ML_2, improved the overall fit significantly for each ratio. Log β values are given in Table 10.6 and the corresponding ECFC and CCFC plots are shown in Figure 10.11.

Although a good fit was obtained for both [L]:[M] = 49 and 100 when the ML_2 complex was used in the species model, a different model was also considered. A hydroxide complex was incorporated, instead of ML_2 the MLOH species was proposed because precipitation occurred at pH values after this species was found (at approximately pH 3), (refer to Figure 10.8). Table 10.7 gives the log β values for

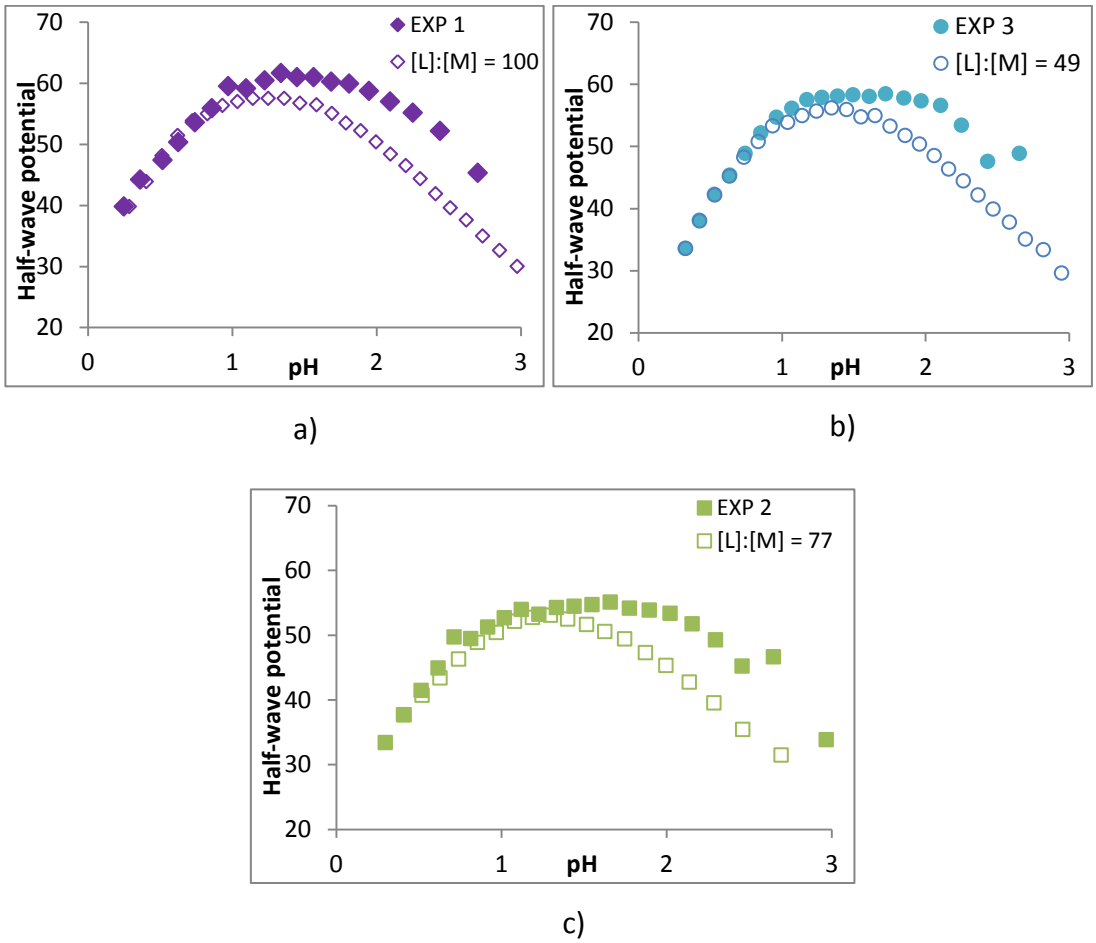


Figure 10.10 Comparison of the ligand-free and corresponding complexation experiment for a) [L]:[M] = 100, b) [L]:[M] = 49 and c) [L]:[M] = 77. (The actual value of the half-wave potential is meaningless because some of the data were manipulated to obtain an overlay of the initial points.)

each ratio with their improved overall fits. In Figure 10.12 it can be seen that the CCFCs pass through the ECFC data much better than in Figure 10.11 when ML_2 was used in the model instead. Although incorporating the MLOH species as opposed to the ML_2 species improves the fit and would be the recommended model here, it is not conclusive as to which species is definitely in solution. Another technique, such

as electrospray ionization-mass spectrometry, would be useful to determine this as the mass/charge ratios of these two species will be significantly different.

Table 10.6 Formation constants calculated using Approach 1 and $E(Bi_{free})_T$ for the MLH, ML and ML_2 species model.

Complex	[L]:[M] = 100		[L]:[M] = 77		[L]:[M] = 49		AVERAGE	
	Log β	Std Dev	Log β	Std Dev	Log β	Std Dev	Log β	Std Dev
MLH	6.47	0.04	*6.53*	*0.05*	6.82	0.05	6.6	0.2
ML	4.78	0.15	*4.2*	*1.0*	5.28	0.12	5.0	0.4
ML_2	9.29	0.04	*9.79*	*0.04*	9.81	0.06	9.6	0.4
OVERALL FIT	0.92		*1.03*		0.19			

Not included in the average values.

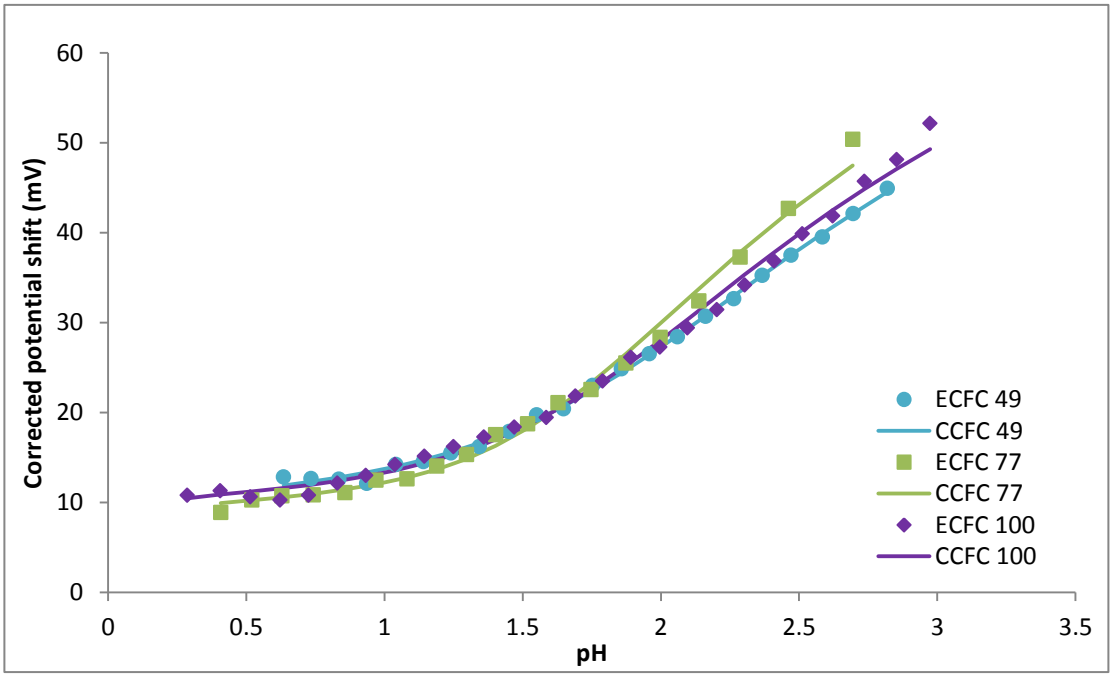


Figure 10.11 ECFC and CCFC calculated using MLH, ML and ML_2 species model at each [L]:[M] ratio.

Table 10.7 Formation constants calculated using Approach 1 and $E(Bi_{free})_T$ for the MLH, ML and MLOH species model.

Complex	[L]:[M] = 100		[L]:[M] = 77		[L]:[M] = 49		AVERAGE	
	Log β	Std Dev	Log β	Std Dev	Log β	Std Dev	Log β	Std Dev
MLH	6.42	0.04	*6.48*	*0.05*	6.76	0.05	6.6	0.2
ML	5.05	0.06	*4.9*	*0.2*	5.45	0.06	5.3	0.3
MLOH	16.69	0.04	*17.19*	*0.04*	16.86	0.07	16.8	0.1
OVERALL FIT	0.28		*0.31*		0.28			

Not included in the average values.

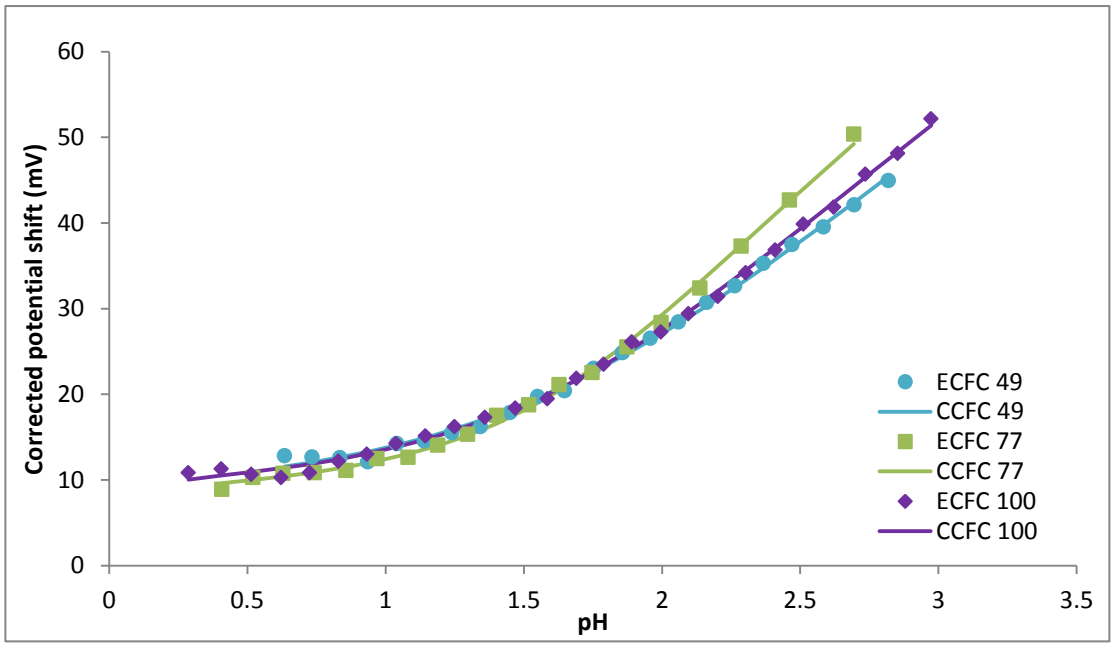


Figure 10.12 ECFC and CCFC calculated using MLH, ML and MLOH species model at each [L]:[M] ratio.

It is important to understand the implications of using the two $E(Bi_{free})$ values on the species predicted and the magnitude of their formation constants. These two values were necessary since the 3D-CFC software cannot incorporate the bismuth(III) nitrate species together with the ligand that is being studied when determining formation constants. The competing equilibria at low pH where the bismuth(III)

nitrates exist in solution cannot thus be accounted for. Figure 10.13 shows the SDD for the bismuth(III) nitrate and hydroxide species formed (a), together with the bismuth(III) reduction potential data vs. pH with the compensations made to determine both $E(Bi_{free})$ values (b). Below pH 2 the combination of all bismuth(III) nitrate species dominates the complexes formed. From pH 2 the nitrate complexes decrease in percentage distribution until pH 3 where they essentially are no longer present in solution. As the pH increases so the formation of various hydroxides species also increases. It is extremely unfortunate that precipitation occurs at about pH 2, where the nitrates stop dominating in solution. Thus in Figure 10.14 b) it is proposed (shown as theoretical data points) that the shift due to nitrate complex formation decreases until pH 3 where it becomes zero, while that due to hydroxides increases. Therefore, if the bismuth-ligand system being studied does not form complexes (or only weak complexes are formed) in the low pH region and thus cannot compete with the formation of the nitrate species, using $E(Bi_{free})_{OH}$ would provide a good estimate of a metal-ligand species existing in this pH range (even though the magnitude of the log β value may be slightly underestimated). Using $E(Bi_{free})_{T}$ would provide better log β estimates for species existing above pH 3. The true value for the formation constants of species formed below about pH 3 therefore lies somewhere between that determined using the two $E(Bi_{free})$ values.

From the polarograms in Figure 10.9 it was clear that no complex formation occurred at the lowest pH. This reflected in the ECFC plotted in Figure 10.7 when the $E(Bi_{free})_{OH}$ value was used in the calculation. However, in Figure 10.12 when the $E(Bi_{free})_{T}$ value was employed a shift of about 10 mV was calculated at the lowest pH, which we know is not the case. When using $E(Bi_{free})_{T}$, the software attributes the shift at low pH due to bismuth(III)-nitrate complex formation to that of bismuth(III)-pyrazinecarboxylic acid complex formation, and particularly the MLH species. To see in what pH region the MLH complex was affecting the CCFC, the log β values for the

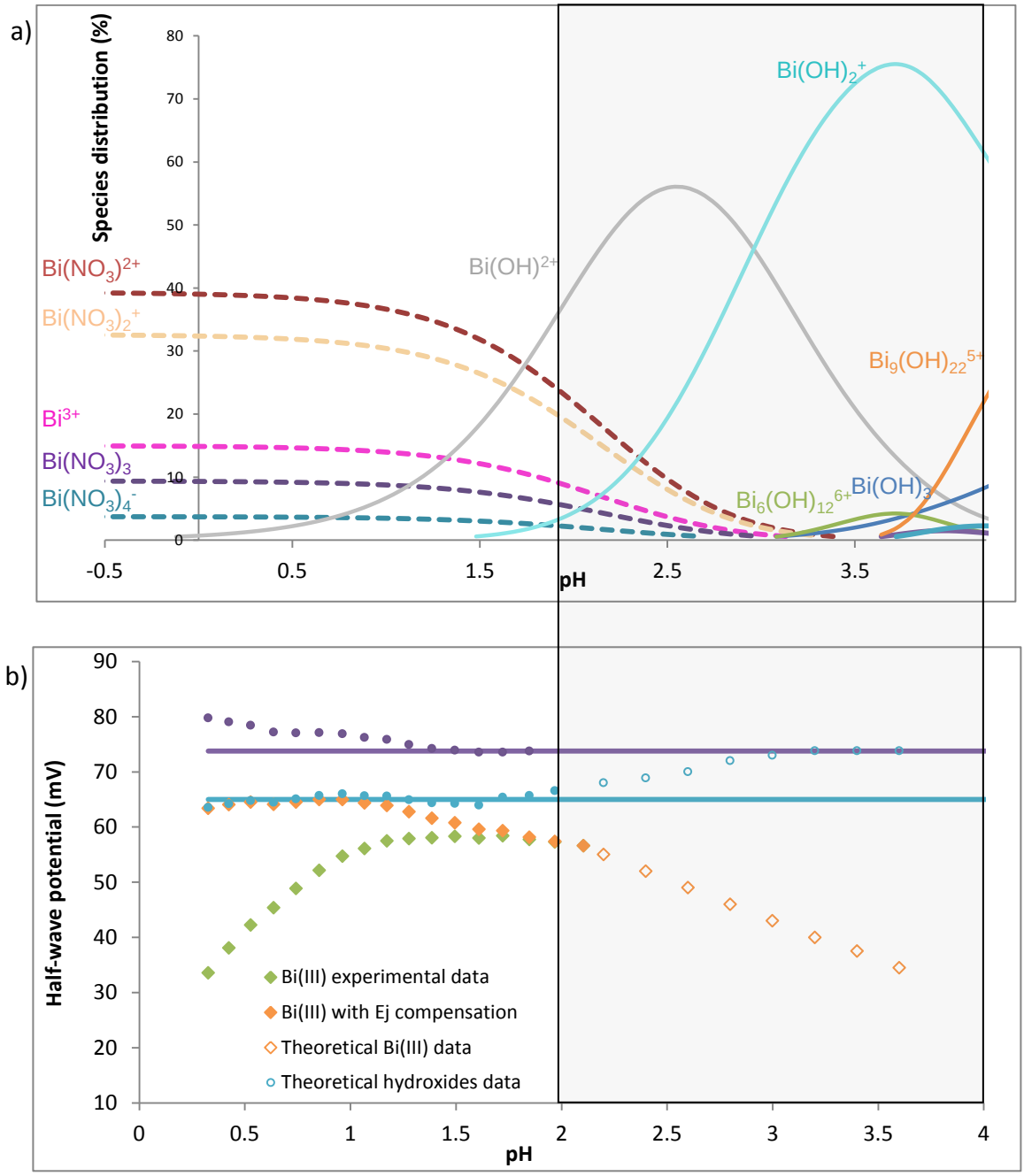


Figure 10.13 Plot showing how the free metal ion potentials (($E(Bi_{free})_{OH}$ and $E(Bi_{free})_T$) (a) are affected by the changing distribution of nitrate and hydroxide species that vary with pH (b) in solution.

ML and MLOH species were fixed (as per Table 10.7) and the MLH complex was deleted. In each experiment the MLH species was found to have an effect up until approximately pH 2 (Figure 10.14) where bismuth(III)-nitrate complexes are still significant in solution. Therefore, it is not conclusive that MLH exists, and if it does, the formation constants would be significantly lower than determined here. The MLH species could only be incorporated into the model when calculating formation constants using $E(Bi_{free})_{OH}$ for the [L]:[M] = 49 ratio, having a log β value of 5.6 ± 0.2. This value would be closer to the true value if this species did exist.

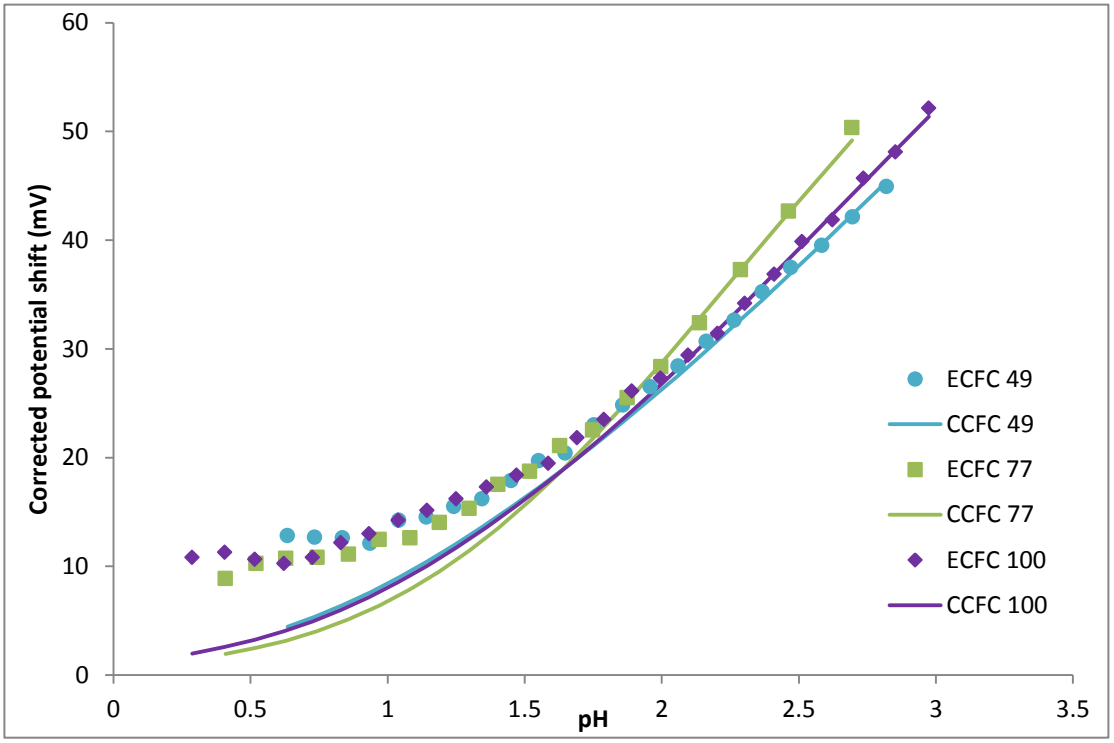


Figure 10.14 ECFC and CCFC for each [L]:[M] ratio showing the pH region where the MLH species affects the CCFC.

A similar process was applied to check in what pH range the MLOH species was affecting the CCFC. The $E(Bi_{free})_T$ value was used and the MLH and ML values were fixed while MLOH was deleted. The CCFC deviated from the ECFC from as low as approximately pH 1.6 for [L]:[M] = 49 and 100. It would be expected that with the

ML species forming from lower pHs already, that the bismuth nitrate species would no longer be competing to a large extent and thus the log β value determined for MLOH would be a good approximation, be it that it may be slightly overestimated. Interestingly, the MLOH species could be fitted to the [L]:[M] = 100 and 49 dataset (a number of points were removed at low pH for [L]:[M] = 49) when using $E(Bi_{free})_{OH}$ giving an average log β value of 15.95 ± 0.03 (in return though the average log β value for ML decreased to 4.4 ± 0.3) The true log β value lies somewhere between that obtained using $E(Bi_{free})_{OH}$ and $E(Bi_{free})_{T}$ (i.e. between 4.4 and 5.3 for ML).

Species distribution diagrams were also plotted using results from Tables 10.6 and 10.7 to show where the MLOH and the ML_2 species would exist in solution under the same conditions (Figure 10.15). According to this, ML_2 starts forming before there is even 10% of ML in solution. Considering that the MLH species is probably not in solution, or certainly not to such great extents, the concentration of ML would be greater than actually depicted here. Still, ML_2 formation beginning so soon after the ML complex starts forming (and increasing so rapidly) is questionable. On the other hand, the MLOH species starts forming at higher pH and is present at about 75% in solution before precipitation occurs. This however is still not a definitive conclusion. According to these SDDs MLH complex formation begins already before pH 0, which cannot be the case since no shift in potential upon addition of the ligand to the sample solution was observed (Figure 10.9). This is further evidence that the log β value (and possibly even the speculation of this MLH species) is incorrect.

Using slope analysis as an indication of possible complexes existing in solution for bismuth(III)-pyrazinecarboxylic acid, possible reduction reactions occurring in the various pH regions have been tabulated (Table 10.8). The pH regions indicated on the ECFC in Figure 10.16 describe the form in which the ligand is found to mainly exist. Two distinct slopes were found between pH 0.5 and 2.7. The first slope of 10 mV occurs between pH 0.5 and 1.5 which could indicate a combination of ML and

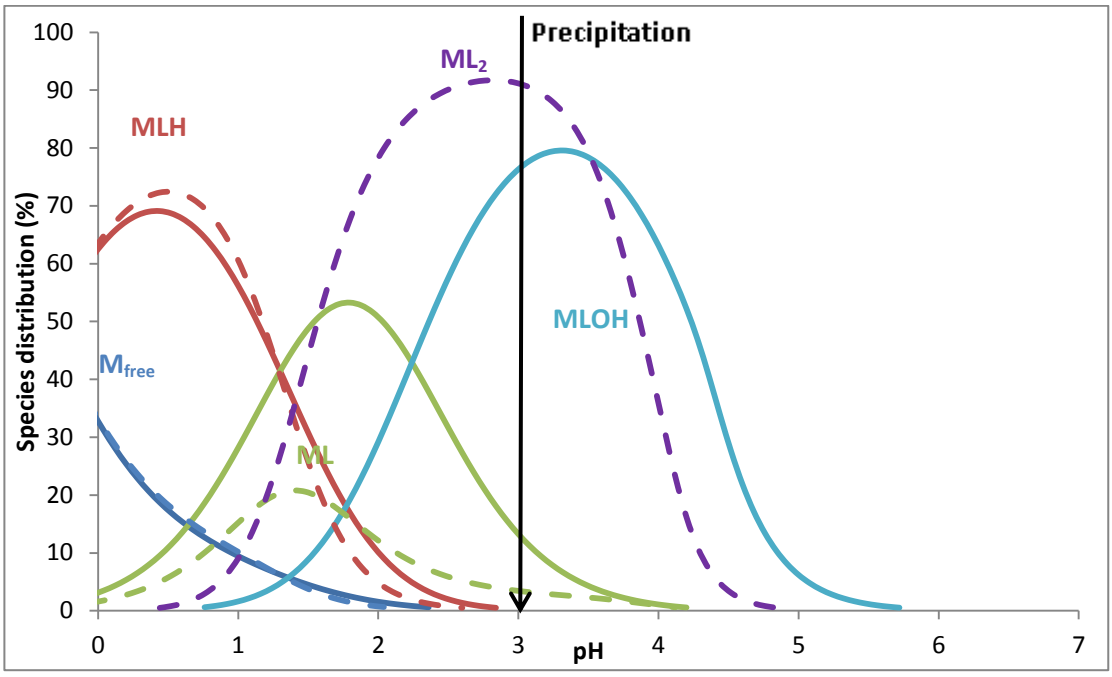


Figure 10.15 Comparative SDDs showing the pH region where MLOH and ML_2 would exist if they were present in solution. Average log β values of 6.6, 5.3 and 16.86 were used for MLH, ML and MLOH, respectively, (solid lines), and 6.6, 5.0 and 9.6 were used for MLH, ML and ML_2, respectively, (dashed lines), both plotted at [L]:[M] = 100. Hydroxide species have been omitted for clarity.

MLH in solution (or simply $M(NO_3)_x$ instead of MLH). Between pH 1.5 and 2.7 the slope increases to 22 mV which indicates that ML probably becomes the dominant species. In this region, both the reduction of ML_2 and MLOH (to produce H_2O instead of OH^- since we are in the acidic region) predict a slope of 40 mV which does not point to either of these species being present in a significant quantity. The slope of 27 mV above pH 2.7 indicates that the MLOH species may exist in solution rather than ML_2.

Table 10.8 Possible reduction reactions in the given pH regions with their respective calculated slopes.

pH range	Possible reduction reactions	Calculated slope
pH < 0.5	$BiLH^{3+} + 3e^- + H^+ \rightleftharpoons Bi^0 + H_2L^+$	20
0.5 < pH < 2.7	$BiLH^{3+} + 3e^- + 0H^+ \rightleftharpoons Bi^0 + HL$	0
	$BiL^{2+} + 3e^- + H^+ \rightleftharpoons Bi^0 + HL$	20
	$BiL_2^+ + 3e^- + 2H^+ \rightleftharpoons Bi^0 + 2HL$	40
	$BiLOH^+ + 3e^- + 2H^+ \rightleftharpoons Bi^0 + +H_2O + HL$	40
	$BiLOH^+ + 3e^- + H^+ \rightleftharpoons Bi^0 + OH^- + HL$	20
pH > 2.7	$BiL^{2+} + 3e^- + 0H^+ \rightleftharpoons Bi^0 + L^-$	0
	$BiL_2^+ + 3e^- + 0H^+ \rightleftharpoons Bi^0 + 2L^-$	0
	$BiLOH^+ + 3e^- + H^+ \rightleftharpoons Bi^0 + +H_2O + L^-$	20
	$BiLOH^+ + 3e^- + 0H^+ \rightleftharpoons Bi^0 + OH^- + L^-$	0

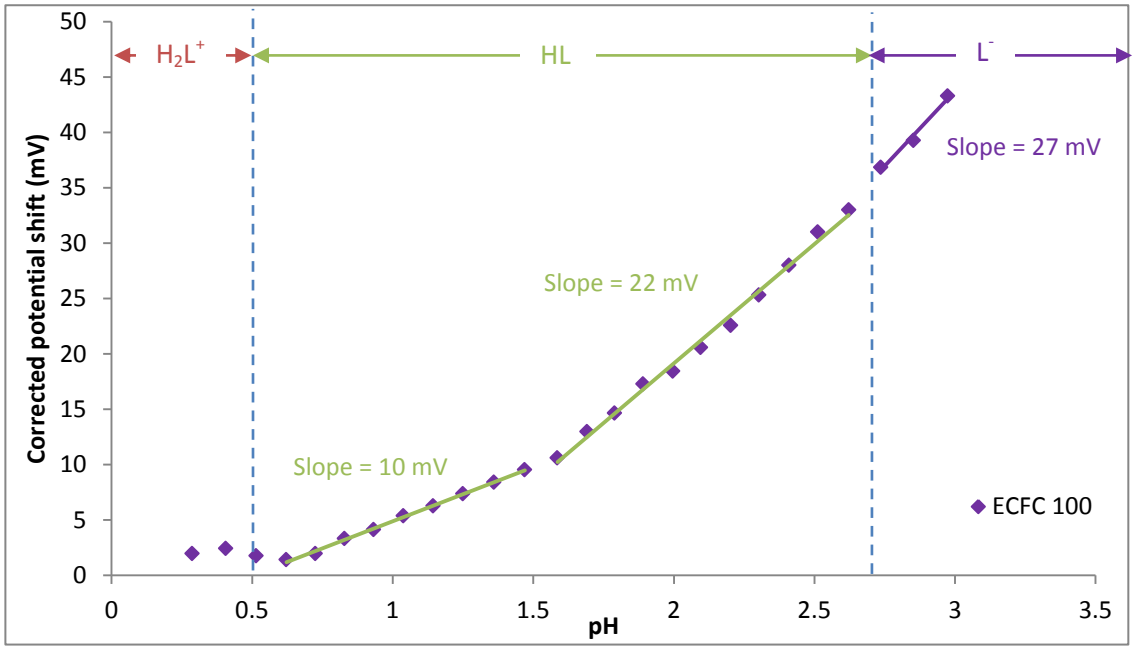


Figure 10.16 Slope analysis performed on the ECFC for [L]:[M] = 100.

10.4.2 Approach 2

Since thallium(I) potential data were only accessible between pH 6 – 10 to calculate $E(Tl_{free})$ in the experiments containing ligand, a second way to determine the $E(Bi_{free})$ values was considered. Approach two (similar to the method described in Chapter Nine section 9.4.1.4) involved calculating the difference between the $E(Bi_{free})$ values and the averaged half-wave reduction potential of thallium(I) for the three overlapping waves that were collected at the lowest pH before the ligand was added. As a reminder, in order to directly relate this difference in the ligand-free experiment to the complexation experiment, the pH at which this difference is determined must be the same, as E_j varies with pH in this region. Thus for each ligand-free experiment the half-wave potential of the actual overlapping waves was not used, but instead the thallium(I) half-wave potential vs. pH data were fitted with a polynomial which best represented the data below pH of about 2 (the same data used in calculating the diffusion junction potential) (see Figure 10.17 for an example using EXP 1). The polynomial was then used to calculate the thallium(I) half-wave potential at the pH at which these data were acquired in the corresponding complexation experiment (see Table 10.9). Again, the difference between this point and the $E(Bi_{free})_{OH}$ and $E(Bi_{free})_T$ values were calculated and are shown in Table 10.10. In this approach the actual difference value obtained for the ligand-free experiment was used with its corresponding complexation experiment (the average model was considered also and the results will be mentioned later in this section). Table 10.10 presents the differences between the $E(Bi_{free})$ potential values and $E_{½}$ for thallium(I) for each ligand-free experiment. It is these differences that will be applied to each corresponding complexation experiment to obtain the two $E(Bi_{free})$ values.

For each complexation experiment the initial overlapping waves for thallium (I) (before ligand was added) were fitted as normal using Equation 2.1, and their half-wave potentials averaged. The differences calculated in Table 10.10 were then

added to these averaged half-wave potential values to obtain the necessary $E(Bi_{free})$ values (see Table 10.11).

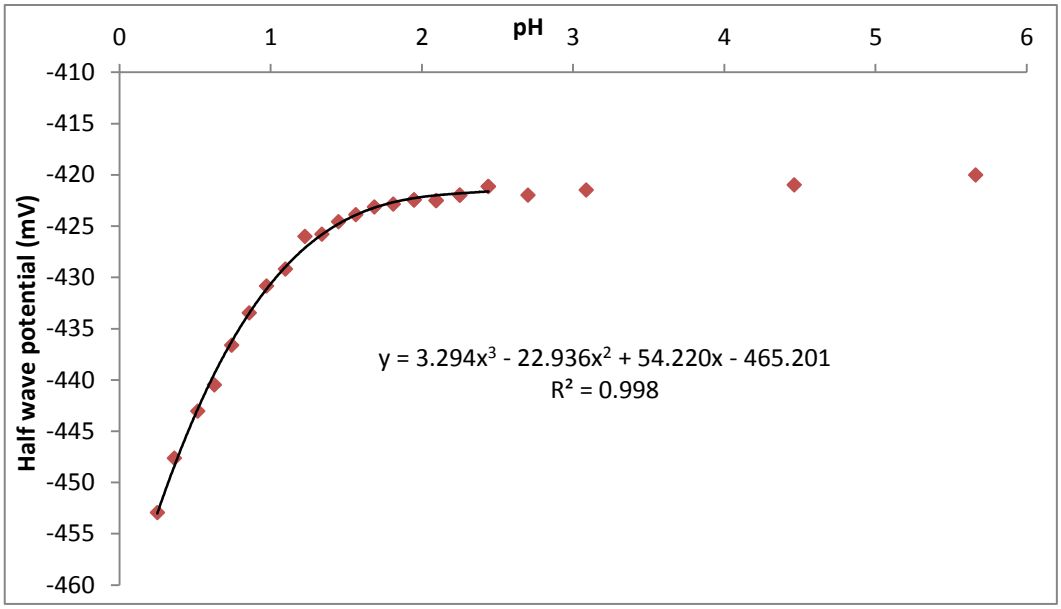


Figure 10.17 Thallium(I) half-wave potential vs. pH data fitted with a polynomial using the same data points that were used in measuring the diffusion junction potential (EXP 1).

Table 10.9 The equation fitted to thallium(I) data in the ligand-free experiments which was used to obtain the $E_{½}$ value for thallium(I) at the initial pH for the corresponding complexation experiment.

Ligand-free experiment		**Complexation experiment**		**Ligand-free experiment**
EXP	**Equation**	**[L]:[M]**	**pH**	$E_{½}$
1	$y = 3.294x^3 - 22.936x^2 + 54.220x - 465.201$	**100**	0.287	-451.45
2	$y = -12.753x^2 + 47.337x - 468.813$	**77**	0.309	-455.40
3	$y = 1.591x^3 - 17.847x^2 + 52.751x - 469.784$	**49**	0.330	-454.26

Table 10.10 Differences calculated between the $E_{½}$ and $E(Bi_{free})$ values for thallium(I), for each ligand-free experiment.

EXP	$E_{½}$	$E(Bi_{free})_{OH}$	$E(Bi_{free})_{T}$	ΔE_{OH} (mV)	ΔE_{OH+NO3} (mV)
1	-451.45	60.0	68.9	519.0	527.9
2	-455.40	62.9	71.8	516.8	525.8
3	-454.26	60.7	69.4	519.3	528.1
			Average	518.4 ± 1.3	527.2 ± 1.3

Table 10.11 Calculated values for the $E(Bi_{free})$ values using background thallium data as the reference point.

[L]:[M]	Initial pH	Average $E_{½}$ for Tl(I) at initial pH (mV)	$E(Bi_{free})_{OH}$ (mV)	$E(Bi_{free})_{T}$ (mV)
100	0.287	-458.94	60.0	68.9
77	0.309	-453.92	62.9	71.8
49	0.33	-458.61	60.7	69.4

For the bismuth data, the shifts due to E_j were compensated for using the E_j that was measured in the corresponding ligand-free experiment, rather than the average E_j. This was done by calculating the magnitude of the E_j at each pH point using the polynomial equations fitted to the diffusion junction potential data for each experiment. Figure 10.18 shows the $E(Bi_{free})_{OH}$ and $E(Bi_{free})_{T}$ values together with the experimental data before and after it was compensated for E_j for the [L]:[M] = 49 dataset.

Determining log β values using these data and $E(Bi_{free})_{OH}$ was not successful even when using the ML species only (as was done for Approach 1). There is no doubt that complex formation with the ligand occurred as differences were observed in the half-wave potential vs. pH plots in Figure 10.10 when ligand was present or

absent. It was found that the corrected potential shift was below 0 at the lowest pHs which

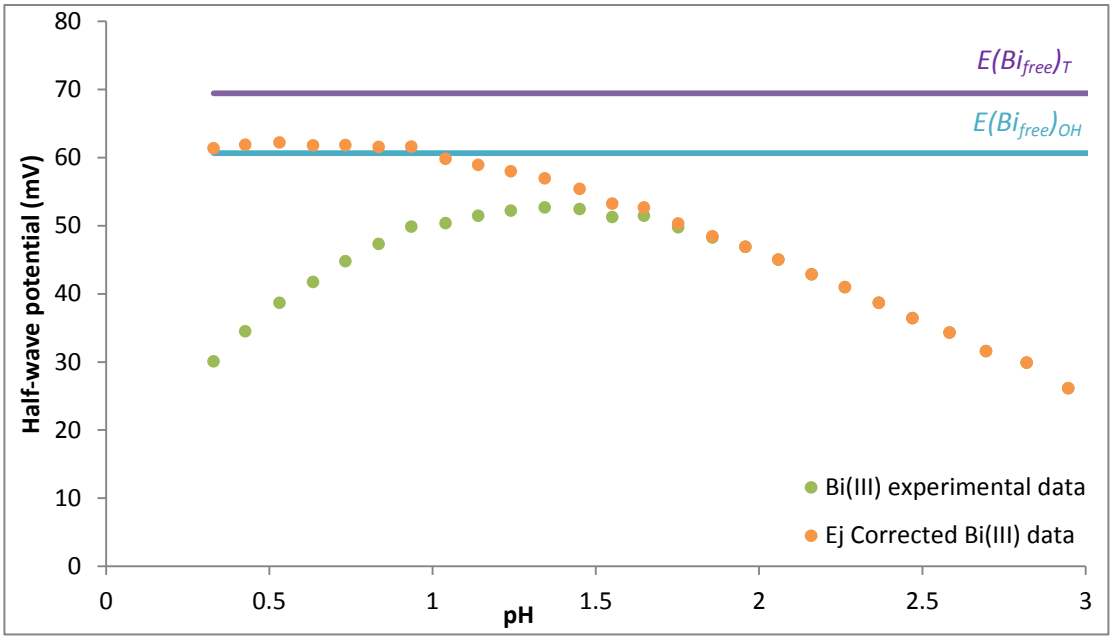


Figure 10.18 Compensation of E_j and calculation of the $E(Bi_{free})$ values obtained using the model for the [L]:[M] = 100 dataset.

indicated that the way in which the free metal ion potential was calculated was inaccurate, which would also affect the $E(Bi_{free})_T$ value in the same way, i.e. producing $E(Bi_{free})$ values that were too low. Nevertheless log β values calculated using $E(Bi_{free})_T$ and a species set of MLH, ML and MLOH are shown in Table 10.12. The average values indicate the shortfall of the $E(Bi_{free})_T$ as their magnitudes are somewhat smaller than those found using Approach 1 (see Table 10.7). Interestingly, the log β values for the two datasets (100 and 49) are significantly more precise than those obtained using Approach 1.

Table 10.12 Formation constants calculated using Approach 2 and $E(Bi_{free})_T$.

Complex	[L]:[M] = 100		[L]:[M] = 77		[L]:[M] = 49		AVERAGE	
	Log β	Std Dev	Log β	Std Dev	Log β	Std Dev	Log β	Std Dev
MLH	6.30	0.04	*5.84*	*0.11*	6.35	0.06	6.32	0.03
ML	4.94	0.07	*4.54*	*0.20*	5.08	0.08	5.01	0.09
MLOH	16.60	0.04	*16.85*	*0.05*	16.52	0.08	16.56	0.05
OVERALL FIT	0.27		*0.51*		0.67			

Not included in the average values.

10.4.3 Comparison of Approach 1 and 2

If the two approaches are scrutinized it can be seen that each has its own advantages and disadvantages. Approach 1 calculates the difference model from an average of a number of points as opposed to Approach 2 which is based on a single point. This single point is calculated from smoothed data (using the equation fitted to the low pH data of the thallium(I) half-wave potentials) which also introduces some discrepancy. However, in the pH region where the difference model for Approach 1 is calculated, there is definitely no complex formation occurring between thallium(I) and the ligand, which may not be the case between pH 6 and 10 where $E(Tl_{free})$ was calculated in Approach 2. For these particular experiments it should be safe to assume that thallium(I) did not form complexes with pyrazinecarboxylic acid because this ligand has shown to form only very weak complexes, and also the magnitude of $E(Bi_{free})$ is somewhat larger than the value found when using Approach 2. If complex formation had taken place the expected value of $E(Bi_{free})$ would have been smaller than in Approach 2 (see the comparative summary of the models and their calculated $E(Bi_{free})$ values, Table 10.13 and 10.14 respectively).

Table 10.13 Summary of the difference models obtained from ligand-free experiments for Approach 1 and 2.

EXP	Approach 1			Approach 2		
	$E(Tl_{free})$	ΔE_{OH} model	ΔE_{OH+NO3} model	$E_{½}(Tl)$	ΔE_{OH} model	ΔE_{OH+NO3} model
1	-421.79	489.3	498.2	-451.45	519.0	527.9
2	-424.67	486.1	495.0	-455.40	516.8	525.8
3	-423.00	488.0	496.8	-454.26	519.3	528.1
Average		487.8	496.7		518.4	527.2
STD DEV		1.6	1.6		1.3	1.3

Table 10.14 Summary of the data $E(Bi_{free})$ values determined for complexation experiments.

[L]:[M]	Approach 1			Approach 2		
	$E(Tl_{free})$	$E(Bi_{free})_{OH}$	$E(Bi_{free})_T$	$E_{½}(Tl)$	$E(Bi_{free})_{OH}$	$E(Bi_{free})_T$
100	-426.25	61.6	70.4	-458.94	60.0	68.9
77	-419.61	68.2	77.1	-453.92	62.9	71.8
49	-422.70	65.1	74.0	-458.61	60.7	69.4

We expected that $E(Bi_{free})$ values would be the same when calculated using the two approaches for each complexation experiment, as was seen for [L]:[M] = 100, but not for the other two experiments. Another major difference between the two approaches is that for Approach 1 an average model was used while for Approach 2 the corresponding ligand-free experiment was used. This discrepancy should be small when compensating for E_j as Figure 10.3 shows that at pH 0.3 the average value is 31 ± 2 mV.

A third approach, Approach 3 was also tried. This was essentially Approach 2 but the average diffusion junction potential (to compensate E_j) and the average model for ΔE_{OH} (518.4 mV) and ΔE_{OH+NO3} (527.2 mV) were used. Approach 3 was tested by determining formation constants. When using the $E(Bi_{free})_{OH}$ values (59.8, 64.5 and

59.5 mV for [L]:[M] = 100, 77 and 49, respectively, the initial data points of the ECFC were still negative (as found for Approach 2) and log β values could not be refined. Using the $E(Bi_{free})_T$ values (68.6, 73.3 and 68.3 mV for [L]:[M] = 100, 77 and 49, respectively) the formation constants for MLH, ML and MLOH were determined and are presented in Table 10.15. The average log β values are slightly smaller than those obtained using Approach 2, but this difference is not significant. These values are also smaller than those determined using Approach 1.

Table 10.15 Formation constants calculated using Approach 3 and $E(Bi_{free})_T$.

Complex	[L]:[M] = 100		[L]:[M] = 77		[L]:[M] = 49		AVERAGE	
	Log β	Std Dev	Log β	Std Dev	Log β	Std Dev	Log β	Std Dev
MLH	6.27	0.04	*6.13*	*0.07*	6.2	0.1	6.24	0.05
ML	4.92	0.07	*4.47*	*0.3*	5	0.09	4.96	0.06
MLOH	16.57	0.04	*16.97*	*0.05*	16.4	0.1	16.5	0.1
OVERALL FIT	0.27		*0.32*		0.3			

No complexes of pyrazinecarboxylic acid with Bi(III) could be found on the NIST database (Martell, Smith and Motekaitis, 2004), and in fact very few metal ions were studied with this ligand, so for interest the La(III)-pyrazinecarboxylic acid complexes were looked at, since the lanthanum(III) metal ion is similar in size (and equivalent in charge) to bismuth(III). Two species were identified for this system, ML and ML_2, where the log β values were 2.3 and 4.1, respectively, at 25 °C and 1.0 M ionic strength using potentiometry. The small magnitudes of these log β values indicate that relatively weak complexes were formed compared to those for Bi(III) as proposed here. A similar trend is observed in the case of quinolinic acid where the log β value for ML is 2.96 for La(III) (at 25 °C and 0.5 M ionic strength) and about 7.5 for Bi(III) (at 25 °C and 0.5 – 0.25 M ionic strength). According to Kim, Kim and Yun (1983) the nitrogen-ligand bond in the pyrazinecarboxylic acid complex is found to be weaker than that of a picolinic acid complex, due to the electron withdrawing

ability of the nitrogen in the *meta* position of the pyrazine ring which results in the reduced basicity of the nitrogen in the *ortho* position.

10.5 CONCLUSIONS

The problem with this particular metal-ligand system was two-fold, complex formation between the ligand and metal ion was very weak and reduction of the ligand interfered with the thallium(I) signal. This meant that the ligand concentration could not be increased to promote complex formation without it further affecting the thallium(I) reduction signal.

In order to obtain a value of $E(Tl_{free})$ for a complexation experiment, the data collection had to be extended to a very high pH which requires a long duration of measurement. Over time the reference system can vary due to changes in the solutions at the various interfaces, which could introduce error in the measurements taken at high pH. Due to the overlap of the thallium(I) data by the ligand reduction at low pHs, we could not establish the trend followed by the thallium(I) data (one which we are familiar with from our ligand-free experiments) and so if there was an error with the reference system it could not be identified.

The data obtained here was not sufficient to make conclusions on the species in solution and their formation constants, although it is predicted that both ML and MLOH is formed in solution. Unfortunately the automated titration system used for the polarographic experiments stopped working so additional experiments could not be run to improve on the reproducibility.

For future work I would suggest repeating the polarographic experiments at [L]:[M] ratios close to 100 and analyzing the data using all approaches again. Further

experiments could also be done using mass spectrometry on solutions at selected pH values, especially between pH 3 and 4, to ascertain if it is the ML_2 or MLOH species existing in solution. Also very importantly is the development of the 3D-CFC software to incorporate competing ligands (such as nitrate) so that the use of the two $E(Bi_{free})$ values is not required and more accurate log β values can be determined.

10.6 REFERENCES

Allen, F. H., 2002. Acta Crystallographica, B58, pp 380-388. Cambridge Structural Database. Version 5.34, November 2012 update.

Anjaneyulu, O., Maddileti, D. and Swamy, K. K., 2012. Structural motifs in phenylbismuth heterocyclic carboxylates–secondary interactions leading to oligomers. *Dalton Transactions,* 41 (3)**,** pp 1004-1012.

Barszcz, B., Masternak, J., Hodorowicz, M. and Jabłońska-Wawrzycka, A., 2012. Cadmium(II) and calcium(II) complexes with N, O-bidentate ligands derived from pyrazinecarboxylic acid. *Journal of Thermal Analysis and Calorimetry,* 108 (3)**,** pp 971-978.

Billing, C. 2012. *Study of bismuth chemistry toward medicinal applications.* Doctor of Philosophy, University of the Witwatersrand.

Cukrowski, I. and Luckay, R. C., 1998. A differential pulse polarographic study of bismuth^{III} complexes with macrocyclic ligands 1,4,7,10-tetraazacyclododecane and 1,4,7,10-tetrakis (2-hydroxypropyl)-1,4,7,10-tetraazacyclododecane. An out-of-cell determination of stability constants of polarographically active and inactive bismuth complexes at fixed ligand to metal ratio and various pH values. *Analytica Chimica Acta,* 372 (3)**,** pp 323-331.

Kim, G. S., Kim, Y. I. and Yun, S. S., 1983. Complexation of the lanthanides by pyrazinecarboxylate. *Polyhedron,* 2 (7)**,** pp 663-668.

Klein, C. L., Majeste, R. J., Trefonas, L. M. and O'Connor, C. J., 1982. Magnetic properties and molecular structure of copper(II) complexes of pyrazinecarboxylic acid. *Inorganic Chemistry,* 21 (5)**,** pp 1891-1897.

Martell, A. E. and Hancock, R. D., 1996. *Metal Complexes in Aqueous Solutions*, New York, Plenum Press.

Martell, A. E., Smith, R. M. and Motekaitis, R. J., 2004. NIST Standard Reference Database 46. 8.0 ed. Gaithersburg, USA: U.S Department of Commerce, National Institute of Standards and Technology.

Powell, K. and Pettit, L., 1997. IUPAC Stability Constants Database. *Academic Software, Otley (UK).*

Premkumar, T. and Govindarajan, S., 2006. Antimicrobial study on trivalent lighter rare-earth complexes of 2-pyrazinecarboxylate with hydrazinium cation. *World Journal of Microbiology and Biotechnology,* 22 (10)**,** pp 1105-1108.

Sun, H., Li, H. and Sadler, P. J., 1997. The Biological and Medicinal Chemistry of Bismuth. *Chemische Berichte/Recueil,* 130**,** pp 669-681.

Zhang, H., Deng, J. Y., Bi, L. J., Zhou, Y. F., Zhang, Z. P., Zhang, C. G., Zhang, Y. and Zhang, X. E., 2008. Characterization of Mycobacterium tuberculosis nicotinamidase/pyrazinamidase. *The Federation of European Biochemical Societies Journal,* 275 (4)**,** pp 753-762.

Zhang, Y., Wade, M. M., Scorpio, A., Zhang, H. and Sun, Z., 2003. Mode of action of pyrazinamide: disruption of Mycobacterium tuberculosis membrane transport and energetics by pyrazinoic acid. *Journal of Antimicrobial Chemotherapy,* 52 (5)**,** pp 790-795.

Chapter Eleven

Concluding Summary

The focus question of this research was whether there is a link between solution species and crystalline complexes. This was investigated by growing crystals under targeted pH, concentration and ligand-to-metal concentration ratio conditions, as predicted from SDDs plotted using species and log β values determined from solution studies. It is clear that there certainly is not a one-to-one correlation between the solution and crystal complexes, as would be expected, but it appears that one could predict with fair success whether the ligand in the complex would be protonated or not.

There was a direct correlation between the pH at which the crystalline complex formed and what the solution results predicted for the following structures: (i) the MLH complex for the cadmium(II)-picolinic acid system, (ii) the ML complex for the cadmium(II)-dipicolinic acid system, (iii) LH_2 found with the cadmium(II)-dipicolinic acid complex and (iv) LH_2 found with the cadmium-quinolinic acid systems, (v) the ML complex for the cadmium-quinolinic acid system and (vi) the MLH complex for the Bi(III)-EDTA system. Unfortunately the crystalline bismuth(III)-quinolinic acid structure was too complicated to be matched to a simple solution species.

The crystalline $M(LH)_3$ complex was found for both the cadmium(II)-picolinic acid and cadmium(II)-quinolinic acid system. In each case it was not initially speculated in solution, but could be included in the species model to an extent to determine a formation constant. This allowed the generation of SDDs which demonstrated that the crystalline complex formed in the pH range where it

showed to exist in solution for both metal-ligand systems. These results highlight that solid state structures can be used (with discretion) to provide a good estimate of the stoichiometry of the species existing in solution. One of the downfalls of polarography, or any other technique used to determine formation constants, is that minor species in solution cannot always be identified. We have shown here that the formation of crystalline complexes could aid in the speculation of species in solution, bearing in mind that predominant species under low concentration conditions are not necessarily the dominant species at high concentrations. The crystalline $M(LH)_3$ complex is a good example here.

The research done towards studying the effect of temperature on formation constants also proved useful in speculating minor species in solution. Determining formation constants for the cadmium(II)-dipicolinic acid system from experiments conducted at various temperatures allowed for the elucidation of a novel species. The effect of temperature on the magnitude of formation constants as well as the types of species that form in solution was demonstrated. The ML_3 complex was identified in solution experiments conducted at 32 and 40 °C and was probably a minor species at 25 °C. Interestingly, the only ML_3 crystalline complex found was grown from solutions at elevated temperatures (60 °C) which again indicates a link between the formation of specific complexes in solution and the solid state.

We are aware of the fact that there are major differences in the solutions for electrochemical experiments and crystallization experiments which do affect the results obtained from each. Ligand is in excess in solution experiments, which promotes complex formation with the metallic cation, according to Le Chatelier's principle. In the crystallization liquor the concentrations of ligand and metal are more similar, but both these concentrations are significantly higher than in the polarographic experiments, which also drives the equilibria forward. This means that in the case of bismuth(III) it hydrolyzes sooner (at lower pH), and in the case of cadmium(II) it allows the formation of complexes with higher stoichiometries.

In general, the polarographic technique and the method of analysis used in this project were not only efficient at identifying species below pH 2, but also accurately determining their formation constants for the cadmium(II)-ligand systems. This research highlights the general complexity of studying bismuth(III) complex formation which is why so little is known about it. Difficulties arise due to two main reasons: firstly, obtaining the free metal ion potential directly is impossible due to complex formation with both hydroxides and nitrates, and secondly, studies have to be conducted from low pH as precipitation occurs under acidic conditions, thus the diffusion junction potential has to be determined (which was generally done using a witness ion) and compensated for. For the Bi(III)-EDTA studies thallium(I) could not be used as an in-situ witness ion to monitor the diffusion junction potential because its reduction potential overlapped with that of bismuth(III). Apart from the chemistry itself, the fact that the software used to calculate formation constants posed limitations as competing ligands could not be included, lead to more complicated procedures to produce the best estimates for these values. All these factors lead to errors which compound within an experiment and affect the calculated formation constants.

The choice of ligand used in studies of bismuth(III) complex formation also complicated matters. In the case of EDTA reliable formation constants could not be obtained due to the irreversibility of the system, and in the case of pyrazinecarboxylic acid the complexes formed with Bi(III) were very weak which meant that the shifts in potential were relatively small. This made it extremely difficult to interpret data in the acidic region where competition with nitrates occurred, but could not be sufficiently accounted for because of software constraints.

In general, this research has also shown how species distribution diagrams can be used so that conditions for growing crystals can be manipulated to target particular crystalline complexes. There obviously is not always a full correlation,

but it must be a better approach than what generally appears to be an almost random attempt at making up solutions in the hope of obtaining a specific complex or merely to see what crystallizes.

Chapter Twelve

Appendix A

12.1 CHAPTER TWO: EXPERIMENTAL

Table A2.1 Reagents used for experimentation

Reagent	Supplier	Manufacturer Assay
Mercury Metal, Triply distilled	Saarchem, UnivAR®	99.80%
Cadmium(II) nitrate tetrahydrate	Fluka	≥ 99%
Bismuth(III) nitrate pentahydrate	Fluka	≥ 98.0%
Thallium(I) nitrate	Merck	≥ 99%
Picolinic acid	Aldrich	≥ 99%
Dipicolinic acid	Sigma-Aldrich	≥ 99%
Quinolinic acid	Aldrich	≥ 99%
Ethylenediaminetetraacetic acid di-sodium salt dihydrate	Saarchem	98.50%
Pyrazinecarboxylic acid	Aldrich	99%
Nitric acid	Merck or Saarchem, UnivAR®	≥ 65%
Sodium hydroxide	Saarchem, UnivAR®	≥ 98%
Potassium hydroxide solution (45%)	Sigma-Aldrich	≤ 0.3%
Sodium nitrate	Sigma-Aldrich	≥ 99.5%
Potassium nitrate	Sigma-Aldrich	≥ 99.0%
Ascarite®	Fluka	5-20 mesh
Soda lime	Merck, uniLAB®	4-8 mesh
Potassium hydrogen pthalate	Merck	99.90%
Gelatine		

Table A2.2 Parameters for standardizing KOH and HNO_3 using the autotitrator

Parameter	Setting
Autotitrator configuration:	
Mode	DisC
Rate of addition	1 mL/min
Rate of filling	30 mL/min (10 mL burette)
Volume increment	
Stop conditions:	
Stop volume	15 mL
Volume after end point	0.5 or 1 mL

Table A2.3 Parameters used for the calibration of the glass electrode.

Parameter	Setting	
	Cadmium	**Bismuth**
Potentiometric Data:		
Initial pause	1800 s	1800 s
Equilibration time	15 s	5 s
Sample rate	2 s	2 s
Criterion for stability	0.04	0.04
Maximum waiting time	15 min	15 min
Number of readings saved	100	100
Stop conditions:		
Stop potential	-400 mV	-400 mV
Stop pH	14	14
Stop volume	50 mL or 35 mL	45 mL
Dosimat configuration:		
Mode	DisC	DisC
Rate of addition	5 mL/min	5 mL/min
Rate of filling	30 mL/min (10 mL burette)	30 mL/min (10 mL burette)
Volume increment	0.5 mL throughout, or else 0.5 mL until 22 mL, 0.1 mL until 28 mL, then 0.5 mL to 35 mL	0.5 mL

Table A2.4 Parameters and their settings used when manually collecting a polarogram.

Parameter	Setting	
	Cadmium	**Bismuth**
Initial potential	-0.2 V	0.18 V
Final potential	-0.75 V	-0.70 V
Step potential	-0.04 V	-0.04 V
Step time (drop life)	1s	1s
Current integration time	100 ms	120 ms
CV-gain	0.005 mA/V	0.005 mA/V
Potential input range	± 1.0 V	± 1.0 V
Current input range	± 1.0 V	± 1.0 V
Purge time	varied	varied
Rest time	10 s	10

12.2 CHAPTER THREE: THE DIFFUSION JUNCTION POTENTIAL

Table A3.1 Data table for students t-test.

t Table

cum. prob	$t_{.50}$	$t_{.75}$	$t_{.80}$	$t_{.85}$	$t_{.90}$	$t_{.95}$	$t_{.975}$	$t_{.99}$	$t_{.995}$	$t_{.999}$	$t_{.9995}$
one-tail	0.50	0.25	0.20	0.15	0.10	0.05	0.025	0.01	0.005	0.001	0.0005
two-tails	1.00	0.50	0.40	0.30	0.20	0.10	0.05	0.02	0.01	0.002	0.001
df											
1	0.000	1.000	1.376	1.963	3.078	6.314	12.71	31.82	63.66	318.31	636.62
2	0.000	0.816	1.061	1.386	1.886	2.920	4.303	6.965	9.925	22.327	31.599
3	0.000	0.765	0.978	1.250	1.638	2.353	3.182	4.541	5.841	10.215	12.924
4	0.000	0.741	0.941	1.190	1.533	2.132	2.776	3.747	4.604	7.173	8.610
5	0.000	0.727	0.920	1.156	1.476	2.015	2.571	3.365	4.032	5.893	6.869
6	0.000	0.718	0.906	1.134	1.440	1.943	2.447	3.143	3.707	5.208	5.959
7	0.000	0.711	0.896	1.119	1.415	1.895	2.365	2.998	3.499	4.785	5.408
8	0.000	0.706	0.889	1.108	1.397	1.860	2.306	2.896	3.355	4.501	5.041
9	0.000	0.703	0.883	1.100	1.383	1.833	2.262	2.821	3.250	4.297	4.781
10	0.000	0.700	0.879	1.093	1.372	1.812	2.228	2.764	3.169	4.144	4.587
11	0.000	0.697	0.876	1.088	1.363	1.796	2.201	2.718	3.106	4.025	4.437
12	0.000	0.695	0.873	1.083	1.356	1.782	2.179	2.681	3.055	3.930	4.318
13	0.000	0.694	0.870	1.079	1.350	1.771	2.160	2.650	3.012	3.852	4.221
14	0.000	0.692	0.868	1.076	1.345	1.761	2.145	2.624	2.977	3.787	4.140
15	0.000	0.691	0.866	1.074	1.341	1.753	2.131	2.602	2.947	3.733	4.073
16	0.000	0.690	0.865	1.071	1.337	1.746	2.120	2.583	2.921	3.686	4.015
17	0.000	0.689	0.863	1.069	1.333	1.740	2.110	2.567	2.898	3.646	3.965
18	0.000	0.688	0.862	1.067	1.330	1.734	2.101	2.552	2.878	3.610	3.922
19	0.000	0.688	0.861	1.066	1.328	1.729	2.093	2.539	2.861	3.579	3.883
20	0.000	0.687	0.860	1.064	1.325	1.725	2.086	2.528	2.845	3.552	3.850
21	0.000	0.686	0.859	1.063	1.323	1.721	2.080	2.518	2.831	3.527	3.819
22	0.000	0.686	0.858	1.061	1.321	1.717	2.074	2.508	2.819	3.505	3.792
23	0.000	0.685	0.858	1.060	1.319	1.714	2.069	2.500	2.807	3.485	3.768
24	0.000	0.685	0.857	1.059	1.318	1.711	2.064	2.492	2.797	3.467	3.745
25	0.000	0.684	0.856	1.058	1.316	1.708	2.060	2.485	2.787	3.450	3.725
26	0.000	0.684	0.856	1.058	1.315	1.706	2.056	2.479	2.779	3.435	3.707
27	0.000	0.684	0.855	1.057	1.314	1.703	2.052	2.473	2.771	3.421	3.690
28	0.000	0.683	0.855	1.056	1.313	1.701	2.048	2.467	2.763	3.408	3.674
29	0.000	0.683	0.854	1.055	1.311	1.699	2.045	2.462	2.756	3.396	3.659
30	0.000	0.683	0.854	1.055	1.310	1.697	2.042	2.457	2.750	3.385	3.646
40	0.000	0.681	0.851	1.050	1.303	1.684	2.021	2.423	2.704	3.307	3.551
60	0.000	0.679	0.848	1.045	1.296	1.671	2.000	2.390	2.660	3.232	3.460
80	0.000	0.678	0.846	1.043	1.292	1.664	1.990	2.374	2.639	3.195	3.416
100	0.000	0.677	0.845	1.042	1.290	1.660	1.984	2.364	2.626	3.174	3.390
1000	0.000	0.675	0.842	1.037	1.282	1.646	1.962	2.330	2.581	3.098	3.300
z	0.000	0.674	0.842	1.036	1.282	1.645	1.960	2.326	2.576	3.090	3.291
	0%	50%	60%	70%	80%	90%	95%	98%	99%	99.8%	99.9%
	Confidence Level										

http://www.sjsu.edu/faculty/gerstman/StatPrimer/t-table.pdf

12.3 CHAPTER FIVE: SOLUTION STUDIES OF CADMIUM(II)-DIPICOLINIC ACID COMPLEXES

Table A5.1 Standard redox potentials of the silver/silver chloride reference electrode ([KCl] = 3 mol/L) as a function of the temperature and concentration (Metrosensor electrodes, 2012).

Temperature (°C)	0	+10	+20	+25	+30	+40	+50	+60
Potential (mV)	+224.2	+217.4	+210.5	+207.0	+203.4	+196.1	+188.4	+180.3

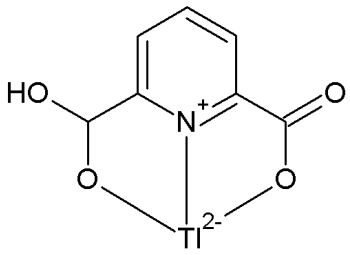


Figure A5.1 Monomeric unit making up the polymers of GIZKEG, WARYEU and WARYEU01.

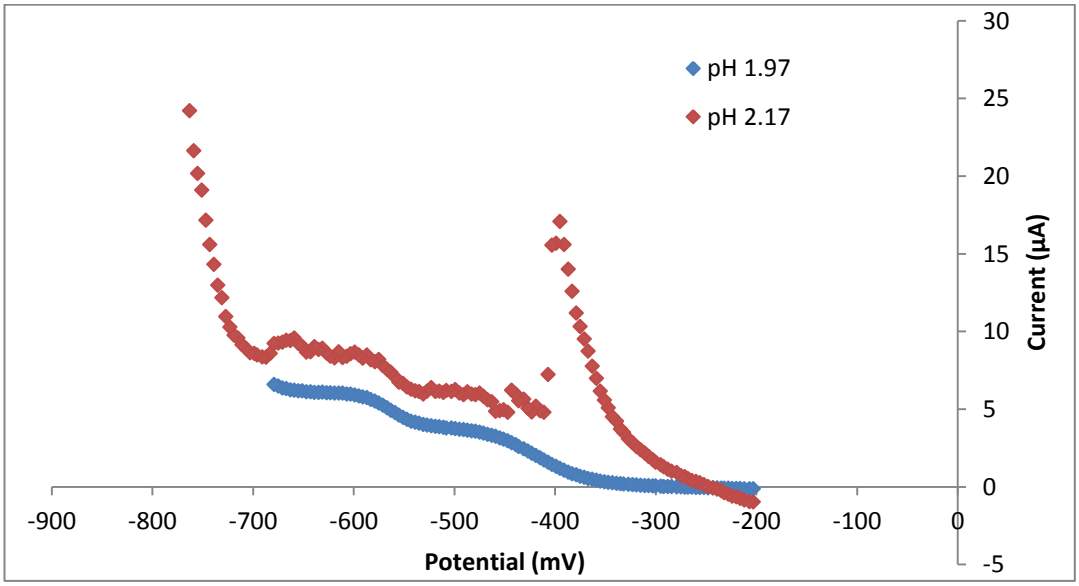


Figure A5.2 Comparison of a normal polarogram with one that is noisy and cannot be used.

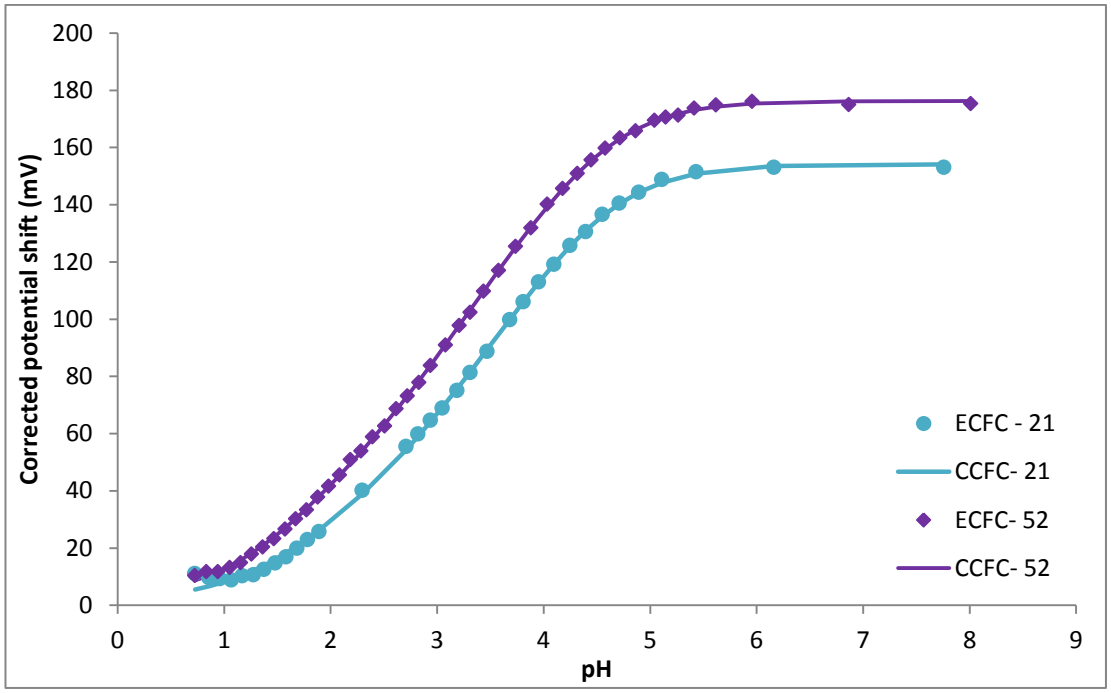


Figure A5.3 ECFC and CCFC for [L]:[M] = 21 and 52 (at 25 °C), fitted with the MLH, ML, ML_2 and ML_3 model.

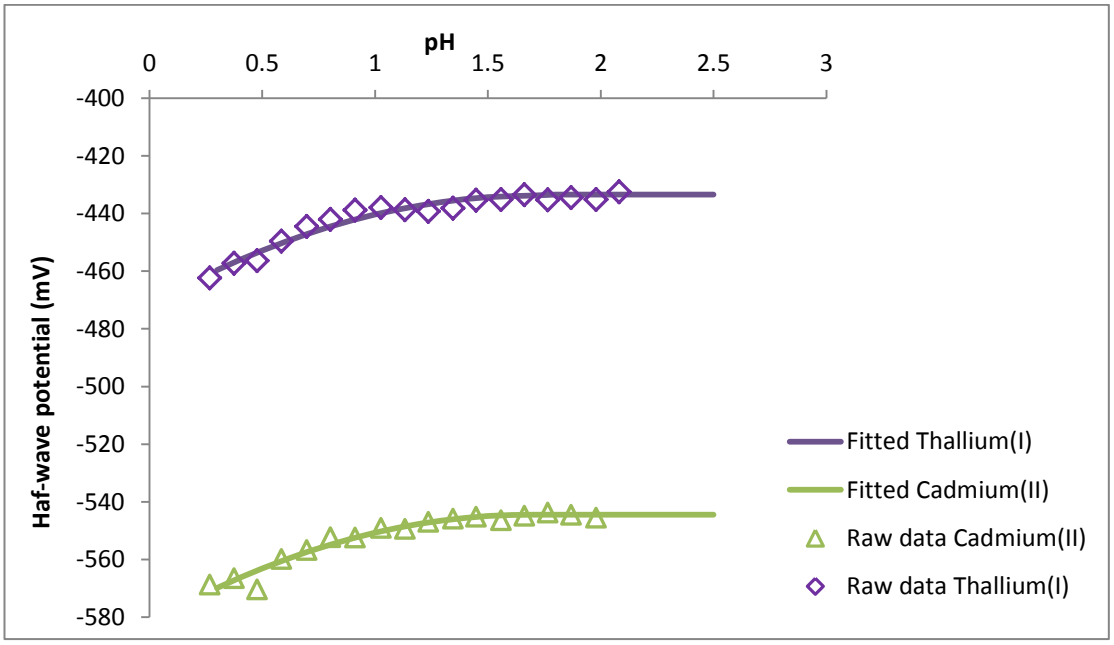


Figure A5.4 Comparison showing the closeness of the raw and fitted half-wave potentials for thallium(I) and cadmium(II) of EXP 3.

Table A5.2 Table highlighting the variation in pH (x-intercept) and potential (y-intercept) of the glass electrode calibration curves at 25, 32 and 40 °C.

Temperature:	25 °C		32 °C		40 °C	
Intercepts:	pH	Potential (mV)	pH	Potential (mV)	pH	Potential (mV)
Calibration 1	6.9	405.45	7	412.54	7.2	425.72
Calibration 2	6.9	408.46	7	412.46	7.1	422.26

12.3.1 Section A.5.1

The four-complex model comprising the MLH, ML, ML_2 and ML_3 complexes was used to fit the ECFC, refining the log β input values to achieve the following formation constants:

Table A5.3 Formation constants and their respective standard deviations for the cadmium(II) dipicolinate system at 32 °C.

Complex	**[L]: [M] = 20**		**[L]: [M] = 38**		**[L]: [M] = 49**		**AVERAGE**	
	Log β	**Std Dev**	**Log β**	**Std Dev**	**Log β**	**Std Dev**	**Log β**	**Std Dev**
MLH	8.27	0.03	8.31	0.02	7.84	0.04	8.1	0.3
ML	6.48	0.02	6.49	0.02	6.33	0.02	6.43	0.09
ML_2	10.90	0.03	10.77	0.02	10.51	0.02	10.7	0.2
ML_3	13.87	0.05	13.06	0.06	12.95	0.04	13.3	0.5
OVERALL FIT	0.35		0.66		0.74			

Formation constants calculated using the four-complex model refined for each [L]:[M] ratio and produced good overall standard deviations for the fit of the CCFC. Overlaying the ECFC with the CCFC shows a good correlation in each case, throughout the pH range (Figure A5.5). The standard deviations of each formation constant for every experiment are all very low, showing that the calculated formation constants fit the experimental data well. However, the average values show relatively high standard deviations, except for that of the ML complex. A high standard deviation for the MLH complex is expected because its presence is at low pH where E_j compensation occurs, as well as the

problem of the overlap of waves due to dipicolinic acid reduction. The ML_2 formation constant decreases with an increase in the ligand concentration.

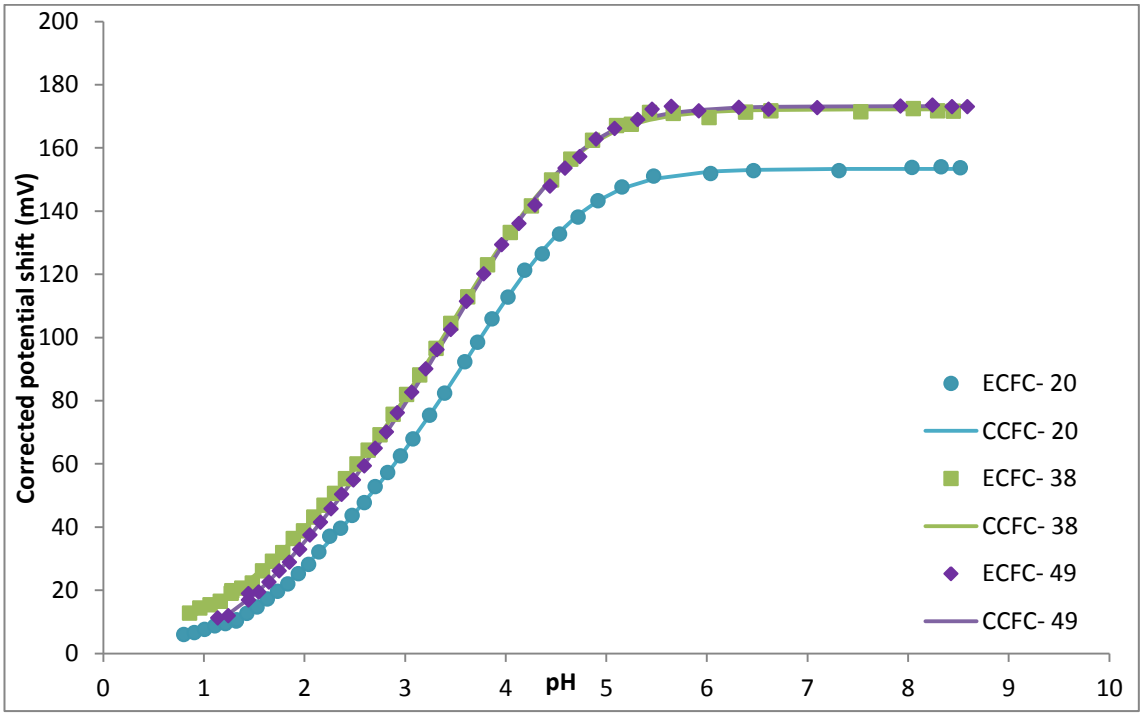


Figure A5.5 ECFC and CCFC fitted using the MLH, ML, ML_2 and ML_3 species model, for each [L]:[M] dataset at 32 °C.

Fitting this same data with the three-complex model – omitting the ML_3 complex – shows an equally good fit of the data, although it causes the overall standard deviation to increase for each [L]:[M] ratio, given in Table A5.4.

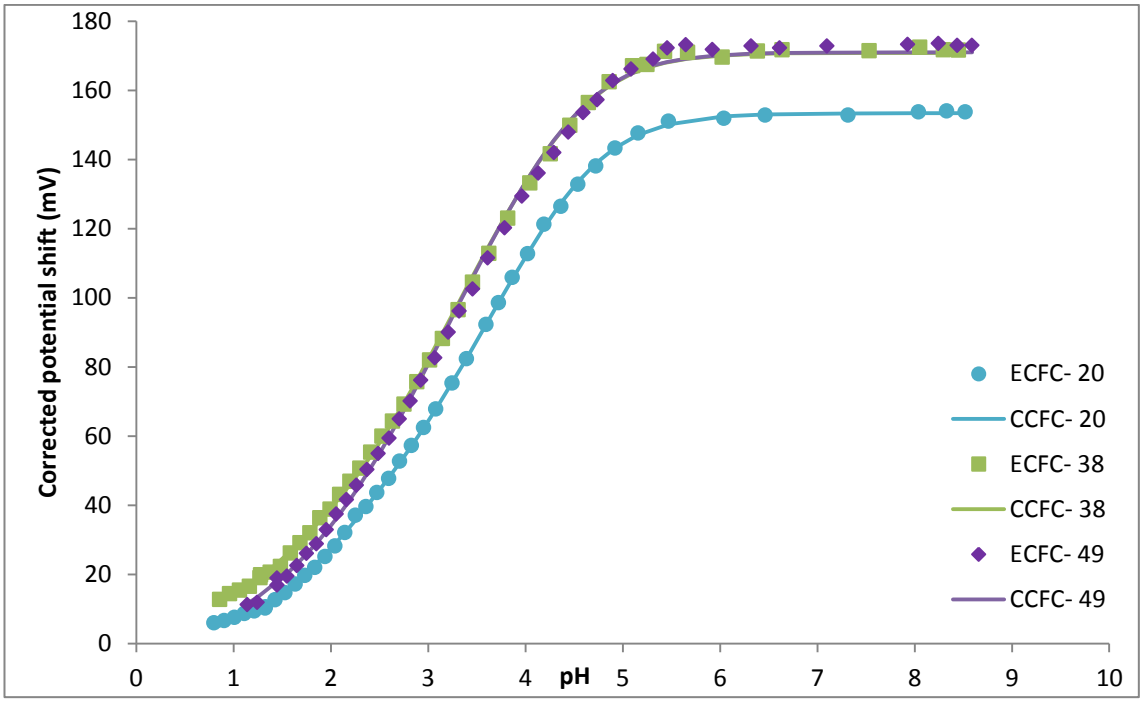


Figure A5.6 ECFC and CCFC fitted using the MLH, ML, and ML_2 species model, for each [L]:[M] dataset at 32 °C.

Table A5.4 Formation constants and their respective standard deviations for the cadmium(II) dipicolinate system at 32 °C.

Complex	[L]:[M] = 20		[L]:[M] = 38		[L]:[M] = 49		AVERAGE	
	Log *β*	Std Dev	Log *β*	Std Dev	Log *β*	Std Dev	Log *β*	Std Dev
MLH	8.33	0.02	8.34	0.02	7.97	0.03	8.2	0.2
ML	6.38	0.02	6.41	0.02	6.19	0.03	6.3	0.1
ML_2	11.072	0.009	10.879	0.008	10.690	0.007	11.0	0.1
OVERALL FIT	2.21		1.70		3.90			

A plot of [L]:[M] = 20 where the ML_3 complex is included and excluded shows that the actual fit of the CCFC barely changes.

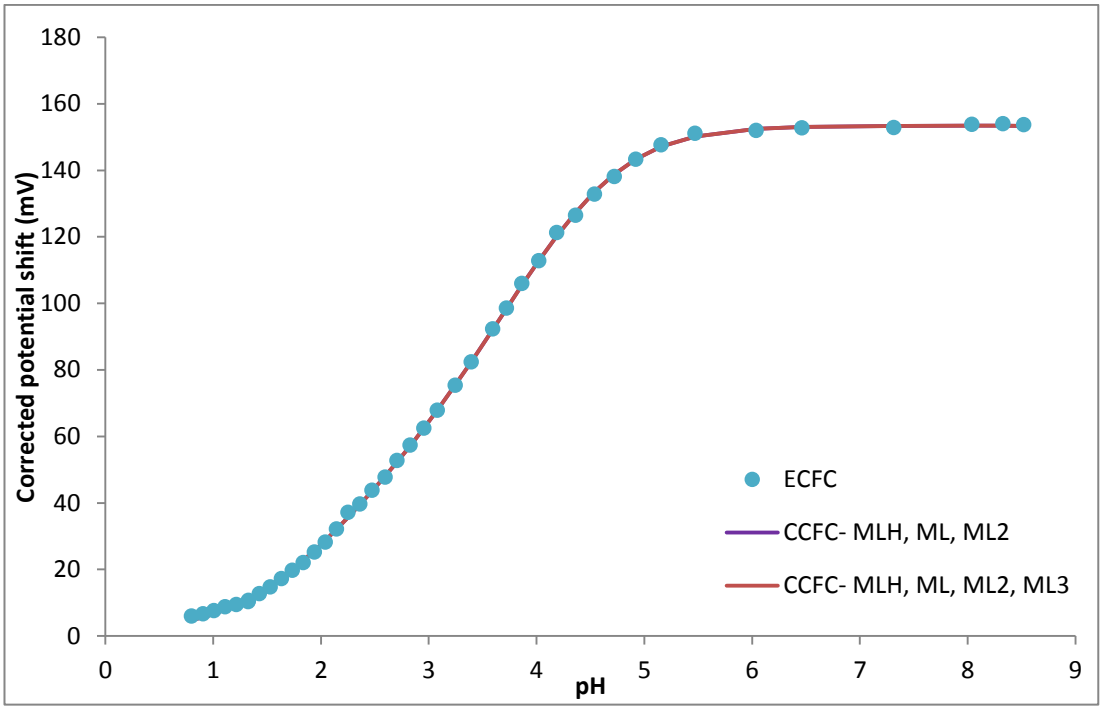


Figure A5.7 Comparison of the CCFC fitted using the MLH, ML, and ML_2 and MLH, ML, ML_2 and ML_3 species models, for the [L]:[M] = 20 dataset at 32 °C.

TableA5.5 Formation constants and their respective standard deviations for the [L]:[M] = 20 ratio at 32 °C.

Complex	Log *β*	Std Dev	Log *β*	Std Dev
MLH	8.33	0.02	8.27	0.03
ML	6.38	0.02	6.48	0.02
ML_2	11.072	0.009	10.9	0.03
ML_3	-	-	13.87	0.05
OVERALL FIT	2.21		0.35	

The overall standard deviation does not indicate which model best suits the data. Comparing the standard deviations or the changes in formation constants, for this case, also does not give any confirmation. The change though in the magnitude of the ML_2 complex is significant when using the three- and four-complex models, and so it is important to be using the correct model. If we based this decision upon what information literature has at hand, we would

probably choose to exclude the ML_3 complex, because it hasn't been shown to exist previously. On closer inspection though, comparing log *K* values for the ML_2 complex, I would say that the four-complex model is better represented because it's log *K* value for the ML_2 complex is 4.3 which is closer to that shown by literature (4.3, 4.40 and 4.26 by Suzuki and Yamasaki (1957), Anderegg (1960) and Evtimova, Scharff and Paris (1969), respectively). The log *K* value calculated for the ML_2 formation constant, acquired using the three-complex model, was 4.7.

-------End of Section A5.1-------

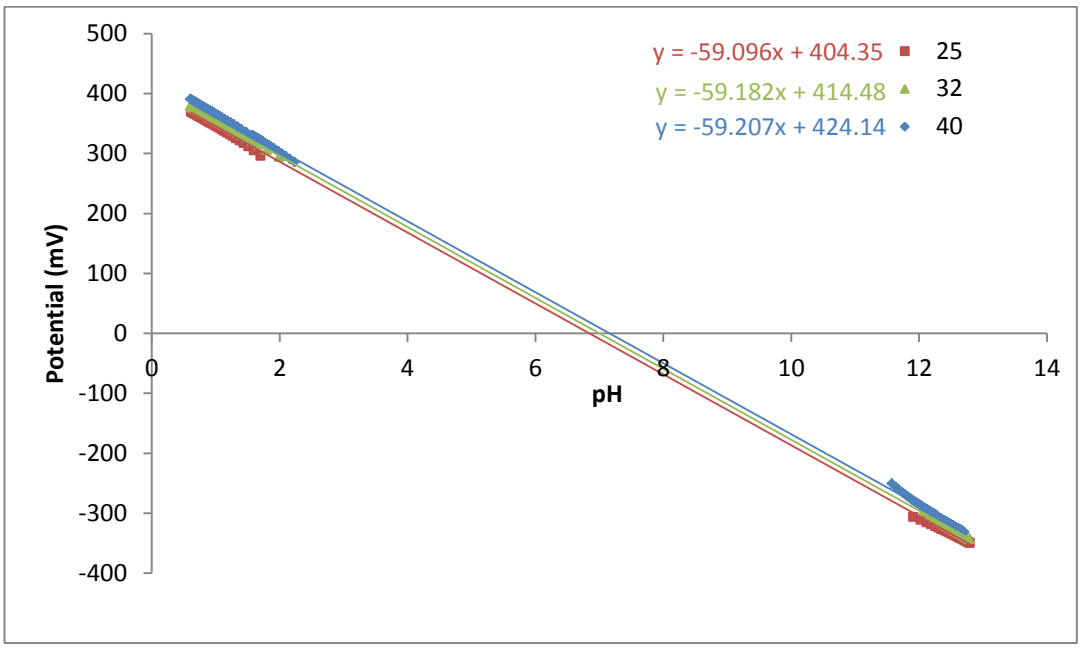


Figure A5.8 Comparison of glass electrode calibration curves at 25, 32 and 40 °C.

12.4 CHAPTER SEVEN: COMPLEX FORMATION OF CADMIUM(II)-QUINOLINIC ACID

Table A7.1 Summary of the data obtained when incorporating the third protonation constant (0.8) and then calculating the CCFC with the following four species: MLH_2, MLH, ML and ML_2.

Complex	[L]:[M] = 21		[L]:[M] = 56		[L]:[M] = 101		[L]:[M] = 196		AVERAGE	
	Log *β*	Std Dev	Log *β*	Std Dev	Log *β*	Std Dev	Log *β*	Std Dev	Log *β*	Std Dev
MLH_2	9.2	0.3	8	0.8	8.67	0.08	8.95	0.04	8.7	0.5
MLH	6.6	0.3	6.3	0.3	6.58	0.09	6.7	0.07	6.6	0.2
ML	3.83	0.05	4.04	0.03	3.83	0.03	3.87	0.04	3.9	0.1
ML_2	6.4	0.2	6.4	0.1	6.78	0.02	6.89	0.01	6.6	0.3
OVERALL FIT	0.091		0.2256		0.5876		2.0848			

Removed points 1-7 for the [L]:[M] = 21 data.

12.5 CHAPTER EIGHT: COMPLEX FORMATION OF BISMUTH(III)-QUINOLINIC ACID

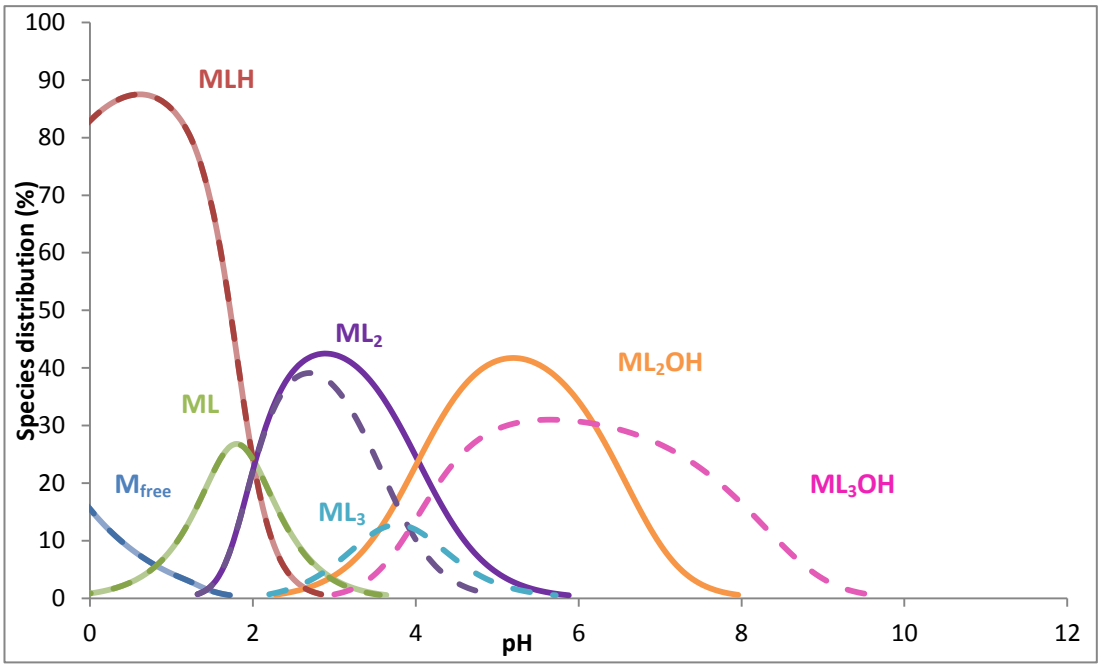


Figure A8.1 Comparison of SDDs plotted using species set 1 (MLH, ML, ML_2 and ML_2OH) (solid lines) and species set 2 (MLH, ML, ML_2, ML_3 and ML_3OH) (dashed lines), where [L]:[M] = 1:1 and [Bi] = 0.05 M. All hydroxides have been omitted for clarity. Refer to Table 8.4, $E(Bi_{free})_T$, for log β values.

12.6 CHAPTER NINE: COMPLEX FORMATION OF BISMUTH(III)-EDTA

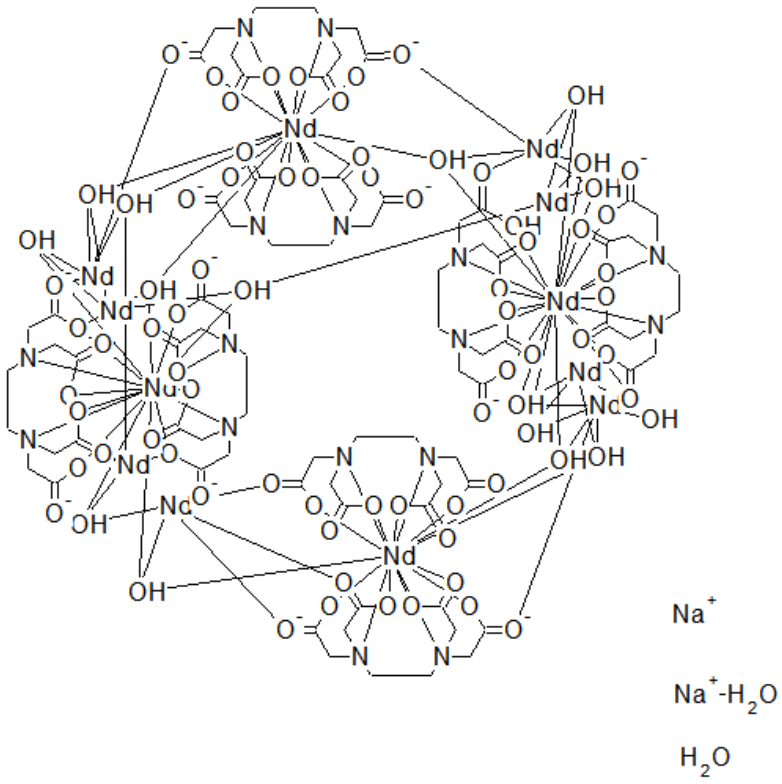


Figure A9.1 Structural diagram of FAFSAH from the CSD (Allen, 2002).

Table A9.1 Experimental conditions used for solving formation constants of the Bi(III)-EDTA system using the 3DCFC program.

Number of electrons transferred:	3
Temperature:	25 °C
Ionic strength:	0.5 M
pKw:	13.74
Concentration of hydroxide species:	0.4969
Slope:	19.720 mV
Experiment mode:	DCT

12.7 REFERENCES

Allen, F. H., 2002. Acta Crystallographica, B58, pp 380-388. Cambridge Structural Database. Version 5.34, November 2012 update.

Anderegg, G., 1960. Pyridinderivate als Komplexbildner I. Pyridincarbonsäuren. *Helvetica Chimica Acta,* 43 (1)**,** pp 414-424.

Evtimova, B., Scharff, J.-P. and Paris, M. R., 1969. *Bulletin de la Societe Chimique de France* pp 81.

Suzuki, K. and Yamasaki, K., 1957. Stabilities of Dipicolinic Acid Complexes with Bivalent Metals. *Die Naturwissenschaften,* 44**,** pp 396.

Chapter Thirteen

Appendix B

Table B13.1 Alphabetized REFCODES of the CSD (Allen, 2002) with corresponding references.

AFEBUI	Tellez, Gaytan, Bernes and Vergara (2002)
AGUBEK	Li, Ha, Chang and Yuan (2008)
BENVEV	Pelizzi and Pelizzi (1981)
BOKRID	Huang *et al.* (2008)
CDPICO	Deloume and Loiseleur (1974)
CEBPEF	Li, Wang, Fu and Chen (2005)
CEXWEI	Mahata and Natarajan (2007)
CONXEJ	Aghabozorg *et al.* (2009)
DARYEB	Wang, Fan, Wang and Chen (2005)
DEQDIN	Wu, Zhang and Lin (2006)
DEQDIN	Wu, Zhang and Lin (2006)
DOCQIW	Prasad and Rajasekharan (2008)
DOCQOC	Prasad and Rajasekharan (2008)
DOZDEC	Starosta and Leciejewicz (2009)
ETUVAR	Dong *et al.* (2011)
ETUYUO	Aghabozorg *et al.* (2011)
FAFSAH	Wang, Jin and Zheng (2000)
FISTOR	Basu, Peng, Lee and Bhattacharya (2005)
FISTUX	Basu, Peng, Lee and Bhattacharya (2005)
GERGOA	Andrews *et al.* (2006)
GETYOU	Wu, Chen and Du (2006)
GISJUO	Aghabozorg *et al.* (2008a)
GIZKEG	Aghabozorg *et al.* (2007)
HAZSIK	Goher, Youssef, Zhou and Mak (1993)
HISSAE	Pons (2007)
IDIFIK	Odoko, Kusano and Okabe (2002)
IDIFIK01	Ranjbar, Aghabozorg, Moghimi and Yanovsky (2001)
IJIYOQ	Lush and Shen (2011)
IJIYOQ01	Jia *et al.* (2012)

ILEJUF	Biswas, Saha, Steele and Mostafa (2011)
IRADAH	Marjit Singh, Jali, Das and Baruah (2011)
KANQOG	Yingfan *et al.* (2004)
KIVROW	Barral *et al.* (1991)
KIVROW01	Xu and Sasaki (1999)
LEHCEI	Tabatabaee, Derikvand and Attar Gharamaleki (2012)
LOBGUF	Kermagoret and Braunstein (2008)
MELYOS	Aghabozorg, Aghajani and Sharif (2006)
NELNIB	Odoko, Isomoto and Okabe (2001)
NISJEE	Karimov and Ismailova (1997)
NOCPUR	Mahata, Ramya and Natarajan (2008)
NOJDOG	Tabatabaee *et al.* (2008)
OBUZOB	Fu, Wang and Liu (2004)
OPOVUL	Zhang, Sulaiman, Tio and Hor (2011)
PEPXOY	Li *et al.* (2006)
PICOLA02	Hamazaki *et al.* (1998)
PYCXMN	Figgis, Raston, Sharma and White (1978)
PYCXMN01	Li, Wang, Wang and Xia (2000)
QUFQUY	Ma *et al.* (2009)
QUGCEB	Hu *et al.* (2009)
RAZXUF	Kang *et al.* (2005)
REHLIA	Onggo, Martak, Yamin and Ng (2006)
REMJOJ	Harrowfield *et al.* (2006)
REMJOJ01	Jia *et al.* (2012)
SAHCOU	Toma *et al.* (2003)
SEFSIG	Wen *et al.* (2006)
TEQTAK	Bermejo *et al.* (1996)
TUXLAA	Barszcz *et al.* (2010)
TUXLEE	Barszcz *et al.* (2010)
UQAKED	Wang *et al.* (2011)
WABJUG	Gharagozlou, Langer and Nemati (2010)
WARYEU	Rafizadeh, Amani and Neumüller (2005)
WARYEU01	Aghabozorg *et al.* (2008b)
XESHOS	Barnett *et al.* (2001)
XESHUY	Barnett *et al.* (2001)
YILBIF	Papatriantafyllopoulou *et al.* (2007)
YIZVAF	Callens, Burton, White and Barrett (2008)
YIZVEJ	Callens, Burton, White and Barrett (2008)

YIZVEJ01	Anjaneyulu, Prasad and Swamy (2010)

13.1 REFERENCES

Aghabozorg, H., Aghajani, Z. and Sharif, M., 2006. Bis (2, 4, 6-triamino-1, 3, 5-triazin-1-ium) bis (pyridine-2, 6-dicarboxylato-κ^3O,N,O')cadmate(II). *Acta Crystallographica Section E: Structure Reports Online,* 62 (8)**,** pp m1930-m1932.

Aghabozorg, H., Khazaie, Z., Agah, A. A., Saemi, M. and Notash, B., 2011. Propane-1,2-diaminium bis(pyridine-2, 6-dicarboxylato-$\kappa^3O^{2,}N,O^6$)cadmate dihydrate. *Acta Crystallographica Section E: Structure Reports Online,* 67 (7)**,** pp m982-m982.

Aghabozorg, H., Manteghi, F., Ghadermazi, M., Mirzaei, M., Salimi, A. R., Shokrollahi, A., Derki, S. and Eshtiagh-Hosseini, H., 2009. A novel supramolecular compound of cadmium(II): Synthesis, characterization, crystal structure,*ab initio HF, DFT* calculations and solution study. *Journal of Molecular Structure,* 919 (1)**,** pp 381-388.

Aghabozorg, H., Motyeian, E., Khadivi, R., Ghadermazic, M. and Manteghi, F., 2008a. catena-Poly[[triaquacadmium(II)]-μ-pyridine-2,3-dicarboxylato-$\kappa^3N,O^2:O^3$]. *Acta Crystallographica,* E64**,** pp m320-m321.

Aghabozorg, H., Ramezanipour, F., Nakhjavan, B., Soleimannejad, J., Attar Gharamaleki, J. and Sharif, M., 2007. Different complexation behavior of a proton transfer compound obtained from 1, 10-phenanthroline and pyridine-2,6-dicarboxylic acid with Sn(IV), Sb(III) and Tl(I). *Crystal Research and Technology,* 42 (11)**,** pp 1137-1144.

Aghabozorg, H., Ramezanipour, F., Soleimannejad, J., Sharif, M. A., Shokrollahi, A., Shamsipur, M., Moghimi, A., Attar Gharamaleki, J., Lippolis, V. and Blake, A. J., 2008b. *Pol. J. Chem. ,* 82**,** pp 487-507.

Allen, F. H., 2002. Acta Crystallographica, B58, pp 380-388. Cambridge Structural Database. Version 5.34, November 2012 update.

Andrews, P. C., Deacon, G. B., Junk, P. C., Kumar, I. and Silberstein, M., 2006. Synthetic and structural comparisons of bismuth(III) carboxylates synthesised under solvent-free and reflux conditions. *Dalton Transactions,* (40)**,** pp 4852-4858.

Anjaneyulu, O., Prasad, T. and Swamy, K. K., 2010. Coordinatively polymeric and monomeric bismuth(III) complexes with pyridine carboxylic acids. *Dalton Transactions,* 39 (8)**,** pp 1935-1940.

Barnett, S. A., Blake, A. J., Champness, N. R., Nicolson, J. E. B. and Wilson, C., 2001. Synthesis and structural characterisation of cadmium(II) and zinc(II) coordination polymers with an angular dipyridyl bridging ligand: parallel interpenetration of two-dimensional sheets with 4.8^2 topology. *Journal of the Chemical Society, Dalton Transactions,* (5)**,** pp 567-573.

Barral, M. C., Jimenez-Aparicio, R., Royer, E. C., Saucedo, M. J., Urbanos, F. A., Gutierrez-Puebla, E. and Ruiz-valero, C., 1991. Reaction of tetraacetatochlorodiruthenium(II,III) with pyridine-2-carboxylic acid. X-Ray crystal structures of tris(pyridine-2-carboxylato-κ*N,O*)ruthenium(III) monohydrate and trans-bis(pyridine-2-carboxylato-κ*N,O*)bis(triphenylphosphine)ruthenium(II)-methanol(1/2). *Journal of the Chemical Society, Dalton Transactions,* 0 (6)**,** pp 1609-1613.

Barszcz, B., Hodorowicz, M., Jabłońska-Wawrzycka, A., Masternak, J., Nitek, W. and Stadnicka, K., 2010. Comparative study on Cd(II) and Ca(II) model complexes with pyridine-2,3-dicarboxylic acid: Synthesis, crystal structure and spectroscopic investigation. *Polyhedron,* 29 (4)**,** pp 1191-1200.

Basu, S., Peng, S.-M., Lee, G.-H. and Bhattacharya, S., 2005. Synthesis, structure and electrochemical properties of tris-picolinate complexes of rhodium and iridium. *Polyhedron,* 24**,** pp 157-163.

Bermejo, E., Castiñeiras, A., Domínguez, R., Strähle, J. and Maichle-Mössmer, C., 1996. Aqua (iodo)(pyridine-1-oxide-2-carboxylate) cadmium (II), [Cd $(C_6H_4NO_3)I(H_2O)$], a compound with bidimensional supramolecular self-organization. *Polyhedron,* 15 (12)**,** pp 1923-1930.

Biswas, S., Saha, R., Steele, I. M. and Mostafa, G., 2011. Planar tetrameric metal cluster formation at room temperature induced by π··· π interactions: 3D supramolecular host containing 1D channel filled with solvent methanol. *Inorganica Chimica Acta,* 368 (1)**,** pp 216-222.

Callens, E., Burton, A. J., White, A. J. and Barrett, A. G., 2008. Mechanistic study on benzylic oxidations catalyzed by bismuth(III) salts: X-ray structures of two bismuth–picolinate complexes. *Tetrahedron Letters,* 49 (23)**,** pp 3709-3712.

Deloume, J.-P. and Loiseleur, H., 1974. Structure Cristalline du Pyridine-2 Carboxylate de Cadmium. *Crystal Chemistry,* B30**,** pp 607.

Dong, G.-Y., Liu, T.-F., He, C.-H., Deng, X.-C. and Shi, X.-G., 2011. Bis(2-propyl-1H-imidazol-3-ium) bis(pyridine-2,6-dicarboxylato-κ^3O^2,N,O^6)cadmate(II). *Acta Crystallographica Section E: Structure Reports Online,* 67 (7)**,** pp m1007.

Figgis, B., Raston, C., Sharma, R. and White, A., 1978. Crystal structure of Tris (pyridine-2-carboxylato) manganese(III) monohydrate. *Australian Journal of Chemistry,* 31 (11)**,** pp 2545-2548.

Fu, A.-Y., Wang, D.-Q. and Liu, A.-Z., 2004. Bis(ethylenediammonium) tris(pyridine-2,6-dicarboxylato-κ_3O,O',N)cadmium(II) hexahydrate. *Acta Crystallographica Section E,* 60 (10)**,** pp m1372-m1373.

Gharagozlou, M., Langer, V. and Nemati, A., 2010. Hexaaquazinc(II) bis[tris (3-carboxypyridine-2-carboxylato)zincate(II)]. *Acta Crystallographica Section E: Structure Reports Online,* 66 (12)**,** pp m1606-m1607.

Goher, M. A. S., Youssef, A. A., Zhou, Z.-Y. and Mak, T. C. W., 1993. Synthesis and characterization of some metal(II) complexes of quinolinic acid (H_2-Quin) and X-ray crystal structures of [Ni(H-Quin)$_2$(H_2O)$_2$] and [Mn(H_2O)$_6$][Mn(H-Quin)$_3$]$_2$. *Polyhedron,* 12 (15)**,** pp 1871-1878.

Hamazaki, H., Hosomi, H., Takeda, S., Kataoka, H. and Ohba, S., 1998. 2-Pyridinecarboxylic acid. *Acta Crystalographica,* 54**,** pp IUC9800049-IUC9800049.

Harrowfield, J. M., Lugan, N., Marandi, F., Shahverdizadeh, G. H. and Soudi, A. A., 2006. *Australian Journal of Chemistry,* 59**,** pp 400.

Hu, J., Li, J., Zhao, J., Hou, H. and Fan, Y., 2009. *Inorg.Chim.Acta,* 362**,** pp 5023.

Huang, Y.-G., Wang, X.-T., Jiang, F.-L., Gao, S., Wu, M.-Y., Gao, Q., Wei, W. and Hong, M.-C., 2008. Cobalt–Lanthanide Coordination Polymers Constructed with Metalloligands: A Ferromagnetic Coupled Quasi-1D Dy^{3+} Chain Showing Slow Relaxation. *Chemistry-A European Journal,* 14 (33)**,** pp 10340-10347.

Jia, Y., Li, H., Guo, Q., Zhao, B., Zhao, Y., Hou, H. and Fan, Y., 2012. Template-Induced Structural Isomerism of Pyridine-2,3-dicarboxylate and PbII with Similar High Stability and Different Fluorescent Properties. *European Journal of Inorganic Chemistry,* 2012 (18)**,** pp 3047-3053.

Kang, Y., Zhang, J., Li, Z.-J., Qin, Y.-Y. and Yao, Y.-G., 2005. Rare 4.8^2 net in a fluorescent Cd-organic framework. *Inorganic Chemistry Communications,* 8 (8)**,** pp 722-724.

Karimov, Z. and Ismailova, G. M., 1997. *Uzb.Khim.Zh.(Russ.)(Uzbek Chem.J.),* 4**,** pp 2.

Kermagoret, A. and Braunstein, P., 2008. Synthesis of nickel complexes with bidentate N, O-type ligands and application in the catalytic oligomerization of ethylene. *Dalton Transactions,* (12)**,** pp 1564-1573.

Li, M., Ha, W., Chang, L. and Yuan, L., 2008. catena-Poly [[[aqua(1,10-phenanthroline-κ^2N,N')cadmium(II)]-μ-pyridine-2,3-dicarboxylato-$\kappa^4N,O^2:O^3,O^{3'}$] dihydrate]. *Acta Crystallographica Section E: Structure Reports Online,* 64 (12)**,** pp m1554-m1555.

Li, M., Xiang, J., Yuan, L., Wu, S., Chen, S. and Sun, J., 2006. Syntheses, Structures, and Photoluminescence of Three Novel Coordination Polymers Constructed from Dimeric d^{10} Metal Units. *Crystal Growth and Design,* 6 (9)**,** pp 2036-2040.

Li, Y.-Z., Wang, M., Wang, L.-F. and Xia, C.-J., 2000. *Acta Crystallogr., Sect.C: Cryst. Struct. Commun.,* 56**,** pp 445.

Li, Z.-X., Wang, D.-Q., Fu, A.-Y. and Chen, D.-H., 2005. Crystal structure of tetraammonium tris(pyridine-2,6-dicarboxylato-O,N,O')cadmate(II) hexahydrate, $(NH_4)_4[Cd(C_7H_3NO_4)_3] \cdot 6H_2O$. *Zeitschrift für Kristallographie,* 220**,** pp 481-482.

Lush, S. F. and Shen, F. M., 2011. Poly [(4-pyridine-2, 3-dicarboxylato) lead (II)]. *Acta Crystallographica Section E: Structure Reports Online,* 67 (2)**,** pp m163-m164.

Ma, K., Shi, Q., Hu, M., Cai, X. and Huang, S., 2009. Two Cd(II) and Ni(II) complexes constructed with dicyanamide and picolinate ligands. *Inorganica Chimica Acta,* 362 (14)**,** pp 4926-4930.

Mahata, P. and Natarajan, S., 2007. A New Series of Three-Dimensional Metal-Organic Framework,$[M_2(H_2O)][C_5N_1H_3(COO)_2]_3 \cdot 2H_2O$, M = La, Pr, and Nd: Synthesis, Structure, and Properties. *Inorganic Chemistry,* 46 (4)**,** pp 1250-1258.

Mahata, P., Ramya, K. V. and Natarajan, S., 2008. *Chem.-Eur.J.,* 14**,** pp 5839.

Marjit Singh, W., Jali, B. R., Das, B. and Baruah, J. B., 2011. Synthesis, characterization, and reactivity of zinc carboxylate complexes of 2,3-pyridine dicarboxylic acid and (3-oxo-2,3-dihydro-benzo[1,4]oxazin-4-yl) acetic acid. *Inorganica Chimica Acta,* 372 (1)**,** pp 37-41.

Odoko, M., Isomoto, N. and Okabe, N., 2001. Di-μ-chloro-bis[(2-pyridinecarboxylato-*N,O*)(2-pyridinecarboxylic acid-*N,O*)cadmium(II)] ethanol solvate. *Acta Crystallographica Section E,* 57 (8)**,** pp m371-m372.

Odoko, M., Kusano, A. and Okabe, N., 2002. Hexaaquabis(μ-pyridine-2,6-dicarboxylato-O,N,O':O)-dicadmium(II)-pyridine-2,6-dicarboxylic acid (1/2). *Acta Crystallographica,* E58 (1)**,** pp m25-m27.

Onggo, D., Martak, F., Yamin, B. and Ng, S. W., 2006. Hemi {tris (picolinic acid-κ^2*N,O*)iron(II)/tris (picolinato-κ^2*N,O*)iron(II)} hemi (tetrafluoroborate). *Acta Crystallographica Section E: Structure Reports Online,* 62 (5)**,** pp m1112-m1113.

Papatriantafyllopoulou, C., Raptopoulou, C. P., Terzis, A., Janssens, J. F., Manessi-Zoupa, E., Perlepes, S. P. and Plakatouras, J. C., 2007. Assembly of a helical zinc(II) chain and a two-dimensional cadmium(II) coordination polymer using picolinate and sulfate anions as bridging ligands. *Polyhedron,* 26 (15)**,** pp 4053-4064.

Pelizzi, C. and Pelizzi, G., 1981. X-Ray structure of tris (picolinato) cobalt(III) monohydrate. *Transition Met Chem,* 6 (5)**,** pp 315-316.

Pons, J., Garcia-Anton, J., Jimenez, R., Solans, X., Font-Bardia, M., and Ros, J, 2007. Preparation and structural characterisation of a Cd(II) complex with unusual geometry. *Inorg.Chem.Commun,* 10**,** pp 1554-1556.

Prasad, T. and Rajasekharan, M., 2008. Solvent dependent crystallization of isomeric chain coordination polymers in the Ce-Zn/Cd-dipic system. *Crystal Growth and Design,* 8 (4)**,** pp 1346-1352.

Rafizadeh, M., Amani, V. and Neumüller, B., 2005. Synthesis, Characterization, and Crystal Structure of Thallium(I) Complex containing Monodeprotonated 2,6-Pyridinedicarboxylic Acid. *Zeitschrift für anorganische und allgemeine Chemie,* 631 (10)**,** pp 1753-1755.

Ranjbar, M., Aghabozorg, H., Moghimi, A. and Yanovsky, A., 2001. Crystal structure of Bi(III) complex of a pyridine containing self-assembling system. *Analytical sciences : the*

international journal of the Japan Society for Analytical Chemistry, 17 (12)**,** pp 1469-1470.

Starosta, W. and Leciejewicz, J., 2009. Catenated polymeric molecular patterns in structures of two calcium(II) complexes with pyridine-2,3-dicarboxylate (quinolinic) and water ligands. *Journal of Coordination Chemistry,* 62 (8)**,** pp 1240-1248.

Tabatabaee, M., Aghabozorg, H., Nasrolahzadeh, R., Roshan, L. and Firoozi, N., 2008. Butane-1,4-diammonium bis(pyridine-2,6-dicarboxylato-κ^3O^2,N,O^6)cadmate(II) dihydrate. *Acta Crystallographica Section E: Structure Reports Online,* 64 (10)**,** pp m1290-m1290.

Tabatabaee, M., Derikvand, Z. and Attar Gharamaleki, J., 2012. Guanidinium hexaaquazinc(II) bis [tris (3-carboxypyridine-2-carboxylato) zincate]. *Acta Crystallographica Section E: Structure Reports Online,* 68 (8)**,** pp m1035-m1035.

Tellez, V. C., Gaytan, B. S., Bernes, S. and Vergara, E. G., 2002. The supramolecular structure of pyridine-2,6-dicarboxylic acid. *Acta Crystallographica Section C,* 58 (4)**,** pp o228-o230.

Toma, M., Sanchez, A., Casas, J. S., Sordo, J., Garcia-Tasende, M. S., Castellano, E. E., Ellena, J. and Berdan, I., 2003. *Central European Journal of Chemistry,* (4)**,** pp 441.

Wang, J., Su, J.-X., Tang, X., Wang, Y.-X. and Cheng, S.-Y., 2011. *Wuji Huaxue Xuebao(Chin.)(Chin.J.Inorg.Chem.),* 27**,** pp 957.

Wang, R.-Y., Jin, T.-Z. and Zheng, Z.-P., 2000. *Acta Chimica Sinica,* 58**,** pp 1481.

Wang, Y.-T., Fan, H.-H., Wang, H.-Z. and Chen, X.-M., 2005. A solvothermally in situ generated mixed-ligand approach for NLO-active metal-organic framework materials. *Inorganic Chemistry,* 44 (12)**,** pp 4148-4150.

Wen, L., Li, Y., Lu, Z., Lin, J., Duan, C. and Meng, Q., 2006. Syntheses and structures of four d10 metal-organic frameworks assembled with aromatic polycarboxylate and bix [bix= 1, 4-Bis (imidazol-1-ylmethyl) benzene]. *Crystal Growth and Design,* 6 (2)**,** pp 530-537.

Wu, C.-D., Zhang, L. and Lin, W., 2006. 1D and 2D Homochiral Metal-Organic Frameworks Built from a New Chiral Elongated Binaphthalene-Derived Bipyridine. *Inorganic Chemistry,* 45 (18)**,** pp 7278-7285.

Wu, H.-F., Chen, X.-D. and Du, M., 2006. A one-dimensional Cd^{II} coordination polymer: poly [[[bis [methanolcadmium (II)]-μ_2-aqua]-bis (μ_3-pyridine-2, 6-dicarboxylato-κ^5O:O, N, O': O')]. *Acta Crystallographica Section E: Structure Reports Online,* 63 (1)**,** pp m126-m128.

Xu, L. and Sasaki, Y., 1999. Syntheses and characterization of a series of carbonylruthenium(I) and (II) complexes containing pyridyl ligands. *Journal of Organometallic Chemistry,* 585 (2)**,** pp 246-252.

Yingfan, L., Dong, Z., Ruina, Y., Jing, Z., Yuan, S. and Chuanjian, S., 2004. *Russian Journal of Coordination Chemistry,* 49**,** pp 1971.

Zhang, W.-H., Sulaiman, N. B., Tio, P. S. and Hor, T. A., 2011. Nuclearity growth towards Ni(II) cubane in self-assembly with 2-hydroxymethyl pyridine (hmpH) and 5-ethoxycarbonyl-2-hydroxymethyl pyridine (5-ehmpH). *Crystal Engineering Communications,* 13 (8)**,** pp 2915-2922.